NASA TECHNICAL TRANSLATION

NASA TT F-771

NASA TT F-771

SCATTERING AND ATTENUATION OF ELECTROMAGNETIC RADIATION BY ATMOSPHERIC PARTICLES

by V. I. Rozenberg

Hydrometeorological Press
Leningrad, 1972

NATIONAL AERONAUTICS AND SPACE ADMINISTRATION • WASHINGTON, D. C. • FEBRUARY 1974

N74-19017

1. Report No. NASA TT F-771	2. Government Accession No.	3. Recipient's Catalog No.
4. Title and Subtitle SCATTERING AND ATTENUATION OF ELECTROMAGNETIC RADIATION BY ATMOSPHERIC PARTICLES		5. Report Date February 1974 6. Performing Organization Code
7. Author(s) V. I. Rozenberg		8. Performing Organization Report No. 10. Work Unit No.
9. Performing Organization Name and Address Techtran Corporation, P.O. Box 729 Glen Burnie, Maryland 21061		11. Contract or Grant No. NASw-2485 13. Type of Report and Period Covered TECHNICAL TRANSLATION
12. Sponsoring Agency Name and Address NATIONAL AERONAUTICS AND SPACE ADMINISTRATION WASHINGTON, D. C. 20546		14. Sponsoring Agency Code

15. Supplementary Notes

Translation of: "Rasseyaniye i Oslableniye Elektromagnitnogo Izlucheniya Atmosfernymi Chastitsami," Leningrad, Hydrometeorlogical Press, 1972, 348 pp.

16. Abstract

This book deals with scattering and attenuation of submillimeter, millimeter and centimeter radio waves by an arbitrary collective of atmospheric particles different in their physical structure and properties taking into account the multiple radiation exchange among them. Particular attention is given to dielectric permeability, radiophysical characteristics and calculation aspects of algorithms development and computer processing.

17. Key Words (Selected by Author(s))	18. Distribution Statement
	UNCLASSIFIED-UNLIMITED CAT. -13

19. Security Classif. (of this report)	20. Security Classif. (of this page)	21. No. of Pages	22. Price
UNCLASSIFIED	UNCLASSIFIED	346	$7.50

EDITOR'S PREFACE

The name of the author of the present monograph, V. I. Rozenberg, is already known to a wide circle of experts in the field of application of radar methods to meteorology, atmospheric optics and radar theory. /3

In his new monograph, V. I. Rozenberg develops his earlier results of studies on the scattering and attenuation of centimeter, millimeter and submillimeter electromagnetic radiation by atmospheric particles. These results are related primarily to a natural generalization of classical theory, considerably extended in the known works of K. S. Shifrina, H. K. van de Hulst, D. Deyrmendzhana, and others, to the case of a nonconcentrically layered spherical particle for an arbitrary location and different dielectric properties of its layers.

Using this theory and modern computers, the author analyzed for the first time the fundamental radar characteristics (scattering cross sections, attenuation cross sections, etc.) of a series of practically important types of hydrometeors, taking into account their surface properties, the layered character of their structure, and various regular aspects of the distribution of density and permittivity.

It is particularly important to note that Rozenberg did not confine himself to a discussion of the radar characteristics of individual particles, but has constructed an extensive theory of the scattering and attenuation of electromagnetic radiation by arbitrary collections of such particles, allowing for multiple radiation exchange between them, a theory from which Mie expressions for a polydisperse medium follow when certain *ad hoc* assumptions are made. This brings the theoretical radiometeorological models very close to the actual processes taking place in the atmosphere.

The author also concentrates a great deal of attention on Mie calculations, pointing out a number of new governing principles and relations. He performs his calculations only after carefully choosing permittivities of hydrometeors by thorough analysis of numerous literature data and his own studies. To our knowledge, most of the numerical values of permittivity of water over a wide range of temperatures (including negative ones) and wave lengths listed in the Appendix have never been published before, They can be successfully used in various geophysical, radioastronomical and oceanographic studies. /4

There can be no question that the methods of investigation proposed by the author and the results obtained through their use, presented in the monograph on a modern mathematical level, will prove very useful to scientists specializing in the field of the theory of scattering and attenuation of electromagnetic radiation, as well as specialists concerned with problems of a broader

introduction of radar into the practice of supplying the national economy of the country with meteorological information and weather forecasts.

V. G. Morachevskiy

TABLE OF CONTENTS

SCATTERING AND ATTENUATION OF ELECTROMAGNETIC RADIATION BY ATMOSPHERIC PARTICLES

Introduction

/5*

The last decade has been characterized by a particularly rapid development and improvement of radar engineering. This in turn offers steadily increasing possibilities for the application of radar methods in different areas of science (meteorology, geophysics, astrophysics, oceanography, spectroscopy, etc.), as well as in the national economy (in the control of ships, aircraft, satellites and rockets, in weather and flood forecasting, mapping of the Earth's surface, etc.).

A major trend in the perfection of radar stations (RS) consists in increasing the transmission range and improving the distinguishability of the objects being detected, this being achieved primarily by increasing the resolving power of the radar equipment, partly as the result of a narrowing of the signal radiation pattern along one or both angular coordinates. However, since the design and technological factors limit the antenna dimensions, the resolving power of RS can be increased and the permissible enlargement of the antennas can be achieved mainly by using a shorter, microwave (centimeter, millimeter and submillimeter) range of radio waves.

However, the operation of microwave RS, particularly in the millimeter and submillimeter range, is affected by various atmospheric formations (precipitation, clouds, fogs), which attenuate the radar signals and decrease the radar detectability of the objects being tracked.

As we know, attenuation of radio waves passing through regions occupied by hydrometeors is due to the fact that a part of the energy of the propagating wave is absorbed by particles and converted into heat, and part is scattered by these particles in different directions.

A decrease in the radar detectability of targets located in the region of hydrometeors is due to the fact that in addition to the attenuation of electromagnetic waves, their scattering by particles in the radar (backscattering) direction also takes place. Radio waves scattered in this manner are received by the RS as noise masking the radar signals reflected from the target.

Thus, the determination of the optimal characteristics of radar systems operating under complex meteorological conditions as well as an appropriate choice of the working frequency and of various circuit modifications to reduce the sensitivity of an RS to the influence of meteorological factors are completely determined by the radar properties of the atmospheric formations.

/6

---

* Numbers in the margin indicate pagination in the foreign text.

This has stimulated a broad front of radiometeorological research which in turn, along with visual, aircraft and network synoptic observations, has provided highly important information on the fundamental problems of atmospheric physics and has also permitted improvements in the techniques of measurements of precipitation intensity, weather content of clouds, speed and direction of wind, microstructural characteristics of hydrometeors, atmospheric turbulence parameters, etc., techniques required for the operation of the weather service.

In many cases, this has resulted in progress in the effectiveness of measures taken to prevent damage done by hail, to disperse fog, to produce artificial rain, etc.

The timeliness of studies of radar characteristics of atmospheric formations has increased even more at the present time in connection with the swift development of aviation and astronautics.

Flights of aircraft at increasingly higher speeds increase their chances of encountering hail or liquid drop precipitation. Because of the presence of strong vertical currents in the atmosphere, the possibility of such an encounter is not excluded even in a completely cloudless sky. The designers of the latest aircraft are therefore faced with the serious problem of developing radar equipment capable of reliably detecting accumulations of atmospheric particles (hydrometeors) of different types. The creation and perfection of such RS is indissolubly tied to progress in the area of research on the radar properties of atmospheric formations.

Until recently, the entire theory of radar reflectivity and attenuation of radio waves by hydrometeors was based on a representation of the latter in the form of a collection of individual, randomly located spherical particles, the mean distances between which are much greater than their own size. In this assumption, the radar characteristics of the collection under consideration were obtained additively from known Mie solutions of the problem of wave diffraction by a single homogeneous sphere.

However, recent experimental data have shown that actual precipitation is more likely to consist of a collection of groups, each of which consists of two or more drops located close to each other.

Moreover, experimental analysis of such particles as hail (see the figure, for example), performed by a number of Soviet and foreign authors has shown that its representation in the form of a homogeneous particle is an unjustified idealization. Thus, a more complete approximation of actual atmospheric formations has led us to the necessity of constructing a more general theory of scattering and attenuation of electromagnetic radiation by a collection of nonconcentrically layered particles arbitrarily located with respect to one another. The development of such theory with computational aspects of the algorithms constructed, and also their numerical realization on modern com- /7

puters with reference to radiometeorological problems is the subject of the present monograph, written on the basis of studies made by the author in the last few years.

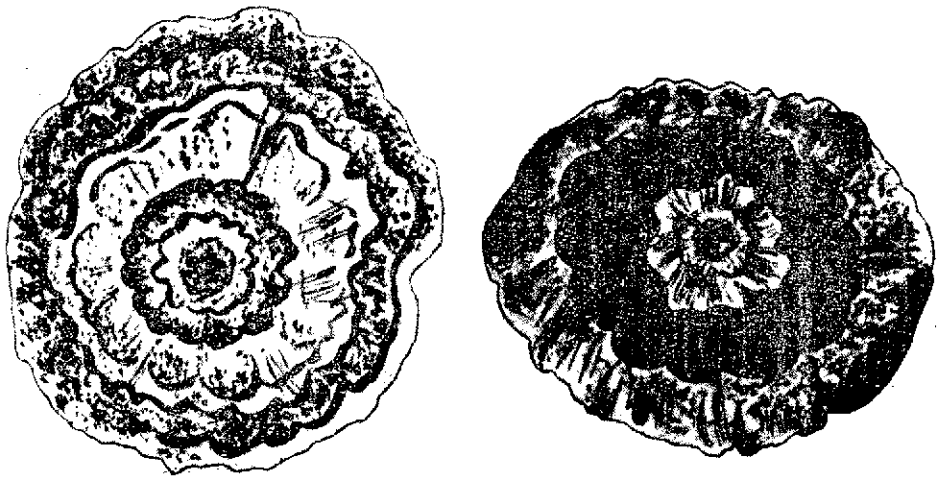

Central Cross Section of a Hailstone with Nonconcentric Layers of Different Densities, After K. A. Browning.

The monograph consists of two parts including six chapters and an Appendix.

The first part is devoted to a development of the theory of scattering and attenuation of electromagnetic radiation by an arbitrary collection of particles differing in physical structure and spherical in shape, taking the multiple reemission between them into consideration. Particular attention is given to radar and radiophysical characteristics such as scattering and attenuation cross sections, scattering indices, etc., and also to computational aspects of the formulated algorithms.

The second part contains an application of the resultant theory in its coherent and noncoherent approximations to specific problems in radiometeorology: scattering and attenuation of submillimeter, millimeter and centimeter radio waves by atmospheric formations. A very detailed study was made of the permittivities of water, ice, homogeneous mixture of water with ice and snow as a function of temperature, state of aggregation and wavelength, and also of the physical conditions determining the different structures and parameters of atmospheric particles.

Considerable attention is given to the analysis of cross sections of scattering and attenuation of microwaves by both individual particles and their collections in relation to the relative location[1] and shape of the particles, /8
their different states of aggregation, dielectric properties and temperature, and for many-layered hailstones, also in relation to the relative location of the layers, the relations of their thicknesses and densities, and also in

[1]Particles located fairly close to one another are taken into account.

relation to the particle size distribution function, maximum and minimum diameters in the spectrum, wave length, and physical conditions in the atmosphere.

The Appendix gives detailed tables of the permittivities of water over a wide range of wavelengths and temperatures. The tables given here may be useful in solving many problems in many areas of science, engineering and national economy, wherever a qualitative or quantitative consideration of the radar properties of hydrometeors is necessary.

The book uses a continuous numbering of the chapters and references, but the numbering of the paragraphs, figures, tables, and formulas is separate for each chapter. Each chapter, and in some cases the subsections begin with a brief survey of the present status of the problem and literature. When this was not necessary, in view of the presence of a similar analysis in the literature, the author confines himself to references to the appropriate sources.

The author is fully aware of the unavoidable presence of various types of errors in a monograph of this size, but there would no doubt have been many more were it not for the severe constructive criticism of its reviewers, on the staff of the A. I. Voyeykov Main Geophysical Observatory and Central Aerological Observatory, for the highly qualified and painstaking efforts of its editors, and for the assistance and support of colleagues and friends. To all of them the author expresses his sincere gratitude.

PART 1

CHAPTER 1.

SCATTERING AND ATTENUATION OF ELECTROMAGNETIC WAVES BY A NONCONCENTRICALLY LAYERED SPHERICAL PARTICLE

§ 1.1. Spheres Arbitrarily Located Inside One Another in the Field of a Dipole Radiator. Statement of the Problem. /9

The beginning of work on the theory of scattering of waves by a homogeneous sphere apparently dates back to the end of the last century [1]. From that time up to the present, the number of publications dealing with various aspects of this theory has continued to increase steadily.

About 20 years ago, K. S. Shifrin [2] and A. L. Aden and M. Kerker [3] almost simultaneously published papers that gave a rigorous solution of the problem of diffraction of electromagnetic waves by a sphere with a concentric spherical inclusion. These solutions were then used as the basis for a whole series of studies related to the theory of multilayered spherically symmetric structures.

The most detailed and complete discussions of the case of more than two layers may be found in [4], and its computational aspects, in [5].

In 1959, B. P. D'yakonov published his results [6] on the diffraction of electromagnetic waves by a sphere with a nonconcentric spherical inclusion under the assumption that the incident field was symmetric with respect to the axis connecting the centers of the two spheres. Unfortunately, this paper contained a number of errors, some of which were noticed and corrected in [7].

A paper by Ye. A. Ivanov [8] was devoted to a rigorous solution of this axisymmetric problem with the condition that the source of the electromagnetic field was an electric dipole located on the line of centers of the diffracting spheres[2]. This author also gave results [9] for the case of arbitrary orientation and location of the dipole. However, in view of the inaccuracy of some /10
of the initial expressions, due to the use of expansions of special functions of other authors with an associated Legendre function determined in different ways, the final results of [9] need to be corrected.

Some of the inaccuracies were pointed out in [10][3], which, in addition to the problem analogous to [9] in formulation, also discusses the diffraction of a plane wave as well as electromagnetic and radar characteristics of diffracting objects.

---

[2] It should be noted that the paper gives an inaccurate demonstration of the incorrectness of the initial expansions and final results of [7].

[3] See also [11], which gives a more comprehensive discussion than [10].

Let us note at this point that rigorous methods of construction of the solution and their validation will be used in these problems to obtain solutions of the problem of diffraction by a sphere with any number of spherical inclusions provided that they all have a common axis of symmetry.[4]

In regard to the problems formulated in its title, the present chapter presents a solution of the problem of scattering and attenuation of electromagnetic waves by a set of spheres arbitrarily (including asymmetrically) located inside one another. Some of these results were published by the author in [12]. Let us now turn to the statement of the problem.

Consider that in an infinite space there are ν spheres arbitrarily located inside one another (Figure 1.1) with centers $O_1, O_2, \ldots, O_\nu$ ($O_1O_2 = h_2$, $O_2O_3 = h_3, \ldots, O_{\nu-1}O_\nu = h_\nu$) and radii $b_1, b_2, \ldots, b_\nu$, respectively.

We will term medium 0 the part of space external to the sphere of radius b_1, medium j the part of the interior of the sphere of radius b_j excluding the region occupied by the sphere with its center at point O_{j+1} ($j = 1, 2, \ldots, \nu - 1$), and medium ν the interior of the sphere of radius b_ν. We will relate with medium j ($j = 0, 1, \ldots, \nu$) its electromagnetic parameters ε (absolute permittivity) and μ (absolute permeability), assuming them to be complex in the general case.[5]

We will also assume that at some point O_0 of medium 0 ($O_0O_1 = h_1 > b_1$) there is a source of excitation of electromagnetic waves constituting an elementary electric dipole[6] of moment $p \exp(-i\omega t)$ arbitrarily oriented in space.

The problem consists in determining the electromagnetic field induced by the electric dipole in each of the indicated media.

---

[4] See for example the comment of the author of [9] on p. 359.

[5] See expressions (4.1)-(4.3).

[6] In the case of a magnetic dipole of moment m, the solution will follow directly from the relations between the Debye potentials of the primary field of the electric (U^e_{00}, V^e_{00}) and magnetic (U^m_{00}, V^m_{00}) dipoles [9]: $U^m_{00} = -\frac{|m|}{|p|}\frac{\mu_0}{\varepsilon_0} V^{(e)}_{00}$, $V^{(m)}_{00} = \frac{|m|}{|p|} U^e_{00}$.

/11

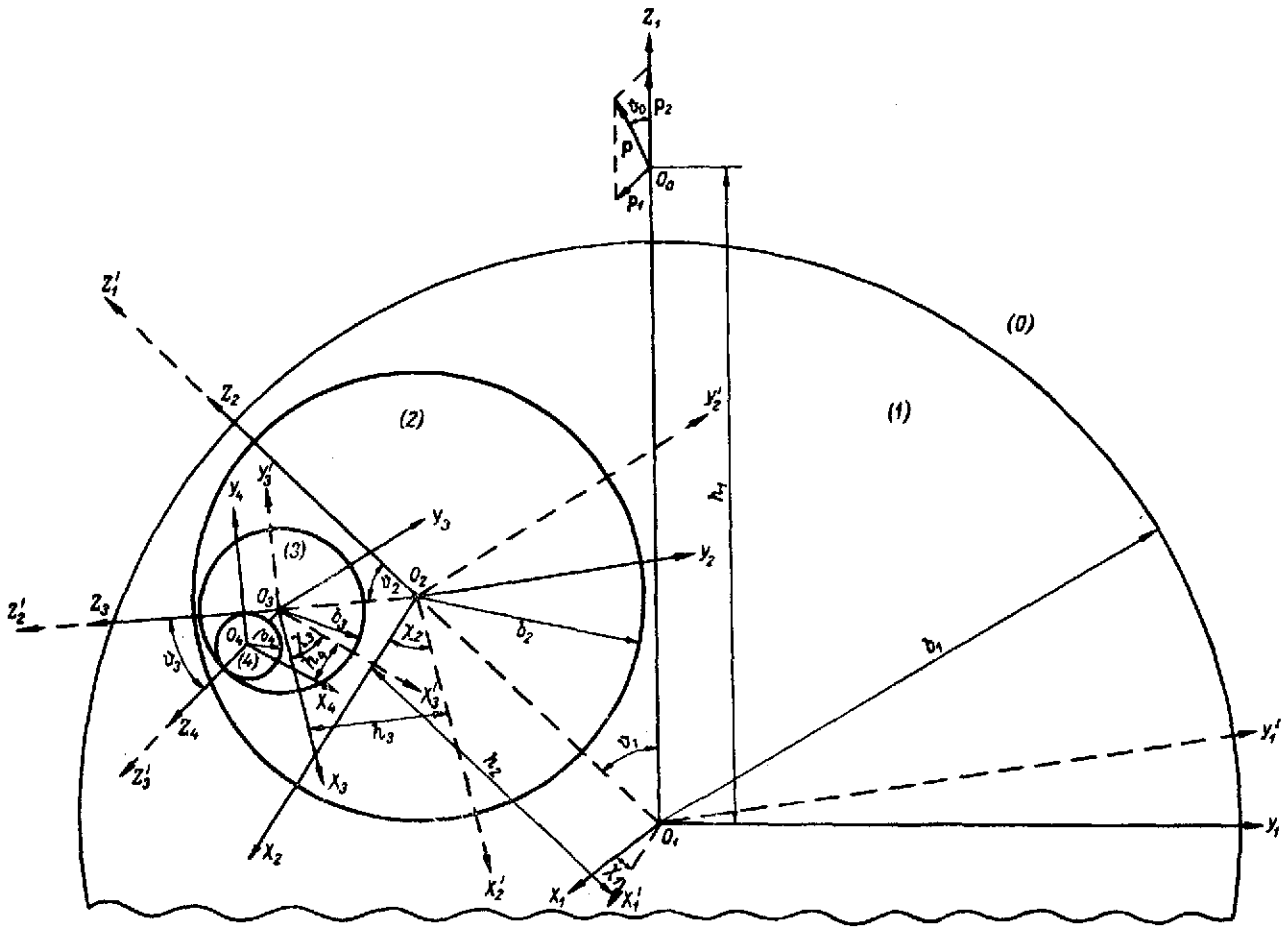

Figure 1.1. Collection Of Spheres Located Inside One Another In the Field of a Dipole Radiatior

/12

A rigorous solution of this problem amounts to solving the Maxwell equation:[7]

$$\begin{cases} \text{curl } H^{(j)} = \alpha_j E^{(j)} \\ \text{curl } E^{(j)} = -\beta_j H^{(j)}, \end{cases}$$

where

$$\alpha_j = -i\omega\varepsilon_j, \quad \beta_j = -i\omega\mu_j, \quad \omega = \frac{2\pi c}{\lambda}, \tag{1.1}$$

[7]The time factor exp(- iωt) is omitted hereinafter. The SI system of units is used.

λ is the wave length, c is the speed of light in medium 0, under certain boundary conditions consisting in the continuity of the tangential components of the resultant fields at the boundaries of the media considered, and with the condition of Sommerfeld radiation at infinity.

We will formulate the problem in the coordinate form, and to do so, will introduce $2\nu - 1$ coordinate systems.

System $X_1Y_1Z_1$. Axis Z_1 will be drawn through point O_1 collinearly to vector O_1O_0; axis X_1, along the line of intersection of the plane perpendicular to O_1O_0 at point O_1 and to the plane passing through axis Z_1 and vector p; axis Y_1, perpendicular to axes X_1 and Z_1 so that the coordinate system $X_1Y_1Z_1$ is a right-handed system. If vector p lies on the straight line O_1O_0 (vertical dipole), the position of axis X_1 is fixed so that plane $X_1O_1Z_1$ passes through point O_2. The angle between the dipole moment p and axis Z_1 will be denoted by θ_0.

Systems $X_j'Y_j'Z_j'$ ($j = 1, 2, \ldots, \nu - 1$). We draw axis Z_j' through O_j collinearly to the vector O_jO_{j+1}; axis X_j', along the line of intersection of the plane perpendicular to axis Z_j' at point O_j with plane $X_jO_jY_j$ and reorient it in the direction from which the observer sees the rotation superimposing axis Z_j on axis Z_j' through an angle smaller than π, taking place counter clockwise; axis Y_j', perpendicular to axis X_j' and Z_j' so that the coordinate system $X_j'Y_j'Z_j'$ has a right-handed orientation. If point O_{j+1} lies on the straight line $O_{j-1}\ O_j$, then axis X_j' will be oriented along axis X_j, Y_j' along axis Y_j, and Z_j' along axis Z_j.

System $X_jY_jZ_j$ ($j = 2, 3, \ldots, \nu$). These are obtained by shifting the systems $X_{j-1}'Y_{j-1}'Z_{j-1}'$ parallel to one another along the positive semiaxis Z_{j-1}' by a distance h_j. The origin O_{j-1} moves to point O_j.[8]

We will define the position of the coordinate system $X_j'Y_j'Z_j'$ ($j = 1, 2, \ldots, \nu - 1$) by means of Euler angles: χ_j -- the angle[9], made by axis X_j with axis

---

[8] The construction of the coordinate systems introduced is carried out in the order $X_1Y_1Z_1$, $X_1'Y_1'Z_1'$, $X_2Y_2Z_2, \ldots$, $X_{\nu-1}'Y_{\nu-1}'Z_{\nu-1}'$, $X_\nu Y_\nu Z_\nu$ by induction.

[9] χ_j and the polar angle χ_j^* of the position of the center O_{j+1} in spherical coordinates of system $X_jY_jZ_j$ are related as follows: $\chi_j^* = \chi_j - \frac{\pi}{2}$, and as χ_j changes from 0 to 2π, χ_j^* ranges over the interval from $-\frac{\pi}{2}$ to $\frac{3\pi}{2}$.

X_j ($0 \leq \chi_j < 2\pi$); Θ_j -- the angle formed by axis Z'_j with axis Z_j ($0 \leq \Theta_j \leq \pi$), /13
by positive angle we mean the angle (in the right-handed coordinate system) through which a counter clockwise rotation takes place for an observer looking from the positive end of the axis about which the rotation takes place. The system $X'_jY'_jZ'_j$ is uniquely defined by the Euler angles χ_j, Θ_j. An exception is the angles corresponding to the position of points O_{j+1} on the positive or negative part of axis Z_j. Then, according to our assumption on the choice of the system $X'_jY'_jZ'_j$, we will assume for both cases that $\Theta_j = 0$ and $\chi_j = 0$.

Considering the characteristics of their mutual arrangement, we introduce into each of the constructed systems ($j = 1, 2, \ldots, \nu$) the following spherical coordinates: in the system $X_jY_jZ_j$ - r_j, Θ_j, ϕ_j ($j = 1, 2, \ldots, \nu$); $X'_jY'_jZ'_j$ - r_j, Θ'_j, ϕ_{j+1} ($j = 1, 2, \ldots, \nu - 1$), using the formulas:

$$\begin{cases} x_j = r_j \sin\theta_j \cos\varphi_j, \\ y_j = r_j \sin\theta_j \sin\varphi_j, \\ z_j = r_j \cos\theta_j, \end{cases}$$

$$\begin{cases} x'_j = r_j \sin\theta'_j \cos\varphi_{j+1}, \\ y'_j = r_j \sin\theta'_j \sin\varphi_{j+1}, \\ z'_j = r_j \cos\theta'_j, \end{cases} \tag{1.1a}$$

$$0 \leqslant \theta_j, \quad \theta'_j \leqslant \pi, \quad 0 \leqslant r_j < \infty, \quad 0 \leqslant \varphi_j < 2\pi.$$

The system of Maxwell's vector equations in spherical coordinates, for example, r, θ, ϕ, is reduced to a single scalar equation by means of the Debye potentials U_j and V_j of the medium j, related to the components of the electromagnetic field by the expressions:

$$E_r^{(j)} = \frac{\partial^2 (rU_j)}{\partial r^2} + k_j^2 (rU_j),$$

$$H_r^{(j)} = \frac{\partial^2 (rV_j)}{\partial r^2} + k_j^2 (rV_j),$$

$$E_\theta^{(j)} = \frac{1}{r} \frac{\partial^2 (rU_j)}{\partial r \partial \theta} - \frac{\beta_j}{r \sin\theta} \frac{\partial (rV_j)}{\partial \varphi},$$

$$H_\theta^{(j)} = \frac{\alpha_j}{r \sin\theta} \frac{\partial (rU_j)}{\partial \varphi} + \frac{1}{r} \frac{\partial^2 (rV_j)}{\partial r \partial \theta},$$

$$E_\varphi^{(j)} = \frac{1}{r \sin\theta} \frac{\partial^2 (rU_j)}{\partial r \partial \varphi} + \frac{\beta_j}{r} \frac{\partial (rV_j)}{\partial \theta},$$

$$H_\varphi^{(j)} = -\frac{\alpha_j}{r} \frac{\partial (rU_j)}{\partial \theta} + \frac{1}{r \sin\theta} \frac{\partial^2 (rV_j)}{\partial r \partial \varphi}, \tag{1.2}$$

where $E^{(j)}_{r,\theta,\phi}$, $H^{(j)}_{r,\theta,\phi}$, are respectively the projections of vectors $E^{(j)}$ and $H^{(j)}$ of medium j in the spherical system r, θ, φ; /14

$$k_j^2 = -\alpha_j\beta_j = \omega^2\varepsilon_j\mu_j, \tag{1.3}$$

with k_j chosen so that

$$\operatorname{Im} k_j \geqslant 0. \tag{1.4}$$

The functions U_j, V_j satisfy one and the same Helmholtz equation:

$$\frac{\partial^2 (rT_j)}{\partial r^2} + \frac{1}{r\sin\theta}\frac{\partial}{\partial\theta}\left(\sin\theta\frac{\partial T_j}{\partial\theta}\right) + \frac{1}{r\sin^2\theta}\frac{\partial^2 T_j}{\partial\varphi^2} + k_j^2 T_j r = 0, \tag{1.4a}$$

where

$$T_j = \{U_j,\ V_j\}, \qquad j = 1,\ 2,\ \ldots,\ \nu. \tag{1.5}$$

Introduction of the Debye potentials makes it possible to reduce the system of Maxwell's vector equations with boundary conditions not separable by coordinates to a system of scalar equations (1.4a) with separated boundary conditions.

To system (1.4a) it is necessary to add the conditions imposed on T_j which result from (1.2), assuming the continuity of the tangential components of vectors E and H at the boundaries of the media considered:

$$\left.\begin{aligned} q_j T_j &= q_{j+1} T_{j+1} \\ \frac{\partial (r_{j+1} T_j)}{\partial r_{j+1}} &= \frac{\partial (r_{j+1} T_{j+1})}{\partial r_{j+1}} \end{aligned}\right\} \qquad \begin{aligned} &\text{where } r_{j+1} = b_{j+1}, \\ &j = 0,\ 1,\ \ldots,\ \nu - 1, \end{aligned} \tag{1.6}$$

where

$$q_j = \{\alpha_j,\ \beta_j\}. \tag{1.7}^{10}$$

$$T_0 = T_{00} + T_{0s},\ T_{00} = \{U_{00},\ V_{00}\},\quad T_{0s} = \{U_{0s},\ V_{0s}\} \tag{1.8}$$

T_{0s} is the solution of equation (1.4a), and the symbols U_{00}, V_{00} and U_{0s}, V_{0s} entering into expressions (1.8) are the Debye potentials corresponding to the primary ($E^{(00)}$, $H^{(00)}$) and secondary ($E^{(0s)}$, $H^{(0s)}$) electromagnetic fields in medium 0. Thus, the problem amounts to solving equations (1.4a) with boundary conditions (1.6) and the condition of Sommerfeld radiation

$$\frac{\partial T_0}{\partial r_1} - ik_0 T_0 = o\left(\frac{1}{r}\right). \tag{1.9}$$

[10] Hereinafter a set of two expressions (separated by a comma) in braces will symbolize the correspondence of the first to the potential U and of the second to the potential V.

To solve the stated problem, it is necessary to have formulas for re-expanding the separated solutions of equations (1.4a), written in one system, in terms of these same solutions in another coordinate system (addition theorems).

§ 1.2. Addition Theorems

/15

Many papers have been devoted to addition theorems of the functions $h_n(kr)P_n^m(\cos\theta)$ and $j_n(kr)P_n^m(\cos\theta)$, where

$$h_n(z) = \sqrt{\frac{\pi}{2z}}\, H^{(1)}_{n+\frac{1}{2}}(z),$$

$$j_n(z) = \sqrt{\frac{\pi}{2z}}\, J_{n+\frac{1}{2}}(z),$$

$$P_n^m(z) = (-1)^m \frac{(1-z^2)^{\frac{m}{2}}}{2^n n!} \frac{d^{n+m}}{dz^{n+m}}(z^2-1)^n, \tag{1.10}$$

$H^{(1)}_{n+\frac{1}{2}}(z)$ is a Hankel function of the first kind of half-integer order,

$J_{n+\frac{1}{2}}(z)$ is a Bessel function of half-integer order, and $P_n^m(z)$ is an associated Legendre function.

Thus, W. Trinks [13, 14] obtained these theorems in the form of a complex algorithm of comparison of the coefficients for the same terms in quintriple and triple series, leaving aside the study of range of validity of these constructions. O. A. Germognova [15] simplified this procedure by finding the analytical form of notation of Trinks' algorithm without discussing the region of convergence of the constructed expansions. We should mention the somewhat related paper of Sato Yasuo [16], who obtained addition theorems of $h_n^{(2)}(kR)P_n^m(\cos\theta)e^{im\phi}$ in the form of expansions, not in Bessel functions, but in degrees of kr; the expansion coefficients are not given by a general formula, but are obtained with the aid of recurrence relations.

In their general formulation, these problems have been treated by B. Friddman and J. Russek [17], A. Ben-Menahem [18], who wrote the principal results of [17] in a shortened operator form, S. Stein [19], who corrected the main errors of [17], O. Crusan [20], who obtained a series of new recurrence relations for expansion coefficients, Ye. A. Ivanov [21], who derived addition theorems for more general spheroidal functions and discusses them in special cases of spherical coordinates in [8, 22], and the author [11], where a rigorous validation of addition theorems is given along with their various representations.[11]

[11] See also the pertinent results published in [9] and [57].

The addition theorems of the functions $P_n^m(\cos\theta)e^{im\phi}$ in the case of rotation of the coordinate system are discussed in detail in [23-26], and the computational aspects, in [27]. /16

In view of the fact that the general transformation of the coordinate system in plane XOZ may be represented as a superposition of the motion along axis Z and rotation about it, we first obtain the addition theorems of the functions $h_n(kr)P_n^m(\cos\theta)$ and $j_n(kr)P_n^m(\cos\theta)$ in the case of a parallel shift of the coordinate system along axis Z.

Addition theorems of functions $h_n(kr)P_n^m(\cos\theta)$. Let the Cartesian coordinate systems $X_1Y_1Z_1$ and $X_2Y_2Z_2$, obtained by shifting the former parallel to itself along axis Z_1 to a new origin O_2 be introduced into a three-dimensional space (Figure 1.2), along with the spherical coordinates r_1, θ_1, ϕ and r_2, θ_2, ϕ respectively, associated with these systems. We will denote the spherical coordinates of the origin O_2 in the coordinates r_1, θ_1, ϕ by l_{12}, θ_{12}, 0. We will assume that at point A, located in plane $X_1O_1Z_1$ at distances b from point O_1 and $\sqrt{l_{12}^2 - b^2}$ from point O_2, the function $\frac{\exp(ikR)}{ikR}$ is given, where R = AP, and P is an arbitrary point in space.

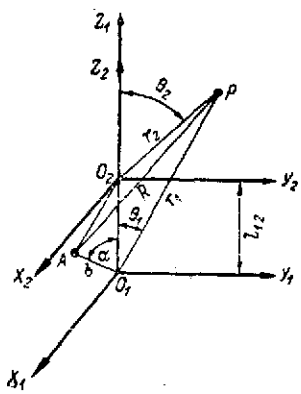

Figure 1.2. Coordinate Systems in Addition Theorems.

Let us consider the case $\theta_{12} = 0$. We have

$$\frac{\exp(ikR_{(O_1)})}{ikR_{(O_1)}} = \frac{\exp(ikR_{(O_2)})}{ikR_{(O_2)}}, \tag{1.11}$$

where

$$R_{(O_1)} = \sqrt{r_1^2 + b^2 - 2r_1 b\cos\gamma_1},$$

$$R_{(O_2)} \sqrt{r_2^2 + b^2 \tan\alpha - 2r_2 b \tan\alpha \cos\gamma_2}$$

$$\alpha = \arccos\frac{b}{l_{12}}, \quad 0 \leqslant \alpha \leqslant \frac{\pi}{2}, \tag{1.12}$$

$$\cos\gamma_1 = \cos\left(\widehat{O_1A,\ O_1P}\right) = \cos\theta_1\cos\alpha + \sin\theta_1\sin\alpha\cos\varphi,$$

$$\cos\gamma_2 = \cos\left(\widehat{O_2A,\ O_2P}\right) =$$

$$= \cos\theta_2\cos\left(\frac{\pi}{2} + \alpha\right) + \sin\theta_2\sin\left(\frac{\pi}{2} + \alpha\right)\cos\varphi.$$

We use the formula

$$\frac{\exp(ikR)}{ikR} = \sum_{n=0}^{\infty}(2n+1)\times$$

$$\times P_n(\cos\theta)\begin{cases} j_n(k\rho_0)\,h_n(k\rho) & \text{for } \rho > \rho_0, \\ j_n(k\rho)\,h_n(k\rho_0) & \text{for } \rho < \rho_0, \end{cases} \tag{1.13}$$

where $R = \sqrt{\rho^2 + \rho_0^2 - 2\rho\rho_0 - \cos\theta}$, and expand both parts of equality (1.11) in /17 series

$$\sum_{n=0}^{\infty} (2n+1) P_n(\cos\gamma_1) j_n(kb) h_n(kr_1) =$$

$$= \sum_{\tau=0}^{\infty} (2\tau+1) P_\tau(\cos\gamma_2) j_\tau(kb\,\mathrm{tg}\,\alpha) h_\tau(kr_2), \tag{1.14}$$

in the range

$$r_1 > b, \quad r_2 > \sqrt{l_{12}^2 - b^2}. \tag{1.15}$$

Using the addition theorms for Legendre polynomials [28] and considering (1.12), we obtain the expressions:

$$P_n(\cos\gamma_1) = \sum_{m=0}^{n} \varepsilon_m (-1)^m P_n^{-m}(\cos\theta_1) P_n^m(\cos\alpha) \cos m\varphi,$$

$$P_\tau(\cos\gamma_2) = \sum_{m=0}^{n} \varepsilon_m (-1)^m P_\tau^{-m}(\cos\theta_2) P_\tau^m\left[\cos\left(\frac{\pi}{2} + \alpha\right)\right] \cos m\varphi, \tag{1.16}$$

$$\varepsilon_m = \begin{cases} 1 & \text{for } m = 0, \\ 2 & \text{for } m \geqslant 1. \end{cases}$$

Substituting these expressions into (1.14), we find

$$\sum_{n=0}^{\infty} (2n+1) j_n(kb) h_n(kr_1) \sum_{m=0}^{n} (-1)^m \varepsilon_m P_n^{-m}(\cos\theta) P_n^m(\cos\alpha) \times$$

$$\times \cos m\varphi = \sum_{\tau=0}^{\infty} (2\tau+1) j_\tau(kb\,\mathrm{tg}\,\alpha) h_\tau(kr_2) \times \tag{1.17}$$

$$\times \sum_{m=0}^{n} (-1)^m \varepsilon_m P_\tau^{-m}(\cos\theta_2) P_\tau^m\left[\cos\left(\frac{\pi}{2} + \alpha\right)\right] \cos m\varphi. \tag{1.17}$$

In order to obtain the required expansion, it is necessary to separate on the right side of (1.17) a factor of the form $j_\tau(kb) P_\tau^m(\cos\alpha)$. For this purpose, using [29] the integral representation

$$j_\tau(kx) P_\tau^m(\cos\beta) = \frac{i^{m-\tau}}{2} \int_0^{\pi} e^{ikx\cos\beta\cos u} \times$$

$$\times J_m(kx\sin\beta\sin u) P_\tau^m(\cos u) \sin u\, du \tag{1.18}$$

and the expansion

$$e^{-ikl_{12}\cos u} = \sum_{\nu=0}^{\infty} i^{-\nu} (2\nu+1) j_\nu(kl_{12}) P_\nu(\cos u), \tag{1.19}$$

after a series of transformations, we obtain: /18

$$j_\tau(kb\operatorname{tg}\alpha)\,P_\tau^m\left[\cos\left(\frac{\pi}{2}+\alpha\right)\right]=\frac{i^{m-\tau}}{2}\sum_{\nu=0}^{\infty}i^{-\nu}(2\nu+1)\,j_\nu(kl_{12})\times$$

$$\times\int_0^{\pi}e^{ikb\cos\alpha\cos u}J_m(kb\sin\alpha\sin u)\,P_\nu(\cos u)\,P_\tau^m(\cos u)\sin u\,du. \qquad (1.19a)$$

Here we have switched the summation and integral signs, which is possible in view of the uniform and absolute convergence of the series.

We will represent the product $P_\nu(\cos u)P_\tau^m(\cos u)$ in the form of a series with respect to associated functions $p_\sigma^m(\cos u)$.

Such an expansion may be obtained as a special case of the Clebsch-Gordan series [26] for generalized spherical functions defined on the surface of a sphere and belonging to a functional space in which an irreducible representation of the weight n of the rotation group of three-dimensional space is realized:

$$P_\nu(\cos u)\,P_\tau^m(\cos u)=\sum_{\sigma=|\nu-\tau|}^{\nu+\tau}{}'\,b_{\sigma\nu\tau}^m P_\sigma^m(\cos u), \qquad (1.20)$$

where the prime in the summation signifies that a letter extends over values of σ having the same parity as the upper index of the summation,

$$b_{\sigma\nu\tau}^m=\frac{2\sigma+1}{2}(-1)^m\int_{-1}^{1}P_\nu(x)\,P_\tau^m(x)\,P_\sigma^{-m}(x)\,dx, \qquad (1.21)$$

$$b_{\sigma\nu\tau}^m=\sqrt{\frac{(\tau+m)!\,(\sigma-m)!}{(\tau-m)!\,(\sigma+m)!}}\,C(\nu,\ \tau,\ \sigma;\ 0,\ m,\ m)\times$$
$$\times C(\nu,\ \tau,\ \sigma;\ 0,\ 0,\ 0), \qquad (1.22)$$

$C(l_1,\ l_2,\ l;\ j,\ k,\ j+k)$ are the Clebsch-Gordan coefficients, whose explicit form and various representations may be found, for example, in [25, 26].

Substituting expression (1.19a) into (1.17) and considering relations (1.20) and (1.18) and the orthogonality properties of trigonometric functions, we obtain

$$\sum_{n=0}^{\infty}(2n+1)\,j_n(kb)\,P_n^m(\cos\alpha)\,h_n(kr_1)\,P_n^{-m}(\cos\vartheta_1)=$$
$$=\sum_{\tau=0}^{\infty}(2\tau+1)\,h_\tau(kr_2)\,P_\tau^{-m}(\cos\vartheta_2)\,i^{-\tau}\sum_{\nu=0}^{\infty}(2\nu+1)\,j_\nu(kl_{12})\times$$
$$\times\sum_{\sigma=|\nu-\tau|}^{\nu+\tau}{}'\,b_{\sigma\nu\tau}^m i^\sigma j_\sigma(kb)\,P_\sigma^m(\cos\alpha). \qquad (1.23)$$

For further considerations, the following lemma will be necessary.

Lemma 1. For every natural n for which the repeated series $\sum_{i=0}^{\infty} \sum_{j=|n-i|}^{n+i}{}' |a_{ij}|$ converges, the following equality applies: /19

$$\sum_{i=0}^{\infty} \sum_{j=|n-i|}^{n+i}{}' a_{ij} = \sum_{i=0}^{\infty} \sum_{j=|n-i|}^{n+i}{}' a_{ji}. \tag{1.24}$$

Proof. It follows from the absolute convergence of the repeated series that the sum will not change if its terms are rearranged. This will be done for the sum to the left of the equality sign in (1.24).

Without detracting from generality, we will assume than n is an even number. We will divide the sum $U_n = \sum_{i=0}^{n-1} \sum_{j=|n-i|}^{n+i}{}' a_{ij}$ into two sums: $U_n^{(1)}$ and $U_n^{(2)}$,

$$U_n = U_n^{(1)} + U_n^{(2)} = \sum_{i=0}^{n-1} \sum_{j=|n-i|}^{n+i}{}' a_{ij} + \sum_{i=n}^{\infty} \sum_{j=|n-i|}^{n+i}{}' a_{ij}. \tag{1.25}$$

We will expand the first sum and rearrange the summands, combining terms with the same second index:

$$\begin{aligned} U_n^{(1)} = {} & a_{0n} + (a_{1n-1} + a_{1n+1}) + (a_{2n-2} + a_{2n} + a_{2n+2}) + \dots + \\ & + (a_{n-22} + a_{n-24} + \dots + a_{n-22n-2}) + (a_{n-11} + a_{n-13} + \\ & + \dots + a_{n-12n-1}) = \sum_{i=n-1}^{n-1} a_{i1} + \sum_{i=n-2}^{n-2} a_{i2} + \sum_{i=n-3}^{n-1}{}' a_{i3} + \\ & + \sum_{i=n-4}^{n-2}{}' a_{i4} + \dots + \sum_{i=2}^{n-2}{}' a_{in-2} + \sum_{i=1}^{n-1}{}' a_{in-1} + \sum_{i=0}^{n-2}{}' a_{in} + \\ & + \sum_{i=1}^{n-1}{}' a_{in+1} + \sum_{i=2}^{n-2}{}' a_{in+2} + \dots + \sum_{i=n-4}^{n-2}{}' a_{i2n-4} + \\ & + \sum_{i=n-3}^{n-1}{}' a_{i2n-3} + \sum_{i=n-2}^{n-2}{}' a_{i2n-2} + \sum_{i=n-1}^{n-1} a_{i2n-1}. \end{aligned} \tag{1.26}$$

We transform the second sum $U_n^{(2)}$, having changed the summation index:

$$\begin{aligned} U_n^{(2)} = {} & \sum_{i=n}^{\infty} a_{ii-n} + \sum_{i=n}^{\infty} a_{ii-n+2} + \dots + \sum_{i=n}^{\infty} a_{ii+n} = \\ = {} & \sum_{i=0}^{\infty} a_{i+ni} + \sum_{i=2}^{\infty} a_{i+n-2i} + \dots + \sum_{i=2n-2}^{\infty} a_{i-n+2i} + \\ & + \sum_{i=2n}^{\infty} a_{i-ni}. \end{aligned} \tag{1.27}$$

Having used expansions (1.25)-(1.27) and collected the terms with the same second index, we obtain /20

$$U_n = a_{n0} + (a_{n-11} + a_{n+11}) + (a_{n-22} + a_{n2} + a_{n+22}) + \ldots + \\ + \sum_{j=|n-l|}^{n+l}{}' a_{jl} + \ldots = \sum_{l=0}^{\infty} \sum_{j=|n-l|}^{n+l}{}' a_{jl},$$

q.e.d.

Applying the lemma to the right side of equality (1.23) and changing the order of summation in τ and ν, we find

$$\sum_{n=0}^{\infty} (2n+1)\, j_n(kb)\, P_n^m(\cos\alpha)\, h_n(kr_1)\, P_n^{-m}(\cos\theta_1) = \\ = \sum_{\nu=0}^{\infty} i^{\nu} j_{\nu}(kb)\, P_{\nu}^m(\cos\alpha) \sum_{\tau=0}^{\infty} \sum_{\sigma=|\nu-\tau|}^{\nu+\tau}{}' (2\tau+1)\, h_{\tau}(kr_2) \times \\ \times P_{\tau}^{-m}(\cos\theta_2)\, i^{-\tau-\sigma}(2\sigma+1)\, j_{\sigma}(kl_{12})\, b_{\nu\sigma\tau}^m. \qquad (1.28)$$

The validity of applying lemma 1 to (1.23) and of transposing the summation signs in (1.28) is based on lemmas 2-4.

Lemma 2. If for complex functions of a natural argument x_n and y_n, defined for each[12] $n \in N$, the equivalence condition $|x_n| \sim |y_n|$ is fulfilled[13], a constant independent of n will be found such that for all $n \in N$ the following inequality is valid:

$$|x_n| < \text{const}\ |y_n|.$$

Proof. It follows from the theorem on the boundedness of a variable having a limit.

Lemma 3. The repeated series $R_{\nu}^m = \sum_{\tau=0}^{\infty} \sum_{\sigma=|\nu-\tau|}^{\nu+\tau}{}' (2\tau+1) h_{\tau}(kr_2) \times P_{\tau}^{-m}(\cos\theta_2) i^{-\tau-\sigma}(2\sigma+1) j_{\sigma}(kl_{12}) b_{\nu\sigma\tau}^m$ converges absolutely for every ν in the range $r_2 > l_{12}$.

---

[12] By N is meant the set of all natural numbers.

[13] This condition is equivalent to the equality $\lim_{n\to\infty} \left|\frac{x_n}{y_n}\right| = 1$.

Proof. It follows from asymptotic expansions of the functions $j_\nu(z)$ and $h_\tau(z)$ for $\nu, \tau \to \infty$ and from lemma 2 that

$$|j_\nu(z_2)| < \text{const}_1 \frac{|z_2|^\nu}{(2\nu+1)!!}, \quad |h_\tau(z_1)| < \text{const}_2 \frac{(2\tau-1)!!}{|z_1|^\tau}, \tag{1.29}$$

and from the estimate of [29]

$$|P_n^{\pm m}(x)| < \frac{2}{\sqrt{n\pi}} \frac{(n+m)!}{n!}(1-x^2)^{-\frac{m+1}{2}}, \quad n \geqslant 1,$$
$$n-m+1>0, \quad m \geqslant 0$$

and from the condition $P_0(x) \equiv 1$ /21

$$|P_n^{\pm m}(x)| < \text{const}_3 \frac{(n+m)!}{n!}. \tag{1.30}$$

Considering inequality (1.30), we obtain from (1.21)

$$|b_{\nu\tau}^m| < \text{const}_4 \frac{(2\nu+1)(\tau+m)!(\nu-m)!}{\tau!\nu!}. \tag{1.31}$$

If we write $\tilde{j}_\sigma(z) = \sqrt{\frac{\pi}{2z}} I_{\sigma+\frac{1}{2}}(z)$, where $I_\nu(z)$ is a Bessel function of an imaginary argument [28], then on the basis of the representation

$$j_\sigma(z) = z^\sigma \sum_{k=0}^{\infty} \frac{(-1)^k z^{2k}}{2^k k!(2\sigma+2k+1)!!}$$

one can show that

$$|j_\sigma(z)| < \tilde{j}_\sigma(|z|). \tag{1.32}$$

By virtue of estimates (1.29)-(1.32) we have

$$|R_\nu^m| < \text{const}_5 \frac{(2\nu+1)(\nu-m)!}{\nu!} \times$$
$$\times \sum_{\tau=0}^{\infty} \frac{(2\tau+1)!!(\tau-m)!(\tau+m)!(\nu+\tau)}{[\tau!]^2 |kr_2|^\tau} \sum_{\sigma=|\nu-\tau|}^{\nu+\tau} \tilde{j}_\sigma(|kl_{12}|). \tag{1.33}$$

Applying A. Jones' inequality $j_n(|z|) \geq j_k(|z|)$ [30] valid for all z and $k > n \geq 0$, to expression (1.33), we obtain the expression[14]

[14]The same result also follows from D. Cochran's more general theory [31].

$$|R_\nu^m| < \text{const}_5 \frac{(2\nu+1)(\nu-m)!}{\nu!} \times$$

$$\times \sum_{\tau=0}^{\infty} \frac{(2\tau+1)!!(\tau-m)!(\tau+m)!(\nu+\tau)^2}{[\tau!]^2 |kr_2|^2} \tilde{j}_{|\nu-\tau|}(|kl_{12}|),$$

from which, if one considers the asymptotic expansion for $\nu \to \infty$ of the function $I_\nu(|z|)$ and lemma 2, the following results:

$$|R_\nu^m| < \text{const}_6 \frac{(2\nu+1)(\nu-m)!}{\nu!} \times$$

$$\times \sum_{\tau=0}^{\infty} \frac{(2\tau+1)!!(\tau-m)!(\tau+m)!(\nu+\tau)^2}{[\tau!]^2 |kr_2|^\tau [2|\nu-\tau|+1]!!} |kl_{12}|^{|\nu-\tau|}. \qquad (1.34)$$

The proof of the lemma is completed by applying d'Alembert's criterion to series /22 (1.34).

Lemma 4. The series $F_m = \sum_{\nu=0}^{\infty} i^\nu j_\nu(kb) P_\nu^m(\cos\alpha) R_\nu^m$ converges absolutely in the range $r_2 > l_{12} + b$.

Proof. It follows from relations (1.29), (1.30), (1.34) that

$$|F_m| < \text{const}_7 (S_1 + S_2),$$

where

$$S_1 = \sum_{\nu=0}^{\infty} |k^2 b l_{12}|^\nu \frac{(\nu+m)!(\nu-m)!}{[\nu!]^2 (2\nu-1)!!} \times$$

$$\times \sum_{\tau=0}^{\nu} \frac{(2\tau+1)!!(\tau-m)!(\tau+m)!(\nu+\tau)^2}{[\tau!]^2 |k^2 r_2 l_{12}|^\tau [2(\nu-\tau)+1]!!},$$

$$S_2 = \sum_{\nu=0}^{\infty} \left(\frac{b}{l_{12}}\right)^\nu \frac{(\nu+m)!(\nu-m)!}{[\nu!]^2 (2\nu-1)!!} \times$$

$$\times \sum_{\tau=\nu+1}^{\infty} \frac{(2\tau+1)!!(\tau-m)!(\tau+m)!(\nu+\tau)^2}{[\tau!]^2 [2(\tau-\nu)+1]!!} \left(\frac{l_{12}}{r_2}\right)^\tau.$$

If in the expressions for S_1 and S_2 one uses the inequalities

$$\frac{(\tau+m)!(\tau-m)!}{[\tau!]^2} < \text{const}_8, \quad \frac{(\nu+m)!(\nu-m)!}{[\nu!]^2} < \text{const}_8,$$

then makes the substitution $n = \nu - \tau$, in the expression for S_1 and $n = \tau - \nu$ in the expression for S_2, and again applies the inequalities

$$\frac{(2\nu-2n+1)!!\,(2\nu-n)^2}{(2\nu-1)!!\,(2n+1)!!}<\text{const}_9\frac{\nu^4}{n!},$$

$$\frac{(2n+2\nu+1)!!\,(n+2\nu)}{(2n+1)!!\,(2\nu-1)!!}<\text{const}_{10}\frac{(n+\nu)^3\,(n+\nu)!}{\nu!\,n!},$$

which follow from the Stirling formula and from lemma 2, one can show that

$$S_1<\text{const}_{11}\sum_{\nu=0}^{\infty}\left(\frac{b}{l_{12}}\right)^{\nu}\left(\frac{l_{12}}{r_2}\right)^{\nu}\nu^4\sum_{n=0}^{\infty}\frac{|k^2r_2l_{12}|^n}{n!}<\infty,$$

$$S_2<\text{const}_{12}\sum_{\nu=0}^{\infty}\left(\frac{b}{r_2}\right)^{\nu}\sum_{n=1}^{\infty}(n+\nu)^3\frac{(n+\nu)!}{\nu!\,n!}\left(\frac{l_{12}}{r_2}\right)^{n}. \tag{1.35}$$

To prove the convergence of series (1.35), we will construct a matrix in ν, n from its coefficients and will perform the summation over its diagonals /23
$n+\nu=s$ -- constant!), the sum of the terms along which is nothing but the Newton binomial. Then

$$S_2<\text{const}_{13}\sum_{s=1}^{\infty}s^3\left(\frac{b+l_{12}}{r_2}\right)^{s}. \tag{1.36}$$

The series in (1.36) converges for $r_2 > l_{12} + b$. This completes the proof.

Let us note at this point that although equality (1.28) was derived by assuming (1.12) $0 \leq \alpha \leq \frac{\pi}{2}$, the series from the analytical functions entering into this equality converge uniformly for all $\alpha \in [0, \pi]$ for any finite b, r_1, r_2, l_{12} in the indicated regions. Then, on the basis of the analytic continuation principle theory, expression (1.28) will also hold for $\alpha \in [\frac{\pi}{2}, \pi]$. On the basis of the arbitrariness of b in (1.15) and orthogonality of the associated Legendre functions for $\alpha \in [0, \pi]$, we arrive at the following result:

$$h_n(kr_1)\,P_n^{-m}(\cos\theta_1)=(-1)^m\sum_{\tau=0}^{\infty}\sum_{\sigma=|n-\tau|}^{n+\tau}{}'(2\tau+1)\,i^{n-\tau-\sigma}\,j_\sigma(kl_{12})\times$$
$$\times a_{\sigma n\tau}^{m}\,h_\tau(kr_2)\,P_\tau^{-m}(\cos\theta_2),\quad r_2>l_{12}, \tag{1.37}$$

where

$$a_{\sigma\nu\tau}^{m}=(-1)^m\frac{2\sigma+1}{2\nu+1}\,b_{\nu\sigma\tau}^{m}=\frac{2\sigma+1}{2}\int_{-1}^{1}P_\tau^m(x)\,P_\nu^{-m}(x)\,P_\sigma(x)\,dx=$$
$$=\sqrt{\frac{(\tau+m)!\,(\nu-m)!}{(\tau-m)!\,(\nu+m)!}}\,C(\tau,\ \nu,\ \sigma;\ m,\ -m,\ 0)\,C(\tau,\ \nu,\ \sigma;\ 0,\ 0,\ 0). \tag{1.38}$$

Relations (1.38) together with (1.20) make it possible to determine $a^m_{\sigma\nu\tau}$ as the coefficient in the expansion

$$P^m_\tau(x)\,P^{-m}_\nu(x) = \sum_{\sigma=|\tau-\nu|}^{\tau+\nu}{}' a^m_{\sigma\nu\tau} P_\sigma(x).$$

If $\theta_{12} = \pi$, a reasoning similar to the above will lead to

$$h_n(kr_1)\,P^{-m}_n(\cos\theta_1) = (-1)^m \sum_{\tau=0}^{\infty} \sum_{\sigma=|n-\tau|}^{n+\tau}{}' (2\tau+1)\, i^{n-\tau+\sigma} j_\sigma(kl_{12}) \times$$
$$\times a^m_{\sigma n\tau} h_\tau(kr_2)\,P^{-m}_\tau(\cos\theta_2), \quad r_2 > l_{12}. \tag{1.39}$$

Combining expressions (1.37) and (1.39) and using the property of associated Legendre functions

$$P^{-m}_n(x) = (-1)^m \frac{(n-m)!}{(n+m)!} P^m_n(x), \tag{1.40}$$

we arrive at the following theorem.

Theorem 1. /24

$$h_n(kr_1)\,P^m_n(\cos\theta_1) = \frac{(n+m)!}{(n-m)!} \sum_{\tau=0}^{\infty} \sum_{\sigma=|n-\tau|}^{n+\tau}{}' (2\tau+1) \times$$
$$\times i^{n-\tau+2\sigma} \sin\frac{\theta_{12}}{2}\, j_\sigma(kl_{12})\,\delta^m_{\sigma n\tau} h_\tau(kr_2)\,P^m_\tau(\cos\theta_2), \quad r_2 > l_{12}, \tag{1.41}$$

where

$$\delta^m_{\sigma n\tau} = (-1)^m \frac{(\tau-m)!}{(\tau+m)!} a^m_{\sigma n\tau} =$$
$$= \frac{2\sigma+1}{2} \int_{-1}^{1} P^{-m}_\tau(x)\,P^{-m}_n(x)\,P_\sigma(x)\,dx. \tag{1.42}$$

To obtain an analogous expansion for $r_2 < l_{12}$, we use another expansion (1.13) in (1.11):

$$\sum_{n=0}^{\infty} (2n+1)\,P_n(\cos\gamma_1)\,j_n(kb)\,h_n(kr_1) =$$
$$= \sum_{\tau=0}^{\infty} (2\tau+1)\,P_\tau(\cos\gamma_2)\,h_\tau(kb\,\tan\alpha)\,j_\tau(kr_2)$$

which applies in the range $r_1 > b$, $r_2 < \sqrt{l_{12}^2 - b^2}$; at the same time, we initially assume that $\theta_{12} = 0$.

Applying the same reasoning as in the derivation of theorem 1, we obtain

$$\sum_{n=0}^{\infty}(2n+1)\,j_n(kb)\,P_n^m(\cos\alpha)\,h_n(kr_1)\,P_n^{-m}(\cos\theta_1)=$$

$$=\sum_{\tau=0}^{\infty}(2\tau+1)\,h_\tau(kb\ \operatorname{tan}\ \alpha)\,P_\tau^m\left[\cos\left(\frac{\pi}{2}+\alpha\right)\right]j_\tau(kr_2)\,P_\tau^{-m}(\cos\theta_2). \qquad (1.43)$$

In order to obtain the required expansions, it is necessary to separate the factor $j_\tau(kb)P_\tau^m(\cos\alpha)$ on the right side of (1.43). We do this by using the following integral representation [9, 32]:

$$h_n(kr)\,P_n^m(\cos\theta)=i^{m-n}\int_0^{-\frac{\pi}{2}-i\infty}e^{ikr\cos\theta\cos u}J_m(kr\sin\theta\sin u)\times$$

$$\times P_n^m(\cos u)\sin u\,du, \qquad \operatorname{Re}k>0;\quad 0\leqslant\theta<\frac{\pi}{2}. \qquad (1.44)$$

Hence we obtain /25

$$h_\tau(kb\ \operatorname{tg}\alpha)\,P_\tau^m\left[\cos\left(\frac{\pi}{2}+\alpha\right)\right]=$$

$$=i^{\tau-m}\int_0^{\frac{\pi}{2}-i\infty}e^{ikl_{12}\cos u}e^{-ikb\cos\alpha\cos u}\times$$

$$\times J_m(kb\sin\alpha\sin u)\,P_\tau^m(\cos u)\sin u\,du. \qquad (1.45)$$

We can show the validity of the expansion

$$e^{ikb\cos\alpha\cos u}J_m(kb\sin\alpha\sin u)=$$

$$=\sum_{\nu=0}^{\infty}(2\nu+1)\,i^{\nu-m}(-1)^\nu\,j_\nu(kb)\,P_\nu^m(\cos\alpha)\,P_\nu^{-m}(\cos u),$$

which, when substituted into (1.45), gives

$$h_\tau(kb\ \operatorname{tan}\ \alpha)\,P_\tau^m\left[\cos\left(\frac{\pi}{2}+\alpha\right)\right]=i^{\tau-m}\sum_{\nu=0}^{\infty}(2\nu+1)\,i^{\nu-m}(-1)^\nu\times$$

$$\times j_\nu(kb)\,P_\nu^m(\cos\alpha)\int_0^{\frac{\pi}{2}-i\infty}e^{ikl_{12}\cos u}P_\nu^{-m}(\cos u)\times$$

$$\times P_\tau^m(\cos u)\sin u\,du. \qquad (1.46)$$

Here we transpose the summation sign and the improper integral sign, the validity of which can be proven by using without any substantial modifications the proof of the addition theorem for the function $h_n(kr)$ given in [33]. Considering relation (1.38) and the expression

$$h_\sigma(z) = i^{-\sigma} \int_0^{\frac{\pi}{2} - i\infty} e^{iz\cos u} P_m(\cos u) \sin u \, du,$$

which is a special case for (1.44), formula (1.46) will take the form

$$h_\tau(kb \tan\alpha) P_\tau^m\left[\cos\left(\frac{\pi}{2}+\alpha\right)\right] = \sum_{\nu=0}^{\infty} (2\nu+1)(-1)^{\nu+m} \times$$

$$\times j_\nu(kb) P_\nu^m(\cos\alpha) \sum_{\sigma=|\tau-\nu|}^{\tau+\nu\prime} a_{\sigma\nu\tau}^m i^{\sigma+\nu+\tau} h_\sigma(kl_{12}). \tag{1.47}$$

Substituting (1.47) into the right side of (1.43) and considering the arbitrariness of b and α, we find /26

$$h_n(kr_1) P_n^{-m}(\cos\theta_1) = (-1)^m \sum_{\tau=0}^{\infty} (2\tau+1) \sum_{\sigma=|\tau-n|}^{\tau+n\prime} a_{\sigma n\tau}^m i^{\sigma-n+\tau} \times$$

$$\times h_\sigma(kl_{12}) j_\tau(kr_2) P_\tau^{-m}(\cos\theta_2), \quad r_2 < l_{12}. \tag{1.48}$$

It is easy to show (by replotting Figure 1.2 and repeating all the preceding arguments) that when $\theta_{12} = \pi$, expression (1.48) takes the form

$$h_n(kr_1) P_n^{-m}(\cos\theta_1) = (-1)^m \sum_{\tau=0}^{\infty} (2\tau+1) \sum_{\sigma=|\tau-n|}^{\tau+n\prime} a_{\sigma n\tau}^m i^{\tau-\sigma-n} \times$$

$$\times h_\sigma(kl_{12}) j_\tau(kr_2) P_\tau^{-m}(\cos\theta_2). \tag{1.49}$$

The following theorem results from (1.48), (1.49) with consideration of (1.42), (1.40).

Theorem 2.

$$h_n(kr_1) P_n^m(\cos\theta_1) = \frac{(n+m)!}{(n-m)!} \sum_{\tau=0}^{\infty} \sum_{\sigma=|n-\tau|}^{n+\tau\prime} (2\tau+1) \times$$

$$\times i^{\sigma+\tau-n-2\sigma} \sin\frac{\theta_{12}}{2} h_\sigma(kl_{12}) \delta_{\sigma n\tau}^m j_\tau(kr_2) P_\tau^m(\cos\theta_2), \quad r_2 < l_{12}. \tag{1.50}$$

Addition theorems (1.42), (1.50) may be given a different form if they are transformed on the basis of lemma 1. We thus obtain

$$h_n(kr_1)P_n^m(\cos\theta_1)=\sum_{\tau=0}^{\infty}\sum_{\sigma=|n-\tau|}^{n+\tau}{}'(2\tau+1)\,i^{n-\sigma-\tau+2\tau\sin\frac{\theta_{12}}{2}}\times$$
$$\times b_{\sigma\tau n}^m j_\tau(kl_{12})h_\sigma(kr_2)P_\sigma^m(\cos\theta_2),\quad r_2>l_{12};$$
$$h_n(kr_1)P_n^m(\cos\theta_1)=\sum_{\tau=0}^{\infty}\sum_{\sigma=|n-\tau|}^{n+\tau}{}'(2\tau+1)\,i^{\tau+\sigma-n-2\tau\sin\frac{\theta_{12}}{2}}\times$$
$$\times b_{\sigma\tau n}^m h_\tau(kl_{12})j_\sigma(kr_2)P_\sigma^m(\cos\theta_2),\quad r_2<l_{12}.$$

We will write theorems 1 and 2 in the coordinates introduced in § 1.1:

$$h_n(k_jr_{j+1})P_n^m(\cos\theta_{j+1})=$$
$$=\sum_{p=0}^{\infty}F_{pnmj}h_p(k_jr_j)P_p^m(\cos\theta_j'),\quad r_j>h_{j+1};\tag{1.51}$$
$$h_n(k_jr_{j+1})P_n^m(\cos\theta_{j+1})=$$
$$=\sum_{p=0}^{\infty}\widetilde{F}_{pnmj}j_p(k_jr_j)P_p^m(\cos\theta_j'),\quad r_j<h_{j+1},\tag{1.52}$$

where /27

$$F_{pnmj}=\frac{(n+m)!}{(n-m)!}(2p+1)\,i^{n-p}\sum_{\sigma=|n-p|}^{n+p}{}'i^{-\sigma+2\sigma\cos\frac{1}{2}\theta_{j\,j+1}'}\times$$
$$\times j_\sigma(k_jh_{j+1})\delta_{\sigma np}^m,\tag{1.53}$$
$$\widetilde{F}_{pnmj}=\frac{(n+m)!}{(n-m)!}(2p+1)\,i^{p-n}\sum_{\sigma=|n-p|}^{n+p}{}'i^{\sigma-2\sigma\cos\frac{1}{2}\theta_{j\,j+1}'}\times$$
$$\times h_\sigma(k_jh_{j+1})\delta_{\sigma np}^m,\quad j=1,\ 2,\ \ldots,\ \nu-1,\tag{1.54}$$

$\theta_{j\,j+1}'$ being the spherical coordinate θ_j' of the origin O_{j+1}.

We will note at this point that formulas (1.51) and (1.52) also apply for $r_j = h_{j+1}$ provided $\theta_j \neq 0$, i.e., these expansions cannot be used for $r_j = h_{j+1}$ at point O_{j+1}, which is the singular point of these expansions.

Addition theorems for the functions $j_n(kr)P_n^m(\cos\theta)$. To obtain the addition theorem of the other separated solution of the Helmholtz equation, we will use its integral representation (1.18), expansion (1.19), and the relations

$$kr_1\cos\theta_1=kr_2\cos\theta_2+kl_{12},$$
$$kr_1\sin\theta_1=kr_2\sin\theta_2.$$

Furthermore, reasoning in the same way as in the derivation of the addition theorem for the modified Bessel function $j_n(z)$ in [33], we come to the

expansion

$$j_n(kr_1)\,P_n^{\lambda}(\cos\theta_1)=\sum_{\tau=0}^{\infty}\sum_{\sigma=|n-\tau|}^{n+\tau}{}' i^{\tau-n+\sigma-2\tau\sin\frac{\theta_{12}}{2}}(2\tau+1)\,j_\tau(kl_{12})\times$$
$$\times\, b_{\sigma\tau n}^{m}\,j_\sigma(kr_2)\,P_\sigma^m(\cos\theta_2),\quad r_2\gtrless l_{12}. \tag{1.55}$$

Applying lemma 1 to expression (1.55) and considering equality (1.38) and also the property of the transposition of indices τ and n resulting from it,

$$a_{\tau\sigma n}^{m}=\frac{(n+m)!\,(\tau-m)!}{(n-m)!\,(\tau+m)!}\,a_{\sigma n\tau}^{m},$$

we obtain the following theorem.

Theorem 3.

$$j_n(kr_1)\,P_n^m(\cos\theta_1)=\frac{(n+m)!}{(n-m)!}\sum_{\tau=0}^{\infty}\sum_{\sigma=|n-\tau|}^{n+\tau}{}'(2\tau+1)\,i^{\tau-n+\sigma-2\tau\sin\frac{\theta_{12}}{2}}\times$$
$$\times\, j_\sigma(kl_{12})\,\delta_{\sigma n\tau}^{m}\,j_\tau(kr_2)\,P_\tau^m(\cos\theta_2),\quad r_2\gtrless l_{12}. \tag{1.56}$$

Expression (1.56) in the coordinates $\mathbf{r_j}$, θ_j', $\mathbf{r_{j+1}}$, θ_{j+1} has the form

$$j_n(k_jr_{j+1})\,P_n^m(\cos\theta_{j+1})=$$
$$=\sum_{p=0}^{\infty}F_{pnmj}\,j_p(k_jr_j)\,P_p^m(\cos\theta_{j+1}'),\quad r_j\gtrless h_{j+1}, \tag{1.57}$$

$$j_p(k_jr_j)\,P_p^m(\cos\theta_j')=\sum_{\tau=0}^{\infty}F_{\tau pmj}^{(-1)}\,j_\tau(k_jr_{j+1})\,P_\tau^m(\cos\theta_{j+1}), \tag{1.58}$$
$$r_{j+1}\gtrless h_{j+1},$$

/28

where

$$F_{\tau pmj+1}^{(-1)}=\frac{(p+m)!}{(p-m)!}(2\tau+1)\,i^{p-\tau}\times$$
$$\times\sum_{\sigma=|p-\tau|}^{p+\tau}{}' i^{-\sigma+2\sigma\sin\frac{1}{2}\theta_{j+1}'}\,j_\sigma(k_jh_{j+1})\,\delta_{\sigma p\tau}^{m}. \tag{1.59}$$

If we first substitute (1.58) into the right side of (1.57), then perform the same operation in reverse order, we obtain

$$\sum_{p=0}^{\infty}F_{pnmj}F_{\tau pmj}^{(-1)}=\sum_{p=0}^{\infty}F_{pnmj}^{(-1)}F_{\tau pmj}=\delta_{\tau n}, \tag{1.60}$$

where $\delta_{\tau n}$ is the Kronecker symbol.

Let us note at this point that if in deriving theorems 1-3 we set m and α equal to zero from the very beginning, we will obtain the theorems and method first indicated in [6].

Addition theorems for the function $P_n^m(\cos\theta)e^{im\phi}$. We will write these theorems in the coordinates introduced in § 1.1, using the results of [25, 26]. The coordinates x_j, y_j, z_j and x_j', y_j', z_j' are related to one another by the Euler angles Θ_j, χ_j by means of the following relations:

$$\left.\begin{aligned} x_j &= x_j' \cos\chi_j - y_j' \sin\chi_j \cos\vartheta_j + z_j' \sin\chi_j \sin\vartheta_j, \\ y_j &= x_j' \cos\chi_j + y_j' \cos\chi_j \cos\vartheta_j - z_j' \cos\chi_j \sin\vartheta_j, \\ z_j &= y_j' \sin\vartheta_j + z_j' \cos\vartheta_j, \end{aligned}\right\} \tag{1.61}$$

$$\left.\begin{aligned} x_j' &= x_j \cos\chi_j + y_j \sin\chi_j, \\ y_j' &= -x_j \sin\chi_j \cos\vartheta_j + y_j \cos\chi_j \cos\vartheta_j + z_j \sin\vartheta_j, \\ z_j' &= x_j \sin\chi_j \sin\vartheta_j - y_j \cos\chi_j \sin\vartheta_j + z_j \cos\vartheta_j. \end{aligned}\right\} \tag{1.62}$$

Substituting (1.1a) into (1.61) and (1.62), we obtain the relation between the coordinates θ_j, ϕ_j and θ_j', ϕ_{j+1}:

$$\left\{\begin{aligned} &\exp\left[i\left(\frac{\pi}{2}+\varphi_j-\chi_j\right)\right] = \\ &= \frac{\cos\theta_j' \sin\vartheta_j - \sin\theta_j' \sin\varphi_{j+1} \cos\chi_j + i \sin\theta_j' \cos\varphi_{j+1}}{\sin\theta_j}, \\ &\cos\theta_j = \cos\theta_j' \cos\vartheta_j + \sin\theta_j' \sin\varphi_{j+1} \sin\vartheta_j, \end{aligned}\right.$$

$$\left\{\begin{aligned} &\cos\theta_j' = \cos\theta_j \cos\vartheta_j - \sin\theta_j \sin\vartheta_j \sin(\varphi_j - \chi_j), \\ &\tan\varphi_{j+1} = \frac{\cos\theta_j \sin\vartheta_j + \sin\theta_j \cos\vartheta_j \sin(\varphi_j-\chi_j)}{\sin\theta_j \cos(\varphi_j-\chi_j)}, \\ &j = 1, 2, \ldots, \nu-1, \end{aligned}\right. \qquad /29$$

whence [26, 25]

$$P_n^m(\cos\theta_j)\, e^{im\varphi_j} = \sum_{l=-n}^{n} b_{lnmj} P_n^l(\cos\theta_j')\, e^{il\varphi_{j+1}}, \tag{1.63}$$

$$P_n^l(\cos\theta_j')\, e^{il\varphi_{j+1}} = \sum_{\lambda=-n}^{n} b_{\lambda nlj}^{(-1)} P_n^\lambda(\cos\theta_j)\, e^{i\lambda\varphi_j}. \tag{1.64}$$

Here

$$b_{lnmj} = e^{im\chi_j} \sqrt{\frac{(n+m)!\,(n-l)!}{(n-m)!\,(n+l)!}}\, P_{ml}^n(\cos\vartheta_j), \tag{1.65}$$

$$b_{\lambda nlj}^{(-1)} = (-1)^{\lambda+l} e^{-il\chi_j} \sqrt{\frac{(n+l)!\,(n-\lambda)!}{(n-l)!\,(n+\lambda)!}}\, P_{l\lambda}^n(\cos\vartheta_j), \tag{1.66}$$

$$j = 1, 2, \ldots, \nu-1;$$

$P_{mr}^n(z)$ are functions in terms of which the matrix elements of the irreducible representations $T_\zeta(G)$ of the group SL(2, C) are expressed.

The function $P^n_{mr}(z)$ is related to classical Jacobi polynomials $P_k^{(\alpha,\ \beta)}(z)$ as follows:

$$P^n_{mr}(z) = 2^{-m} i^{m-r} \sqrt{\frac{(n-m)!\,(n+m)!}{(n-r)!\,(n+r)!}} \times$$
$$\times (1-z)^{\frac{m-r}{2}} (1+z)^{\frac{m+r}{2}} P_{n-m}^{(m-r,\ m+r)}(z).$$

By analogy with the manner in which we obtained equality (1.60), it follows from expressions (1.63), (1.64) that

$$\sum_{l=-n}^{n} b^{(-1)}_{lnmj} b_{\lambda nlj} = \sum_{l=-n}^{n} b_{lnmj} b^{(-1)}_{\lambda nlj} = \delta_{\lambda m}. \tag{1.67}$$

Addition theorems for the functions $j_n(kr)P^m_n(\cos\theta)e^{im\phi}$, $h_n(kr)P^m_n(\cos\theta)e^{im\phi}$.

From expressions (1.58) and (1.63) with the aid of superposition one can readily obtain

$$j_n(k_j r_j)\, P_n^m(\cos\theta_j)\, e^{im\varphi_j} =$$
$$= \sum_{\tau=0}^{\infty} \sum_{l=-n}^{n} K_{\tau lnmj} j_\tau(k_j r_{j+1})\, P_\tau^l(\cos\theta_{j+1})\, e^{il\varphi_{j+1}}, \tag{1.68}$$

where

$$K_{\tau lnmj} = b_{lnmj} F^{(-1)}_{\tau nlj},$$
$$j = 1,\ 2,\ \ldots,\ \nu - 1. \tag{1.69}$$

Similar operations with relations (1.51) and (1.64) and also (1.64) and (1.52) will respectively lead to the following expressions: /30

$$h_n(k_j r_{j+1})\, P_n^m(\cos\theta_{j+1})\, e^{im\varphi_{j+1}} =$$
$$= \sum_{p=0}^{\infty} \sum_{\lambda=-p}^{p} K^{(-1)}_{p\lambda nmj} h_p(k_j r_j)\, P_p^\lambda(\cos\theta_j)\, e^{i\lambda\varphi_j}, \quad r_j > h_{j+1}, \tag{1.70}$$

$$h_n(k_j r_{j+1})\, P_n^m(\cos\theta_{j+1})\, e^{im\varphi_{j+1}} =$$
$$= \sum_{p=0}^{\infty} \sum_{\lambda=-p}^{p} R_{p\lambda nmj} j_p(k_j r_j)\, P_p^\lambda(\cos\theta_j)\, e^{i\lambda\varphi_j}, \quad r_j < h_{j+1}, \tag{1.71}$$

where

$$K^{(-1)}_{p\lambda nmj} = b^{(-1)}_{\lambda pmj} F_{pnmj}, \tag{1.72}$$

$$R_{p\lambda nmj} = b^{(-1)}_{\lambda pmj} \widetilde{F}_{pnmj},$$
$$j = 1,\ 2,\ \ldots,\ \nu - 1. \tag{1.73}$$

The following important identity follows from equalities (1.60), (1.67), (1.69) and (1.72):

$$\sum_{n=0}^{\infty}\sum_{m=-n}^{n} K^{(-1)}_{nmp\lambda j}K_{\tau lmj}=\delta_{\tau p}\delta_{l\lambda},\quad j=1,\ 2,\ \ldots,\ \nu-1. \tag{1.74}$$

§ 1.3. General Solution of the Problem. Components of the Electromagnetic Field.

We will divide the dipole moment vector p into two components (relative to a sphere of radius b_1): a horizontal one p_1 ($|p_1| = |p| \sin\Theta_0$) and a vertical one p_2 ($|p_2| = |p| \cos\Theta_0$). Then in the coordinates r_1, θ_1, ϕ_1 for $r_1 < h_1$, T_{00} will take the form:

$$T_{00}=\sum_{n=0}^{\infty}\sum_{m=-1}^{1} A^{(0)}_{nm} j_n(k_0 r_1)\, P_n^m(\cos\theta_1)\, e^{im\varphi_1}, \tag{1.75}$$

where

$$A^{(0)}_{nm}=\begin{cases} -n(n+1)\beta_{00}A_{1n} & \text{for } m=-1,\\ A_{2n} & \text{for } m=0,\\ \alpha_{00}A_{1n} & \text{for } m=1,\\ 0 & \text{for } |m|>1, \end{cases} \tag{1.76}$$

$$n=0,\ 1,\ \ldots$$

$$A_{1n}=\left\{\frac{ik_0|\mathbf{p}_1|(2n+1)}{h_1 n(n+1)}\zeta_n'(k_0h_1),\right.$$

$$\left.-\frac{ik_0\varkappa_0|\mathbf{p}_1|(2n+1)}{n(n+1)}h_n(k_0h_1)\right\},\quad n\geqslant 1, \tag{1.77}$$

$$A_{10}\{0,\ 0\}, \tag{1.78}$$

$$A_{2n}=\left\{\frac{ik_0|\mathbf{p}_2|(2n+1)}{h_1}h_n(k_0h_1),\ 0\right\}, \tag{1.79}$$

/31

$$\alpha_{00}=\left\{\frac{1}{2},\quad -\frac{i}{2}\right\},$$

$$\beta_{00}=\left\{\frac{1}{2},\quad \frac{i}{2}\right\}, \tag{1.80}$$

$$\zeta_n(z)=zh_n(z),$$

$$\zeta_n'(z)=\frac{d}{dz}\zeta_n(z). \tag{1.81}$$

If however $r > h_1$, then

$$T_{00}=\sum_{n=0}^{\infty}\sum_{m=-1}^{1} t^{(0)}_{nm} h_n(k_0r_1)\, P_n^m(\cos\theta_1)\, e^{im\varphi_1},$$

where

$$t_{nm}^{(0)} = \begin{cases} -n(n+1)\beta_{00}t_{1n} & \text{for } m=-1, \\ t_{2n} & \text{for } m=0, \\ \alpha_{00}t_{1n} & \text{for } m=1, \\ 0 & \text{for } |m|>1, \end{cases}$$

$$n = 0, 1, \ldots$$

$$t_{1n} = \left\{ -\frac{ik_0 |\mathbf{p}_1| (2n+1)}{h_1 n(n+1)} \psi_n'(k_0 h_1), \right.$$

$$\left. -\frac{ik_0 \alpha_0 |\mathbf{p}_1| (2n+1)}{n(n+1)} j_n(k_0 h_1) \right\}, \quad n \geqslant 1,$$

$$t_{10} = \{0, 0\}, \qquad t_{2n} = \left\{ \frac{ik_0 |\mathbf{p}_2| (2n+1)}{h_1} j_n(k_0 h_1), 0 \right\},$$

$$\psi_n(z) = z j_n(z), \quad \psi_n'(z) = \frac{d}{dz}\psi_n(z). \tag{1.82}$$

We will seek the solutions of equations (1.4a) in the corresponding regions by taking (1.9) into account in the following form:

$$T_j = \begin{cases} T_{00} + \sum\limits_{n=0}^{\infty} \sum\limits_{m=-n}^{n} B_{nm}^{(0)} h_n(k_0 r_1) P_n^m(\cos\theta_1) e^{im\varphi_1} & \text{for } j=0, \\ \sum\limits_{n=0}^{\infty} \sum\limits_{m=-n}^{n} A_{nm}^{(j)} j_n(k_j r_j) P_n^m(\cos\theta_j) e^{im\varphi_j} + B_{nm}^{(j)} \times \\ \times h_n(k_j r_{j+1}) P_n^m(\cos\theta_{j+1}) e^{im\varphi_{j+1}} \\ \qquad\qquad \text{for } j=1, 2, \ldots, \nu-1, \\ \sum\limits_{n=0}^{\infty} \sum\limits_{m=-n}^{n} A_{nm}^{(\nu)} j_n(k_\nu r_\nu) P_n^m(\cos\theta_\nu) e^{im\varphi_\nu} & \text{for } j=\nu. \end{cases} \tag{1.83}$$

The expressions for T_j when $j = 1, 2, \ldots, \nu$ may be written in more compact form if we set /32

$$B_{nm}^{(\nu)} \equiv 0. \tag{1.84}$$

Then

$$T_j = \sum_{n=0}^{\infty} \sum_{m=-n}^{n} A_{nm}^{(j)} j_n(k_j r_j) P_n^m(\cos\theta_j) e^{im\varphi_j} + B_{nm}^{(j)} h_n(k_j r_{j+1}) P_n^m(\cos\theta_{j+1}) e^{im\varphi_{j+1}}, \quad j = 1, 2, \ldots, \nu. \tag{1.85}$$

This is the expression which we will use hereinafter, taking assumption (1.84) into consideration.

Making solutions (1.83) satisfy the boundary conditions (1.6) and using the addition theorems on (1.68), (1.70) and the property of orthogonality of tesseral functions, we obtain:

$$
\begin{cases}
q_0 j_n(k_0 b_1) A_{nm}^{(0)} + q_0 h_n(k_0 b_1) B_{nm}^{(0)} = q_1 j_n(k_1 b_1) A_{nm}^{(1)} + \\
\quad + q_1 h_n(k_1 b_1) \sum\limits_{\tau=0}^{\infty} \sum\limits_{l=-\tau}^{\tau} B_{\tau l}^{(1)} K_{nm\tau l\,1}^{(-1)}, \\
\psi_n'(k_0 b_1) A_{nm}^{(0)} + \zeta_n'(k_0 b_1) B_{nm}^{(0)} = \psi_n'(k_1 b_1) A_{nm}^{(1)} + \\
\quad + \zeta_n'(k_1 b_1) \sum\limits_{\tau=0}^{\infty} \sum\limits_{l=-\tau}^{\tau} B_{\tau l}^{(1)} K_{nm\tau l\,1}^{(-1)}, \\
\ldots\ldots\ldots\ldots\ldots\ldots\ldots\ldots\ldots\ldots\ldots\ldots \\
q_j j_n(k_j b_{j+1}) \sum\limits_{\tau=0}^{\infty} \sum\limits_{l=-\tau}^{\tau} A_{\tau l}^{(j)} K_{nm\tau lj} + q_j h_n(k_j b_{j+1}) B_{nm}^{(j)} = q_{j+1} \times \\
\quad \times j_n(k_{j+1} b_{j+1}) A_{nm}^{(j+1)} + q_{j+1} h_n(k_{j+1} b_{j+1}) \times \\
\quad \times \sum\limits_{\tau=0}^{\infty} \sum\limits_{l=-\tau}^{\tau} B_{\tau l}^{(j+1)} K_{nm\tau l\,j+1}^{(-1)}, \\
\psi_n'(k_j b_{j+1}) \sum\limits_{\tau=0}^{\infty} \sum\limits_{l=-\tau}^{\tau} A_{\tau l}^{(j)} K_{nm\tau lj} + \zeta_n'(k_j b_{j+1}) B_{nm}^{(j)} = \\
\quad = \psi_n'(k_{j+1} b_{j+1}) A_{nm}^{(j+1)} + \zeta_n'(k_{j+1} b_{j+1}) \times \\
\quad \times \sum\limits_{\tau=0}^{\infty} \sum\limits_{l=-\tau}^{\tau} B_{\tau l}^{(j+1)} K_{nm\tau l\,j+1}^{(-1)},
\end{cases}
\tag{1.86}
$$

$$
j = 1, 2, \ldots, \nu - 1; \quad n = 0, 1, \ldots; \quad m = -n, \ldots, n.
$$

We write system (1.86) as follows: /33

$$
\begin{aligned}
B_{nm}^{(0)} &= \frac{q_1 j_n(k_1 b_1)}{q_0 h_n(k_0 b_1)} A_{nm}^{(1)} + \frac{q_1 h_n(k_1 b_1)}{q_0 h_n(k_0 b_1)} \times \\
&\times \sum_{\tau=0}^{\infty} \sum_{l=-\tau}^{\tau} B_{\tau l}^{(1)} K_{nm\tau l\,1}^{(-1)} - \frac{j_n(k_0 b_1)}{h_n(k_0 b_1)} A_{nm}^{(0)}, \\
A_{nm}^{(1)} &= \frac{\zeta_n'(k_0 b_1)}{\psi_n'(k_1 b_1)} B_{nm}^{(0)} - \frac{\zeta_n'(k_1 b_1)}{\psi_n'(k_1 b_1)} \times \\
&\times \sum_{\tau=0}^{\infty} \sum_{l=-\tau}^{\tau} B_{\tau l}^{(1)} K_{nm\tau l\,1}^{(1)} + \frac{\psi_n'(k_0 b_1)}{\psi_n'(k_1 b_1)} A_{nm}^{(0)}, \\
B_{nm}^{(j)} &= \frac{q_{j+1} j_n(k_{j+1} b_{j+1})}{q_j h_n(k_j b_{j+1})} A_{nm}^{(j+1)} - \\
&- \frac{j_n(k_j b_{j+1})}{h_n(k_j b_{j+1})} \sum_{\tau=0}^{\infty} \sum_{l=-\tau}^{\tau} A_{\tau l}^{(j)} K_{nm\tau lj} + \\
&+ \frac{q_{j+1} h_n(k_{j+1} b_{j+1})}{q_j h_n(k_j b_{j+1})} \sum_{\tau=0}^{\infty} \sum_{l=-\tau}^{\tau} B_{\tau l}^{(j+1)} K_{nm\tau l\,j+1}^{(-1)}, \\
A_{nm}^{(j+1)} &= \frac{\psi_n'(k_j b_{j+1})}{\psi_n'(k_{j+1} b_{j+1})} B_{nm}^{(j)} +
\end{aligned}
\tag{1.87}
$$

$$+\frac{\psi_n'(k_jb_{j+1})}{\psi_n'(k_{j+1}b_{j+1})}\sum_{\tau=0}^{\infty}\sum_{l=-\tau}^{\tau}A_{\tau l}^{(j)}K_{nm\tau lj}-$$

$$-\frac{\zeta_n'(k_{j-1}b_{j+1})}{\psi_n'(k_{j+1}b_{j+1})}\sum_{\tau=0}^{\infty}\sum_{l=-\tau}^{\tau}B_{\tau l}^{(j+1)}K_{nm\tau l\,j+1},$$

$$n=0,\ 1,\ 2,\ \ldots;\quad m=-n,\ \ldots,\ n;\quad j=1,\ \ldots,\ \nu-1. \tag{1.87}$$

It is assumed that

$$h_n(k_jb_{j+1})\neq 0, \tag{1.88}$$

$$\psi_n'(k_{j+1}b_{j+1})\neq 0, \tag{1.89}$$

$$n=0,\ 1,\ \ldots;\quad j=0,\ 1,\ \ldots,\ \nu-1.$$

Inequality (1.88) in the problem at hand is always valid by virtue of inequality (1.4) and of H. Falkenberg's theorem [34], which states that the equation $h_n(z) = 0$ has no zeros in the half-plane $0 \leq \arg z \leq \pi$.

For certain n and j, inequality (1.89) may fail to be fulfilled. This case will therefore be analyzed separately.

If in system (1.87) we make the substitution /34

$$A_{nm}^{(j)}=Z_{nm}^{(2j-1)}\sqrt{\frac{(n-m)!}{(n+m)!}}\,h_n^*(k_jb_j),\quad j=1,\ 2,\ \ldots,\ \nu;$$

$$B_{nm}^{(j)}=Z_{nm}^{(2j)}\sqrt{\frac{(n-m)!}{(n+m)!}}\,j_n^*(k_jb_{j+1}),\quad j=0,\ 1,\ \ldots,\ \nu-1;$$

$$A_{nm}^{(0)}=X_{nm}^{(0)}\sqrt{\frac{(n-m)!}{(n+m)!}}, \tag{1.90}$$

where[15]

$$h_n^*(k_jb_j)=\frac{(2n-1)!!}{(k_jb_j)^n},\qquad j_n^*(k_jb_j)=\frac{(k_jb_j)^n}{(2n+1)!!}, \tag{1.91}$$

---

[15] In analogous cases, other transformations of variables are usually employed (see for example [9, 57] and others), in which the expressions $h_n^*(k_jb_j)$ and $j_n^*(k_jb_j)$ in (1.90) are replaced by the functions $h_n(k_jb_j)$ and $j_n(k_jb_j)$, respectively. In addition to complicating the computational aspects of the problem, such substitution loses meaning and does not lead to definitive results when k_jb_j is the root of the equation $j_n(z) = 0$.

it is rewritten in the form

$$\begin{cases} Z_{nm}^{(0)} = a_n^{(0)} Z_{nm}^{(1)} + \sum\limits_{\tau=0}^{\infty} \sum\limits_{l=-\tau}^{\tau} Z_{\tau l}^{(2)} a_{\tau l n m 0}^{(2)} - \Phi_{nm}^{(0)}, \\ Z_{nm}^{(1)} = a_n^{(1)} Z_{nm}^{(0)} + \sum\limits_{\tau=0}^{\infty} \sum\limits_{l=-\tau}^{\tau} Z_{\tau l}^{(2)} a_{\tau l n m 1}^{(2)} - \Phi_{nm}^{(1)}, \\ \ldots\ldots\ldots\ldots\ldots\ldots\ldots\ldots\ldots\ldots \\ Z_{nm}^{(2j)} = a_n^{(2j)} Z_{nm}^{(2j+1)} + \sum\limits_{\tau=0}^{\infty} \sum\limits_{l=-\tau}^{\tau} Z_{\tau l}^{(2j-1)} a_{\tau l n m\, 2j}^{(2j-1)} + \\ \quad + \sum\limits_{\tau=0}^{\infty} \sum\limits_{l=-\tau}^{\tau} Z_{\tau l}^{(2j+2)} a_{\tau l n m\, 2j}^{(2j+2)} - \Phi_{nm}^{(2j)}, \\ Z_{nm}^{(2j+1)} = a_n^{(2j+1)} Z_{nm}^{(2j)} + \sum\limits_{\tau=0}^{\infty} \sum\limits_{l=-\tau}^{\tau} Z_{\tau l}^{(2j-1)} a_{\tau l n m\, 2j+1}^{(2j-1)} + \\ \quad + \sum\limits_{\tau=0}^{\infty} \sum\limits_{l=-\tau}^{\tau} Z_{\tau l}^{(2j+2)} a_{\tau l n m\, 2j+1}^{(2j+2)} - \Phi_{nm}^{(2j+1)}. \end{cases} \tag{1.92}$$

$$n = 0, 1, \ldots; \quad m = -n, \ldots, n; \quad j = 1, 2, \ldots, \nu - 1.$$

Here

$$a_n^{(2j)} = \frac{q_{j+1} j_n(k_{j+1} b_{j+1}) h_n^*(k_{j+1} b_{j+1})}{q_j h_n(k_j b_{j+1}) j_n^*(k_j b_{j+1})};$$

$$a_n^{(2j+1)} = \frac{\zeta_n'(k_j b_{j+1}) j_n^*(k_j b_{j+1})}{\psi_n'(k_{j+1} b_{j+1}) h_n^*(k_j b_{j+1})};$$

$$\Phi_{nm}^{(j)} = \begin{cases} \dfrac{j_n(k_0 b_1)}{h_n(k_0 b_1) j_n^*(k_0 b_1)} X_{nm}^{(0)}, & j = 0, \\ -\dfrac{\psi_n'(k_0 b_1)}{\psi_n'(k_1 b_1) h_n^*(k_1 b_1)} X_{nm}^{(0)}, & j = 1, \\ 0, & j > 1; \end{cases}$$

$$a_{\tau l n m\, 2j}^{(2j-1)} = -\sqrt{\frac{(n+m)!(\tau-l)!}{(n-m)!(\tau+l)!}} \times$$

$$\times \frac{j_n(k_j b_{j+1}) h_\tau^*(k_j b_j)}{h_n(k_j b_{j+1}) j_n^*(k_j b_{j+1})} K_{nm\tau l j}, \quad j = 1, 2, \ldots, \nu - 1;$$

$$a_{\tau l n m\, 2j}^{(2j+2)} = \sqrt{\frac{(n+m)!(\tau-l)!}{(n-m)!(\tau+l)!}} \times$$

$$\times \frac{q_{j+1} h_n(k_{j+1} b_{j+1}) j_\tau^*(k_{j+1} b_{j+2})}{q_j h_n(k_j b_{j+1}) j_n^*(k_j b_{j+1})} K_{nm\tau l\, j+1}^{(-1)}, \quad j = 0, 1, \ldots, \nu - 2;$$

$$a^{(2j-1)}_{\tau l n m\, 2j+1} = \sqrt{\frac{(n+m)!\,(\tau-l)!}{(n-m)!\,(\tau+l)!}} \times$$

$$\times \frac{\psi_n'(k_j b_{j+1})\, h_\tau^*(k_j b_j)}{\psi_n'(k_{j+1} b_{j+1})\, h_n^*(k_{j+1} b_{j+1})} K_{nm\tau l j}, \quad j = 1, 2, \ldots, \nu - 1;$$

$$a^{(2j+2)}_{\tau l n m\, 2j+1} = -\sqrt{\frac{(n+m)!\,(\tau-l)!}{(n-m)!\,(\tau+l)!}} \times$$

$$\times \frac{\zeta_n'(k_{j+1} b_{j+1})\, j_\tau^*(k_{j+1} b_{j+2})}{\psi_n'(k_{j+1} b_{j+1})\, h_n^*(k_{j+1} b_{j+1})} K^{(-1)}_{nm\tau l\, j+1}, \quad j = 0, 1, \ldots, \nu - 2. \quad (1.93) \qquad (1.93)$$

System (1.92) may also be written in the more general form:

$$Z^{(s)}_{nm} = a_n^{(s)} Z^{(s+(-1)^s)}_{nm} + \sum_{i=0}^{2\nu-1} \sum_{\tau=0}^{\infty} \sum_{l=-\tau}^{\tau} Z^{(i)}_{\tau l} a^{(i)}_{\tau l n m s} - \Phi^{(s)}_{nm}, \qquad (1.94)$$

$$s = 0, 1, \ldots, 2\nu - 1; \quad n = 0, 1, \ldots; \quad m = -n, \ldots, n,$$

where the expression for $a^{(i)}_{\tau l n m s}$ for indices i and s satisfying one of the relations

$$\begin{aligned} &i = 2j-1, \quad s = 2j, && j = 1, 2, \ldots, \nu-1; \\ &i = 2j+2, \quad s = 2j, && j = 0, 1, \ldots, \nu-2; \\ &i = 2j-1, \quad s = 2j+1, && j = 1, 2, \ldots, \nu-1; \\ &i = 2j+2, \quad s = 2j+1, && j = 0, 1, \ldots, \nu-2, \end{aligned}$$

is determined by formulas (1.93) and is equal to zero for all the remaining relations. /36

To study the solvability and uniqueness of the solution, it is useful to give the following form to system (1.94):

$$\sum_{l=0}^{2\nu-1} Z^{(i)}_{nm} \alpha^{(n)}_{ls} + \sum_{i=0}^{2\nu-1} \sum_{\tau=0}^{\infty} \sum_{l=-\tau}^{\tau} Z^{(i)}_{\tau l} a^{(i)}_{\tau l n m s} = \Phi^{(s)}_{nm}, \qquad (1.95)$$

$$s = 0, 1, \ldots, 2\nu - 1; \quad n = 0, 1, \ldots; \quad m = -n, \ldots, n.$$

In system (1.95)

$$\alpha^{(n)}_{ls} = a_n^{(s)} \delta_{ls+(-1)^s} - \delta_{ls}. \qquad (1.96)$$

In the form of (1.95), system (1.92) permits a simple functional treatment.

We introduce into consideration the space $\tilde{l}_2$, consisting of infinite three-dimensional matrices $Z = \{Z^{(j)}_{nm}\}$, n = 0, 1,...; m = - n, ..., n; j = 0, 1,..., 2ν - 1 c $Z^{(j)}_{nm} = 0$ for $|m| > n$ and with the norm

$$\|Z\| = \sqrt{\sum_{j=0}^{2\nu-1} \sum_{n=0}^{\infty} \sum_{m=-n}^{n} |Z_{nm}^{(j)}|^2} < \infty.$$

The operations of addition and multiplication by a number are introduced naturally.

Since any three-dimensional matrix from $\tilde{l}_2$ contains only an even number of constituent elements, by appropriately renumbering them it is easy to establish the algebraic isomorphism and isometry of the spaces $\tilde{l}_2$ and l_2 (the spaces of the sequences $\{Z_k\}$, k = 0, 1, 2, ...), whence it follows that the space $\tilde{l}_2$ introduced is a Banach space [35].

In terms of the space l_2, system (1.95) may be written with the aid of matrix operators W and T:

$$(W + T) Z = \Phi, \tag{1.97}$$

where $\alpha_{is}^{(n)}$ and $a_{\tau l nms}^{(i)}$ are the kernels of operator W and T, respectively. It will be shown that $\Phi \in \tilde{l}_2$, i.e.,

$$\|\Phi\| < \infty. \tag{1.98}$$

To do so, it is sufficient to show that

$$\sum_{n=0}^{\infty} \sum_{m=-n}^{n} |\Phi_{nm}^{(0)}|^2 < \infty, \tag{1.99}$$

since

$$|\Phi_{nm}^{(1)}| < \text{const}_1 |\Phi_{nm}^{(0)}|. \tag{1.100}$$

Inequality (1.100) results from estimates (1.29), lemma 2 of § 1.2 and expressions (1.81), (1.93). /37

Similarly, we obtain the inequalities

$$|A_{1n}| < \text{const}_2 \frac{(2n+1)!!}{|k_0 h_1|^n}, \qquad |A_{2n}| < \text{const}_3 \frac{(2n+1)!!}{|k_0 h_1|^n},$$

which lead to the following:

$$|A_{nm}^{(0)}| < \text{const}_4 \frac{(2n+1)!!}{|k_0 h_1|^n}. \tag{1.101}$$

If we use the estimates from (1.101) and

$$\frac{|j_n(k_0b_1)|}{|h_n(k_0b_1)||j_n^*(k_0b_1)|}<\text{const}_5\frac{|k_0b_1|^n}{(2n-1)!!}$$

in (1.99) taking (1.93) into consideration, we will have

$$\sum_{n=0}^{\infty}\sum_{m=-n}^{n}|\Phi_{nm}^{(0)}|^2<\text{const}_6\sum_{n=1}^{\infty}n^4\left(\frac{b_1}{h_1}\right)^{2n}. \tag{1.102}$$

The series on the right in expression (1.102) converges for $b_1 < h_1$. Thus, inequality (1.98) was proven under the assumption that the dipole is located above the sphere of radius of b_1 and does not touch it.

To prove the solvability of equation (1.97), we will have to use Fredholm's alternative. The way to this is opened up by the theorem of S. M. Nikol'skiy [36], which for our case may be formulated as follows.

Theorem. If: 1) W and T are linear operators defined in $\tilde{l}_2$ and representing it in their part; 2) W is a reversible operator and T is a completely continuous operator, and $\Phi \in \tilde{l}_2$, then Fredholm's alternative applies to equation (1.97).

Let us consider the operators W and T.

Operator W places each $Z \in l_2$ in correspondence with a certain U = WZ with the aid of the transformation

$$U_{nm}^{(s)}=\sum_{i=0}^{2\nu-1}Z_{nm}^{(i)}\alpha_{is}^{(n)}. \tag{1.103}$$

The additivity of operator W follows directly from (1.103).

We will use Bunyakovskiy's inequality [35] in expression (1.103):

$$|U_{nm}^{(s)}|^2<\sum_{i=0}^{2\nu-1}|Z_{nm}^{(i)}|^2\sum_{i=0}^{2\nu-1}|\alpha_{is}^{(n)}|^2. \tag{1.104}$$

By virtue of the estimate $|a_n^{(s)}| < \text{const}_6$ (resulting from lemma 2 of § 1.2), Stirling's formula and expressions (1.93), (1.96), (1.104), we have

$$|U_{nm}^{(s)}|^2<\text{const}_7\sum_{i=0}^{2\nu-1}|Z_{nm}^{(i)}|^2,$$

whence

$$\| U \| < \text{const}_7 \| Z \|. \tag{1.105}$$

/38

Inequality (1.105) indicates the boundedness of the additive operator W and hence, its linearity [37]. From (1.105) it also follows that operator W acts from $\tilde{l}_2$ into $\tilde{l}_2$.

It will be shown that W is an operator reversible in $\tilde{l}_2$.

The matrix $\alpha^{(n)} = \{\alpha_{is}^{(n)}\}$ of the transform W of (1.103) has the form

$$\alpha^{(n)} = \left(\begin{array}{cccc|c|cc} -1 & a_n^{(1)} & 0 & 0 & \dots & 0 & 0 \\ a_n^{(0)} & -1 & 0 & 0 & \dots & 0 & 0 \\ \hline 0 & 0 & -1 & a_n^{(3)} & \dots & 0 & 0 \\ 0 & 0 & a_n^{(2)} & -1 & \dots & 0 & 0 \\ \hline \cdot & \cdot & \cdot\ \cdot\ \cdot & & \dots & \cdot & \cdot \\ \cdot & \cdot & \cdot\ \cdot\ \cdot & & \dots & \cdot & \cdot \\ \hline 0 & 0 & 0 & 0 & \dots & -1 & a_n^{(2\nu-2)} \\ 0 & 0 & 0 & 0 & \dots & a_n^{(2\nu-1)} & -1 \end{array}\right). \tag{1.106}$$

Partitioning matrix (1.106) by dotted lines into second order square cells, we conclude that this matrix is quasi-diagonal [38] with the determinant

$$\det \alpha^{(n)} = \prod_{j=0}^{\nu-1} (1 - a_n^{(2j)} a_n^{(2j+1)}). \tag{1.107}$$

We will prove that

$$\det \alpha^{(n)} \neq 0, \tag{1.108}$$

or the equivalent statement that

$$1 - a_n^{(2j)} a_n^{(2j+1)} \neq 0, \quad n = 0, 1, \dots; \quad j = 0, 1, \dots, \nu - 1. \tag{1.109}$$

Substituting expressions (1.93) into the left member of inequality (1.109), we obtain

$$1 - a_n^{(2j)} a_n^{(2j+1)} = - \frac{\Delta_n^{(j)}}{q_j h_n (k_j b_{j+1}) \psi_n' (k_{j+1} b_{j+1})}, \tag{1.110}$$

where

$$\Delta_n^{(j)} = q_{j+1} h_n (k_{j+1} b_{j+1}) \psi_n' (k_j b_{j+1}) - q_j h_n (k_j b_{j+1}) \psi_n' (k_{j+1} b_{j+1}). \tag{1.111}$$

In view of the validity of inequality (1.88) and of the assumption (1.89), /39
it follows that relation (1.108) is equivalent to the following:

$$\Delta_n^{(j)} \neq 0. \tag{1.112}$$

We will prove the validity of (1.112). To this end, we will consider the following auxiliary problem.

Let there be a sphere of radius b_{j+1} (medium j + 1) in infinite space. The following scalar problem of mathematical physics is posed:

$$\begin{gathered}
\Delta T_j + k_j^2 T_j = 0 \text{ (medium j)} \\
\Delta T_{j+1} + k_{j+1}^2 T_{j+1} = 0 \text{ (medium j + 1)} \\
\left.\begin{aligned} q_j T_j &= q_{j+1} T_{j+1} \\ \frac{\partial (rT_j)}{\partial r} &= \frac{\partial (rT_{j+1})}{\partial r} \end{aligned}\right\} \text{ for } r = b_{j+1}, \\
\lim_{r \to \infty} r\left[\frac{\partial T_j}{\partial r} - ik_j T_j\right] = 0.
\end{gathered} \tag{1.113}$$

Here the expanded equation for medium (j) is identical to equation (1.4a). System (1.113) is homogeneous, and by virtue of the uniqueness theorem [39] has only a trivial (zero) solution, i.e.,

$$T_j \equiv 0 \equiv T_{j+1}. \tag{1.114}$$

We will seek the solution of problem (1.113) in the form

$$\begin{aligned}
T_j &= a_n h_n(k_j r) P_n(\cos\theta), \\
T_{j+1} &= b_n j_n(k_{j+1} r) P_n(\cos\theta).
\end{aligned} \tag{1.115}$$

Making expressions (1.115) satisfy the boundary conditions (1.113), we come to the following algebraic system for coefficients a_n and b_n:

$$\begin{cases} a_n q_0 h_n(k_j b_{j+1}) - b_n q_1 j_n(k_{j+1} b_{j+1}) = 0, \\ a_n \zeta_n'(k_j b_{j+1}) - b_n \psi_n'(k_{j+1} b_{j+1}) = 0. \end{cases} \tag{1.116}$$

It follows from equalities (1.114) and (1.115) that a_n and b_n can be only identical zeroes. Hence, it follows for the determinant (1.116) that

$$\begin{vmatrix} q_j h_n(k_j b_{j+1}) & -q_{j+1} j_n(k_{j+1} b_{j+1}) \\ \zeta_n'(k_j b_{j+1}) & -\psi_n'(k_{j+1} b_{j+1}) \end{vmatrix} \neq 0. \tag{1.117}$$

Since the left member of expressions (1.117) is nothing but $\Delta_n^{(j)}$, determined from formula (1.111), inequalities (1.112) and consequently (1.108) as well may be considered proven.

It is easy to write the matrix $\tilde{\alpha}^{(n)}$, the inverse of matrix (1.106): /40

$$\alpha^{(n)} = \left(\begin{array}{cccc|c|cc} -1 & a_n^{(1)} & 0 & 0 & \dots & 0 & 0 \\ a_n^{(0)} & -1 & 0 & 0 & \dots & 0 & 0 \\ \hline 0 & 0 & -1 & a_n^{(3)} & \dots & 0 & 0 \\ 0 & 0 & a_n^{(2)} & -1 & \dots & 0 & 0 \\ \hline \cdot & \cdot & \cdot & \cdot & \dots & \cdot & \cdot \\ \cdot & \cdot & \cdot & \cdot & \dots & \cdot & \cdot \\ \hline 0 & 0 & 0 & 0 & \dots & -1 & a_n^{(2\nu-2)} \\ 0 & 0 & 0 & 0 & \dots & a_n^{(2\nu-1)} & -1 \end{array}\right) \tag{1.118}$$

It follows from expressions (1.118), (1.106), (1.108) that W is an operator reversible in $\tilde{l}_2$.

Operator T places each $Z \in \tilde{l}_2$ in correspondence with a certain V = TZ with the aid of the transformation

$$V_{nm}^{(s)} = \sum_{l=0}^{2\nu-1} \sum_{\tau=0}^{\infty} \sum_{l=-\tau}^{\tau} Z_{\tau l}^{(i)} a_{\tau lnms}^{(i)}. \tag{1.119}$$

We will find the conditions which must be imposed on the kernel of operator T in order that the latter act from $\tilde{l}_2$ into $\tilde{l}_2$ and at the same time be completely continuous.

From Bunyakovskiy's inequality applied to (1.119) we obtain the estimate

$$\|V\| < \sqrt{\sum_{s=0}^{2\nu-1} \sum_{n=0}^{\infty} \sum_{m=-n}^{n} \sum_{l=0}^{2\nu-1} \sum_{\tau=0}^{\infty} \sum_{l=-\tau}^{\tau} |a_{\tau lnms}^{(i)}|^2}\, \|Z\|, \tag{1.120}$$

from which it follows that

$$\|T\| < \sqrt{\sum_{s=0}^{2\nu-1} \sum_{n=0}^{\infty} \sum_{m=-n}^{n} \sum_{l=0}^{2\nu-1} \sum_{\tau=0}^{\infty} \sum_{l=-\tau}^{\tau} |a_{\tau lnms}^{(i)}|^2}, \tag{1.121}$$

where $\|T\|$ is the norm of operator T.

From inequality (1.120) it is easy to obtain the condition

$$\sum_{n=0}^{\infty}\sum_{m=-n}^{n}\sum_{\tau=0}^{\infty}\sum_{l=-\tau}^{\tau}|a_{\tau lnms}^{(l)}|^2<\infty, \tag{1.122}$$

which is sufficient for the statement that operator T acts from $\tilde{l}_2$ into $\tilde{l}_2$. /41

We will show that condition (1.122) also guarantees its complete continuity.

We introduce into $\tilde{l}_2$ the linear operators T_k (k = 0, 1, 2, ...): $\tilde{V} = T_k Z$, realizing the transformation

$$\tilde{V}_{nm}^{(s)}=\sum_{i=0}^{2\nu-1}\sum_{\tau=0}^{\infty}\sum_{l=-\tau}^{\tau}Z_{\tau l}^{(i)}a_{\tau lnms}^{(ik)}, \tag{1.123}$$

where

$$a_{\tau lnms}^{(ik)}=\begin{cases}a_{\tau lnms}^{(l)} & \text{for } n\leqslant k,\\ 0 & \text{for } n>k.\end{cases} \tag{1.124}$$

It follows from (1.124) and (1.123) that no matter what $Z \in \tilde{l}_2$ is, $\tilde{V}_{nm}^{(s)} = 0$ when n > k. Consequently, the set of values of each of the operators T_k is finite-dimensional, and therefore operators T_k are completely continuous. By analogy with estimate (1.121) it may be shown that

$$\|T-T_k\|\leqslant\sqrt{\sum_{s=0}^{2\nu-1}\sum_{n=k+1}^{\infty}\sum_{m=-n}^{n}\sum_{i=0}^{2\nu-1}\sum_{\tau=0}^{\infty}\sum_{l=-\tau}^{\tau}|a_{\tau lnms}^{(l)}|^2}. \tag{1.125}$$

By virtue of inequality (1.122), the right member of expression (1.125) tends to zero when $k \to \infty$, leading to the relationship

$$\lim_{k\to\infty}\|T-T_k\|=0.$$

It follows[16] that T is a completely continuous operator. Obviously, condition (1.122) will be fulfilled for system (1.95) if

$$L_1^{(j)}=\sum_{n=0}^{\infty}\sum_{m=-n}^{n}\sum_{\tau=0}^{\infty}\sum_{l=-\tau}^{\tau}|a_{\tau lnm2j}^{(2j+2)}|^2<\infty,\quad j=0,1,\ldots,\nu-2; \tag{1.126}$$

$$L_2^{(j)}=\sum_{n=0}^{\infty}\sum_{m=-n}^{n}\sum_{\tau=0}^{\infty}\sum_{l=-\tau}^{\tau}|a_{\tau lnm\,2j+1}^{(2j+2)}|^2<\infty,\quad j=0,1,\ldots,\nu-2; \tag{1.127}$$

[16] In view of the completeness of space $\tilde{l}_2$.

$$L_3^{(j)}=\sum_{n=0}^{\infty}\sum_{m=-n}^{n}\sum_{\tau=0}^{\infty}\sum_{l=-\tau}^{\tau}|a_{\tau lnm2j}^{(2j-1)}|^2<\infty,\quad j=0,\ 1,\ \ldots,\ \nu-1; \tag{1.128}$$

$$L_4^{(j)}=\sum_{n=0}^{\infty}\sum_{m=-n}^{n}\sum_{\tau=0}^{\infty}\sum_{l=-\tau}^{\tau}|a_{\tau lnm\,2j+1}^{(2j-1)}|^2<\infty,\quad j=0,\ 1,\ \ldots,\ \nu-1. \tag{1.129}$$

We will prove inequality (1.126). Using the estimate /42

$$|P_{km}^{n}(\cos\vartheta)|<1, \tag{1.130}$$

resulting from the unitarity of the matrix [26] of generalized spherical functions of n-th order, the relation

$$|P_{km}^{n}(\cos\vartheta)|<1,$$

resulting from the integral representation (1.42) with consideration of the property of the associated Legendre function relative to the superscript, and also lemma 2 of § 1.2, and inequalities (1.29), (1.32), we will have

$$L_1^{(j)}<\text{const}_8\sum_{n=0}^{\infty}\sum_{\tau=0}^{\infty}(\tau+n)^5\times$$
$$\times\frac{|k_{j+1}b_{j+2}|^{2\tau}|k_{j+1}h_{j+2}|^{2|n-\tau|}}{|k_{j+1}b_{j+1}|^{2n}}\left[\frac{(2n+1)!!}{(2\tau+1)!!(2|n-\tau|+1)!!}\right]^2. \tag{1.131}$$

In the course of derivation of relation (1.131), an estimate for the function $P_n^m(x)$ finer than (1.30) was used, i.e.,

$$|P_n^m(x)|<\sqrt{\frac{(n+m)!}{(n-m)!}}, \tag{1.132}$$

which is obtained from the representation [26]

$$P_n^m(x)=i^m\sqrt{\frac{(n+m)!}{(n-m)!}}P_{m0}^{n}(x)$$

and inequality (1.130).

Dividing the sum with respect to τ in (1.131) into two parts: $\tau<n$ and $\tau\geq n$, performing the appropriate substitutions by analogy with the proof of lemma 4 of § 1.2, we will come to the validity of inequality (1.126) under the condition that

$$b_{j+2}+h_{j+2}<b_{j+1},\quad j=0,\ 1,\ \ldots,\ \nu-2. \tag{1.133}$$

Inequality (1.133) imposes limitations on the arrangement of the spheres: they must not touch each other.

We now turn to the proof of inequality (1.127). From the estimate

$$\left|\frac{q_{j+1}h_n(k_{j+1}b_{j+1})\,j_\tau^*(k_{j+1}b_{j+2})}{q_jh_n(k_jb_{j+1})\,j_n^*(k_jb_{j+1})}\right|<\text{const}_9\left|\frac{\zeta_n'(k_{j+1}b_{j+1})\,j_\tau^*(k_{j+1}b_{j+2})}{\psi_n'(k_{j+1}b_{j+1})\,h_n^*(k_{j+1}b_{j+1})}\right|,$$

obtained from lemma 2 of § 1.2, we have

$$|a_{\tau lnm2j+1}^{(2j+2)}|<\text{const}_9|a_{\tau lnm2j}^{(2j+2)}|. \tag{1.134}$$

Relations (1.134) and (1.126) demonstrate the validity of relation (1.127).

Inequalities (1.128) and (1.129) are proven exactly as expressions (1.126) and (1.127), respectively.

Thus, conditions (1.126)-(1.129) take place, and therefore T in system (1.97) acts from $\tilde{l}_2$ into $\tilde{l}_2$ and is completely continuous. /43

Hence, all the conditions of Nikol'skiy's theorems have been fulfilled, and consequently, Fredholm's alternative applies. We will formulate it with reference to the problem at hand.

Fredholm's Alternative. In order for equation (1.97) to have a solution for any Φ, it is necessary and sufficient that the homogeneous equation

$$(W + T)Z = 0 \tag{1.135}$$

have only a trivial solution.

Before proving that equation (1.135), corresponding to the homogeneous system (1.92) and (1.94) (when $\Phi_{nm}^{(i)} \equiv 0$) has only a zero solution, we will prove the following theorem.

Theorem 1. It follows from the condition $Z = \left\{Z_{nm}^{(s)}\right\} \in \tilde{l}_2$ (s = 0, 1, ..., 2ν - 1; n = 0, 1, ...; m = -n, ..., n) that both the series (1.83) and the series obtained from them by differentiating with respect to spherical coordinates a finite number of times converge absolutely and uniformly.

Proof. It follows from the condition $Z\in\tilde{l}_2$ that the coefficients $Z_{nm}^{(s)}$ are absolutely and uniformly limited, i.e., $|Z_{nm}^{(s)}| < \text{const}_{10}$, which according to relations (1.90) and lemma 2 of § 1.2 leads to the following estimates for the coefficients $A_{nm}^{(j)}$ and $B_{nm}^{(j)}$:

$$|A_{nm}^{(j)}| < \text{const}_{11} \sqrt{\frac{(n-m)!}{(n+m)!}} \frac{(2n-1)!!}{|k_j b_j|^n}, \quad j=1, 2, \ldots, \nu;$$

$$|B_{nm}^{(j)} < \text{const}_{12} \sqrt{\frac{(n-m)!}{(n+m)!}} \frac{|k_j b_{j+1}|^n}{(2n+1)!!}, \quad j=0, 1, \ldots, \nu-1. \tag{1.136}$$

On the other hand, from the recurrance relations for associated Legendre functions and their derivatives one can deduce the equality

$$\frac{d}{d\theta} P_n^m(\cos\theta) = \frac{1}{2}\left[P_n^{m+1}(\cos\theta) - (n-m+1)(n+m) P_n^{m-1}(\cos\theta)\right], \tag{1.137}$$

which by virtue of inequality (1.132) gives

$$\left|\frac{d}{d\theta} P_n^m(\cos\theta)\right| < \text{const}_{13}\, n \sqrt{\frac{(n+m)!}{(n-m)!}}. \tag{1.138}$$

Differentiating the right and left members of expression (1.137) (s - 1) times and using inequalities (1.138), it is easy to estimate by mathematical induction the derivative of s-th order of the function $P_n^m(\cos\theta)$:

$$\left|\frac{d^s}{d\theta^s} P_n^m(\cos\theta)\right| < \text{const}_{14}\, n^s \sqrt{\frac{(n+m)!}{(n-m)!}}. \tag{1.139}$$

Relations (1.136), (1.139) and

$$\left|\frac{d^s}{dr_j^s} j_n(k_j r_j)\right| < \text{const}_{15}\, n^s \frac{|k_j r_j|^n}{(2n+1)!!},$$

$$\left|\frac{d^s}{dr_j^s} h_n(k_j r_j)\right| < \text{const}_{16}\, n^s \frac{(2n-1)!!}{|k_j r_j|^n}, \tag{1.140}$$

obtained like inequalities (1.29), make it possible to estimate the derivative $\frac{\partial^{s_1+s_2+s_3}}{\partial r_j^{s_1} \partial\theta_j^{s_2} \partial\phi_j^{s_3}}$ of the common terms of series (1.83):

$$\left|\frac{\partial^{s_1+s_2+s_3}}{\partial r_j^{s_1} \partial\theta_j^{s_2} \partial\varphi_j^{s_3}} A_{nm}^{(j)} j_n(k_j r_j) P_n^m(\cos\theta_j) e^{im\varphi_j}\right| < \text{const}_{17}\, n^{s_1+s_2+s_3} \left|\frac{r_j}{b_j}\right|^n,$$

$$\left|\frac{\partial^{s_1+s_2+s_3}}{\partial r_j^{s_1} \partial\theta_j^{s_2} \partial\varphi_j^{s_3}} B_{nm}^{(j)} h_n(k_j r_{j+1}) P_n^m(\cos\theta_j) e^{im\varphi_{j+1}}\right| < \text{const}_{18}\, n^{s_1+s_2+s_3} \times$$

$$\times \left|\frac{b_{j+1}}{r_{j+1}}\right|^n. \tag{1.141}$$

It follows that the series obtained from the expressions (1.83) by differentiating s_1, s_2, s_3 times with respect to the coordinates r_j, θ_j, ϕ_j respectively are majorized by the convergent numerical series

$$|T_j| < \text{const}_{19} \sum_{n=0}^{\infty} \left(\left| \frac{r_j}{b_j} \right|^n + \left| \frac{b_{j+1}}{r_{j+1}} \right|^n \right) n^{s_1+s_2+s_3}, \quad j = 1, 2, \ldots, \nu,$$

since for j the regions $r_j < b_j$ and $r_{j+1} > b_{j+1}$. For T_0, an analogous result is obtained from estimates (1.101) and (1.141). Thus, the theorem has been proven.

We will now show that equation (1.135) has only a trivial solution in $\tilde{\mathcal{Z}}_2$.

We will assume the opposite, i.e., that in $\tilde{\mathcal{Z}}_2$ there will be a $\tilde{\bar{Z}} = \tilde{\bar{Z}}^{(j)}_{nm}$ not identically equal to zero and at the same time satisfying equation (1.135).[17] This means that there exists at least one $j = j_0$ for which $\tilde{\bar{Z}}^{(j_0)}_{nm} \neq 0$, and hence, by virtue of relations (1.90), also

$$\tilde{\bar{A}}^{(j_0)}_{nm} \neq 0 \tag{1.142}$$

or

$$\tilde{\bar{B}}^{(j_0)}_{nm} \neq 0 \tag{1.143}$$

System (1.135) corresponds to a homogeneous boundary value deflection problem, which in the absence of a source and with the condition of radiation at infinity, and also owing to the contribution of the tangential components of the field and the theorem of uniqueness of the solution of the homogeneous system of Maxwell equations in a multiply connected region has only a zero solution.[18]

Hence, by virtue of the theorem just proven, it follows that in the first medium, for example, $\tilde{\bar{T}}_1 \equiv 0$, or, what amounts to the same thing

$$\sum_{n=0}^{\infty} \sum_{m=-n}^{n} \bar{\bar{A}}^{(1)}_{nm} j_n(k_1 r_1) P_n^m(\cos\theta_1) e^{im\varphi_1} + \bar{\bar{B}}^{(1)}_{nm} h_n(k_1 r_2) P_n^m(\cos\theta_2) e^{im\varphi_2} \equiv 0. \tag{1.144}$$

[17]The two dashes above the symbol will denote the quantities pertaining to the homogeneous boundary value problem (1.135).

[18]In reference to this question, see for example [9].

We will apply the addition theorem (1.70) to the second sum in (1.144) and change the order of summation.[19]

$$\sum_{n=0}^{\infty}\sum_{m=-n}^{n}\left[\overline{\overline{A}}^{(1)}_{nm}j_n(k_1r_1)+h_n(k_1r_1)\sum_{p=0}^{\infty}\sum_{\lambda=-p}^{p}\overline{\overline{B}}^{(1)}_{p\lambda}K^{(-1)}_{nmp\lambda 1}\right]\times$$
$$\times P_n^{\lambda}(\cos\theta_1)e^{i\lambda\varphi_1}\equiv 0.$$

Hence, in view of the orthogonality of the Tesseral functions, we obtain

$$\overline{\overline{A}}^{(1)}_{nm}j_n(k_1r_1)+h_n(k_1r_1)\sum_{p=0}^{\infty}\sum_{\lambda=-p}^{p}\overline{\overline{B}}^{(1)}_{p\lambda}K^{(-1)}_{nmp\lambda 1}\equiv 0. \tag{1.145}$$

Since the functions $j_n(z)$ and $h_n(z)$ are linearly independent, identity (1.145) can take place only provided that

$$\overline{\overline{A}}^{(1)}_{nm}\equiv 0, \tag{1.146}$$

$$\sum_{p=0}^{\infty}\sum_{\lambda=-p}^{p}\overline{\overline{B}}^{(1)}_{p\lambda}K^{(-1)}_{nmp\lambda 1}\equiv 0. \tag{1.147}$$

Multiplying equality (1.147) by $K_{\tau\zeta nml}$, then summing it over m from -n to n and over n from 0 to infinity (using formula (1.74)), we will obtain

$$\overline{\overline{B}}^{(1)}_{p\lambda}\equiv 0 \tag{1.148}$$

The following theorem will be required for further consideration.

Theorem 2. It follows from the condition $\overline{\overline{A}}^{(j)}_{nm}\equiv 0\equiv\overline{\overline{B}}^{(j)}_{nm}$ that $\overline{\overline{A}}^{(j+1)}_{nm}\equiv 0\equiv\overline{\overline{B}}^{(j+1)}_{nm}$.

Proof. Assuming that $A^{(0)}_{nm}=0$, condition (1.148) reduces system (1.86) to the following: /46

$$q_{j+1}j_n(k_{j+1}b_{j+1})\overline{\overline{A}}^{(j+1)}_{nm}+q_{j+1}h_n(k_{j+1}b_{j+1})\times$$
$$\times\sum_{\tau=0}^{\infty}\sum_{l=-\tau}^{\tau}\overline{\overline{B}}^{(j+1)}_{\tau l}K^{(-1)}_{nm\tau l\,j+1}=0,$$

$$\psi_n'(k_{j+1}b_{j+1})\overline{\overline{A}}^{(j+1)}_{nm}+\zeta_n'(k_{j+1}b_{j+1})\sum_{\tau=0}^{\infty}\sum_{l=-\tau}^{\tau}\overline{\overline{B}}^{(j+1)}_{\tau l}K^{(-1)}_{nm\tau l\,j+1}=0,$$

$$j=1,\ 2,\ \ldots,\ \nu-1;\quad n=0,\ 1,\ \ldots;\quad m=-n,\ \ldots,\ n. \tag{1.149}$$

Excluding the coefficient $\overline{\overline{B}}^{(j+1)}_{\tau\zeta}$ from system (1.149) and considering that the Wronskian of the functions $\psi n(z)$, $\zeta n(z)$ is

---

[19]The validity of this operation is guaranteed by theorem 1 of the present paragraph.

$$\psi_n(z)\zeta_n'(z) - \zeta_n(z)\psi_n'(z) = i. \tag{1.149a}$$

we will obtain $\bar{\bar{A}}_{nm}^{(j+1)} \equiv 0$.

The same identity $\bar{\bar{B}}_{nm}^{(j+1)} \equiv 0$ is obtained from system (1.149) by excluding $\bar{\bar{A}}_{nm}^{(j)}$ by the same method as was used to obtain relation (1.148) from (1.147). The theorem has been proven.

From the theorem and equalities (1.146), (1.148) it follows by induction that for any $j = j_0$

$$\bar{\bar{A}}_{nm}^{(j_0)} \equiv 0 \equiv \bar{\bar{B}}_{nm}^{(j_0)}.$$

We have reached a contradiction with the assumption of (1.142), (1.143). Thus, equation (1.135) has only a trivial solution, and system (1.97) is uniquely solvable in $\tilde{l}_2$.

Let us note at this point that by analogy with the reasoning in [40, 41], pertaining to l_2, it can be shown that system (1.97) or, what amounts to the same thing, (1.95), is also solvable in l_2 by reduction.

If follows from the above that solutions (1.83) via relations (1.2) satisfy the Maxwell equations, the boundary conditions on the interfaces, the Sommerfeld condition, and hence, realize the solution of the problem formulated in § 1.1.

Let us now consider the case

$$\psi_n'(k_{j+1}b_{j+1}) = 0, \tag{1.150}$$

i.e., remove the limitation (1.89) imposed on all the preceding discussions.

According to Lommel's theorem [42], the equation $\Psi_n'(z) = 0$ has only real roots. Therefore, the question of unfulfillability of inequality (1.89) makes sense only when k_{j+1} is real.

Let the following equality be valid for a certain $n = n_0$ and $j = j_0$:

$$\psi_{n_0}'(k_{j_0+1}b_{j_0+1}) = 0. \tag{1.151}$$

Without detracting from the generality of our arguments, we will postulate that $j_0 \geqslant 1$. Then, transposing the equations in system (1.86) corresponding to $j = j_0$, $n = n_0$, and taking (1.151) into account, we will write them as follows:

$$B_{n_0m}^{(j_0)} = 0 \cdot A_{n_0m}^{(j_0+1)} - \frac{\psi_{n_0}'(k_{j_0}b_{j_0+1})}{\zeta_{n_0}'(k_{j_0}b_{j_0+1})} \sum_{\tau=0}^{\infty} \sum_{l=-\tau}^{\tau} A_{\tau l}^{(j_0)} K_{n_0m\tau l j_0} +$$

$$+ \frac{\zeta_{n_0}'(k_{j_0+1}b_{j_0+1})}{\zeta_{n_0}'(k_{j_0}b_{j_0+1})} \sum_{\tau=0}^{\infty} \sum_{l=-\tau}^{\tau} B_{\tau l}^{(j_0+1)} K_{n_0m\tau l\, j_0+1}^{(-1)}. \tag{1.152}$$

$$A_{n_0m}^{(j_0+1)}=\frac{q_{j_0}h_{n_0}(k_{j_0}b_{j_0+1})}{q_{j_0+1}j_{n_0}(k_{j_0+1}b_{j_0+1})}B_{n_0m}^{(j_0)}+\frac{q_{j_0}j_{n_0}(k_{j_0}b_{j_0+1})}{q_{j_0+1}j_{n_0}(k_{j_0+1}b_{j_0+1})}\times$$

$$\times\sum_{\tau=0}^{\infty}\sum_{l=-\tau}^{\tau}A_{\tau l}^{(j_0)}K_{n_0m\tau lj_0}-\frac{h_{n_0}(k_{j_0+1}b_{j_0+1})}{j_{n_0}(k_{j_0+1}b_{j_0+1})}\sum_{\tau=0}^{\infty}\sum_{l=-\tau}^{\tau}B_{\tau l}^{(j_0+1)}K_{n_0m\tau l\,j_0+1}. \qquad (1.152)$$

With the a

With the aid of the substitution (1.90) and consideration of relations (1.152), system (1.95) for the case (1.150) will become

$$\sum_{l=0}^{2\nu-1}Z_{nm}^{(s)}a_{ls*}^{(n)}+\sum_{l=0}^{2\nu-1}\sum_{\tau=0}^{\infty}\sum_{l=-\tau}^{\tau}Z_{\tau l}^{(l)}a_{\tau lnms*}^{(l)}=\Phi_{nm}^{(s)}, \qquad (1.153)$$

$$s=0,\ 1,\ \ldots,\ 2\nu-1;\quad n=0,\ 1,\ \ldots;\quad m=-n,\ \ldots,\ n,$$

where

$$a_{ls_*}^{(n)}=(b_{ls}^{(n)}-\delta_{ls})(1-\delta_{nn_0})+(b_{ls0}^{(n)}-\delta_{ls})\delta_{nn_0},$$

$$b_{ls0}^{(n)}=a_{n0}^{(s)}\delta_{ls+(-1)^s},$$

$$a_{n0}^{(s)}=\begin{cases}a_{n*}^{(2j_0+1)} & \text{for}\quad s=2j_0+1,\\ 0 & \text{for}\quad s=2j_0,\\ a_n^{(s)} & \text{for}\quad s\neq 2j_0,\quad 2j_0+1,\end{cases}$$

$$a_{n*}^{(2j_0+1)}=\frac{q_jh_n(k_jb_{j+1})j_n^*(k_jb_{j+1})}{q_{j+1}j_n(k_{j+1}b_{j+1})h_n^*(k_jb_j)}\delta_{jj_0},$$

$a_{\tau l nms*}^{(i)}$ is defined for indices i, s, not respectively equal to $2j_0$ - 1, $2j_0$; $2j_0+2$, $2j_0$; $2j_0-1$, $2j_0+1$; $2j_0+2$, $2j_0+1$ as $a_{\tau l nms}^{(i)}$, according to expressions (1.93), for the other relations of i and s as follows:

$$a_{\tau ln_0m2j_0*}^{(2j_0-1)}=-\sqrt{\frac{(\tau-l)!(n+m)!}{(\tau+l)!(n-m)!}}\times$$

$$\times\frac{\psi_n'(k_jb_{j+1})h_\tau^*(k_jb_j)}{\zeta_n'(k_jb_{j+1})j_n^*(k_jb_{j+1})}K_{nm\tau lj}\delta_{jj_0}\delta_{nn_0}, \qquad (1.154)$$

$$a_{\tau ln_0m2j_0*}^{(2j_0+2)}=\sqrt{\frac{(\tau-l)!(n+m)!}{(\tau+l)!(n-m)!}}\times \qquad \text{/48}$$

$$\times\frac{\zeta_n'(k_{j+1}b_{j+1})j_\tau^*(k_{j+1}b_{j+1}')}{\zeta_n'(k_jb_{j+1})j_n^*(k_jb_{j+1})}K_{nm\tau lj+1}^{(-1)}\delta_{jj_0}\delta_{nn_0},$$

$$a_{\tau ln_0m\,2j_0+1*}^{(2j_0-1)}=\sqrt{\frac{(\tau-l)!(n+m)!}{(\tau+l)!(n-m)!}}\times$$

$$\times\frac{q_jj_n(k_jb_{j+1})h_\tau^*(k_jb_j)}{q_{j+1}j_n(k_{j+1}b_{j+1})h_n^*(k_jb_j)}K_{nm\tau lj}\delta_{jj_0}\delta_{nn_0},$$

$$a^{(2j_0+2)}_{\tau l n_0 m\, 2j_0+1^*} = -\sqrt{\frac{(\tau-l)!\,(n+m)!}{(\tau+l)!\,(n-m)!}}\times$$

$$\times\frac{h_n(k_{j+1}b_{j+1})\,j^*_\tau(k_{j+1}b_{j+2})}{j_n(k_{j+1}b_{j+2})\,h^*_n(k_jb_j)}K^{(-1)}_{nmd\,j+1}\delta_{jj_0}\delta_{nn_0}. \tag{1.154}$$

If by analogy with (1.135), system (1.153) is written in the form

$$(W_* + T)Z = \Phi \tag{1.155}$$

where W_* is an operator with kernel $\alpha^{(n)}_{is^*}$, and T_* is an operator with kernel $a^{(i)}_{\tau lnms^*}$, it can be shown that W_* is a reversible operator and T_* is a completely continuous operator in $\tilde{l}_2$. For this it is obviously sufficient to show that

$$\det\alpha^{(n_0)}_* \neq 0 \quad (\alpha^{(n)}_* = \{\alpha^{(n)}_{is^*}\}), \tag{1.156}$$

$$\sum_{\tau=0}^{\infty}\sum_{l=-\tau}^{\tau}|a^{(l)}_{\tau l n_0 m s^*}|^2 < \infty. \tag{1.157}$$

We will prove the validity of condition (1.156). It is easy to see that the matrix $\alpha^{(n_0)}_*$ will also be quasi-diagonal and may be obtained from matrix (1.106) $\alpha^{(n)}$ for $n=n_0$, if the j_0 cell of the main diagonal is replaced by the determinant

$$\begin{vmatrix} -1 & a^{(2j_0+1)}_{n_0^*} \\ 0 & -1 \end{vmatrix}.$$

Moreover

$$\det\alpha^{(n_0)}_* = \prod_{j=0}^{\nu-1}{}'^{(j_0)}\left(1 - a^{(2j)}_{n_0}a^{(2j+1)}_{n_0}\right), \tag{1.158}$$

where the prime of the product with index j_0 means that the time corresponding to $j=j_0$ has been eliminated from the product.

According to inequality (1.108), the validity of relation (1.156) follows from (1.158). If however, condition (1.151) is fulfilled for a given n_0 for

several j: j_0, j_1, ..., j_p, then, applying all of the above reasoning without any substantial modification, we will obtain /49

$$\det \alpha^{(n_0)} = \prod_{j=0}^{\nu-1} (j_0, j_1, \ldots, j_p)^r \left(1 - a_{n_0}^{(2j)} a_{n_0}^{(2j+1)}\right) \neq 0,$$

i.e., relation (1.156) takes place in this case as well.

In order to prove statement (1.157), it is sufficient to show, as can be readily seen from expressions (1.154) and inequalities (1.126)-(1.129), that

$$\sum_{\tau=1}^{\infty} \sum_{l=-\tau}^{\tau} \sqrt{\frac{(\tau-l)!}{(\tau+l)!}} \left| h_\tau^* (k_{j_0} b_{j_0}) K_{n_0 m \tau l j_0} \right| < \infty, \tag{1.159}$$

$$\sum_{\tau=1}^{\infty} \sum_{l=-\tau}^{\tau} \sqrt{\frac{(\tau-l)!}{(\tau+l)!}} \left| j_\tau^* (k_{j_0+1} b_{j_0+2}) K_{n_0 m \tau l j_0+1} \right| < \infty. \tag{1.160}$$

Thus, relation (1.159) follows from the estimate

$$\sum_{\tau=1}^{\infty} \sum_{l=-\tau}^{\tau} \sqrt{\frac{(\tau-l)!}{(\tau+l)!}} \left| h_\tau^* (k_{j_0} b_{j_0}) K_{n_0 m \tau l j_0} \right| < \text{const}_{20} \sum_{\tau=1}^{\infty} \frac{(2\tau-1)!! \tau^2}{(2|\tau-n_0|+1)!!} \frac{|k_j h_{j+1}|^{|\tau-n_0|}}{|k_{j_0} b_{j_0}|^{\tau}}, \tag{1.161}$$

obtained with the aid of the same inequalities that were used in proving statement (1.122). The convergence of the series to the right of the inequality sign in (1.161) is established by means of d'Alembert's criterion under the condition $h_{j0} + 1 < b_{j0}$, which always applies.

Relation (1.160) is also valid by virtue of the following estimate:

$$\sum_{\tau=1}^{\infty} \sum_{l=-\tau}^{\tau} \sqrt{\frac{(\tau-l)!}{(\tau+l)!}} \left| j_\tau^* (k_{j_0+1} b_{j_0+2}) K_{n_0 m \tau l j_0+1}^{(-1)} \right| <$$

$$< \text{const}_{21} \sum_{\tau=1}^{\infty} \tau^2 \frac{|k_{j_0+1} b_{j_0+1}|^{\tau} |k_{j_0+1} h_{j_0+2}|^{|\tau-n_0|}}{(2\tau+1)!! (2|\tau-n_0|+1)!!}.$$

If several n exist for which equality (1.151) becomes an identity, then for each such n, system (1.86) is rearranged by analogy with the above discussed case of (1.152) when $n = n_0$, and all the existence and uniqueness theorems hold for this case as well.

Let us note at this point that in the course of transformations of system (1.86) to the form (1.152), it was assumed that

$$j_{n0}(k_{j0+1} b_{j0+1}) \neq 0, \tag{1.162}$$

which is always valid.

Indeed, an assumption opposed to inequality (1.162) together with inequality (1.151) would mean that $(k_{j0+1}b_{j0+1})$ is a double root of the equation $\psi n_0(z) = 0$, which is incorrect, since cylindrical functions have no multiple roots [42], different from zero. /50

This completes the case discussed above.

From the very beginning of the solution of the problem, in order to avoid cumbersome operations in constructing the solution and in its validation, the desired Debye potentials u_j and v_j were combined into a single generalized potential T_j (1.5) with the aid of appropriate notation (see reference on p. 14). However, later on, in order to write the component intensities of the electromagnetic field in each of the media, we will have to separate again all the expressions under consideration. We will therefore agree to provide all the quantities pertaining to the potential U with the subscript (u), and those pertaining to V, with the subscript (v). In this case, for example, the solutions of system (1.95) and the coefficients $A_{nm}^{(j)}$, $B_{nm}^{(j)}$ expressed in terms of them, depending on the type of potential considered will have the form of either $Z_{nm(u)}^{(j)}$, $A_{nm(u)}^{(j)}$, $B_{nm(u)}^{(j)}$, or $Z_{nm(v)}^{(j)}$, $A_{nm(v)}^{(j)}$, $B_{nm(v)}^{(j)}$.

Then, taking the designations (1.5), (1.8), (1.75)-(1.85) into account, we have:

$$\left.\begin{aligned} U_{00} &= \sum_{n=0}^{\infty}\sum_{m=-1}^{1} A_{nm(u)}^{(0)} j_n(k_0 r_1) P_n^m(\cos\theta_1) e^{im\varphi_1} \\ V_{00} &= \sum_{n=0}^{\infty}\sum_{m=-1}^{1} A_{nm(v)}^{(0)} j_n(k_0 r_1) P_n^m(\cos\theta_1) e^{im\varphi_1} \end{aligned}\right\} \quad \text{for} \quad r_1 < h_1;$$

$$\left.\begin{aligned} U_{00} &= \sum_{n=0}^{\infty}\sum_{m=-1}^{1} t_{nm(u)}^{(0)} h_n(k_0 r_1) P_n^m(\cos\theta_1) e^{im\varphi_1} \\ V_{00} &= \sum_{n=0}^{\infty}\sum_{m=-1}^{1} t_{nm(v)}^{(0)} h_n(k_0 r_1) P_n^m(\cos\theta_1) e^{im\varphi_1} \end{aligned}\right\} \quad \text{for} \quad r_1 > h_1; \qquad (1.163)$$

$$U_{0s}=\sum_{n=0}^{\infty}\sum_{m=-n}^{n}B^{(0)}_{nm\,(u)}h_n(k_0r_1)\,P_n^m(\cos\theta_1)\,e^{im\varphi_1},$$

$$V_{0s}=\sum_{n=0}^{\infty}\sum_{m=-n}^{n}B^{(0)}_{nm\,(v)}h_n(k_0r_1)\,P_n^m(\cos\theta_1)\,e^{im\varphi_1};$$

$$U_j=\sum_{n=0}^{\infty}\sum_{m=-n}^{n}A^{(j)}_{nm\,(u)}j_n(k_jr_j)\,P_n^m(\cos\theta_j)\,e^{im\varphi_j}+$$
$$+B^{(j)}_{nm\,(u)}h_n(k_jr_{j+1})\,P_n^m(\cos\theta_{j+1})\,e^{im\varphi_{j+1}}, \qquad (1.164)$$

$$V_j=\sum_{n=0}^{\infty}\sum_{m=-n}^{n}A^{(j)}_{nm\,(v)}j_n(k_jr_j)\,P_n^m(\cos\theta_j)\,e^{im\varphi_j}+$$
$$+B^{(j)}_{nm\,(v)}h_n(k_jr_{j+1})\,P_n^m(\cos\theta_{j+1})\,e^{im\varphi_{j+1}};$$
$$j=1,\ 2,\ \ldots,\ \nu;\quad B^{(\nu)}_{nm\,(u)}=B^{(\nu)}_{nm\,(v)}=0. \qquad (1.165)$$ /51

Using relations (1.2) from expression (1.163)-(1.164), we will obtain the components of the primary $E^{(00)}$, $H^{(00)}$ and secondary $E^{(0s)}$, $H^{(0s)}$ electromagnetic fields in medium 0, and also, by means of addition theorems (1.70)-(1.71), the field vector components $E^{(j)}$, $H^{(j)}$ of medium j. Since we will need only the vector components $E^{(0s)}$, $H^{(0s)}$, we will give their expressions below:

$$E^{(0s)}_{r_1}=\frac{1}{r_1}\sum_{n=0}^{\infty}\sum_{m=-n}^{n}B^{(0)}_{nm\,(u)}n(n+1)\,h_n(k_0r_1)\,P_n^m(\cos\theta_1)\,e^{im\varphi_1},$$

$$E^{(0s)}_{\theta_1}=\frac{1}{r_1}\sum_{n=0}^{\infty}\sum_{m=-n}^{n}B^{(0)}_{nm\,(u)}\zeta_n'(k_0r_1)\,\tau_n^m(\theta_1)\,e^{im\varphi_1}-$$
$$-i\beta_0\sum_{n=0}^{\infty}\sum_{m=-n}^{n}\tilde{B}^{(0)}_{nm\,(v)}m\,h_n(k_0r_1)\,\pi_n^m(\theta_1)\,e^{im\varphi_1},$$

$$E^{(0s)}_{\varphi_1}=\frac{i}{r_1}\sum_{n=0}^{\infty}\sum_{m=-n}^{n}B^{(0)}_{nm\,(u)}m\zeta_n'(k_0r_1)\,\pi_n^m(\theta_1)\,e^{im\varphi_1}+$$
$$+\beta_0\sum_{n=0}^{\infty}\sum_{m=-n}^{n}B^{(0)}_{nm\,(v)}h_n(k_0r_1)\,\tau_n^m(\theta_1)\,e^{im\varphi_1}, \qquad (1.166)$$

$$H^{(0s)}_{r_1}=\frac{1}{r_1}\sum_{n=0}^{\infty}\sum_{m=-n}^{n}B^{(0)}_{nm\,(v)}n(n+1)\,h_n(k_0r_1)\,P_n^m(\cos\theta_1)\,e^{im\varphi_1},$$

$$H_{\theta_1}^{(0s)} = i\alpha_0 \sum_{n=0}^{\infty} \sum_{m=-n}^{n} B_{nm\,(u)}^{(0)} m h_n(k_0 r_1)\, \pi_n^m(\theta_1)\, e^{im\varphi_1} +$$

$$+ \frac{1}{r_1} \sum_{n=0}^{\infty} \sum_{m=-n}^{n} B_{nm\,(v)}^{(0)} \zeta_n'(k_0 r_1)\, \tau_n^m(\theta_1)\, e^{im\varphi_1},$$

$$H_{\phi_1}^{(0s)} = -\alpha_0 \sum_{n=0}^{\infty} \sum_{m=-n}^{n} B_{nm\,(u)}^{(0)} h_n(k_0 r_1)\, \tau_n^m(\theta_1)\, e^{im\varphi_1} +$$

$$+ \frac{i}{r_1} \sum_{n=0}^{\infty} \sum_{m=-n}^{n} B_{nm\,(v)}^{(0)} m \zeta_n'(k_0 r_1)\, \pi_n^m(\theta_1)\, e^{im\varphi_1}. \qquad (1.166)$$

Here /52

$$\tau_n^m(\theta) = \frac{d}{d\theta} P_n^m(\cos\theta),$$

$$\pi_n^m(\theta) = \frac{P_n^m(\cos\theta)}{\sin\theta}, \qquad (1.167)$$

α_0, β_0 are defined by formulas (1.1).

We will find the expressions for the components of secondary field (1.166) in the long-range zone, using representations of the functions $h_n(z)$ and $\xi'_n(z)$ asymptotic with respect to the argument

$$h_n(z) \sim i^{-(n+1)} \frac{e^{iz}}{z},$$

$$\zeta_n'(z) \sim i^{-n} e^{iz} \qquad (1.168)$$

and introducing the following notation:

$$S_1(\theta_1,\ \varphi_1)=\sum_{n=0}^{\infty}\sum_{m=-n}^{n}B^{(0)}_{nm\,(u)}i^{-n}n(n+1)P_n^m(\cos\theta_1)e^{im\varphi_1},$$

$$S_2(\theta_1,\ \varphi_1)=\sum_{n=0}^{\infty}\sum_{m=-n}^{n}B^{(0)}_{nm\,(u)}i^{-n}\tau_n^m(\theta_1)e^{im\varphi_1},$$

$$S_3(\theta_1,\ \varphi_1)=\sum_{n=0}^{\infty}\sum_{m=-n}^{n}B^{(0)}_{nm\,(v)}i^{-n}m\pi_n^m(\theta_1)e^{im\varphi_1},$$

$$S_4(\theta_1,\ \varphi_1)=\sum_{n=0}^{\infty}\sum_{m=-n}^{n}B^{(0)}_{nm\,(u)}i^{-n}m\pi_n^m(\theta_1)e^{im\varphi_1},$$

$$S_5(\theta_1,\ \varphi_1)=\sum_{n=0}^{\infty}\sum_{m=-n}^{n}B^{(0)}_{nm\,(v)}i^{-n}\tau_n^m(\theta_1)e^{im\varphi_1},$$

$$S_6(\theta_1,\ \varphi_1)=\sum_{n=0}^{\infty}\sum_{m=-n}^{n}B^{(0)}_{nm\,(v)}i^{-n}n(n+1)P_n^m(\cos\theta_1)e^{im\varphi_1},$$

$$\varkappa_0=\sqrt{\frac{\mu_0}{\varepsilon_0}}.$$

(1.169)

Then, after suitable transformations taking into account relations (1.1), (1.3) for the long-range zone of medium 0, we will have:

$$E^{(0s)}_{r_1}\sim\frac{e^{ik_0r_1}}{ik_0r_1^2}S_1(\theta_1,\ \varphi_1),\quad H^{(0s)}_{r_1}\sim\frac{e^{ik_0r_1}}{ik_0r_1^2}S_6(\theta_1,\ \varphi_1),$$

$$E^{(0s)}_{\theta_1}\sim\frac{e^{ik_0r_1}}{r_1}[S_2(\theta_1,\ \varphi_1)+i\varkappa_0S_3(\theta_1,\ \varphi_1)],$$

$$H^{(0s)}_{\theta_1}\sim\frac{e^{ik_0r_1}}{r_1}\left[-\frac{1}{\varkappa_0}S_4(\theta_1,\ \varphi_1)+S_5(\theta_1,\ \varphi_1)\right],$$

$$E^{(0s)}_{\varphi_1}\sim\frac{e^{ik_0r_1}}{r_1}[iS_4(\theta_1,\ \varphi_1)-\varkappa_0S_5(\theta_1,\ \varphi_1)],$$

$$H^{(0s)}_{\varphi_1}\sim\frac{e^{ik_0r_1}}{r_1}\left[\frac{1}{\varkappa_0}S_2(\theta_1,\ \varphi_1)+iS_3(\theta_1,\ \varphi_1)\right].$$

(1.170)

/53

The following relations may be obtained from expressions (1.170):

$$E_{\theta_1}^{(0s)} = x_0 H_{\phi 1}^{(0s)}, \quad E_{r_1}^{(0s)} = 0$$
$$E_{\phi_1}^{(0s)} = -x_0 H_{\theta 1}^{(0s)}, \quad H_{r_1}^{(0s)} = 0 \tag{1.171}$$

whence

$$E_{\theta_1}^{(0s)} E_{\phi 1}^{(0s)} + H_{\theta 1}^{(0s)} H_{\phi 1}^{(0s)} = 0 \tag{1.172}$$

i.e., as in the case of a single sphere, in the long-range zone approximation, the electromagnetic field of a nonconcentrically layered spherical particle also has a transverse character, and the electric and magnetic factors are mutually perpendicular.

We will mention a number of simplifying features for cases of vertical ($\theta_0 = 0$) and horizontal ($\theta_0 = \frac{\pi}{2}$) dipoles that are most important in theory and applications.

Verticle Dipole. By agreement[20] on the choice of the coordinate system $X_1Y_1Z_1$ in this particular case we have $\chi_1 = \frac{\pi}{2}$. Taking this into consideration, together with the fact that $p_1 = 0$ in expressions (1.76)-(1.77), (1.82), we will obtain:

$$A_{nm(v)}^{(0)} = 0,$$
$$A_{nm(u)}^{(0)} = \frac{ik_0 |p_2|}{h_1} (2n+1) h_n(k_0 h_1) \delta_{m0},$$
$$t_{nm(u)}^{(0)} = \frac{ik_0 |p_2|}{h_1} (2n+1) j_n(k_0 h_1) \delta_{m0}, \tag{1.173}$$
$$t_{nm(v)}^{(0)} = 0.$$

It also follows from relations (1.173), (1.90), (1.93) that

$$\Phi_{nm(v)}^{(j)} \equiv 0. \tag{1.174}$$

Condition (1.174) converts system (1.97), corresponding to potential V, to homogeneous system (1.135). Since it was shown previously that equation (1.135) has only a trivial solution in $\tilde{z}_2$, then $Z_{nm(v)}^{(j)} \equiv 0$, whence by relations (1.90) it follows that

---

[20]See page 12.

The quantity $\sigma'_D(0, 0)$, calculated in the direction of the incident wave, is called the backscattering cross-section σ'_B. Consequently, we have

$$\sigma'_B = \frac{4\pi}{k_0^4}(|S_7(0, 0)|^2 + |S_8(0, 0)|^2). \tag{1.206}$$

Having transformed expression (1.206) by using for this purpose the values of functions (1.167) $\tau_n^m(\theta)$ and $\pi_n^m(\theta)$ at zero

$$\tau_n^m(0) = \pi_n^m(0) = \begin{cases} \frac{1}{2} & \text{for } m = -1, \\ -\frac{n(n+1)}{2} & \text{for } m = 1, \\ 0 & \text{for } |m| \neq 1, \end{cases} \tag{1.207}$$

obtained with the aid of representations (1.137), and

$$\pi_n^m(\theta) = -\frac{1}{2m\cos\theta}\left[P_n^{m+1}(\cos\theta) + \right.$$
$$\left. + (n-m+1)(n+m)P_n^{m-1}(\cos\theta)\right], \tag{1.208}$$

and also the identity $|z_1+z_2|^2 + |z_1-z_2|^2 = 2|z_1|^2 + 2|z_2|^2$, we will have

$$\sigma'_B = \frac{2\pi}{k_0^4}\left[\left|\sum_{n=1}^{\infty} i^{-n}\left(\widetilde{B}^{(0)}_{n,-1(u)} - i\varkappa_0\widetilde{B}^{(0)}_{n,-1(v)}\right)\right|^2 + \right.$$
$$\left. + \left|\sum_{n=1}^{\infty} i^{-n}n(n+1)\left(\widetilde{B}^{(0)}_{n1(u)} + i\varkappa_0\widetilde{B}^{(0)}_{n1(v)}\right)\right|^2\right]. \tag{1.209}$$

We introduce the notation:

$$\Xi^{(1)}_{nm} = -\frac{2i^{n-1}\operatorname{sign} m}{k_0(2n+1)}\sqrt{\frac{(n+m)!\,n(n+1)}{(n-m)!}}\,\widetilde{B}^{(0)}_{nm(u)},$$
$$\Xi^{(2)}_{nm} = -\frac{2i^{n-1}\beta_0}{k_0^2(2n+1)}\sqrt{\frac{(n+m)!\,n(n+1)}{(n-m)!}}\,\widetilde{B}^{(0)}_{nm(v)}, \tag{1.210}$$

Then, expression (1.209) for σ'_B will take the form

$$\sigma'_B = \frac{\pi}{2k_0^2}\sum_{m=\pm1}\left|\sum_{n=1}^{\infty}(-1)^n(2n+1)\left(\Xi^{(1)}_{nm} - \Xi^{(2)}_{nm}\right)\right|^2. \tag{1.211}$$

we come to

$$\Upsilon_0 = \frac{4\pi}{k_0^2} \sum_{n=1}^{\infty} \sum_{m=-n}^{n} \left[\left| \widetilde{B}^{(0)}_{nm\,(u)} \right|^2 + \varkappa_0^2 \left| \widetilde{B}^{(0)}_{nm\,(v)} \right|^2 \right] \frac{n(n+1)(n+m)!}{(2n+1)(n-m)!}.$$

In terms of notation (1.210) the expression for γ_0 will assume the simple form

$$\Upsilon_0 = \pi \sum_{n=1}^{\infty} \sum_{m=-n}^{n} (2n+1)\left(\left| \Xi^{(1)}_{nm} \right|^2 + \left| \Xi^{(2)}_{nm} \right|^2 \right). \tag{1.216}$$

Directly following from the above are the expressions for the indicatrix and effective area of scattering:

$$\Upsilon(\theta_1, \varphi_1) = \frac{|S_7(\theta_1, \varphi_1)|^2 + |S_8(\theta_1, \varphi_1)|^2}{\pi k_0^2 \sum_{n=1}^{\infty} \sum_{m=-n}^{n} (2n+1)\left(\left| \Xi^{(1)}_{nm} \right|^2 + \left| \Xi^{(2)}_{nm} \right|^2 \right)} \tag{1.217}$$

$$\sigma_1 = \frac{1}{(k_0 b_1)^2} \sum_{n=1}^{\infty} \sum_{m=-n}^{n} (2n+1)\left(\left| \Xi^{(1)}_{nm} \right|^2 + \left| \Xi^{(2)}_{nm} \right|^2 \right). \tag{1.218}$$

Another important characteristic of the particle under consideration is the effective attenuation cross-section σ_2.[21] To calculate it, according to the optical theorem [44-- p. 204, 48--p. 72], it suffices to find the imaginary part of the amplitude of the electric field in the long-range zone, observed behind the particle in the direction of polarization of the primary field. More accurately, considering the adopted notation,

$$\sigma_2 = \frac{4}{k_0 (k_0 b_1)^2} (-\mathrm{Im}) S_7(\pi, 0). \tag{1.219}$$[22]

This in turn, by virtue of the relations

$$\tau_n^m(\pi) = -\pi_n^m(\pi) = (-1)^n \tau_n^m(0), \tag{1.220}$$

---

[21] Referred to πb_1^2.

[22] Usually σ_2 is determined by means of the surface integral over a sphere located in the distance zone (see for example [47, 10]). The optical theorem essentially consists in transforming this integral by the stationary phase method to the form of (1.219).

$$A^{(j)}_{nm\,(v)} = 0 = B^{(j)}_{nm\,(v)},\quad j = 1,\ 2,\ \ldots,\ \nu.$$

(1.175)

Horizontal Dipole. Here it is necessary to set $|p_2| = 0$, which, in view of relations (1.79), (1.82) leads to the equality

$$\left.\begin{aligned} A_{2n} &= 0, \\ t_{2n} &= 0, \end{aligned}\right\} \tag{1.176}$$

or, if the notations in (1.76), (1.82) are considered, to the following:

$$\left.\begin{aligned} A^{(0)}_{n0} &= 0, \\ t^{(0)}_{n0} &= 0. \end{aligned}\right\}$$

(1.177)

These are the only simplifications in the general expressions of the problem that can be made in this case.

To conclude this section, let us note that if the relations of parameters k_j and b_j are such that equality (1.151) applies, all the expressions (1.163)--(1.165) will remain valid if one assumes that the unknowns $Z^{(j)}_{nm*}$ are found from system (1.153).[23] The expressions relating to coefficients $A^{(j)}_{nm*}$, $B^{(j)}_{nm*}$ with the quantity $Z^{(j)}_{nm*}$ will remain the same as before.[24]

§ 1.4. Spheres Arbitrarily Located Inside One Another in a Field of the Plane Wave

It is well known that Maxwell equations can be reduced by means of the substitution

$$\begin{aligned} E^{(j)} &= \operatorname{curl}\operatorname{curl}\Pi^{(j)} \\ H^{(j)} &= \alpha_j \operatorname{curl}\Pi^{(j)} \end{aligned} \tag{1.178}$$

to the equation

$$\Delta\Pi^{(j)} + k_j^2\Pi^{(j)} = 0.$$

---

[23] All the expressions for this case are provided with an asterisk (*).
[24] See relation (1.90).

Here $\Pi^{(j)}$ is the Hertz vector of medium j, and Δ is the 3-dimensional Laplace operator. The Hertz vector, corresponding to the primary $E^{(00)}$, $H^{(00)}$ field of a dipole radiator with moment p_1 has the following projections in the $X_1Y_1Z_1$ coordinate system:

$$\mathbf{\Pi}^{(00)} = \{\Pi_0, 0, 0\}, \tag{1.179}$$

where

$$\Pi_0 = |\mathbf{p}_1| \frac{e^{ik_0R}}{R}, \quad R = \sqrt{h_1^2 + r_1^2 - 2r_1h_1\cos\theta_1}. \tag{1.180}$$

The solution of the problem formulated in the title of the present section will be obtained by means of the limiting conversion of the solution already discussed in § 1.3 for the case in which the source of electromagnetic waves is a horizontal electric dipole with moment p_1 (see Figure 1.1). To this end, we will direct the dipole p_1 to infinity without changing its orientation (parallel to axis X_1).

We will also correspondingly transform the expressions for the electromagnetic field compounds. Thus, if in the expansion

$$\Pi_0 = |\mathbf{p}_1| ik_0 \sum_{n=0}^{\infty} (2n+1) j_n(k_0r_1) h_n(k_0h_1) P_n(\cos\theta_1),$$

obtainable from expressions (1.13), (1.180) for $r_1 < h_1$ we separate the principal term of the asymptotic series for $h_1 \to \infty$ with the aid of representation (1.168), we will obtain:

$$\Pi_0 \sim |\mathbf{p}_1| \frac{e^{ik_0h_1}}{h_1} \sum_{n=0}^{\infty} (2n+1) i^{-n} j_n(k_0r_1) P_n(\cos\theta_1). \tag{1.181}$$

Since the series on the right in (1.181) is merely the expansion of the plane wave $e^{-ik_0r_1\cos\theta_1}$, the expression for Π_0 may be written as follows:

$$\Pi_0 \sim E_0 e^{-ik_0z}, \tag{1.182}$$

where

$$E_0 = |\mathbf{p}_1| \frac{e^{ik_0h_1}}{h_1}. \tag{1.183}$$

Using expressions (1.182), (1.179) in (1.178), we will have in the given approximation the following component of the primary field:

$$E_{x_1}^{(00)} \sim k_0^2 E_0 e^{-ik_0 z}, \quad H_{x_1}^{(00)} \sim 0, \quad H_{z_1} \sim 0,$$
$$E_{y_1}^{(00)} \sim 0, \quad E_{z_1}^{(00)} \sim 0, \quad H_{y_1}^{(00)} \sim -ik_0 \alpha_0 E_0 e^{-ik_0 z_1}, \tag{1.184}$$

and also the relation between them

$$E_{x_1}^{(00)} \sim -\varkappa_0 H_{y_1}^{(00)}. \tag{1.185}$$

Formulas (1.184), (1.185) show that we have obtained a plane wave propagating along the negative portion of axis Z_1, whose electric vector is polarized along axis X_1 (horizonal polarization).

We will now assume that the components of the primary field have the form

$$E_{x_1}^{(00)} = k_0^2 E_0 e^{-ik_0 z_1}, \quad H_{x_1}^{(00)} = H_{z_1}^{(00)} = 0,$$
$$E_{y_1}^{(00)} = E_{z_1}^{(00)} = 0, \quad H_{y_1}^{(00)} = -ik_0 \alpha_0 E_0 e^{-ik_0 z_1}, \tag{1.186}$$

which differs from the form of (1.184) in that the sign ~ has been replaced by an equality sign. Hence, it is obvious that in order to obtain the solution of the general problem of scattering of a plane electromagnetic wave by the body under consideration, it is sufficient[25] in all the expressions of the solution for the case of a horizontal dipole (§ 1.3) to separate the principal terms of the asymptotic series for $h_1 \to \infty$, which after suitable transformations by determining factors of the type of (1.183) will give us the desired solution. /56

We will introduce the following notation:[26]

$$g_n = \left\{ i^{-n-1} k_0 \frac{2n+1}{n(n+1)}, \quad -i^{-n} \alpha_0 \frac{2n+1}{n(n+1)} \right\},$$

$$\widetilde{A}_{nm}^{(0)} = \begin{cases} -n(n+1)\beta_{00} g_n & \text{for } m = -1, \\ \alpha_{00} g_n & \text{for } m = 1, \\ 0 & \text{for } |m| \neq 1, \end{cases}$$

$$\widetilde{X}_{nm}^{(0)} = \sqrt{\frac{(n+m)!}{(n-m)!}}\, \widetilde{A}_{nm}^{(0)},$$

$$\widetilde{\Phi}_{nm}^{(j)} = \begin{cases} \dfrac{j_n(k_0 b_1)}{h_n(k_0 b_1)\, j_n^*(k_0 b_1)} \widetilde{X}_{nm}^{(0)}, & j = 0, \\ -\dfrac{\psi_n'(k_0 b_1)}{\psi_n'(k_1 b_1)\, h_n^*(k_1 b_1)} \widetilde{X}_{nm}^{(0)}, & j = 1, \\ 0, & j > 1. \end{cases} \tag{1.187}$$

---

[25] By virtue of the linearity of the equations and boundary conditions of the problem.

[26] Concerning the use of braces, see the reference on p. 14.

Then from relations (1.77), (1.76), (1.168) we will obtain:

$$A_{1n} \sim E_0 g_n, \quad A^{(0)}_{nm} \sim E_0 \widetilde{A}^{(0)}_{nm},$$

$$X^{(0)}_{nm} \sim E_0 \widetilde{X}^{(0)}_{nm}, \quad \Phi^{(j)}_{nm} \sim E_0 \widetilde{\Phi}^{(j)}_{nm}. \tag{1.188}$$

If in system (1.95) we now switch to new unknowns in accordance with the formula

$$Z^{(j)}_{nm} = E_0 \widetilde{Z}^{(j)}_{nm}, \tag{1.189}$$

then, taking relations (1.188) into account, we will obtain

$$\sum_{l=0}^{2\nu-1} \widetilde{Z}^{(l)}_{nm} a^{(n)}_{ls} + \sum_{l=0}^{2\nu-1} \sum_{\tau=0}^{\infty} \sum_{l=-\tau}^{\tau} \widetilde{Z}^{(l)}_{\tau l} a^{(l)}_{\tau lnms} = \widetilde{\Phi}^{(s)}_{nm}. \tag{1.190}$$

Like (1.95), this infinite system is uniquely solvable in $\widetilde{l}_2$, since the kernels of the operators have remained the same, and for the free term, by virtue of the estimate (resulting from lemma 2 of § 1.2)

$$\left|\widetilde{\Phi}^{(j)}_{nm}\right| < \text{const}_1 \left|\Phi^{(j)}_{nm}\right| \qquad /5$$

and inequality (1.98), $\phi \in \widetilde{l}_2$ is valid.

According to the relations of the equality (=) and equivalence (~) signs specified above, the solution of the problem for the case of a plane wave in each of (ν + 1) media will be determined from expressions for the case of a dipole radiator if $A^{(j)}_{nm(u)}$, $B^{(j)}_{nm(u)}$, $B^{(j)}_{nm(v)}$ is replaced by $E_0\widetilde{A}^{(j)}_{nm(u)}$, $E_0\widetilde{A}^{(j)}_{nm(v)}$, $E_0\widetilde{B}^{(j)}_{nm(u)}$, $E_0\widetilde{B}^{(j)}_{nm(v)}$ respectively in these expressions. The coefficients $\widetilde{A}^{(j)}_{nm}$, $\widetilde{B}^{(j)}_{nm}$ are related to $\widetilde{Z}^{(j)}_{nm}$ by expressions (1.90), (1.189), and subscripts u, v have the same meaning here as in symbols without the tilde (see p. 50).

The components of the secondary field (1.170) in the approximation of the long-range zone of medium 0 are similarly obtained.

Thus,

$$E^{(0s)}_{r_1} \sim E_0 \frac{e^{ik_0 r_1}}{ik_0 r_1^2} \widetilde{S}_1(\theta_1, \varphi_1), \quad H^{(0s)}_{r_1} \sim E_0 \frac{e^{ik_0 r_1}}{ik_0 r_1} \widetilde{S}_6(\theta_1, \varphi_1),$$

$$E^{(0s)}_{\theta_1} \sim E_0 \frac{e^{ik_0 r_1}}{r_1}\left[\widetilde{S}_2(\theta_1, \varphi_1) + i\varkappa_0 \widetilde{S}_3(\theta_1, \varphi_1)\right],$$

$$H^{(0s)}_{\theta_1} \sim E_0 \frac{e^{ik_0 r_1}}{r_1}\left[\widetilde{S}_5(\theta_1, \varphi_1) - \frac{i}{\varkappa_0}\widetilde{S}_4(\theta_1, \varphi_1)\right],$$

$$E^{(0s)}_{\phi_1} \sim E_0 \frac{e^{ik_0 r_1}}{r_1}\left[i\widetilde{S}_4(\theta_1, \varphi_1) - \varkappa_0 \widetilde{S}_5(\theta_1, \varphi_1)\right], \tag{1.191}$$

$$H_{\varphi_1}^{(0s)} \sim E_0 \frac{e^{ik_0 r_1}}{r_1}\left[\frac{1}{\varkappa_0}\widetilde{S}_2(\theta_1,\ \varphi_1) + i\widetilde{S}_3(\theta_1,\ \varphi_1)\right], \tag{1.191}$$

where

$$\widetilde{S}_1(\theta_1,\ \varphi_1) = \sum_{n=0}^{\infty}\sum_{m=-n}^{n} \widetilde{B}_{nm\,(u)}^{(0)}\, i^{-n}\, n(n+1)\, P_n^m(\cos\theta_1)\, e^{im\varphi_1},$$

$$\widetilde{S}_2(\theta_1,\ \varphi_1) = \sum_{n=0}^{\infty}\sum_{m=-n}^{n} \widetilde{B}_{nm\,(u)}^{(0)}\, i^{-n}\tau_n^m(\theta_1)\, e^{im\varphi_1},$$

$$\widetilde{S}_3(\theta_1,\ \varphi_1) = \sum_{n=0}^{\infty}\sum_{m=-n}^{n} \widetilde{B}_{nm\,(v)}^{(0)}\, i^{-n} m\pi_n^m(\theta_1)\, e^{im\varphi_1},$$

$$\widetilde{S}_4(\theta_1,\ \varphi_1) = \sum_{n=0}^{\infty}\sum_{m=-n}^{n} \widetilde{B}_{nm\,(u)}^{(0)}\, i^{-n} m\pi_n^m(\theta_1)\, e^{im\varphi_1},$$

$$\widetilde{S}_5(\theta_1,\ \varphi_1) = \sum_{n=0}^{\infty}\sum_{m=-n}^{n} \widetilde{B}_{nm\,(v)}^{(0)}\, i^{-n}\tau_n^m(\theta_1)\, e^{im\varphi_1},$$

$$\widetilde{S}_6(\theta_1,\ \varphi_1) = \sum_{n=0}^{\infty}\sum_{m=-n}^{n} \widetilde{B}_{nm\,(v)}^{(0)}\, i^{-n}\, n(n+1)\, P_n^m(\cos\theta_1)\, e^{im\varphi_1}. \tag{1.192}$$

/58

It is evident from expressions (1.191) that the relations (1.171) also apply when the primary field is given in the form of a plane wave.

Let us note at this point that all of the above applies under condition (1.89). If the latter does not hold, however, i.e., equality (1.150) is fulfilled, the only change which must obviously be introduced into the above discussion consists in determining the unknown coefficients $\widetilde{Z}_{nm}^{(j)}$, not from equation (1.190), but from the following equation:

$$\sum_{l=0}^{2\nu-1} \widetilde{Z}_{nm}^{(s)} a_{ls*}^{(n)} + \sum_{i=0}^{2\nu-1}\sum_{\tau=0}^{\infty}\sum_{l=-\tau}^{\tau} \widetilde{Z}_{\tau l}^{(i)} a_{\tau lnms*}^{(i)} = \widetilde{\Phi}_{nm}^{(s)}, \tag{1.193}$$

where $\alpha_{is*}^{(n)}$ and $a_{\tau lnms*}^{(i)}$ are defined by expressions (1.154).

§ 1.5 Electromagnetic and Radar Characteristics

In this section, with a view to specific applications, we will consider k_0 to be a real number.

The transverse character of the electromagnetic field scattered by the body under consideration in the long-range zone of medium 0, established in

§ 1.3, §11.4, leads to the fact that the corresponding Poynting vector

$$P^{(0_s)} = E^{(0_s)} \times H^{(0_s)} \tag{1.194}$$

has only the radial component $p_r^{(0_s)}$ in the given approximation. Therefore, the intensity of the scattered field $I'(\theta_1, \phi_1)$ in the long-range zone is defined [43] as the absolute value of the real part of the time-averaged scattered field directed along the radius of the Poynting vector, and is numerically equal to the energy transferred by the wave per unit time through a unit area of the surface normal to the direction of propagation of the wave. This definition is equivalent to the following formula:

$$I'(\theta_1, \varphi_1) = \left| R \frac{1}{T} \int_0^T P_r^{(0s)} dt \right|, \tag{1.195}$$

where $T = \frac{2\pi}{\omega}$, ω having the same meaning as in expression (1.1).

Substituting relations (1.171) into (1.194), we come to the expression for $P_r^{(0_s)}$:

$$P_r^{(0s)} = E_{\theta_1}^{(0s)} H_{\phi_1}^{(0s)} - E_{\theta_1}^{(0s)}. \tag{1.196}$$

Using the identity of [43]

$$R \frac{1}{T} \int_0^T E_{\theta_1}^{(0s)} H_{\phi_1}^{(0s)} dt = \frac{1}{4} \left(E_{\theta_1}^{(0s)} \overline{H}_{\phi_1}^{(0s)} + \overline{E}_{\theta_1}^{(0s)} H_{\phi_1}^{(0s)} \right).$$

from equality (1.195), taking expressions (1.196) and (1.171) into consideration, we will obtain[27]

$$I'(\theta_1, \phi_1) = \frac{1}{2x_0} \left(\left| E_{\theta_1}^{(0s)} \right|^2 + \left| E_{\phi_1}^{(0s)} \right|^2 \right). \tag{1.197}$$

If the notation

$$\begin{aligned} S_7(\theta_1, \varphi_1) &= \widetilde{S}_2(\theta_1, \varphi_1) + i x_0 \widetilde{S}_3(\theta_1, \varphi_1), \\ S_8(\theta_1, \varphi_1) &= i \widetilde{S}_4(\theta_1, \varphi_1) - x_0 \widetilde{S}_5(\theta_1, \varphi_1), \end{aligned} \tag{1.198}$$

---

[27]Here and below, the dash over the symbol denotes a complex conjugate.

is introduced, and relations (1.191) are taken into account, formula (1.197) may be given the form

$$I'(\theta_1, \varphi_1)=\frac{|E_0|^2}{2\varkappa_0 r_1^2}(|S_7(\theta_1, \varphi_1)|^2+|S_8(\theta_1, \varphi_1)|^2). \tag{1.199}$$

We will find the expressions for the intensity $I_0(\theta_1, \phi_1)$ of the primary field. To do so, in formulas (1.194)-(1.196) we will replace $P_r^{(0s)}$ by $P_r^{(00)}$ and, using relations (1.186), (1.185), by analogy with the above we will obtain

$$I_0(\theta_1, \varphi_1)=\frac{k_0^4|E_0|^2}{2\varkappa_0}. \tag{1.200}$$

The ratio $\frac{I'(\theta_1, \phi_1)}{I_0(\theta_1, \phi_1)}$ will give us the relative values of the intensity

$$I(\theta_1, \varphi_1)=\frac{1}{k_0^4 r_1^2}(|S_7(\theta_1, \varphi_1)|^2+|S_8(\theta_1, \varphi_1)|^2). \tag{1.201}$$

A number of important characteristics of the electromagnetic field are connected with the intensity $I(\theta_1, \phi_1)$. One of them is the dimensionless direction function $F(\theta_1, \phi_1)$, defined as [44]:

$$F(\theta_1, \varphi_1)=(k_0 r_1)^2 I(\theta_1, \varphi_1). \tag{1.202}$$

The quantity $\frac{1}{k_0^2} F(\theta_1, \phi_1)$ has the dimension of area. The relative /60 values of $I(\theta_1, \phi_1)$ or $F(\theta_1, \phi_1)$ may be plotted on a polar diagram against angle θ_1 for a fixed ϕ_1. This diagram is called the scattering diagram of the given body.

The following formula follows from (1.201), (1.202):

$$F(\theta_1, \varphi_1)=\frac{1}{k_0^2}(|S_7(\theta_1, \varphi_1)|^2+|S_8(\theta_1, \varphi_1)|^2). \tag{1.203}$$

Another quantity related to $I(\theta_1, \phi_1)$ is the differential two-position scattering cross-section defined [45, 46] as follows:

$$\sigma_D'(\theta_1, \varphi_1)=4\pi r_1^2 I(\theta_1, \varphi_1), \tag{1.204}$$

or, taking relation (1.201) into account,

$$\sigma_D'(\theta_1, \varphi_1)=\frac{4\pi}{k_0^4}(|S_7(\theta_1, \varphi_1)|^2+|S_8(\theta_1, \varphi_1)|^2). \tag{1.205}$$

In practice, however, use is frequently made of the differential two-position scattering cross-section (σ_D) and backscattering cross-section (σ_B), written in dimensionless form.[28] This is usually accomplished by dividing σ_D' and σ_B' respectively by the area of the central section of the large sphere (πb_1^2). Formulas (1.205) and (1.211) will then become

$$\sigma_D(\theta_1, \varphi_1) = \frac{4}{k_0^2 b_1^2}(|S_7(\theta_1, \varphi_1)|^2 + |S_8(\theta_1, \varphi_1)|^2), \tag{1.212}$$

$$\sigma_B = \frac{1}{2(k_0 b_1)^2} \sum_{m=\pm 1} \left| \sum_{n=1}^{\infty} (-1)^n (2n+1)(\Xi_{nm}^{(1)} - \Xi_{nm}^{(2)}) \right|^2. \tag{1.213}$$

The scattering indicatrix $\gamma(\theta_1, \phi_1)$ and the effective area of total scattering σ_1, referred[29] to πb_1^2, are defined [44] respectively as

$$\begin{gathered} \Upsilon(\theta_1, \varphi_1) = \frac{1}{\Upsilon_0} F(\theta_1, \varphi_1), \\ \sigma_1 = \frac{1}{\pi (k_0 b_1)^2} \Upsilon_0, \\ \Upsilon_0 = \int_0^{2\pi} \int_0^{\pi} F(\theta_1, \varphi_1) \sin\theta_1 \, d\theta_1 \, d\varphi_1, \end{gathered} \tag{1.214}$$

We first transform γ_0. Replacing in expression (1.203) the squares of the absolute values by the product of two complex conjugates and considering relations (1.198), (1.192) and also the values of the integrals[30]

$$\begin{gathered} \int_0^{\pi} [\tau_{n'}^m(\theta_1)\tau_n^m(\theta_1) + m^2 \pi_n^m(\theta_1)\pi_{n'}^m(\theta_1)] \sin\theta_1 \, d\theta_1 = \\ = \frac{2}{2n+1} \frac{(n+m)!}{(n-m)!} n(n+1)\delta_{nn'}, \\ \int_0^{\pi} [\pi_n^m(\theta_1)\tau_{n'}^m(\theta_1) + \pi_{n'}^m(\theta_1)\tau_n^m(\theta_1)] \sin\theta_1 \, d\theta_1 = 0 \text{ for } m \neq 0, \end{gathered} \tag{1.215}$$

---

[28] In this case we will hereinafter denote such quantities by the same symbols, but without a dash.

[29] And therefore dimensionless.

[30] The first of these integrals is given in [47], and the second is obtained from (1.167) by integrating by parts.

resulting from functions (1.137), (1.207), (1.208), reduces formula (1.219) to the form /63

$$\sigma_2 = \frac{2}{k_0 (k_0 b_1)^2} (-\mathrm{Im}) \sum_{n=1}^{\infty} \sum_{m=\pm 1} i^n \sqrt{\frac{(n+m)!\, n(n+1)}{(n-m)!}} \times \times \left[\widetilde{B}^{(0)}_{nm\,(u)} - i x_0 m \widetilde{B}^{(0)}_{nm\,(v)} \right]. \tag{1.221}$$

If in equality (1.221) we switch to the new variables $\Xi^{(1)}_{nm}$ and $\Xi^{(2)}_{nm}$ in accordance with formulas (1.210), taking into consideration the relation (Im)iA = =(-R)A, we will obtain the final expression[31] for σ_2:

$$\sigma_2 = \frac{1}{(k_0 b_1)^2} (-\mathrm{Re}) \sum_{n=1}^{\infty} \sum_{m=\pm 1} (2n+1) (\Xi^{(1)}_{nm} + \Xi^{(2)}_{nm}). \tag{1.222}$$

A linearly polarized wave incident on an obstacle usually generates an eliptically polarized scattered wave containing both $E_\theta^{(0_s)}$, and $E_\phi^{(0_s)}$. As a rule, radar units which emit and receive radio waves are as sensitive to that part of the field scattered by the obstacles which is polarized in the same way as the field of the plane wave.

In this case [46], the two-position scattering cross-section[32] is calculated from the form

$$\sigma'(\theta_1, \varphi_1) = \lim_{r_1 \to \infty} 4\pi r_1^2 \frac{|E^{(0_s)}|}{|E^{(00)}|} \tag{1.223}$$

where $E^{(0_s)}$ is the component of the field of scattering at the point of reception in the direction θ_1, ϕ_1, polarized in the same way as the field $E^{(00)}$ of the plane wave striking the obstacle from the direction θ_0, ϕ_0; r_1 is the distance from the origin, at which the diffracting body is located, to the receiver, located in the long-range zone of the field.

If in formula (1.223) $\theta_1 = \theta_0$, $\phi_1 = \phi_0$, the value of σ' is called the radar cross-section and denoted by $\sigma'0$. Both σ' and σ'_0 have the dimensions of an area.

Since in our case (see § 1.4), the plane wave propagating in the negative direction of axis Z_1 has the electric vector $E^{(00)}$ polarized along axis X_1,

---

[31] A different derivation of formula (1.222) is given in [12].
[32] In contrast to σ_D, the word "differential" is omitted here.

expression (1.223) is equivalent to the following:

$$\sigma'(\theta_1, \varphi_1) = \lim_{r_1 \to \infty} 4\pi r_1^2 \frac{\left| E_{x_1}^{(0s)} \right|^2}{\left| E_{x_1}^{(00)} \right|^2}. \tag{1.224}$$

If we substitute the quantities which, as can be readily seen, have the form

$$|E_{x_1}^{(0s)}| = |E_{\theta_1}^{(0s)} \cos\theta_1 \cos\phi_1 - E_{\phi_1}^{(0s)} \sin\phi_1|; \quad |E_{x_1}^{(00)}| = k_0^4 |E_0|^2 ,$$

into formula (1.224) and take relations (1.191), (1.198) into account, we obtain

$$\sigma'(\theta_1, \varphi_1) = \frac{4\pi}{k_0^4} |S_7(\theta_1, \varphi_1) \cos\theta_1 \cos\varphi_1 - S_8(\theta_1, \varphi_1) \sin\varphi_1|^2. \tag{1.225}$$

Hence, the expression for the radar scattering cross-section:

$$\sigma_0' = \frac{4\pi}{k_0^4} |S_7(0, 0)|^2, \tag{1.226}$$

or, by virtue of relations (1.198), (1.192), (1.207)

$$\sigma_0' = \frac{\pi}{k_0^4} \left| \sum_{n=1}^{\infty} i^{-n} \left[\widetilde{B}_{n,-1(u)}^{(0)} - \widetilde{B}_{n1(u)}^{(0)} n(n+1) - \right. \right.$$
$$\left. \left. - ix_0 \widetilde{B}_{n,-1(v)}^{(0)} - ix_0 \widetilde{B}_{n1(v)}^{(0)} n(n+1) \right] \right|^2. \tag{1.227}$$

In the notation of (1.210), formula (1.227) assumes the more compact form

$$\sigma_0' = \frac{\pi}{4k_0^2} \left| \sum_{n=1}^{\infty} \sum_{m=\pm 1} (-1)^n (2n+1) \left(\Xi_{nm}^{(1)} - \Xi_{nm}^{(2)} \right) \right|^2. \tag{1.228}$$

Normalizing $\sigma'(\theta_1, \phi_1)$ and σ'_0 by dividing by πb_1^2, we obtain the dimensionless quantities $\sigma(\theta_1, \phi_1)$ and σ_0:

$$\sigma(\theta_1, \varphi_1) = \frac{4}{k_0^4 b_1^2} |S_7(\theta_1, \varphi_1) \cos\theta_1 \cos\varphi_1 - S_8(\theta_1, \varphi_1) \sin\varphi_1|^2, \tag{1.229}$$

$$\sigma_0 = \frac{1}{4(k_0 b_1)^2} \left| \sum_{n=1}^{\infty} \sum_{m=\pm 1} (-1)^n (2n+1) \left(\Xi_{nm}^{(1)} - \Xi_{nm}^{(2)} \right) \right|^2. \tag{1.230}$$

§ 1.6. Scattering and Attenuation of Electromagnetic Waves by a Spherical Particle for Different Special Relative Positions of Its Layers.

We will consider different special cases of the general solution of the problem (§ 1.3, 1.4) and the corresponding (§ 1.5) electromagnetic and radar characteristics. The discussion will also involve cases in which the centers of all the spheres are located on the same straight line (line of centers), and cases of concentric arrangements of the spheres.

Case, Where the Centers Of All ν Spheres Lie On the Same Straight Line.

Mathematically, this condition (Figure 1.3) is equivalent to the following

$$\vartheta_j = 0, \quad j = 2, 3, \ldots, \nu - 1. \tag{1.231}$$

According to the remarks on page 12 on the introduction of the coordinate systems $X_j^! Y_j^! Z_j^!$, we also have in this case

$$X_j = 0, \quad j = 2, 3, \ldots, \nu - 1. \tag{1.232}$$

Relations (1.231), (1.232) considerably simplify expressions /65
(1.65), (1.66) if one considers that [26] $P_{ml}^n(1) = \delta_{ml}$, where δ_{ml} is the Kronaecker symbol.

$$b_{lnmj} = \delta_{ml}, \quad b_{\lambda nlj}^{(-1)} = \delta_{l\lambda}, \quad j = 2, 3, \ldots, \nu - 1; \tag{1.233}$$

Hence, formulas (1.69), (1.72), (1.93) will assume the form:

$$\left.\begin{aligned} K_{nm\tau lj} &= F_{n\tau mj}^{(-1)} \delta_{lm}, \\ K_{nm\tau lj}^{(-1)} &= F_{n\tau lj} \delta_{lm}, \end{aligned}\right\} j = 2, 3, \ldots, \nu - 1; \tag{1.234}$$

$$a_{\tau lnm2j}^{(2j-1)} = -\sqrt{\frac{(n+m)!\,(\tau-l)!}{(n-m)!\,(\tau+l)!}} \frac{j_n(k_j b_{j+1})\, h_\tau^*(k_j b_j)}{h_n(k_j b_{j+1})\, j_n^*(k_j b_{j+1})} \times$$
$$\times F_{n\tau mj}^{(-1)} \delta_{lm}, \quad j = 2, 3, \ldots, \nu - 1; \tag{1.235}$$

$$a_{\tau lnm2j}^{(2j+2)} = \sqrt{\frac{(n+m)!\,(\tau-l)!}{(n-m)!\,(\tau+l)!}} \frac{q_{j+1} h_n(k_{j+1} b_{j+1})\, j_\tau^*(k_{j+1} b_{j+2})}{q_j h_n(k_j b_{j+1})\, j_n^*(k_j b_{j+1})} \times$$
$$\times F_{n\tau lj+1} \delta_{lm}, \quad j = 1, 2, \ldots, \nu - 2; \tag{1.236}$$

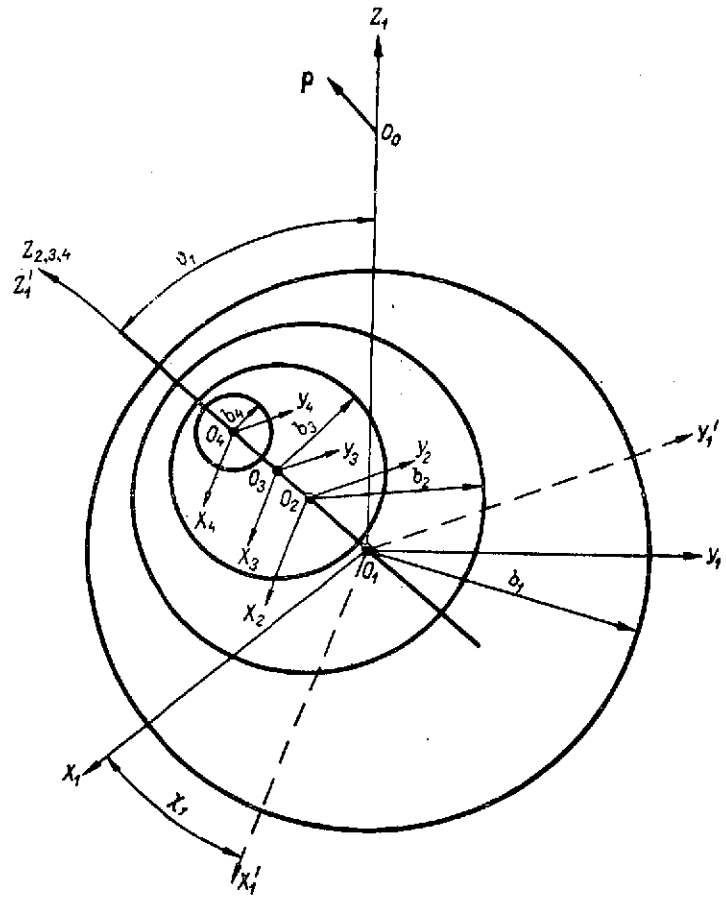

Figure 1.3. Case of Location of the Centers of All the Spheres on the Same Straight Line.

$$a_{\tau lnm\,2j+1}^{(2j-1)} = \sqrt{\frac{(n+m)!\,(\tau-l)!}{(n-m)!\,(\tau+l)!}}\,\frac{\psi_n'(k_j b_{j+1})\,h_\tau^*(k_j b_j)}{\psi_n'(k_{j+1}b_{j+1})\,h_n^*(k_{j+1}b_{j+1})}\times$$

$$\times F_{n\tau mj}^{(-1)}\delta_{lm},\quad j=2,\ 3,\ \ldots,\ \nu-1; \tag{1.237}$$

$$a_{\tau lnm\,2j+1}^{(2j+2)} = -\sqrt{\frac{(n+m)!\,(\tau-l)!}{(n-m)!\,(\tau+l)!}}\,\frac{\zeta_n'(k_{j+1}b_{j+1})\,j_\tau^*(k_{j+1}b_{j+2})}{\psi_n'(k_{j+1}b_{j+1})\,h_n^*(k_{j+1}b_{j+1})}\times$$

$$\times F_{n\tau l\,j+1}\delta_{lm},\quad j=1,\ 2.\ \ldots,\ \nu-2. \tag{1.238}$$

This in turn reduces system (1.92) to the form:

$$
\begin{cases}
Z_{nm}^{(0)} = a_n^{(0)} Z_{nm}^{(1)} + & + \sum_{\tau=0}^{\infty} \sum_{l=-\tau}^{\tau} Z_{\tau l}^{(2)} a_{\tau l n m 0}^{(2)} - \Phi_{nm}^{(0)}, \\
Z_{nm}^{(1)} = a_n^{(1)} Z_{nm}^{(0)} + & + \sum_{\tau=0}^{\infty} \sum_{l=-\tau}^{\tau} Z_{\tau l}^{(2)} a_{\tau l n m 1}^{(2)} - \Phi_{nm}^{(1)}, \\
Z_{nm}^{(2)} = a_n^{(2)} Z_{nm}^{(3)} + \sum_{\tau=0}^{\infty} \sum_{l=-\tau}^{\tau} Z_{\tau l}^{(1)} a_{\tau l n m 2}^{(1)} & + \sum_{\tau=0}^{\infty} Z_{\tau m}^{(4)} a_{\tau m n m 2}^{(4)}, \\
Z_{nm}^{(3)} = a_n^{(3)} Z_{nm}^{(2)} + \sum_{\tau=0}^{\infty} \sum_{l=-\tau}^{\tau} Z_{\tau l}^{(1)} a_{\tau l n m 3}^{(1)} & + \sum_{\tau=0}^{\infty} Z_{\tau m}^{(4)} a_{\tau m n m 3}^{(4)}, \\
Z_{nm}^{(2j)} = a_n^{(2j)} Z_{nm}^{(2j+1)} + \sum_{\tau=0}^{\infty} Z_{\tau m}^{(2j-1)} a_{\tau m n m 2j}^{(2j-1)} + \sum_{\tau=0}^{\infty} Z_{\tau}^{(2j+2)} a_{\tau m n m 2j}^{(2j+2)}, \\
Z_{nm}^{(2j+1)} = a_n^{(2j+1)} Z_{nm}^{(2j)} + \\
\quad + \sum_{\tau=0}^{\infty} Z_{nm}^{(2j-1)} a_{\tau m n m 2j+1}^{(2j-1)} + \sum_{\tau=0}^{\infty} Z_{\tau m}^{(2j+2)} a_{\tau m n m 2j+1}^{(2j+2)},
\end{cases}
\tag{1.239}
$$

$$
j = 2, 3, \ldots, \nu - 1; \quad n = 0, 1, \ldots; \quad m = -n, \ldots, n,
$$

where $a_n^{(s)}$ and $\Phi_{nm}^{(s)}$ are defined by formulas (1.93), and $a_{\tau l n m s}^{(i)}$, by formulas (1.235)-(1.238).

If in system (1.239) $Z_{nm}^{(s)}$ is replaced by $\tilde{A}_{nm}^{(s)}$, and $\Phi_{nm}^{(s)}$ by $\tilde{\Phi}_{nm}^{(s)}$, in accordance with expressions (1.187), we will obtain the simplified system (1.190) corresponding to the case of a plane wave. /67

Let us note here that the case where relation (1.150) applies is completed by systems (1.153), (1.193) provided that the appropriate changes are made in expressions (1.154), in accordance with equalities (1.234).

Case Where the Line of Centers of All ν Spheres Coincides with Axis Z_1.

This case is characterized by the fact that the line of centers of spheres under consideration passes through point O_0 (Figure 1.4), at which the source of the electromagnetic field is located. Hence, to the conditions (1.231), (1.232) already discussed in the preceding case it is necessary to add $\Theta_1 = 0$. Then expressions (1.233), (1.235), (1.237) will also be valid for $j = 1$, and (1.236), (1.238) for $j = 0$. System (1.239) will then assume the form:

$$
\begin{cases}
Z_{nm}^{(0)} = a_n^{(0)} Z_{nm}^{(1)} + & + \sum_{\tau=0}^{\infty} Z_{\tau m}^{(2)} a_{\tau mnm0}^{(2)} - \Phi_{nm}^{(0)}, \\
Z_{nm}^{(1)} = a_n^{(1)} Z_{nm}^{(0)} + & + \sum_{\tau=0}^{\infty} Z_{\tau m}^{(2)} a_{\tau mnm1}^{(2)} - \Phi_{nm}^{(1)}, \\
Z_{nm}^{(2j)} = a_n^{(2j)} Z_{nm}^{(2j+1)} + \sum_{\tau=0}^{\infty} Z_{\tau m}^{(2j-1)} a_{\tau mnm2j}^{(2j-1)} & + \sum_{\tau=0}^{\infty} Z_{\tau m}^{(2j+2)} a_{\tau mnm2j}^{(2j+2)}, \\
Z_{nm}^{(2j+1)} = a_n^{(2j+1)} Z_{nm}^{(2j)} + \sum_{\tau=0}^{\infty} Z_{\tau m}^{(2j-1)} a_{\tau mnm2j+1}^{(2j-1)} + \sum_{\tau=0}^{\infty} Z_{\tau m}^{(2j+2)} a_{\tau mnm2j+1}^{(2j+2)}, & \qquad (1.240)
\end{cases}
$$

$$j = 1, 2, \ldots, \nu - 1; \quad n = 0, 1, \ldots; \quad m = -n, \ldots, n.$$

Replacing in equations (1.240) $Z_{nm}^{(s)}$ by $\tilde{Z}_{nm}^{(s)}$, and $\Phi_{nm}^{(s)}$ by $\tilde{\Phi}_{nm}^{(s)}$ according to (1.187), we will obtain a system corresponding to the case of a plane wave. If however relation (1.150) applies, the coefficients (1.154) of the unknowns in systems (1.153) and (1.193) are transformed by taking into account expressions (1.234), which, as was shown above, are also valid when j = 1.

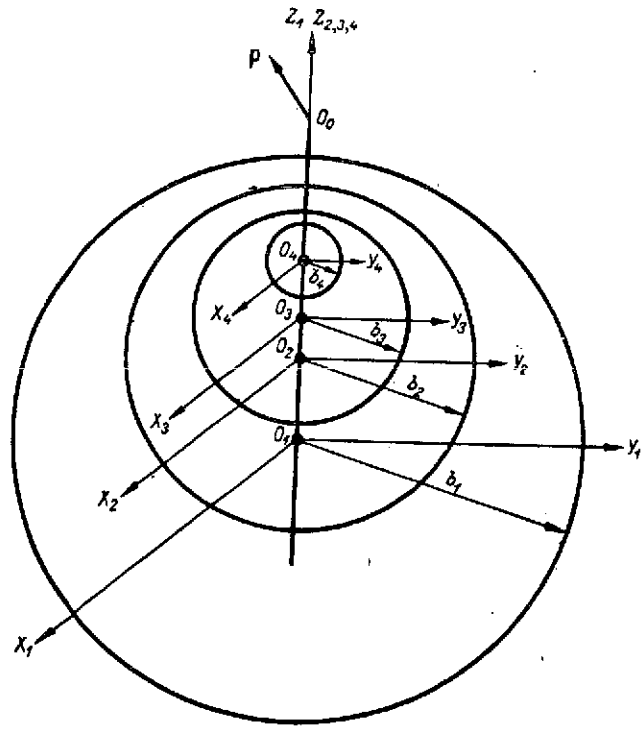

Figure 1.4. Case of Location of the Line of Centers of All the Spheres on Axis Z_1.

Case of Concentric Arrangement of ν Spheres.

This case (Figure 1.5) may be obtained most simply, for example, from the preceeding case if in the latter the quantities $h_2, h_3, \ldots, h_\nu$ are made to tend to zero. By virtue of the easily verifiable relations

$$j_\sigma(0)=\delta_{\sigma 0},$$
$$\delta^m_{0np}=\frac{1}{2n+1}\frac{(n-m)!}{(n+m)!}\delta_{pn},$$

and (1.233) for $j = 1, 2, \ldots, \nu - 1$ leads to the following values of $k_{nm\tau lj}$ and $K^{-1}_{nm\tau lj}$:

$$K_{nm\tau lj}=K^{(-1)}_{nm\tau lj}=\delta_{n\tau}\delta_{lm}, \quad j=1, 2, \ldots, \nu-1. \tag{1.241}$$

Using these values, one can represent equations (1.240) in the form of the finite algebraic system:

$$\begin{cases} Z^{(0)}_{nm}=a^{(0)}_n Z^{(1)}_{nm}+ & +Z^{(2)}_{nm}a^{(2)}_{nmnm0}-\Phi^{(0)}_{nm}, \\ Z^{(1)}_{nm}=a^{(1)}_n Z^{(0)}_{nm}+ & +Z^{(2)}_{nm}a^{(2)}_{nmnm1}-\Phi^{(1)}_{nm}, \\ Z^{(2j)}_{nm}=a^{(2j)}_n Z^{(2j+1)}_{nm}+Z^{(2j-1)}_{nm}a^{(2j-1)}_{nmnm2j} & +Z^{(2j+2)}_{nm}a^{(2j+2)}_{nmnm2j}, \\ Z^{(2j+1)}_{nm}=a^{(2j+1)}_n Z^{(2j)}_{nm}+Z^{(2j-1)}_{nm}a^{(2j-1)}_{nmnm2j+1}+Z^{(2j+2)}_{nm}a^{(2j+2)}_{nmnm2j+1}, \end{cases}$$

$$j=1, 2, \ldots, \nu-1; \quad n=0, 1, \ldots; \quad m=-n, \ldots, n, \tag{1.242}$$

where $a^{(s)}_n$ and $\Phi^{(s)}_{nm}$ are given by formulas (1.93), and $a^{(i)}_{\tau lnms}$ are given by formulas (1.235)-(1.238) taking relations (1.241) into account. /69

If we introduce the notation

$$\Omega^{(2j-1)}_{n2j}=-\frac{(2n-1)!!(2n+1)!!}{(k_j^2 b_j b_{j+1})^n}\frac{j_n(k_j b_{j+1})}{h_n(k_j b_{j+1})}, \quad j=1, 2, \ldots, \nu-1;$$
$$\Omega^{(2j+2)}_{n2j}=\frac{q_{j+1}}{q_j}\left(\frac{k_{j+1}b_{j+2}}{k_j b_{j+1}}\right)^n\frac{h_n(k_{j+1}b_{j+1})}{h_n(k_j b_{j+1})}, \quad j=0, 1, \ldots, \nu-2; \tag{1.243}$$

$$\mathfrak{Q}_{n2j+1}^{(2j-1)} = \left(\frac{k_{j+1}b_{j+1}}{k_j b_j}\right)^n \frac{\psi_n'(k_j b_{j+1})}{\psi_n'(k_{j+1}b_{j+1})}, \quad j=1,\ 2,\ \ldots,\ \nu-1;$$

$$\mathfrak{Q}_{n2j+1}^{(2j+2)} = -\frac{\left(k_{j+1}^2 b_{j+1} b_{j+2}\right)^n}{(2n-1)!!\,(2n+1)!!}\,\frac{\zeta_n'(k_{j+1}b_{j+1})}{\psi_n'(k_{j+1}b_{j+1})},$$

$$j=0,\ 1,\ \ldots,\ \nu-2, \tag{1.243}$$

system (1.242) may be transformed to the form[33]

$$\begin{cases}
-Z_{nm}^{(0)} + Z_{nm}^{(1)} a_n^{(0)} + Z_{nm}^{(2)} \mathfrak{Q}_{n0}^{(2)} = \Phi_{nm}^{(0)}, \\
Z_{nm}^{(0)} a_n^{(1)} - Z_{nm}^{(1)} + Z_{nm}^{(2)} \mathfrak{Q}_{n1}^{(2)} = \Phi_{nm}^{(1)}, \\
Z_{nm}^{(1)} \mathfrak{Q}_{n2}^{(1)} - Z_{nm}^{(2)} + Z_{nm}^{(3)} a_n^{(2)} + Z_{nm}^{(4)} \mathfrak{Q}_{n2}^{(4)} = 0, \\
Z_{nm}^{(1)} \mathfrak{Q}_{n3}^{(1)} + Z_{nm}^{(2)} a_n^{(3)} - Z_{nm}^{(3)} + Z_{nm}^{(4)} \mathfrak{Q}_{n3}^{(4)} = 0, \\
\cdots\cdots\cdots\cdots\cdots\cdots\cdots\cdots \\
Z_{nm}^{(2j-1)} \mathfrak{Q}_{n2j}^{(2j-1)} - Z_{nm}^{(2j)} + \\
\quad + Z_{nm}^{(2j+1)} a_n^{(2j)} + Z_{nm}^{(2j+2)} \mathfrak{Q}_{n2j}^{(2j+2)} = 0, \\
Z_{nm}^{(2j-1)} \mathfrak{Q}_{n2j-1}^{(2j-1)} + Z_{nm}^{(2j)} a_n^{(2j+1)} - \\
\quad - Z_{nm}^{(2j+1)} + Z_{nm}^{(2j+2)} \mathfrak{Q}_{n2j+1}^{(2j+2)} = 0, \\
\cdots\cdots\cdots\cdots\cdots\cdots\cdots\cdots \\
Z_{nm}^{(2\nu-3)} \mathfrak{Q}_{n2\nu-2}^{(2\nu-3)} - Z_{nm}^{(2\nu-2)} + Z_{nm}^{(2\nu-1)} a_n^{(2\nu-2)} = 0, \\
Z_{nm}^{(2\nu-3)} \mathfrak{Q}_{n2\nu-1}^{(2\nu-3)} + Z_{nm}^{(2\nu-2)} a_n^{(2\nu-1)} - Z_{nm}^{(2\nu-1)} = 0,
\end{cases} \tag{1.244}$$

$$j=2,\ 3,\ \ldots,\ \nu-2; \quad n=0,\ 1,\ \ldots; \quad m=-n,\ \ldots\ n.$$

Since from expressions((1.93), (1.76) it follows that when $|m| > 1$ $\Phi_{nm}^{(j)} = 0$, it may be concluded that for these m, system (1.244) is homogeneous.

[33]Assuming that $\nu > 2$.

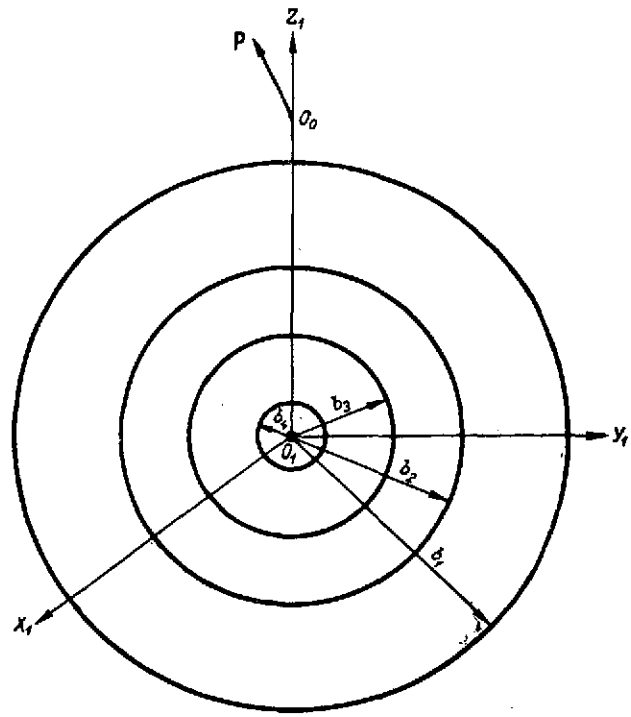

Figure 1.5. Case of Concentric Arrangement of the Spheres.

By virtue of the unique solvability proven in § 1.3, it follows from the homogeneity of the system that

$$Z_{nm}^{(j)}=0;\ |m|>1;\ n=0,\ 1,\ \ldots;\quad j=0,\ 1,\ \ldots,\ 2\nu-1, \tag{1.245}$$

or in terms of notation (1.90)

$$\left.\begin{aligned} A_{nm}^{(j)}&=0,\ j=1,\ 2,\ \ldots,\ \nu,\\ B_{nm}^{(j)}&=0,\ j=0,\ 1,\ \ldots,\ \nu-1 \end{aligned}\right\}|m|>1,\ n=0,\ 1,\ \ldots \tag{1.246}$$

We will denote the column of free terms of system (1.244) by Φ_{nm}:

$$\Phi_{nm}=\begin{pmatrix} \Phi_{nm}^{(0)}\\ \Phi_{nm}^{(1)}\\ 0\\ \cdot\\ \cdot\\ \cdot\\ 0 \end{pmatrix}, \tag{1.247}$$

The determinant of the system by Δ_n:

$$\begin{vmatrix} -1 & a_n^{(0)} & \Omega_{n0}^{(2)} & \cdots & 0 & 0 & 0 & 0 & \cdots & 0 & 0 & 0 \\ a_n^{(1)} & -1 & \Omega_{n1}^{(2)} & \cdots & 0 & 0 & 0 & 0 & \cdots & 0 & 0 & 0 \\ \cdots & \cdots & \cdots & \cdots & \cdots & \cdots & \cdots & \cdots & \cdots & \cdots & \cdots & \cdots \\ 0 & 0 & 0 & \cdots & \Omega_{n2j}^{(2j-1)} & -1 & a_n^{(2j)} & \Omega_{n2j}^{(2j+2)} & \cdots & 0 & 0 & 0 \\ 0 & 0 & 0 & \cdots & \Omega_{n2j+1}^{(2j-1)} & a_n^{(2j+1)} & -1 & \Omega_{n2j+1}^{(2j+2)} & \cdots & 0 & 0 & 0 \\ \cdots & \cdots & \cdots & \cdots & \cdots & \cdots & \cdots & \cdots & \cdots & \cdots & \cdots & \cdots \\ 0 & 0 & 0 & \cdots & 0 & 0 & 0 & 0 & \cdots & \Omega_{n2\nu-2}^{(2\nu-3)} & -1 & a_n^{(2\nu-2)} \\ 0 & 0 & 0 & \cdots & 0 & 0 & 0 & 0 & \cdots & \Omega_{n2\nu-1}^{(2\nu-3)} & a_n^{(2\nu-1)} & -1 \end{vmatrix} \tag{1.248}$$

$$n = 0, 1, \ldots; \quad j = 1, \ldots, \nu - 2.$$

and the determinant obtained from (1.248) by replacing the s-th column (s = 0, 1, ..., 2ν - 1) by the column of free terms (1.247), by $\Delta_{sn}^{(m)}$. From Cramer's theorem, we then have

$$Z_{nm}^{(s)} = \frac{\Delta_{sn}^{(m)}}{\Delta_n}, \quad s = 0, 1, \ldots, 2\nu - 1, \tag{1.249}$$

or, taking notations (1.90), (1.91) into account

$$\left.\begin{aligned} A_{nm}^{(j+1)} &= \frac{\Delta_{2j+1n}^{(m)}}{\Delta_n} \sqrt{\frac{(n-m)!}{(n+m)!}} \frac{(2n-1)!!}{(k_{j+1}b_{j+1})^n}, \\ B_{nm}^{(j)} &= \frac{\Delta_{2jn}^{(m)}}{\Delta_n} \sqrt{\frac{(n-m)!}{(n+m)!}} \frac{(k_j b_{j+1})^n}{(2n+1)!!}, \end{aligned}\right\} \quad j = 0, 1, \ldots, \nu - 1. \tag{1.250}$$

By analogy with the coefficients $Z_{nm}^{(j)}$, $A_{nm}^{(j)}$, $B_{nm}^{(j)}$, we will agree to denote by $\Delta_{n(u)}$, $\Delta_{sn(u)}^{(m)}$ the determinants Δ_n, $\Delta_{sn}^{(m)}$ corresponding to the potential U, and by $\Delta_{n(v)}$, $\Delta_{sn(v)}^{(m)}$, the determinants corresponding to the potential V. We will have in this case:

$$A^{(j+1)}_{nm\,(u)} = \frac{\Delta^{(m)}_{2j+1n\,(u)}}{\Delta_{n\,(u)}} \sqrt{\frac{(n-m)!}{(n+m)!}} \frac{(2n-1)!!}{(k_{j+1}b_{j+1})^n},$$

$$A^{(j+1)}_{nm\,(v)} = \frac{\Delta^{(m)}_{2j+1n\,(v)}}{\Delta_{n\,(v)}} \sqrt{\frac{(n-m)!}{(n+m)!}} \frac{(2n-1)!!}{(k_{j+1}b_{j+1})^n},$$

(1.251)

$$B^{(j)}_{nm\,(u)} = \frac{\Delta^{(m)}_{2jn\,(u)}}{\Delta_{n\,(u)}} \sqrt{\frac{(n-m)!}{(n+m)!}} \frac{(k_j b_{j+1})^n}{(2n+1)!!}, \quad (1.251)$$

$$B^{(j)}_{nm\,(v)} = \frac{\Delta^{(m)}_{2jn\,(v)}}{\Delta_{n\,(v)}} \sqrt{\frac{(n-m)!}{(n+m)!}} \frac{(k_j b_{j+1})^n}{(2n+1)!!}.$$

At the same time, relations (1.246) will become

$$A^{(j)}_{nm\,(u)} = A^{(j)}_{nm\,(v)} = B^{(j)}_{nm\,(u)} = B^{(j)}_{nm\,(v)} = 0 \text{ при } |m| > 1. \quad (1.252)$$

From expressions (1.247), (1.76)-(1.80), (1.90) it is easy to obtain the following relations:

$$\Phi_{n,\,-m\,(u)} = (-1)^m \Phi_{nm\,(u)}, \quad (1.253)$$
$$\Phi_{n,\,-m\,(v)} = \Phi_{nm\,(v)},$$

which in turn lead to the equalities

$$\Delta^{(-m)}_{sn\,(u)} = (-1)^m \Delta^{(m)}_{sn\,(u)},$$
$$\Delta^{(-m)}_{sn\,(v)} = \Delta^{(m)}_{sn\,(v)}. \quad (1.254)$$

The dependence of the expressions for $\Phi_{nm(u)}$ and $\Delta^{(m)}_{sn}$ on the index m, revealed in relations (1.253), (1.254), makes it possible to establish this dependence for the coefficients $A^{(j)}_{nm}$, $B^{(j)}_{nm}$ as well.

$$A^{(j+1)}_{n,\,-m\,(u)} = (-1)^m \frac{(n+m)!}{(n-m)!} A^{(j+1)}_{nm\,(u)},$$

$$B^{(j)}_{n,\,-m\,(u)} = (-1)^m \frac{(n+m)!}{(n-m)!} B^{(j)}_{nm\,(u)},$$

$$A^{(j+1)}_{n,\,-m\,(v)} = \frac{(n+m)!}{(n-m)!} A^{(j+1)}_{nm\,(v)},$$

$$B^{(j)}_{n,\,-m\,(v)} = \frac{(n+m)!}{(n-m)!} B^{(j)}_{nm\,(v)},$$

$$j = 0,\ 1,\ \ldots,\ \nu - 1. \quad (1.255)$$

To formulas (1.255) it is necessary to add the following ones:

$$A^{(j+1)}_{n0\,(v)} = B^{(j)}_{n0\,(v)} = 0, \quad j = 0, 1, \ldots, \nu - 1, \tag{1.256}$$

which are readily obtained from expressions (1.76), (1.79), (1.247), (1.249) and from the uniqueness theorem of § 1.3.

If in equations (1.244) $Z^{(s)}_{nm}$ is replaced by $\widetilde{Z}^{(s)}_{nm}$, and $\Phi^{(s)}_{nm}$ by $\widetilde{\Phi}^{(s)}_{nm}$, in accordance with expressions (1.187), the system corresponding to the case of a plane wave will be obtained.

The determinant of the system thus obtained will remain the same (1.248), and the column of these free terms will assume the form

$$\widetilde{\Phi}_{nm} = \begin{pmatrix} \widetilde{\Phi}^{(0)}_{nm} \\ \widetilde{\Phi}^{(1)}_{nm} \\ 0 \\ \cdot \\ \cdot \\ \cdot \\ 0 \end{pmatrix}. \tag{1.257}$$

Operating in the same way as in the derivation of expressions (1.251)-(1.256), we will have the following relations corresponding to this case:

$$\begin{aligned}
\widetilde{A}^{(j+1)}_{nm\,(u)} &= \frac{\widetilde{\Delta}^{(m)}_{2j+1n\,(u)}}{\Delta_{n\,(u)}} \sqrt{\frac{(n-m)!}{(n+m)!}} \frac{(2n-1)!!}{(k_j b_j)^n}, \\
\widetilde{A}^{(j+1)}_{nm\,(v)} &= \frac{\widetilde{\Delta}^{(m)}_{2j+1n\,(v)}}{\Delta_{n\,(v)}} \sqrt{\frac{(n-m)!}{(n+m)!}} \frac{(2n-1)!!}{(k_j b_j)^n}, \\
\widetilde{B}^{(j)}_{nm\,(u)} &= \frac{\widetilde{\Delta}^{(m)}_{2jn\,(u)}}{\Delta_{n\,(u)}} \sqrt{\frac{(n-m)!}{(n+m)!}} \frac{(k_j b_{j+1})^n}{(2n+1)!!}, \\
\widetilde{B}^{(j)}_{nm\,(v)} &= \frac{\widetilde{\Delta}^{(m)}_{2jn\,(v)}}{\Delta_{n\,(v)}} \sqrt{\frac{(n-m)!}{(n+m)!}} \frac{(k_j b_{j+1})^n}{(2n+1)!!},
\end{aligned} \tag{1.258}$$

$$\widetilde{A}^{(j)}_{nm\,(u)} = \widetilde{A}^{(j)}_{nm\,(v)} = \widetilde{B}^{(j)}_{nm\,(u)} = \widetilde{B}^{(j)}_{nm\,(v)} = 0 \text{ при } |m| \neq 1, \tag{1.259}$$

$$\left\{\begin{matrix}\widetilde{A}^{(j)}_{n,\,-1\,(u)}\\ \widetilde{B}^{(j)}_{n,\,-1\,(u)}\end{matrix}\right\}=-n(n+1)\left\{\begin{matrix}\widetilde{A}^{(j)}_{n1\,(u)}\\ \widetilde{B}^{(j)}_{n1\,(u)}\end{matrix}\right\},$$

$$\left\{\begin{matrix}\widetilde{A}^{(j)}_{n,\,-1\,(v)}\\ \widetilde{B}^{(j)}_{n,\,-1\,(v)}\end{matrix}\right\}=n(n+1)\left\{\begin{matrix}\widetilde{A}^{(j)}_{n1\,(v)}\\ \widetilde{B}^{(j)}_{n1\,(v)}\end{matrix}\right\},$$

$$j=0,\ 1,\ \ldots,\ 2\nu-1. \qquad (1.260)$$

From formulas (1.258)-(1.260) it is now easy to obtain the relations for the coefficients $\Xi^{(1)}_{nm}$, $\Xi^{(2)}_{nm}$. Thus, taking notation (1.210) into account, we have:

$$\Xi^{(1)}_{n,\,-1}=\Xi^{(1)}_{n1},\quad \Xi^{(2)}_{n,\,-1}=\Xi^{(2)}_{n1},\quad \Xi^{(1)}_{nm}=\Xi^{(2)}_{nm}\ \text{при}\ |m|\neq 1; \qquad (1.261)$$

$$\Xi^{(1)}_{n1}=-\frac{2\sqrt{n(n+1)}}{k_0(2n+1)}\,\frac{\widetilde{\Delta}^{(1)}_{0n\,(u)}}{\Delta_{n\,(u)}}\,\frac{(k_0b_1)^n}{(2n+1)!!}\,i^{n-1},$$

$$\Xi^{(2)}_{n1}=-\frac{2\beta_0\sqrt{n(n+1)}}{k_0^2(2n+1)}\,\frac{\widetilde{\Delta}^{(1)}_{0n\,(v)}}{\Delta_{n\,(v)}}\,\frac{(k_0b_1)^n}{(2n+1)!!}\,i^{n-1}, \qquad (1.262)$$

where the determinant $\widetilde{\Delta}^{(1)}_{0n}=\left\{\widetilde{\Delta}^{(u)}_{0n(u)},\ \widetilde{\Delta}^{(1)}_{0n(v)}\right\}$ may be written in the following form: /74

$$\begin{vmatrix}
\widetilde{\Phi}^{(0)}_{n1} & a_n^{(0)} & \Omega^{(2)}_{n0} & \cdot & 0 & 0 & 0 & 0 & \cdot & 0 & 0 & 0\\
\widetilde{\Phi}^{(1)}_{n1} & -1 & \Omega^{(2)}_{n1} & \cdot & 0 & 0 & 0 & 0 & \cdot & 0 & 0 & 0\\
\cdot & \cdot & \cdot & \cdot & \cdot & \cdot & \cdot & \cdot & \cdot & \cdot & \cdot & \cdot\\
0 & 0 & 0 & \cdot & \Omega^{(2j-1)}_{n2j} & -1 & a_n^{(2j)} & \Omega^{(2j+2)}_{n2j} & \cdot & 0 & 0 & 0\\
0 & 0 & 0 & \cdot & \Omega^{(2j-1)}_{n2j+1} & a_n^{(2j+1)} & -1 & \Omega^{(2j+2)}_{n2j+1} & \cdot & 0 & 0 & 0\\
\cdot & \cdot & \cdot & \cdot & \cdot & \cdot & \cdot & \cdot & \cdot & \cdot & \cdot & \cdot\\
0 & 0 & 0 & \cdot & 0 & 0 & 0 & 0 & \cdot & \Omega^{(2\nu-3)}_{n2\nu-2} & -1 & a_n^{(2\nu-2)}\\
0 & 0 & 0 & \cdot & 0 & 0 & 0 & 0 & \cdot & \Omega^{(2\nu-3)}_{n2\nu-1} & a_n^{(2\nu-1)} & -1
\end{vmatrix} \qquad (1.263)$$

$$n=0,\ 1,\ \ldots;\quad j=1,\ 2,\ \ldots,\ \nu-2.$$

Relations (1.258)-(1.262), which apply in this case, permit a substantial simplification of the formula describing the field of the plane wave and its various characteristics in the long-range zone.

At this point, having further applications in mind, we will turn to the electromagnetic and radar characteristics exclusively. For this purpose, we

need expressions (1.192) for $\widetilde{S}_i(\theta_1, \phi_1)$, i = 2, 3, 4, 5 transformed to a simpler form by means of the above mentioned relations. They are:

$$\widetilde{S}_2(\theta_1, \varphi_1) = 2\sum_{n=1}^{\infty} i^{-n}\widetilde{B}^{(0)}_{n1\,(u)}\tau^1_n(\theta_1)\cos\varphi_1,$$

$$\widetilde{S}_3(\theta_1, \varphi_1) = 2\sum_{n=1}^{\infty} i^{-n}B^{(0)}_{n1\,(v)}\pi^1_n(\theta_1)\cos\varphi_1,$$

$$\widetilde{S}_4(\theta_1, \varphi_1) = 2i\sum_{n=1}^{\infty} i^{-n}\widetilde{B}^{(0)}_{n1\,(u)}\pi^1_n(\theta_1)\sin\varphi_1, \qquad (1.264)$$

$$\widetilde{S}_5(\theta_1, \varphi_1) = 2i\sum_{n=1}^{\infty} i^{-n}\widetilde{B}^{(0)}_{n1\,(v)}\tau^1_n(\theta_1)\sin\varphi_1.$$

From the above and from equality (1.198), the formulas for $S_{7,\ 8}(\theta_1, \phi_1)$ follow directly: /7

$$S_7(\theta_1, \varphi_1) = 2\cos\varphi_1\sum_{n=1}^{\infty} i^{-n}\left[\widetilde{B}^{(0)}_{n1\,(u)}\tau^1_n(\theta_1) + i\varkappa_0\widetilde{B}^{(0)}_{n1\,(v)}\pi^1_n(\theta_1)\right],$$

$$S_8(\theta_1, \varphi_1) = -2\sin\varphi_1\sum_{n=1}^{\infty} i^{-n}\left[\widetilde{B}^{(0)}_{n1\,(u)}\pi^1_n(\theta_1) + i\varkappa_0\widetilde{B}^{(0)}_{n1\,(v)}\tau^1_n(\theta_1)\right], \qquad (1.265)$$

which in terms of notation (1.210) and

$$W_1(\theta_1) = \sum_{n=1}^{\infty}(-1)^n\frac{2n+1}{n(n+1)}\left[\Xi^{(1)}_{n1}\tau^1_n(\theta_1) - \Xi^{(2)}_{n1}\pi^1_n(\theta_1)\right],$$

$$W_2(\theta_1) = \sum_{n=1}^{\infty}(-1)^n\frac{2n+1}{n(n+1)}\left[\Xi^{(1)}_{n1}\pi^1_n(\theta_1) - \Xi^{(2)}_{n1}\tau^1_n(\theta_1)\right] \qquad (1.266)$$

may be written as follows:

$$S_7(\theta_1, \varphi_1) = -ik_0W_1(\theta_1)\cos\varphi_1,$$
$$S_8(\theta_1, \varphi_1) = ik_0W_2(\theta_1)\sin\varphi_1. \qquad (1.267)$$

It is now easy to write the expressions for the electromagnetic and radar characteristics corresponding to the case at hand (see Figure 1.4). The same notation as in § 1.5 will be used. We thus have:

a. the intensity of the scattered field in the long-range zone

$$I(\theta_1, \varphi_1) = \frac{1}{(k_0r_1)^2}(|W_1(\theta_1)|^2\cos^2\varphi_1 + |W_2(\theta_1)|^2\sin^2\varphi_1); \qquad (1.268)$$

b. the diagram of the scattered field in the long-range zone

$$F(\theta_1,\ \varphi_1)=|W_1(\theta_1)|^2\cos^2\varphi_1+|W_2(\theta_1)|^2\sin^2\varphi_1; \tag{1.269}$$

c. the differential two-position scattering cross-section

$$\sigma_D(\theta_1,\ \varphi_1)=\frac{4}{(k_0b_1)^2}(|W_1(\theta_1)|^2\cos^2\varphi_1+|W_2(\theta_1)|^2\sin^2\varphi_1); \tag{1.270}$$

d. the backscattering cross-section

$$\sigma_B=\frac{1}{(k_0b_1)^2}\left|\sum_{n=1}^{\infty}(-1)^n(2n+1)(\Xi_{n1}^{(1)}-\Xi_{n1}^{(2)})\right|^2; \tag{1.271}$$

e. the scattering indicatrix

$$\Gamma(\theta_1,\ \varphi_1)=\frac{1}{2\pi}\frac{|W_1(\theta_1)|^2\cos^2\varphi_1+|W_2(\theta_1)|^2\sin^2\varphi_1}{\sum_{n=1}^{\infty}(2n+1)(|\Xi_{n1}^{(1)}|^2+|\Xi_{n1}^{(2)}|^2)}; \tag{1.272}$$

f. the effective area of total scattering

$$\sigma_1=\frac{2}{(k_0b_1)^2}\sum_{n=1}^{n}(2n+1)(|\Xi_{n1}^{(1)}|^2+|\Xi_{n1}^{(2)}|^2); \tag{1.273}$$

/76

g. the effective area of attenuation

$$\sigma_2=\frac{2}{(k_0b_1)^2}(-\mathrm{Re})\sum_{n=1}^{\infty}(2n+1)(\Xi_{n1}^{(1)}+\Xi_{n1}^{(2)}); \tag{1.274}$$

h. the two-position scattering cross-section

$$\sigma(\theta_1,\ \varphi_1)=\frac{4}{(k_0b_1)^2}|W_1(\theta_1)\cos\theta_1\cos^2\varphi_1+W_2(\theta_1)\sin^2\varphi_1|; \tag{1.275}$$

i. the radar scattering cross-section

$$\sigma_0=\frac{1}{(k_0b_1)^2}\left|\sum_{n=1}^{\infty}(-1)^n(2n+1)(\Xi_{n1}^{(1)}-\Xi_{n1}^{(2)})\right|^2, \tag{1.276}$$

which in this case coincides with the effective backscattering area in view of the symmetry of the body under consideration.

Thus, the expressions obtained for the characteristics, generalizing the expressions already known for a two-layer or single-layer particle, may be used in calculations of a ν-layer spherically symmetric spherical particle.

Let us note in conclusion that if the parameters of the media in the case under consideration are such that identity (1.150) applies, the determinants (1.248) and (1.263) must be replaced by the corresponding determinants of systems (1.153), (1.193). The coefficients of the unknowns of (1.93) must then be simplified by considering equality (1.241).[34]

---

[34]This remark applies equally to the two cases discussed below.

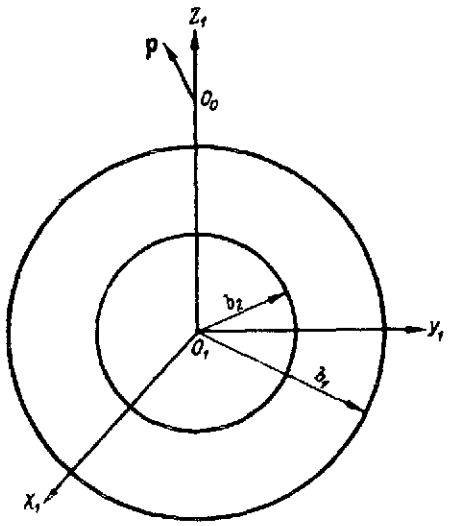

Figure 1.6. Case of Two Concentric Spheres.

Case of Two Concentric Spheres. This case (Figure 1.6) is realized from the preceeding case when $\nu = 2$. For unknown $Z_{nm}^{(j)}$ ($j = 0, 1, 2, 3$), system (1.244) becomes: /77

$$\begin{cases} -Z_{nm}^{(0)} + Z_{nm}^{(1)} a_n^{(0)} + Z_{nm}^{(2)} \Omega_{n0}^{(2)} = \Phi_{nm}^{(0)}, \\ Z_{nm}^{(0)} a_n^{(1)} - Z_{nm}^{(1)} + Z_{nm}^{(2)} \Omega_{n1}^{(2)} = \Phi_{nm}^{(1)}, \\ Z_{nm}^{(1)} \Omega_{n2}^{(1)} - Z_{nm}^{(2)} + Z_{nm}^{(3)} a_n^{(2)} = 0, \\ Z_{nm}^{(1)} \Omega_{n3}^{(1)} + Z_{nm}^{(2)} a_n^{(3)} - Z_{nm}^{(3)} = 0, \end{cases} \tag{1.277}$$

$n = 0, 1, \ldots; m = -n, \ldots, n,$

where the coefficients of the unknowns are defined by formulas (1.243), (1.93). The solution of the system may be written in the form (1.219). The coefficients $A_{nm}^{(j)}$ and $B_{nm}^{(j)}$ are found from relations (1.250)-(1.256), which include only the determinants $\Delta_{jn(u)}^{(0)}$, $\Delta_{jn(u)}^{(1)}$, $\Delta_{jn(v)}^{(1)}$ and Δ_n, where

$$\Delta_{0n}^{(m)} = \begin{vmatrix} \Phi_{nm}^{(0)} & a_n^{(0)} & \Omega_{n0}^{(2)} & 0 \\ \Phi_{nm}^{(1)} & -1 & \Omega_{n1}^{(2)} & 0 \\ 0 & \Omega_{n2}^{(1)} & -1 & a_n^{(2)} \\ 0 & \Omega_{n3}^{(1)} & a_n^{(3)} & -1 \end{vmatrix}, \quad \Delta_{1n}^{(m)} = \begin{vmatrix} -1 & \Phi_{nm}^{(0)} & \Omega_{n0}^{(2)} & 0 \\ a_n^{(1)} & \Phi_{nm}^{(1)} & \Omega_{n1}^{(2)} & 0 \\ 0 & 0 & -1 & a_n^{(2)} \\ 0 & 0 & a_n^{(3)} & -1 \end{vmatrix},$$

$$\Delta_{2n}^{(m)} = \begin{vmatrix} -1 & a_n^{(0)} & \Phi_{nm}^{(0)} & 0 \\ a_n^{(1)} & -1 & \Phi_{nm}^{(1)} & 0 \\ 0 & \Omega_{n2}^{(1)} & 0 & a_n^{(2)} \\ 0 & \Omega_{n3}^{(1)} & 0 & -1 \end{vmatrix}, \quad \Delta_{3n}^{(m)} = \begin{vmatrix} -1 & a_n^{(0)} & \Omega_{n0}^{(2)} & \Phi_{nm}^{(0)} \\ a_n^{(1)} & -1 & \Omega_{n1}^{(2)} & \Phi_{nm}^{(1)} \\ 0 & \Omega_{n2}^{(1)} & -1 & 0 \\ 0 & \Omega_{n3}^{(1)} & a_n^{(3)} & 0 \end{vmatrix}, \tag{1.278}$$

$$\Delta_n = \begin{vmatrix} -1 & a_n^{(0)} & \Omega_{n0}^{(2)} & 0 \\ a_n^{(1)} & -1 & \Omega_{n1}^{(2)} & 0 \\ 0 & \Omega_{n2}^{(1)} & -1 & a_n^{(2)} \\ 0 & \Omega_{n3}^{(1)} & a_n^{(3)} & -1 \end{vmatrix}.$$

The coefficients $\tilde{A}_{nm}^{(j)}$, $\tilde{B}_{nm}^{(j)}$, however, corresponding to the case of a plane wave, may be obtained from expressions (1.258)-(1.260) with the aid of the determinants:

$$\widetilde{\Delta}_{0n}^{(1)}=\begin{vmatrix} \widetilde{\Phi}_{n1}^{(0)} & a_n^{(0)} & \Omega_{n0}^{(2)} & 0 \\ \widetilde{\Phi}_{n1}^{(1)} & -1 & \Omega_{n1}^{(2)} & 0 \\ 0 & \Omega_{n2}^{(1)} & -1 & a_n^{(2)} \\ 0 & \Omega_{n3}^{(1)} & a_n^{(3)} & -1 \end{vmatrix}, \quad \widetilde{\Delta}_{1n}^{(1)}=\begin{vmatrix} -1 & \widetilde{\Phi}_{n1}^{(0)} & \Omega_{n0}^{(2)} & 0 \\ a_n^{(1)} & \widetilde{\Phi}_{n1}^{(1)} & \Omega_{n1}^{(2)} & 0 \\ 0 & 0 & -1 & a_n^{(2)} \\ 0 & 0 & a_n^{(3)} & -1 \end{vmatrix}$$

/78

$$\widetilde{\Delta}_{2n}^{(1)}=\begin{vmatrix} -1 & a_n^{(0)} & \Phi_{n1}^{(0)} & 0 \\ a_n^{(1)} & -1 & \Phi_{n1}^{(1)} & 0 \\ 0 & \Omega_{n2}^{(1)} & 0 & a_n^{(2)} \\ 0 & \Omega_{n3}^{(1)} & 0 & -1 \end{vmatrix}, \quad \widetilde{\Delta}_{3n}^{(1)}=\begin{vmatrix} -1 & a_n^{(0)} & \Omega_{n0}^{(2)} & \widetilde{\Phi}_{n1}^{(0)} \\ a_n^{(1)} & -1 & \Omega_{n1}^{(2)} & \widetilde{\Phi}_{n1}^{(1)} \\ 0 & \Omega_{n2}^{(1)} & -1 & 0 \\ 0 & \Omega_{n3}^{(1)} & a_n^{(3)} & 0 \end{vmatrix} \tag{1.279}$$

Here as in the preceeding paragraph, we will deal only with the transformation of the electromagnetic and radar characteristics of a two-layer sphere. Since their analytical expressions will remain the same as in the case of a multi-layer sphere, i.e., (1.268)-(1.276), the transformation will apply to the coefficients $\Xi_{n1}^{(1)}$, $\Xi_{n1}^{(2)}$, written in (1.262) in terms of the determinants (1.263), (1.279)

It can be shown that after numerous and cumbersome transformations based on the properties of the determinant, these coefficients will take the form:

$$\Xi_{n1}^{(1)}=\frac{\begin{vmatrix} \alpha_0 j_n(k_0b_1) & \alpha_1 j_n(k_1b_1) & \alpha_1 h_n(k_1b_1) & 0 \\ \psi_n'(k_0b_1) & \psi_n'(k_1b_1) & \zeta_n'(k_1b_1) & 0 \\ 0 & -\alpha_1 j_n(k_1b_2) & -\alpha_1 h_n(k_1b_2) & \alpha_2 j_n(k_2b_2) \\ 0 & \psi_n'(k_1b_2) & \zeta_n'(k_1b_2) & -\psi_n'(k_2b_2) \end{vmatrix}}{\begin{vmatrix} -\alpha_0 h_n(k_0b_1) & \alpha_1 j_n(k_1b_1) & \alpha_1 h_n(k_1b_2) & 0 \\ -\zeta_n'(k_0b_1) & \psi_n'(k_1b_1) & \zeta_n'(k_1b_1) & 0 \\ 0 & -\alpha_1 j_n(k_1b_2) & -\alpha_1 h_n(k_1b_2) & \alpha_2 j_n(k_2b_2) \\ 0 & \psi_n'(k_1b_2) & \zeta_n'(k_1b_2) & -\psi_n'(k_2b_2) \end{vmatrix}},$$

$$\Xi_{n1}^{(2)}=\frac{\begin{vmatrix} \beta_0 j_n(k_0b_1) & \beta_1 j_n(k_1b_1) & \beta_1 h_n(k_1b_1) & 0 \\ \psi_n'(k_0b_1) & \psi_n'(k_1b_1) & \zeta_n'(k_1b_1) & 0 \\ 0 & -\beta_1 j_n(k_1b_2) & -\beta_1 h_n(k_1b_2) & \beta_2 j_n(k_2b_2) \\ 0 & \psi_n'(k_1b_2) & \zeta_n'(k_1b_2) & -\psi_n'(k_2b_2) \end{vmatrix}}{\begin{vmatrix} -\beta_0 h_n(k_0b_1) & \beta_1 j_n(k_1b_1) & \beta_1 h_n(k_1b_1) & 0 \\ -\zeta_n'(k_0b_1) & \psi_n'(k_1b_1) & \zeta_n'(k_1b_1) & 0 \\ 0 & -\beta_1 j_n(k_1b_2) & -\beta_1 h_n(k_1b_2) & \beta_2 j_n(k_2b_2) \\ 0 & \psi_n'(k_1b_2) & \zeta_n'(k_1b_2) & -\psi_n'(k_2b_2) \end{vmatrix}}. \tag{1.280}$$

If we introduce the notation

$$\alpha = k_0 b_2,\ \nu = k_0 b_1,\ \frac{k_2}{k_0} = N_2,\ \frac{k_1}{k_0} = N_1,$$

$$y_i = \sqrt{\frac{\varepsilon_i}{\mu_i}},\ i = 0,\ 1,\ 2, \tag{1.281}$$

$$\eta_n^{(1)}(x) = \frac{\varphi_n'(x)}{x},\ \eta_n^{(2)}(x) = \frac{\zeta_n'(x)}{x},$$

then carry out transformations similar to those which led to expressions (1.280), and consider the relations

$$k_2 b_2 = N_2\alpha,\ k_1 b_2 = N_1\alpha,\ k_1 b_1 = N_1\nu, \tag{1.282}$$

which may be obtained from (1.281) by using formulas (1.1), (1.3), we will obtain another representation for the coefficients $\Xi_{n1}^{(1),(2)}$:

$$\Xi_{n1}^{(1)} = \frac{\begin{vmatrix} 0 & -\eta_n^{(1)}(N_2\alpha) & \eta_n^{(1)}(N_1\alpha) & \eta_n^{(2)}(N_1\alpha) \\ 0 & -y_2 j_n(N_2\alpha) & y_1 j_n(N_1\alpha) & y_1 h_n(N_1\alpha) \\ \eta_n^{(1)}(\nu) & 0 & \eta_n^{(1)}(N_1\nu) & \eta_n^{(2)}(N_1\nu) \\ y_0 j_n(\nu) & 0 & y_1 j_n(N_1\nu) & y_1 h_n N_1\nu) \end{vmatrix}}{\begin{vmatrix} 0 & -\eta_n^{(1)}(N_2\alpha) & \eta_n^{(1)}(N_1\alpha) & \eta_n^{(2)}(N_1\alpha) \\ 0 & -y_2 j_n(N_2\alpha) & y_1 j_n(N_1\alpha) & y_1 h_n(N_1\alpha) \\ -\eta_n^{(2)}(\nu) & 0 & \eta_n^{(1)}(N_1\nu) & \eta_n^{(2)}(N_1\nu) \\ -y_0 h_n(\nu) & 0 & y_1 j_n(N_1\nu) & y_1 h_n(N_1\nu) \end{vmatrix}}$$

$$\Xi_{n1}^{(2)} = \frac{\begin{vmatrix} 0 & -j_n(N_2\alpha) & j_n(N_1\alpha) & h_n(N_1\alpha) \\ 0 & -y_2\eta_n^{(1)}(N_2\alpha) & y_1\eta_n^{(1)}(N_1\alpha) & y_1\eta_n^{(2)}(N_1\alpha) \\ j_n(\nu) & 0 & j_n(N_1\nu) & h_n(N_1\nu) \\ y_0\eta_n^{(1)}(\nu) & 0 & y_1\eta_n^{(1)}(N_1\nu) & y_1\eta_n^{(2)}(N_1\nu) \end{vmatrix}}{\begin{vmatrix} 0 & -j_n(N_2\alpha) & j_n(N_1\alpha) & h_n(N_1\alpha) \\ 0 & -y_2\eta_n^{(1)}(N_2\alpha) & y_1\eta_n^{(1)}(N_1\alpha) & y_1\eta_n^{(2)}(N_1\alpha) \\ -h_n(\nu) & 0 & j_n(N_1\nu) & h_n(N_1\nu) \\ -y_0\eta_n^{(2)}(\nu) & 0 & y_1\eta_n^{(1)}(N_1\nu) & y_1\eta_n^{(2)}(N_1\nu) \end{vmatrix}} \tag{1.283}$$

In this form the coefficients of (1.283) coincide to within the designations with the analogous coefficients given in [3]. As was done in [3], we will also write them in a form convenient for calculations: /80

$$\Xi_{n1}^{(1)} = -\frac{\eta_n^{(1)}(\nu) A_1 + y_0 j_n(\nu) A_2}{\eta_n^{(2)}(\nu) A_1 + y_0 h_n(\nu) A_2}, \qquad (1.284)$$

$$\Xi_{n1}^{(2)} = -\frac{j_n(\nu) A_3 + y_0 \eta_n^{(1)}(\nu) A_4}{h_n(\nu) A_3 + y_0 \eta_n^{(2)}(\nu) A_4},$$

where

$$A_1 = y_1^2 \eta_n^{(1)}(N_2\alpha)\left[j_n(N_1\nu) h_n(N_1\alpha) - j_n(N_1\alpha) h_n(N_1\nu)\right] + \\ + y_1 y_2 j_n(N_2\alpha)\left[\eta_n^{(1)}(N_1\alpha) h_n(N_1\nu) - \eta_n^{(2)}(N_1\alpha) j_n(N_1\nu)\right],$$

$$A_2 = y_1 \eta_n^{(1)}(N_2\alpha)\left[j_n(N_1\alpha)\eta_n^{(2)}(N_1\nu) - h_n(N_1\alpha)\eta_n^{(1)}(N_1\nu)\right] + \\ + y_2 j_n(N_2\alpha)\left[\eta_n^{(1)}(N_1\nu)\eta_n^{(2)}(N_1\alpha) - \eta_n^{(1)}(N_1\alpha)\eta_n^{(2)}(N_1\nu)\right],$$

$$A_3 = y_1^2 j_n(N_2\alpha)\left[\eta_n^{(1)}(N_1\nu)\eta_n^{(2)}(N_1\alpha) - \eta_n^{(1)}(N_1\alpha) \times \right. \\ \left. \times \eta_n^{(2)}(N_1\nu)\right] + y_1 y_2 \eta_n^{(1)}(N_1\alpha)\left[j_n(N_1\alpha)\eta_n^{(2)}(N_1\nu) - h_n(N_1\alpha)\eta_n^{(1)}(N_1\nu)\right],$$

$$A_4 = y_1 j_n(N_2\alpha)\left[\eta_n^{(1)}(N_1\alpha) h_n(N_1\nu) - \eta_n^{(2)}(N_1\alpha) j_n(N_1\nu)\right] + \\ + y_2 \eta_n^{(1)}(N_2\alpha)\left[j_n(N_1\nu) h_n(N_1\alpha) - j_n(N_1\alpha) h_n(N_1\nu)\right]. \qquad (1.285)$$

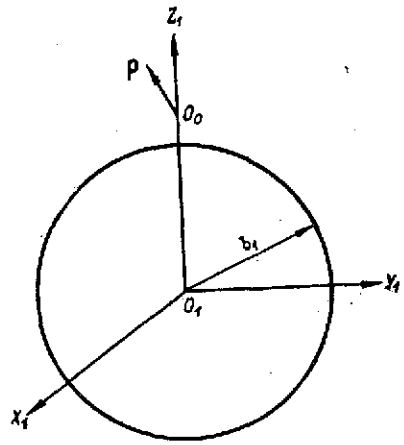

Figure 1.7. Case of a Single Sphere.

Case of a Single Sphere. In this case (Figure 1.7), $\nu = 1$ and system (1.244) becomes:

$$\begin{cases} -Z_{nm}^{(0)} + Z_{nm}^{(1)} a_n^{(0)} = \Phi_{nm}^{(0)}, \\ Z_{nm}^{(0)} a_n^{(1)} - Z_{nm}^{(1)} = \Phi_{nm}^{(1)}. \end{cases}$$

Hence, considering relations (1.249)- /81
-(1.263), (1.149a), notation (1.281) and with condition (1.150), as a result of a series of transformations we will obtain the values of the unknown coefficients:

$$A_{nm(u)}^{(1)} = \frac{y_0 i A_{nm(u)}^{(0)}}{y_1 \psi_n(N_1\nu)\zeta_n'(\nu) - y_0 \zeta_n(\nu)\psi_n'(N_1\nu)},$$

$$A^{(1)}_{nm\,(v)} = \frac{y_1 i A^{(0)}_{nm\,(v)}}{y_0\psi_n(N_1\nu)\zeta_n'(\nu) - y_1\zeta_n(\nu)\psi_n'(N_1\nu)},$$

$$B^{(0)}_{nm\,(u)} = \frac{y_1\psi_n(N_1\nu)\psi_n'(\nu) - y_0\psi_n'(N_1\nu)\psi_n(\nu)}{y_0\zeta_n(\nu)\psi_n'(N_1\nu) - y_1\psi_n(N_1\nu)\zeta_n'(\nu)} A^{(0)}_{nm\,(u)},$$

$$B^{(0)}_{nm\,(v)} = \frac{y_0\psi_n(N_1\nu)\psi_n'(\nu) - y_1\psi_n'(N_1\nu)\psi_n(\nu)}{y_1\zeta_n(\nu)\psi_n'(N_1\nu) - y_0\psi_n(N_1\nu)\zeta_n'(\nu)} A^{(0)}_{nm\,(v)},$$

where $A^{(0)}_{nm(u)}$ and $A^{(0)}_{nm(v)}$ are defined by formulas (1.76)-(1.80). The coefficients $\tilde{A}^{(1)}_{nm}$ and $\tilde{B}^{(1)}_{nm}$, corresponding to the case of a plane wave, are similarly obtained:

$$\tilde{A}^{(1)}_{n1\,(u)} = \frac{2n+1}{2n(n+1)} \frac{i^{-n}k_0 y_0}{y_1\psi_n(N_1\nu)\zeta_n'(\nu) - y_0\zeta_n(\nu)\psi_n'(N_1\nu)},$$

$$\tilde{A}^{(1)}_{n1\,(v)} = -\frac{2n+1}{2n(n+1)} \frac{i^{-n}\alpha_0 y_1}{y_0\psi_n(N_1\nu)\zeta_n'(\nu) - y_1\zeta_n(\nu)\psi_n'(N_1\nu)},$$

$$\tilde{B}^{(0)}_{n1\,(u)} = i^{-(n+1)} k_0 \frac{2n+1}{2n(n+1)} \frac{y_1\psi_n(N_1\nu)\psi_n'(\nu) - y_0\psi_n'(N_1\nu)\psi_n(\nu)}{y_0\zeta_n(\nu)\psi_n'(N_1\nu) - y_1\psi_n(N_1\nu)\zeta_n'(\nu)}, \qquad (1.286)$$

$$\tilde{B}^{(0)}_{n1\,(v)} = i^{-n+1}\alpha_0 \frac{2n+1}{2n(n+1)} \frac{y_1\psi_n'(N_1\nu)\psi_n(\nu) - y_0\psi_n(N_1\nu)\psi_n'(\nu)}{y_1\zeta_n(\nu)\psi_n'(N_1\nu) - y_0\psi_n(N_1\nu)\zeta_n'(\nu)}.$$

Using relation (1.286) in (1.210), we come to expressions for the coefficients $\Xi^{(1),\ (2)}_{n1}$, known in the literature as Mie coefficients:

$$\Xi^{(1)}_{n1} = -\frac{y_0\psi_n'(N_1\nu)\psi_n(\nu) - y_1\psi_n(N_1\nu)\psi_n'(\nu)}{y_0\zeta_n(\nu)\psi_n'(N_1\nu) - y_1\psi_n(N_1\nu)\zeta_n'(\nu)},$$

$$\Xi^{(2)}_{n1} = -\frac{y_0\psi_n(N_1\nu)\psi_n'(\nu) - y_1\psi_n'(N_1\nu)\psi_n(\nu)}{y_0\psi_n(N_1\nu)\zeta_n'(\nu) - y_1\zeta_n(\nu)\psi_n'(N_1\nu)}, \qquad (1.287)$$

the electromagnetic and radar characteristics being defined by formulas (1.286)-(1.276). Let us note that the same relations (1.287) but in a somewhat different form may be obtained from expressions (1.283), (1.284) if in the latter one sets $b_2 = b_1$ ($\alpha = \nu$), or $b_2 = 0$. /82

$$\Xi^{(1)}_{n1} = -\frac{y_0\eta^{(1)}_n(N_s\alpha)j_n(\alpha) - y_2\eta^{(1)}_n(\alpha)j_n(N_s\alpha)}{y_0\eta^{(1)}_n(N_s\alpha)h_n(\alpha) - y_2\eta^{(2)}_n(\alpha)j_n(N_s\alpha)},$$

$$\Xi^{(2)}_{n1} = -\frac{y_0\eta^{(1)}_n(\alpha)j_n(N_s\alpha) - y_2\eta^{(1)}_n(N_s\alpha)j_n(\alpha)}{y_0\eta^{(2)}_n(\alpha)j_n(N_s\alpha) - y_2\eta^{(1)}_n(N_s\alpha)h_n(\alpha)}, \qquad (1.288)$$

where

$$\alpha=\frac{2\pi b_2}{\lambda},\ s=2 \quad \text{for} \quad b_2=b_1;$$

$$\alpha=\frac{2\pi b_1}{\lambda},\ s=1 \quad \text{for} \quad b_2=0.$$

§ 1.7. Scattering and Attenuation of Electromagnetic Waves by an Ideally Conducting Sphere With a Nonconcentrically Layered Cover.

It is evident that the solution of the problem formulated in the title of the present paragraph should follow from the general solution of § 1.3. if in the latter one sets $k_\nu^2 = i\infty$. However, this method turns out to be more cumbersome and much more complex than the direct solution of the problem.

Let us have in the field of a dipole radiator (Figure 1.1) ν spheres arbitrarily located inside one another, the ν-th sphere (of radius b_ν) being ideally conducting. In terms of the notation of § 1.1, we introduce the generalized potential T_j of medium j, which satisfies equation (1.4a) and is related to the electromagnetic field components by relations (1.5), (1.2), (1.7), (1.8). The problem under consideration is stated as follows: to find the solutions of equations (1.4a) at each of $j = 0, 1, \ldots, \nu - 1$ media under conditions (1.9) and

$$\left.\begin{aligned} q_j T_j &= q_{j+1} T_{j+1} \\ \frac{\partial (r_{j+1} T_j)}{\partial r_{j+1}} &= \frac{\partial (r_{j+1} T_{j+1})}{\partial r_{j+1}} \end{aligned}\right\} \text{for } r_{j+1} = b_{j+1},\ j = 0, 1, \ldots, \nu-2,$$

$$\alpha_{01} \frac{\partial (r_\nu T_{\nu-1})}{\partial r_\nu} + \beta_{01} T_{\nu-1} = 0 \text{ for } r_\nu = b_\nu, \tag{1.289}$$

where[35]

$$\alpha_{01} = \{1, 0\},\quad \beta_{01} = \{0, 1\}. \tag{1.290}$$

The solution of the stated problem is sought in the form of the same (1.75)- /84
(1.85) expansions as in the general case. Satisfaction by the latter of conditions (1.289) by analogy with (1.92) leads to a system for unknown $Z_{nm}^{(j)}$, related to the coefficients $A_{nm}^{(j)}$, $B_{nm}^{(j)}$, by relations (1.90):

---

[35]The same notation as in the preceding sections will be used here. Since in the ν-th medium, because of absence of the electromagnetic field, $E_\theta^{(\nu-1)} = E_\phi^{(\nu-1)} = 0$, $T_\nu = 0$.

$$
\begin{cases}
Z_{nm}^{(0)} = a_n^{(0)} Z_{nm}^{(1)} + \sum\limits_{\tau=0}^{\infty} \sum\limits_{l=-\tau}^{\tau} Z_{\tau l}^{(2)} a_{\tau l n m 0}^{(2)} - \Phi_{nm}^{(0)}, \\
Z_{nm}^{(1)} = a_n^{(1)} Z_{nm}^{(0)} + \sum\limits_{\tau=0}^{\infty} \sum\limits_{l=-\tau}^{\tau} Z_{\tau l}^{(2)} a_{\tau l n m 1}^{(2)} - \Phi_{nm}^{(1)}, \\
Z_{nm}^{(2j)} = a_n^{(2j)} Z_{nm}^{(2j+1)} + \sum\limits_{\tau=0}^{\infty} \sum\limits_{l=-\tau}^{\tau} Z_{\tau l}^{(2j-1)} a_{\tau l n m 2j}^{(2j-1)} + \sum\limits_{\tau=0}^{\infty} \sum\limits_{l=-\tau}^{\tau} Z_{\tau l}^{(2j+2)} \times a_{\tau l n m 2j}^{(2j+2)}, \\
Z_{nm}^{(2j+1)} = a_n^{(2j+1)} Z_{nm}^{(2j)} + \sum\limits_{\tau=0}^{\infty} \sum\limits_{l=-\tau}^{\tau} Z_{\tau l}^{(2j-1)} a_{\tau l n m 2j+1}^{(2j-1)} + \sum\limits_{\tau=0}^{\infty} \sum\limits_{l=-\tau}^{\tau} Z_{\tau l}^{(2j+2)} a_{\tau l n m 2j+1}^{(2j+2)}, \\
Z_{nm}^{(2\nu-3)} = \sum\limits_{\tau=0}^{\infty} \sum\limits_{l=-\tau}^{\tau} Z_{\tau l}^{(2\nu-3)} a_{\tau l n m 2\nu-2}^{(2\nu-3)},
\end{cases}
\tag{1.291}
$$

$$
n = 0, 1, \ldots; \quad m = -n, \ldots, n; \quad j = 1, 2, \ldots, \nu - 2.
$$

Here $a_n^{(s)}$, $\Phi_{nm}^{(s)}$, $a_{\tau l n m s}^{(i)}$ are defined by formulae (1.93):

$$
\begin{aligned}
a_{\tau l n m 2\nu-2}^{(2\nu-3)} &= -\sqrt{\frac{(n+m)!\,(\tau-l)!}{(n-m)!\,(\tau+l)!}} \frac{\Gamma_n(k_{\nu-1}b_\nu)\, h_\tau^*(k_{\nu-1}b_{\nu-1})}{G_n(k_{\nu-1}b_\nu)\, j_n^*(k_{\nu-1}b_\nu)} K_{nm\tau l\nu-1}, \\
\Gamma_n(k_{\nu-1}r_\nu) &= \alpha_{01} \frac{d}{dr_\nu} [r_\nu j_n(k_{\nu-1}r_\nu)] + \beta_{01} j_n(k_{\nu-1}r_\nu), \\
G_n(k_{\nu-1}r_\nu) &= \alpha_{01} \frac{d}{dr_\nu} [r_\nu h_n(k_{\nu-1}r_\nu)] + \beta_{01} h_n(k_{\nu-1}r_\nu).
\end{aligned}
\tag{1.292}
$$

In the course of the transformations, the fulfillment of inequalities (1.88), (1.89) was assumed for j = 0, 1, ..., ν - 2, and

$$
\zeta_n'(k_{\nu-1}b_\nu) \neq 0. \tag{1.293}
$$

By virtue of (1.4), condition (1.293) always applies, and the proof is carried out by analogy with the proof of statement (1.88). However, condition (1.89) may also not be fulfilled. This case will be discussed below.

If by analogy with the general case (p. 36) we introduce a Banach space /84 $\tilde{l}'_2$, consisting of three-dimensional matrices $Z = \{Z_{nm}^{(j)}\}$, $n = 0, 1, \ldots, m = -n, \ldots, j = 0, 1, \ldots, 2\nu - 2$, with $Z_{nm}^{(j)} = 0$ or $|m| > n$ and the norm

$$\|Z\| = \sqrt{\sum_{j=0}^{2\nu-2} \sum_{n=0}^{\infty} \sum_{m=-n}^{n} |Z_{nm}^{(j)}|^2} < \infty,$$

then system (1.219) may be written in the form of a single functional equation of type (1.97):

$$(\mathbf{W} + \mathbf{T}) Z = \Phi. \tag{1.294}$$

Fredholm's alternative is valid for equation (1.294), since the linear operators W and T act from $\tilde{l}'_2$ to $\tilde{l}'_2$, the former being reversible and the latter completely continuous, and $\Phi \in \tilde{l}'_2$.

Indeed, the transformation matrix of W

$$\begin{pmatrix} -1 & a_n^{(1)} & \cdot & 0 & 0 & 0 \\ a_n^{(0)} & -1 & \cdot & 0 & 0 & 0 \\ \cdot & \cdot & \cdot & \cdot & \cdot & \cdot \\ 0 & 0 & \cdot & -1 & a_n^{(2\nu-4)} & 0 \\ 0 & 0 & \cdot & a_n^{(2\nu-3)} & -1 & 0 \\ 0 & 0 & \cdot & 0 & 0 & -1 \end{pmatrix} \tag{1.295}$$

is a square matrix of order (2v-1) × (2v-1) with nonzero determinant, which can be easily demonstrated by the aid of inequality (1.108) by expanding the determinant of matrix (1.295) with respect to the elements of the last row. The total continuity of the operator T devolves from inequalities (1.126) - (1.129) and

$$\sum_{n=0}^{\infty} \sum_{m=-n}^{n} \sum_{\tau=0}^{\infty} \sum_{l=-\tau}^{\tau} |a_{\tau l n m 2\nu-2}^{(2\nu-3)}|^2 < \infty.$$

This results from relation (1.128) and from the estimate

$$\left| \frac{\psi_n'(z)}{\zeta_n'(z)} \right| < \text{const} \left| \frac{j_n(z)}{h_n(z)} \right|,$$

obtainable by means of lemma 2 of § 1.2. Further, by analogy with the general case, it is shown without any appreciable changes that the homogeneous system

$$(\mathbf{W} + \mathbf{T}) Z = 0$$

has only a trivial solution.

Hence we conclude that system (1.291) is uniquely solvable in $\tilde{l}_2'$ and by virtue of theorem 1 of § 1.3, that expansions (1.83) together with relations (1.2) realize the solution of this problem.

If the paramters of the media are such that equality (1.151) applies, then by using relation $j_0 \leqslant \nu - 2$, which holds for the problem at hand, we arrive at a system corresponding to this case:

$$\begin{cases} \sum\limits_{l=0}^{2\nu-3} Z_{nm}^{(s)} \alpha_{ls*}^{(n)} + \sum\limits_{l=0}^{2\nu-3} \sum\limits_{\tau=0}^{\infty} \sum\limits_{l=-\tau}^{\tau} Z_{\tau l}^{(l)} a_{\tau l n m s *}^{(l)} = \Phi_{nm}^{(s)}, \\ Z_{nm}^{(2\nu-2)} = \sum\limits_{\tau=0}^{\infty} \sum\limits_{l=-\tau}^{\tau} Z_{\tau l}^{(2\nu-3)} \alpha_{\tau l n m 2\nu-2}^{(2\nu-3)}, \end{cases} \tag{1.296}$$

$$s = 0, 1, \ldots, 2\nu - 3; \quad n = 0, 1, \ldots; \quad m = -n, \ldots, n.$$

where $\alpha_{is**}^{(n)}$, $a_{\tau l n m s *}^{(i)}$ are defined by expressions (1.154).

The unique solvability of equations (1.296) is shown as in the general case.

In the case where the primary field is the plane wave field (1.186), system (1.291) becomes:

$$\begin{cases} \tilde{Z}_{nm}^{(0)} = a_n^{(0)} \tilde{Z}_{nm}^{(1)} + \sum\limits_{\tau=0}^{\infty} \sum\limits_{l=-\tau}^{\tau} \tilde{Z}_{\tau l}^{(2)} a_{\tau l n m 0}^{(2)} - \Phi_{nm}^{(0)}, \\ \tilde{Z}_{nm}^{(1)} = a_n^{(1)} \tilde{Z}_{nm}^{(0)} + \sum\limits_{\tau=0}^{\infty} \sum\limits_{l=-\tau}^{\tau} \tilde{Z}_{\tau l}^{(2)} a_{\tau l n m 1}^{(2)} - \Phi_{nm}^{(1)}, \\ \tilde{Z}_{nm}^{(2j)} = a_n^{(2j)} \tilde{Z}_{nm}^{(2j+1)} + \sum\limits_{\tau=0}^{\infty} \sum\limits_{l=-\tau}^{\tau} \tilde{Z}_{\tau l}^{(2j-1)} a_{\tau l n m 2j}^{(2j-1)} + \sum\limits_{\tau=0}^{\infty} \sum\limits_{l=-\tau}^{\tau} \tilde{Z}_{\tau l}^{(2j+2)} a_{\tau l n m 2j}^{(2j+2)}, \\ \tilde{Z}_{nm}^{(2j+1)} = a_n^{(2j+1)} \tilde{Z}_{nm}^{(2j)} + \sum\limits_{\tau=0}^{\infty} \sum\limits_{l=-\tau}^{\tau} \tilde{Z}_{\tau l}^{(2j-1)} a_{\tau l n m 2j+1}^{(2j-1)} + \sum\limits_{\tau=0}^{\infty} \sum\limits_{l=-\tau}^{\tau} \tilde{Z}_{\tau l}^{(2j+2)} a_{\tau l n m 2j+2}^{(2j+2)}, \\ \tilde{Z}_{nm}^{(2\nu-2)} = \sum\limits_{\tau=0}^{\infty} \sum\limits_{l=-\tau}^{\tau} \tilde{Z}_{\tau l}^{(2\nu-3)} a_{\tau l n m 2j+2}^{(2\nu-3)}, \end{cases} \tag{1.297}$$

$$j=1, 2, \ldots, \nu-2; \quad n=0, 1, \ldots; \quad m=-n, \ldots, n,$$

where $\widetilde{\Phi}_{nm}^{(j)}$ is defined by formula (1.187). All the expressions of § 1.4, 1.5 for the field components and also their electromagnetic and radar characteristics in each of the media will remain unchanged. However, the only exceptions are the coefficients $\widetilde{A}_{nm}^{(j)}$ and $\widetilde{B}_{nm}^{(j)}$, related to $\widetilde{Z}_{nm}^{(j)}$ by a dependence equivalent to (1.90). If identity (1.151) also applies to the case of the plane wave, system (1.297) is no longer suitable for determining $\widetilde{Z}_{nm}^{(j)}$. It must be converted to the form: /86

$$\begin{cases} \sum\limits_{l=0}^{2\nu-3} \widetilde{Z}_{nm}^{(s)} a_{ls*}^{(n)} + \sum\limits_{l=0}^{2\nu-3} \sum\limits_{\tau=0}^{\infty} \sum\limits_{l=-\tau}^{\tau} \widetilde{Z}_{\tau l}^{(i)} a_{\tau lnms_*}^{(i)} = \widetilde{\Phi}_{nm}^{(s)}, \\ \widetilde{Z}_{nm}^{(2\nu-2)} = \sum\limits_{\tau=0}^{\infty} \sum\limits_{l=-\tau}^{\tau} \widetilde{Z}_{\tau l}^{(2\nu-3)} a_{\tau lnm2\nu-2}^{(2\nu-3)}. \end{cases} \tag{1.298}$$

We will consider special cases of the relative positions of the layers of the cover.[36]

Case Where the Centers of All the ν Spheres Lie on the Same Straight Line. In this case (Figure 1.3), relations (1.234) apply, and in system (1.291) and the series of binary sums is converted to unary ones:

$$\begin{cases} Z_{nm}^{(0)} = a_n^{(0)} Z_{nm}^{(1)} + \sum\limits_{\tau=0}^{\infty} \sum\limits_{l=-\tau}^{\tau} Z_{\tau l}^{(2)} a_{\tau lnm\,0}^{(2)} - \Phi_{nm}^{(0)}, \\ Z_{nm}^{(1)} = a_n^{(1)} Z_{nm}^{(0)} + \sum\limits_{\tau=0}^{\infty} \sum\limits_{l=-\tau}^{\tau} Z_{\tau l}^{(2)} a_{\tau lnm\,1}^{(2)} - \Phi_{nm}^{(1)}, \\ Z_{nm}^{(2)} = a_n^{(2)} Z_{nm}^{(3)} + \sum\limits_{\tau=0}^{\infty} \sum\limits_{l=-\tau}^{\tau} Z_{\tau l}^{(1)} a_{\tau lnm\,2}^{(1)} + \sum\limits_{\tau=0}^{\infty} Z_{nm}^{(4)} a_{\tau mnm\,2}^{(4)}, \\ Z_{nm}^{(3)} = a_n^{(3)} Z_{nm}^{(2)} + \sum\limits_{\tau=0}^{\infty} \sum\limits_{l=-\tau}^{\tau} Z_{\tau l}^{(1)} a_{\tau lnm\,3}^{(1)} + \sum\limits_{\tau=0}^{\infty} Z_{\tau m}^{(4)} a_{\tau minm\,3}^{(4)}, \\ Z_{nm}^{(2j)} = a_n^{(2j)} Z_{nm}^{(2j+1)} + \sum\limits_{\tau=0}^{\infty} Z_{\tau m}^{(2j-1)} a_{\tau mnm\,2j}^{(2j-1)} + \sum\limits_{\tau=0}^{\infty} Z_{\tau m}^{(2j+2)} a_{\tau mnm\,2j}^{(2j+2)}, \end{cases} \tag{1.299}$$

[36]Cases where equality (1.151) applies and the unknowns are determined either from system (1.296) or from (1.298) are treated like the corresponding cases in § 1.6, and are therefore omitted here.

$$\begin{cases} Z_{nm}^{(2j+1)} = a_n^{(2j+1)} Z_{nm}^{(2j)} + \sum\limits_{\tau=0}^{\infty} Z_{\tau m}^{(2j-1)} a_{\tau m n m\, 2j+1}^{(2j-1)} + \sum\limits_{\tau=0}^{\infty} Z_{\tau m}^{(2j+2)} a_{\tau m n m\, 2j+1}^{(2j+2)}, \\ Z_{nm}^{(2\nu-2)} = \sum\limits_{\tau=0}^{\infty} Z_{\tau m}^{(2\nu-3)} a_{\tau m n m\, 2\nu-2}^{(2\nu-3)}. \end{cases}$$

Here $a_n^{(s)}$ are defined by formulas (1.93), $a_{\tau mnms}^{(i)}$ by (1.235)-(1.238), and $\alpha_{\tau mnm2\nu-2)}^{(2\nu-3)}$ by the formula

$$\alpha_{\tau m n m\, 2\nu-2}^{(2\nu-3)} = -\sqrt{\frac{(n+m)!\,(\tau-m)!}{(n-m)!\,(\tau+m)!}} \times \times \frac{\Gamma_n(k_{\nu-1}b_\nu)\, h_\tau^*(k_{\nu-1}b_{\nu-1})}{G_n(k_{\nu-1}b_\nu)\, j_n^*(k_{\nu-1}b_\nu)} F_{n\tau m\nu-1}^{(-1)}. \qquad (1.300)$$

If in system (1.299) $\Phi_{nm}^{(s)}$ is replaced by $\tilde{\Phi}_{nm}^{(s)}$, in accordance with expressions (1.187), and $Z_{nm}^{(s)}$ by $\tilde{Z}_{nm}^{(s)}$, we will obtain system (1.297), simplified for the case under consideration.

Case Where the Line of Centers of All the ν Spheres Coincides With Axis Z. Providing that the centers of all the spheres and the point of application of the dipole are located on the same straight line, expressions (1.233), (1.235), (1.237) are valid also for $j = 1$, and (1.236), (1.238), also for $j = 0$. When this fact is taken into account, system (1.299) becomes even more simplified.

$$\begin{cases} Z_{mn}^{(0)} = a_n^{(0)} Z_{nm}^{(1)} + \quad + \sum\limits_{\tau=0}^{\infty} Z_{\tau m}^{(2)} a_{\tau m n m\, 0}^{(2)} - \Phi_{nm}^{(0)}, \\ Z_{nm}^{(1)} = a_n^{(1)} Z_{nm}^{(0)} + \quad + \sum\limits_{\tau=0}^{\infty} Z_{\tau m}^{(2)} a_{\tau m n m 1}^{(2)} - \Phi_{nm}^{(1)}, \\ Z_{nm}^{(2j)} = a_n^{(2j)} Z_{nm}^{(2j+1)} + \sum\limits_{\tau=0}^{\infty} Z_{\tau m}^{(2j-1)} a_{\tau m n m 2j}^{(2j-1)} + \sum\limits_{\tau=0}^{\infty} Z_{\tau m}^{(2j+2)} a_{\tau m n m 2j}^{(2j+2)}, \\ Z_{nm}^{(2j+1)} = a_n^{(2j+1)} Z_{nm}^{(2j)} + \sum\limits_{\tau=0}^{\infty} Z_{\tau m}^{(2j-1)} a_{\tau m n m 2j+1}^{(2j-1)} + \sum\limits_{\tau=0}^{\infty} Z_{\tau m}^{(2j+2)} a_{\tau m n m 2j+1}^{(2j+2)}, \\ Z_{nm}^{(2\nu-2)} = \sum\limits_{\tau=0}^{\infty} Z_{\tau m}^{(2\nu-3)} a_{\tau m n m 2\nu-2}^{(2\nu-3)}, \end{cases} \qquad (1.301)$$

$$n = 0, 1, \ldots; \quad m = -n, \ldots, n; \quad j = 2, 3, \ldots, \nu - 2.$$

The case of the plane wave is completed by system (1.301) if in the latter $Z_{nm}^{(j)}$ is replaced by $\widetilde{Z}_{nm}^{(j)}$, and $\Phi_{nm}^{(s)}$ by $\widetilde{\Phi}_{nm}^{(s)}$, in accordance with relation (1.187).

Case of Concentric Arrangement of ν Spheres. In this case (see Figure 1.5) from equality (1.241) with the aid of notation (1.243) and

$$\widetilde{\Omega}_{n2\nu-2}^{(2\nu-3)} = -\frac{\Gamma_n(k_{\nu-1}b_\nu)(2n-1)!!(2n+1)!!}{G_n(k_{\nu-1}b_\nu)(k_{\nu-1}^2 b_{\nu-1}b_\nu)^n} \tag{1.302}$$

the unknown $Z_{nm}^{(j)}$ are determined from the following system: /88

$$\begin{cases} -Z_{nm}^{(0)} + Z_{nm}^{(1)}a_n^{(0)} + Z_{nm}^{(2)}\Omega_{n0}^{(2)} = \Phi_{nm}^{(0)}, \\ Z_{nm}^{(0)}a_n^{(1)} - Z_{nm}^{(1)} + Z_{nm}^{(2)}\Omega_{n1}^{(2)} = \Phi_{nm}^{(1)}, \\ Z_{nm}^{(2j-1)}\Omega_{n2j}^{(2j-1)} - Z_{nm}^{(2j)} + Z_{nm}^{(2j+1)}a_n^{(2j)} + Z_{nm}^{(2j+2)}\Omega_{n2j}^{(2j+2)} = 0, \\ Z_{nm}^{(2j-1)}\Omega_{n2j+1}^{(2j-1)} + Z_{nm}^{(2j)}a_n^{(2j+1)} - Z_{nm}^{(2j+1)} + Z_{nm}^{(2j+2)}\Omega_{n2j+1}^{(2j+2)} = 0, \\ Z_{nm}^{(2\nu-3)}\widetilde{\Omega}_{n2\nu-2}^{(2\nu-3)} - Z_{nm}^{(2\nu-2)} = 0, \end{cases} \tag{1.303}$$

$$n = 0, 1, \ldots; \quad m = -n, \ldots, n; \quad j = 1, 2, \ldots, \nu-2.$$

The determinant Δ_n of this system, in contrast to (1.248) has the form:

$$\begin{vmatrix} -1 & a_n^{(0)} & \Omega_{n0}^{(2)} & \cdots & 0 & 0 & 0 & 0 & \cdots & 0 & 0 \\ a_n^{(1)} & -1 & \Omega_{n1}^{(2)} & \cdots & 0 & 0 & 0 & 0 & \cdots & 0 & 0 \\ \cdots & \cdots & \cdots & \cdots & \cdots & \cdots & \cdots & \cdots & \cdots & \cdots & \cdots \\ 0 & 0 & 0 & \cdots & \Omega_{n2j}^{(2j-1)} & -1 & a_n^{(2j)} & \Omega_{n2j}^{(2j+2)} & \cdots & 0 & 0 \\ 0 & 0 & 0 & \cdots & \Omega_{n2j+1}^{(2j-1)} & a_n^{(2j+1)} & -1 & \Omega_{n2j+1}^{(2j+2)} & \cdots & 0 & 0 \\ \cdots & \cdots & \cdots & \cdots & \cdots & \cdots & \cdots & \cdots & \cdots & \cdots & \cdots \\ 0 & 0 & 0 & \cdots & 0 & 0 & 0 & 0 & \cdots & \widetilde{\Omega}_{n2\nu-2}^{(2\nu-3)} & -1 \end{vmatrix} \tag{1.304}$$

$$n = 0, 1, \ldots; \quad j = 1, 2, \ldots, \nu-2.$$

If hereinafter we have this determinant in mind, formulas (1.249)-(1.256) will remain in force. The determinant $\widetilde{\Delta}_n$ is obtained by replacing the first column of determinant (1.304) by the column $\widetilde{\Phi}_{nm}$, in accordance with equality (1.257). Then expressions (1.258)-(1.276) will apply here as well.

Case of Two Spheres. In the case where the ideally conducting sphere has one concentric spherical dielectric covering (Figure 1.6), we have a system of three equations to find the unknowns $Z_{nm}^{(j)}$, j = 0, 1, 2:

$$\begin{cases} -Z_{nm}^{(0)} + Z_{nm}^{(1)} a_n^{(0)} + Z_{nm}^{(2)} \Omega_{n0}^{(2)} = \Phi_{nm}^{(0)}, \\ Z_{nm}^{(0)} a_n^{(1)} - Z_{nm}^{(1)} + Z_{nm}^{(2)} \Omega_{n1}^{(2)} = \Phi_{nm}^{(1)}, \\ Z_{nm}^{(1)} \widetilde{\Omega}_{n2}^{(1)} - Z_{nm}^{(2)} = 0, \end{cases}$$

where the coefficients of the unknowns are defined by formulas (1.243), (1.322).

Because of the presence of a single covering, both the order of the determinants (1.278), characteristic of the general case, and their number decrease. We will write them out: /8.

$$\Delta_{0n}^{(1)} = \begin{vmatrix} \Phi_{n1}^{(0)} & a_n^{(0)} & \Omega_{n0}^{(2)} \\ \Phi_{n1}^{(1)} & -1 & \Omega_{n1}^{(2)} \\ 0 & \widetilde{\Omega}_{n2}^{(1)} & -1 \end{vmatrix},$$

$$\Delta_{1n}^{(1)} = \begin{vmatrix} -1 & \Phi_{n1}^{(0)} & \Omega_{n0}^{(2)} \\ a_n^{(1)} & \Phi_{n1}^{(1)} & \Omega_{n1}^{(2)} \\ 0 & 0 & -1 \end{vmatrix}, \qquad (1.305)$$

$$\Delta_{2n}^{(1)} = \begin{vmatrix} -1 & a_n^{(0)} & \Phi_{n1}^{(0)} \\ a_n^{(1)} & -1 & \Phi_{n1}^{(1)} \\ 0 & \widetilde{\Omega}_{n2}^{(1)} & 0 \end{vmatrix},$$

$$\Delta_n = \begin{vmatrix} -1 & a_n^{(0)} & \Omega_{n0}^{(2)} \\ a_n^{(1)} & -1 & \Omega_{n1}^{(2)} \\ 0 & \widetilde{\Omega}_{n2}^{(1)} & -1 \end{vmatrix}.$$

If the primary field is the plane wave field (1.186), then the determinants $\widetilde{\Delta}_{in}^{(1)}$ (i = 0, 1, 2) in terms of which the field components are expressed are formed from determinants (1.305) $\Delta_{in}^{(1)}$ by replacing $\Phi_{n1}^{(0)}$ and $\widetilde{\Phi}_{n1}^{(1)}$ by $\widetilde{\Phi}_{n1}^{(0)}$ and $\widetilde{\phi}_{n1}^{(1)}$ respectively.

It can also be shown if one takes into account relations (1.292), in expressions (1.262) and notation (1.281), that the coefficients $\Xi_{nm}^{(1),(2)}$ in the case at hand have the form:

$$\Xi_{n1}^{(1)}=\frac{\begin{vmatrix} y_0\zeta_n(\nu) & y_1\psi_n(N_1\nu) & y_1\zeta_n(N_1\nu) \\ \zeta_n'(\nu) & \psi_n'(N_1\nu) & \zeta_n'(N_1\nu) \\ 0 & \psi_n'(N_1\alpha) & \zeta_n'(N_1\alpha) \end{vmatrix}}{\begin{vmatrix} y_0\psi_n(\nu) & y_1\psi_n(N_1\nu) & y_1\zeta_n(N_1\nu) \\ \psi_n'(\nu) & \psi_n'(N_1\nu) & \zeta_n'(N_1\nu) \\ 0 & -\psi_n'(N_1\alpha) & -\zeta_n'(N_1\alpha) \end{vmatrix}},$$

$$\Xi_{n1}^{(2)}=\frac{\begin{vmatrix} y_1\zeta_n(\nu) & y_0\psi_n(N_1\nu) & y_0\zeta_n(N_1\nu) \\ \zeta_n'(\nu) & \psi_n'(N_1\nu) & \zeta_n'(N_1\nu) \\ 0 & \psi_n(N_1\alpha) & \zeta_n(N_1\alpha) \end{vmatrix}}{\begin{vmatrix} y_1\psi_n(\nu) & y_0\psi_n(N_1\nu) & y_0\zeta_n(N_1\nu) \\ \psi_n'(\nu) & \psi_n'(N_1\nu) & \zeta_n'(N_1\nu) \\ 0 & -\psi_n(N_1\alpha) & -\zeta_n(N_1\alpha) \end{vmatrix}}. \qquad (1.306)$$

After expanding the determinants and transforming expression (1.306), we can write in the form analogous to (1.284): /90

$$\Xi_{n1}^{(1)}=-\frac{y_0\zeta_n'(\nu)A_1+\zeta_n'(\nu)A_2}{y_0\psi_n(\nu)A_1+\psi_n'(\nu)A_2},$$

$$\Xi_{n1}^{(2)}=-\frac{y_1\zeta_n(\nu)A_3+\zeta_n'(\nu)A_4}{y_1\psi_n(\nu)A_3+\psi_n'(\nu)A_4},$$

where

$$A_1=\psi_n'(N_1\nu)\zeta_n'(N_1\alpha)-\psi_n'(N_1\alpha)\zeta_n'(N_1\nu),$$

$$A_2=y_1[\zeta_n(N_1\nu)\psi_n'(N_1\alpha)-\psi_n(N_1\nu)\zeta_n'(N_1\alpha)],$$

$$A_3=\psi_n'(N_1\nu)\zeta_n(N_1\alpha)-\psi_n(N_1\alpha)\zeta_n'(N_1\nu),$$

$$A_4=y_0[\zeta_n(N_1\nu)\psi_n(N_1\alpha)-\psi_n(N_1\nu)\zeta_n(N_1\alpha)].$$

Case of a Single Sphere. This case is characterized by the absence of any covering on an ideally conducting sphere (Figure 1.7) of radius b_1. Using relation (1.69) with $\nu = 1$, and assuming by definition that

$$K_{\tau lnm0}=\delta_{\tau n}\delta_{lm}\delta_{r_1r_0}\delta_{\theta_1\theta_0}\delta_{\varphi_1\varphi_0},$$

we come to the equality

$$B_{nm}^{(0)}=-\frac{\Gamma_n(k_0b_1)}{G_n(k_0b_1)}A_{nm}^{(0)}, \qquad (1.307)$$

into which system (1.291) degenerates.

From formula (1.307) it is now easy to obtain the expressions for the coefficient $B_{nm}^{(0)}$, $\tilde{B}_{nm}^{(0)}$, and also $\Xi_{nm}^{(1)}$, $\Xi_{n1}^{(2)}$;

$$B^{(0)}_{n0\,(u)} = -\frac{ik_0|\mathbf{p}_2|}{h_1}(2n+1)\frac{\psi_n'(k_0b_1)}{\zeta_n'(k_0b_1)}h_n(k_0h_1),$$

$$B^{(0)}_{n1\,(u)} = \frac{ik_0|\mathbf{p}_1|}{h_1}\frac{2n+1}{2n(n+1)}\frac{\psi_n'(k_0b_1)}{\zeta_n'(k_0b_1)}\zeta_n'(k_0h_1),$$

$$\widetilde{B}^{(0)}_{n1\,(u)} = -i^{-(n+1)}k_0\frac{2n+1}{2n(n+1)}\frac{\psi_n'(k_0b_1)}{\zeta_n'(k_0b_1)},$$

$$B^{(0)}_{n1\,(v)} = \frac{\alpha_0k_0|\mathbf{p}_1|(2n+1)}{2n(n+1)}\frac{j_n(k_0b_1)}{h_n(k_0b_1)}h_n(k_0h_1),$$

$$\widetilde{B}^{(0)}_{n1\,(v)} = -i^{-n+1}\alpha_0\frac{2n+1}{2n(n+1)}\frac{j_n(k_0b_1)}{h_n(k_0b_1)},$$

$$\Xi^{(1)}_{n1} = -\frac{\psi_n'(k_0b_1)}{\zeta_n'(k_0b_1)}, \qquad \text{/91}$$

$$\Xi^{(2)}_{n1} = -\frac{j_n(k_0b_1)}{h_n(k_0b_1)}.$$

Here, for the coefficients $B^{(0)}_{nm}$ for other values of index m, relations (1.255), (1.256) are valid; for $\widetilde{B}^{(0)}_{nm}$, (1.259), (1.260); for $\Xi^{(1),(2)}_{nm}$, (1.261).

Let us note in conclusion that in this special case as well, formulas and expressions coinciding with those known from the literature were obtained.

§ 1.8. Computational Aspects

The chief difficulty in solving the above discussed problems is the solution of infinite algebraic systems (1.95), (1.153), (1.190), (1.193), as well as systems corresponding to different special cases of relative positions of the spheres and their dielectric properties, discussed in § 1.6 and 1.7.

In view of the identity of the approaches in the numerical realization of the solutions of all the indicated systems, we will indicate it only for system (1.95).

We first transform this system. Thus, multiplying both sides of equality (1.95) by matrix (1.118) $\widetilde{\alpha}^{(n)}\{\beta^{(n)}_{sj}\}$, $s, j=0, 1, \ldots, 2\nu-1$; $n=0, 1, \ldots$,

$$\beta^{(n)}_{sj} = \frac{(-1)^{s+j}\left[a_n^{(j)}\delta_{sj+(-1)^j} - \delta_{sj}\right]}{\prod_{j=0}^{\nu-1}\left(1-a_n^{(2j)}a_n^{(2j+1)}\right)} \qquad (1.308)$$

and summing up over s from 0 to 2ν - 1, by virtue of the relation

$$\sum_{s=0}^{2\nu-1} \alpha_{ls}^{(n)} \beta_{sj}^{(n)} = \delta_{lj},$$

resulting from expressions (1.106) and (1.118), we will obtain

$$Z_{nm}^{(j)} - \sum_{l=0}^{2\nu-1} \sum_{\tau=0}^{\infty} \sum_{l=-\tau}^{\tau} Z_{\tau l}^{(l)} \mathrm{E}_{\tau lnm}^{(lj)} = \Lambda_{nm}^{(j)}, \tag{1.309}$$

$$n = 0, 1, \ldots; \quad m = -n, \ldots, n; \quad j = 0, 1, \ldots, 2\nu - 1,$$

where

$$\mathrm{E}_{\tau lnm}^{(lj)} = -\sum_{s=0}^{2\nu-1} a_{\tau lnms}^{(l)} \beta_{sj}^{(n)}, \tag{1.310}$$

$$\Lambda_{nm}^{(j)} = \sum_{s=0}^{2\nu-1} \Phi_{nm}^{(s)} \beta_{sj}^{(n)}.$$

System (1.309) may also be written in the form of a single functional equation in Banach space $\tilde{l}_2$. /92

$$Z + \mathrm{E}Z = \Lambda. \tag{1.311}$$

Indeed, from asymptotic representations of modified Bessel and Hankel functions, lemma 2 of § 1.2 and expression (1.308), we have the inequality

$$|\beta_{sj}^{(n)}| < \mathrm{const}_1, \tag{1.312}$$

which in turn, by means of representations (1.310) and estimates (1.122), (1.102) with limitations (1.133) and $b_1 < h_1$, leads to the following:

$$\|\Lambda\| < \mathrm{const}_2, \tag{1.313}$$

$$\sum_{\tau=0}^{\infty} \sum_{l=-\tau}^{\tau} \sum_{n=0}^{\infty} \sum_{m=-n}^{n} |\mathrm{E}_{\tau lnm}^{(lj)}|^2 < \mathrm{const}_3. \tag{1.314}$$

The last of relations (1.314) signifies that E is a completely continuous operator in $\tilde{l}_2$.

The chief requirement placed on the numerical algorithm of the solution of system (1.309) is the presence at each step of computations of *a priori* estimates of the convergence of the operations performed.

Thus, on the basis of the fact that any completely continuous operator in Banach space admits of representation in the form of a sum of a finite-dimensional operator and a convergence operator, determined in the corresponding subspaces as a result of standard [40, 41] transformations which are omitted here we arrive at the following computational scheme for solving system (1.309).

1. An n_0 is chosen such that

$$\sum_{l=0}^{2\nu-1}\sum_{j=0}^{2\nu-1}\sum_{\tau=n_0+1}^{\infty}\sum_{l=-\tau}^{\tau}\sum_{n=n_0+1}^{\infty}\sum_{m=-n}^{n}|\mathrm{E}_{\tau lnm}^{(lj)}|^2=q<1. \tag{1.315}$$

2. Systems of algebraic equations with respect to the unknown $f_{nm}^{(j)}$ and $G_{\tau l nm}^{(sj)}$ are solved:

$$f_{nm}^{(j)}-\sum_{s=0}^{2\nu-1}\sum_{\tau=n_0+1}^{\infty}\sum_{l=-\tau}^{\tau}f_{\tau l}^{(s)}\mathrm{E}_{\tau lnm}^{(sj)}=\Lambda_{nm}^{(j)}, \tag{1.316}$$

$$n=n_0+1,\quad n_0+2,\ \ldots;\quad m=-n,\ \ldots,\ n;\quad j=1,\ 2,\ \ldots,\ 2\nu-1,$$

$$G_{\tau lnm}^{(sj)}-\sum_{d=1}^{2\nu-1}\sum_{p=n_0+1}^{\infty}\sum_{r=-p}^{p}G_{\tau lpr}^{(sd)}\mathrm{E}_{prnm}^{(dj)}=\mathrm{E}_{\tau lnm}^{(sj)}, \tag{1.317}$$

$$n=n_0+1,\quad n+2,\ \ldots;\quad m=-n,\ \ldots,\ n;\quad \tau=0,\ 1,\ \ldots,\ n_0;$$

$$l=-\tau,\ \ldots,\ \tau;\quad s,\ j=1,\ 2,\ \ldots,\ 2\nu-1.$$

By virtue of inequality (1.315), the operators of equations (1.316), (1.317) /93 are convergence operators in space $\tilde{l}_2$. The solution is found by the method of successive approximations. It is known that the inequality

$$\|x_k-x^*\|<\delta \tag{1.138}$$

will be fulfilled [49] when

$$n>\frac{1}{\ln q}\,\frac{\delta(1-q)}{\|x_0-x_1\|}, \tag{1.319}$$

where x_k is the k-th approximation, x* is the exact solution, δ is the specified computational error, and q is a parameter defined by equality (1.315).

3. We calculate $R_{\tau l nm}^{(sj)}$ and $F_{nm}^{(j)}$:

$$R_{\tau lnm}^{(sj)}=\mathrm{E}_{\tau lnm}^{(sj)}+\sum_{d=0}^{2\nu-1}\sum_{p=n_0+1}^{\infty}\sum_{l=-p}^{p}G_{\tau lpr}^{(sd)}\mathrm{E}_{\tau lnm}^{(dj)}, \tag{1.320}$$

$$\tau=0,\ 1,\ \ldots,\ n_0;\quad l=-\tau,\ \ldots,\ \tau;\quad s,\ j=0,\ 1,\ \ldots,\ 2\nu-1;$$

$$F_{nm}^{(j)}=\Lambda_{nm}^{(j)}+\sum_{s=0}^{2\nu-1}\sum_{\tau=n_0+1}^{\infty}\sum_{l=-\tau}^{\tau}f_{\tau l}^{(s)}\mathrm{E}_{\tau lnm}^{(sj)}, \tag{1.321}$$

$$n=0,\ 1,\ \ldots,\ n_0;\quad m=-n,\ \ldots,\ n;\quad j=0,\ 1,\ \ldots,\ 2\nu-1.$$

4. A finite system [50, 38] is solved with respect to the desired unknowns $z_{nm}^{(j)}$ for $n \leqslant n_0$;

$$Z_{nm}^{(j)} - \sum_{s=1}^{\nu} \sum_{\tau=0}^{n_0} \sum_{l=-\tau}^{\tau} Z_{\tau l}^{(s)} R_{\tau l n m}^{(sj)} = F_{nm}^{(j)},$$
$$n = 0, 1, \ldots, n_0; \quad m = -n, \ldots, n; \quad j = 0, 1, \ldots, 2\nu - 1. \tag{1.322}$$

5. The unknown $Z_{nm}^{(j)}$ for $n > n_0$ are found in terms of the $z_{nm}^{(j)}$ already found in par. 4 with the aid of expression

$$Z_{nm}^{(j)} = f_{nm}^{(j)} + \sum_{s=1}^{\nu} \sum_{\tau=0}^{n_0} \sum_{l=-\tau}^{\tau} Z_{\tau l}^{(s)} G_{\tau l n m}^{(sj)}, \tag{1.323}$$
$$n = n_0 + 1, \quad n_0 + 2, \ldots; \quad m = -n, \ldots, n; \quad j = 0, 1, \ldots, 2\nu - 1.$$

It is convenient to check the final result by applying the reduction method directly to system (1.95).

CHAPTER 2

SCATTERING AND ATTENUATION OF ELECTROMAGNETIC WAVES BY AN ARBITRARY SET OF SPHERICAL PARTICLES

§ 2.1. Set Of ν Spheres In A Dipole Radiator Field. Statement Of The Problem.

Theoretical studies dealing with the scattering of electromagnetic waves by spheres arbitrarily arranged in space, with consideration of their mutual influences, were initiated by the well-known work of W. Trinks [13], in which this problem was solved for the case of two spheres under the condition that the incident plane wave propagates in the direction of their common axis of symmetry. O. A. Germogenova [15] extended Trink's solution to the case of two spheres of arbitrary diameters arbitrarily arranged in relation to the wave vector of the incident wave.

G. A. Shebeko [51] treated the same problem by assuming that the incident field is produced by a dipole radiator located at some point of space outside the spheres. Limitations were imposed on both the dipole orientation (moment p of dipole assumed to be collinear with the common axis of the spheres) and the electromagnetic parameters of the spheres (the spheres are assumed to be ideally conducting). In [52, 9], Ye. A. Ivanov removed these limitations, and obtained expressions for the radiophysical characteristics of two spheres in the wave zone.[37] Thus, the problem of scattering of electromagnetic waves by two spheres may be considered solved in a theoretical sense.

The solution of the problem of scattering by an arbitrary number of spheres was treated in two studies: [22], which solves the problem of diffraction of a linearly polarized plane electromagnetic wave by several ideally conducting spheres with their centers on the same straight line; [55], which constructed a solution for the case of a dipole radiator arbitrarily situated and oriented in space under the condition that the spheres are ideally conducting; [56], in which the problem under consideration was solved in general form without imposing any limitations on the dielectric properties, size and arrangement of the spheres, or on the type and orientation of the incident radiation.[38] In addition, [56] gives expressions for various electromagnetic and radar characteristics of a set of spheres in the long-range zone.

[37] See also [53, 54].

[38] See also [57].

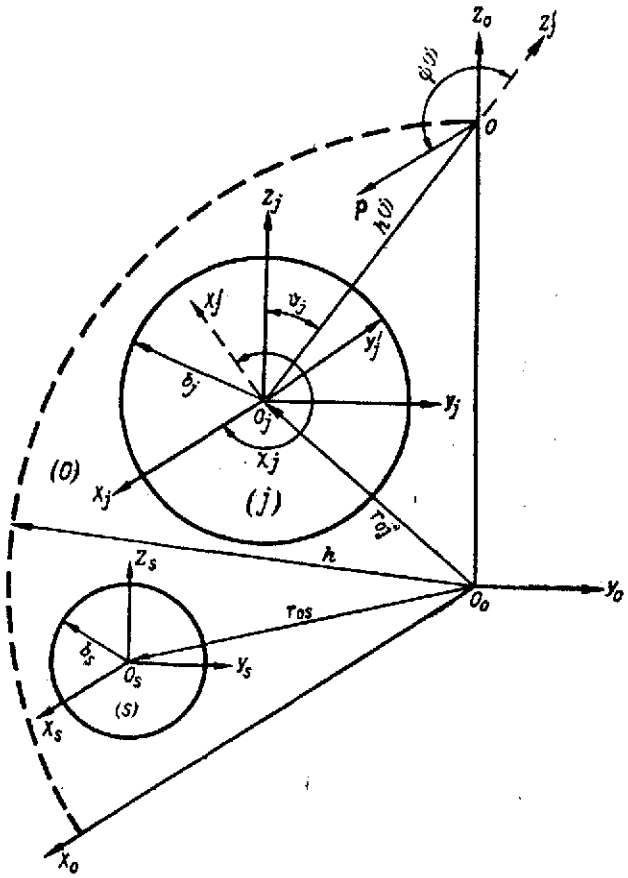

Figure 2.1. Set of Spheres in a Dipole Radiator Field.

Let us turn directly to the problem formulated in the title of this section.

Let ν spheres (Figure 2.1) be arbitrarily arranged in infinite space (medium zero), the j-th sphere (medium j) having radius b_j, the center at point O_j, and complex permittivity and permeability ε_j and μ_j respectively ($j = 1, 2, \ldots, \nu$). We will also assume that at some point 0 of medium 0 there is an electric dipole of moment p arbitrarily oriented in space.[39] The problem of determining the electromagnetic fields in each of these media is raised. /96

We introduce $2\nu + 1$ rectangular Cartesian coordinate systems.

System $X_0Y_0Z_0$. Axis Z_0 will be drawn through point o perpendicular to vector p, and axis X_0 parallel to vector p. The origin of system O_0 is chosen arbitrarily on axis Z_0. We will denote the distance O_0O_j by r_{0j} and O_0O by h.

Systems $X_jY_jZ_j$ ($j = 1, 2, \ldots, \nu$) are obtained by a parallel shift of system $X_0Y_0Z_0$ into origin O_j.

In each of the Cartesian systems $X_jY_jZ_j$, the spherical coordinates r_j, θ_j, ϕ_j ($j = 0, 1, \ldots, \nu$) are introduced; $0 < r_j < \infty$, $0 \leqslant \theta_j \leqslant \pi$, $0 \leqslant \phi_j < 2\pi$. In addition, by r_{sj}, θ_{sj}, ϕ_{sj} are denoted the spherical coordinates of origin O_j in a system with origin O_s ($s, j = 0, 1, \ldots, \nu$; $s \neq j$). We will also agree on the numbering of the media considered ($j = 1, 2, \ldots, \nu$). Thus, we will

[39] The same remarks apply here as in the statement of the problem in § 1.1 (see references on p. 5).

number in the order of nondecreasing r_{0j}, i.e., the first medium taken will be the sphere whose polar radius is the smallest of all r_{0j} ($j = 1, 2, \ldots, \nu$), the second medium will have the smallest of all r_{0j} ($j = 2, 3, \ldots, \nu$), and so on.

Systems $X_j'Y_j'Z_j'$ ($j = 1, 2, \ldots, \nu$). Axis Z_j' will be drawn along the straight line O_jO, axis X_j' in plane $X_jO_jY_j$ perpendicular to Z_j' and will be directed toward the side from which the observer sees the rotation which superposes axis Z_j on axis Z_j' at an angle smaller than π taking place counterclockwise, and axis Y_j', perpendicular to axis X_j' and Z_j' so that system $X_j'Y_j'Z_j'$ has a right-handed orientation.

We will denote distance O_jO by $h^{(j)}$, the angles between axis Z_j' and vector p by $\psi^{(j)}$, and the angles between axis Z_j', Z_j and X_j', X_j by ϑ_j and χ_j respectively.

Relating to medium j ($j = 0, 1, \ldots, \nu$) the function T_j (1.5), (1.8) in terms of which the components of the electromagnetic fields in each of the media are expressed by formulas (1.2), we can formulate the problem under consideration as follows:[40]

$$\Delta T_j + k_j^2 T_j = 0, \quad j = 0, 1, 2, \ldots, \nu, \tag{2.1}$$

$$\left.\begin{aligned} q_0 T_0 &= q_j T_j \\ \frac{\partial (r_j T_0)}{\partial r_j} &= \frac{\partial (r_j T_j)}{\partial r_j} \end{aligned}\right\} \text{ for } r_j = b_j, \quad j = 1, 2, \ldots, \nu; \tag{2.2}$$

$$\frac{\partial T_0}{\partial r_0} - ik_0 T_0 = o\left(\frac{1}{r_0}\right).$$

To solve the problem, we will require more general addition theorems than those obtained in § 1.2.

§ 2.2. Addition Theorems

/97

We have the problem of obtaining formulas for reexpanding the functions $j_n(kr_s)P_n^m(\cos\theta_s)e^{im\phi_s}$ and $h_n(kr_s)P_n^m(\cos\theta_s)e^{im\phi_s}$, given in the coordinate system $X_sY_sZ_s$ (Figure 2.2) with respect to the same functions in system $X_jY_jZ_j$.

To solve this problem, we will use the same reasoning as in the derivation of analogous theorems in § 1.2. The difference lies only in the fact that in the case at hand, we choose point A (in the notation of § 1.2) in plane Π drawn through the straight line O_sO_j at some angle β to plane $Z_jO_jO_sZ_s$. As in § 1.2, we assume that angle O_sAO_j is a right angle.

[40] Here q_j and k_j are defined by expressions (1.7), (1.1).

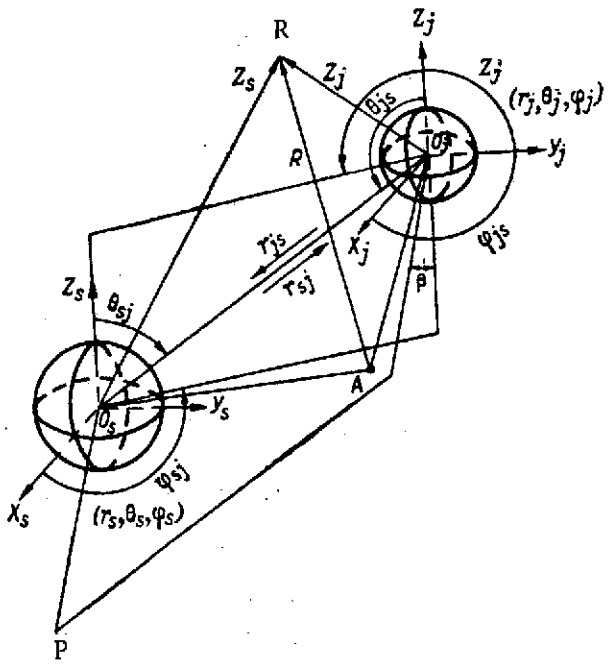

Figure 2.2. Coordinate Systems in the Addition Theorems.

Continuing to follow the reasoning of § 1.2 with the necessary correction of the operations, in accordance with the present selection of the position of point A, by virtue of the arbitrariness of distances AO_s, angle β and orthogonality of the tesseral functions, we arrive at the additional theorems for the functions $h_n(kr_s)P_n^m(\cos\theta_s)e^{im\phi_s}$. However, for the functions $j_n(kr_s)P_n^m(\cos\theta_s)e^{im\phi_s}$, one can make use of the integral representation [9, 29]

$$j_n(kr_j)\,P_n^m(\cos\theta_j)\,e^{im\varphi_j} =$$

$$= \frac{i^{-n}}{4\pi}\int_0^{2\pi}\int_0^{\pi} e^{ikr_j\cos\gamma_j}P_n^m(\cos\alpha)\,e^{im\beta}\sin\alpha\,d\alpha\,d\beta,$$

the readily obtainable conversion relations /98

$$r_j\cos\gamma_j = r_s\cos\gamma_s + r_{js}\cos\gamma_{js},$$

where $$\cos\gamma_0 = \cos\theta_p\cos\alpha + \sin\theta_p\sin\alpha\cos(\varphi_p-\beta),\quad p = j,\ s,\ js,$$

and also the expansion

$$e^{ikr_s\cos\gamma_s} = \sum_{\tau=0}^{\infty}\sum_{l=-\tau}^{\tau}(2\tau+1)\,\frac{(\tau-l)!}{(\tau+l)!}\,i^{\tau}j_{\tau}(kr_s)\,P_{\tau}^{l}(\cos\theta_s)\times$$
$$\times P_{\tau}^{l}(\cos\alpha)\,e^{il(\varphi_s-\beta)},$$

and

$$P_n^m(\cos\alpha)\,P_{\tau}^{l}(\cos\alpha) = \sum_{\sigma=|n-\tau|}^{n+\tau}{}' \frac{(\tau+l)!}{(\tau-l)!}\,\delta_{\sigma n\tau}^{ml}P_{\sigma}^{m-l}(\cos\alpha), \qquad (2.3)$$

where[41]

$$\delta_{\sigma n\tau}^{ml} = \frac{2\sigma+1}{2}(-1)^m\int_{-1}^{1}P_n^m(x)\,P_{\tau}^{-l}(x)\,P_{\sigma}^{l-m}(x)\,dx =$$
$$= (-1)^l\sqrt{\frac{(n+m)!\,(\tau-l)!\,(\sigma-m+l)!}{(n-m)!\,(\tau+l)!\,(\sigma+m-l)!}}\;C(n,\ \tau,\ \sigma;\ m,\ -l,\ m-l)\times \qquad (2.4)$$
$$\times C(n,\ \tau,\ \sigma;\ 0,\ 0,\ 0).$$

[41] Concerning the functions C $(l_1, l_2, l;$ j, k, j + k) see p. 14.

Thus we have:

Theorem 1.

$$j_n(kr_s)P_n^m(\cos\theta_s)e^{im\varphi_s} = \sum_{\tau=0}^{\infty}\sum_{l=-\tau}^{\tau}\Omega_{\tau lnm}^{(sj)}j_\tau(kr_j)P_\tau^l(\cos\theta_j)e^{il\varphi_j}, \quad r_j \leqslant r_{sj},$$

where

$$\Omega_{\tau lnm}^{(sj)} = (2\tau+1)\sum_{\sigma=|\tau-n|}^{\tau+n}{}' i^{\sigma+\tau-n}j_\sigma(kr_{sj})P_\sigma^{m-l}(\cos\theta_{sj})\times \times\exp[i(m-l)\varphi_{sj}]\delta_{\sigma n\tau}^{ml}. \tag{2.5}$$

Theorem 2.

$$h_n(kr_s)P_n^m(\cos\theta_s)e^{im\varphi_s} = \sum_{\tau=0}^{\infty}\sum_{l=-\tau}^{\tau}\Psi_{\tau lnm}^{(sj)}j_\tau(kr_j)P_\tau^l(\cos\theta_j)e^{il\varphi_j}, \quad r_j < r_{sj},$$

where

$$\Psi_{\tau lnm}^{(sj)} = (2\tau+1)\sum_{\sigma=|\tau-n|}^{\tau+n}{}' i^{\sigma+\tau-n}h_\sigma(kr_{sj})P_\sigma^{m-l}(\cos\theta_{sj})\times \times\exp[i(m-l)\varphi_{sj}]\delta_{\sigma n\tau}^{ml}. \tag{2.6}$$

Theorem 3.

$$h_n(kr_s)P_n^m(\cos\theta_s)e^{im\varphi_s} = \sum_{\tau=0}^{\infty}\sum_{l=-\tau}^{\tau}R_{\tau lnm}^{(sj)}h_\tau(kr_j)P_\tau^{m-l}(\cos\theta_j)e^{i(m-l)\varphi_j}, \quad r_j > r_{sj}, \tag{2.7}$$

/99

where

$$R_{\tau lnm}^{(sj)} = (2\tau+1)\sum_{\sigma=|\tau-n|}^{\tau+n}{}' i^{\sigma+\tau-n}j_\sigma(kr_{sj})P_\sigma^l(\cos\theta_{sj})\exp(il\varphi_{sj})\delta_{\tau n\sigma}^{ml}, \tag{2.8}$$

Let us note in conclusion that analogous theorems are also given in [9]; they differ from ours in the derivation.

§ 2.3. General Solution of the Problem. Components of Electromagnetic Field

We will seek the solution of problem (2.2) in the form

$$T_j = \begin{cases} T_{00} + \sum_{s=1}^{\nu}\sum_{n=0}^{\infty}\sum_{m=-n}^{n}B_{nm}^{(s)}h_n(k_0r_s)P_n^m(\cos\theta_s)e^{im\varphi_s} & \text{for } j=0, \\ \sum_{n=0}^{\infty}\sum_{m=-n}^{n}A_{nm}^{(j)}j_n(k_jr_j)P_n^m(\cos\theta_j)e^{im\varphi_j} & \text{for } j=1,2,\ldots,\nu. \end{cases} \tag{2.9}$$

Here the expression for T_{00} is determined by formulas (1.75)-(1.82), but in coordinates r_0, θ_0, ϕ_0:

$$T_{00} = \sum_{n=1}^{\infty}\sum_{m=\pm1}A_{nm}^{(0)}j_n(k_0r_0)P_n^m(\cos\theta_0)e^{im\varphi_0}, \quad r_0 < h, \tag{2.10}$$

where

$$A_{nm}^{(0)}=\begin{cases}-n(n+1)\beta_{00}A_{1n} & \text{for } m=-1,\\ \alpha_{00}A_{1n} & \text{for } m=1;\\ 0 & \text{for } |m|\neq 1,\\ & n=1,\ 2,\ \ldots\end{cases} \tag{2.11}$$

$$A_{1n}=\left\{-\frac{ik_0|\mathbf{p}|(2n+1)}{hn(n+1)}\zeta_n'(k_0h),\quad -\frac{ik_0z_0|\mathbf{p}|(2n+1)}{n(n+1)}h_n(k_0h)\right\},$$

α_{00}, β_{00} being defined by formulas (1.80). For $r_0 > h$ the expression for T_{00} has the form

$$T_{00}=\sum_{n=1}^{\infty}\sum_{m=\pm 1}t_{nm}^{(0)}h_n(k_0r_0)P_n^m(\cos\theta_0)e^{im\varphi_0}, \tag{2.12}$$

where

$$t_{nm}^{(0)}=\frac{A_{nm}^{(0)}}{A_{1n}}t_{1n},$$

$$t_{1n}=\left\{-\frac{ik_0|\mathbf{p}|(2n+1)}{hn(n+1)}\psi_n'(k_0h),\quad -\frac{ik_0z_0|\mathbf{p}|(2n+1)}{n(n+1)}j_n(k_0h)\right\}. \tag{2.13}$$

/100

In order to make solutions (2.9) satisfy the boundary equations (2.2), we also need the expressions for function T_{00} in coordinates r_j, θ_j, ϕ_j ($j = 1, 2, \ldots, \nu$) for $r_j < h^{(j)}$.

We will use the coordinate system $X_j'Y_j'Z_j'$ for this purpose. We resolve the dipole moment vector p into two components relative to axis Z_j': a horizontal component p_{1j} and a vertical component p_{2j}:

$$|\mathbf{p}_{1j}|=|\mathbf{p}|\sin\psi^{j},\quad |\mathbf{p}_{2j}|=|\mathbf{p}|\cos\psi^{(j)}. \tag{2.14}$$

It is easy to show that angle $\psi^{(j)}$ may be determined from the equality

$$\cos\psi^{(j)}=-\frac{r_{0j}\sin\theta_{0j}\cos\varphi_{0j}}{\sqrt{r_{0j}^2+h^2-2hr_{0j}\cos\theta_{0j}}}. \tag{2.15}$$

Then by analogy with expressions (1.75)-(1.82) in spherical coordinates of system $X_j'Y_j'Z_j'$, function T_{00} will take the form

$$T_{00}=\sum_{n=0}^{\infty}\sum_{m=-1}^{1}D_{nmj}^{(0)}j_n(k_0r_j)\bar{P}_n^m(\cos\theta_j')e^{im\varphi_j'},\quad r_j<h^{(j)}, \tag{2.16}$$

where

$$D_{nmj}^{(0)}=\begin{cases}-n(n+1)\beta_{00}D_{1nj} & \text{for } m=-1,\\ D_{2nj} & \text{for } m=0,\\ \alpha_{00}D_{1nj} & \text{for } m=1,\\ 0 & \text{for } |m|>1.\end{cases} \tag{2.17}$$

$$D_{1nj}=\left\{-\frac{ik_0|\mathbf{p}_{1j}|(2n+1)}{h^{(j)}n(n+1)}\zeta_n'(k_0h^{(j)}),\quad -\frac{ik_0z_0|\mathbf{p}_{1j}|(2n+1)}{n(n+1)}h_n(k_0h^{(j)})\right\} \tag{2.18}$$

$$D_{2nj} = \left\{ \frac{ik_0 |\mathbf{p}_{2j}| (2n+1)}{h^{(j)}} h_n(k_0 h^{(j)}),\ 0 \right\}. \tag{2.19}$$

If we now switch to spherical coordinates of system $X_jY_jZ_j$ with the aid of addition theorems[42] (1.64), we obtain

$$T_{00} = \sum_{n=0}^{\infty} \sum_{m=-1}^{1} \sum_{\lambda=-n}^{n} D^{(0)}_{nmj} b^{(-1)}_{\lambda nmj} j_n(k_0 r_j) P_n^{\lambda}(\cos\theta_j) e^{i\lambda\varphi_j}, \quad r_j < h^{(j)}, \tag{2.20}$$

where $b^{(-1)}_{\lambda nmj}$ is defined by relation (1.66).

Making solutions (2.9) satisfy the boundary conditions (2.2) with the aid of addition theorems (2.3)-(2.6) and considering the orthogonality properties of the Tesseral functions and also the substitution /101

$$B^{(j)}_{nm} = Z^{(j)}_{nm} \sqrt{\frac{(n-m)!}{(n+m)!}}\, j^*_n(k_0 b_j), \tag{2.21}$$

after transformations we arrive at the system[43]

$$Z^{(j)}_{nm} = \sum_{s=1}^{\nu} \sum_{\tau=0}^{\infty} \sum_{l=-\tau}^{\tau} Z^{(s)}_{\tau l} L^{(sj)}_{\tau l n m} + \Phi^{(j)}_{nm}, \tag{2.22}$$

$$j = 1, 2, \ldots, \nu; \quad n = 0, 1, \ldots; \quad m = -n, \ldots, n;$$

where

$$L^{(sj)}_{\tau l n m} = \frac{\Delta^{(2)}_{nj}}{\Delta^{(1)}_{nj}} \sqrt{\frac{(\tau-l)!\,(n+m)!}{(\tau+l)!\,(n-m)!}}\, \frac{j^*_\tau(k_0 b_s)}{j_n(k_0 b_j)} \Psi^{(sj)}_{nm\tau l} (1-\delta_{sj}),$$

$$\Phi^{(j)}_{nm} = \frac{\Delta^{(3)}_{nj}}{\Delta^{(1)}_{nj}} \sqrt{\frac{(n+m)!}{(n-m)!}}\, \frac{1}{j^*_n(k_0 b_j)} \sum_{l=-1}^{1} D^{(0)}_{nlj} b^{(-1)}_{mnlj},$$

$$\Delta^{(1)}_{nj} = q_j j_n(k_j b_j) \zeta'_n(k_0 b_j) - q_0 h_n(k_0 b_j) \psi'_n(k_j b_j),$$

$$\Delta^{(2)}_{nj} = q_0 j_n(k_0 b_j) \psi'_n(k_j b_j) - q_j j_n(k_j b_j) \psi'_n(k_0 b_j), \tag{2.23}$$

$$\Delta^{(3)}_{nj} = q_0 j_n(k_0 b_j) \psi'_n(k_j b_j) - q_j j_n(k_j b_j) \psi'_n(k_0 b_j).$$

$A^{(j)}_{nm}$ is determined by any of the equalities:

$$A^{(j)}_{nm} = \frac{q_0 h_n(k_0 b_j)}{q_j j_n(k_j b_j)} B^{(j)}_{nm} + \frac{q_0 j_n(k_0 b_j)}{q_j j_n(k_j b_j)} \times$$

$$\times \sum_{s=1}^{\nu} \sum_{\tau=0}^{\infty} \sum_{l=-\tau}^{\tau} B^{(s)}_{\tau l} \Psi^{(sj)}_{nm\tau l} (1-\delta_{sj}) + \frac{q_0 j_n(k_0 b_j)}{q_j j_n(k_j b_j)} \sum_{l=-1}^{1} D^{(0)}_{nlj} b^{(-1)}_{mnlj}. \tag{2.24}$$

---

[42] By replacing $\phi_j + 1$ by ϕ'_j.

[43] The function $j^*_n(z)$ is defined by expression (1.91).

$$A_{nm}^{(j)}=\frac{\zeta_n'(k_0b_j)}{\psi_n'(k_jb_j)}B_{nm}^{(j)}+\frac{\psi_n'(k_0b_j)}{\psi_n'(k_jb_j)}\sum_{s=1}^{\nu}\sum_{\tau=0}^{\infty}\sum_{l=-\tau}^{\tau}B_{\tau l}^{(s)}\times$$

$$\times\Psi_{nm\tau l}^{(sj)}(1-\delta_{sj})+\frac{\psi_n'(k_0b_j)}{\psi_n'(k_jb_j)}\sum_{l=-1}^{1}D_{nlj}^{(0)}b_{mnlj}^{(-1)}. \tag{2.25}$$

In the course of the transformation, we assumed:

$$\Delta_{nj}^{(1)}\neq 0, \tag{2.26}$$

$$\psi_n(k_jb_j)\neq 0, \tag{2.27}$$

$$\psi_n'(k_jb_j)\neq 0. \tag{2.28}$$

Inequality (2.26) is unconditional and fulfilled for all j and n. Proof /102
of this statement follows from the proof of inequality (1.112), if in the latter one replaces q_j, k_j, k_{j+1}, b_{j+1} by q_0, k_0, k_j, b_j, respectively. As far as relations (2.27), (2.28) are concerned, they are valid only provided that $\operatorname{Im} k_j \neq 0$. If, however, $\operatorname{Im} k_j = 0$ for a certain j, then one of the inequalities (2.27), (2.28) may fail to be fulfilled.[44] This case will subsequently be analyzed separately.

System (2.22) admits a simple functional treatment if by analogy with § 1.3 we introduce[45] into consideration the Banach space $\tilde{l}_2$, consisting of infinite three-dimensional matrices $Z=\left\{Z_{nm}^{(j)}\right\}$, $n = 0, 1, \ldots$; $m = -n, \ldots, n$; $j = 1, 2, \ldots, \nu$ with $Z_{nm}^{(j)} = 0$ when $|m| > n$, with the norm

$$\|Z\|=\sqrt{\sum_{j=1}^{\nu}\sum_{n=0}^{\infty}\sum_{m=-n}^{n}|Z_{nm}^{(j)}|^2}<\infty.$$

In terms of space $\tilde{\tilde{l}}_2$, the following operator equation corresponds to system (2.22):

$$Z=TZ+\Phi. \tag{2.29}$$

It is known [41] that for equations of type (2.29), where T is a linear operator defined in space $\tilde{\tilde{l}}_2$ and representing it in its part, and $\Phi\in\tilde{\tilde{l}}_2$

---

[44]The two equalities $\psi_n(k_jb_j) = 0$ and $\psi_n'(k_jb_j) = 0$ are impossible simultaneously, since otherwise this would signify the presence of multiple roots in the function $\psi_n^{(z)}$, which is incorrect [42].

[45]See p. 32.

the Fredholm alternative is valid stating that either equation (2.29) is solvable for any $\Phi \in \mathfrak{F}_2$ or the homogeneous equation

$$Z = TZ \tag{2.30}$$

has nontrivial solutions.

By analogy with the reasoning[46] given in § 1.3, it can be shown that operator T and the free term Φ will meet the above requirements if

$$\sum_{n=0}^{\infty} \sum_{m=-n}^{n} \sum_{\tau=0}^{\infty} \sum_{l=-\tau}^{\tau} |L_{\tau l n m}^{(sj)}|^2 < \infty, \tag{2.31}$$

$$\sum_{n=0}^{\infty} \sum_{m=-n}^{n} |\Phi_{nm}^{(j)}|^2 < \infty \tag{2.32}$$

respectively.

Thus, from the estimates /103

$$\left| \frac{\Delta_{nj}^{(2)}}{\Delta_{nj}^{(1)}} \right| < \text{const}_1 \frac{|k_0 b_j|^{2n}}{[(2n+1)!!]^2},$$

$$|\Psi_{nm\tau l}^{(sj)}| < \text{const}_2 (2n+1) \sqrt{\frac{(n-m)!\,(\tau+l)!}{(n+m)!\,(\tau-l)!}}\, (n+\tau)^2 \frac{(2n+2\tau-1)!!}{|k_0 r_{sj}|^{n+\tau}}, \tag{2.33}$$

resulting from asymptotic with respect to the index expansions of the modified Bessel functions, from lemma 2 of § 1.2, and from Stirling's formula and inequality (1.132), we have

$$|L_{\tau l n m}^{(sj)}| < \text{const}_3 (n+\tau)^5 \left(\frac{b_j}{r_{sj}}\right)^n \left(\frac{b_s}{r_{sj}}\right)^\tau \frac{(n+\tau)!}{\tau!\, n!}. \tag{2.34}$$

From relation (2.34) by analogy with the proof of inequalities (1.35) we have the validity of statement (2.31) for $b_s + b_j < r_{sj}$, i.e., when the spheres do not touch.

It can be shown that by using estimate (1.132) in the integral representation (2.4) of $\delta_{\sigma n \tau}^{m l}$ and estimate (1.130) in expression (1.66), and also estimates analogous to those which were used in deriving relation (2.34), we will get

$$\left| \frac{\Delta_{nj}^{(3)}}{\Delta_{nj}^{(1)}} \right| < \text{const}_4 \frac{|k_0 b_j|^{2n}}{[(2n+1)!!]^2},$$

$$|b_{mnlj}^{(-1)}| < \sqrt{\frac{(n+l)!\,(n-m)!}{(n-l)!\,(n+m)!}}$$

$$|D_{nmj}^{(0)}| < \text{const}_5 \frac{(2n+1)!!}{|k_0 h^{(j)}|^n}. \tag{2.35}$$

[46] See pp. 37, 38, 32.

These inequalities in turn lead to the relation

$$|\Phi_{nm}^{(j)}| < \text{const}_6 \left| \frac{b_j}{h^{(j)}} \right|^n n. \tag{2.36}$$

If one considers estimate (2.36) on the left of inequality (2.32), then, provided that

$$b_j < h_j, \quad j = 1, 2, \ldots, \nu, \tag{2.37}$$

we will arrive at the required relation (2.32). Let us note at this point that condition (2.37) is equivalent to the condition that the dipole does not touch any of the spheres considered.

Thus, Fredholm's alternative is applicable to system (2.29). We will show that the homogeneous system (2.30), or, what amounts to the same thing,[47] /104

$$\overline{\overline{B}}_{nm}^{(j)} = \frac{\Delta_{nj}^{(2)}}{\Delta_{nj}^{(1)}} \sum_{s=1}^{\nu} \sum_{\tau=0}^{\infty} \sum_{l=-\tau}^{\tau} \overline{\overline{B}}_{\tau l}^{(s)} \Psi_{nm\tau l}^{(sj)} (1 - \delta_{sj}),$$
$$j = 1, 2, \ldots, \nu; \quad n = 0, 1, \ldots; \quad m = -n, \ldots, n, \tag{2.38}$$

has only a trivial solution.

System (2.38) corresponds to the homogeneous boundary value problem (2.1), (2.2) provided $T_{00} \equiv 0$. From the uniqueness theorem of the solution of this problem in the multiply connected region and from theorem 1 of § 1.3, slightly corrected for the case at hand, it follows that there can be no relations other than $\overline{T}_0 = 0$.

This means according to formula (2.9) that

$$\sum_{s=1}^{\nu} \sum_{n=0}^{\infty} \sum_{m=-n}^{n} \overline{\overline{B}}_{nm}^{(s)} h_n(k_0 r_s) P_n^m(\cos\theta_s) e^{im\varphi_s} \equiv 0. \tag{2.39}$$

If we now write expression (2.39) in the coordinates of the j-th sphere with the aid of addition theorem (2.5) and correspondingly change the order of the summation, we will obtain (2.40)

$$\sum_{\tau=0}^{\infty} \sum_{l=-\tau}^{\tau} [\overline{\overline{B}}_{\tau l}^{(j)} h_\tau(k_0 r_j) + j_\tau(k_0 r_j) \sum_{s=1}^{\nu} \sum_{n=0}^{\infty} \sum_{m=-n}^{n} \overline{\overline{B}}_{(s)}^{nm} \times$$
$$\times \Psi_{\tau lnm}^{(sj)} (1 - \delta_{sj})] P_\tau^l(\cos\theta_j) e^{il\varphi_j} = 0. \tag{2.40}$$

In this case, the validity of the change of the summation order is substantiated by the analogy with theorem 1 of § 1.3 with consideration of relations (2.33), (1.29), (1.132).

---

[47] The two dashes above the symbol will denote quantities pertaining to the homogeneous boundary value problem for equations (2.30).

It follows from equality (2.40) that the expression in square brackets becomes zero:

$$\overline{\overline{B}}_{\tau l}^{(j)} h_\tau(k_0 r_j) + j_\tau(k_0 r_j) \sum_{s=1}^{\nu} \sum_{n=0}^{\infty} \sum_{m=-n}^{n} \overline{\overline{B}}_{nm}^{(s)} \Psi_{\tau lnm}^{(sj)} (1 - \delta_{sj}) = 0. \tag{2.41}$$

Comparing relations (2.41) and (2.38), we find

$$\overline{\overline{B}}_{\tau l}^{(j)} \left[h_\tau(k_0 r_j) + j_\tau(k_0 r_j) \frac{\Delta_{\tau j}^{(1)}}{\Delta_{\tau j}^{(2)}} \right] = 0, \tag{2.42}$$

whence $\overline{\overline{B}}_{\tau l}^{(j)} \equiv 0$.

Indeed, if $\Delta_{\tau j}^{(2)} = 0$, the required result follows directly from system (2.38); however, the case $\Delta_{\tau j}^{(2)} \neq 0$ is completed by inequality (2.26) and by the linear independency of the functions in square brackets of equality (2.42). /10

Thus, it has been shown that system (2.22) is uniquely solvable in $\tilde{\tilde{l}}_2$.

Here, as in the case of $\tilde{\tilde{l}}_2$, it can be shown that system (2.22) is also solvable in $\tilde{\tilde{l}}_2$ by reduction.

If we now perform the substitution

$$A_{nm}^{(j)} = Y_{nm}^{(j)} \sqrt{\frac{(n-m)!}{(n+m)!}}\, h_n^*(k_j b_j),$$

in expressions (2.24), (2.25), then, proceeding from the condition that $Z = \{Z_{nm}^{(j)}\} \in \tilde{\tilde{l}}_2$, taking into consideration notation (2.21), one can easily obtain the following estimate:

$$Y = \{Y_{nm}^{(j)}\} \in \tilde{\tilde{l}}_2.$$

By virtue of Theorem 1 of § 1.3[48] these estimates prove that expressions (2.9), (1.5), (1.8) together with relation (1.2) are the desired solutions of the problem formulated in § 2.1.

Let us now consider the case in which one of equalities (2.27), (2.28) does not hold. Consider, for example, for certain $j = j_0$ and $n = n_q$ ($q = 0, 1, \ldots, p$)

$$\psi_{n_q}(k_{j_0} b_{j_0}) = 0. \tag{2.43}$$

[48] Slightly corrected for this case.

Rearranging equations (2.22) by considering relations (2.43) to resemble (1.152), (1.153), we obtain a system corresponding to a case under consideration:

$$Z_{nm}^{(j)} = \sum_{s=1}^{\nu} \sum_{\tau=0}^{\infty} \sum_{l=-\tau}^{\tau} Z_{\tau l}^{(s)} L_{\tau lnm}^{(sj)*} + \Phi_{nm}^{(j)}, \tag{2.44}$$

$$j = 1, 2, \ldots, \nu; \quad n = 0, 1, \ldots; \quad m = -n, \ldots, n,$$

where

$$L_{\tau lnm}^{(sj)*} = \sqrt{\frac{(\tau - l)!\,(n+m)!}{(\tau + l)!\,(n-m)!}}\, \frac{j_\tau^*(k_0 b_s)}{j_n^*(k_0 b_j)}\, \Psi_{nm\tau l}^{(sj)}\,(1 - \delta_{sj}) \times$$

$$\times \left[\frac{\Delta_{nj}^{(2)}}{\Delta_{nj}^{(1)}} \left(1 - \delta_{jj_0} \prod_{q=0}^{p} \delta_{nn_q} \right) - \frac{j_n(k_0 b_j)}{h_n(k_0 b_j)}\, \delta_{jj_0} \prod_{q=0}^{p} \delta_{nn_q} \right], \tag{2.45}$$

$A_{nm}^{(j)}$ being found from equation (2.25).

If, however, inequality (2.28) is not fulfilled, i.e., for certain $j = j_0$ /106 and $n = n_q$ ($q = 0, 1, \ldots, p$) the relation

$$\psi'_{n_q}(k_{j_0} b_{j_0}) = 0, \tag{2.46}$$

holds, as a result of the same transformation as in the preceding case we arrive at the same system (2.44) but with a different expression for $L_{\tau lnm}^{(sj)*}$:

$$L_{\tau lnm}^{(sj)*} = \sqrt{\frac{(\tau - l)!\,(n+m)!}{(\tau + l)!\,(n-m)!}}\, \frac{j_\tau^*(k_0 b_s)}{j_n^*(k_0 b_j)}\, \Psi_{nm\tau l}^{(sj)}\,(1 - \delta_{sj}) \times$$

$$\times \left[\frac{\Delta_{nj}^{(2)}}{\Delta_{nj}^{(1)}} \left(1 - \delta_{jj_0} \prod_{q=0}^{p} \delta_{nn_q} \right) - \frac{\psi'_n(k_0 b_j)}{\zeta'_n(k_0 b_j)}\, \delta_{jj_0} \prod_{q=0}^{p} \delta_{nn_q} \right]. \tag{2.47}$$

In this case (2.46), $A_{nm}^{(j)}$ will be determined from equation (2.24). The expressions for the electromagnetic field vector components for each of the ν spheres are obtained from formulas (2.9)-(2.13), (1.5), (1.2); for medium 0, by dividing the entire region 0 (Figure 2.3) into concentric spheres of radii r_{0j} ($j = 1, 2, \ldots, \nu$) with center a point O_0, with subsequent application of the addition theorems of § 2.2 to each of the regions $0_{j\,j+1}$ ($j = 0, 1, \ldots, \nu$). Here, $0_{j\,j+1}$ ($j = 1, 2, \ldots, \nu - 1$) denotes the region defined by inequalities $r_{0j} < r_0 < r_{0j+1}$, $r_j > b_j$, $r_{j+1} > b_{j+1}$, 0_{01} denotes the region defined by inequalities $r_0 > r_{0\nu}$, $r_\nu > b_\nu$, $0_{\nu\nu+1}$, the region defined by inequalities $r_0 > r_{0\nu}$, $r_\nu > b_\nu$. On the other hand, the expressions for

vectors $E^{(0_s)}$ and $H^{(0_s)}$ in medium 0 may be obtained in the same manner if the potentials of the secondary field in medium 0

$$\left.\begin{aligned} U_{0_s} &= \sum_{s=1}^{\nu}\sum_{n=0}^{\infty}\sum_{m=-n}^{n} B^{(s)}_{nm(u)} h_n(k_0 r_s) P_n^m(\cos\theta_s) e^{im\varphi_s}, \\ V_{0_s} &= \sum_{s=1}^{\nu}\sum_{n=0}^{\infty}\sum_{m=-n}^{n} B^{(s)}_{nm(v)} h_n(k_0 r_s) P_n^m(\cos\theta_s) e^{im\varphi_s} \end{aligned}\right\} \qquad (2.48)$$

are substituted into relations (1.2), written in coordinates r_0, θ_0, ϕ_0, and the indicated differentiations of the expressions $h_n(k_0 r_s)P_n^m(\cos\theta_s)e^{im\phi_s}$ are performed according to the rules of a complex function. Moreover, instead of different representations following from the use of addition theorems, we will have a single expression for the entire medium 0. To realize this approach, it is necessary to have formulas of the type

$$[r_s,\ \cos\theta_s,\ e^{im\varphi_s}] = f(r_0\ \theta_0,\ \varphi_0).$$

These formulas are easily obtained (Figure 2.4) by methods of analytical geometry. They are:

$$\left.\begin{aligned} r_s &= \sqrt{\left(r_0 - r_{0s}\cos\tilde{\theta}_s\right)^2 + r_{0s}^2\sin^2\tilde{\theta}_s}, \\ \cos\tilde{\theta}_s &= \cos\theta_0\cos\theta_{0s} + \sin\theta_0\sin\theta_{0s}\cos(\varphi_0 - \varphi_{0s}), \\ \cos\theta_s &= \frac{r_0\cos\theta_0 - r_{0s}\cos\theta_{0s}}{r_s}, \\ e^{im\varphi_s} &= \frac{\left[r_0\sin\theta_0 e^{i\varphi_0} - r_{0s}\sin\theta_{0s}e^{i\varphi_{0s}}\right]^m}{\left[r_0^2\sin^2\theta_0 - 2r_0r_{0s}\sin\theta_0\sin\theta_{0s}\cos(\varphi_0-\varphi_{0s}) + r_{0s}^2\sin^2\theta_s\right]^{\frac{m}{2}}} \end{aligned}\right\} \qquad (2.49)$$

We will find the components of the secondary electromagnetic field in the long-range zone of medium 0. /10

Thus, it is easy to determine from expressions (2.49) that when $r_0 \gg h$, the following relations apply:

$$\varphi_s \sim \varphi_0, \quad \theta_s \sim \theta_0, \quad r_s \sim r_0 - r_{0s}\cos\tilde{\theta}_s. \qquad (2.50)$$

Hence, considering relations (1.68), (2.48) and (1.2), as a result of transformations we have in the long-range zone:

$$\left.\begin{aligned} E^{(0s)}_{r_0} &\sim 0, \\ E^{(0s)}_{\theta_0} &\sim \frac{e^{ik_0r_0}}{r_0}\left[S_2(\theta_0,\ \varphi_0) + i\varkappa_0 S_3(\theta_0,\ \varphi_0)\right], \\ E^{(0s)}_{\varphi_0} &\sim \frac{e^{ik_0r_0}}{r_0}\left[iS_4(\theta_0,\ \varphi_0) - \varkappa_0 S_5(\theta_0,\ \varphi_0)\right], \\ H^{(0s)}_{r_0} &\sim 0, \end{aligned}\right\} \qquad (2.51)$$

$$H_{\theta_0}^{(0s)} \sim \frac{e^{ik_0 r_0}}{r_0}\left[S_5(\theta_0, \varphi_0) - \frac{i}{\varkappa_0} S_4(\theta_0, \varphi_0)\right],$$
$$H_{\varphi_0}^{(0s)} \sim \frac{e^{ik_0 r_0}}{r_0}\left[\frac{1}{\varkappa_0} S_2(\theta_0, \varphi_0) + iS_3(\theta_0, \varphi_0)\right], \qquad (2.51)$$

where $\varkappa_0$ is defined by formula (1.169),

$$S_2(\theta_0, \varphi_0) = \sum_{s=1}^{\nu}\sum_{n=0}^{\infty}\sum_{m=-n}^{n} B_{nm(u)}^{(s)} i^{-n} W_{nms}^{(1)}(\theta_0, \varphi_0),$$
$$S_3(\theta_0, \varphi_0) = \sum_{s=1}^{\nu}\sum_{n=0}^{\infty}\sum_{m=-n}^{n} B_{nm(v)}^{(s)} i^{-n} W_{nms}^{(2)}(\theta_0, \varphi_0), \qquad (2.52)$$
$$S_4(\theta_0, \varphi_0) = \sum_{s=1}^{\nu}\sum_{n=0}^{\infty}\sum_{m=-n}^{n} B_{nm(u)}^{(s)} i^{-n} W_{nms}^{(2)}(\theta_0, \varphi_0),$$
$$S_5(\theta_0, \varphi_0) = \sum_{s=1}^{\nu}\sum_{n=0}^{\infty}\sum_{m=-n}^{n} B_{nm(v)}^{(s)} i^{-n} W_{nms}^{(1)}(\theta_0, \varphi_0),$$
$$W_{nms}^{(1)}(\theta_0, \varphi_0) = \frac{\partial}{\partial\theta_0} W_{nms}(\theta_0, \varphi_0), \qquad (2.53)$$
$$W_{nms}^{(2)}(\theta_0, \varphi_0) = \frac{1}{i\sin\theta_0}\frac{\partial}{\partial\varphi_0} W_{nms}(\theta_0, \varphi_0),$$
$$W_{nms}(\theta_0, \varphi_0) = \exp\left(-ik_0 r_{0s}\cos\tilde{\theta}_s\right) P_n^m(\cos\theta_0)\, e^{im\varphi_0}.$$

From expressions (2.49), (2.53) it also follows that /109

$$W_{nms}^{(1)}(\theta_0, \varphi_0) = ik_0 r_{0s} e^{-ik_0 r_{0s}\cos\tilde{\theta}_s}[\sin\theta_0\cos\theta_{0s} -$$
$$- \cos\theta_0\sin\theta_{0s}\cos(\varphi_0 - \varphi_{0s})]\, P_n^m(\cos\theta_0)\, e^{im\varphi_0} +$$
$$+ e^{-ik_0 r_{0s}\cos\tilde{\theta}_s}\tau_n^m(\theta_0)\, e^{im\varphi_0},$$
$$W_{nms}^{(2)}(\theta_0, \varphi_0) = k_0 r_{0s} e^{-ik_0 r_{0s}\cos\tilde{\theta}_s}\sin\theta_{0s}\sin(\varphi_0 - \varphi_{0s}) \times \qquad (2.54)$$
$$\times P_n^m(\cos\theta_0)\, e^{im\varphi_0} + e^{-ik_0 r_{0s}\cos\tilde{\theta}_s} m\pi_n^m(\theta_0)\, e^{im\varphi_0}.$$

$$\left.\begin{aligned} E_{\theta_0}^{(0s)} &= \varkappa_0 H_{\varphi_0}^{(0s)}, \quad E_{r_0}^{(0s)} = 0, \\ E_{\varphi_0}^{(0s)} &= -\varkappa_0 H_{\theta_0}^{(0s)} \quad H_{r_0}^{(0s)} = 0, \\ E_{\theta_0}^{(0s)} E_{\varphi_0}^{(0s)} &+ H_{\theta_0}^{(0s)} H_{\varphi_0}^{(0s)} = 0. \end{aligned}\right\} \qquad (2.55)$$

Relations (2.55) show that as in the case of one or two spheres, the field in the long-range zone has a transverse character, and vectors $E^{(0s)}$ and $H^{(0s)}$ are mutually perpendicular.

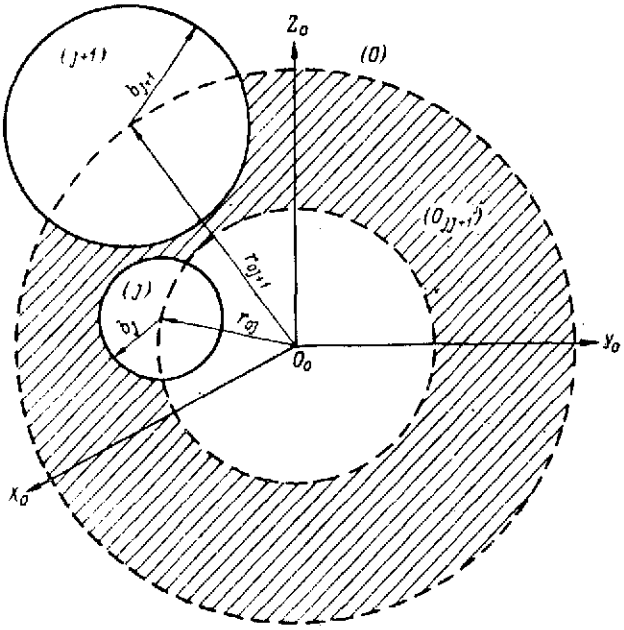

Figure 2.3. In Reference to the Determination of the Components of the Secondary Electromagnetic Field in Region $0_{j\ j+1}$ of Medium 0.

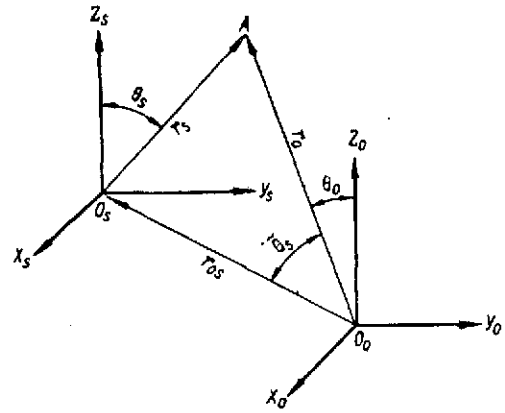

Figure 2.4. In Reference to the Expression for r_s, $\cos\theta_s$, $e^{im\phi s}$ in Terms of Spherical Coordinates r_0, θ_0, ϕ_0.

§ 2.4. Arbitrary Set of Spheres in the Field of a Plane Wave.

The case of a plane wave is the limiting case for the solution constructed in the preceding paragraph. We will direct dipole p along axis Z_0 to infinity while preserving its orientation. We thus obtain a plane wave propagating along negative axis Z_0, whose electric vector is polarized along axis X_0. The components of the incident field of the plane wave will, according to relations (1.190)-(1.196), have the form[49]

$$\begin{gathered} E_{x_0}^{(00)} = k_0^2 E_1 e^{-ik_0 z_0}, \\ H_{x_0}^{(00)} = H_{z_0}^{(00)} = E_{y_0}^{(00)} = E_{z_0}^{(00)} = 0, \\ H_{y_0}^{(00)} = -ik_0 a_0 E_1 e^{-ik_0 z_0}, \end{gathered} \tag{2.56}$$

where

$$E_1 = |\mathbf{p}| \frac{e^{ik_0 h}}{h}. \tag{2.57}$$

[49]Considering the notation used in this chapter.

Essentially following the reasoning given in § 1.4, one can obtain the electromagnetic field components in each of the media in the case where the primary field is a plane wave field of the form of (2.56).

To this end, in the expressions corresponding to the dipole radiator it is necessary to replace $A^{(s)}_{nm(u)}$, $A^{(s)}_{nm(v)}$, $B^{(s)}_{nm(u)}$, $B^{(s)}_{nm(v)}$ by $E_1\widetilde{A}^{(s)}_{nm(u)}$, $E_1\widetilde{A}^{(s)}_{nm(v)}$, $E_1\widetilde{B}^{(s)}_{nm(u)}$, $E_1\widetilde{B}^{(s)}_{nm(v)}$, respectively. /110

$$\widetilde{A}^{(s)}_{nm}=\frac{q_0h_n(k_0b_s)}{q_sj_n(k_sb_s)}\widetilde{B}^{(s)}_{nm}+\frac{q_0j_n(k_0b_s)}{q_sj_n(k_sb_s)}\times$$

$$\times\sum_{j=1}^{\nu}\sum_{\tau=0}^{\infty}\sum_{l=-\tau}^{\tau}\widetilde{B}^{(j)}_{\tau l}\Psi^{(js)}_{nm\tau l}(1-\delta_{sj})+\frac{q_0j_n(k_0b_s)}{q_sj_n(k_sb_s)}\sum_{l=-1}^{1}\widetilde{D}^{(0)}_{nls}\widetilde{b}^{(-1)}_{mnls},$$

$$s=1,\ 2,\ \ldots,\ \nu;$$

$$\widetilde{B}^{(j)}_{nm}=\widetilde{Z}^{(j)}_{nm}\sqrt{\frac{(n-m)!}{(n+m)!}}\,j^*_n(k_0b_j), \tag{2.58}$$

where $\widetilde{Z}^{(j)}_{nm}$ is determined from the system

$$\widetilde{Z}^{(j)}_{nm}=\sum_{s=1}^{\nu}\sum_{\tau=0}^{\infty}\sum_{l=-\tau}^{\tau}\widetilde{Z}^{(s)}_{\tau l}L^{(sj)}_{\tau lnm}+\widetilde{\Phi}^{(j)}_{nm}, \tag{2.59}$$

$$j=1,\ 2,\ \ldots,\ \nu;\quad n=0,\ 1,\ \ldots;\quad m=-n,\ \ldots,\ n.$$

$L^{(sj)}_{\tau lnm}$ is given by formula (2.23), and expressions analogous to (1.188) are denoted by $\widetilde{\Phi}^{(j)}_{nm}$, $\widetilde{D}^{(0)}_{nlj}$, $\widetilde{b}^{(-1)}_{mnls}$.

Let us find their explicit form. Thus, from equalities (2.14), (2.15) it is easy to find the following estimates for $h\to\infty$:

$$|\mathbf{p}_{1j}|=|\mathbf{p}|\left[1+0\left(\frac{1}{h^2}\right)\right],$$

$$|\mathbf{p}_{2j}|=|\mathbf{p}|\left[0\left(\frac{1}{h}\right)\right], \tag{2.60}$$

whence in the long-range zone approximation one can obtain

$$|p_{1j}|\sim|p|,\ |p_{2j}|\sim 0 \tag{2.61}$$

If now in expressions (2.18) we use an asymptotic expansion of the functions $\frac{\zeta'_n(k_0h^{(j)})}{h^{(j)}}$ and $h_n(k_0h^{(j)}$ for $h^{(j)}\to\infty$ according to relations (1.168); considering

the equality

$$h^{(j)} = \sqrt{h^2 + r_{0j}^2 - 2r_{0j}h\cos\theta_{0j}},$$

we expand in a series of type (1.13) in the functions $j_\tau(k_0r_0)P_\tau(\cos\theta_{0j})$ for $r_{0j} < h^{(j)}$; then use relation (1.168) again this time, however for $h \to \infty$; then contract the series obtained as the result of the indicated transformations, allowing for the expansion

$$e^{-ik_0r_{0j}\cos\theta_{0j}} = \sum_{\tau=0}^{\infty} i^{-\tau}(2\tau+1)\,j_\tau(k_0r_{0j})\,P_\tau(\cos\theta_{0j}),$$

we obtain

$$D_{lnj} \sim E_l e^{-ik_0r_{0j}\cos\theta_{0j}} g_n, \tag{2.62}$$

where g_n is defined by formula (1.187).

By virtue of relations (1.187), (2.17), (2.19), (2.61), expression (2.62) in turn leads to the following:

$$\widetilde{D}^{(0)}_{nmj} = e^{-ik_0r_{0j}\cos\theta_{0j}}\widetilde{A}^{(0)}_{nm}. \tag{2.63}$$

Hence, we obtain from formula (2.23)

$$\widetilde{\Phi}^{(j)}_{nm} = \frac{\Delta^{(3)}_{nj}}{\Delta^{(1)}_{nj}}\sqrt{\frac{(n+m)!}{(n-m)!}}\,\frac{\exp(-ik_0r_{0j}\cos\theta_{0j})}{j_n^*(k_0b_j)}\sum_{l=\pm1}\widetilde{A}^{(0)}_{nl}\widetilde{b}^{(-1)}_{mnlj}, \tag{2.64}$$

where $\widetilde{b}^{(-1)}_{mn\ell j}$ is the principal term of the asymptotic expansion of $b^{(-1)}_{mn\ell j}$ when $h \to \infty$. However, when $h \to \infty$, $\theta_j \sim 0$, $\chi_j \sim 0$ and $P^n_{\ell m}(\cos\theta_j) \sim \delta_{\ell m}$ [26]. Hence, $\widetilde{b}^{(-1)}_{mn\ell j}$. Thus

$$\widetilde{\Phi}^{(j)}_{nm} = \frac{\Delta^{(3)}_{nj}}{\Delta^{(1)}_{nj}}\sqrt{\frac{(n+m)!}{(n-m)!}}\,\frac{\exp(-ik_0r_{0j}\cos\theta_{0j})}{j_n^*(k_0b_j)}\widetilde{A}^{(0)}_{nm} \tag{2.65}$$

and

$$\widetilde{A}^{(s)}_{nm} = \frac{q_0h_n(k_0b_s)}{q_sj_n(k_sb_s)}\widetilde{B}^{(s)}_{nm} + \frac{q_0j_n(k_0b_s)}{q_sj_n(k_sb_s)} \times$$

$$\times\sum_{j=1}^{\nu}\sum_{\tau=0}^{\infty}\sum_{l=-\tau}^{\tau}\widetilde{B}^{(j)}_{\tau l}\Psi^{(js)}_{nm\tau l}(1-\delta_{sj}) + \frac{q_0j_n(k_0b_s)}{q_sj_n(k_sb_s)}\exp(-ik_0r_{0s}\cos\theta_{0s})\widetilde{A}^{(0)}_{nm}.$$

System (2.59) differs from system (2.22) only in the form of the right member. By analogy with inequality (2.32), it can be shown that

$$\sum_{n=1}^{\infty}\sum_{m=-n}^{n}\left|\widetilde{\Phi}^{(1)}_{nm}\right|^2 < \infty,$$

whence follows the unique solvability of equations (2.59) as well.

The validation of the solution, performed for the case of the dipole radiator in § 2.3, is used here without any modifications.

It is now easy on the basis of expression (2.51) to write the components of the secondary field in the long-range zone of medium 0 under the condition that the incident field is given by relation (2.56). We have: /112

$$
\begin{aligned}
E_{r_0}^{(0s)} &\sim 0,\\
E_{\theta_0}^{(0s)} &\sim E_1 \frac{e^{ik_0 r_0}}{r_0}\left[\widetilde{S}_2(\theta_0,\ \varphi_0) + i\varkappa_0 \widetilde{S}_3(\theta_0,\ \varphi_0)\right],\\
E_{\varphi_0}^{(0s)} &\sim E_1 \frac{e^{ik_0 r_0}}{r_0}\left[i\widetilde{S}_4(\theta_0,\ \varphi_0) - \varkappa_0 \widetilde{S}_5(\theta_0,\ \varphi_0)\right],\\
H_{r_0}^{(0s)} &\sim 0,\\
H_{\theta_0}^{(0s)} &\sim E_1 \frac{e^{ik_0 r_0}}{r_0}\left[\widetilde{S}_5(\theta_0,\ \varphi_0) - \frac{i}{\varkappa_0}\widetilde{S}_4(\theta_0,\ \varphi_0)\right],\\
H_{\varphi_0}^{(0s)} &\sim E_1 \frac{e^{ik_0 r_0}}{r_0}\left[\frac{1}{\varkappa_0}\widetilde{S}_2(\theta_0,\ \varphi_0) + i\widetilde{S}_3(\theta_0,\ \varphi_0)\right],
\end{aligned}
\tag{2.66}
$$

where

$$
\begin{aligned}
\widetilde{S}_2(\theta_0,\ \varphi_0) &= \sum_{s=1}^{\nu}\sum_{n=0}^{\infty}\sum_{m=-n}^{n} \widetilde{B}_{nm\,(u)}^{(s)} i^{-n} W_{nms}^{(1)}(\theta_0,\ \varphi_0),\\
\widetilde{S}_3(\theta_0,\ \varphi_0) &= \sum_{s=1}^{\nu}\sum_{n=0}^{\infty}\sum_{m=-n}^{n} \widetilde{B}_{nm\,(v)}^{(s)} i^{-n} W_{nms}^{(2)}(\theta_0,\ \varphi_0),\\
\widetilde{S}_4(\theta_0,\ \varphi_0) &= \sum_{s=1}^{\nu}\sum_{n=0}^{\infty}\sum_{m=-n}^{n} \widetilde{B}_{nm\,(u)}^{(s)} i^{-n} W_{nms}^{(2)}(\theta_0,\ \varphi_0),\\
\widetilde{S}_5(\theta_0,\ \varphi_0) &= \sum_{s=1}^{\nu}\sum_{n=0}^{\infty}\sum_{m=-n}^{n} \widetilde{B}_{nm\,(v)}^{(s)} i^{-n} W_{nms}^{(1)}(\theta_0,\ \varphi_0).
\end{aligned}
$$

To conclude the present section let us note that all the arguments and operations given above are valid only under conditions (2.27), (2.28). If one of them is not fulfilled, either relations (2.43) or (2.46) apply. Accordingly, in the system

$$
\widetilde{Z}_{nm}^{(j)} = \sum_{s=1}^{\nu}\sum_{\tau=0}^{\infty}\sum_{l=-\tau}^{\tau} \widetilde{Z}_{\tau l}^{(j)} \widetilde{L}_{\tau l nm}^{(sj)*} + \widetilde{\Phi}_{nm}^{(j)},
\tag{2.68}
$$

$$
j = 1,\ 2,\ \ldots,\ \nu;\quad n = 0,\ 1,\ \ldots;\quad m = -n,\ \ldots,\ n,
$$

which in this case replaces system (2.59), it is necessary to use expression (2.45) or (2.47) for $L_{\tau l nm}^{(sj)*}$. All the remaining formulas and relations remain unchanged.

§ 2.5. Electromagnetic and Radar Characteristics

Here we will follow the terminology and symbols used in § 1.5.

The intensity $I(\theta_0, \phi_0)$ of the secondary electromagnetic field in the long-range zone of medium 0 will have the form

$$I(\theta_0, \varphi_0) = \frac{1}{k_0^4 r_0^2}(|S_7(\theta_0, \varphi_0)|^2 + |S_8(\theta_0, \varphi_0)|^2), \tag{2.69}$$

where

$$\begin{aligned} S_7(\theta_0, \varphi_0) &= \widetilde{S}_2(\theta_0, \varphi_0) + i\varkappa_0 \widetilde{S}_3(\theta_0, \varphi_0), \\ S_8(\theta_0, \varphi_0) &= i\widetilde{S}_4(\theta_0, \varphi_0) - \varkappa_0 \widetilde{S}_5(\theta_0, \varphi_0). \end{aligned} \tag{2.70}$$

Expressions (2.67), (2.70) being considered, expression (2.69) will take the form

$$I(\theta_0, \varphi_0) = \frac{1}{k_0^4 r_0^2} \sum_{t=1}^{2} \left| \sum_{s=1}^{\nu} \sum_{n=0}^{\infty} \sum_{m=-n}^{n} i^{-n} \left[\widetilde{B}^{(s)}_{nm\,(u)} W^{(t)}_{nms}(\theta_0, \varphi_0) + i\varkappa_0 \widetilde{B}^{(s)}_{nm\,(v)} W^{(3-t)}_{nms}(\theta_0, \varphi_0) \right] \right|^2. \tag{2.71}$$

Such important field characteristics as the scattering diagram $F(\theta_0, \phi_0)$ are also related to the field intensity (2.71)

$$F(\theta_0, \varphi_0) = (k_0 r_0)^2 I(\theta_0, \varphi_0) \tag{2.72}$$

and the differential two-position scattering cross-section $\sigma'_D(\theta_0, \phi_0)$

$$\sigma'_D(\theta_0, \varphi_0) = 4\pi r_0^2 I(\theta_0, \varphi_0), \tag{2.73}$$

To determine the backscattering cross-section σ'_B, we introduce the following notation:

$$\begin{aligned} W^{(1)}_{nms}(0, 0) &= V^{(1)}_{nms} \frac{1}{2} e^{-ik_0 r_{0s} \cos\theta_{0s}}, \\ W^{(2)}_{nms}(0, 0) &= V^{(2)}_{nms} \frac{1}{2} e^{-ik_0 r_{0s} \cos\theta_{0s}}, \end{aligned} \tag{2.74}$$

where

$$V^{(1)}_{nms} = \begin{cases} 1 & \text{for } m = -1,\ n > 0, \\ -2ik_0 r_{0s} \sin\theta_{0s} \cos\varphi_{0s} & \text{for } m = 0,\ n \geqslant 0, \\ -n(n+1) & \text{for } m = 1,\ n > 0, \\ 0 & \text{for } \begin{cases} |m| = 1,\ n = 0, \\ |m| > 1,\ n \geqslant 0, \end{cases} \end{cases}$$

$$V_{nms}^{(2)}=\begin{cases}1 & \text{for } m=-1,\ n>0,\\ 2k_0r_{0s}\sin\theta_{0s}\sin\varphi_{0s} & \text{for } m=0,\ n\geqslant 0,\\ n(n+1) & \text{for } m=1,\ n>0,\\ 0 & \text{for } \begin{cases}|m|=1,\ n=0,\\ |m|>1,\ n\geqslant 0,\end{cases}\end{cases} \tag{2.75}$$

/114

Expressions (2.75) are obtained from formulas (2.54), (2.49) by considering relations (1.207) and

$$P_n^m(1)=\delta_{m0}$$

Then by virtue of notation (2.70), (2.52) we will have

$$\sigma_B'=\frac{\pi}{k_0^4}\sum_{l=1}^{2}\left|\sum_{s=1}^{\nu}\sum_{n=0}^{\infty}\sum_{m=-1}^{1}i^{-n}e^{-ik_0r_{0s}\cos\tilde{\theta}_{0s}}\times\right.$$
$$\left.\times\left[\tilde{B}_{nm(u)}^{(s)}V_{nms}^{(l)}+ix_0\tilde{B}_{nm(v)}^{(s)}V_{nms}^{(3-l)}\right]\right|^2. \tag{2.76}$$

The effective attenuation area[50] σ_2' is defined in terms of expressions (1.129), (2.70) as follows

$$\sigma'_2=\sigma_2(\pi b_1^2) \tag{2.77}$$

Using relations (2.67) and also

$$W_{nms}^{(j)}(\pi,\ 0)=\frac{(-1)^{n+m+1}}{2}e^{ik_0r_{0s}\cos\theta_{0s}}V_{nms}^{(j)},$$
$$j=1,\ 2.$$

obtained from expressions (2.54), (1.220), $P_n^m(-1)=(-1)^n\delta_{m0}$ and (2.75), after transformations we will have

$$\sigma_2'=\frac{2\pi}{k_0^3}(-\mathrm{Re})\sum_{s=1}^{\nu}\sum_{n=0}^{\infty}\sum_{m=-1}^{1}e^{ik_0r_{0s}\cos\theta_{0s}}i^{n+1}(-1)^m\times$$
$$\times\left[\tilde{B}_{nm(u)}^{(s)}V_{nms}^{(1)}+ix_0\tilde{B}_{nm(v)}^{(s)}V_{nms}^{(2)}\right]. \tag{2.78}$$

By analogy with (1.210) we introduce the notation:

---

[50] In contrast to (1.219), not normalized.

$$\Xi^{(1)}_{nms} = \begin{cases} -\dfrac{2i^{n-1}\operatorname{sign} m}{(2n+1)k_0}\sqrt{\dfrac{(n+m)!\,n(n+1)}{(n-m)!}}\,\widetilde{B}^{(s)}_{nm(u)} & \text{for } m=\pm 1, \\ \dfrac{4i^n r_{0s}\sin\theta_{0s}\cos\varphi_{0s}}{2n+1}\,\widetilde{B}^{(s)}_{n0(u)} & \text{for } m=0; \end{cases}$$

$$\Xi^{(2)}_{nms} = \begin{cases} -\dfrac{2i^{n-1}}{2n+1}\dfrac{\beta_0}{k_0^2}\sqrt{\dfrac{(n+m)!\,n(n+1)}{(n-m)!}}\,\widetilde{B}^{(s)}_{nm(v)} & \text{for } m=\pm 1, \\ \dfrac{4i^{n-1}\beta_0 r_{0s}\sin\theta_{0s}\sin\varphi_{0s}}{k_0(2n+1)}\,\widetilde{B}^{(s)}_{n0(v)} & \text{for } m=0. \end{cases} \qquad (2.79)$$

Then formula (2.78) for the effective attenuation area σ'_2 may be written more concisely:

$$\sigma'_2 = \frac{\pi}{k_0^2}(-\mathrm{Re})\sum_{s=0}^{\nu}\sum_{n=0}^{\infty}\sum_{m=-1}^{1} e^{ik_0 r_{0s}\cos\theta_{0s}}(2n+1)(\Xi^{(1)}_{nms}+\Xi^{(2)}_{nms}). \qquad (2.80)$$

Let us note at this point that when $\theta_{0s} = 0; \pi$, i.e., when all the spheres are on axis Z_0, the sum corresponding to $m = 0$ disappears in expression (2.80).

By analogy with expressions (1.223)-(1.225), the two-position scattering cross-section $\sigma'(\theta_0, \phi_0)$ will be defined by the formula

$$\sigma'(\theta_0, \varphi_0) = \frac{4\pi}{k_0^4}|S_7(\theta_0, \varphi_0)\cos\theta_0\cos\varphi_0 - S_8(\theta_0, \varphi_0)\sin\varphi_0|. \qquad (2.81)$$

According to expressions (1.227), (2.74), (2.75), after transformations, the radar scattering cross-section takes the form

$$\sigma'_0 = \frac{\pi}{4k_0^2}\left|\sum_{s=1}^{\nu}\sum_{n=0}^{\infty}\sum_{m=-1}^{1}(-1)^n(2n+1)e^{-ik_0 r_{0s}\cos\theta_{0s}}\times\right. \qquad (2.82)$$

$$\left.\times\left[\frac{i^{n-1}2}{(2n+1)k_0}\widetilde{B}^{(s)}_{nm(u)}V^{(1)}_{nms} - \frac{i^{n-1}2\beta_0}{(2n+1)k_0}\widetilde{B}^{(s)}_{nm(v)}V^{(2)}_{nms}\right]\right|^2.$$

If in expression (2.82) we switch to the coefficients $\Xi^{(1)}_{nms}$ and $\Xi^{(2)}_{nms}$ according to formulas (2.79), σ'_0 may also be written as follows:

$$\sigma'_0 = \frac{\pi}{4k_0^2}\left|\sum_{s=1}^{\nu}\sum_{n=0}^{\infty}\sum_{m=-1}^{1} e^{-ik_0 r_{0s}\cos\theta_{0s}}(-1)^n\times\right.$$

$$\left.\times(2n+1)(\Xi^{(1)}_{nms}-\Xi^{(2)}_{nms})\right|^2. \qquad (2.83)$$

The scattering indicatrix $\gamma(\theta_0, \phi_0)$ and the dimensionless σ'_1 are determined by relations (1.214). In this case /116

$$\gamma_0 = \frac{1}{k_0^2} \sum_{l=1}^{2} \int_0^{2\pi} \int_0^{\pi} \left| \sum_{s=1}^{\nu} \sum_{n=0}^{\infty} \sum_{m=-n}^{n} i^{-n} \left[\widetilde{B}^{(s)}_{nm\,(u)} W^{(l)}_{nms}(\theta_0, \varphi_0) + \right. \right.$$
$$\left. \left. + i\varkappa_0 \widetilde{B}^{(s)}_{nm\,(v)} W^{(3-l)}_{nms}(\theta_0, \varphi) \right] \right|^2 \sin\theta_0 \, d\varphi_0 \, d\theta_0. \qquad (2.48)^{51}$$

§ 2.6. Scattering and Attenuation of Electromagnetic Waves by an Arbitrary Set of Ideally Conducting Particles

The solution of the problem formulated in the title of this section is an important special case of the general problem, obtained from the solution of § 2.3 - -2.5 for $k_j^2 = i\infty$, $j = 1, 2, \ldots, \nu$.

However, this method proves to be somewhat more complex than the direct solution examined in § 1.7. We will therefore start again with the statement of the problem.

Let ν spheres arbitrarily arranged in space be located in a dipole radiator field (Figure 2.1). Using the notation of § 2.1, we introduce the generalized potential of medium 0, T_0, which satisfies equation (2.1) and is related to the electromagnetic field components by relations (1.5), (1.2), (1.7), (1.8).[52]

The problem under consideration is stated as follows: to find the solution of equation (2.1) in medium 0 under the condition of radiation at infinity and

$$\alpha_{01} \frac{\partial (r_j T_0)}{\partial r_j} + \beta_{01} T_0 = 0 \text{ for } r_j = b_j, \; j = 1, 2, \ldots, \nu, \qquad (2.85)$$

where α_{01} and β_{01} are defined by formulas (1.29). The solution is sought in the form

$$T_0 = T_{00} + \sum_{s=1}^{\nu} \sum_{n=0}^{\infty} \sum_{m=-n}^{n} B^{(s)}_{nm} h_n(k_0 r_s) P_n^m(\cos\theta_s) e^{im\varphi_s}. \qquad (2.86)$$

Here the expression for T_{00} has the form (2.10)-(2.13) or (2.16)-(2.20).

---

[51] Expression (2.84) admits of integration in finite form. However, the extremely cumbersome final relations obtained in the course of the transformations could not be represented in the form of formulas of type (2.80), (2,83), and they are therefore omitted.

[52] In medium j, $j = 1, 2, \ldots, \nu$, in view of the ideal conductivity of the spheres, the electromagnetic field is absent and therefore $T_j \equiv 0$.

Making the solution of (2.86) satisfy the boundary conditions (2.85), using the addition theorems and properties of orthogonality of Tesseral functions, and also the substitution

$$B_{nm}^{(j)} = Z_{nm}^{(j)} \sqrt{\frac{(n-m)!}{(n+m)!}}\, j_n^*(k_0 b_j), \tag{2.87}$$

after transformations we arrive at an infinite algebraic system corresponding to the case at hand: /11

$$Z_{nm}^{(j)} = \sum_{s=1}^{\nu} \sum_{\tau=0}^{\infty} \sum_{l=-\tau}^{\tau} T_{\tau l n m}^{(sj)} Z_{\tau l}^{(s)} + \Phi_{nm}^{(j)}, \tag{2.88}$$

$$n = 0, 1, \ldots; \quad m = -n, \ldots, n; \quad j = 1, 2, \ldots, \nu$$

where

$$T_{\tau l n m}^{(sj)} = -\frac{\Gamma_n(k_0 b_j)}{G_n(k_0 b_j)} \sqrt{\frac{(n+m)!\,(\tau-l)!}{(n-m)!\,(\tau+l)!}} \times$$

$$\times \frac{j_\tau^*(k_0 b_s)}{j_n^*(k_0 b_j)} \Psi_{nm\tau l}^{(sj)} (1 - \delta_{sj}),$$

$$\Phi_{nm}^{(j)} = -\sqrt{\frac{(n+m)!}{(n-m)!}} \frac{\Gamma_n(k_0 b_j)}{G_n(k_0 b_j)\, j_n^*(k_0 b_j)} \sum_{l=-1}^{1} D_{nlj}^{(0)} b_{mnlj}^{(-1)},$$

$$\Gamma_n(z) = \alpha_{01} \psi_n'(z) + \beta_{01} j_n(z), \tag{2.89}$$

$$G_n(z) = \alpha_{01} \zeta_n'(z) + \beta_{01} h_n(z),$$

$j_n^*(z)$, $\Psi_{nm\tau l}^{(sj)}$, $D_{nlj}^{(0)}$, $b_{mnlj}^{(-1)}$ being defined by expressions (1.91), (2.6), (2.17), (1.66), respectively.

In the course of derivation of equations (2.88), it was assumed that

$$h_n(k_0 b_j) \neq 0, \quad \zeta_n'(k_0 b_j) \neq 0.$$

These inequalities always hold under the conditions of the given problem. Proof of this statement is carried out by analogy with the proof of relations (1.89), (1.293). Hence, in contrast to the case of dielectric spheres, no limitations of the type of (2.27), (2.28) are placed on system (2.88).

In terms of space $\tilde{\tilde{l}}_2$ introduced into § 2.5, system (2.88) will be written in the form

$$Z = TZ + \Phi \tag{2.90}$$

The right side of equation (2.90) Φ is an element of space $\tilde{\tilde{l}}_2$, which follows from estimates (2.25) and

$$\left|\frac{\Gamma_n(k_0b_j)}{G_n(k_0b_j)}\right| < \text{const}\,\frac{|k_0b_j|^{2n}}{[(2n+1)!!]} \tag{2.91}$$

under condition (2.37).

As in system (2.29), operator T is completely continuous. Proof of this statement follows from estimates (2.33) and (2.91), which in turn lead to inequality (2.34) if symbol L is replaced by T in the left member of this inequality.

Thus, Fredholm's alternative is applicable to operator equation (2.90). /118 Proof of only trivial solutions in space $\approx{l}_2$ in the homogeneous system Z = TZ, and also the substantiation of solution (2.86) are carried out without any changes in comparison with the case of dielectric spheres discussed in § 2.4. Hence, system (2.90) as well as (2.88) is uniquely solvable in space $\approx{l}_2$, and representation (2.86) realizes the solution of the stated problem. The components of the electromagnetic fields in medium 0 will be described by the same expressions as in the general case (§ 2.4). In the long-range zone, these expressions may be represented by relations (2.51)-(2.54).

Let us now start moving the dipole p along axis Z_0 toward infinity while preserving its orientation. We thus obtain the plane wave (2.56), which propagates along negative axis Z_0 with an electric vector polarized along axis X_0. The components of the electromagnetic field will be obtained from expressions corresponding to the case of the dipole radiator by substituting $B^{(s)}_{nm(u)}$, $B^{(s)}_{nm(v)}$, by $E_1\widetilde{B}^{(s)}_{nm(u)}$, $E_1\widetilde{B}^{(s)}_{nm(v)}$. Here E_1 is defined by expression (2.57), $\widetilde{B}^{(s)}_{nm(u)}$ and $\widetilde{B}^{(s)}_{nm(v)}$ are the coefficients $\widetilde{B}^{(s)}_{nm}$ corresponding to the Debye potentials U and V,

$$\widetilde{B}^{(s)}_{nm} = \widetilde{Z}^{(s)}_{nm}\sqrt{\frac{(n-m)!}{(n+m)!}}\,j_n^*(k_0b_s), \tag{2.92}$$

$\widetilde{Z}^{(s)}_{nm}$ is found from the system

$$\widetilde{Z}^{(j)}_{nm} = \sum_{s=1}^{\nu}\sum_{\tau=0}^{\infty}\sum_{l=-\tau}^{\tau} T^{(sj)}_{\tau lnm}\widetilde{Z}^{(s)}_{\tau l} + \widetilde{\Phi}^{(j)}_{nm}, \tag{2.93}$$

$$n=0,\ 1,\ \ldots;\quad m=-n,\ \ldots,\ n;\quad j=1,\ 2,\ \ldots,\ \nu;$$

where

$$\widetilde{\Phi}^{(j)}_{nm} = -\sqrt{\frac{(n+m)!}{(n-m)!}}\,\frac{\Gamma_n(k_0b_j)\exp(-ik_0r_{0j}\cos\theta_{0j})}{G_n(k_0b_j)\,j_n^*(k_0b_j)}\,\widetilde{A}^{(0)}_{nm},$$

$\tilde{A}^{(0)}_{nm}$ is defined by expression (1.187).

System (2.93) is obtained from system (2.88) by a passage to the limit was done in § 1.4.

Under the condition that the primary field is the field of the plane wave of the form (2.56), the components of the electromagnetic field of medium 0 in the long-range zone are described by the same expressions (2.66), (2.67) as in the case of dielectric spheres, the only difference being that here $\tilde{B}^{(s)}_{nm}$ is determined from system (2.93) in terms of relations (2.92)

The electromagnetic and radar characteristics of an arbitrary set of ideally conducting spheres are given by expressions (2.71)-(2.84). /1

§ 2.7. Computational Aspect

The most complex stage in the numerical realization of the solutions constructed in the preceding paragraphs is the finding of the solutions of infinite algebraic equations (2.20), (2.44), (2.59), (2.93).

All of the above mentioned systems may be written in terms of space $\tilde{\tilde{l}}_2$ in the form of a single operator equation (2.29) with a completely continuous operator T. In this form, this equation resembles equation (1.311) with a completely continuous operator E, the latter equation corresponding to the case of a single nonconcentrically layered particle. For this reason, the entire computational algorithm described in sections 1-5 of § 1.8 may be transposed here without any modifications.

The final results of the computations are conveniently checked by the reduction method. Thus, if we denote by $\tilde{\tilde{l}}_{2(0)}$ and $\tilde{\tilde{l}}_{2(1)}$ the subspaces $\tilde{\tilde{l}}_2$ of the matrices respectively

$$Z^{(0p)} = \{Z^{(j)}_{nm}\},\ n=0,\ 1,\ \ldots,\ p;\quad m=-n,\ \ldots,\ n;\quad j=1,\ 2,\ \ldots,\ \nu$$

and

$$Z^{(1p)} = \{X^{(j)}_{nm}\},\ n=0,\ 1,\ \ldots;\quad m=-n,\ \ldots,\ n;\quad j=1,\ 2,\ \ldots,\ \nu$$

with

$$X^{(j)}_{nm} = \begin{cases} Z^{(j)}_{nm} & \text{for } n \leqslant p \\ 0 & \text{for } n > p \end{cases}$$

and by R the operator mutually uniquely mapping space $\tilde{\tilde{l}}_{2(0)}$ in $\tilde{\tilde{l}}_{2(1)}$

$$Z^{(1p)} = RZ^{(0p)}$$

it can be shown[53] that the rate of convergence to the exact solution Z of the reduction method for system (2.22) for trunction or order p is determined by the inequality

$$\|Z-\mathbf{R}Z^{(0p)}\|<\text{const}_1\left[\sum_{s=1}^{\nu}\sum_{j=1}^{\nu}\sum_{n=p+1}^{\infty}\sum_{m=-n}^{n}\sum_{\tau=0}^{\infty}\sum_{l=-\tau}^{\tau}\left|L_{\tau lnm}^{(sj)}\right|^2\right]^{\frac{1}{2}}+$$

$$+\text{const}_2\left[\sum_{j=1}^{\nu}\sum_{n=p+1}^{\infty}\sum_{m=-n}^{n}\left|\Phi_{nm}^{(j)}\right|^2\right]^{\frac{1}{2}},$$

which, when estimates (2.34), (2.36) are considered and as result of cumbersome transformations with convolusion of sums, may be represented in the form /120

$$\|Z-\mathbf{R}Z^{(0p)}\|<\text{const}_3\sum_{n=p+1}^{\infty}n^6\left(\tilde{b}_0\right)^n+\text{const}_4\sum_{n=p+1}^{\infty}n\left(\tilde{b}_1\right)^n,$$

where

$$\tilde{b}_0=\max_{s,\,j=1,\,2,\,\ldots,\,\nu}\frac{b_j+b_s}{r_{sj}},\qquad \tilde{b}_1=\max_{s,\,j=1,\,2,\,\ldots,\,\nu}\frac{b_j}{h_j}. \tag{2.94}$$

For system (2.59), estimate (2.94) should be replaced by the following:

$$\|\tilde{Z}-\mathbf{R}\tilde{Z}^{(0p)}\|<\text{const}_5\sum_{n=p+1}^{\infty}n^6\left(\tilde{b}_0\right)^6. \tag{2.95}$$[54]

Let us note here that the series in the right-hand members of inequalities (2.94), (2.95) may be represented in finite form by means of the relation

$$\sum_{n=p+1}^{\infty}n^m x^n=D^{(m)}\left[\frac{x^{p+1}}{1-x}\right],$$

where $D^{(m)}$ is the operator $\left\{x\frac{d}{dx}\right\}$ used m times in the function in square brackets.

If instead of equations (2.22), (2.59) we solve systems (2.44), (2.93), then a suitable correction of the notation should be made in the estimates given above.

In the case of sufficiently small $\tilde{b}_0$, such that an inequality of type (1.315) is fulfilled for all $n \geqslant 0$, the iteration method with estimates (1.318), (1.319) of the convergence rate can be applied directly to equations (2.22), (2.59),

---

[53]Using reasoning similar to that applied in analogous cases by the authors of [41].

[54]The term with the factorial convergence rate was omitted on the right of inequality (2.95).

(2.93), thus substantially reducing the volume of the necessary computational operations.

CHAPTER 3

SCATTERING AND ATTENUATION OF ELECTROMAGNETIC WAVES BY AN ARBITRARY SET OF NONCONCENTRICALLY LAYERED SPHERICAL PARTICLES

§ 3.1. Set of Nonconcentrically Layered Spheres in a Dipole Radiator Field

Chapter 1 discussed the case of a single nonconcentrically layered particle. /121
Here, however, we assume that there is a certain number of such particles, arbitrarily located relative to one another. This problem is a direct extension of the problems of Chapters 1 and 2 and was discussed by the author in [58]. Let us consider the statement of the problem. Let ν spheres with centers O_{s1} and radii b_{s1} ($s = 1, 2, \ldots, \nu$) be arbitrarily located (Figure 3.1) in infinite space, in medium 0. In turn, inside the s-th sphere there is a set of $(\nu_s - 1)$ spheres arbitrarily located inside one another with centers O_{sp} and radii b_{sp} ($p = 2, 3, \ldots, \nu_s$).

We will call medium sp the interior of the sphere of radius b_{sp}, excluding the region occupied by the sphere of radius b_{sp+1}. We will assume that medium sp has complex dielectric and magnetic permeabilities ε_{sp} and μ_{sp} respectively, and medium 0 has ε_0, μ_0.

We will also assume that at some point O of medium 0 there is an electric dipole of moment p, arbitrarily oriented in space (see also the references on p. 6). The problem is to find the electromagnetic fields in each of the media.

We introduce the following systems of Cartesian coordinates

System $X_0Y_0Z_0$. Axiz Z_0 and X_0 are drawn through point O, respectively, perpendicular and parallel to vector p through an arbitrary point O_0 on axis Z_0, and axis Y_0 is drawn perpendicular to axes X_0, Z_0 so that the coordinate system $X_0Y_0Z_0$ is a right-handed one.

Systems $X_{s1}Y_{s1}Z_{s1}$ ($s = 1, 2, \ldots, \nu$) are obtained by a parallel shift of system $X_0Y_0Z_0$ into origins O_{s1}.

Systems $X'_{sp}Y'_{sp}Z'_{sp}$ (s = 1, 2, ..., ν; p = 2, 3, ..., ν_s - 1). Axis Z'_{sp} is drawn along the straight line $O_{sp}O_{sp+1}$; axis X'_{sp}, along the line of intersection of the plane perpendicular to axis Z'_{sp} at point O_{s1} with plane $Z_{sp}O_{sp}Z'_{sp}$ and is directed toward the side from which the observer sees the rotation superimposing axis Z_{sp} on axis Z'_{sp} through an angle smaller than π and taking place counterclockwise. If point O_{sp+1} lies on the straight line $O_{sp-1}O_{sp}$, then axes $X'_{sp}Y'_{sp}Z'_{sp}$ will be directed along axes X_{sp}, Y_{sp}, Z_{sp}, respectively. /12

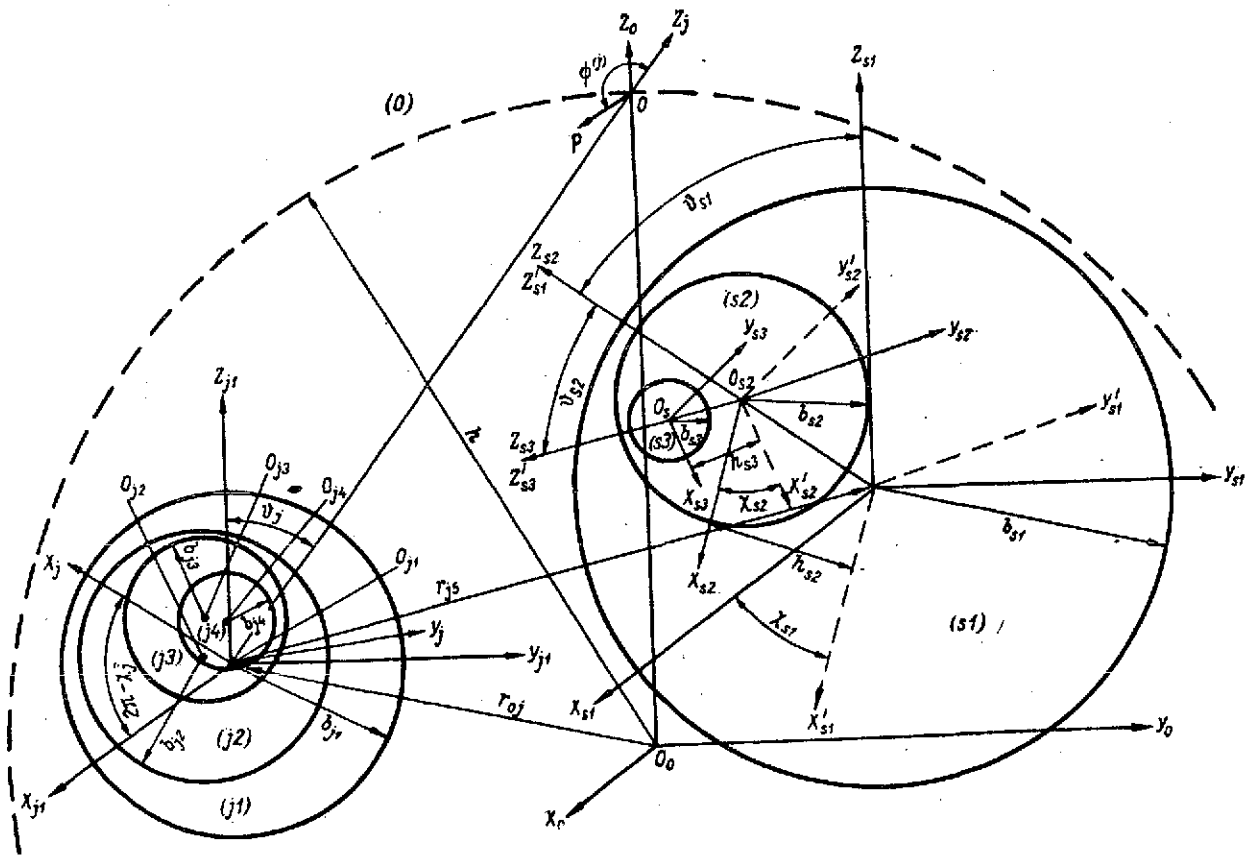

Figure 3.1. Set of Nonconcentrically Layered Spheres in A Dipole Radiator Field.

/

Systems $X_{sp}Y_{sp}Z_{sp}$ ($s = 1, 2, \ldots, \nu$; $p = 2, 3, \ldots, \nu_s - 1$) are obtained by shifting system $X'_{sp-1}Y'_{sp-1}Z'_{sp-1}$ parallel to itself by a distance h_{sp} along the positive semiaxis Z'_{sp-1}.

Systems $X_sY_sZ_s$ ($s = 1, 2, \ldots, \nu$). Axis Z_s will be drawn along straight line $O_{s1}O$, axis X_s, in plane $Z_{s1}O_{s1}Y_{s1}$ perpendicular to axis Z_s and will be directed toward the side from which the observer sees the rotation superimposing axis Z_{s1} on axis Z_s through an angle smaller than π, taking place counterclockwise.

We will specify the position of coordinate systems $X'_{sp}Y'_{sp}Z'_{sp}$ and $X_sY_sZ_s$ with the aid of Euler angles: χ_{sp}--the angle made by axis X'_{sp} with axis X_{sp}; θ_{sp}--the angle made by axis Z'_{sp} with Z_{sp}; χ_s--the angle made by axis X_s with axis X_{s1}; θ_s--the angle between axes Z_s and Z_{s1} ($0 \leqslant \chi_s, \chi_{sp} \leqslant 2\pi$, $0 \leqslant \theta_{sp}$, $\theta_s \leqslant \pi$).

Into each of the systems constructed, we introduce the spherical coordinates $X_sY_sZ_s$ - r_s, θ_s, ϕ_s; $X_{sp}Y_{sp}Z_{sp}$ - r_{sp}, θ_{sp}, ϕ_{sp}, $X'_{sp}Y'_{sp}Z'_{sp}$ - r_{sp}, θ'_{sp}, $\phi sp + 1$.

By $\tilde{r}_{sj}, \tilde{\theta}_{sj}, \tilde{\phi}_{sj}$ are denoted the spherical coordinates of the origin O_{j1} in the system with origin O_{s1}, and by $h^{(s)}$, the distance $\overline{O_{s1}O}$; the angle between vector p and axis Z_s is denoted by $\psi^{(s)}$; the spheres with center O_{s1} ($s = 1, 2, \ldots, \nu$) are numbered in the order of nondecreasing $\tilde{r}_{0s}$. Relating to media sp ($s = 1, 2, \ldots, \nu$; $p = 2, 3, \ldots, \nu_s - 1$) and 0 the generalized scale of potentials T_{sp} and T_0, respectively, by analogy with relations (1.5), (1.8), we formulate the problem at hand as follows:

$$\left.\begin{gathered}\Delta T_{sp} + k_{sp}^2 T_{sp} = 0, \quad s = 1, 2, \ldots, \nu; \quad p = 1, 2, \ldots, \nu_s, \\ \left.\begin{gathered} q_{sp} T_{sp} = q_{sp+1} T_{sp+1} \\ \frac{\partial (r_{sp+1} T_{sp})}{\partial r_{sp+1}} = \frac{\partial (r_{sp+1} T_{sp+1})}{\partial r_{sp+1}} \end{gathered}\right\} \text{for } r_{sp+1} = b_{sp+1}, \\ s = 1, 2, \ldots, \nu; \quad p = 1, 2, \ldots, \nu_s - 1, \\ \Delta T_{0s} + k_0^2 T_{0s} = 0, \\ \left.\begin{gathered} q_0 T_0 = q_{s1} T_{s1} \\ \frac{\partial (r_{s1} T_0)}{\partial r_{s1}} = \frac{\partial (r_{s1} T_{s1})}{\partial r_{s1}} \end{gathered}\right\} \text{for } r_{s1} = b_{s1}, \quad s = 1, 2, \ldots, \nu, \\ \frac{\partial T_0}{\partial r_{s1}} - ik_0 T_0 = o\left(\frac{1}{r_{s1}}\right), \end{gathered}\right. \tag{3.1}$$

where $k_{sp}^2 = -\alpha_{sp}\beta_{sp}$; $\alpha_{sp} = -i\varepsilon_{sp}\omega$; $\beta_{sp} = -i\mu_{sp}\omega$, ω is the angular frequency: $q_{sp} = \{\alpha_{sp}, \beta_{sp}\}$, $s = 1, 2, \ldots, \nu$; $p = 1, 2, \ldots, \nu_s$; $q_0 = \{\alpha_0, \beta_0\}$; $\alpha_0 = -i\varepsilon_0\omega$; $\beta_0 = -i\mu_0\omega$. [The braces have the same meaning as in expression (1.7)]. /12

$$T_0 = T_{00} + T_{0s} \tag{3.2}$$

T_{00} is the generalized scale of potential of the primary field given in the coordinate system $X_0Y_0Z_0$ with the aid of expressions (2.10)-(2.13), or in the coordinate system $X_jY_jZ_j$

$$T_{00} = \sum_{n=0}^{\infty} \sum_{m=-1}^{1} D_{nmj}^{(0)} j_n(k_0 r_j) P_n^m(\cos\theta_j) e^{im\varphi_j}, \tag{3.3}$$

$D_{nmj}^{(0)}$ is determined by formulas (2.17)-(2.19), (2.14); T_{0s} is the generalized scale of potential of the secondary field in medium 0.

We will seek the solution of problem (3.1) in the form:

$$\begin{aligned} T_{sj} = &\sum_{n=0}^{\infty} \sum_{m=-n}^{n} A_{nm}^{(sj)} j_n(k_{sj} r_{sj}) P_n^m(\cos\theta_{sj}) e^{im\varphi_{sj}} + \\ &+ B_{nm}^{(sj)} h_n(k_{sj} r_{sj+1}) P_n^m(\cos\theta_{sj+1}) e^{im\varphi_{sj+1}}, \\ &s = 1, 2, \ldots, \nu; \quad j = 1, 2, \ldots, \nu_s; \\ T_{0s} = &\sum_{s=1}^{\nu} \sum_{n=0}^{\infty} \sum_{m=-n}^{n} B_{nm}^{(s0)} h_n(k_0 r_{s1}) P_n^m(\cos\theta_{s1}) e^{im\varphi_{s1}}, \end{aligned} \tag{3.4}$$

under the assumption that

$$B_{nm}^{(s\nu_s)} = 0, \quad s = 1, 2, \ldots, \nu. \tag{3.5}$$

Making expression (3.4) satisfy the boundary conditions in (3.1), having first used the addition theorems of § 2.2 and considering the orthogonality of the Tesseral functions, after the substitution

$$\begin{aligned} A_{nm}^{(sj)} &= Z_{nm}^{(s2j-1)} \sqrt{\frac{(n-m)!}{(n+m)!}}\, h_n^*(k_{sj} b_{sj}), \quad j = 1, 2, \ldots, \nu_s; \\ B_{nm}^{(sj)} &= Z_{nm}^{(s2j)} \sqrt{\frac{(n-m)!}{(n+m)!}}\, j_n^*(k_{sj} b_{sj+1}), \quad j = 0, 1, \ldots, \nu_s - 1, \end{aligned} \tag{3.6}$$

where the functions $h_n^*(z)$, $j_n^*(z)$ are given by expressions (1.91), and after transformations, we arrive at the system: /

$$
\begin{cases}
Z_{nm}^{(s0)} = a_{ns}^{(0)} Z_{nm}^{(s1)} + \sum_{i=1}^{\nu} \sum_{\tau=0}^{\infty} \sum_{l=-\tau}^{\tau} Z_{\tau l}^{(i0)} f_{\tau l n m\, 0}^{(is)} (1 - \delta_{is}) + \\
\quad + \sum_{\tau=0}^{\infty} \sum_{l=-\tau}^{\tau} Z_{\tau l}^{(s2)} a_{\tau l n m\, 0}^{(s2)} - \Phi_{nm}^{(s0)}, \\
Z_{nm}^{(s1)} = a_{ns}^{(1)} Z_{nm}^{(s0)} + \sum_{i=1}^{\nu} \sum_{\tau=0}^{\infty} \sum_{l=-\tau}^{\tau} Z_{\tau l}^{(i0)} f_{\tau l n m\, 1}^{(is)} (1 - \delta_{is}) + \\
\quad + \sum_{\tau=0}^{\infty} \sum_{l=-\tau}^{\tau} Z_{\tau l}^{(s2)} a_{\tau l n m\, 1}^{(s2)} - \Phi_{nm}^{(s1)}, \\
\cdots\cdots\cdots\cdots\cdots\cdots\cdots\cdots \\
Z_{nm}^{(s2j)} = a_{ns}^{(2j)} Z_{nm}^{(s2j+1)} + \sum_{\tau=0}^{\infty} \sum_{l=-\tau}^{\tau} Z_{\tau l}^{(s2j-1)} a_{\tau l n m 2j}^{(s2j-1)} + \\
\quad + \sum_{\tau=0}^{\infty} \sum_{l=-\tau}^{\tau} Z_{\tau l}^{(s2j+2)} a_{\tau l n m\, 2j}^{(s2j+2)}, \\
Z_{nm}^{(s2j+1)} = a_{ns}^{(2j+1)} Z_{nm}^{(s2j)} + \sum_{\tau=0}^{\infty} \sum_{l=-\tau}^{\tau} Z_{\tau l}^{(s2j-1)} a_{\tau l n m\, 2j+1}^{(s2j-1)} + \\
\quad + \sum_{\tau=0}^{\infty} \sum_{l=-\tau}^{\tau} Z_{\tau l}^{(s2j+2)} a_{\tau l n m\, 2j+1}^{(s2j+2)},
\end{cases}
$$

$$
s = 1, 2, \ldots, \nu; \quad j = 1, 2, \ldots, \nu_s - 1; \quad n = 0, 1, \ldots; \quad m = -n, \ldots, n, \tag{3.7}
$$

where $Z_{nm}^{(s2\nu_s)} = 0$, $s = 1, 2, \ldots, \nu$ by virtue of (3.5).

It was assumed that

$$
\psi_n'(k_{sj} b_{sj}) \neq 0, \quad n = 0, 1, \ldots; \quad s = 1, 2, \ldots, \nu; \quad j = 1, 2, \ldots, \nu_s. \tag{3.8}
$$

Here[55]

$$
a_{\tau l n m\, 2j}^{(s2j+2)} = \sqrt{\frac{(n+m)!\,(\tau-l)!}{(n-m)!\,(\tau+l)!}} \times
$$

$$
\times \frac{q_{sj+1} h_n(k_{sj+1} b_{sj+1})\, j_\tau^*(k_{sj+1} b_{sj+2})}{q_{sj} h_n(k_{sj} b_{sj+1})\, j_n^*(k_{sj} b_{sj+1})} K_{nm\tau l s j+1}^{(-1)},
$$

$$
j = 0, 1, \ldots, \nu_s - 2;
$$

[55]By q_{s0}, k_{s0} are meant q_0, k_0, respectively.

$$a_{\tau lnm\,2j+1}^{(s2j+2)} = -\sqrt{\frac{(n+m)!\,(\tau-l)!}{(n-m)!\,(\tau+l)!}}\times$$

$$\times\frac{\zeta_n'(k_{sj+1}b_{sj+1})\,j_\tau^*(k_{sj+1}b_{sj+2})}{\psi_n'(k_{sj+1}b_{sj+1})\,h_n^*(k_{sj+1}b_{sj+1})}K_{nm\tau ls\,j+1}^{(-1)},\quad j=0,\ 1,\ \ldots,\ \nu_s-2;$$

$$a_{\tau lnm\,2j}^{(s\,2j-1)} = -\sqrt{\frac{(n+m)!\,(\tau-l)!}{(n-m)!\,(\tau+l)!}}\times$$

$$\times\frac{j_n(k_{sj}b_{sj+1})\,h_\tau^*(k_{sj}b_{sj})}{h_n(k_{sj}b_{sj+1})\,j_n^*(k_{sj}b_{sj+1})}K_{nm\tau lsj},\quad j=1,\ 2,\ \ldots,\ \nu_s-1;$$

$$a_{\tau lnm\,2j+1}^{(s\,2j-1)} = \sqrt{\frac{(n+m)!\,(\tau-l)!}{(n-m)!\,(\tau+l)!}}\times$$

$$\times\frac{\psi_n'(k_{sj}b_{sj+1})\,h_\tau^*(k_{sj}b_{sj})}{\psi_n'(k_{sj+1}b_{sj+1})\,h_n^*(k_{sj+1}b_{sj+1})}K_{nm\tau lsj},\quad j=1,\ 2,\ \ldots,\ \nu_s-1;$$

$$K_{\tau lnmsj} = b_{lnmsj}F_{\tau nlsj}^{(-1)};$$

$$K_{p\lambda nmsj}^{(-1)} = b_{\lambda pmsj}^{(-1)}F_{pnmsj};$$

$$b_{lnmsj} = e^{im\chi_{sj}}\sqrt{\frac{(n+m)!\,(n-l)!}{(n-m)!\,(n+l)!}}P_{-ml}^n(\cos\vartheta_{sj});$$

$$b_{\lambda nlsj}^{(-1)} = (-1)^{\lambda+l}e^{-il\chi_{sj+1}}\sqrt{\frac{(n+l)!\,(n-\lambda)!}{(n-l)!\,(n+\lambda)!}}P_{-l\lambda}^n(\cos\vartheta_{sj});$$

$$F_{pnmsj} = \frac{(n+m)!}{(n-m)!}(2p+1)\,i^{n-p}\times$$

$$\times\sum_{\sigma=|n-p|}^{n+p}{}'\,i^{-\sigma+2\sigma\cos\frac{1}{2}\theta'_{sjj+1}}j_\sigma(k_{sj}h_{sj+1})\,\delta_{\sigma np}^m;$$

$$F_{\tau pmsj}^{(-1)} = \frac{(p+m)!}{(p-m)!}(2\tau+1)\,i^{p-\tau}\times$$

$$\times\sum_{\sigma=|p-\tau|}^{p+\tau}{}'\,i^{-\sigma+2\sigma\sin\frac{1}{2}\theta'_{sj\,j+1}}j_\sigma(k_{sj}h_{s\,j+1})\,\delta_{\sigma p\tau}^m;$$

$\delta_{\sigma np}^m$ is defined by expression (1.42); $\theta'_{sj\ j+1}$ is the spherical coordinate θ'_{sj} of the origin O_{sj+1}, and the prime of the summation signs means that the summation extends only to those values of σ that have the same parity as the upper summation index; δ_{is} is the Kronecker symbol;

$$f_{\tau lnm\,0}^{(is)} = -\frac{j_n(k_0b_{s1})\,j_\tau^*(k_0b_{s1})}{h_n(k_0b_{s1})\,j_n^*(k_0b_{s1})}\sqrt{\frac{(\tau-l)!\,(n+m)!}{(\tau+l)!\,(n-m)!}}\Psi_{nm\tau l}^{(is)};$$

$$f_{\tau lnm\,1}^{(is)} = \frac{\psi_n'(k_0b_{s1})\,j_\tau^*(k_0b_{s1})}{\psi_n'(k_{s1}b_{s1})\,h_n^*(k_{s1}b_{s1})}\sqrt{\frac{(\tau-l)!\,(n+m)!}{(\tau+l)!\,(n-m)!}}\Psi_{nm\tau l}^{(is)};$$

/127

$$\Phi_{nm}^{(s0)} = \frac{j_n(k_0 b_{s1})}{h_n(k_0 b_{s1})\, j_n^*(k_0 b_{s1})} \sqrt{\frac{(n+m)!}{(n-m)!}} \sum_{l=-1}^{1} D_{nls}^{(0)} b_{mnls}^{(-1)};$$

$$\Phi_{nm}^{(s1)} = -\frac{\psi_n'(k_0 b_{s1})}{\psi_n'(k_{s1} b_{s1})\, h_n^*(k_{s1} b_{s1})} \sqrt{\frac{(n+m)!}{(n-m)!}} \sum_{l=-1}^{1} D_{nls}^{(0)} b_{mnls}^{(-1)};$$

$$a_{ns}^{(2j)} = \frac{q_{sj+1}\, j_n(k_{sj+1} b_{sj+1})\, h_n^*(k_{sj+1} b_{sj+1})}{q_{sj}\, h_n(k_{sj} b_{sj+1})\, j_n^*(k_{sj} b_{sj+1})}, \qquad j = 0, 1, \ldots, \nu_s - 1;$$

$$a_{ns}^{(2j+1)} = \frac{\zeta_n'(k_{sj} b_{sj+1})\, j_n^*(k_{sj} b_{sj+1})}{\psi_n'(k_{sj+1} b_{sj+1})\, h_n^*(k_{sj+1} b_{sj+1})}, \qquad (3.8a)$$

$$j = 0, 1, \ldots, \nu_s - 1.$$

For convenience of the discussion, we will represent system (3.7) in the following form:

$$\sum_{p=0}^{2\nu_s-1} Z_{nm}^{(sp)} a_{psk}^{(n)} + \sum_{i=1}^{\nu} \sum_{p=0}^{2\nu_s-1} \sum_{\tau=0}^{\infty} \sum_{l=-\tau}^{\tau} Z_{\tau l}^{(ip)} C_{\tau lnmsk}^{(ip)} = \Phi_{nm}^{(sk)}, \qquad (3.9)$$

$$s = 1, 2, \ldots, \nu; \quad k = 0, 1, \ldots, 2\nu_s - 1; \quad n = 0, 1, \ldots;$$

$$m = -n, \ldots, n;$$

where

$$C_{\tau lnmsk}^{(ip)} = \begin{cases} a_{\tau lnmk}^{(sk+2)} & \text{for } i = s;\ p = k+2;\ k = 0, 2, 4, \ldots, 2\nu_s - 2; \\ a_{\tau lnmk}^{(sk+1)} & \text{for } i = s;\ p = k+1;\ k = 1, 3, 5, \ldots, 2\nu_s - 1; \\ a_{\tau lnmk}^{(sk-1)} & \text{for } i = s;\ p = k-1;\ k = 2, 4, \ldots, 2\nu_s - 2; \\ a_{\tau lnmk}^{(sk-2)} & \text{for } i = s;\ p = k-2;\ k = 3, 5, \ldots, 2\nu_s - 1; \\ f_{\tau lnm0}^{(is)}(1 - \delta_{ls}) & \text{for } p = 0;\ k = 0;\ i = 1, 2, \ldots, \nu; \\ f_{\tau lnm1}^{(is)}(1 - \delta_{ls}) & \text{for } p = 0;\ k = 1;\ i = 1, 2, \ldots, \nu; \\ 0 \text{ in all remaining cases;} \end{cases}$$

$$\Phi_{nm}^{(sk)} = \begin{cases} \Phi_{nm}^{(s0)} & \text{for } k = 0; \\ \Phi_{nm}^{(s1)} & \text{for } k = 1; \\ 0 & \text{for } k > 1; \end{cases}$$

$$a_{psk}^{(n)} = a_{ns}^{(k)} \delta_{p\,[k+(-1)^k]} - \delta_{pk}. \qquad (3.10)$$

To substantiate the solvability of system (3.9) and find its solution by analogy with § 1.3 we construct a Banach functional space l_2 whose elements are /128
the infinite four-dimensional matrices $Z = \{Z_{nm}^{(sk)}\}$ $n = 0, 1, \ldots; m = -n, \ldots, n;$ $s = 1, 2, \ldots, \nu;$ $k = 0, 1, \ldots, 2\nu_s - 1,$ с $Z_{nm}^{(sk)} \equiv 0$ with $|m| > n$ and the norm

$$\|Z\| = \sqrt{\sum_{s=1}^{\nu} \sum_{k=0}^{2\nu_s-1} \sum_{n=0}^{\infty} \sum_{m=-n}^{n} |Z_{nm}^{(sk)}|^2} < \infty.$$

In terms of space $\overline{l}_2$, system (3.9) may be written by means of matrix operators W and T

$$(W + T)Z = \Phi. \tag{3.11}$$

Here $\alpha_{psk}^{(n)}$ and $C_{\tau l nmsk}^{(ip)}$ are respectively the kernels of operators W and T; Φ is the free term.

On the basis of estimates (2.35) and similar ones, it can be shown that when

$$b_{s1} < h^{(s)}, \quad s = 1, 2, \ldots, \nu, \tag{3.12}$$

the following inequality holds:

$$\sum_{n=0}^{\infty} \sum_{m=-n}^{n} |\Phi_{nm}^{(sk)}|^2 < \infty,$$
$$s = 1, 2, \ldots, \nu; \quad k = 0, 1, \ldots, 2\nu_s - 1,$$

from which it follows that the right side of equation (3.11) is an element of $\overline{l}_2$.

Relation (3.12) is equivalent to the condition that point 0, at which dipole p is located, does not lie on any of the spheres.

As was done in § 1.3, it is shown without any substantial modifications that:

1. W and T are linear operators defined in space $\overline{l}_2$ and representing it in their part.

2. W is a reversible operator and T is a completely continuous operator.

The complete continuity of operator T follows from the inequality

$$\sum_{n=0}^{\infty} \sum_{m=-n}^{n} \sum_{\tau=0}^{\infty} \sum_{l=-\tau}^{\tau} |C_{\tau l nmsk}^{(ip)}|^2 < \infty,$$

which is fulfilled under the conditions:

$$b_{s1} + b_{j1} < \widetilde{r}_{sj}, \quad s = 1, 2, \ldots, \nu; \quad j = 1, 2, \ldots, \nu;$$
$$b_{sj+1} + h_{sj+1} < b_{sj}, \quad s = 1, 2, \ldots, \nu; \quad j = 1, 2, \ldots, \nu_s - 1. \tag{3.13}$$

Conditions (3.13) are adequate to the requirement that both the spheres and their inner layers have no common points.

Thus, all the conditions of Nikol'skiy's theorem [36] have been met for equation (3.11), and hence, Fredholm's alternative applies. /12

We will show that the homogeneous equation

$$(W + T)Z = 0 \tag{3.14}$$

has only a trivial solution.

Let us assume the opposite, i.e., let in space $\bar{l}_2$ a $\bar{\bar{Z}}$ not identically equal to zero[56] exist such that

$$(W + T)\bar{\bar{Z}} = 0.$$

This means that for certain $s = s_0$, $k = k_0$, $\bar{\bar{Z}}^{(s_0k_0)}_{nm} \neq 0$, or in terms of relation (3.6):

$$\bar{\bar{A}}^{(s_0k_0)}_{nm} \neq 0 \text{ or } \bar{\bar{B}}^{(s_0k_0)}_{nm} \neq 0 \tag{3.15}$$

System (3.14) corresponds to a homogeneous boundary value problem which in the absence of a source and under the condition of radiation at infinity, and also owing to the conjugation of the tangential components of the field and theorem of uniqueness of the solution of the Maxwell homogeneous system in the multiply connected region has only a zero solution.

From the above and from theorem 1 of § 1.3 it follows that $s = s_0$ and $k = k_0$

$$\bar{\bar{T}}_{s_0 1} = 0, \tag{3.16}$$[57]

i.e.,

$$\sum_{n=0}^{\infty}\sum_{m=-n}^{n} \bar{\bar{A}}^{(s_0 1)}_{nm} j_n(k_{s_0 1} r_{s_0 1}) P_n^m(\cos\theta_{s_0 1}) e^{im\varphi_{s_0 1}} + \\ + \bar{\bar{B}}^{(s_0 1)}_{nm} h_n(k_{s_0 1} r_{s_0 2}) P_n^m(\cos\theta_{s_0 2}) e^{im\varphi_{s_0 2}} \equiv 0. \tag{3.17}$$

Applying addition theorem (1.70) to identity (3.17)

$$h_n(k_{s1} r_{s2}) P_n^m(\cos\theta_{s2}) e^{im\varphi_{s2}} = \\ = \sum_{p=0}^{\infty}\sum_{\lambda=-p}^{p} K^{(-1)}_{p\lambda nms1} h_p(k_{s1} r_{s1}) P_p^{\lambda}(\cos\theta_{s1}) e^{i\lambda\varphi_{s1}},$$

after some simple transformations we obtain

$$\bar{\bar{A}}^{(s_0 1)}_{nm} j_n(k_{s_0 1} r_{s_0 1}) + h_n(k_{s_0 1} r_{s_0 1}) \sum_{p=0}^{\infty}\sum_{\lambda=-p}^{p} \bar{\bar{B}}^{(s_0 1)}_{p\lambda} K^{(-1)}_{nmp\lambda s_0 1} \equiv 0. \tag{3.18}$$

Just as relation (1.148) follows from identity (1.145), we have from (3.18) /130

$$\bar{\bar{A}}^{(s_0 1)}_{nm} \equiv 0 \text{ or } \bar{\bar{B}}^{(s_0 1)}_{nm} \equiv 0 \tag{3.19}$$

---

[56]The zero element of space $\bar{l}_2$ is considered to be the matrix

[57]By $\bar{\bar{T}}_{sj}$ is meant the solution of homogeneous problem (3.14) in region sj.

By analogy with the reasoning used in proving theorem 2 of § 1.3, condition (3.18) with $k_0 \neq 0$ leads to the following:

$$\bar{\bar{A}}_{nm}^{(s_0k_0)} \equiv 0 \text{ or } \bar{\bar{B}}_{nm}^{(s_0k_0)} \equiv 0 \tag{3.19a}$$

If $k_0 = 0$, instead of identity (3.16) it is better to proceed from the identity $T_{0s} \equiv 0$, or

$$\sum_{s=1}^{\nu}\sum_{n=0}^{\infty}\sum_{m=-n}^{n} B_{nm}^{(s_0 0)} h_n(k_0 r_{s_0 l}) P_n^m(\cos\vartheta_{s_0 l}) e^{im\varphi_{s_0 l}} \equiv 0,$$

which with an accuracy to the symbols is the same as (2.39). By virtue of relation (2.42), it can be stated here as well that

$$B_{nm}^{(s_0 0)} \equiv 0 \tag{3.20}$$

Identities (3.19)-(3.20) are in contradiction with assumption (3.15). Hence, we conclude that equation (3.14) has only a zero solution, and hence, system (3.7) is uniquely solvable in space $\overline{l}_2$.

It can be shown that both series (3.4) and the series obtained from them by differentiating a finite number of times with respect to the spherical coordinates converge absolutely and uniformly. Thus, representations (3.4) in terms of relation (1.2) realized the solution of the stated problem.

Let us now consider the case in which condition (3.8) is not fulfilled. Let for certain $n = n_0$, $j = j_0$, $s = s_0$ the following relation apply:

$$\psi_{n_0}'(k_{s_0 j_0+1} b_{s_0 j_0+1}) = 0. \tag{3.21}$$

without decreasing the generality, we will assume that it is fulfilled when $j \geqslant 1$.

Then, rearranging the system which is the initial one for (3.7), after transformations analogous to (1.152), we obtain

$$\sum_{p=0}^{2\nu_s-1} Z_{nm}^{(sp)} a_{psk}^{(n)*} + \sum_{l=1}^{\nu}\sum_{p=0}^{2\nu_s-1}\sum_{\tau=0}^{\infty}\sum_{l=-\tau}^{\tau} Z_{\tau l}^{(lp)} C_{\tau lnmsk}^{(lp)*} = \Phi_{nm}^{(sk)}, \tag{3.22}$$

$$s = 1, 2, \ldots, \nu; \quad k = 0, 1, \ldots, 2\nu_s - 1; \quad n = 0, 1, \ldots;$$

$$m = -n, \ldots, n;$$

where

/13

$$C_{\tau lnmsk}^{(lp)*} = C_{\tau lnmsk}^{(lp)}(1 - \delta_{nn_0}\delta_{ss_0}) + \overline{C}_{\tau lnmsk}^{(lp)}\delta_{nn_0}\delta_{ss_0}, \tag{3.23}$$

$$\overline{C}^{(lp)}_{\tau lnmsk}=\begin{cases}\overline{a}^{(sk+2)}_{\tau lnmk} & \text{for } i=s;\ p=k+2;\ k=0,\ 2,\ 4,\ \ldots,\ 2\nu_s-2,\\ \overline{a}^{(sk+1)}_{\tau lnmk} & \text{for } i=s;\ p=k+1;\ k=1,\ 3,\ 5,\ \ldots,\ 2\nu_s-1,\\ \overline{a}^{(sk-1)}_{\tau lnmk} & \text{for } i=s;\ p=k-1;\ k=2,\ 4,\ \ldots,\ 2\nu_s-2,\\ \overline{a}^{(sk-2)}_{\tau lnmk} & \text{for } i=s;\ p=k-2;\ k=3,\ 5,\ \ldots,\ 2\nu_s-1,\\ f^{(is)}_{\tau lnm0}(1-\delta_{is}) & \text{for } p=0;\ k=0;\ i=1,\ 2,\ \ldots,\ \nu;\\ f^{(is)}_{\tau lnm1}(1-\delta_{is}) & \text{for } p=0;\ k=1;\ i=1,\ 2,\ \ldots,\ \nu.\\ 0 & \text{in all the remaining cases}\end{cases}$$

$$\alpha^{(n)*}_{psk}=\alpha^{(n)}_{psk}(1-\delta_{nn_0}\delta_{ss_0})+\overline{\alpha}^{(n)}_{psk}\delta_{nn_0},$$

$$\overline{\alpha}^{(n)}_{psk}=\overline{a}^{(k)}_{ns}\delta_{p\,[k+(-1)^k]}-\delta_{pk},$$

$$\overline{a}^{(k)}_{ns}=\begin{cases}\dfrac{q_{sj}h_n(k_{sj}b_{sj+1})\,j^*_n(k_jb_{j+1})}{q_{sj+1}j_n(k_{sj+1}b_{sj+1})\,h^*_n(k_{sj}b_{sj})}\delta_{jj_0} & k=2j_0+1,\\ 0 & k=2j_0,\\ a^{(k)}_{ns} & \text{in all the remaining cases.}\end{cases}$$

$$\overline{a}^{(s2j-1)}_{\tau lnm2j}=-\sqrt{\frac{(\tau-l)!\,(n+m)!}{(\tau+l)!\,(n-m)!}}\,\frac{\psi'_n(k_{sj}b_{sj+1})\,h^*_\tau(k_{sj}b_{sj})}{\zeta'_n(k_{sj}b_{sj+1})\,j^*_n(k_{sj}b_{sj+1})}K_{nm\tau lsj},$$

$$j=1,\ 2,\ \ldots,\ \nu_s-1,$$

$$\overline{a}^{(s2j+2)}_{\tau lnm2j}=\sqrt{\frac{(\tau-l)!\,(n+m)!}{(\tau+l)!\,(n-m)!}}\,\frac{\zeta'_n(k_{sj+1}b_{sj+1})\,j^*_\tau(k_{sj+1}b_{sj+2})}{\zeta'_n(k_{sj}b_{sj+1})\,j^*_n(k_{sj}b_{sj+1})}K^{(-i)}_{nm\tau lsj+1},$$

$$j=0,\ 1,\ \ldots,\ \nu_s-2,$$

$$\overline{a}^{(s2j+2)}_{\tau lnm2j+1}=-\sqrt{\frac{(\tau-l)!\,(n+m)!}{(\tau+l)!\,(n-m)!}}\,\frac{h_n(k_{sj+1}b_{sj+1})\,j^*_\tau(k_{sj+1}b_{sj+2})}{j_n(k_{sj+1}b_{sj+1})\,h^*_n(k_{sj}b_{sj})}\times$$

$$\times K^{(-1)}_{nm\tau lsj+1},$$

$$j=0,\ 1,\ \ldots,\ \nu_s-2,$$

$$\overline{a}^{(s2j-1)}_{\tau lnm2j+1}=\sqrt{\frac{(\tau-l)!\,(n+m)!}{(\tau+l)!\,(n-m)!}}\,\frac{q_{sj}j_n(k_{sj}b_{sj+1})\,h^*_\tau(k_{sj}b_{sj})}{q_{sj+1}j_n(k_{sj+1}b_{sj+1})\,h^*_n(k_{sj}b_{sj})}K_{nm\tau lsj},\qquad(3.24)$$

$$j=1,\ 2,\ \ldots,\ \nu_s-1.$$

If by analogy with system (3.7), system (3.22) is written in the form of a single operator equation /132

$$(W_* + T)Z = \Phi$$

where W_* is an operator with kernel $\alpha^{(n)*}_{psk}$ and T_* is an operator with kernel $C^{(ip)*}_{\tau\zeta nmsk}$, it can be shown, just as was done in the general case, that W_* is a reversible operator and T_* is a completely continuous operator in space $\overline{l}_2$.

We will note at this point[58] that if the parameters of the media are such that equality (3.21) is fulfilled when $j = j_0$ and for several n and j, i.e., when $n = n_q$ and $s = s_q$, $q = 0, 1, \ldots, p$, then the following formula should be used instead of formula (3.23):

$$C^{(ip)*}_{\tau\zeta nmsk} = C^{(ip)}_{\tau\zeta nmsk}\left(1 - \prod_{q=0}^{p} \delta_{nn_q}\delta_{ss_q}\right) + \overline{C}^{(ip)}_{\tau\zeta nmsk}\prod_{q=0}^{p}\delta_{nn_q}\delta_{ss_0}. \tag{3.25}$$

All the remaining relations of (3.24) will remain unchanged.

The components of the electromagnetic field in medium 0 will be determined by the same formulas as in § 2.3 if $B^{(s)}_{nm(u)}$, $B^{(s)}_{nm(v)}$ are replaced by $B^{(s0)}_{nm(u)}$, $B^{(s0)}_{nm(v)}$. In medium sj ($s = 1, 2, \ldots, \nu$; $j = 1, 2, \ldots, \nu_s$) if $A^{(j)}_{nm(u)}$, $A^{(j)}_{nm(v)}$, $B^{(j)}_{nm(u)}$, $B^{(j)}_{nm(v)}$ are replaced by $A^{(sj)}_{nm(u)}$, $A^{(sj)}_{nm(v)}$, $B^{(sj)}_{nm(u)}$, $B^{(sj)}_{nm(v)}$, respectively.

The scattered field in the long-range zone of medium 0 is then described by the same relations (2.51) as in the case of homogeneous spheres if $S_i(\theta_0, \phi_0)$, $i = 2, 3, 4, 5$ stands for

$$\begin{aligned}
S_2(\theta_0, \varphi_0) &= \sum_{s=1}^{\nu}\sum_{n=0}^{\infty}\sum_{m=-n}^{n} B^{(s0)}_{nm(u)} i^{-n} W^{(1)}_{nms}(\theta_0, \varphi_0),\\
S_3(\theta_0, \varphi_0) &= \sum_{s=1}^{\nu}\sum_{n=0}^{\infty}\sum_{m=-n}^{n} B^{(s0)}_{nm(v)} i^{-n} W^{(2)}_{nms}(\theta_0, \varphi_0),\\
S_4(\theta_0, \varphi_0) &= \sum_{s=1}^{\nu}\sum_{n=0}^{\infty}\sum_{m=-n}^{n} B^{(s0)}_{nm(u)} i^{-n} W^{(2)}_{nms}(\theta_0, \varphi_0),\\
S_5(\theta_0, \varphi_0) &= \sum_{s=1}^{\nu}\sum_{n=0}^{\infty}\sum_{m=-n}^{n} B^{(s0)}_{nm(v)} i^{-n} W^{(1)}_{nms}(\theta_0, \varphi_0).
\end{aligned} \tag{3.25a}$$

The transverse character of the field in the long-range zone approximation, resulting from expressions (2.55), also applies to the case of an arbitrary set of nonconcentrically layered spheres.

---

[58] In the course of the construction of the system it was also assumed that condition (1.162) applies, which also holds in the case at hand by virtue of assumption (3.21).

We will be moving dipole p (Figure 3.1) along axis Z_0 while perserving its orientation. As a result, we will obtain a plane wave (2.56) propagating along the negative axis Z_0, whose electric vector is polarized along axis X_0.

Essentially following the reasoning given in Chapters 1 and 2, we will obtain the components of the electromagnetic field in each of the media considered: in medium 0, if the coefficients $B^{(s)}_{nm(u)}$, $B^{(s)}_{nm(v)}$ from § 2.3 are replaced by $E_1 B^{(s0)}_{nm(u)}$, $E_1 \widetilde{B}^{(s0)}_{nm(v)}$; in medium sj, if the coefficients $A^{(j)}_{nm(u)}$, $A^{(j)}_{nm(v)}$, $B^{(j)}_{nm(v)}$, $B^{(j)}_{nm(v)}$ from § 1.3 are replaced by $E_1 A^{(sj)}_{nm(u)}$, $E_1 \widetilde{A}^{(sj)}_{nm(v)}$, $E_1 \widetilde{B}^{(sj)}_{nm(u)}$, $E_1 \widetilde{B}^{(sj)}_{nm(v)}$.

At the same time, we will assume that

$$\widetilde{A}^{(sj)}_{nm} = \widetilde{Z}^{(s2j+1)}_{nm} \sqrt{\frac{(n-m)!}{(n+m)!}}\, h_n(k_{sj}b_{sj}), \quad j=1, 2, \ldots, \nu_s,$$

$$\widetilde{B}^{(sj)}_{nm} = \widetilde{Z}^{(s2j)}_{nm} \sqrt{\frac{(n-m)!}{(n+m)!}}\, j^*_n(k_{sj}b_{sj+1}),$$

$$j=0, 1, \ldots, \nu_s-1; \quad s=1, 2, \ldots, \nu; \tag{3.26a}$$

and $\widetilde{Z}^{(sp)}_{nm}$ satisfies the infinite algebraic system

$$\sum_{p=0}^{2\nu_s-1} \widetilde{Z}^{(sp)}_{nm}\alpha^{(n)}_{psk} + \sum_{l=1}^{\nu}\sum_{p=0}^{2\nu_s-1}\sum_{\tau=0}^{\infty}\sum_{t=-\tau}^{\tau} \widetilde{Z}^{(tp)}_{\tau t} C^{(tp)}_{\tau lnmsk} = \widetilde{\Phi}^{(sk)}_{nm}, \tag{3.26}$$

$$n=0, 1, \ldots; \quad m=-n, \ldots, n; \quad s=1, 2, \ldots, \nu;$$
$$k=0, 1, \ldots, 2\nu_s-1,$$

where

$$\widetilde{\Phi}^{(s0)}_{nm} = \frac{j_n(k_0b_{s1})}{h_n(k_0b_{s1})\, j^*_n(k_0b_{s1})} \sqrt{\frac{(n+m)!}{(n-m)!}} \exp\left(-ik_0\widetilde{r}_{0j}\cos\widetilde{\theta}_{0j}\right)\widetilde{A}^{(0)}_{nm},$$

$$\widetilde{\Phi}^{(s1)}_{nm} = -\frac{\psi'_n(k_0b_{s1})}{\psi'_n(k_{s1}b_{s1})\, h^*_n(k_{s1}b_{s1})} \sqrt{\frac{(n+m)!}{(n-m)!}} \exp\left(-ik_{0j}\widetilde{r}_{0j}\cos\widetilde{\theta}_{0j}\right)\widetilde{A}^{(0)}_{nm}.$$

$\widetilde{\Phi}^{(sk)}_{nm} = 0$ when $k > 1$, $\widetilde{A}^{(0)}_{nm}$ is found from formula (1.187).

System (3.26), which applies in the case of a plane wave under condition (3.8), differs from system (3.9) only in the free term. It is easy to show that

$$\sum_{n=0}^{\infty}\sum_{m=-n}^{n} \left|\widetilde{\Phi}^{(sk)}_{nm}\right|^2 < \infty, \tag{3.27}$$

$$s=1, 2, \ldots, \nu; \quad k=0, 1, \ldots, 2\nu_s-1.$$

By virtue of the same arguments as those used in proving the unique solvability in space $\overline{l}_2$ of system (3.9), inequality (3.27) leads to an analogous statement for sytem (3.26). The validation of the solution performed in § 3.1 is also applied here without any modifications.

The components of the scattered field in the long-range zone of medium 0 have the form (2.66), where

$$\widetilde{S}_2(\theta_0, \varphi_0)=\sum_{s=1}^{\nu}\sum_{n=0}^{\infty}\sum_{m=-n}^{n}\widetilde{B}^{(s0)}_{nm\,(u)}i^{-n}W^{(1)}_{nms}(\theta_0, \varphi_0),$$

$$\widetilde{S}_3(\theta_0, \varphi_0)=\sum_{s=1}^{\nu}\sum_{n=0}^{\infty}\sum_{m=-n}^{n}\widetilde{B}^{(s0)}_{nm\,(v)}i^{-n}W^{(2)}_{nms}(\theta_0, \varphi_0),$$

$$\widetilde{S}_4(\theta_0, \varphi_0)=\sum_{s=1}^{\nu}\sum_{n=0}^{\infty}\sum_{m=-n}^{n}\widetilde{B}^{(s0)}_{nm\,(u)}i^{-n}W^{(2)}_{nms}(\theta_0, \varphi_0),$$

$$\widetilde{S}_5(\theta_0, \varphi_0)=\sum_{s=1}^{\nu}\sum_{n=0}^{\infty}\sum_{m=-n}^{n}\widetilde{B}^{(s0)}_{nm\,(v)}i^{-n}W^{(1)}_{nms}(\theta_0, \varphi_0).$$

However, if condition (3.8) is not fulfilled, then the following system must be used for determining the unknown coefficients:

$$\sum_{p=0}^{2\nu_s-1}\widetilde{Z}^{(sp)}_{nm}\alpha^{(n)*}_{psk}+\sum_{l=1}^{\nu}\sum_{p=0}^{2\nu_s-1}\sum_{\tau=0}^{\infty}\sum_{l=-\tau}^{\tau}\widetilde{Z}^{(lp)}_{\tau l}C^{(lp)*}_{\tau lnmsk}=\widetilde{\Phi}^{(sk)}_{nm}, \tag{3.27a}$$

$$n=0, 1, \ldots; \quad m=-n, \ldots, n; \quad s=1, 2, \ldots, \nu;$$

$$k=0, 1, \ldots, 2\nu_s-1,$$

where $\alpha^{(n)*}_{psk}$, $C^{(ip)*}_{\tau l nmsk}$ are given by relations (3.23), or (3.25) and (3.24).

§ 3.3. Electromagnetic and Radar Characteristics

The derivation of the electromagnetic and radar characteristics coincides in this case with the analogous conclusion discussed in § 2.5. and will therefore be omitted. We will give only the final expressions. The terminology and symbols used in § 1.5 will be kept.

The intensity $I(\theta_0, \phi_0)$ of the scattered electromagnetic field of medium 0 in the long-range zone is:

$$I(\theta_0, \varphi_0)=\frac{1}{k_0^4 r_0^2}\sum_{l=1}^{2}\left|\sum_{s=1}^{\nu}\sum_{n=0}^{\infty}\sum_{m=-n}^{n}i^{-n}\left[\widetilde{B}^{(s0)}_{nm\,(u)}W^{(l)}_{nms}(\theta_0, \varphi_0)+\right.\right.$$

$$\left.\left.+ik_0\widetilde{B}^{(s0)}_{nm\,(v)}W^{(3-l)}_{nms}\right]\right|^2;$$

The scattering diagram $F(\theta_0, \phi_0)$ is:

$$F(\theta_0, \varphi_0)=(k_0 r_0)^2 I(\theta_0, \varphi_0);$$

The differential two-position scattering cross-section $\sigma'_D(\theta_0, \phi_0)$ is:

$$\sigma'_D(\theta_0, \varphi_0) = 4\pi r_0^2 I(\theta_0, \varphi_0);$$

The effective backscattering area σ'_s is:

$$\sigma'_s = \frac{\pi}{k_0^4} \sum_{l=1}^{2} \left| \sum_{s=1}^{\nu} \sum_{n=0}^{\infty} \sum_{m=-1}^{1} i^{-n} e^{-ik_0 \tilde{r}_{0s} \cos \tilde{\vartheta}_{0s}} \times \right.$$
$$\left. \times \left[\tilde{B}^{(s0)}_{nm\,(u)} V^{(l)}_{nms} + i\varkappa_0 \tilde{B}^{(s0)}_{nm\,(v)} V^{(3-l)}_{nms} \right] \right|^2,$$

where $V^{(l)}_{nms}$ is defined by formulas (2.75);

The effective attenuation area σ'_2 is:

$$\sigma'_2 = \frac{\pi}{k_0^2} (-\mathrm{Re}) \sum_{s=1}^{\nu} \sum_{n=0}^{\infty} \sum_{m=-n}^{n} e^{ik_0 \tilde{r}_{0s} \cos \tilde{\vartheta}_{0s}} (2n+1) \left(\Xi^{(1)}_{nms} + \Xi^{(2)}_{nms} \right);$$

The effective radar scattering area σ'_0 is:

$$\sigma'_0 = \frac{\pi}{4k_0^2} \left| \sum_{s=1}^{\nu} \sum_{n=0}^{\infty} \sum_{m=-1}^{1} e^{-ik_0 \tilde{r}_{0s} \cos \tilde{\vartheta}_{0s}} (-1)^n (2n+1) \left(\Xi^{(1)}_{nms} - \Xi^{(2)}_{nms} \right) \right|^2,$$

where

$$\Xi^{(1)}_{nms} = \begin{cases} -\dfrac{2i^{n-1} \operatorname{sign} m}{(2n+1) k_0} \sqrt{\dfrac{(n+m)!\, n(n+1)}{(n-m)!}}\, \tilde{B}^{(s0)}_{nm\,(u)} & \text{for} \quad m = \pm 1, \\ \dfrac{4i^n \tilde{r}_{0s} \sin \tilde{\vartheta}_{0s} \cos \tilde{\varphi}_{0s}}{(2n+1)} \tilde{B}^{(s0)}_{n0\,(u)} & \text{при} \quad m = 0, \end{cases}$$

$$\Xi^{(2)}_{nms} = \begin{cases} -\dfrac{2i^{n-1}}{(2n+1)} \dfrac{\vartheta_0}{k_0^2} \sqrt{\dfrac{(n+m)!\, n(n+1)}{(n-m)!}}\, \tilde{B}^{(s0)}_{nm\,(v)} & \text{for} \quad m = \pm 1, \\ \dfrac{4i^{n-1} \vartheta_0 \tilde{r}_{0s} \sin \tilde{\vartheta}_{0s} \sin \tilde{\varphi}_{0s}}{k_0 (2n+1)} \tilde{B}^{(s0)}_{n0\,(v)} & \text{for} \quad m = 0; \end{cases}$$

The two-position scattering cross-section $\sigma'(\theta_0, \phi_0)$ is:

$$\sigma'(\theta_0, \varphi_0) = \frac{4\pi}{k_0^4} \left| S_7(\theta_0, \varphi_0) \cos \theta_0 \cos \varphi_0 - S_8(\theta_0, \varphi_0) \sin \varphi_0 \right|;$$

the scattering indicatrix $\gamma(\theta_0, \phi_0)$ is:

$$\Upsilon(\theta_0, \varphi_0) = \frac{1}{\Upsilon_0} F(\theta_0, \varphi_0);$$

The effective area of total scattering σ'_1 is: /136

$$\sigma'_1 = \frac{1}{k_0^2} \Upsilon_0,$$

where

$$\Upsilon_0 = \frac{1}{k_0^2} \sum_{l=1}^{2} \int_0^{2\pi} \int_0^{\pi} \left| \sum_{s=1}^{\nu} \sum_{n=0}^{\infty} \sum_{m=-n}^{n} i^{-n} \left[\tilde{B}^{(s0)}_{nm\,(u)} W^{(l)}_{nms}(\theta_0, \varphi_0) + \right. \right.$$
$$\left. \left. + i\varkappa_0 \tilde{B}^{(s0)}_{nm\,(v)} W^{(3-l)}_{nms}(\theta_0, \varphi_0) \right] \right|^2.$$

§ 3.4 Scattering and Attenuation of Electromagnetic Waves by an Arbitrary Set Of Ideally Conducting Spheres with a Nonconcentrically Layered Covering

The case discussed in the present section (all the spheres of radius $b_{s\nu_s}$, $s = 1, 2, \ldots, \nu$ are ideally conducting) results from the general solution constructed in § 3.1-3.3 for nonconcentrically layered dielectric spheres for $k^2_{s\nu_s} = i\infty$, $s = 1, 2, \ldots, \nu$. However, the difficulties involved in substantiating the limiting conversion oblige us to select a simpler method of direct solution.

We will formulate the problem in terms of the coordinates and symbols introduced in the preceding paragraphs of this chapter.

$$
\begin{gathered}
\Delta T_{sp} + k^2_{sp} T_{sp} = 0, \quad s = 1, 2, \ldots, \nu; \quad p = 1, 2, \ldots, \nu_s, \\
\left.\begin{aligned} q_{sp} T_{sp} &= q_{sp+1} T_{sp+1} \\ \frac{\partial (r_{sp+1} T_{sp})}{\partial r_{sp+1}} &= \frac{\partial (r_{sp+1} T_{sp+1})}{\partial r_{sp+1}} \end{aligned}\right\} \begin{array}{l} \text{for } r_{sp+1} = b_{sp+1}, \\ s = 1, 2, \ldots, \nu; \\ p = 1, 2, \ldots, \nu_s - 2; \end{array} \\
\alpha_{01} \frac{\partial \left(r_{s\nu_s} T_{s\nu_s - 1}\right)}{\partial r_{s\nu_s}} + \beta_{01} T_{s\nu_s - 1} = 0 \\
\text{for } r_{s\nu_s} = b_{s\nu_s}, \quad s = 1, 2, \ldots, \nu; \\
\Delta T_0 + k_0^2 T_0 = 0, \\
\left.\begin{aligned} q_0 T_0 &= q_{s1} T_{s1} \\ \frac{\partial (r_{s1} T_0)}{\partial r_{s1}} &= \frac{\partial (r_{s1} T_{s1})}{\partial r_{s1}} \end{aligned}\right\} \begin{array}{l} \text{for } r_{s1} = b_{s1}, \\ s = 1, 2, \ldots, \nu. \end{array} \\
\frac{\partial T_0}{\partial r_{s1}} - i k_0 T_0 = o\left(\frac{1}{r_{s1}}\right),
\end{gathered}
\tag{3.28}
$$

where α_{01}, β_{01} are defined by expressions (1.290).

The solution of the problem is sought for $s = 1, 2, \ldots, \nu$; $j = 1, 2, \ldots, \nu_s - 1$ in the form (3.4). Making the latter satisfy the boundary conditions (3.28), after transformations and substitution (3.6) we arrive at the system /13

$$
\left\{
\begin{aligned}
Z^{(s0)}_{nm} &= a^{(0)}_{ns} Z^{(s1)}_{nm} + \sum_{l=1}^{\nu} \sum_{\tau=0}^{\infty} \sum_{l=-\tau}^{\tau} Z^{(i0)}_{\tau l} f^{(is)}_{\tau l n m 0} (1 - \delta_{is}) + \\
&\quad + \sum_{\tau=0}^{\infty} \sum_{l=-\tau}^{\tau} Z^{(s2)}_{\tau l} a^{(s2)}_{\tau l n m 0} - \Phi^{(s0)}_{nm}, \\
Z^{(s1)}_{nm} &= a^{(1)}_{ns} Z^{(s0)}_{nm} + \sum_{l=1}^{\nu} \sum_{\tau=0}^{\infty} \sum_{l=-\tau}^{\tau} Z^{(i0)}_{\tau l} f^{(is)}_{\tau l n m 1} (1 - \delta_{is}) + \\
&\quad + \sum_{\tau=0}^{\infty} \sum_{l=-\tau}^{\tau} Z^{(s2)}_{\tau l} a^{(s2)}_{\tau l n m 1} - \Phi^{(s1)}_{nm},
\end{aligned}
\right.
\tag{3.29}
$$

$$\begin{cases} \cdots\cdots\cdots\cdots\cdots\cdots\cdots\cdots \\ Z_{nm}^{(s\,2j)} = a_{ns}^{(2j)} Z_{nm}^{(s\,2j+1)} + \sum_{\tau=0}^{\infty} \sum_{l=-\tau}^{\tau} Z_{\tau l}^{(s\,2j-1)} a_{\tau lnm2j}^{(s\,2j-1)} + \\ \quad + \sum_{\tau=0}^{\infty} \sum_{l=-\tau}^{\tau} Z_{\tau l}^{(s\,2j+2)} a_{\tau lnm2j}^{(s\,2j+2)}, \\ Z_{nm}^{(s\,2j+1)} = a_{ns}^{(2j+1)} Z_{nm}^{(s\,2j)} + \sum_{\tau=0}^{\infty} \sum_{l=-\tau}^{\tau} Z_{\tau l}^{(s\,2j-1)} a_{\tau lnm\,2j+1}^{(s\,2j-1)} + \\ \quad + \sum_{\tau=0}^{\infty} \sum_{l=-\tau}^{\tau} Z_{\tau l}^{(s\,2j+2)} a_{\tau lnm\,2j+1}^{(s\,2j+2)}, \\ Z_{nm}^{(s\,2\nu_s-2)} = \sum_{\tau=0}^{\infty} \sum_{l=-\tau}^{\tau} Z_{\tau l}^{(s\,2\nu_s-3)} \alpha_{\tau lnm\,2\nu_s-2}^{(s\,2\nu_s-3)}, \end{cases} \tag{3.29}$$

$$n=0,\ 1,\ \ldots;\quad m=-n,\ \ldots,\ n;\quad j=1,\ 2,\ \ldots,\ \nu_s-2;$$
$$s=1,\ 2,\ \ldots,\ \nu.$$

Here $a_{ns}^{(k)}$, $\Phi_{nm}^{(sk)}$, $a_{\tau lnmk}^{(si)}$ are defined by formulas (3.8a)

$$\alpha_{\tau lnm\,2\nu_s-2}^{(s\,2\nu_s-3)} = -\sqrt{\frac{(n+m)!\,(\tau-l)!}{(n-m)!\,(\tau+l)!}} \times$$
$$\times \frac{\Gamma_n\left(k_{s\nu_s-1} b_{s\nu_s}\right) h_\tau^*\left(k_{s\nu_s-1} b_{s\nu_s-1}\right)}{G_n\left(k_{s\nu_s-1} b_{s\nu_s}\right) j_n^*\left(k_{s\nu_s-1} b_{s\nu_s}\right)} K_{nm\tau ls\,\nu_s-1}, \tag{3.30}$$

$\Gamma n(z)$, $Gn(z)$ are found from formulas (2.89).

In the course of the transformations it was assumed that

$$\psi_n'(k_{sj} b_{sj}) \neq 0,\quad n=0,\ 1,\ \ldots;\quad s=1,\ 2,\ \ldots,\ \nu; \tag{3.31}$$
$$j=1,\ 2,\ \ldots,\ \nu_s-1.$$

If by analogy with the general case (p. 128) we introduce into consideration the linear Banach space $\overline{l}'_2$, consisting of four-dimensional matrices with $|m| > n$ and the norm /138

$$\|Z\| = \sqrt{\sum_{s=1}^{\nu} \sum_{k=0}^{2\nu_s-2} \sum_{n=0}^{\infty} \sum_{m=-n}^{n} |Z_{nm}^{(sk)}|^2} < \infty,$$

system (3.29) may be written in the form of a single operator in equation

$$(W + T)Z = \Phi \tag{3.32}$$

As in the general case, it can be shown that under conditions (3.12), (3.13) $\Phi \in \overline{l}'_2$, and W and T are linear operators acting from $\overline{l}'_2$ into $\overline{l}'_2$, W being reversible, and T completely continuous in $\overline{l}'_2$. Hence, Fredholm's alternative is applicable to equation (3.32).

Proof of the existence in the homogeneous system

$$(W + T)Z = 0$$

of a trivial solution only is carried out according to a general scheme by contradiction on the basis of the uniqueness theorem for Maxwell equations in the multiply connected region and the addition theorem of § 2.2.

Thus, system (3.29) is uniquely solvable in $\overline{l}'_2$, and representation (3.4) when $s = 1, 2, \ldots, \nu$; $j = 1, 2, \ldots, \nu_s - 1$ in terms of relation (1.2) realizes the solution of the problem on the scattering of the electromagnetic waves of a dipole radiator by ideally conducting spheres with a nonconcentrically layered covering.

In the case where for certain $j = j_0$ and $n = n_q$, $s = s_q$, $q = 0, 1, \ldots, p$, inequality (3.31) is not fulfillable, system (3.29) must be replaced by the following system:

$$\begin{cases} \sum\limits_{p=0}^{2\nu_s-3} Z_{nm}^{(sp)}\alpha_{psk}^{(n)*} + \sum\limits_{l=1}^{\nu}\sum\limits_{p=0}^{2\nu_s-3}\sum\limits_{\tau=0}^{\infty}\sum\limits_{l=-\tau}^{\tau} Z_{\tau l}^{(ip)}C_{\tau lnmsk}^{(ip)*} = \Phi_{nm}^{(sk)}, \\ Z_{nm}^{(s\,2\nu_s-2)} = \sum\limits_{\tau=0}^{\infty}\sum\limits_{l=-\tau}^{\tau} Z_{\tau l}^{(s\,2\nu_s-3)}\alpha_{\tau lnm\,2\nu_s-2}^{(s\,2\nu_s-3)}. \end{cases} \tag{3.33}$$

$$s=1, 2, \ldots, \nu; \quad k=0, 1, \ldots, 2\nu_s-3; \quad n=0, 1, \ldots; \quad m=-n, \ldots, n.$$

where $C_{\tau l nmsk}^{(ip)*}$ is given by relation (3.25), and all the remaining ones, by expression (3.24), (3.30).

System (3.33) is also uniquely solvable in $\overline{l}'_2$. /1

The components of the electromagnetic field in medium 0 will be determined by the corresponding formulas from § 2.3 if in these formulas $B_{nm}^{(s)}$ is replaced by $B_{nm}^{(s0)}$; in medium sj ($s = 1, 2, \ldots, \nu$; $j = 1, 2, \ldots, \nu_s - 1$) by replacing $A_{nm}^{(j)}$ and $B_{nm}^{(j)}$ from § 1.3 by $A_{nm}^{(sj)}$ and $B_{nm}^{(sj)}$. The scattered field in the long-range zone of medium 0 is described by expressions (2.41), and $S_i(\theta_0, \phi_0)$, $i = 2, 3, 4, 5$, by relations (3.25a).

In the case where the primary field is the field of a plane wave (2.56), systems (3.29) and (3.33) become (3.34) and (3.35), respectively:

$$\begin{cases} \sum\limits_{p=0}^{2\nu_s-3} \widetilde{Z}_{nm}^{(sp)} \alpha_{psk}^{(n)} + \sum\limits_{i=1}^{\nu} \sum\limits_{p=0}^{2\nu_s-3} \sum\limits_{\tau=0}^{\infty} \sum\limits_{l=-\tau}^{\tau} \widetilde{Z}_{\tau l}^{(ip)} C_{\tau lnmsk}^{(ip)} = \widetilde{\Phi}_{nm}^{(sk)}, \\ \widetilde{Z}_{nm}^{(s2\nu_s-2)} = \sum\limits_{\tau=0}^{\infty} \sum\limits_{l=-\tau}^{\tau} Z_{\tau l}^{(s2\nu_s-3)} \alpha_{\tau lnm\,2\nu_s-2}^{(s2\nu_s-3)}, \end{cases} \tag{3.34}$$

$$n=0,\ 1,\ \ldots;\quad m=-n,\ \ldots,\ n;\quad s=1,\ 2,\ \ldots,\ \nu;$$

$$k=0,\ 1,\ \ldots,\ 2\nu_s-3.$$

$$\begin{cases} \sum\limits_{p=0}^{2\nu_s-3} \widetilde{Z}_{nm}^{(sp)} \alpha_{psk}^{(n)*} + \sum\limits_{i=1}^{\nu} \sum\limits_{p=0}^{2\nu_s-3} \sum\limits_{\tau=0}^{\infty} \sum\limits_{l=-\tau}^{\tau} \widetilde{Z}_{\tau l}^{(ip)} C_{\tau lnmsk}^{(ip)*} = \widetilde{\Phi}_{nm}^{(sk)}, \\ \widetilde{Z}_{nm}^{(s2\nu_s-2)} = \sum\limits_{\tau=0}^{\infty} \sum\limits_{l=-\tau}^{\tau} \widetilde{Z}_{\tau l}^{(s2\nu_s-3)} \alpha_{\tau lnm\,2\nu_s-2}^{(s2\nu_s-3)}, \end{cases} \tag{3.35}$$

$$n=0,\ 1,\ \ldots;\quad m=-n,\ \ldots,\ n;\quad s=1,\ 2,\ \ldots,\ \nu;$$

$$k=0,\ 1,\ \ldots,\ 2\nu_s-3.$$

The electromagnetic and radar characteristics of an arbitrary set of ideally conducting spheres with a nonconcentrically layered covering will be determined by analogous expressions from § 3.3, obviously with the only difference that here the coefficients $\widetilde{Z}_{nm}^{(s0)}$ related to $\widetilde{B}_{nm}^{(s0)}$ by relations (3.26a) satisfy (3.34) or (3.35), but not longer (3.26) or (3.27a).

The above enumerated aspects of the numerical realization of the solution of the problem discussed in the present chapter do not differ essentially from the corresponding aspects presented in § 1.8, and are therefore omitted.

PART II
CHAPTER 4

DIELECTRIC CONSTANTS OF HYDROMETEORS

§ 4.1. Dielectric Constant of Water

The electromagnetic properties of matter are characterized by three parameters: electrical conductivity γ, absolute dielectric constant ε, and absolute permeability μ. The electrical conductivity of free space (vacuum) is equal to zero, and the absolute dielectric constant and permeability are:

$$\varepsilon = \varepsilon^{(0)} = 8{,}854 \cdot 10^{-12} \text{ F/m},$$
$$\mu = \mu^{(0)} = 1{,}257 \cdot 10^{-6} \text{ G/m}. \tag{4.1}$$

As we know, by using these values one can write the absolute electromagnetic parameters ε and μ of an arbitrary medium by using dimensionless complex relative dielectric constant ε and permeability μ:

$$\varepsilon = \varepsilon^{(0)}\varepsilon; \quad \mu = \mu^{(0)}\mu, \tag{4.2}$$

where

$$\varepsilon = \varepsilon' - i\frac{\gamma}{\omega\varepsilon^{(0)}} = \varepsilon' - i\varepsilon''. \tag{4.3}$$

In paramagnetic and diamagnetic substances such as water, ice, and snow, the magnetic properties are usually weakly expressed: for them as for a vacuum, one can assume that $\mu = 1$. The parameters ε' and ε'', however, are, generally speaking, functions of temperature and frequency.

In studying the dielectric properties of a substance, they are usually divided into polar and nonpolar properties depending on whether the molecules have a constant dipole moment or not. The most common examples of a polar substance are water and ideal aqueous solutions.

In a study of the dielectric properties of polar media, P. Debye [59, 60] obtained the following relation for ε of a substance for alternating fields by assuming the existence of a single relaxation time:

$$\frac{\varepsilon - 1}{\varepsilon + 2} = \frac{N}{3\varepsilon^{(0)}}\left(\alpha + \frac{1}{3}\frac{p^2}{kT}\frac{1}{1 + i\omega\tau_0}\right), \tag{4.4}$$

where N is the number of molecules per unit volume, α is the polarizability of the molecule, p is the dipole moment of the molecule, k is Boltzmann's constant,

T is the absolute temperature, τ_0 is the relaxation time of the molecule, and ω is the cyclic frequency.

Debye treated the molecules of a liquid as spheres of radius a having constant dipole moments and rotating under the influence of an electric field in a medium of viscosity η. In this assumption, τ_0 is defined in terms of the friction coefficient with the aid of Stokes' law:[59]

$$\tau_0 = \frac{\xi}{2kT} = \frac{0{,}4\pi a^3 \eta}{kT}. \tag{4.5}$$

It follows[60] from equations (4.4), (4.5) that the values of the complex dielectric constant of water depend on the frequency and temperature. At low frequencies ($\omega \to 0$), ε is a real number, called the static relative dielectric constant, and is denoted by ε_s. Hence,

$$\frac{\varepsilon_s - 1}{\varepsilon_s + 2} = \frac{N}{3\varepsilon^{(0)}}\left(\alpha + \frac{1}{3}\frac{p^2}{kT}\right). \tag{4.6}$$

At high frequencies ($\omega \to \infty$), ε is also real and is called the optical dielectric constant ε_0. From relation (4.4) we have:

$$\frac{\varepsilon_0 - 1}{\varepsilon_0 + 2} = \frac{N}{3\varepsilon^{(0)}}\alpha. \tag{4.7}$$

From equations (4.4)-(4.7) it is easy to obtain an expression for ε in terms of ε_s, ε_0:

$$\varepsilon = \varepsilon_0 + \frac{\varepsilon_s - \varepsilon_0}{1 + i\omega\left(\tau_0 \frac{\varepsilon_s + 2}{\varepsilon_0 + 2}\right)},$$

or

$$\varepsilon = \varepsilon_0 + \frac{\varepsilon_s - \varepsilon_0}{1 + i\omega\tau}, \tag{4.8}$$

where τ is the relaxation time of the dielectric constant, /142

$$\tau = \frac{\varepsilon_s + 2}{\varepsilon_0 + 2}\tau_0 = \frac{\varepsilon_s + 2}{\varepsilon_0 + 2}\frac{\xi}{2kT}. \tag{4.9}$$

The temperature dependence of ε now enters into relation (4.8) via relations (4.6), (4.7), (4.9).

R. Cole [61] using the results of studies by L. Onsager [62] and Van Vleck [63], found that the experimental values of ε are in better agreement with the theoretical values if one assumes that the relaxation time of the dielectric

---

[59] η is measured in poises, and a in meters.

[60] When $f = \frac{\omega}{2\pi} < 10^{13}$ Hz, α = const.

constant in relation (4.8) is not described by expression (4.9), but by the formula

$$\tau = \frac{\tau_1}{1-\delta}, \tag{4.10}$$

where

$$\delta = \frac{Np^2}{27\varepsilon^{(0)}kT}(\varepsilon_0+2)(1-q).$$

Here q is determined from the relation

$$\frac{\varepsilon_s-1}{\varepsilon_s+2} - \frac{\varepsilon_0-1}{\varepsilon_0+2} - \frac{Np^2}{9\varepsilon^{(0)}kT} = \\ = q\frac{Np^2}{9\varepsilon^{(0)}kT}\left[\frac{3\varepsilon_s(\varepsilon_0+2)}{(2\varepsilon_s+\varepsilon_0)(\varepsilon_s+2)} - 1\right] \tag{4.11}$$

and hence, is temperature dependent.

Formulas for the real and imaginary parts of ε result from expressions (4.8) and (4.3):

$$\varepsilon' = \varepsilon_0 + \frac{\varepsilon_s-\varepsilon_0}{1+(\omega\tau)^2}, \\ \varepsilon'' = \frac{(\varepsilon_s-\varepsilon_0)\omega\tau}{1+(\omega\tau)^2}, \tag{4.12}$$

as does the formula for the complex refractive index

$$N = \sqrt{\varepsilon} = n - i\varkappa, \tag{4.13}$$

where

$$n = \sqrt{\frac{\varepsilon' + \sqrt{(\varepsilon')^2+(\varepsilon'')^2}}{2}}, \\ \varkappa = \sqrt{\frac{-\varepsilon' + \sqrt{(\varepsilon')^2+(\varepsilon'')^2}}{2}} \tag{4.14}$$

In expressions (4.14), n is the refractive index, and κ is the absorption index of the substance.

In practice, instead of ω and τ, use is frequently made of wavelengths /14
λ and λ_s, corresponding respectively to frequencies ω and $\frac{1}{\tau}$, i.e.,

$$\lambda = \frac{2\pi c}{\omega}, \quad \lambda_s = 2\pi c\tau, \tag{4.15}$$

where c is the speed of light in vacuum.

When relations (4.15) are considered, formulas (4.12) take the form:

$$\varepsilon' = \varepsilon_0 + \frac{\varepsilon_s-\varepsilon_0}{1+\left(\frac{\lambda_s}{\lambda}\right)^2}, \tag{4.16}$$

$$\varepsilon'' = \frac{(\varepsilon_s - \varepsilon_0)\frac{\lambda_s}{\lambda}}{1 + \left(\frac{\lambda_s}{\lambda}\right)^2}. \qquad (4.16)$$

The start of extensive experimental and theoretical studies of the dielectric properties of water at $\lambda \leqslant 20$ cm apparently dates back to the 1950s.

A detailed bibliography of this work, contained mainly in papers and reports at conferences held during 1940-1945 is given in [64]. Since most of them were later published in scientific journals, we will not dwell on them here. Let us note only the papers of R. Hippel [65] and N. Dorsey [66], which gave experimental values of n and κ for wavelengths of 9.72 and 10 cm (Table 4.1) and 1.25 cm (Table 4.2).

TABLE 4.1. EXPERIMENTAL VALUES OF n AND κ OF WATER AT λ = 9.72 CM AND λ = 10 CM AFTER [65].

t° C	λ = 9.72 cm		λ = 10 cm	
	n	$\varkappa$	n	$\varkappa$
0	8,95	1,35	—	—
10	9,00	1,10	—	—
20	8,88	0,90	8,84	0,66
30	8,75	0,73	8,69	0,54
40	8,60	0,60	8,56	0,40

Note: Commas indicate decimal points.

TABLE 4.2. EXPERIMENTAL VALUES OF DIELECTRIC CONSTANTS OF WATER AT λ = 1.25 CM AFTER [66].

t° C	n	$\varkappa$	ε'	ε''
3	—	—	27	27
25	6,84	2,63	35	23

Note: Commas indicate decimal points.

In 1946, J. Saxton and J. Lane published in [67] the results of measurement of the complex refractive index (4.13) of water at wavelengths of 1,24 and 1.58 cm as a function of temperature (Table 4.3). In [68], Saxton studied their agreement with theoretical values by using Debye's theoretical model (4.12) with relaxation time of the dielectric constant, defined by both expression (4.9) and (4.10), (4.11). As a result, values of all the parameters entering into equalities (4.9)-(4.12) were found (Table 4.4). Moreover, it was assumed in relation (4.11) that $\varepsilon_s \gg \varepsilon_0$, which immediately leads to the estimate /144

$$\frac{3\varepsilon_s}{2\varepsilon_s + \varepsilon_0} \sim \frac{3}{2},$$

which always holds for the parameters of water. When this is taken into account, expression (4.11) takes the form

$$\frac{\varepsilon_s - 1}{\varepsilon_s + 2} - \frac{\varepsilon_0 - 1}{\varepsilon_0 + 2} - \beta = q\left[\frac{1{,}45(\varepsilon_0 + 2)}{\varepsilon_s + 2} - 1\right]\beta, \qquad (4.17)$$

where

$$\beta = \frac{Np^2}{9\varepsilon^{(0)}kT} = \frac{1180}{T}.$$

TABLE 4.3. EXPERIMENTAL VALUES OF DIELECTRIC CONSTANTS OF WATER AT λ = 1.24 CM AND λ = 1.58 CM AFTER [67]

t° C	λ = 1,24 cm				λ = 1,58 cm			
	n	$\varkappa$	ε'	ε''	n	$\varkappa$	ε'	ε''
0	4,68	2,73	14,4	25,5	5,24	2,90	19,0	30,4
5	5,24	2,89	19,1	30,3	5,84	2,97	25,3	34,7
10	5,74	2,92	24,4	33,5	6,36	2,91	32,0	37,1
15	6,17	2,88	29,8	35,5	6,77	2,78	38,1	37,6
20	6,53	2,77	34,9	36,2	7,13	2,61	44,0	37,2
25	6,84	2,63	35,0	23,0	7,40	2,41	49,0	35,7
30	7,10	2,48	44,2	35,2	7,59	2,21	52,7	33,5
35	7,30	2,30	48,0	33,6	7,72	2,01	55,5	31,0
40	7,47	2,11	—	—	7,81	1,80	37,7	28,1

TABLE 4.4. VALUES OF THE PARAMETERS OF EXPRESSIONS (4.19)-(4.12) AFTER [68]

t° C	q	$\tau \cdot 10^{12}$ C	$\tau_1 \cdot 10^{12}$ C	ε_s	ε_∞
0	1,045	19,05	28,3	88,0	5,5
5	1,047	14,6	21,9	86,0	5,5
10	1,049	11,85	17,8	84,0	5,5
15	1,051	9,6	14,6	82,0	5,5
20	1,053	8,1	12,35	80,0	5,5
25	1,055	6,8	10,5	78,2	5,5
30	1,058	5,95	9,2	76,4	5,5
35	1,061	5,2	8,15	74,7	5,5
40	1,064	4,55	7,3	73,0	5,5

TABLE 4.5. VALUES OF DIELECTRIC CONSTANTS OF WATER CALCULATED [68, 64] FROM THE PARAMETERS OF TABLE 4.4

t° C	λ = 0,5 cm				λ = 3,2 cm			
	n	$\varkappa$	ε'	ε''	n	$\varkappa$	ε'	ε''
0	3,18	1,76	7,01	11,2	7,10	2,89	42,0	41,1
5	3,50	2,03	8,13	14,2	7,63	2,62	51,3	40,0
10	3,80	2,25	9,38	17,1	8,00	2,33	58,6	37,3
15	4,10	2,41	11,0	19,7	8,22	2,00	63,6	32,9
20	4,39	2,54	12,8	22,3	8,33	1,72	66,4	28,7
25	4,67	2,62	14,9	24,4	8,38	1,50	68,0	25,1
30	4,94	2,67	17,3	26,4	8,39	1,31	68,7	22,0
35	5,21	2,69	19,9	28,0	8,38	1,16	68,9	19,4
40	5,47	2,69	22,7	29,4	8,35	1,02	68,7	17,0

Note: In tables above, commas indicate decimal points.

The paper [68] also indicates that the constant (1.45) taken in (4.17) (instead of $\frac{3}{2}$) better satisfies the experimental data, and that its variations with temperature at $0 \leqslant t \leqslant 40°$ C do not exceed 0.003. /145

On the basis of the parameter values listed in Table 4.4, Saxton calculated the refractive and absorption indices n and κ for water at λ = 10.0, 3.2, 1.24, and 1.58 cm, and found them to be in satisfactory agreement with the experimental data reported in the literature. Theoretical curves of n and κ as functions of temperature for λ = = 0.5 cm and as functions of wavelength for $\lambda \geqslant 0.2$ cm at t = 20°C were also plotted in [68].

Table 4.5 lists the results of these calculations, presented in the form of numbers in [64].

In [69], taking the measurements of [67] into consideration and utilizing the fundamental similarity between the mechanisms of dipole rotation and motion of particles in a viscous liquid, Saxton obtained theoretical values of the parameters ε_0, τ and τ_1. (Table 4.6) and experimental values of the refractive index of water in the upper portion of the millimeter range was also made in [69]. /147

As is evident from Figure 4.1, the agreement is completely satisfactory. Extensive calculations (Table 4.7) of the dielectric constants of water with consideration of the values of the parameters given in Table 4.6 were made in [70]. The close

agreement between the values of Tables 4.7 and 4.5 confirms the correct choice of the theoretical model in [69].

TABLE 4.6. VALUES OF THE PARAMETERS OF EXPRESSIONS (4.9)-(4.12) AFTER [69].

t° C	ε_s	ε_0	$\tau \cdot 10^{12}$ c	$\tau_1 \cdot 10^{12}$ c	δ
0	88,0	4,5	21,0	23,1	—0,10
5	86,0	5,0	15,1	—	—0,28
10	84,0	5,5	11,6	15,9	—0,37
15	82,0	5,5	8,9	—	—0,44
20	80,0	5,4	7,7	11,4	—0,48
30	76,4	5,3	5,85	8,5	—0,45
40	73,0	5,2	4,68	6,6	—0,41

Note: Commas indicate decimal points.

In 1947, K. Lindman [71] published a detailed survey of studies, started in 1880, dealing with measurements of the refractive index n, and also the results of his own experiments at wavelengths of 0,015-10.4 cm (Table 4.8). As he noted, these values are in good agreement with the results of a large number of other studies.

TABLE 4.7. VALUES OF DIELECTRIC CONSTANTS OF WATER CALCULATED [70] FROM THE PARAMETERS OF TABLE 4.6. /146

λ cm	$t=0$° C		$t=10$° C		$t=18$° C		$t=20$° C		$t=30$° C		$t=40$° C	
	ε'	ε''	ε'	ε''	ε'	ε''	ε'	ε''	ε'	ε''	ε'	ε''
0,1	—	—	—	—	5,75	4,87	—	—	—	—	—	—
0,2	4,72	4,21	6,15	7,13	—	—	6,82	10,02	7,58	12,56	8,51	14,62
0,3	—	—	—	—	8,18	14,13	—	—	—	—	—	—
0,4	5,34	8,35	8,06	14,00	—	—	10,75	19,25	13,61	22,84	16,72	25,50
0,5	—	—	—	—	12,60	22,12	—	—	—	—	—	—
0,6	6,37	12,38	11,04	20,18	—	—	16,43	26,50	21,59	29,80	26,58	31,45
0,75	—	—	—	—	19,85	29,65	—	—	—	—	—	—
0,8	7,78	16,22	14,82	25,48	—	—	23,05	31,78	29,90	33,82	35,70	33,70
1,0	9,50	19,80	19,18	29,83	27,75	34,41	29,75	35,00	37,50	35,42	43,30	33,61
1,2	11,52	23,20	23,78	33,24	—	—	36,00	36,70	44,01	35,48	49,15	32,35
1,4	13,65	26,09	28,45	35,80	—	—	41,70	37,26	49,30	34,55	53,70	30,60
1,6	16,02	29,00	33,00	37,56	—	—	46,65	37,18	53,58	33,10	57,20	28,71
1,8	18,81	31,47	37,44	38,68	—	—	50,92	36,50	57,10	31,62	59,80	26,82
2,0	21,50	33,68	41,58	39,40	—	—	54,50	35,42	59,88	30,04	61,90	25,05
2,5	28,30	37,69	50,20	39,10	—	—	61,65	32,28	64,80	26,20	65,45	21,41
3,0	34,99	40,22	57,08	37,60	65,05	30,64	66,10	29,18	68,04	22,98	67,60	18,37
3,5	41,08	41,47	62,50	35,50	—	—	69,40	26,38	70,10	20,35	68,98	16,13
4,0	46,68	41,70	66,30	33,25	—	—	71,65	23,82	71,30	18,14	69,88	14,32
5,0	55,82	40,65	71,70	28,95	74,76	21,22	74,20	19,80	73,32	14,97	70,72	11,58
6,0	62,66	38,42	75,05	25,38	—	—	76,00	16,95	74,01	12,68	71,40	9,74
7,5	—	—	—	—	77,76	14,87	—	—	—	—	—	—
8,0	71,55	33,25	78,95	20,04	—	—	77,62	13,00	75,28	9,62	72,18	7,40
10,0	76,70	28,60	80,90	16,47	79,05	11,35	78,10	10,47	75,50	7,72	72,46	5,94
15,0	82,52	20,62	82,60	11,22	—	—	79,61	7,02	76,13	5,15	72,77	3,99
20,0	84,95	15,92	83,47	8,49	—	—	79,92	5,35	76,26	3,91	72,87	2,98

Note: Commas indicate decimal points.

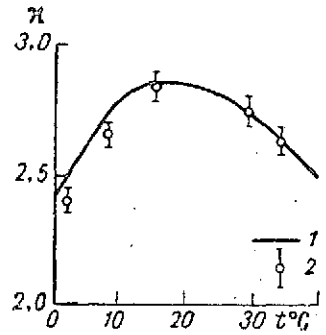

Figure 4.1. Theoretical (1) and Experiment (2) Values of κ at λ= 8.9 mm and t = 20°C After [69].

In 1948, C. Collie, J. Hasted, and D. Ritson [72] performed a careful experiment at 3 wavelengths of the centimeter range in the 0-75°C temperature range. The values of n and κ were measured within ± 1% for each frequency at 10°C temperature intervals with an accuracy of ± 0.4°C. The measurements also showed that ε_0 = 5.5 (±1), and the temperature dependences of λ_s and ε_s were obtained (Table 4.9).

The experiment of [72] was repeated with even greater accuracy by M. Buchanan [73] at wavelengths of 1.26 and 3.2 cm and temperatures from 0-60°C. The n and κ values of water that he obtained differ from the n and κ listed in Table 4.9 by no more than 1%. As is evidenced by the curves plotted in [73], Buchanan's experimental data are in even better agreement with the Debye relations at ε_0 = 5.5 than those of Collie, Hasted and Ritson.

TABLE 4.8. EXPERIMENTAL DEPENDENCE OF THE REFRACTIVE INDEX n ON λ AT t = 17°C AFTER [71].

λ cm	10,4	4,6	2,5	1,5	0,66	0,24	0,10	0,05	0,014
n	9,0	8,77	8,41	7,84	6,02	3,63	2,62	2,22	2,15

On the basis of analysis of a large number of experimental values of dielectric constants of water at t = 20°C (Table 4.10), M. Magat came to the conclusion[61] that Debye's relations (4.16) satisfactorily describe ε of water and in the submillimeter range at the values of ε_s, ε_0, λ_s given in Table 4.11. As will be shown below[62] at ε_0 = 4.1, the errors of the calculated values of n are of the order 3-5%, and those of κ, of the order 40-60% in comparison with the experimental values (Table 4.10).

In [79], using the parameter values from Table 4.4, Saxton continued his calculation of the dielectric constant of water at t = 20°C by carrying it into the submillimeter region up to λ = 300 μm. However, the data thus obtained are not at all in agreement with the experimental values given in Tables 4.8 and 4.10. /14

In 1950, D. Kiely [80] published his measurements at 8.7 mm wavelengths at t = 11.1°C; n = 4.40 + 0.24; κ = 2.91 + 0.06.

Let us note that the value of κ given here is in good agreement with the value obtained by Saxton [69] at λ = 8.9 mm.

[61] Measurements at λ equal to 313 and 109 μm were made by H. Rubens [75], and the remaining ones at λ < 313 μm, by C. Cartwright [76-78].
[62] See Table 4.28.

TABLE 4.9. EXPERIMENTAL AND THEORETICAL VALUES OF n AND κ AFTER [72].

t° C	ε_0	ε_s	λ_s cm	$\tau \cdot 10^{12}$ c	λ = 1,27 cm		λ = 3,21 cm		λ = 10 cm	
					n	κ	n	κ	n	κ
0	5,5	88,2	3,34	17,72	4,94 4,92	2,86 2,81	7,28 7,31	2,86 2,83	9,03 9,04	1,37 1,37
10	5,5	84,2	2,39	12,68	5,55 5,60	2,91 2,92	7,73 7,88	2,43 2,39	8,89 9,00	0,982 0,989
20	5,5	80,36	1,80	9,55	6,25 6,20	2,86 2,83	8,08 8,16	1,97 1,96	8,83 8,87	0,739 0,737
30	5,5	76,7	1,39	7,37	6,75 6,71	2,67 2,64	8,11 8,25	1,57 1,58	8,78 8,70	0,558 0,559
40	5,5	73,1	1,12	5,94	7,00 7,02	2,40 2,39	8,20 8,21	1,29 1,28	8,53 8,51	0,442 0,440

Note: The numerator gives the data obtained experimentally, and the denominator, those obtained by calculation. The column $\tau \cdot 10^{12}$ C gives the values which we calculated from formula (4.15).
Note: Commas indicate decimal points.

TABLE 4.10. EXPERIMENTAL VALUES OF DIELECTRIC CONSTANTS OF WATER AT t = 20°C, OBTAINED BY VARIOUS AUTHORS AFTER [74].

λ cm	ε′	ε″	λ cm	ε′	ε″	λ, мм	n	κ	ε′	ε″
23,6	76,6	5,20	3,58	61,5	26,4	0,313	2,07	0,54	4,0	2,33
11,0	78,9	10,9	3,48	68,5	28,6	0,152	2,03	0,385	3,95	1,57
10,4	78,6	12,1	3,0	65,1	31,6	0,117	2,05	0,350	4,09	1,43
10,0	78,2	13,1	2,8	54,6	33,9	0,109	2,03	0,303	4,02	1,24
9,7	78,1	15,2	1,57	44,1	37,2	0,092	1,98	0,340	3,80	1,35
9,35	78,0	12,1	1,27	30,6	35,7	0,063	1,74	0,53	2,74	1,84
6,16	75,8	18,5	1,24	35,0	36,2	0,052	1,67	0,47	2,57	1,57
6,1	73,2	18,1								

Note: Commas indicate decimal points.

In 1951, K. S. Shifrin's book [81] was published, which gave the refractive and absorption indices of water in the lower portion of the submillimeter range, similar to the data of Rubens [75] and Cartwright [76-78] .

In 1952 Lane and Saxton published a paper [82] which presented the results of measurements of the absorption index of water at temperatures of -8 and +50°C at wavelengths of 0.62, 1.24, and 3.21 cm (Table 4.12).

[63] See Table 4.10.

TABLE 4.11. VALUES OF PARAMETERS ε_s, ε_0, λ_s IN DEBYE'S RELATION AFTER [74].

t° C	ε_s	ε_0	λ_s cm
0	87,8	4,1	3,15
20	80,1	4,1	1,75 ± 0,05
40	73,0	4,1	1,05

Note: Commas indicate decimal points.

As is evident from a comparison of Tables 4.12 and 4.9, the close agreement between the results of theoretical calculations [82] and measurements [72] is observed not only in the centimeter range, but also in the millimeter range of radio waves. This also follows from the data of Table 4.13, which we calculated from formulas (4.16) by using the parameters of Table 4.9 at λ = = 0.62 CM.

When expression (4.14) is taken into consideration, the ε' and ε'' values of Table 4.7 lead to much greater differences of κ from the data of [72]. An important step forward in [82] in comparison with previous studies was the investigation of the dielectric properties of supercooled water. Lane and Saxton [82] found that the dielectric constants of supercooled water change continuously in the range from 0 to -8°C. This is explained by the fact that the absorption and dispersion of water are related to the mechanism of dipole relaxation, and this relaxation in turn is determined by the viscosity of the liquid. As was shown by J. Goe and T. Godfrey [83], there is a continuous dependence between viscosity and temperature. /150

TABLE 4.12. EXPERIMENTAL VALUES OF κ AFTER [82].

t° C	λ=0,62 cm	λ=1,24 cm	λ=3,21cm	t° C	λ=0,62 cm	λ=1,24 cm	λ=3,21 cm
—8	1,77	2,55	—	20	2,59	2,86	2,00
0	2,04	2,77	2,89	30	2,70	2,67	1,60
10	2,37	2,90	2,44	40	2,70	2,41	1,29

Note: Commas indicate decimal points.

TABLE 4.13. VALUES OF κ OF WATER AT λ = 0.62 CM, CALCULATED FROM THE PARAMETERS OF TABLE 4.9.

t° C	0	10	20	30	40
κ	2,05	2,36	2,58	2,67	2,68

Note: Commas indicate decimal points.

In the paper [84], which was a continuation of [82], on the basis of available experimental data [82] in the millimeter range of change in λ, Saxton refined the parameters ε_s, ε_0, τ and τ_1 entering into Debye's expressions (4.12), (4.10). Using these refined parameters (Table 4.14), he plotted the dependences of ε' and ε'' of water on λ (Figure 4.2) at t = 20°C and 0.1 cm $\leqslant \lambda \leqslant$ 10 cm. Some curves are also given in [85].

TABLE 4.14. REFINED VALUES OF THE PARAMETERS ε_s, ε_0, AND τ OF WATER AFTER [84].

NOTE. VALUES AT t = -10°C OBTAINED [82] BY EXTRAPOLATING THE DATA AT t = -8°C.

t° C	ε_s	ε_0	$\tau \cdot 10^{-12}$ sec	$\tau \cdot 10^{12}$ sec
—10	92,3	4,9	27,5	32,3
0	88,2	4,9	18,7	22,4
10	84,2	4,9	13,6	16,6
20	80,4	4,9	10,1	12,6
30	76,7	4,9	7,5	9,5
40	73,1	4,9	5,9	7,5

Note: Commas indicate decimal points.

TABLE 4.15. ε' AND ε'' VALUES OF WATER CALCULATED AT t = 20°C FROM THE PARAMETERS OF TABLE 4.14.

λ cm	10,0	3,0	0,6	0,3	0,1
ε'	77,76	58,72	10,72	5,73	5,11
ε''	13,87	34,15	21,64	11,61	4,00

Note: Commas indicate decimal points.

TABLE 4.16. EXPERIMENTAL VALUES OF ε', ε'' AND ε_s OF WATER AT λ = 3 CM AND λ = 10 CM AFTER [87].

t° C	ε_s	λ=3 cm		λ=10 cm	
		ε'	ε''	ε'	ε''
1,5	87,57	38,0	39,1	80,5	25,0
5	86,13	41,0	39,0	80,2	22,1
15	82,23	49,0	34,3	78,8	16,2
25	78,54	55,0	29,7	76,7	12,0
35	75,04	58,0	25,5	74,0	9,4
45	71,70	59,0	23,6	70,7	7,5

Note: Commas indicate decimal points.

To compare the dielectric constants of water given in [84] with other experimental and theoretical values, Table 4.15 lists ε' and ε'' values at t = = 20°C, which we calculated from the data of Table 4.14. It is evident from a comparison of the data of Tables 4.15 and 4.10 that the dielectric constants calculated from the new parameters are in satisfactory agreement with the experimental data at λ = 10 cm and in poor agreement at λ = 3 cm. However, the best approximation to ε from Table 4.10 at both wavelengths is given by the calculation[64] made by using the parameters of Table 4.4. Moreover, the values of Table 4.5 are also in good agreement with the experimental data given in Table 4.1 for λ = 10 cm and in poor agreement with the data shown in Figure 4.2 for λ = = 0.6 cm. /151

As was noted by Saxton, the refined parameters of Table 4.14 describe the dielectric properties of water much better in the range $\lambda \geqslant 10$ cm.

Saxton [84] also made an attempt to plot the dependences of ε' and ε'' of water at $\lambda <$ < 0.1 cm. As is evident from Figure 4.3, the Debye model is unsuitable for obtaining such dependences. Saxton used G. Froehlich's theory of resonance absorption [86] as the basis for the study of the dielectric properties of water in the submillimeter range of radiowaves. The calculations were formed by using the formulas

[64] See Table 4.5.

$$\varepsilon'_{res} = \varepsilon_{0f} + \frac{\Delta\varepsilon}{2}\left\{\frac{1+\omega_0(\omega+\omega_0)\tau_r^2}{1+(\omega+\omega_0)^2\tau_r^2} + \frac{1-\omega_0(\omega-\omega_0)\tau_r^2}{1+(\omega-\omega_0)^2\tau_r^2}\right\},$$

$$\varepsilon''_{res} = \frac{\Delta\varepsilon}{2}\left\{\frac{\omega\tau_r}{1+(\omega+\omega_0)^2\tau_r^2} + \frac{\omega\tau_r}{1+(\omega-\omega_0)^2\tau_r^2}\right\}, \qquad (4.17a)$$

where /152

$$\omega_0 = 6{,}67 \cdot 10^{12}, \quad \tau_r = 3{,}84 \cdot 10^{-14},$$
$$\Delta\varepsilon = \varepsilon_0 - \varepsilon_{01}, \quad \varepsilon_0 = 4{,}9, \quad \varepsilon_{01} = 1{,}8. \qquad (4.17b)$$

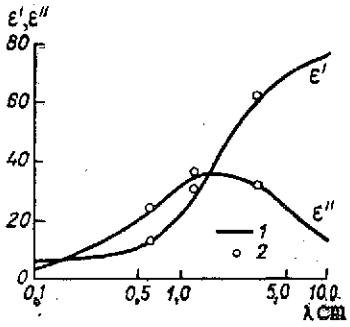

Figure 4.2. Theoretical (1) and Experimental (2) ε' and ε'' Values at t = = 20°C After [84].

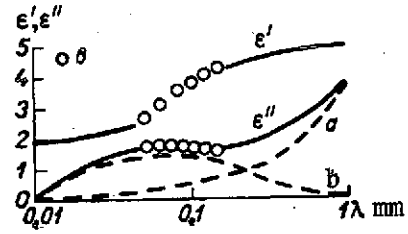

Figure 4.3. ε' and ε'' of Water vs. λ at t = 20°C After [84]. a, Component ε'' of Debye dispersion; b, Component ε'' of Froehlich resonance absorption; c, Experimental data [76-78].

From Figure 4.3 it is also evident that formulas (4.17a) give a complex dielectric constant of water that is in good agreement with the data of [76-78].

Maryott and Buckley [87] gave experimental values of ε', ε'' and ε_s of water as functions of temperature at λ = 3 and 10 cm, obtained at the Insulation Research Laboratory of the Massachusetts Institute of Technology during the period 1948-1953. These values are listed in Table 4.16.

Let us note that some ε' and ε'' values in Table 4.16 are in poor agreement with the calculated values given in Tables 4.7 and 4.15, and also with certain other experimental data mentioned above.

In 1953, P. Hertel, A. Straiton and C. Tolbert published a paper [88] in which they reported that the ε values of water measured at 8.6 mm wavelength practically coincided with Saxton's calculated data [85] obtained with the

parameter values given in Table 4.14. In the same year, V. Little [89] published results of his experiments at wavelengths of 9.16-11.12 cm at t = 21°C (Table 4.17). His results at λ = 10 cm were in good agreement with the data of Tables 4.15, 4.10, 4.9 and 4.5 only for ε'.

Two years later, J. Poley [90] presented measurements of ε of water in the range 0.802-3.99 cm at t = 20°C (Table 4.18) which were close to the ε values listed in Tables 4.3, 4.9, 4.10, etc.

TABLE 4.17. EXPERIMENTAL DATA ON ε' AND ε'' OF WATER AT t = 21°C AFTER [89].

λ cm	ε'	ε''
9,16	77,0	14,8
9,75	77,6	14,0
10,00	78,0	13,5
10,57	78,1	13,0
11,12	78,5	12,2

TABLE 4.18. EXPERIMENTAL DATA ON ε' AND ε'' OF WATER AT t = 20°C AFTER [90].

λ cm	ε'	ε''
3,99	70,1	24,6
3,55	67,7	27,1
3,20	61,8	32,0
1,25	31,5	35,5
0,802	21,34	29,6

Note: Commas indicate decimal points.

G. Strivasava and Y. Varshni [91] performed a careful experiment to determine the temperature dependence of the static dielectric constant ε_s. They also attempted an analytical description of the function $\varepsilon_s = f(T)$, where T is the absolute temperature (T = 273 + t). In so doing, they used the Debye representation (4.6). Finding ε_s from the latter, it is easy to obtain

$$\varepsilon_s = A + \frac{B}{T+C}, \qquad (4.18)$$

where A, B, C are some constants.

Treatment of the experimental data gave the relation /153

$$\varepsilon_s = \frac{62445}{T + 120} - 70.91. \qquad (4.19)$$

As is evident from Table 4.19, the calculated and the experimental values are in good mutual agreement.

Later, the same authors found [92] that the relation

$$\varepsilon_s = \frac{60677.53}{T + 112.95} - 69.03 \qquad (4.20)$$

better describes the results of their measurements.

We will cite at this point the paper [93], which is somewhat related to the studies of [91, 92], in which the following dependence of ε_s on temperature t°C was found:

$$\varepsilon_s = 78.57\ [1 - 0.00461\ (t - 25) + 0.0000155\ (t - 25)^2].$$

However, as was noted by the authors of [93], in the range of t from 4-10°C, this formula is unsuitable for specific calculations.

TABLE 4.19. CALCULATED (ε_{sc}) AND EXPERIMENTAL (ε_{se}) VALUES OF THE DIELECTRIC CONSTANT OF WATER AFTER [91].

T K	ε_{sp}	ε_{se}	Error
273	87,98	88,01	+0,034
287	82,51	82,70	+0,23
298	78,48	78,57	+0,11
323	70,05	70,28	+0,32

Note: Commas indicate decimal points.

TABLE 4.20. EXPERIMENTAL ε VALUES OF WATER AT t = 20°C AFTER [94].

λ cm	ε'	ε''	n	κ
1,36	28,0	34,1	6,0	2,84
0,85	17,5	27,3	5,0	2,73
0,63	14,7	24,4	4,6	2,62
0,43	8,9	16,9	3,75	2,26

Note: Commas indicate decimal points.

In 1959, N. S. Zinchenko [94] performed measurements of ε at t = = 20°C and λ = 0.43 to 1.36 cm (Table 4.20). Results of the measurements were compared with those of calculation using formulas (4.12). As reported in [95], the parameter ε_0 was assumed equal to 5.5, and the remaining parameters were chosen from Table 4.14. The experimental values were found to differ from the calculated ones by no more than 5-10%. If one compares the data of Tables 4.20 and 4.7, one can see that at λ = 0.43 and 0.63 cm, the ε' and ε'' values agree to within 8-15%, whereas at λ = 0.85 cm, within 30%. At the same time, the experimental data of [94] differed from the results of [90] at λ = 0.85 cm by 8-30%, and from the results calculated from the parameters of Table 4.14 by 15-38% at all the wavelengths considered.

In the same year, R. Rampolla, R. Miller, C. Smyth [96] published results of a measurement of the dielectric properties of water at t = 20°C at a wavelength of 0.31 cm. These values were: ε' = 8.5, ε'' = 12.0, n = 3.31, κ= 1.76. The errors in the determination of ε' and ε'' were 0.5 and 2.5% respectively.

These values differ from the data on ε' and ε'' given in Table 4.5 by 0.3 and 16%, and data on ε' and ε'' given in Table 4.14 by 32 and 3%.

Thus, the values measured in [96] at λ = 0.31 mm are in better agreement with the calculated values obtained by means of the parameters of Table 4.4.

In the same year, L. D. Kislovskiy [97], who performed measurements of absorption and reflection of water under conditions of model representations which he developed, calculated n and κ of water at t = 20°C and 2 μm ≤ λ ≤ 200 μm. Results of this calculation are presented in Figure 4.4.

Two years later, A. Ye. Stanevich and N. G. Yaroslavskiy [98] used direct experimental measurements of the absorption of water to study the dependence of κ on λ for 42 μm ≤ λ ≤ 2000 μm at 25°C (Figure 4.5).

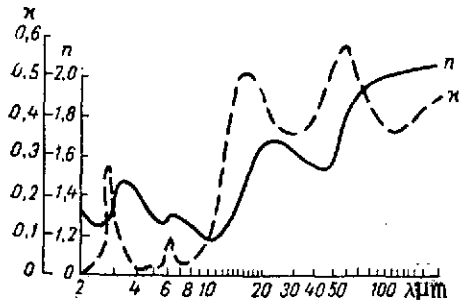

Figure 4.4. Experimental Dependence of n and κ of Water on λ at t = 20°C [97].

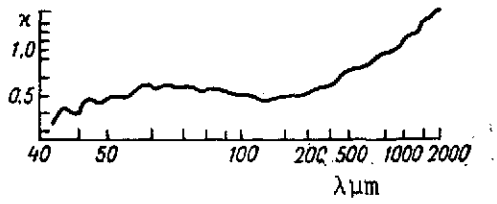

Figure 4.5. Experimental Dependence of κ on λ at t = 25°C After [98].

The data shown in Figure 4.5 are in good agreement with those of Table 4.10 and Figure 4.4.

In 1966, Lane [99] analyzed the agreement in the submillimeter range between the new experimental data [100, 98], and the data obtained by Saxton [84] from formulas (4.16) and presented in Figure 4.3.

Figure 4.6, taken from [99], shows a completely satisfactory agreement of the curves under consideration.

In the same year, K. A. Goronina, R. K. Belov and E. P. Sorokina [101] measured the dielectric constant of water for 1.6-1.2 mm wavelengths at t = 16°C (Table 4.21) and also the dependence of the loss tangent and of the expression $\sqrt{(\varepsilon')^{65} + (\varepsilon'')^{65}}$ on temperature at λ = 1.6 mm (Figure 4.7). /155

TABLE 4.21. EXPERIMENTAL ε' AND ε'' VALUES OF WATER AT t = 16°C AFTER THE DATA OF [101].

λ mm	1,2	1,25	1,42	1,47	1,53	1,6
ε' ± 0,5	5,7	6,2	5,4	5,4	5,7	5,8
ε'' ± 0,5	5,5	6,4	6,9	6,9	7,4	7,4

Note: Commas indicate decimal points.

The paper [202] pointed out the inaccuracy of the calculation made in [101], which led its authors to the incorrect assertion that a good agreement existed between the results of measurements and the values obtained f from the Debye formula.

Let us also mention the important paper by A. I. Khvostova [103], in which the dielectric constant of water was measured at 0.85 mm wavelengths: ε' = 6.2, ε'' = 3.6. This is equivalent to the fact that n = 2.58, κ = 0.696.

These values are in good agreement with the data [98-100] . In addition to studies of the electrical properties of water at increasingly shorter wavelengths

[65] The water temperature was not indicated in [103].

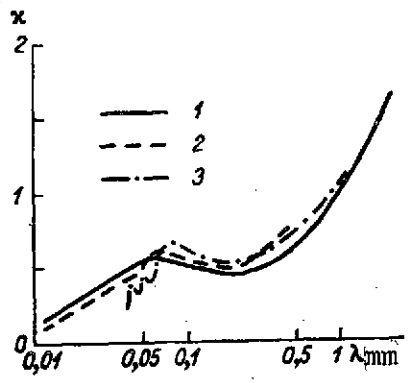

Figure 4.6. Dependence of κ of Water On λ According to Data of Different Authors.
1, Data of Saxton [84]; 2, Measurements of Draegert et al., [100]; 3, Measurements of Stanevich and Yaroslavskiy [98].

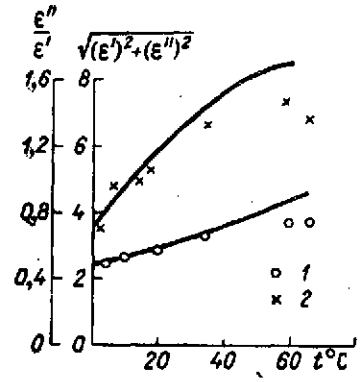

Figure 4.7. Experimental Values of $\sqrt{(\varepsilon')^2 + (\varepsilon'')^2}$ (1) and $\frac{\varepsilon'}{\varepsilon''}$ (2) of Water at Different Temperatures for λ = 1.6 mm After [101].

more accurate experiments were also set up in the region 10 cm ≤ λ ≤ 20 cm. /15
One of such rare studies in which ε' and ε'' of water were closely studied at t = 20°C is that of H. Hoffman [104] (Table 4.22). The ε' and ε'' values which he measured agree with the data of Table 4.15 to within 1.8 and 10% and with the data of Table 4.7, to within 10 and 8%, respectively.

TABLE 4.22. EXPERIMENTAL ε' AND ε'' VALUES OF WATER AT t = 20°C AFTER [104].

λ cm	ε'	ε''
9,00	76,0 ± 0,7	12,1 ± 0,4
10,00	76,35 ± 0,5	11,4 ± 0,25
10,80	76,4 ± 0,5	10,9 ± 0,25
17,76	77,6 ± 0,5	6,7 ± 0,15
22,52	77,9 ± 0,5	5,2 ± 0,15

Note: Commas indicate decimal points.

It should be noted that as the experimental data were gradually refined, attempts were also made to describe them better by means of the so-called generalized Debye equation proposed by K. Cole and R. Cole [105]:

$$\varepsilon = \varepsilon_0 + \frac{\varepsilon_s - \varepsilon_0}{1 + (i\omega\tau)^{1-\alpha}} \qquad (4.21)$$

where α is an empirical parameter taking values between 0 and 1. Separating the real part from the imaginary part in expression (4.21), we obtain:

$$\varepsilon' = \varepsilon_0 + \frac{(\varepsilon_s - \varepsilon_0)\left\{1 + (\omega\tau)^{1-\alpha}\sin\frac{\pi\alpha}{2}\right\}}{1 + 2(\omega\tau)^{1-\alpha}\sin\frac{\pi\alpha}{2} + (\omega\tau)^{2(1-\alpha)}},$$

$$\varepsilon'' = \frac{(\varepsilon_s - \varepsilon_0)(\omega\tau)^{1-\alpha}\cos\frac{\pi\alpha}{2}}{1 + 2(\omega\tau)^{1-\alpha}\sin\frac{\pi\alpha}{2} + (\omega\tau)^{2(1-\alpha)}}. \qquad (4.22)$$

when α = 0, relations (4.22) become (4.12).

It is easy to see that when the parameter α is introduced into the Debye relations, the frequency dependence of ε decreases somewhat.

When $\omega \to 0$, according to formulas (4.22), the dielectric constant is equal to ε_s, and when $\omega \to \infty$, to ε_0.

While studying the dielectric properties of polar liquids, R. Fuoss and J. Kirkwood found [106] that when the value of parameter α is suitably chosen, equation (4.21) better reflects the frequency of ε.

Treatment of the experimental data for water with the aid of relations (4.22), performed by E. Grant, T. Buchanan, and H. Cook [107] showed that a better agreement is obtained for $\alpha = 0.02$ and $\varepsilon_0 = 4.5$ with λ_s and ε_s practically the same as the corresponding data of Table 4.9. These authors note that the dielectric constants determined from equations (4.22) better describe ε of water at $\lambda = 313$ and $\lambda = 152$ μm (see Table 4.10). However, our analysis has shown that the values calculated for $\lambda < 313$ μm differ from the experimental ones (see Table 4.10) by 7-12% in n and 30-70% in κ.

Let us note at this point that treatment of experimental data showed in [108] that the values $\varepsilon_0 = 5.0$, $\alpha = 0.02$ better describe the measurement results than similar values obtained by the authors of [107].

We should also consider the generalizing studies [109] and [110]. Thus, E. Nora [109] averaged the data of [82, 111, 107, 96] on the Debye parameters ε_0 and ε_s (Table 4.23) and obtained an average ε_0 equal to 5.0 ±0.4 (independently of temperature).

Using an analogous approach, J. Hasted [110] arrived at λ_s values that practically coincided with the data of Table 4.9: $\varepsilon_0 = 5.5 \pm 1$, $\alpha = 0.02 \pm 0.007$.

TABLE 4.23. AVERAGE VALUES OF THE PARAMETERS ε_0 AND ε_s AFTER [109].

t°C	ε_0	ε_s	t°C	ε_0	ε_s
0	4,91 ± 0,45	87,90	30	4,93 ± 0,52	76,58
10	5,14 ± 0,50	83,95	40	4,77 ± 0,59	73,15
20	5,86 ± 0,74	80,18	50	4,42 ± 1,12	69,88

Note; Commas indicate decimal points.

/157

We will also mention the study [112], in which on the basis of theoretical treatment of experimental findings it was determined that the Debye equation (4.16) with the parameters of Collie, Hasted and Ritson (see Table 4.9) very adequately describes the permittivity of water in the range 0.1 cm $\leqslant \lambda \leqslant$ 14 cm (Figures 4.8 and 4.9).

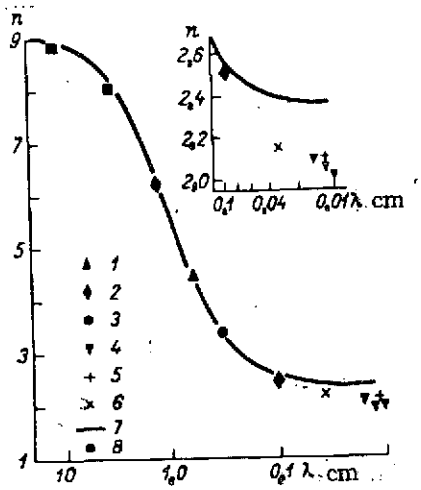

Figure 4.8. Experimental and Theoretical Values of the Refractive Index n of Water at t = 20°C after [112]. 1, after [82]; 2, [113]; 3, [96]; 4, [76]; 5, [112]; 6, [112]; 7, Debye curve; 8, after [72].

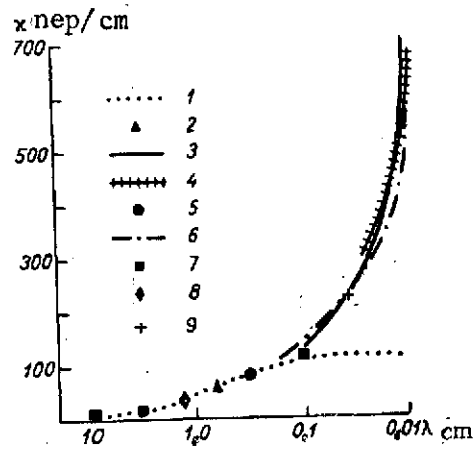

Figure 4.9. Experimental and Theoretical Values of the Absorption Index κ of Water at t = 20°C After [112]. 1, Debye curve; 2, after [82]; 3, 9, [112], 24°C; 4, [100], 30°C; 5, [96]; 6, [98]; 7, [72]; 8, after [113].

Comparison of the experimental and Debye curves in the submillimeter range, however, shows that n and κ calculated from formulas (4.16) with the parameters ε_0, ε_s, λ_s from Table 4.9 contain an error of the order of 20 and 60% respectively.

The paper [112] also gives results of experimental studies of the temperature dependence of n and κ of water at a wavelength of 337 μm (Table 4.24)[66].

TABLE 4.24. EXPERIMENTAL n AND κ VALUES OF WATER AT λ = 337 μm AFTER [112] /158

t° C	n	κ	t° C	n	κ
0	2,15	—	20	2,16	0,514
10	2,15	—	30	2,17	0,648
18	2,16	0,469	40	2,20	0,737

Note: Commas indicate decimal points.

On the basis of the experimental studies surveyed above, the following analytical dependences of ε_s and λ_s on temperature were obtained on a computer by means of the least squares method [102]:

[66] In [112], the data of Table 4.24 are presented in the form of curves and κ is given in nep/cm.

$$\varepsilon_s = 0{,}00081t^2 - 0{,}40885t + 88{,}2, \quad (4.23)$$

$$\lambda_s = 1.4662^{-0.0634t} + 0.000136t^2 - 0{,}027296t + 1.8735116, \quad (4.24)$$

which apply over a wide temperature range, from -40 to +75°C. Let us note that in deriving relations (4.23), (4.24) only those measurements which were made at subzero temperatures were taken into consideration. In addition, we proceeded from the assumption that if relations (4.23), (4.24) correctly describe the behavior of ε_s and λ_s at $t \geqslant 0$, they should also automatically apply at $t < 0$. This follows from purely experimental studies by Saxton [82], in which he showed and proved[67] that when t changes continuously from 0 to -8°C, all the constants change continuously.

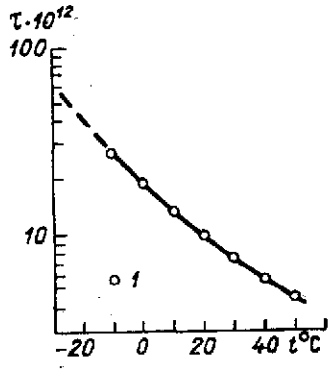

Figure 4.10. Temperature Dependence of τ After [84, 114]. 1, Experimental points.

Table 4.25 lists values of ε_s and λ_s calculated from formulas (4.23) and (4.24).

If the values of ε_s at $t \geqslant 0$ in Table 4.25 are compared with experimental data of other authors (see Tables 4.4, 4.9, 4.11, 4.14, 4.16, 4.19 and 4.23), the differences amount to no more than 1%. Thus follows the subzero temperatures are concerned, Saxton's data (see Table 4.14) for t = -10°C, ε_s = = 92.3 practically coincide with ours (Table 4.25): ε_s = 92.37.

If one extrapolates the approximation [91] of ε_s (4.19)-(4.20) into the region of subzero temperatures, ε_s values differing from ours (Table 4.25) by not more than 0.8% are obtained. From the standpoint of the calculations, (formula (4.19) must evidently be acknowledged to be simpler and more valid than (4.23).

The λ_s values listed in Tables 4.25 and 4.9 all coincide and differ from t /159 the data of Table 4.14 and Figure 4.10, plotted from the values of Table 4.14 extrapolated into the region of low temperatures according to [114], by not more than 7%. Such a difference may be explained only by a low choice of ε_0 in [84], as was pointed out, for example, in [112].

---

[67] For more detail see p. 150.

TABLE 4.25. TEMPERATURE DEPENDENCE OF THE PARAMETERS ε_s AND λ_s AFTER [102].

t° C	ε_s	λ_s	t° C	ε_s	λ_s	t° C	ε_s	λ_s
—40	105,85	20,97	1	87,80	3,22	22	79,60	1,70
—38	104,90	18,81	2	87,89	3,11	23	79,23	1,66
—36	103,97	16,89	3	86,99	3,01	24	78,86	1,62
—34	103,03	15,19	4	86,58	2,90	25	78,49	1,58
—32	102,11	13,69	5	86,18	2,81	26	78,12	1,54
—30	101,19	12,35	6	85,78	2,72	27	77,76	1,50
—28	100,28	11,16	7	85,38	2,63	28	77,39	1,46
—26	99,38	10,10	8	84,99	2,55	29	77,03	1,43
—24	98,48	9,16	9	84,59	2,47	30	76,67	1,40
—22	97,59	8,33	10	84,20	2,39	31	76,31	1,36
—20	96,70	7,58	11	83,81	2,32	32	75,95	1,33
—18	95,82	6,92	12	83,42	2,25	33	75,60	1,30
—16	94,95	6,32	13	83,03	2,18	34	75,24	1,27
—14	94,08	5,79	14	82,04	2,12	35	74,89	1,24
—12	93,22	5,32	15	82,26	2,06	36	74,54	1,22
—10	92,37	4,90	16	81,87	2,00	37	74,19	1,19
—8	91,52	4,52	17	81,49	1,95	38	73,84	1,17
—6	90,68	4,17	18	81,11	1,89	39	73,49	1,14
—4	89,85	3,87	19	80,73	1,84	40	73,15	1,12
—2	89,02	3,59	20	80,35	1,79			
0	88,20	3,34	21	79,98	1,75			

Note: Commas indicate decimal points.

Among the studies enumerated above, we should mention particularly that of A. Ye. Basharinov and B. G. Kutuza [115], which gave experimental value[68] of τ_0 of supercooled water at temperatures from -2.5 to -12.5°C (Table 4.26).

TABLE 4.26. EXPERIMENTAL τ_0 VALUES OF WATER AFTER [115].

observation sessions	1	2	3	4	5	6	7	8
t° C	—12,5	—8	—7	—4	—2,5	+2	+2	+3
$\tau_0 \cdot 10^{12}$ c	2,60	2,20	2,07	1,91	1,67	1,75	1,27	1,20

On the basis of treatment of experimental data[69] [72], the temperature dependence of the relaxation time τ_0 of the molecule was obtained in the same paper to within 5%:

$$\tau_0 = e^{\left(\frac{2074,8}{273+t} - 7,22\right)} \cdot 10^{-12} \text{ sec}, t > 0. \quad (4.25)$$

For $t < 0$, the authors of [115] propose another temperature dependence: /16

$$\tau_0 = e^{\left(\frac{2457}{273+t} - 8,55\right)} \cdot 10^{-12} \text{ sec}, t < 0. \quad (4.26)$$

The λ_s values calculated from formulas (4.9), (4.15) with consideration of expressions (4.25) (Table 4.27a) and (4.26) (Table 4.27b) show that the data of

[68] See expression (4.9).
[69] See Table 4.9.

[115] differ from ours (Table 4.25) by several percent (not more than 7%). At the same time, the same values of [72] are approximated 80-100 times more accurately[70] by relation (4.24), continuous in t [102]. The final n and κ values of water determined from formulas (4.12), (4.9), (4.23), (4.25), (4.26) agree with ours to within 5%.

At the same time, our calculated κ values of supercooled water (see appendix) differ from those measured experimentally by Lane and Saxton (see Table 4.12) at t = -8°C at wavelengths 0.62 and 1.24 cm by 1.7 and 0.7% respectively.

TABLE 4.27. VALUES OF λ_s CALCULATED ON THE BASIS OF DATA OF [115].

a)		b)	
t° C	λ_s	t° C	λ_s
0	3,54	0	3,30
—10	5,21	10	2,41
—20	7,88	20	1,79
—30	12,29	30	1,35
—40	19,82	40	1,04

Note: Commas indicate decimal points.

Let us examine ε_0 somewhat more closely. The survey of theoretical studies given above indicated ε_0 values obtained by different authors in the course of a mathematical description of resultant experimental studies of dielectric constants of water in various portions of variation of λ. Thus, for approximately the same ε_s, λ values, the following ε_0 values were obtained: 5.5 [72-112]; 4.5-5.5 as a function of t [69]; 4.1 [74]; 4.9 [84]; 5.0-6.6 [111]; 5.0 ±0.4 [108]; 1.77 [116]; 1.8 [117], etc.

In order to explain the dependence of the refractive index n and absorption index κ on ε_0 and α entering into the generalized Debye equation, a numerical calculation was performed using formulas (4.16) for ε_0 = 1.8 to 5.5, temperatures of 0, 20, 40°C and λ = 10 to 0.0152 cm. Results of this calculation at t = 20°C are shown in Table 4.28. It is apparent from the table that the maximum variations of n and κ as functions of changing ε_0 amount to respectively: 1.6 and 6% in the lower portion of the centimeter range, 28 and 35% in the millimeter range, and 50 and 80% in the submillimeter range.

Analysis of the refractive and absorption indices calculated at 0 and 40°C and their comparison with the data listed in Table 4.28 lead to the conclusion that as the temperature rises, the dependence of n and κ on ε_0 weakens somewhat, and in the centimeter range of change in λ, the variations in ε_0 in the range from 1.8 to 5.5 at all the temperatures considered essentially do not affect n and κ of water. This apparently also explains the fact that large differences in ε_0 values used to calculate the dielectric constants of water by many investigators led to approximately the same final results. /161

[70] In contrast to relations (4.25), (4.26).

TABLE 4.28. DEPENDENCE OF DEBYE RELATIONS OF n AND κ OF WATER AT t = 20°C on ε_0.

ε_0	λ = 10 cm		λ = 3 cm		λ = 1,25 cm		λ = 0,8 cm	
	n	κ	n	κ	n	κ	n	κ
1,8	8,86	0,77	8,02	2,16	6,06	3,04	4,88	2,99
2,3	8,86	0,77	8,02	2,14	6,07	3,01	4,90	2,96
2,8	8,86	0,76	8,03	2,12	6,09	2,99	4,92	2,93
3,3	8,86	0,76	8,03	2,11	6,10	2,96	4,95	2,90
3,8	8,86	0,75	8,04	2,10	6,12	2,93	4,97	2,86
4,2	8,86	0,75	8,04	2,09	6,13	2,91	4,99	2,84
4,5	8,86	0,74	8,04	2,08	6,14	2,90	5,00	2,82
4,7	8,86	0,74	8,04	2,07	6,14	2,89	5,01	2,81
4,9	8,86	0,74	8,05	2,07	6,15	2,88	5,02	2,79
5,1	8,86	0,74	8,05	2,06	6,16	2,87	5,03	2,78
5,3	8,86	0,74	8,05	2,05	6,16	2,86	5,04	2,77
5,5	8,86	0,73	8,05	2,05	6,17	2,85	5,05	2,76

ε_0	λ = 0,1 cm		λ = 0,08 cm		λ = 0,0337 cm		λ = 0,0152 cm	
	n	κ	n	κ	n	κ	n	κ
1,8	1,85	1,18	1,73	1,01	1,44	0,51	1,37	0,24
2,3	1,95	1,11	1,83	0,95	1,59	0,46	1,53	0,21
2,8	2,04	1,06	1,94	0,89	1,73	0,42	1,69	0,19
3,3	2,13	1,00	2,04	0,84	1,86	0,39	1,83	0,18
3,8	2,22	0,96	2,14	0,80	1,99	0,36	1,96	0,17
4,2	2,30	0,92	2,22	0,76	2,08	0,34	2,06	0,16
4,5	2,35	0,90	2,28	0,74	2,15	0,33	2,13	0,15
4,7	2,39	0,88	2,32	0,73	2,20	0,32	2,17	0,15
4,9	2,42	0,86	2,36	0,71	2,24	0,32	2,22	0,14
5,1	2,46	0,85	2,40	0,70	2,29	0,31	2,26	0,14
5,3	2,50	0,84	2,43	0,69	2,33	0,30	2,31	0,14
5,5	2,51	0,83	2,47	0,67	2,37	0,30	2,35	0,14

Note: Commas indicate decimal points.

Treatment on the computer of all the above results of measurements of the dielectric constant of water in the range $0.08 \leqslant \lambda \leqslant 20$ cm at different temperatures confirms the conclusion reached in [112] and elsewhere that $\varepsilon_0 = 5.5$ is the best constant from the standpoint of agreement of the theoretical and experimental data.

Thus, calculating n and κ of water from formulas (4.16), (4.23), (4.24) for $\varepsilon_0 = 5.5$, λ = 0.08 cm, t - 22°C, we obtain n = 2.48, κ = 0.70. Comparing these values with n = 2.58 and κ = 0.696, obtained by A. I. Khvostova [103] experitally at λ = 0.085 cm (see p. 155) we see that even in the upper portion of the submillimeter range, the discrepancies of the calculated and experimental values do not exceed 5% in n and that there are no discrepancies at all in κ. /16

If these coefficients are calculated with our formulas for λ = 0.3 cm, t = 20°C, we obtain n = 3.31, κ = 1.84, against the experimental values of Rampolla, Miller and Smyth [96], n = 3.31, κ = 1.76 (see p. 154). In this case, our values of n given in [96] agree, and κ differ by not more than 3.3%.

Analysis of the generalized Debye equation (4.22) and calculations of n and κ for different ε_0, α and t°C show that it is impossible, by introducing the parameter α into expressions (4.16), to substantially decrease the accuracy of the agreement between the theoretical and the experimental results, or, for approximately the same accuracy as in the case of $\alpha = 0$, to expand the range of change of λ toward wavelengths shorter than 0.08 cm.

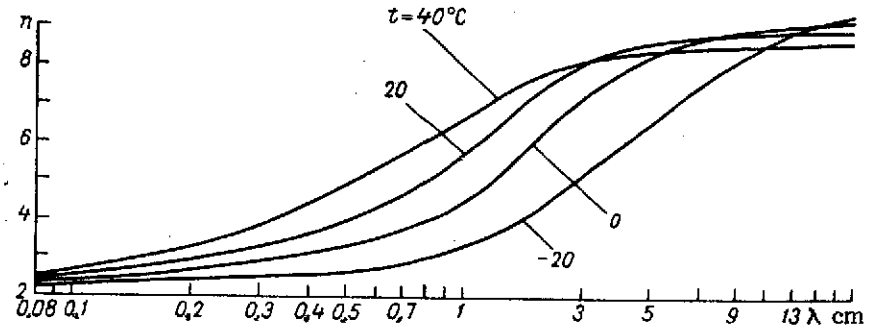

Figure 4.11. Dependence of n of Water on Wavelength λ at Different Temperatures.

Figures 4.11 and 4.12 show individual results[71] of our calculations of n and κ of water from formulas (4.14), (4.16), (4.23), (4.24) for $\varepsilon_0 = 5.5$.

Analysis of the dependence of n on λ and t (Figures 4.11) show that the refractive index of water at each temperature depends on the wavelength in the range of its change from 0.1 cm to a certain magnitude of $\lambda_{max}^{(t)}$. The latter in turn depends on t: the lower the water temperature, the greater the maximum value of $\lambda_{max}^{(t)}$, starting at which the refractive index practically ceases to change with increasing wavelengths. For example, $\lambda_{max}^{(40)} = 9$ cm; $\lambda_{max}^{(20)} = 14$ cm; $\lambda_{max}^{(0)} = 20$ cm; $\lambda_{max}^{(-20)} = 27$ cm.

For the range $0.08 \text{ cm} \leqslant \lambda \leqslant 0.1$ cm, n may be considered independent of both wavelengths and temperature. /163

From Figure 4.11 it is also evident that at a fixed temperature, the dependence of n on λ is increasing. A similar character is exhibited by the dependence t at $-40°C \leqslant t \leqslant 40°C$ and a fixed wavelength in the range $0.08 \leqslant \lambda_{max}^{(40)}$. At $\lambda > \lambda_{max}^{(40)}$, the character of the dependence becomes somewhat more complicated,

[71] Detailed values of ε', ε'', n, κ of water at wavelengths of 0.08 to 20 cm at temperatures from -40 to 40°C are given in the appendix.

and the magnitude of the highest value of n as a function of λ increases with rising temperature. /163

As shown in Figure 4.12, the absorption index κ depends more on the wavelength and temperature than n, this being true of the entire range of change in λ and t under consideration. To each temperature there corresponds a wavelength at which this index has a maximum value κ_{max}. Moreover, the higher the temperature, the lower κ_{max} and the smaller the wavelength at which the maximum of κ is reached.

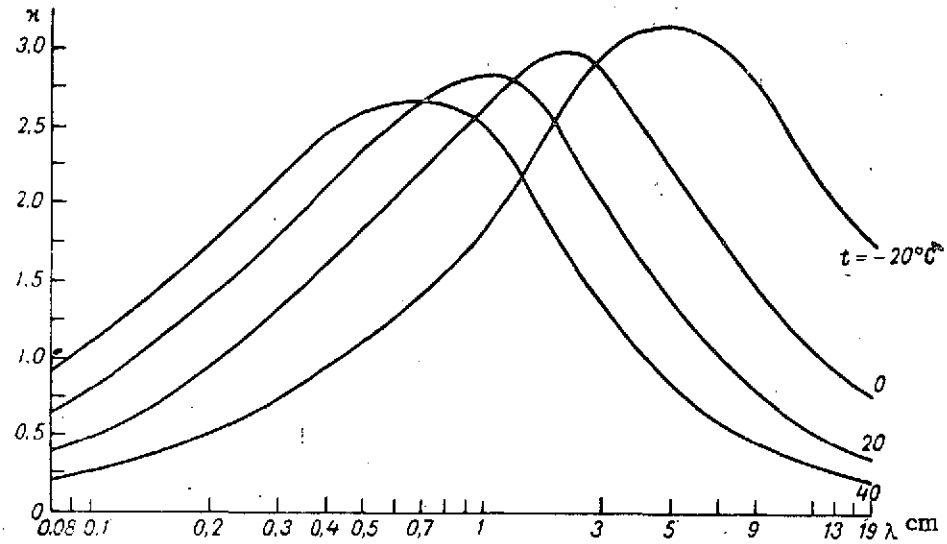

Figure 4.12. Dependence of κ of Water on Wavelength λ at Different Temperatures.

In 1969, a paper by V. M. Zolotarev et al. was published [118] which gave results of a study of n and κ of water at t = 25°C by means of four independent methods (transmission, reflection, NPVO and Kramers-Kronig methods) over a wide spectral range, $1\text{-}10^6$ μm, results which agreed with an accuracy of not more than 3% with those reported in the literature. Table 4.29 lists only values of λ from 50 μm to 10 cm. The corresponding values of n and κ for λ < 50 μm may be found in [118-124].

We will also note the paper [125], in which measurements of the dielectric constant of water were made at 2.0-0.8 mm wavelengths at t = 21°C. The results are shown in Table 4.30.

TABLE 4.29. VALUES OF n AND κ OF WATER AT t = 25°C AFTER [118]. /164

λ	n	κ	λ	n	κ
50,0 μm	1,582	0,503	250,0 μm	2,157	0,536
60,0	1,715	0,593	500,0	2,409	0,74
62,5	1,750	0,595	0,1 см	2,663	1,02
75,0	1,868	0,563	0,5	4,162	2,33
100,0	1,986	0,527	1,0	5,697	2,90
150,0	2,074	0,486	5,0	8,553	1,48
200,0	2,120	0,500	10,0	8,856	0,74

Note: Commas indicate decimal points.

The authors of [125] state that at $\lambda < 2$ mm, the experimental ε values of water are in poor agreement with the values obtained from the Debye relations. Noting that the data of [125] disagree with the measurements of [101] given in Table 4.21, [103] and Table 4.29, the authors indicate that these differences cannot be explained by measurement errors.

TABLE 4.30. EXPERIMENTAL ε' AND ε'' VALUES OF WATER AT t = 21°C AFTER [125].

λ mm	1,5	1,3	1,0	0,8
$\varepsilon' \pm 0,3$	5,35	4,98	4,43	4,46
$\varepsilon'' \pm 0,25$	6,60	5,80	4,45	3,96

Note: Commas indicate decimal points.

Finally, we will mention the paper [126], which recommends the use of the Debye equation in the submillimeter range after a suitable correction allowing for the dielectric dispersion of water in the infrared region. The following expressions are thus obtained:

$$\varepsilon' = \varepsilon'_{res} + \frac{\varepsilon_s - \varepsilon'_{res}}{1 + \left(\frac{\lambda_s}{\lambda}\right)^2}, \qquad \varepsilon'' = \varepsilon''_{res} + \frac{\varepsilon_s - \varepsilon'_{res}}{1 + \left(\frac{\lambda_s}{\lambda}\right)^2}, \tag{4.26a}$$

where ε'_{res}, ε''_{res} are determined from formulas (4.17a), (4.17b), $\tau_r = 3.2858 \cdot 10^{-14}$, $\omega_0 = 7.793 \cdot 10^{12}$ at t = 20°C, expressions that adequately describe the experimental data and are in agreement with the Debye expressions (4.16) at $\lambda \geqslant 0.8$ mm (Figure 4.13).

On the basis of [100], the authors of [126] found that the dependence of ε of water on temperature t in the submillimeter range is close to linear:

$$\varepsilon'(t) = \varepsilon'(t_0) + k_1(t - t_0),$$
$$\varepsilon''(t) = \varepsilon''(t_0) + k_2(t - t_0); \tag{4.26b}$$

the k_1 and k_2 values for different λ being shown in Figure 4.14. Figure 4.15 /165 illustrates the temperature dependence of the dielectric constant of water in

the submillimeter range. It is evident ε' is practically independent of t, and that ε" changes a little more markedly, but still very slightly (increases) with rising t.

The paper [126] also gives results of measurements of ε at λ = 0.86 mm and t = 20°C (ε' = 4.9, ε" = 4.2, 20% error), λ = 0.98 mm and λ = 1.5 mm at t = 8 ÷ ÷ 65°C (10-12% error), which satisfactorily agree with the calculated data.

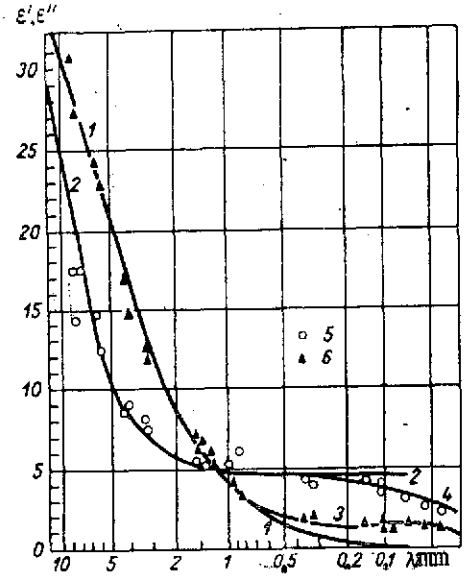

Figure 4.13. Dielectric Constant of Water at t = 20°C After [126].
ε' (1) and ε" (2) calculated after Debye (4.16); ε' (3) and ε" (4) calculated from formulas (4.26a); ε' (5) and ε" (6) obtained in [126].

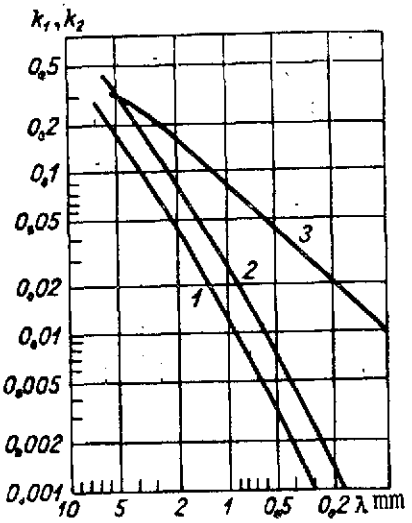

Figure 4.14. Dependence of k_1 and k_2 on λ.
1, k_1 at t < 40°C; 2, k_1 at t > 40°C; 3, k_2

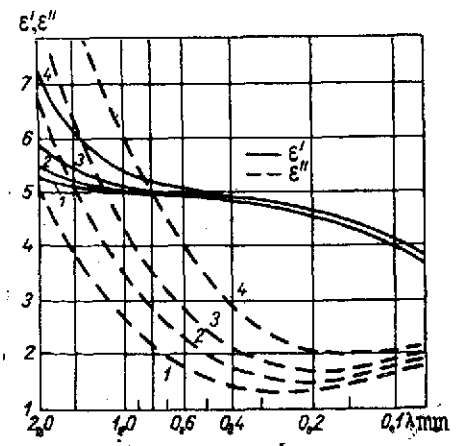

Figure 4.15. Dependence of ε' and ε" of Water on Temperature After [126].
1, 0°C; 2, 10°C; 3, 20°C; 4, 40°C.

Let us also note that the ε values of water at λ = 0.86 mm [126] agree with little experimental error with the data which we calculated from the Debye equations (see appendix).

§ 4.2. Dielectric Constant of Ice and of a Homogeneous Mixture of Water With Ice and Snow.

/166

There are only a few studies [120-132, 135, 1936][72], which give results of measurements of the dielectric constant of ice for wavelengths below 20 cm.

Thus, E. Yonker [130], who performed an experiment at 3.01 and 9.18 cm wavelengths at temperatures from 0 to -50°C found that n of ice changes from 1.75 at λ = 3.01 cm to 1.72 at λ = 9.18 cm, and κ is independent of wavelength and increases (Figure 4.16) from 0.0001 to 0.0010 as t rises.

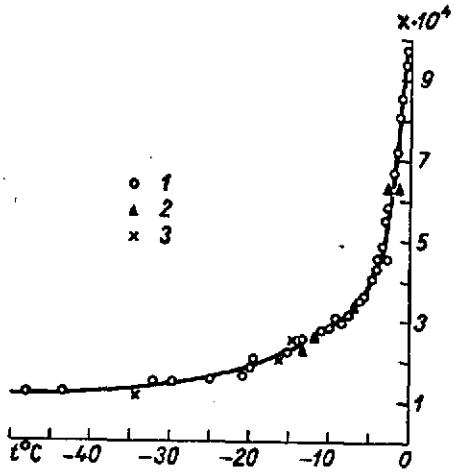

Figure 4.16. Temperature Dependence of κ of Ice After [130].
1,2, Experiment at λ = 3.01 cm, two different samples; 3, experiment at λ = = 9.18 cm.

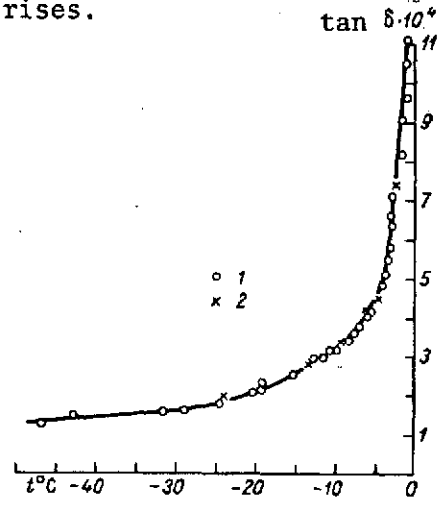

Figure 4.17. Loss Tangent of Ice at λ = 3 cm as a Function Temperature After [132].
1,2, Two different samples.

In addition, in [130], Yonker gives values of the real and imaginary parts of the dielectric constant of ice, which he measured at 1.25 cm wavelengths at t = -15°C: ε' = 3.3; ε'' = 0.0011.

Later, R. Dunsmuir and J. Lamb [131] at 3 and 9 cm wavelengths, then Lamb [132] at λ = 3 cm repeated the experiment mentioned in [130] and arrived at practically the same dependence of n and κ on λ and t. The data of these papers are reflected in Table 4.33 and Figure 4.17.

[72]See also the reviews [127-129].

In addition, Lamb showed in [132] that Debye's equations (4.12) suitable for describing the dielectric properties of ice in the low frequency region of the spectrum are completely inapplicable in its centimeter region.

The same conclusion can be reached if one compares the data of calculations of [133] at λ = 3 cm with the experimental values cited above. We also made an attempt to describe the experimental data given in [130-132] by means of the generalized Debye equation (4.22) for ε_s and τ_s values taken from [134]. Comparison of ε_0 and α values calculated with a wide grid with the experimental values of n and κ [130-132] showed that no satisfactory description uniform in λ of these data can be achieved by expression (4.22) for any fixed ε_0 and λ. /167

In 1949, J. Lamb and A. Turney [135] published measurements of ε' and loss tangent of ice at 1.25 cm wavelength (Figure 4.18) for temperatures from -200 to 0°C. Figure 4.18 clearly shows a marked dependence of the loss tangent at 1.25 and 3 cm wavelengths in the temperature range from -50 to 0°C. In 1952, the paper of W. Cumming [136] was published in which the temperature dependence of the dielectric properties of ice and snow covers of different densities was studied at 3.2 cm wavelength.

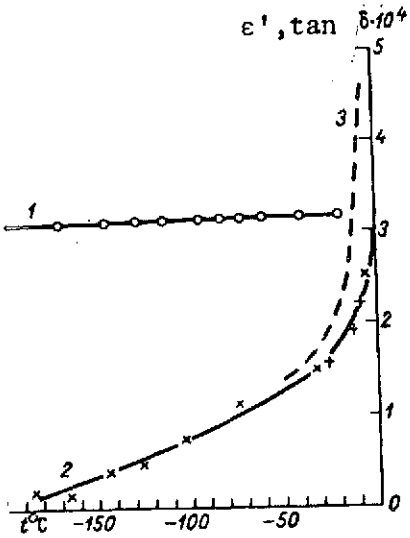

Figure 4.18. ε' (Curve 1) and Loss Tangent (Curve 2) of Ice as Functions of Temperature at λ = 1.25 cm After [135]. 1,2, Experimental points; 3, loss tangent at λ = 3 cm after [132].

Results of these measurements, which we recalculated for n and κ, are shown in the form of Tables 4.31 and 4.32.[73] Table 4.33, compiled from data of many authors, shows that at 1.25 cm $\leqslant \lambda \leqslant$ cm and t $\leqslant$ -20°C, the dielectric properties of ice are independent of wavelength. A similar conclusion for t > -20°C may apparently be reached only for the range λ = 3 to 9 cm.

It is noted in [136] that the measurement results are not affected by ε, whether the ice used was prepared from fresh, distilled, or tap water. Hence, such a difference in the κ values of ice [130-132, 135] and [136] should probably be attributed to its anisotropy. This problem is discussed in detail in [138, 110].

[73] In [136], these data for $\rho \leqslant 0.76$ g/cm^3 are referred to a snow cover of corresponding density. However, as will be shown below, a snow cover and ice of the same density have essentially the same dielectric constant.

Only three papers [101, 97, 76] devoted to measurements of the dielectric constant of ice for waves shorter than 1 cm are known.

TABLE 4.31. EXPERIMENTAL n AND κ VALUES OF ICE AT DIFFERENT DENSITIES ρ, TEMPERATURES t°C AND λ = 3.2 cm AFTER [136]. /168

ρ g/cm³	n	κ·10⁴ at t° C									
		0	−2	−4	−6	−8	−10	−12	−14	−16	−18
0,916	1,78	23,0	1,6	12,0	10,5	8,9	7,7	7,1	6,6	6,3	6,1
0,76	1,65	14,8	10,7	8,7	7,4	6,4	5,8	5,4	4,9	4,7	4,4
0,60	1,50	10,3	7,5	6,0	5,2	4,5	4,3	3,9	3,7	3,3	3,0
0,46	1,38	6,9	4,8	4,1	3,4	3,1	2,8	2,6	2,5	2,5	2,5
0,38	1,31	5,2	3,9	3,3	2,6	2,4	2,3	2,2	2,1	2,0	1,8
0,34	1,27	5,0	3,7	3,0	2,3	2,0	1,9	1,8	1,6	1,4	1,3

TABLE 4.32. EXPERIMENTAL n AND κ VALUES OF WET SNOW COVER AT 0°C AS FUNCTIONS OF THE PERCENTAGE (BY WEIGHT) CONTENT OF WATER p AFTER [136].

ρ g/cm³	n	κ·10⁴ at P %								
		0	0,2	0,4	0,6	0,8	1,0	1,2	1,4	1,6
0,38	1,31	5,2	13,7	26,2	38,0	54,4	73,4	89,7	112,0	134,0
0,76	1,65	14,8	33,8	55,3	90,1	131,3	179,0	242,0	304,0	371,0

TABLE 4.33. REFRACTIVE INDICES n AND ABSORPTION INDICES κ OF ICE IN THE 1.25-9 cm WAVELENGTH RANGE BASED ON DATA OF VARIOUS AUTHORS.

Author and Reference	λ cm	n	κ·10⁴ at t° C							
			0	−10	−15	−20	−30	−40	−50	−60
Yonker [130]	3,01; 9,18	1,75—1,72	10,0	2,9	—	2,0	1,4	1,3	1,1	—
Dunsmuir,	1,25	1,82	—	—	3,0	—	—	—	—	—
Lamb [131]	3,0; 9,0	1,75—1,72	10,5	2,85	2,29	—	1,45	—	1,1	—
Lamb [132]	3,0	1,75	12,0	2,8	—	1,9	1,4	1,3	1,2	—
Lamb, Turney [135]	1,25	1,77—1,78	2,7	1,9	—	1,6	1,4	1,28	1,1	1,04
Cumming [136] [74]	3,2	1,78	24	7,9	—	5,5	—	—	—	—

Note: In tables above commas indicate decimal points.

[74] The data of [136] were linearly extrapolated to unit density by J. Marshall and K. Gunn [137].

Thus, in [101], only the value of the refractive index n = 1.6 was obtained at /169 a temperature close to zero and 1.6 mm wavelengths, in [97], values of n and κ at t = -10°C in the wave length range from 2 to 200 μm (Figure 4.19), and in [76], values of κ at t = -10°C for several wavelengths from 52 to 152 μm (Table 4.34).

TABLE 4.34. EXPERIMENTAL κ VALUES OF ICE AT t = 10°C AFTER [76].

λ μm	52	63	83	100	117	152
κ	0,27	0,30	0,22	0,08	0,03	0,03

The first studies of radar signals from melting hailstones were made by J. Ryde [139] under the assumption that these hailstones were so small that they constitute a homogeneous mixture of water and ice. The dielectric constant of the mixture was calculated from the formula

$$\frac{\varepsilon_{mix}-1}{\varepsilon_{mix}+2}=\frac{M_w}{M_{mix}}\frac{\rho_{mix}}{\rho_w}\frac{\varepsilon_1-1}{\varepsilon_1+u}=\frac{M_i}{M_{mix}}\frac{\rho_{mix}}{\rho_i}\frac{\varepsilon_i-1}{\varepsilon_i+2}, \tag{4.27}$$

where ε_{mix}, ε_w, and ε_i, M_{mix}, M_w and M_i, ρ_{mix}, ρ_w and ρ_i are the dielectric constants, masses and densities of the mixture, water and ice respectively.

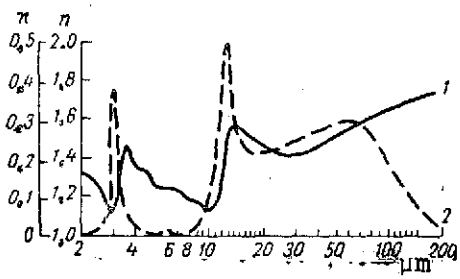

Figure 4.19. Dependence of n (1) and κ (2) of Ice on Wavelength λ at t = 10°C After [97].

Formula (4.27) is a special case of Weiner's general equation [140] for u = 2.

$$\frac{\varepsilon_{mix}-1}{\varepsilon_{mix}+u}=\frac{M_1}{M_{mix}}\frac{\rho_{mix}}{\rho 1}\frac{\varepsilon_1-1}{\varepsilon_1+u}=\frac{M_2}{M_{mix}}\frac{\rho_{mix}}{\rho 2}\frac{\varepsilon_2-1}{\varepsilon_2+u}, \tag{4.28}$$

where subscripts 1 correspond to quantities of the first substance, subscripts 2 to quantities of the second substance, and u is the so-called shape parameter.

K. Wagner [141] showed that relation (4.27) may be used when the first substance is in a homogeneous mixture in the form of spherical particles.[75]

[75] If the particles have a different shape, the u values and other aspects corresponding to this shape may be found in [142, 143].

A theoretical validation of formula (4.27) in the case where the components of the homogeneous mixture have real values of the dielectric constant was also given by R. Dichburn [144]. For complex ε with Im $\varepsilon \neq 0$, expression (4.27) was used by K. Gunn and T. East [145], L. Battan and B. Herman [146] and others in calculations of the reflectivity and attenuation capacity of a melting spherical ice particle; results thus obtained were in fairly good agreement with the experimental data. /170

However, in light of the latest measurements of J. Joss and R. List [147] and also those of Joss [148], the extension of formula (4.27) to melting ice particles is somewhat dubious. Nevertheless, D. Atlas [149] notes the usefulness of estimates and theoretical results obtained with the aid of relation (4.27).

Assuming in expression (4.27) that $\rho_{mix} \approx \rho_w \approx \rho_i \approx 1$, and denoting $\frac{M_w}{M_{mix}}$ by δ_w, we obtain

$$\frac{\varepsilon_{mix} - 1}{\varepsilon_{mix} + 2} = \frac{\varepsilon_w - 1}{\varepsilon_w + 2}\delta_w + \frac{\varepsilon_i - 1}{\varepsilon_i + 2}(1 - \delta_w), \qquad (4.29)$$

where δ_w is the relative percentage (by weight) of water in the mixture.

On the basis of formulas (4.29), (4.14), (4.16), (4.23), (4.24) and dielectric constants of ice, n and κ of a homogeneous mixture of water and ice at $t° = 0°C$ (Figures 4.20, 4.21) and $t = -10°C$ (Table 4.35) were calculated [150].

TABLE 4.35. VALUES OF n AND κ OF A HOMOGENEOUS MIXTURE OF SUPERCOOLED WATER AND ICE FOR $t = -10°C$ AND DIFFERENT δ_w.

δ_w	$\lambda = 1{,}24$ cm		$\lambda = 0{,}62$ cm		δ_w	$\lambda = 1{,}24$ cm		$\lambda = 0{,}62$ cm	
	n	$\varkappa$	n	$\varkappa$		n	$\varkappa$	n	$\varkappa$
0,0	1,78	$7{,}9 \cdot 10^{-4}$	1,78	$7{,}9 \cdot 10^{-4}$	0,6	2,95	0,41	—	—
0,1	1,92	0,030	—	—	0,7	3,28	0,63	—	—
0,2	2,07	0,067	2,02	0,11	0,8	3,66	0,99	2,97	1,02
0,3	2,24	0,12	—	—	0,9	4,03	1,60	—	—
0,4	2,44	0,18	—	—	1,0	4,15	2,55	3,10	1,77
0,5	2,68	0,28	2,47	0,39					

Note: Commas indicate decimal points.

It is evident from Figure 4.20 that the refractive index of the homogeneous mixture of water and ice at $\lambda > 2$ cm is practically independent from wavelength. There is an indefinite maximum of the function $n = f(\lambda)$ for each δ_w, and as δ_w increases, this maximum shifts toward longer wavelengths. At $\lambda < 2$ cm, a marked dependence of the refractive index on wavelength is observed, especially in the millimeter portion of the spectrum[76]. /171

[76] Under the assumption that the dielectric constants of ice at a given temperature are constant over the entire range of λ from 0.1 to 20 cm.

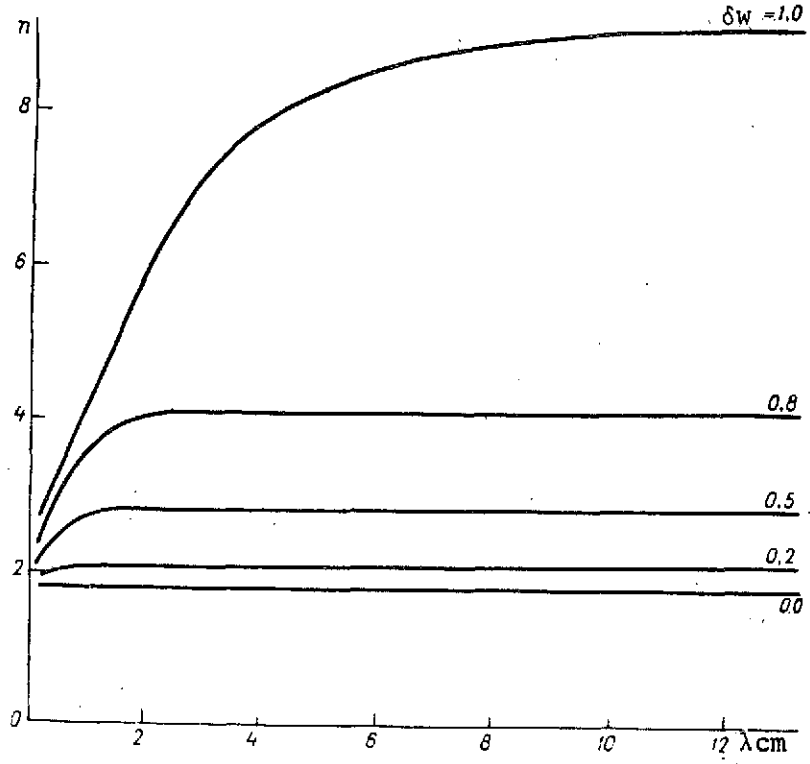

Figure 4.20. n of Homogeneous Water-Ice Mixture For Different Relative Values (δ_w) of the Percentage of Water at t = 0°C.

It is evident from Figure 4.21 that the absorption index κ of a homogeneous water-ice mixture depends substantially on wavelength and water content of the mixture. A particularly marked dependence of κ on λ is observed in the millimeter range, and of κ on δ_w, when $\delta_w > 0.5$. Comparison of Figures 4.20 and 4.21 with the data of Table 4.34 shows that the dependence of n and κ of the homogeneous ice-water mixture on temperature t°C is not very distinct.

Other relations for calculating mixtures of two-phase substances also exist. Thus, if a mixture consists of two finely dispersed, thoroughly mixed phases, /172 the dielectric constant of the mixture is calculated from Lichtenecker's formula [151, 152]

$$\ln\varepsilon_{mix} = x_1 \ln \varepsilon_1 + (1 - \varepsilon_1)\ln \varepsilon_2, \tag{4.30}$$

where x_1, x_2 are the volume concentrations of the first and second substance in the mixture.

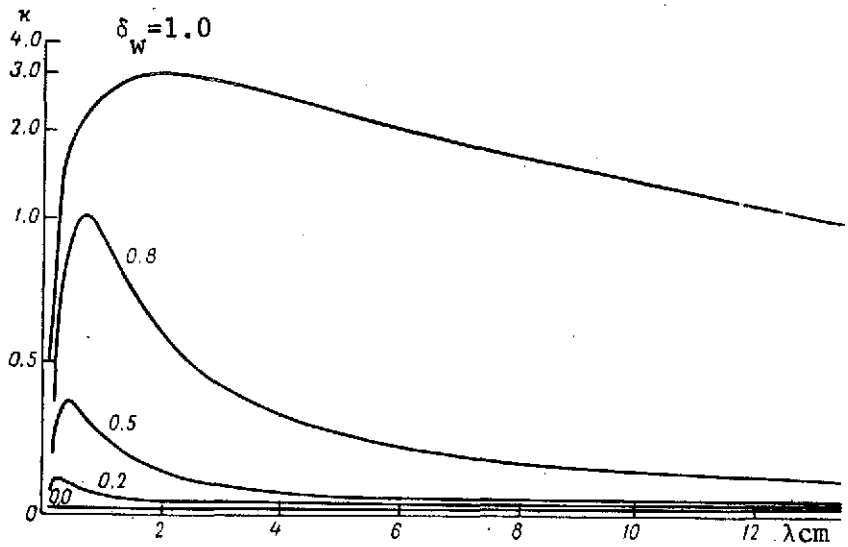

Figure 4.21. Variation of κ of Homogeneous Water-Ice Mixture with δ_w at t = 0°C.

For the case of a static two-component mixture in which the particles are arranged at random, V. I. Odelevskiy [151, 152] proposed the formula:

$$\varepsilon_{mix} = A + \sqrt{A^2 + \frac{\varepsilon_1 \varepsilon_2}{2}}, \tag{4.31}$$

where

$$A = \frac{(3x_1 - 1)\,\varepsilon_1 + (3x_2 - 1)\,\varepsilon_2}{4}.$$

If, however, a two-component mixture constitutes a matrix system whose first component uniformly surrounds the elongated inclusions of the second component distributed through it, then according to Odelevskiy ε is found from the formula

$$\varepsilon_{mix} = \varepsilon_1 \left(1 + \frac{x_2}{\frac{1 - x_2}{3} + \frac{x_2}{\varepsilon_2 - \varepsilon_1}}\right) \tag{4.32}$$

when $x_2 \neq 1$.

In the presence of a low concentration C of the second substance in the first, the following relation is proposed in [153]: /173

$$\varepsilon_{mix} = \varepsilon_1 + c\,\frac{3(\varepsilon_2 - \varepsilon_1)\,\varepsilon_1}{\varepsilon_2 + 2\varepsilon_1}. \tag{4.32a}$$

We will also recall the relations used in [11] to calculate the dielectric constant of seawater, treated as a homogeneous mixture of water and its solutes. Analysis of individual values of the radar cross-section, calculated on the basis of dielectric constants ε_{mix} from formulas (4.30)-(4.32a) and from relations of § 1.4 taken from [11], showed that they were in worse agreement with

the experimental values than with those determined from formula (4.29). However, detailed experimental studies of the homogeneous water-ice mixture over a wide range of λ are necessary in order to solve the problem of the best approximation of ε_{mix}.

We will use expression (4.28) for $u = 2$ to calculate ε of ice and snow of different densities, treating them as a homogeneous mixture of ice and air. In this case, equation (4.38) becomes (4.27) if in the latter M_w, ρ_w and ε_w are taken to mean the mass, density and dielectric constant of air (instead of water) respectively. If in addition we assume that $M_w \approx 0$ and $\rho_i \approx 1$ g/cm^3, $M_{mix} = M_i$, expression (4.27) will take the form

$$\frac{\varepsilon_{mix} - 1}{\varepsilon_{mix} + 2} = \frac{\varepsilon_i - 1}{\varepsilon_i + 2} \rho_{mix} \qquad (4.33)$$

D. Atlas [137] tested expression (4.33) experimentally and found that it satisfactorily described the measurement results (to within 7%).

Table 4.36 lists ε_{mix} values representing ε_i of different densities, calculated from formula (4.33) on the basis of refractive and absorption indices of ice with a density of 0.916 g/cm^3 (Table 4.31). Comparison of the data of Tables 4.36 and 4.31 shows them to be in completely satisfactory agreement.

TABLE 4.36. VALUES OF n AND κ OF ICE, CALCULATED FOR DIFFERENT DENSITIES ρ AND TEMPERATURES t.

ρ g/cm^3	n	$\kappa \cdot 10^4$ at t° C			
		0	−6	−12	−18
0,76	1,55	14,57	6,65	4,50	3,86
0,46	1,31	7,43	3,39	2,29	1,97
0,34	1,22	5,21	2,38	1,61	1,38

At the same time, if the dielectric constant of wet ice of 0.38 g/cm^3 density is calculated from formula (4.29) (Table 4.37) and compared with the data of Table 4.32, one can observe a discrepancy in the absorption indices κ of a wet snow cover and wet ice of the same density. All this obviously applies if expression (4.29) correctly reflects the dielectric properties of wet ice. /17

Treating snow as ice with 10^{-2}–10^{-3} g/cm^3 density, we will use formula (4.33) to calculate the dielectric constant of a snowflake[77] (Table 4.38).

[77]Assuming that a wet snowflake is dielectrically equivalent to a wet snow cover, its ε as a function of the water content may be calculated [154-156] from formula (4.29) by replacing ε_i in the latter by ε of snow according to Table 4.38.

TABLE 4.37. CALCULATED VALUES OF n (IN NUMERATOR) AND $\kappa \cdot 10^4$ (IN DENOMINATOR) OF WET ICE WITH 0.38 g/cm^3 DENSITY AS FUNCTIONS OF WAVELENGTH λ AND PERCENTAGE p OF WATER AT 0°C.

λcm	p%			
	0,4	0,8	1,2	1,6
0,1	1,31 / 12,6	1,32 / 20,0	1,32 / 27,5	1,32 / 35,0
0,4	1,31 / 17,6	1,32 / 30,1	1,32 / 42,6	1,33 / 55,2
0,86	1,32 / 13,4	1,32 / 21,7	1,33 / 30,0	1,33 / 38,3
3,2	1,32 / 7,7	1,32 / 10,2	1,33 / 12,7	1,33 / 15,2
11,0	1,32 / 5,9	1,32 / 6,7	1,33 / 7,4	1,33 / 8,1
17,0	1,32 / 5,7	1,32 / 6,1	1,33 / 6,6	1,33 / 7,1

TABLE 4.38. VALUES OF n (IN NUMERATOR) AND $\kappa \cdot 10^4$ (IN DENOMINATOR) OF ICE WITH DIFFERENT DENSITIES ρ AND AT TEMPERATURES t.

ρ g/cm^3	t° C				
	0	−6	−10	−12	−18
0,03	1,01895 / 0,416	1,01895 / 0,190	1,01895 / 0,143	1,01895 / 0,129	1,01895 / 0,110
0,01	1,00630 / 0,138	1,00630 / 0,0631	1,00630 / 0,0474	1,00630 / 0,0426	1,00630 / 0,0356
0,005	1,00315 / 0,0690	1,00315 / 0,0135	1,00315 / 0,0237	1,00315 / 0,0213	1,00315 / 0,0182

Note: commas indicate decimal points in above tables

The data of Table 4.38 indicate a weak dependence of the absorption index κ of snow on temperature at $t < -6°C$ and a complete independence from t of its refractive index.[78]

[78]Values of the real part of the dielectric constant and loss tangent of freshly precipitated snow are given in [157] for $t = -6°C$ and $\lambda = 3$ cm, which in terms of N gives $1.12\text{-}2.36 \cdot 10^{-4}$ i. Comparing this value of N with the data of Tables 4.31, 4.36, we find that it corresponds to snow with ~0.3-0.4 g/cm^3 density.

CHAPTER 5

SCATTERING AND ATTENUATION OF MICRORADIOWAVES BY ONE HYDROMETEORIC PARTICLE

§ 5.1. Physical Structure and Parameters of a Hydrometeoric Particle.

Hailstone. It is well-known [158, 159] that the most complex representative of hydrometeors from the standpoint of physical structure and phase state is a hailstone.

Measurements of hailstone density immediately after precipitation showed [158, 160][79] that on the average, for hailstones 3-18 mm in diameter, it ranges from 0.5-0.9 g/m^3, and for fine hail and graupel amounts to approximately 0.3 g/cm^3.

Frequently, hailstones (particularly the largest ones) consist of 2-20 nonconcentric layers of ice of different crystal structures and densities (Figure 5.1, Table 5.1).[80]

TABLE 5.1. STRUCTURE OF HAILSTONES FALLEN IN DENVER (USA)

Diameter (mm)	No. of Hailstones	Type of Core	Number of Layers								
			3	4	5	6	7	8	9	10	11
21	9	Dull 9	2	0	2	0	3	0	1	0	1
24	10	Dull 5	2	2	3	1	0	1	1	0	0
		Transparent 2									
		Mixed 2									
27	6	Dull 5	0	1	3	0	1	1	0	0	0
		Transparent 1	0	0	0	1	1	0	0	0	0
30	2	Dull 1	4	3	8	2	5	2	2	0	1
Total	27										

[79] See also [313-317].

[80] See also [318-321], the figure on p. 3 and [314].

The conditions determining the formation of a given ice crystal structure in a hailstone have been discussed in many theoretical and experimental papers [161-173 and others]. Thus, according to [171-173], the conditions of the crystallization process and the structure of growing ice are determined by the critical value h_{cr} of the parameter h_g: /163

$$h_g = \frac{\rho_w \lambda_w (t_0 - t)}{\rho_i L v q \bar{E}} \left[1 - \frac{2{,}96}{t_0 - t}\left(\frac{v q \bar{E}}{\rho_w}\right)^{0{,}592}\right], \qquad (5.1)$$

where ρ_w, ρ_i are the densities of water and growing ice, respectively; λ_w is the molar thermoconductivity coefficient of water; t_0, t are the temperatures of stable phase equilibrium and supercooled droplets, respectively; L is the specific heat of fusion of ice; v is the velocity of the flow of the water aerosol relative to the hailstone[81]; q is the water content; $\bar{E}$ is the average integral coefficient of capture of the droplets by the hailstone.

The supercritical (dry) regime of hailstone growth is achieved when $h_g > h_{cr}$. In this case, the liquid film rapidly disappears, and on reaching the hailstone, the supercooled droplets will crystallize without forming a continuous and stable film. The ice thus formed is of comparitively low density ($\rho_i < 0.92$ g/cm^3), dull, and inhomogeneous in structure, and the surface of the hailstone remains virtually dry.

The subscritical ("wet") growth regime is achieved when $h_g < h_{cr}$. In this case, the crystallization proceeds under a stable film of water with the formation of a very dense ($\rho_i \approx 0.9$ g/cm^3) transparent ice of homogeneous structure. The thickness of the liquid film of water on the surface of such wet hailstones may be calculated from the formula

$$h_{wet} = \left[\frac{5{,}1 \cdot 10^6 \rho_i L q \bar{E} \sigma \mu_i^3 \mathrm{Re}^{0{,}6}}{\alpha_0^3 c_w \rho_w^3 a v^5 (t_0 - t)\left[1 - \frac{2{,}96}{t_0 - t}\left(\frac{v q \bar{E}}{\rho_w}\right)^{0{,}592}\right]}\right]^{\frac{1}{4}}, \qquad (5.2)$$

where σ is the specific surface tension of water; μ_d is the dynamic viscosity of water; R is the Reynolds number for the airflow around the object; α_0 is the relative turbulence intensity in the liquid film, equal to the ratio of the mean

[81]For a hailstone growing in a cloud, v is equal to the difference of the fall velocity of the hailstone v_h and cloud droplets v_d. In most cases $v_h \gg v_d$, so that $v \approx v_h$.

square fluctuation of the velocity to the mean velocity of the water in the film; c_w is the specific heat capacity of water; ρ_a is the air density.

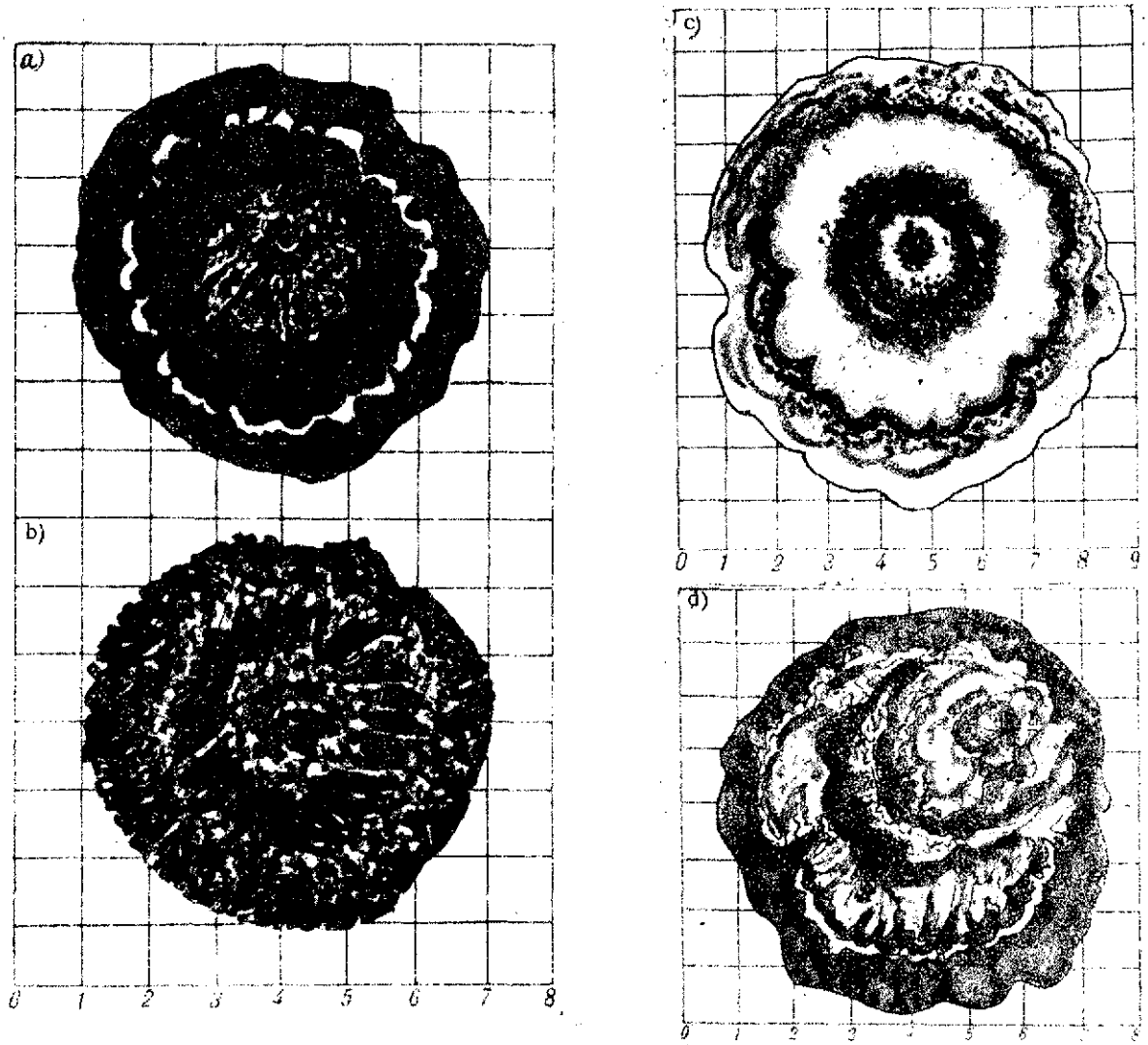

/178

/179

Figure 5.1. Central Cross-section of Layered Hailstone.
a, After [161]; b, After [162]; c, After [163]; d, After [164].

In order to determine the magnitude of parameter h_{cr} at which one structure of growing ice changes to another, observations were made [172] on the icing of objects in a flow of supercooled water droplets. Results of the experiments /180 are presented in Figure 5.2. The figure shows that when $h_{cr} = 0.1$ cm, there is a fairly distinct boundary separating two types of ice: transparent (when $h_g < 0.1$ cm) and dull ($h_g > 0.1$ cm) ice. In order to determine the dependence of the structure of ice on temperature t, liquid water content $q\bar{E}$ and flow velocity of the supercooled droplets, the experimental conditions were varied [175] so

that several layers of ice of different structures would successively form on the object.[82]. A model of such an artificially grown layered boundary is shown in Figure 5.3.

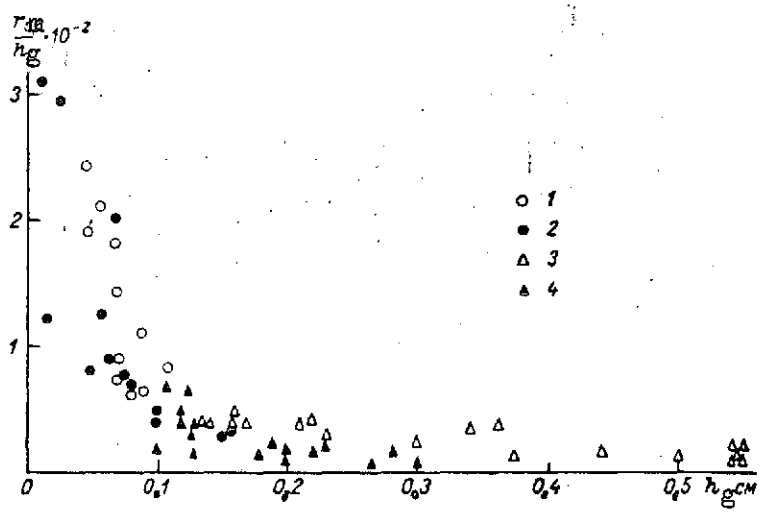

Figure 5.2. Structure of Ice During Icing For Different Values of h_g and Mean Radius of Aerosol Droplets r_m. 1, 3, Laboratory experiments (points with $h_g \geqslant 0.6$ cm were placed on the ordinate h_g = 0.6 cm); 2,4, Observations in clouds after [174]; 1,2, Homogeneous transparent ice; 3,4, Inhomogeneous dull ice.

Layers 1 and 3 were obtained at h_g = 0.07 cm < h_{cr}, t = -6°C, v = 33 m/s, $q\overline{E}$ = 0.5 g/m^3; layer 2 - at h_g = 0.22 cm > h_{cr}, v = 11 m/s, t = -6°C, $q\overline{E}$ = 0.5 g/m^3.

Let us also note that the magnitude of parameter h_g determines not only the structure, but also the density of growing ice. This is clearly illustrated in Figure 5.4, taken from [173]. The analytical form of the function $\rho_i = f(h_g)$ is completely satisfactorily approximated by the formula

$$\rho_i = \rho_0 \left[1 - \exp\left(-\frac{a}{h_g}\right)\right], \tag{5.3}$$

where ρ_0 is the limiting density of ice (0.92 g/cm^3), a = 0.4 cm.

[82] As in natural hailstones, shown in Figure 5.1.

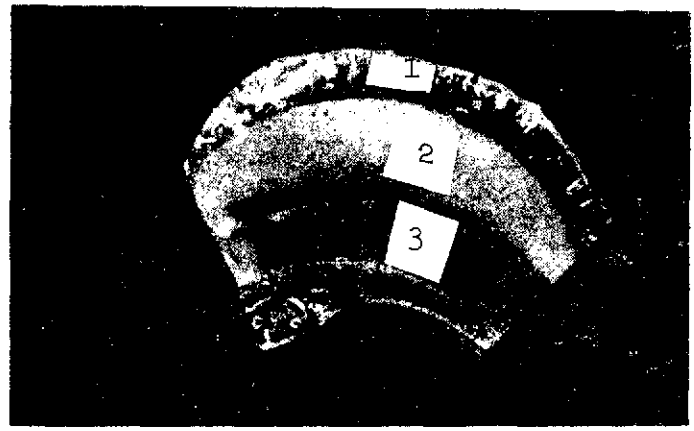

Figure 5.3. Model of Artificially Grown Layered Hailstone After [175].
1,3, Transparent ice; 2, Dull ice.

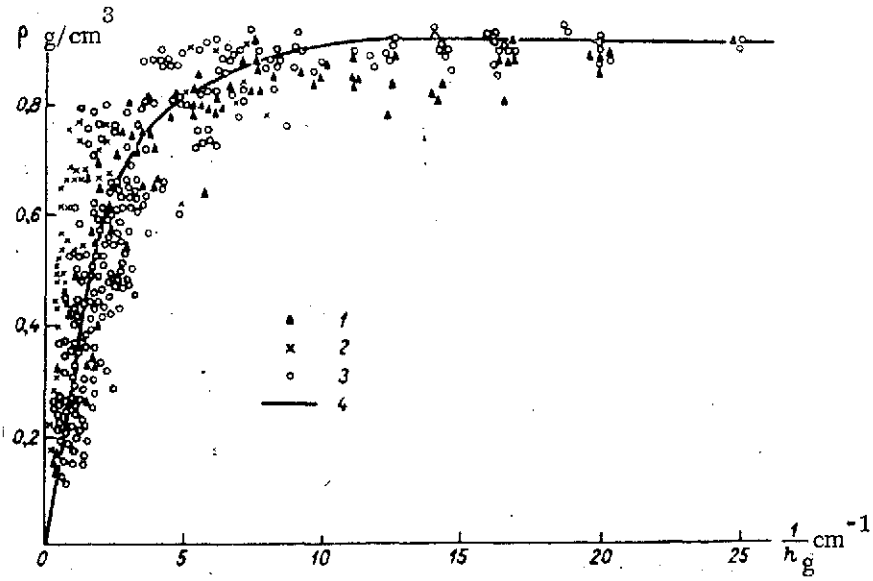

Figure 5.4. Ice Density Versus h_g.
1, Laboratory experiment; 2, Experiments under natural conditions; 3, Data of [170]; 4, Calculation according to formula (5.3).

The results obtained were used in a study of the formation of a layered hailstone in thick cumulus clouds. As follows from [176, 177, 179, 180], strong ascending motions with velocities of 10-20 m/s or greater are observed for fairly long periods of time in such clouds. Hail nuclei formed as a result of freezing of the largest cloud droplets [180] rise upward in such a flow, During their motion, they capture finer cloud droplets and thus grow in size. The /182

ascent continues until the hailstone reaches the level of the zero isotherm. Whether such hailstones eventually fall to earth, or whether they are converted into fine graupel and rain depends in turn on the set of conditions determining the process of melting of the hail during its fall in the warm part of the cloud and the subcloud layer of air.

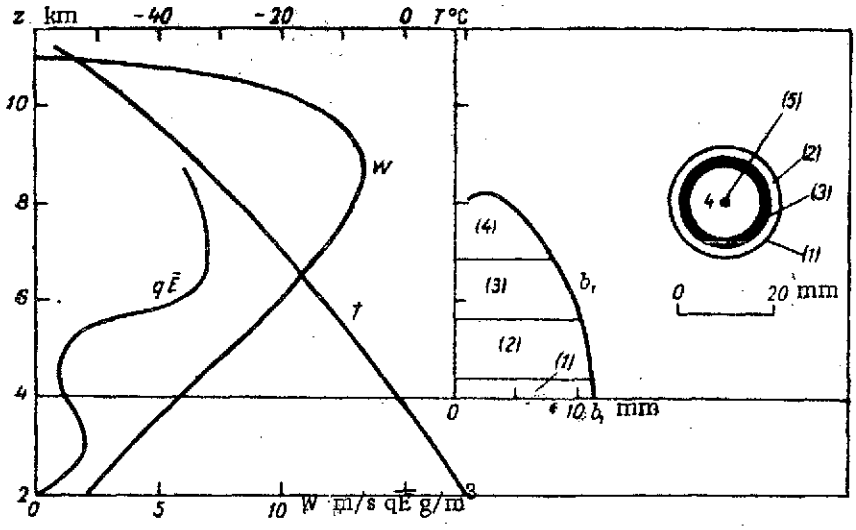

Figure 5.5. Example of Calculation of a Multilayered Hailstone Formed In A Cumulus Cloud After [180, 181].

The formation of the layered structure of hailstones formed in this manner takes place if the combination of cloud parameters (T, q, $\bar{E}$, ρ_a) and hailstone parameters ($v = f(r, \rho_i)$) is such that as the hailstone moves through the supercooled part of the cloud, the value of h_g will go several times through the critical value h_{cr} = 0.1 cm.

A specific example of calculation of a multilayered hailstone for typical parameters of a cumulus cloud is shown in Figure 5.5.

The hailstone of radius b_1 considered in Figure 5.5 was formed at a height /18
of 8 km from a large frozen drop (transparent nucleus (5)). This was followed by growth on the hailstone of dull ice (layer (4)), transparent ice (layer (3)), dull ice again (layer (2)) and thinnest outer layer (1) of transparent ice. Such a hailstone is shown schematically in Figure 5.5 on the right. Here t is the cloud temperature, W is the velocity of ascending motions, $q\bar{E}$ is the effective liquid water content in the cumulus cloud, and z is the height.

Above, we discussed the structure of growing hailstones in the course of their motion in the supercooled part of a cumulus cloud and showed that depending on the cloud parameters, the hailstone surface may be either dry or wet.

Let us consider a melting hailstone. When hailstones fall through cloud and subcloud layers with a positive temperature, their surface heats up and thaws. The water formed becomes distributed over the hailstone surface either in the form of a film of water [149] or in the form of a homogeneous mixture of water and ice (loose ice). Since the inner structure of thawing hailstones is formed in the course of their growth in the supercooled part of the cloud, the new elements in this case in comparison with the case already discussed will be the structure and dimensions of the outer shell of the hailstone.

Published data on this question are quite scarce[83], but even these are usually very approximate and qualitative in character. Thus, while comparing the results of measurements with calculations of radar cross-sections after Mie, D. Atlas [149] found that the maximum thickness of the water film on the hailstone was 0.01 cm; having performed high-speed filming of an artificial spherical particle 3 cm in diameter during its melting in a wind tunnel at blowing speeds of 15-20 m/s, A. Gvelesiani [182] obtained a thickness of the water shell at its equator of 1.7-1.5 mm.

In addition to hailstones consisting of alternating ice layers of different densities, either coated with a film of water or completely homogeneous, hollow hailstones have also been described in the literature [183]. The diameter of the largest ones reached almost 1 cm. Air is not the only foreign substance in a hailstone. Thus, the book [184] mentions hailstones whose cores consist of sand, dust, plant particles, stones, asphalt gravel, etc., as well as hailstones consisting of snow grains coated with an ice shell or of glassy transparent ice drops.

The hailstone is more or less spherical in shape. For example, according to the data of 1,000 observations [158] of hailstones fallen in the course of a number of years in France, hailstones of a particular shape constitute less than 10% of the total number.

The falling velocities of hailstones of different densities are shown in Figure 5.6.

Snow Crystal. Many investigators have collected and photographed snow crystals and catalogued them. Particularly well-known in this area has become the book of W. Bentley and W. Humphreys [185], which contains over 3,000 photomicrographs. /184

However, as was noted by B. Mason [159], this book showed a tendency to include only crystals of the most regular and well-defined shape. Actually, an extremely great variety of the shapes of snow crystals is observed [186 and others]. The following shapes are most frequently distinguished (Figure 5.7): needles, plane, and spatial dendrites, crystals with nonfrozen droplets, etc.

---

[83] See for example the survey in [149] and [182].

The largest linear dimensions are usually exhibited by spatial dendrites. Their diameter reaches 8-10 mm, and the shape is characterized by a marked branchiness. The diameters of plane dendrites do not exceed 4-5 mm. Under certain conditions, coalescence of snow crystals with drops takes place. At sufficiently low temperature, fine droplets freeze upon striking the surface of the snow crystals, almost retaining their shape. The snow crystals thus formed are rimed. A characteristic modification of heavily rimed crystals is grain. Grain is spherical or conical in shape. Its diameter ranges from fractions of a millimeter to 10-15 mm.

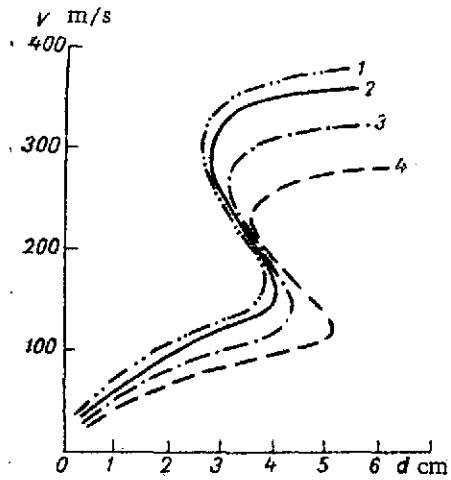

Figure 5.6. Falling Velocity V of Hailstones of Different Densities ρ After [159].

1, $\rho = 0.915$ g/cm^3; 2, $\rho = 0.800$ g/cm^3; 3, $\rho = 0.600$ g/cm^3; 4, $\rho = 0.400$ g/cm^3.

Coalescence of snow crystals leads to the formation of flakes. They may reach 10 mm or more in size. Flakes are formed most frequently at an air temperature close to 0°C. However, cases of precipitation of flakes have also been observed at lower temperatures, for example, at -20 to -30°C.

The density of snow crystals and flakes is relatively low and amounts [187-196, 137, 184] to about 10^{-3}-10^{-2} g/cm^3, in contrast to snow pellets, whose density is as high as 0.1-0.2 g/cm^3.

In [193, 196], a dependence of the density of snow crystals (ρ g/cm^3) on their diameter (d_{cm}) was found to be

$$\rho = \beta d^{-\alpha}, \tag{5.4}$$

where β and α are parameters which we found in [197] by approximating the experimental data of [193, 198]:

$$\beta = 0.012; \quad \alpha = 0.73 \tag{5.5}$$

Empirical dependences of the mass of snow crystals (mg) of different shapes /18. on their linear dimension (mm) are given in Table 5.2. The falling velocities of snow crystals of different types and diameters are listed in Figures 5.8-5.10.

A drop of water is a mechanically stable particle, since the surface forces acting at its boundary continually strive to minimize its surface. If, however, the surface tension forces are predominant, the shape of the drop corresponds to the minimum ratio of the surface area to the volume, i.e., it is spherical. This is observed [159] in the case of cloud drops, drizzle and fine rain drops (with a diameter under 3-4 mm).

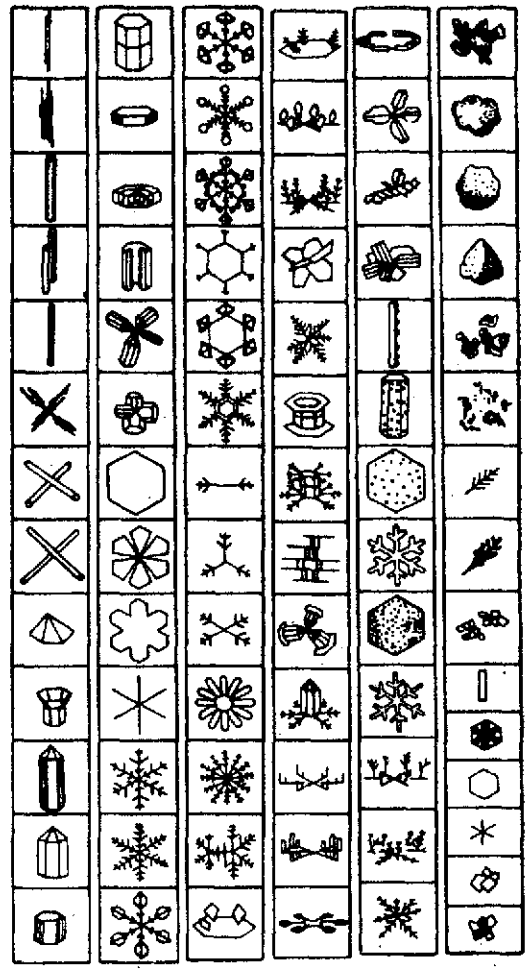

Figure 5.7. Meteorological Classification Of Snow Crystals After [186].

TABLE 5.2. DEPENDENCE OF THE MASS OF SNOW CRYSTALS ON THEIR LINEAR DIMENSIONS d AFTER [159]

Crystals	Formulas
Pellets	$m = 0{,}065d_2^3$
Rimed plates and star-like dendrites	$m = 0{,}077d$
Snowdust and spatial dendrites	$m = 0{,}010d^2$
Plane dendrites	$m = 0{,}0038d^2$
Needles	$m = 0{,}0029d$

Commas indicate decimal points.

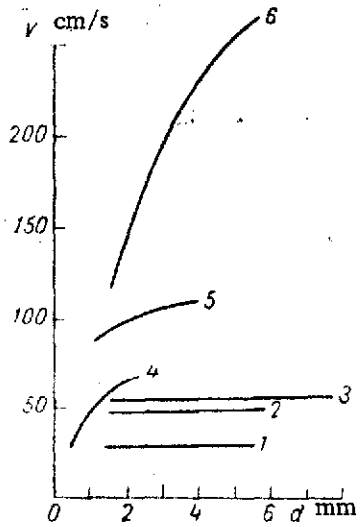

Figure 5.8. Falling Velocities V of Snow Crystals vs. Their Linear Dimensions d After [159].
1, Plane dendrites; 2, Snow powder; 3, Spatial dendrites; 4, Needles 5, Crystals with frozen-on droplets; 6, Pellets.

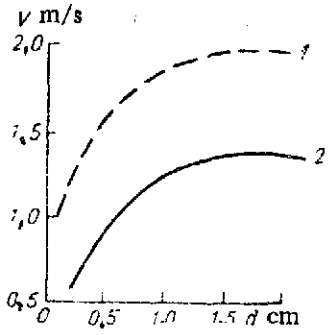

Figure 5.9. Falling Velocities V of Rimed Snow Crystals and Fine Rimed Snowflakes vs. Their Linear Dimensions d After [159].

1, Snowflakes; 2, Simple snow crystals.

However, when in addition to the surface forces, other commensurate forces due to various external factors are acting, the total energy minimum may become incompatible with the spherical shape of the drop. The literature contains many pictures from high-speed photography showing that large water drops falling at a steady velocity have a substantially flattened lower surface and a smooth round upper surface (Figure 5.11). /1

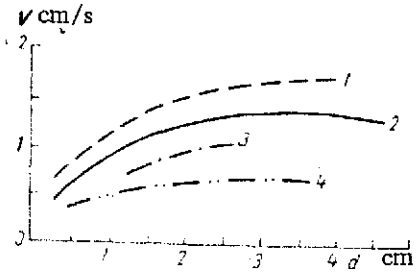

Figure 5.10. Falling Velocities V of Rimed and Nonrimed Snowflakes vs. Their Linear Dimensions d After [159].

Rimed snowflakes: 1, Vertically elongated, 2, Horizontally elongated; nonrimed snowflakes: 3, Vertically elongated, 4, Horizontally elongated.

These photographs also show that during their fall, large drops undergo [199] oscillatory motions along their vertically oriented axis. At the start of the fall, the drop flattens, and the flattening continues until the vertical dimension of the drop amounts to about 1/4 of its horizontal dimension. The drop then returns to its original shape and again becomes round.

The steady falling velocities V in still air of a single water drop of diameter d at temperature t = 20°C, p = 1,000 mb and t = 0°C, p = 900 mb are shown in Tables 5.3 and 5.4, respectively.

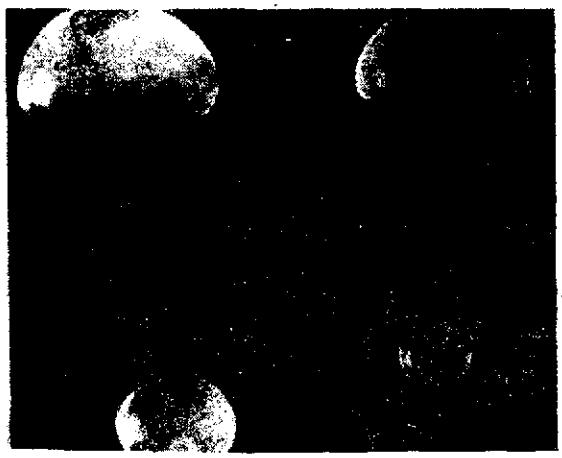

Figure 5.11. Large Water Drops Falling At a Steady Velocity After [159]. The equivalent diameter of the spherical particle and the measured falling velocities are equal: 6.5 mm and 8.9 m/s; 6.0 mm and 8.8 m/s; 4.8 mm and 8.3 m/s; 2.8 mm and 6.8 m/s.

In the free atmosphere, v increase somewhat because of its lower density. /188

In studying the fall of drops from great heights, it is necessary to consider the dependence of the falling velocity on the height. The corresponding numerical data and curves may be found in [204].

As was shown by V. G. Khorguani [205], the falling velocity v_s of a collection of particles differs substantially from v of a single particle. Thus, based

TABLE 5.3. FALLING VELOCITY OF DROP AT p = 1,000 mb AND t = 20°C AFTER [200-202].

d cm	v cm/s	d cm	v cm/s	d cm	v cm/s
0,004	5	0,20	649	0,44	898
0,01	27	0,24	727	0,45	900
0,02	72	0,25	741	0,48	907
0,04	162	0,28	782	0,50	909
0,05	206	0,30	806	0,52	912
0,08	327	0,32	826	0,55	913
0,10	403	0,35	853	0,60	914
0,12	464	0,36	860	0,65	914
0,15	540	0,40	883	0,70	914
0,16	565				

TABLE 5.4. FALLING VELOCITY OF DROP AT p = 900 mb AND t = 0°C AFTER 159].

d cm	v cm/s	d cm	v cm/s	d cm	v cm/s
0,002	1,3	0,06	260	0,18	645
0,003	3,0	0,07	302	0,20	690
0,004	5,4	0,08	344	0,24	769
0,006	11,3	0,09	386	0,28	825
0,008	18,3	0,10	426	0,32	870
0,01	26,5	0,11	462	0,40	925
0,02	76	0,12	493	0,48	955
0,03	125	0,14	551	0,56	970
0,04	172	0,16	601	0,60	976
0,05	217				

Note: Commas indicate decimal points.

on results of some 200 laboratory measurements [205], the velocity of a system of particles of equal size is on the whole greater than the velocity of a single particle. In particular, if the initial distance between the particle centers is less than 10 diameters, the velocity v_s is 2.5-3 times as high as v. Other things being equal, as the Reynolds number increases, the velocity of the collection of particles decreases. For example, when N = 100 and $\frac{L}{d} = 3.18$ (N being the number of particles and L, the distance between the particle centers) for R = 0.0023 v_s is 3.2 times the velocity of a single particle and for R = 0.192, 1.71 times this velocity. Moreover, if the Reynolds number is constant, as the distance between the particles increases, the falling velocity of a collection of particles decreases.

Khorguani [205] also cites data showing that for the same distance between the particles, the velocity v_s of a collection consisting of a large number of particles is greater. For example, when $\frac{L}{d} = 3.18$, N = 100, $\frac{v_s}{v} = 3.20$, and when N = 25, $\frac{v_s}{v} = 2.20$.

These facts, which require further detailed investigations, must be considered in calculations of radar characteristics of hydrometeors.

§ 5.2. Effect of Dielectric Constants of a Hydrometeoric Particle On Its Radar Characteristics. /18.

As was noted in Chapter 4, values of dielectric constants of hydrometeors obtained by different authors are different.

A particularly marked difference in ε is observed for ice (Table 4.33) at λ = 1 to 10 cm. In addition, because of the major advantage involved, many experimental studies are usually made, not on atmospheric aerosol particles,

but on models that are dielectrically similar to them. For example, instead of ice of unit density at t = 0°C (N = 1.78-0.0024i) and λ = 1 to 10 cm, uses frequently made [206] of plexiglas (N = 1.61-0.0025i) etc. [207].

If account is taken of the fact that the radar characteristics considered are of fluctuating character, it becomes evident that it is necessary to study the problem formulated in the title of this paragraph.

A computer was used to carry out calculations of the effective areas of radar σ_0 (1.276) and total σ_1 (1.273) scattering, and also attenuation[84] σ_2 (1.274) for ice spheres at temperatures of 0 and -10°C. The dielectric constants were chosen from Table 4.33 after Dunsmuir and Lamb [131] and Cumming [136]. The calculations were performed in accordance with a procedure generally resembling the one described in [70, 208-213].

Results of the calculations of [214] are listed in Table 5.5, from which it is evident that the σ_0 values in the denominator are smaller than the σ_0 indicated in the numerator by not more than 10% and $\alpha = \frac{\pi d}{\lambda} \leqslant 30$ and amount to 20-65% when $100 \geqslant \alpha > 30$. Differences in σ_1 do not exceed 20% in the entire range of variation of α. As far as the attenuation is concerned, a marked difference in dielectric constants does not result in any substantial change of σ_2 for $\alpha \leqslant 100$.

It follows from the above that in a theoretical study of the radar scattering of radiowaves by large hailstones, particular attention should be given to the accuracy of the ε values chosen.

In a study of the errors introduced into scattering cross-sections by dielectrically equivalent models, D. Atlas et al., [206] calculated σ_0 for N equal to 1.60 and 1.61 and N = 1.61-0.0025 i (plexiglas) for α from 0.1-100. For $\alpha \leqslant 7$, the difference between σ_0 for the N considered is small, and when $7 < \alpha < 20$, the overall minimum is essentially the same, and the maximum increases in the order N = 1.61-0.0025 i; N = 1.60; N = 1.61.

It also follows from the above data that in the region $\alpha \geqslant 7$, the radar cross-section σ_0 for the plexiglas sphere is one order of magnitude greater than for a metal sphere of the same size. This is explained by the focusing action of the dielectric sphere: a major part of the incident energy is focused /191 on the reverse side of the sphere and is reflected from it in a narrower beam.

---

[84] With the coefficients defined by expressions (1.288).

TABLE 5.5. EFFECTIVE AREAS OF RADAR σ_0 AND TOTAL σ_1 SCATTERING AND ALSO ATTENUATION σ_2 OF A HAILSTONE WITH DIFFERENT DIELECTRIC CONSTANTS.

NOTE. THE NUMERATOR GIVES σ_0, σ_1, AND σ_2 OF HAILSTONES WITH ε TAKEN FROM [131], AND THE DENOMINATOR, WITH ε TAKEN FROM [136].

a	σ_0		σ_1		σ_2	
	0	−10° C	0	−10° C	0	−10° C
0,1	$\frac{7\cdot10^{-5}}{7\cdot10^{-5}}$	$\frac{7\cdot10^{-5}}{7\cdot10^{-5}}$	$\frac{5\cdot10^{-5}}{5\cdot10^{-5}}$	$\frac{5\cdot10^{-5}}{5\cdot10^{-5}}$	$\frac{22\cdot10^{-5}}{23\cdot10^{-5}}$	—
5	$\frac{13,22}{12,31}$	$\frac{13,78}{13,41}$	$\frac{2,15}{2,05}$	$\frac{2,21}{2,17}$	$\frac{2,21}{2,19}$	$\frac{2,22}{2,21}$
10	$\frac{10,94}{10,04}$	$\frac{11,46}{11,11}$	$\frac{2,34}{2,28}$	$\frac{2,87}{2,35}$	$\frac{2,39}{2,40}$	$\frac{2,89}{2,39}$
15	$\frac{11,04}{10,44}$	$\frac{11,00}{11,07}$	$\frac{2,49}{2,34}$	$\frac{2,65}{2,53}$	$\frac{2,53}{2,57}$	$\frac{2,71}{2,66}$
20	$\frac{27,02}{22,09}$	$\frac{30,18}{28,06}$	$\frac{2,23}{2,12}$	$\frac{2,29}{2,25}$	$\frac{2,32}{2,32}$	$\frac{2,32}{2,32}$
25	$\frac{24,78}{21,04}$	$\frac{27,38}{25,45}$	$\frac{1,93}{1,83}$	$\frac{2,00}{1,96}$	$\frac{2,05}{2,06}$	$\frac{2,05}{2,05}$
30	$\frac{50,13}{35,84}$	$\frac{61,42}{53,65}$	$\frac{2,02}{1,87}$	$\frac{2,13}{2,05}$	$\frac{2,17}{2,16}$	$\frac{2,17}{2,17}$
35	$\frac{43,76}{30,05}$	$\frac{53,91}{46,99}$	$\frac{2,17}{2,01}$	$\frac{2,28}{2,21}$	$\frac{2,32}{2,31}$	$\frac{2,32}{2,32}$
40	$\frac{35,13}{32,41}$	$\frac{42,87}{37,54}$	$\frac{2,01}{1,86}$	$\frac{2,11}{2,04}$	$\frac{2,17}{2,17}$	$\frac{2,16}{2,17}$
45	$\frac{73,01}{45,52}$	$\frac{98,07}{80,17}$	$\frac{1,92}{1,74}$	$\frac{2,07}{1,96}$	$\frac{2,13}{2,12}$	$\frac{2,14}{2,13}$
50	$\frac{49,87}{31,04}$	$\frac{64,89}{54,56}$	$\frac{1,91}{1,74}$	$\frac{2,04}{1,95}$	$\frac{2,09}{2,10}$	$\frac{2,09}{2,09}$
55	$\frac{45,67}{27,00}$	$\frac{61,74}{50,49}$	$\frac{1,95}{1,76}$	$\frac{2,10}{2,00}$	$\frac{2,17}{2,17}$	$\frac{2,16}{2,17}$
60	$\frac{73,28}{38,57}$	$\frac{106,74}{83,19}$	$\frac{1,96}{1,74}$	$\frac{2,12}{2,01}$	$\frac{2,19}{2,17}$	$\frac{2,19}{2,19}$
65	$\frac{45,60}{25,50}$	$\frac{63,27}{50,97}$	$\frac{1,83}{1,64}$	$\frac{1,97}{1,87}$	$\frac{2,05}{2,07}$	$\frac{2,04}{2,05}$
70	$\frac{50,66}{24,43}$	$\frac{74,50}{58,00}$	$\frac{1,82}{1,61}$	$\frac{2,00}{1,87}$	$\frac{2,02}{2,09}$	$\frac{2,09}{2,09}$
75	$\frac{55,10}{26,48}$	$\frac{82,84}{63,39}$	$\frac{1,88}{1,66}$	$\frac{2,06}{1,94}$	$\frac{2,14}{2,14}$	$\frac{2,14}{2,14}$

Note: Commas indicate decimal points.

TABLE 5.5 CONT'D

α	σ_0		σ_1		σ_2	
	0	−10° C	0	−10° C	0	−10° C
80	35,00 / 18,88	46,08 / 38,86	1,85 / 1,62	2,03 / 1,91	2,12 / 2,12	2,12 / 2,12
85	48,86 / 17,96	91,48 / 60,05	1,79 / 1,56	2,00 / 1,85	2,09 / 2,09	2,10 / 2,10
90	37,81 / 15,59	63,14 / 44,98	1,77 / 1,54	1,96 / 1,82	2,06 / 2,07	2,05 / 2,06
95	26,77 / 13,72	36,53 / 29,93	1,80 / 1,55	2,01 / 1,96	2,12 / 2,11	2,12 / 2,12
100	40,38 / 13,57	73,29 / 50,35	1,80 / 1,54	2,02 / 1,86	2,13 / 2,12	2,13 / 2,13

Note: Commas indicate decimal points.

Figure 5.12 shows curves of normalized cross-sections of plexiglas and ice spheres. When $\alpha > 20$, the curve for ice runs much higher than that for plexiglas, although the imaginary parts of the indices of ice and plexiglas practically coincide, while the real parts differ by not more than 6%.

At the same time, comparison of σ_0 data for N = 1.78-0.00055 i and N = 1.78-0.00079 i [216] shows that when the imaginary part of the refractive index changes by 30-50%, σ_0 change by not more than 10-20% in the range of $0.1 \leqslant \alpha \leqslant 100$.

The influence of variations of the real refractive index is manifested with particular clarity when $\alpha > 100$, as can be seen from Table 5.6, which gives calculated σ_0 values for N = 1.6 and N = 1.78. This is due to an increase in the focusing effect of the sphere as N increases.

TABLE 5.6. EFFECTIVE AREA OF RADAR SCATTERING σ_0 FOR N = 1.6 AND N = 1.78

N	α				
	200	400	600	800	1000
1,6	8,53	14,04	22,12	38,62	29,70
1,78	340,15	377,67	359,59	705,66	992,96

Note: Commas indicate decimal points.

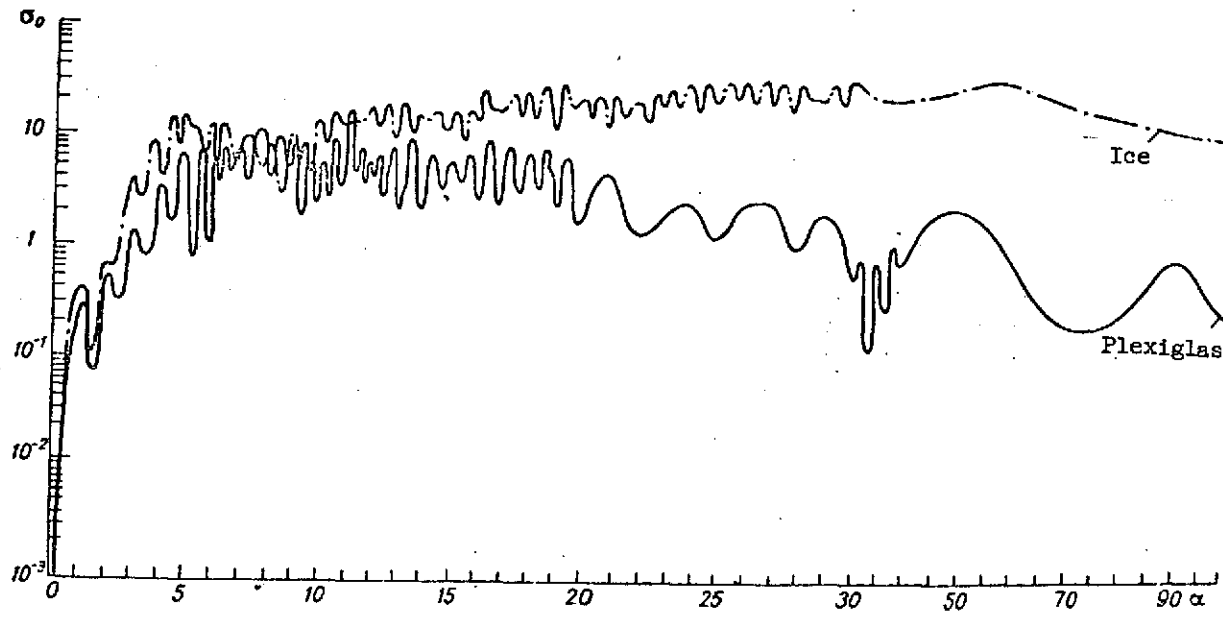

Figure 5.12. Effective Area of Radar Scattering σ_0 of Spheres With N = 1.61-0.0025 i (plexiglas) and N = 1.78-0.0024 i (ice at 0°C) After [215].

In [216], in order to study the influence of the imaginary part of the refractive index on the reflecting and attenuating properties of an ice sphere, σ_0, σ_1, and σ_2 were calculated for $N = 1.78\text{-}10^{-m}i$ over a side range of α values (from 0.01-5,000) and m = 0, 1, ..., 9, ∞. Results of the calculations are presented in Tables 5.7-5.9. Analysis of the values of radar cross-section σ_0 (Table 5.7) shows that if the absorption index κ = Im N is smaller than 10^{-4}, its variations have practically no effect on σ_0 over the entire range considered. For the indicated ($\kappa \leqslant 10^4$) imaginary parts of N as α increases, σ_0 also increases. Moreover, for $\alpha \geqslant 5$, σ_0 exceeds not only its asymptotic value, but also the asymptotic value corresponding to an ideally conducting sphere ($\sigma_0^{(id)} = 1$). /19

If, however, the magnitude of the imaginary part is appreciable, as the electromagnetic wave passes through the interior of the sphere in both directions, energy is lost, and the focusing action of the sphere will be insignificant. In that case, as α increases, σ_0, while fluctuating, increases slightly at first,

and reaches a maximum, then begins to decrease, approaching its limiting value σ_0^*. The limiting values of σ_0^* for $\alpha \to \infty$ are listed in Table 5.10.

It follows from a comparison of Tables 5.7 and 5.10 that when $m \geqslant 4$, as α increases over the entire range considered, σ_0 moves further and further away from its asymptotic value. When $m = 3$ and $\alpha > 400$, σ_0 begins to approach its limiting value, but even when $\alpha = 800$, σ_0 still exceeds the limiting value by a factor of 25 and reaches it only when $\alpha = 4{,}000$. If, however, $\kappa = 10^{-2}$, σ_0 reaches its limiting value when $\alpha = 400$, and in the case of $\kappa = 0.1$ to 1, when $\alpha \approx 10$.

Thus, as the imaginary part of the refractive index of the substance of the sphere increases, a decrease takes place in the maximum value and in the range of normalized radii of the sphere α at which σ_0 substantially exceeds its limiting value.

An examination of σ_1 (Table 5.8) and σ_2 (Table 5.9) shows that they are stable at small variations of the imaginary part of N and when $\alpha > 5$ to 10, differ very little from their limiting values σ_1^* (Table 5.10) and $\sigma_2^* = 2$.

In contrast to ice, the effective scattering and attenuation areas of water spheres depend considerably less on the variations of dielectric constants. To illustrate this statement, σ_0, σ_1, and σ_2 were calculated for water spheres with the dielectric constants given in the appendix and obtained by many authors.

Table 5.11 lists the results of such a calculation at $\lambda = 1$ mm. The numerator gives the σ_0, σ_1, and σ_2 values calculated by Ch.-M. Chu [70] at $t = 18°C$ (see Table 4.7), and the denominator, our calculations at $t = 20°C$ (the N values were taken from the appendix). Analysis of Table 5.11 and other such calculations shows that the error in σ_0, σ_1, and σ_2 values for water spheres are no greater, and as a rule, much smaller in the percentage ratio than the error of dielectric constants. This fact is also confirmed by comparative calculations of the scattering and attenuation cross-sections for water spheres in the submillimeter range[85] from N values calculated from Debye formulas (4.10), (4.14), (4.23), (4.24) (4.24) and experimental values (see Table 4.29). /198 /199

[85] It is shown in § 4.1 that in the submillimeter range, the Debye values N of water appreciably differ from experimental values.

TABLE 5.7. DEPENDENCE OF EFFECTIVE RADAR SCATTERING AREA σ_0 ON VARIATIONS OF THE ABSORPTION INDEX AT N = 1.78 - 10^{-m}i [Table Continued].

m	σ_0 at α					
	0,01	0,1	1	5	10	20
∞	7,040694·10⁻⁹	7,022653·10⁻⁵	0,393789	13,998175	11,666644	31,424563
9	7,040694·10⁻⁹	7,022653·10⁻⁵	0,393789	13,998174	11,666643	31,424558
8	7,040694·10⁻⁹	7,022653·10⁻⁵	0,393789	13,998167	11,666637	31,424518
7	7,040694·10⁻⁹	7,022653·10⁻⁵	0,393789	13,998097	11,666573	31,424118
6	7,040694·10⁻⁹	7,022653·10⁻⁵	0,393789	13,997401	11,665935	31,420120
5	7,040694·10⁻⁹	7,022653·10⁻⁵	0,393785	13,990437	11,659557	31,380156
4	7,040694·10⁻⁹	7,022653·10⁻⁵	0,393749	13,921093	11,595887	30,982592
3	7,040702·10⁻⁹	7,022661·10⁻⁵	0,393389	13,255310	10,970410	27,214968
2	7,041872·10⁻⁹	7,023801·10⁻⁵	0,389894	8,559040	6,020235	6,581344
1	7,159385·10⁻⁹	7,140899·10⁻⁵	0,364107	0,363425	0,074141	0,074281
0	1,866806·10⁻⁸	1,869309·10⁻⁴	0,661979	1,360824	0,183873	0,181626

m	σ_0 at α					
	50	100	200	400	600	800
∞	71,466744	101,40058	340,15653	377,66503	359,58971	705,65841
9	71,466720	101,40049	340,15588	377,66399	359,58874	705,65298
8	71,466503	101,39965	340,15002	377,65360	359,57995	705,60404
7	71,464333	101,39124	340,09138	377,55070	359,49210	705,11491
6	71,442636	101,30713	339,50558	376,52297	358,61359	700,25313
5	71,226001	100,47038	333,70299	366,37815	349,83193	654,48390
4	69,091988	92,517162	281,06330	280,20713	266,34879	374,16221
3	50,739725	42,114354	60,099522	22,632266	8,387565	2,047032
2	1,976196	0,110814	0,080940	0,078741	0,078735	0,078735
1	0,079938	0,079916	—	—	—	--
0	0,187972	0,184111	—	—	—	—

Note: Commas indicate decimal points.

TABLE 5.7 CONT'D

m	σ_0 at α					
	1000	1400	2000	2500	4000	5000
∞	992,96487	1231,8001	2310,9123	2247,4941	—	—
9	—	—	—	—	—	—
8	—	—	—	—	—	—
7	—	—	—	—	—	—
6	984,90805	1223,2301	2272,7463	2213,3820	3455,0708	5041,1393
5	915,71182	1104,8761	1959,9719	1888,8507	2673,2471	3535,5129
4	453,95785	432,0172	486,1043	393,4236	202,2790	138,0191
3	0,305879	0,221216	0,064263	0,080782	0,078733	0,078723
2	—	—	—	—	—	—
1	—	—	—	—	—	—
0	—	—	—	—	—	—

Note: Commas indicate decimal points

TABLE 5.8. DEPENDENCE OF EFFECTIVE TOTAL SCATTERING AREA σ_1 ON VARIATIONS OF THE ABSORPTION INDEX AT $N = 1.78 - 10^{-m}i$ [TABLE CONTINUED].

m	σ_1 at α		
	0,01	0,1	1
∞	4,6938347·10⁻⁹	4,7066127·10⁻⁵	0,50454619
9	4,6939347·10⁻⁹	4,7066127·10⁻⁵	0,50454619
8	4,6938347·10⁻⁹	4,7066127·10⁻⁵	0,50454618
7	4,6938352·10⁻⁹	4,7066127·10⁻⁵	0,50454615
6	4,6938349·10⁻⁹	4,7066127·10⁻⁵	0,50454585
5	4,6938348·10⁻⁹	4,7066127·10⁻⁵	0,50454284
4	4,6938348·10⁻⁹	4,7066128·10⁻⁵	0,50451268
3	4,6938129·10⁻⁹	4,7066184·10⁻⁵	0,50421207
2	4,6945828·10⁻⁹	4,7073822·10⁻⁵	0,50129708
1	4,1129218·10⁻⁹	4,7858265·10⁻⁵	0,48072059
0	1,2457884·10⁻⁸	1,2518949·10⁻⁴	0,79763200

/196

Note: Commas indicate decimal points.

TABLE 5.8 CONT'D

m	σ_1 at α				
	5	10	20	50	100
∞	2,2286991	2,3873253	2,3203220	2,0865701	2,1347510
9	2,2286990	2,3873252	2,3203219	2,0865699	2,1347507
8	2,2286983	2,3873248	2,3203210	2,0865683	2,1347470
7	2,2286908	2,3873207	2,3203124	2,0867718	2,1347096
6	2,2286165	2,3872796	2,3202267	2,0863873	2,1343359
5	2,2278729	2,3868681	2,3193699	2,0847443	2,1306091
4	2,2204738	2,3827617	2,3108420	2,0684838	2,0943070
3	2,1499746	2,3424878	2,2295121	1,9216791	1,8088196
2	1,6826263	2,0093241	1,7022562	1,3089814	1,1984944
1	1,0596653	1,2419140	1,2069719	1,1867928	1,1738744
0	1,3608240	1,3537214	1,33331391	1,3037924	1,2851813

m	σ_1 at α				
	200	400	600	800	1000
∞	2,0770611	2,0267223	2,0265029	2,0307315	2,0144871
9	2,0770603	2,0267209	2,0265029	2,0307314	—
8	2,0770532	2,0267075	2,0265031	2,0307304	—
7	2,0769816	2,0265735	2,0265046	2,0307207	—
6	2,0762662	2,0252351	2,0265204	2,0306259	2,0107676
5	2,0681543	2,0119811	2,0266728	2,0298130	1,9781525
4	2,0019509	1,8915074	2,0227130	2,0265866	1,7198765
3	1,5721955	1,3329758	2,0281932	1,1887332	1,1639663
2	1,1625542	1,1529761	2,0278301	1,1464185	—
1	—	—	—	—	—
0	—	—	—	—	—

m	σ_1 at α			
	1400	2000	2500	4000
∞	2,0179434	2,0129720	2,0125004	—
9	—	—	—	—
8	—	—	—	—
7	—	—	—	—
6	2,0126347	2,0055278	2,0032023	1,9924124
5	1,9672596	1,9420275	1,9249191	1,8728851
4	1,6382326	1,5304087	1,4613439	1,3187885
3	1,1471467	1,1409606	1,1394354	1,1374306
2	—	—	—	—
1	—	—	—	—
0	—	—	—	—

Note: Commas indicate decimal points.

TABLE 5.9. DEPENDENCE OF EFFECTIVE ATTENUATION SCATTERING CROSS-SECTIONS ON VARIATIONS OF THE OBSORPTION INDEX AT N = $= 1.78 - 10^{-m}i$ [Table Continued].

/197

m	σ_1 at α		
	0,01	0,1	1
∞	4,6937397·10⁻⁹	4,7066127·10⁻⁵	0,50454619
9	4,6943406·10⁻⁹	4,7066132·10⁻⁵	0,50454619
8	4,6988941·10⁻⁹	4,7000877·10⁻⁵	0,50454621
7	6,6261296·10⁻⁶	4,7033222·10⁻⁵	0,50454645
6	4,8432443·10⁻⁶	4,7253404·10⁻⁵	0,50454883
5	2,7422255·10⁻⁶	4,8680731·10⁻⁵	0,50457259
4	1,7715668·10⁻⁶	6,3057273·10⁻⁵	0,50481021
3	2,3082940·10⁻⁶	2,0831996·10⁻⁴	0,50718597
2	1,5619941·10⁻⁴	1,6599668·10⁻³	0,53089276
1	1,5979343·10⁻³	1,6162411·10⁻²	0,76252767
0	1,4218939·10⁻²	0,1438572	2,44995763

m	σ_2 at α				
	5	10	20	50	00
∞	2,2286991	2,3873253	2,3203220	2,0865701	2,1347511
9	2,2286991	2,3873253	2,3203220	2,0865701	2,1347511
8	2,2286989	2,3873253	2,3203220	2,0865702	2,1334751
7	2,2286971	2,3873257	2,3203222	2,0865708	2,1334750
6	2,2286790	2,3873296	2,3203238	2,0865775	2,1334743
5	2,2284981	2,3873685	2,3203406	2,0866442	2,1346648
4	2,2266995	2,3877569	2,3205023	2,0873091	2,1338914
3	2,2096757	3,3915427	2,3216524	2,0936183	2,1263554
2	2,1095440	2,4120246	2,3092534	2,1258394	2,0958077
1	2,3299283	2,4020065	2,1424445	2,1424445	2,0906061
0	2,6212837	2,4238180	2,2798120	2,1563632	2,0989855

/198

m	σ_2 at α				
	200	400	600	800	1000
∞	2,0770611	2,0267223	2,0265029	2,0307315	2,0144871
9	2,0770611	2,0267224	2,0265006	2,0307282	—
8	2,0770612	2,0267226	2,0264803	2,0306990	—
7	2,0770621	2,0267244	2,0262771	2,0304065	—
6	2,0770715	2,0267433	2,0242483	2,0274974	2,0145314
5	2,0771591	2,0269262	2,0042829	1,9997115	2,0148888
4	2,0775849	2,0280425	1,8319596	1,7809362	2,0164554
3	2,0715164	2,0321867	1,2358388	2,0237459	2,0192774
2	2,0578246	2,0363919	1,1489006	2,0229994	—
1	—	—	—	—	—
0	—	—	—	—	—

Commas indicate decimal points.

TABLE 5.9 CONT'D

m	σ_3 at α			
	1400	2000	2500	4000
∞	2,0179434	2,0129720	2,0125004	—
9	—	—	—	—
8	—	—	—	—
7	—	—	—	—
6	2,0180527	2,0130127	2,0125667	2.0071557
5	2,0179827	2,0131387	2,0124628	2.0072355
4	2,0171970	2,0130490	2,0117670	2.0075523
3	2,0159656	2,0125312	2,0108014	2.0078930
2	—	—	—	—
1	—	—	—	—
0	—	—	—	—

Commas indicate decimal points.

TABLE 5.10. LIMITING VALUES OF EFFECTIVE AREA RADAR σ_0^* AND TOTAL σ_1^* SCATTERING FOR $N = 1.78 - 10^{-m}i$ AT $m = 0, 1, \ldots, 9, \infty$. /199

m	σ_0^*	σ_1^*	m	σ_0^*	σ_1^*
∞	0,078722	1,079	4	0,078722	1,079
9	0,078722	1,079	3	0,078722	1,079
8	0,078722	1,079	2	0,078735	1,079
7	0,078722	1,079	1	0,078578	1,080
6	0,078722	1,079	0	0,184272	1,184
5	0,078722				

Commas indicate decimal points.

Table 5.12 also lists data for $\lambda = 500$ μm. It is obvious that although the difference in the imaginary parts of N is substantial (three-fold), the σ_0 and σ_2 values calculated from the Debye and experimental N values differ from one another by not more than 30%. Moreover, the magnitude of the indicated error also includes the error due to the difference in the temperatures considered. The error in calculations of σ_0 and σ_2 from the Debye values of N at $\lambda = 0.03$ cm is slightly greater.

Let us consider the influence of errors in the determination of the dielectric constants of snow on its scattering and attenuation cross-sections.

TABLE 5.11. EFFECTIVE AREAS OF RADAR σ_0 AND TOTAL σ_1 SCATTERING AND ATTENUATION σ_2 OF ELECTROMAGNETIC WAVE OF 01. cm LENGTH BY A WATER SPHERE AT N = 2.58 - 0.95 i (IN THE NUMERATOR) AND N = 2.53 - 0.82 i (IN THE DENOMINATOR)

a	σ_0	σ_1	σ_2
0,1	$\frac{2,2 \cdot 10^{-4}}{2,1 \cdot 10^{-4}}$	$\frac{1,5 \cdot 10^{-4}}{1,4 \cdot 10^{-4}}$	$\frac{0,070}{0,061}$
0,3	$\frac{0,018}{0,017}$	$\frac{0,013}{0,013}$	$\frac{0,260}{0,239}$
0,7	$\frac{0,477}{0,413}$	$\frac{0,433}{0,402}$	$\frac{1,444}{1,320}$
1,0	$\frac{1,021}{0,905}$	$\frac{1,378}{1,343}$	$\frac{3,128}{3,048}$
2,0	$\frac{0,473}{0,466}$	$\frac{1,459}{1,450}$	$\frac{3,024}{3,049}$
3,0	$\frac{0,213}{0,207}$	$\frac{1,443}{1,411}$	$\frac{2,808}{2,803}$
4,0	$\frac{0,161}{0,152}$	$\frac{1,436}{1,412}$	$\frac{2,690}{2,688}$
5,0	$\frac{0,195}{0,182}$	$\frac{1,428}{1,405}$	$\frac{2,608}{2,605}$

Note: Commas indicate decimal points.

TABLE 5.12. EFFECTIVE AREAS OF RADAR SCATTERING σ_0 AND ATTENUATION σ_2 OF AN ELECTROMAGNETIC WAVE OF 500 μm LENGTH BY WATER VAPOR WITH CALCULATED (DEBYE) AND EXPERIMENTAL [118] N VALUES FOR WATER.

d	σ_0	σ_2	d	σ_0	σ_2
0,01	$\frac{0,221}{0,259}$	$\frac{0,624}{0,925}$	0,10	$\frac{0,151}{0,172}$	$\frac{2,526}{2,532}$
0,03	$\frac{0,209}{0,202}$	$\frac{3,472}{3,177}$	0,25	$\frac{0,178}{0,204}$	$\frac{2,297}{2,308}$
0,07	$\frac{0,199}{0,269}$	$\frac{2,660}{2,656}$	0,45	$\frac{0,181}{0,209}$	$\frac{2,206}{2,215}$

Note. The calculated values (in the numerator) were determined at t = 20°C (N = = 2.36 - 0.26 i), and the experimental values (in the denominator), at t = 25°C (N = 2.409 - 0.74 i). Commas indicate decimal points.

Figure 5.13 illustrates the influence of the imaginary part of N on the σ_0 and σ_2 values. The values of the refractive index chosen here are close /200
(with an error of less than 0.6%) to N of snow (see Table 4.38) at t = 0°C for densities of 0.005 and 0.01 g/cm^3. It would seem that such a small error in N should have practically no effect on the scattering and attenuating cross-section. However, as we will see below, the functions $\sigma_0 = f(N, \alpha)$ and $\sigma_2 = \phi(N, \alpha)$ are unstable relative to small variations of Ren when N is close to unity in absolute value. Thus, it is evident from Figure 5.13 that a twofold /201
decrease in Im N at constant Ren leads to an increase in σ_0 and σ_2 values by not more than a factor of 5 and 2, respectively.

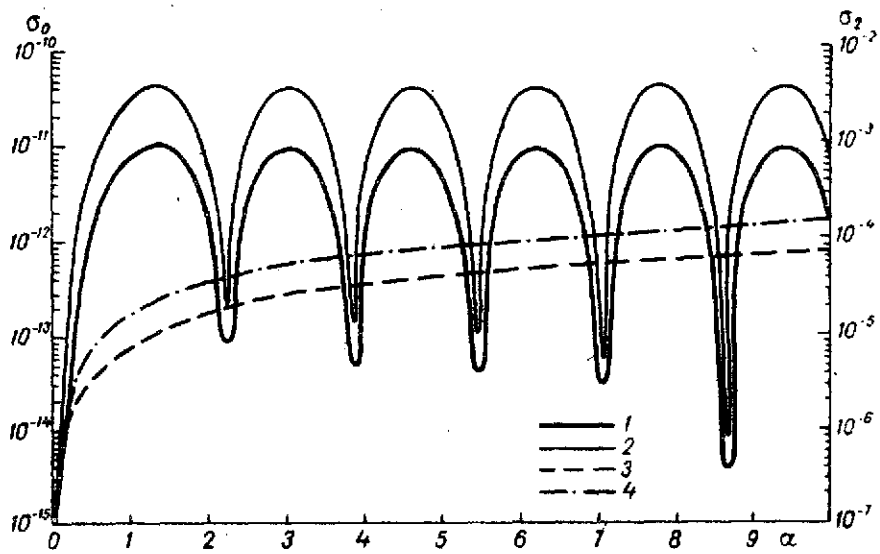

Figure 5.13. Effective Areas of Radar Scattering σ_0 (1, 2) and Attenuation σ_2 (3, 4) of a Spherical Snow Crystal with N = 1.00-0.969 · 10^{-4} i (1, 3) and N = 1.00-0.14 · 10^{-4} i (2, 4) vs. α.

At the same time, if the real part of N is changed by only 2%, the magnitude of the imaginary part being practically the same, the final σ_0 and σ_2 values will differ very greatly (Table 5.13).

TABLE 5.13. CROSS-SECTIONS OF RADAR SCATTERING σ_0 AND ATTENUATION σ_2 OF A SNOW CRYSTAL FOR DIFFERENT α

α	σ_0 at N		σ_2 at N	
	1,00—0,14 · 10^{-4} i	1,02—0,19 · 10^{-4} i	1,00—0,14 · 10^{-4} i	1,02—0,19 · 10^{-4} i
0,1	3,45 · 10^{-14}	7,01 · 10^{-8}	3,71 · 10^{-6}	4,97 · 10^{-6}
0,5	1,78 · 10^{-11}	3,62 · 10^{-5}	1,86 · 10^{-5}	5,21 · 10^{-5}
1,0	1,16 · 10^{-10}	3,05 · 10^{-4}	3,73 · 10^{-5}	3,77 · 10^{-4}
3,0	1,99 · 10^{-10}	4,43 · 10^{-4}	1,12 · 10^{-4}	6,08 · 10^{-3}
6,0	1,55 · 10^{-10}	3,70 · 10^{-4}	2,24 · 10^{-4}	2,76 · 10^{-2}
8,0	1,73 · 10^{-10}	2,52 · 10^{-4}	2,99 · 10^{-4}	5,02 · 10^{-2}
10,0	2,57 · 10^{-11}	2,09 · 10^{-6}	3,73 · 10^{-4}	7,91 · 10^{-2}

Note: Commas indicate decimal points.

The mechanism of such a strong dependence of the scattering and attenuation cross-sections on a slight variation of the real part of the complex index N of low density snow can best be followed in the Rayleigh approximation. Thus, at a sufficiently small α

$$\sigma_0 = 4\left|\frac{N^2-1}{N^2+2}\right|^2\alpha^4. \tag{5.6}$$

We will consider two basic cases corresponding to the dielectric constants of snow of 10^{-2}-10^{-3} g/cm^3 density (see Table 4.38): $N = 1 - i\xi$ and $N = (1 + \delta) - i\xi$, where $1 > \delta \gg \xi$, and ξ has the order of magnitude 10^{-5}-10^{-6}. Then, substituting the expressions for N into formula (5.6) and neglecting quantities of second-order or smallness in comparison with the first, we will have

$$\text{for} \quad N = 1 - i\xi \qquad \sigma_0 = \frac{\alpha^4}{9}\xi^2, \tag{5.7}$$

$$\text{for} \quad N = (1+\delta) - i\xi \qquad \sigma_0 = \frac{\alpha^4}{9}\delta^2. \tag{5.8}$$

We now set $\xi = 10^{-6}$ and $\delta = 10^{-3}$. As follows from expressions (5.7), (5.8), a 0.1% error in N leads to a decrease in σ_0 by six orders of magnitude. Comparing two other cases $\delta = \delta_1$ and $\delta = \delta_2$, i.e., when $R\,N \neq 1$, we obtain a ratio of the corresponding σ_0 values equal to $\left(\frac{\delta_2}{\delta_1}\right)^2$.

Thus, if $\delta_1 = 10^{-3}$, and $\delta_2 = 6 \cdot 10^{-3}$ (the error in N is 0.6%), the radar scattering cross-sections differ by a factor of 36. /202

The cross-sections of total scattering σ_1 and attenuation σ_2 are similarly treated. We will note here that since for σ_2 the indicated instability takes place at somewhat larger values of α than for σ_0, it is necessary to consider the first few terms.

§ 5.3. Scattering and Attenuation of Microradiowaves by a Homogeneous Hydrometeoric Particle.

Hailstone. The first rigorous calculations after Mie of the effective areas of radar scattering σ_0 and attenuation σ_2 of centimeter electromagnetic waves by homogeneous ice spheres at $\alpha \leqslant 4$ were performed by J. Ryde[86]. Later, in connection with R. Donaldson's study [217], who noted a comparitively high reflectivity of hail by means of a 3.2 cm radar unit, B. Herman and L. Battan [210, 218] performed more detailed calculations of σ_0 and σ_2 of homogeneous

[86]A survey of papers in which the calculations were performed in the Rayleigh approximation may be found in [145, 64, 114].

ice spheres of 1 g/cm^3 density at t = 0°C for α from 0.1 to 500. Results of these calculations, which were in good agreement with the experimental data [219, 220, etc.], led to one of the key conclusions of radiometeorology: the scattering by dry ice spheres whose size is not smaller than the wavelength is approximately one order of magnitude greater than the scattering by spherical water drops of the same radius. This fact was experimentally and theoretically demonstrated in [215, 221].

Data on further studies along these lines may be found in the comprehensive survey of D. Atlas [149]. Here, however, we will consider exclusively questions that were not dealt with in the above mentioned works.

Accurate diffraction formulas were used to calculate σ_0, σ_1 and σ_2 of homogeneous ice spheres of 1 g/cm^3 density at temperatures[87] from 0 to -50°C and α from 0.1 to 100. Figures 5.14-5.16 show the σ_0, σ_1 and σ_2 curves plotted on the basis of the results of these calculations for t = 0°C.

The σ_0, σ_1 and σ_2 curves at other temperatures may be found in [214, 11]. Since the dielectric constants of ice in the lower portion of the centimeter range are independent of wavelength, by assuming λ equal to π and replacing α by d cm in Figures 5.14-5.16, we will obtain the scattering and attenuation cross-section curves at 3.14 cm wavelength as functions of hailstone diameter at 0°C.

Analysis of the temperature dependence of σ_0 shows that at all α, a temperature below -30°C has practically no effect on the σ_0 values. The temperature correction applied to σ_0 at $\alpha \leqslant 10$ and $t < -30$°C does not exceed 25%. /204
Hence, for small α and any temperature one can use with a sufficient degree of accuracy the σ_0 values obtained at 0°C. At large α, the temperature change in the range from 0 to -30°C may lead to a two-threefold increase or decrease in the radar scattering cross-section.

The total scattering cross-section σ_1 at all α is found in the range of 10-20% of σ_1 at t = 0°C and for $\alpha \leqslant 25$, the dependence of σ_1 on temperature may be neglected altogether.

For all $\alpha < 100$, the effective attenuation area σ_2 is independent of temperature with an accuracy of less than 4%.

---

[87] The dielectric constants of ice were selected from Table 4.33, the data of W. Cumming [136] being used at 0, -10 and -20°C, and the values given by D. Lamb and A. Turney [35] being used at -30, -40, and -50°C.

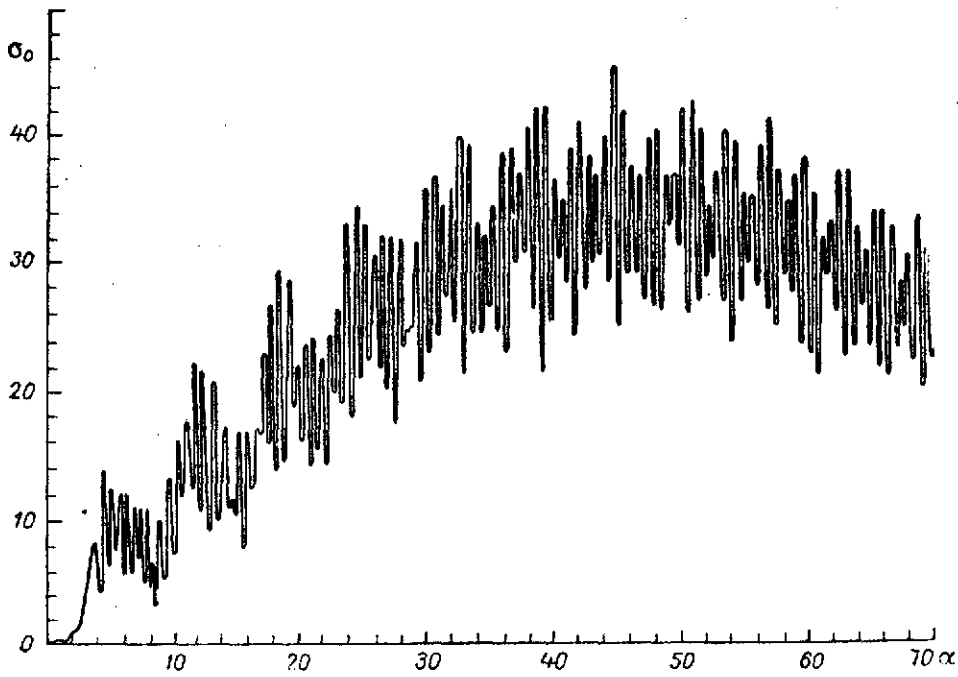

Figure 5.14. Effective Area of Radar Scattering σ_0 of a Spherical Hailstone of Unit Density at t = 0°C.

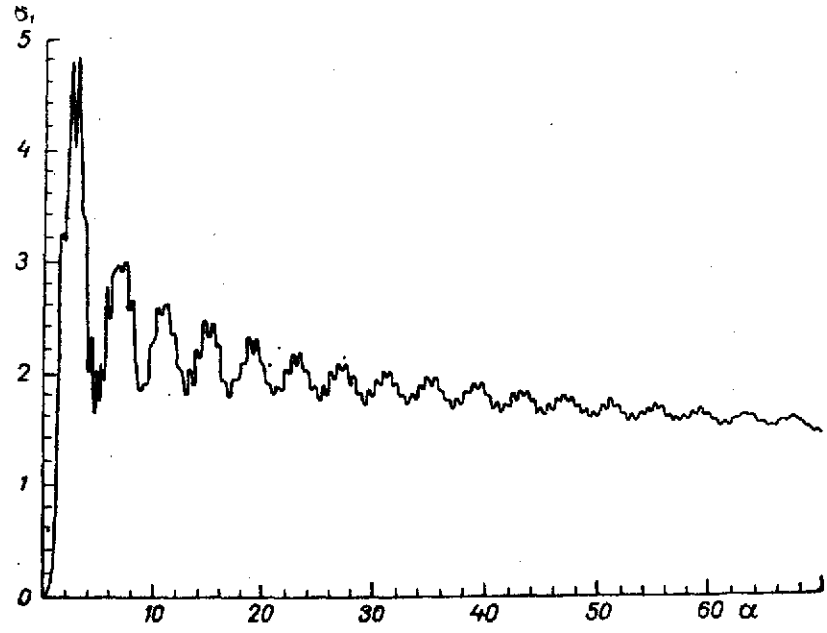

Figure 5.15. Effective Area of Total Scattering σ_1 of a Hailstone of Unit Density at t = 0°C.

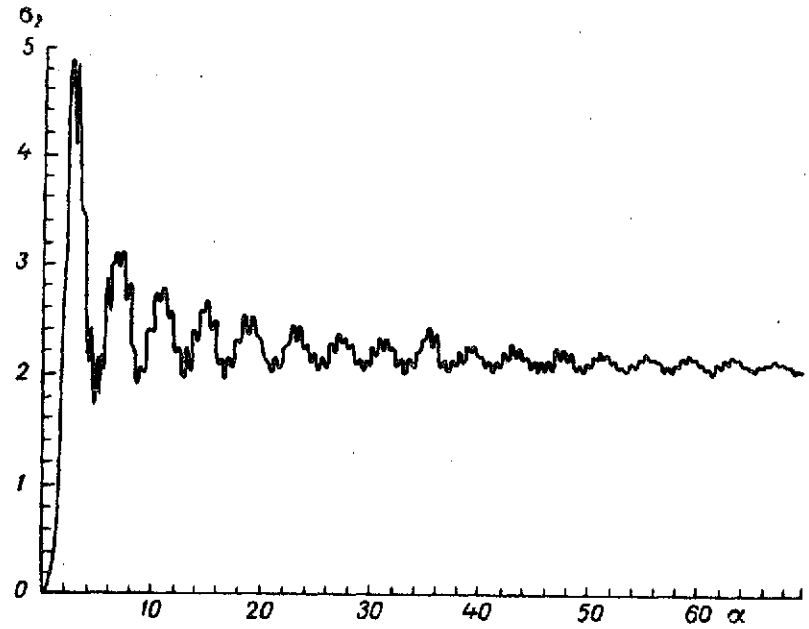

Figure 5.16. Effective Attenuation Area σ_2 of Spherical Hailstones of Unit Density t = 0°C.

Analysis of radar scattering and attenuation cross-sections for hailstones with density ρ of less than unity (Figures 5.17-5.19) shows that as the density decreases, the temperature dependences of σ_0 and σ_2 become still weaker. Thus, at $\alpha \leqslant 13$ (Figure 5.17), a greater σ_0 corresponds to a hailstone of higher density. For $\alpha > 13$, a hailstone of 0.380 g/cm^3 density reflects back 1.2-5 times as much energy as a hailstone of 0.600 g/cm^3 density, σ_0 of both hailstones being 5-10 times smaller than σ_0 of a hailstone with ρ = 0.916 g/cm^3. Thus, over the entire segment of variation of α under consideration, the effective area of radar scattering depends substantially on density.

Since the character of the dependences of σ_1 and σ_2 on ρ (Figures 5.18, 5.19) is complex, we will consider the function of σ_2. It is apparent that the /206 effect of density ρ on the values of the effective attenuation area is somewhat less distinct than on σ_0, particularly at $\alpha > 10$, where the σ_2 values of hailstones with densities of 0.600 g/cm^3 and 0.380 g/cm^3 may be considered equal to within 7-8%. At ρ = 0. 916 g/cm^3, σ_2 differs by less than 30% from the σ_2 at the remaining densities in this range. At $\alpha < 3.4$, a monotonic dependence of σ_2 on ρ occurs: to a lower density there corresponds a smaller σ_2. A fairly substantial influence of ρ on the magnitude of σ_2 is observed at these values of α. For example, at α = 2.4, the corresponding σ_2 values for densities of 0.916, 0.600, and 0.380 g/cm^3 are 4.901, 2.340, and 0.996.

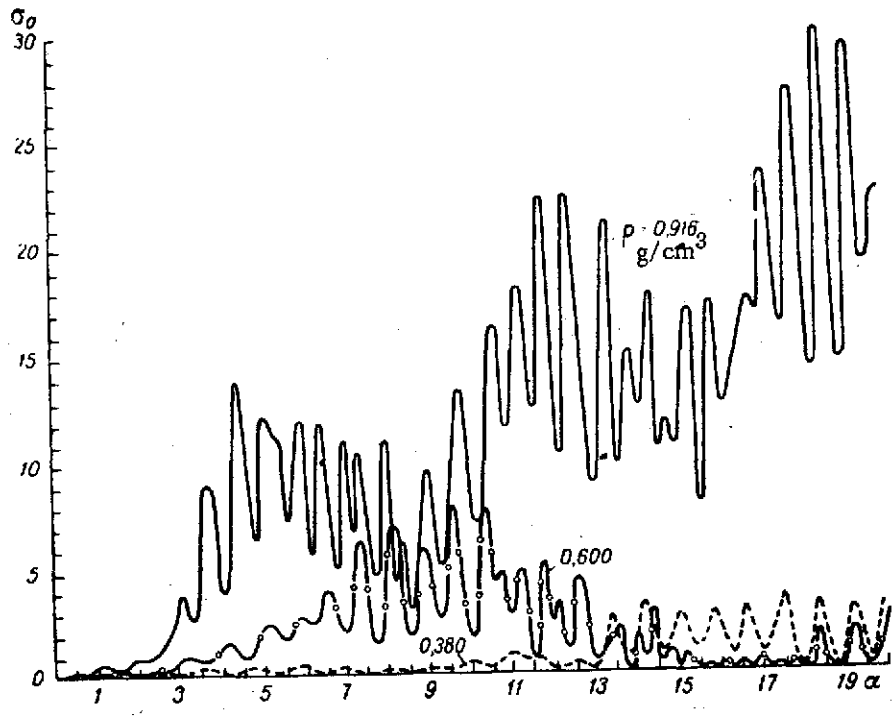

Figure 5.17. Effective Area of Radar Scatter σ_0 of a Spherical Hailstone Having Varying Density with t = 0°C.

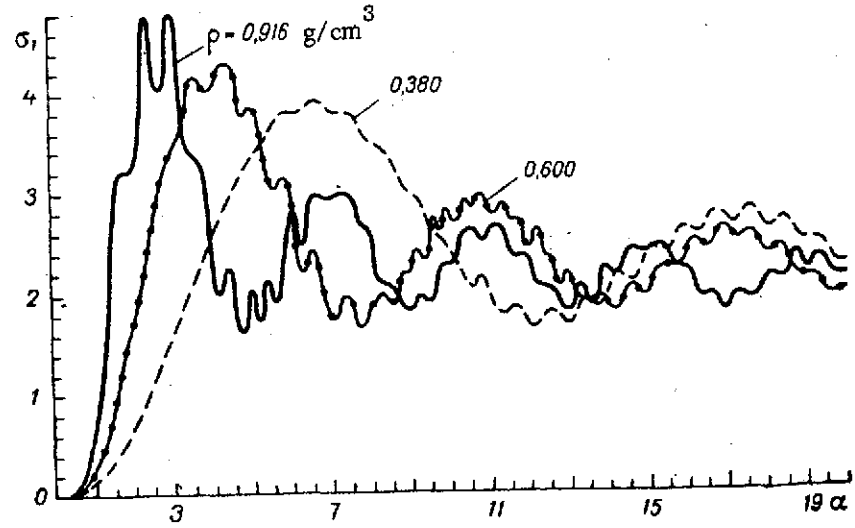

Figure 5.18. Effect Area of Total Scatter σ_1 of a Spherical Hailstone Having Varying Density with t - 0°C.

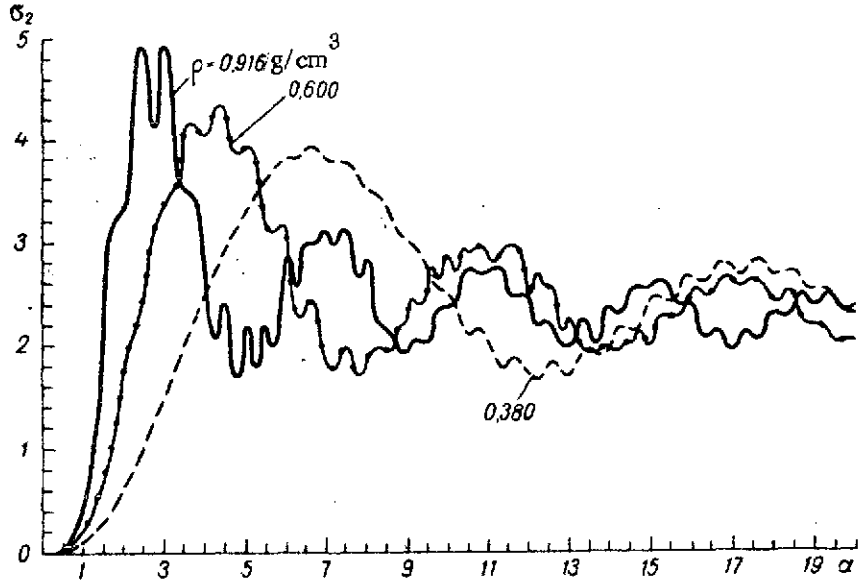

Figure 5.19. Effective Attenuation Area σ_2 of Spherical Hailstones of Different Densities at t = 0°C.

As is evident from Figure 5.19, for $3.4 < \alpha < 10$, the dependence of σ_2 on ρ has a more complex variable character.

Analysis of calculated values of the scattering and attenuation cross-sections of a hailstone as functions of its radius b_1 at different λ shows that for a hailstone smaller than 4.6 cm in diameter, the dependence of σ_0 on λ in the 0.86-17 cm range decreases monotonically[88]. If, however, its size is no greater than 6.0 cm and no smaller than 4.6 cm, this property is preserved only at λ = 0.86 to 11 cm. For the effective attenuation area σ_2, the monotonicity condition of the function $\sigma_2 = f(\lambda)$ with $\lambda \in [0.86, 17\text{ cm}]$ takes place when the hailstone diameter is under 1 cm. When $d > 1$ cm, an oscillatory character of the dependence of σ_2 on λ is observed. Let us also note that the /207 shape of the curve $\sigma_1 = \phi(\lambda)$ in the range λ = 0.86 to 17 cm practically duplicates the function $\sigma_2 = f(\lambda)$.

Figures 5.20 and 5.21 show σ_0 and σ_2 curves of a wet hailstone (snow grain) of 0.38 g/cm³ density. The calculations were made by taking into account model

[88]It is assumed that the dielectric constants of ice in the range λ = 0.86 to 17 cm are the same as at λ = 1 to 10 cm.

representations of dielectric constants (see § 4.2) on the basis of the experimental data of Table 4.32.

It is evident from Figure 5.20 that for $\alpha \leqslant 10$, the differences in σ_0 at different values of the percentage (p) of water in the hailstone are not substantial. For $\alpha > 10$ and in the presence of 1.6% of water in the hailstone, the radar scattering cross-section decreases by a factor of 1.8-3. The attenuation cross-sections of the wet hailstone σ_2 at $p \leqslant 1.6\%$ and all $\alpha < 20$ (Figure 5.21) are practically the same as the σ_2 values for a dry hailstone of the same density.

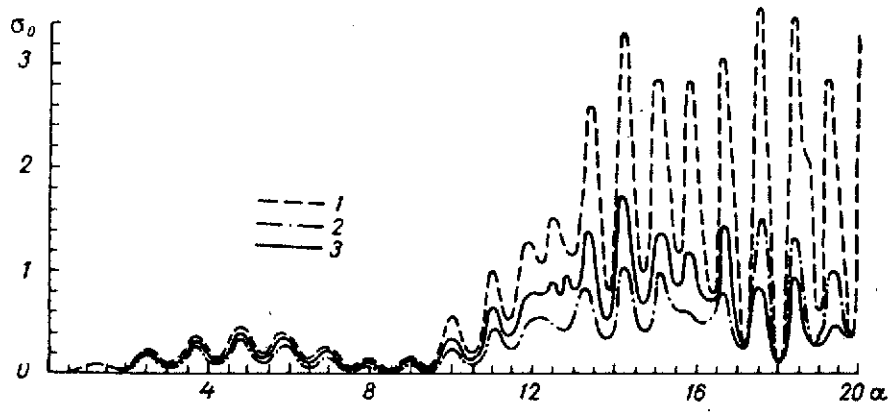

Figure 5.20. Effective Radar Scattering Area σ_0 of Wet Hailstone of 0.380 g/cm³ Density For Different Contents of Water (p), t = 0°C, λ = 3.2 cm. 1, p = 0.0%; 2, p = 1.0%; 3, p = 1.6%.

Snow Crystal. In § 5.2 it was shown that variations in the dielectric constants of snow (see Table 4.38) of 10^{-2}-10^{-3} g/cm³ density in the range of 1% cause very significant changes in scattering and attenuation cross-sections. Since the N values themselves in Table 4.38 were obtained by calculation, on the basis of the concepts of § 4.2 [see formulas (4.27), (4.28), (4.33)] which agreed to within 7% with experimental studies [137], they can hardly be used in calculations of σ_0, σ_1, and σ_2.

It is necessary to perform careful measurements of N of snow, particularly of its real part, as a function of density and wavelength, before the above mentioned calculations are possible.[89]

[89]The aforesaid should be fully applied to the results of [322, 197, etc.].

Water Drop. During the period 1940-1954, calculations after Mie were performed to determine the effective areas of scattering and attenuation of centimeter and millimeter electromagnetic radiation [64, 145, 70][90] by a spherical/208 water drop with a size $\alpha = \frac{\pi d}{\lambda}$ not exceeding[91] five.

Later, calculations were also performed [222 etc.] for $\alpha \geqslant 5$ by means of computers and programs for the calculation of hailstones.

J. R. Gerhardt et al. [219-220] found that the calculated and experimental σ_0 values of water drops in the centimeter and millimeter ranges of λ were in good agreement.

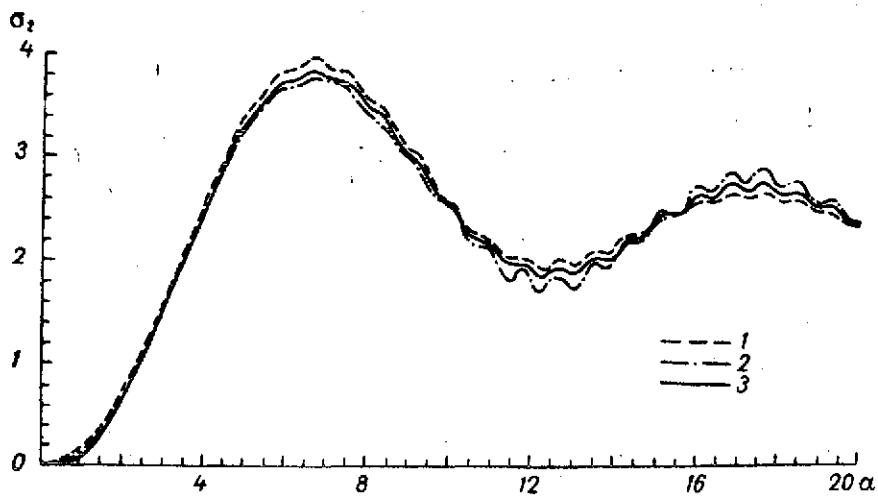

Figure 5.21. Effective Attenuation Area σ_2 of a Wet Hailstone of 0.380 g/cm³ Density For Different Water Contents p. t = 0°C, λ = 3.2 cm.

1, p = 0.0%; 2, p = 1,0%; 3, p = 1.6%.

Referring to various appendices, we use formulas (1.276), (1.273), and (1.274) to calculate σ_0, σ_1 and σ_2 of water spheres of different sizes at different temperatures and λ of microwave and submillimeter range. The dielectric constants of water for $\lambda \geqslant 0.08$ cm at the corresponding temperatures were chosen from the appendix, and for $\lambda < 0.08$ cm, from Tables 4.29, 4.24.

[90] Detailed surveys of such studies are given in [64], [145].

[91] The first calculations of this kind in this country were made by O. Ya. Usikov, V. L. German, and I. Kh. Vakser [95].

Thus, Figure 5.22 shows σ_0, σ_1 and σ_2 curves for different α, but for fixed values of temperature and wavelength. It is evident that the radar scattering curve is definitely more oscillatory in character than the σ_1 and σ_2 curves. As α increases, all the curves tend to their limiting values [11].

Figures 5.23 and 5.24 illustrate the temperature dependence of σ_0 and σ_2. /209 Analysis shows that σ_0 of a water drop with temperature t°C differs from σ_0 of a drop with t = 20°C by not more than 20-40%. Under the same conditions, the σ_2 values differ by less than 5%. Moreover, as the wavelength decreases, the temperature dependence of the scattering and attenuation cross-sections diminishes, and in the submilimeter range we can assume that $\frac{\partial \sigma_i}{\partial t} \sim 0$, i = 0, 1, 2. The observed temperature variations of the radar characteristics of a water drop are a direct consequence of the character of the temperature dependence of the complex refractive index (4.13) (see Figures 4.11, 4.12).

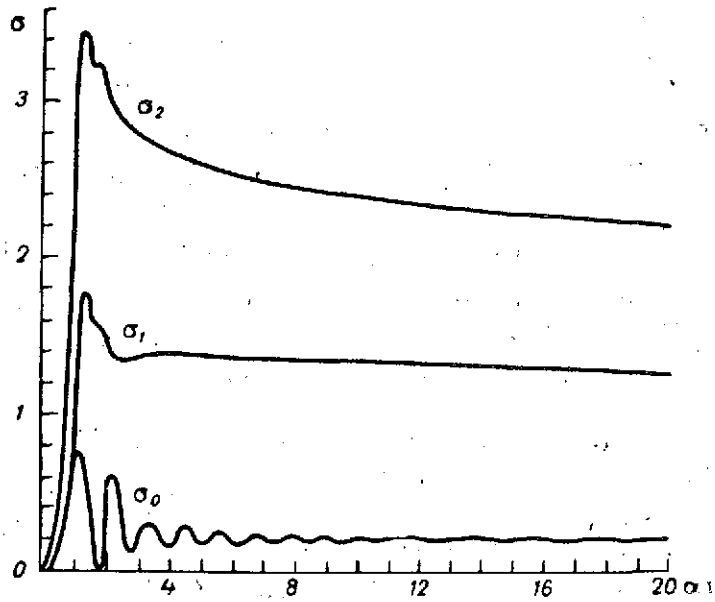

Figure 5.22 Effective Areas of Radar σ_0 and Total σ_1 Scattering and Attenuation σ_2 of a Spherical Water Drop At t = 10°C and λ = 1 mm.

The effect of wavelength λ on the cross-sections of radar scattering σ_0 and attenuation σ_2 of a water drop of different normalized sizes is clearly

evident from the curves of Figures 5.25 and 5.26. Thus, in the centimeter range the dependence of σ_0 and σ_2 on λ is weakly manifested, but this cannot in general be said for the millimeter range and certainly not for the submillimeter range.

The various aspects of radar characteristics for limiting cases of "small" and "large" water drops have been discussed in detail in [45, 81, 145, 125, 70, 222-228, 64, 114, etc.], and are therefore omitted here.

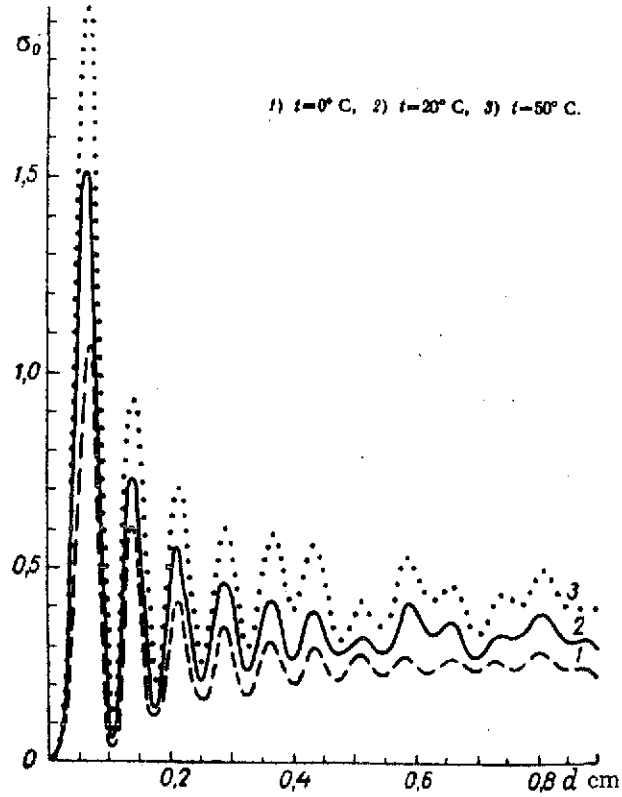

Figure 5.23. Effective Radar Scattering Area σ_0 of a Water Drop at λ = 0.2 cm at Different Temperatures. 1, t = 0°C; 2, t = 20°C; 3, t = 50°C. /210

§ 5.4. Scattering and Attenuation of Microwaves by a Layered Hailstone /212

The radar characteristics of hailstones, representing homogeneous ice spheres, with different dielectric properties and temperatures, are discussed in the preceding section. However, as was noted in § 5.1, a natural hailstone is a layered substance, generally with a nonconcentric arrangement of layers of different densities. In the approximation of a spherical two-layer hailstone (see Figure 1.6) and a spherical nonconcentrically layered (see

Figure 1.4) three-layer hailstone, these characteristics were partially studied by the author [227, 12].

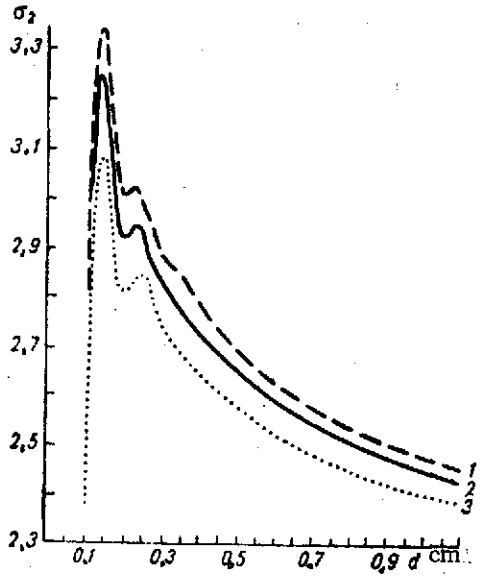

Figure 5.24. Effective Attenuation Area σ_2 of a Water Drop at λ = 4 mm at Different Temperatures, 1, t = 0°C; 2, t = 20°C; 3, t = 50°C.

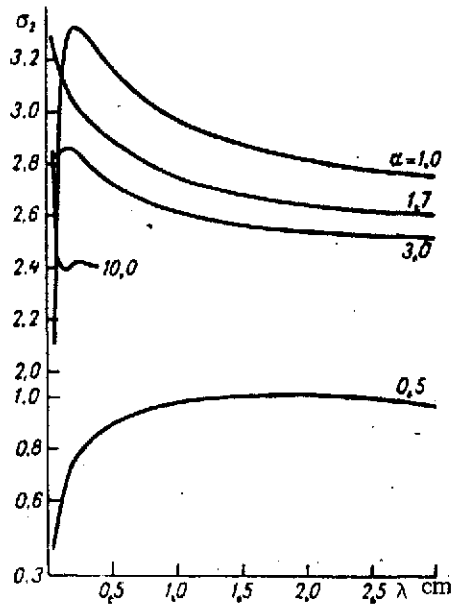

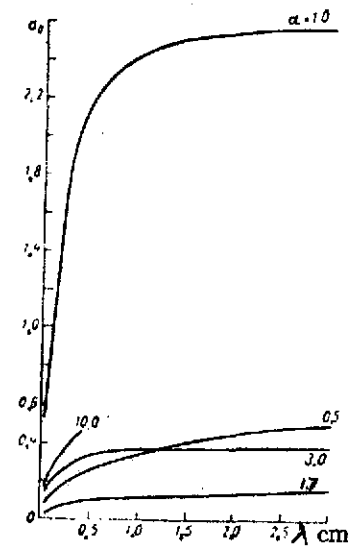

Figure 5.25. Dependence of σ_0 of a Water Drop at t = 20°C on λ at Different α. /211

Figure 5.26. Dependence of σ_2 of Water Drop at t = 20°C on λ at Different α.

Below, in addition to two-layer particles, a much broader representation will be given to studies pertaining to the scattering and attenuation of microwaves by multi-layered hailstones with the actual arrangement and dimensions of the layers.

We begin with the two-layer hailstone. We introduce the following symbols (see Figure 1.6): ρ_2 — density of core (spherical inclusion) in g/cm^3; ρ_1 — density of shell (region inside the particle and

external to its inclusion) in g/cm^3; b_2 – radius of core in cm; b_1 – radius of particle in cm; $h_{sh} = b_1 - b_2$ – thickness of shell in cm; ρ – density of homogeneous spherical hailstone of radius b_1; $\nu - \frac{2\pi b_1}{\lambda}$; λ – wavelength of the lower and a part of the centimeter range.

Calculations were performed for the effective areas of radar scattering σ_0 and attenuation σ_2 of microwaves[92] by a two-layer hailstone by using the exact diffraction formulas 1.276 and 1.274 as functions of ν, taking into account the symbols (1.281-1.283), for different combinations of layer densities from 0.380 to 0.916 g/cm^3 and ratios of their dimensions $\frac{b_2}{b_1}$, and using the dielectric constants from Table 4.31 and t = 0°C.

Layered Hailstone with $\rho_1 < \rho_2$. Cases of the following density combinations are considered: $\rho_2 = 0.916$ g/cm^3, $\rho_1 = 0.600$ g/cm^3; $\rho_2 = 0.916$ g/cm^3, $\rho_1 = 0.380$ g/cm^3; $\rho_2 = 0.600$ g/cm^3, $\rho_1 = 0.380$ g/cm^3; and ratios $\frac{b_2}{b_1}$: 0.00; 0.05' 0.10' 0.25; 0.50; 0.80; 0.90; 0.96; 1.00, values of $\frac{b_2}{b_1}$ equal to 0.00 and 1.00 being deferred to the limiting cases of a homogeneous sphere of radius b_1 with $\rho = \rho_1$ and $\rho = \rho_2$ respectively.

Table 5.14 lists values of σ_0, and Table 5.15, σ_0 at h_{sh} equal to 0.00 b_1; 0.04 b_1; 0.10 b_1 for all three pairs of densities. It is of this that for $\nu \leqslant 1$, softening of the hailstone from the outside, i.e., the appearance on the hailstone of the layer with $h_{sh} \leqslant 0.1\ b_1$ softer than the core has practically no effect on σ_0. Similar conclusion can also be reached with regard to σ_2. However, as follows from Table 5.15, this conclusion will apply with an accuracy of 20-30% for all ν. /21

$\rho_2 = 0.916$ g/cm^3; $\rho_1 = 0.600$ g/cm^3. For $\nu > 1$, the shell of thickness of 0.04 b_1 substantially decreases σ_0, particularly for large ν ($15 < \nu < 30$), where the radar cross-section values amount to approximately 1/3 of σ_0 of the homogeneous hailstone with $\rho = 0.916$ g/cm^3. At $\nu > 40$, their leveling takes

---

[92] According to § 4.2, the dielectric constants of ice in the centimeter range are practically independent of wavelength. Assuming that the same values of the dielectric constants will hold in the milimeter region of change of λ, these results will also apply to this range of λ.

place to a certain extent around their asymptotic values ($\nu \to \infty$), which, as shown by calculations, differ only slightly. A further enlargement of the shell to $h_{sh} = 0.10\ b_1$ results in a sharper decrease of σ_0 for $1 < \nu \leqslant 11$ with further oscillation about its limiting value. Starting at $\nu > 50$, the σ_0 curve becomes stable, and at $\nu > 80$ it occupies an intermediate position between the curves with $\frac{b_2}{b_1}$ equal to 0.96 and 1.00.

The character of the behavior of radar scattering as a function of the growth of the shell to sizes $0.2\ b_1$ and $0.5\ b_1$, i.e., for a comparatively large and less dense layer of the shell for $\nu \leqslant 10$ is evident from Figure 5.27. Thus, for $\nu \leqslant 3.0$, the difference in σ_0 of the two-layer hailstone with $\frac{b_2}{b_1}$ equal to 0.8 and 0.5, and a homogeneous hailstone with $\rho_0 = 0.600$ g/cm^3 /216 is slight. At $3 < \nu < 9$, as h_{sh} grows from 0.2 to $0.5\ b_1$, σ_0 has a tendency to increase and approaches the corresponding values of σ_0 of the homogeneous hailstone with $\rho = 0.916$ g/cm^3. Results of calculations for $9 \leqslant \nu \leqslant 15.5$ show that the σ_0 curve of the hailstone with $\frac{b_2}{b_1} = 0.8$ fluctuates around values corresponding to the hailstone with $\rho = 0.916$ g/cm^3, and in some intervals substantially exceeds them. This apparently accounts for the fact that in many cases the magnitude of radar reflection observed by various authors considerably exceeds the theoretically calculated magnitude for a spectrum of homogeneous hailstones with $\rho = 1$ g/cm^3.

It follows from an analysis of the σ_0 curves of hailstones with $\frac{b_2}{b_1} = 0.5$ that for $10 < \nu < 15.5$, σ_0 slightly oscillates around the curve for the homogeneous hailstone. It may be assumed, therefore, that for these ν, the hailstone with a shell of the order of $0.5\ b_1$ behaves as a homogeneous hailstone whose density is equal to that of the shell.

At $\nu > 15.5$, the function σ_0 corresponding to the case $\frac{b_2}{b_1} = 0.8$ decreases sharply in comparison with σ_0 for $\rho = 0.916$ g/cm^3, approaching closer to σ_0 for $\frac{b_2}{b_1} = 0.5$ and $\rho = 0.600$ g/cm^3, and at $\nu > 18$, the σ_0 values of the curve with $\frac{b_2}{b_1}$ equal to 0.8 and 0.5 already differ little from the asymptotic values.

TABLE 5.14. VALUES OF τ_0 OF A TWO-LAYER HAILSTONE FOR DIFFERENT COMBINATIONS OF DENSITIES OF THE CORE (ρ_2) AND SHELL (ρ_1) AT $\frac{b_2}{b_1}$ = 0.90, 0.96, AND 1.00, t = 0°C.

	$\rho_2=0{,}916$ g/cm^3, $\rho_1=0{,}600$ g/cm^3		$\rho_2=0{,}916$ g/cm^3, $\rho_1=0{,}380$ g/cm^3		$\rho_2=0{,}600$ g/cm^3, $\rho_1=0{,}380$ g/cm^3		$\rho_2=0{,}380$ g/cm^3, $\rho_1=0{,}600$ g/cm^3		$\rho_2=0{,}380$ g/cm^3, $\rho_1=0{,}916$ g/cm^3		$\rho_2=0{,}600$ g/cm^3, $\rho_1=0{,}916$ g/cm^3		$\rho=0{,}916$ g/cm^3	$\rho=0{,}600$ g/cm^3	$\rho=0{,}380$ g/cm^3
	$\frac{b_2}{b_1}=0{,}90$	$\frac{b_2}{b_1}=0{,}96$	$\frac{b_2}{b_1}=0{,}90$	$\frac{b_2}{b_1}=0{,}96$	$\frac{b_2}{b_1}=0{,}90$	$\frac{b_2}{b_1}=0{,}96$	$\frac{b_2}{b_1}=0{,}90$	$\frac{b_2}{b_1}=0{,}96$	$\frac{b_2}{b_1}=0{,}90$	$\frac{b_2}{b_1}=0{,}96$	$\frac{b_2}{b_1}=0{,}90$	$\frac{b_2}{b_1}=0{,}96$	$\frac{b_2}{b_1}=1{,}00$	$\frac{b_2}{b_1}=1{,}00$	$\frac{b_2}{b_1}=1{,}00$
0,1	0,000	0,000	0,000	0,000	0,000	0,000	0,000	0,000	0,000	0,000	0,000	0,000	0,000	0,000	0,000
0,3	0,005	0,005	0,004	0,005	0,002	0,003	0,001	0,001	0,002	0,002	0,003	0,003	0,006	0,002	0,001
0,5	0,035	0,038	0,031	0,037	0,016	0,018	0,010	0,009	0,014	0,011	0,024	0,021	0,041	0,019	0,008
0,8	0,196	0,211	0,175	0,202	0,087	0,095	0,051	0,045	0,068	0,051	0,121	0,109	0,221	0,102	0,041
1,0	0,369	0,385	0,339	0,374	0,165	0,178	0,090	0,081	0,110	0,088	0,209	0,195	0,393	0,186	0,075
3,0	1,810	3,100	1,278	2,749	0,279	0,410	0,134	0,078	0,652	0,154	1,474	0,810	0,840	0,524	0,078
5,0	3,468	4,676	5,254	4,174	0,549	1,233	0,160	0,227	1,535	0,238	5,044	4,199	12,375	2,120	0,336
8,0	0,511	4,227	3,138	4,544	0,861	1,191	1,309	0,208	10,108	1,286	5,403	7,907	11,047	4,404	0,151
10,0	1,429	7,802	2,251	7,970	2,640	3,050	7,714	1,396	5,432	7,371	0,312	8,420	10,105	1,666	0,354
13,0	5,725	7,708	0,668	13,602	0,760	1,890	9,167	7,428	2,966	2,635	1,411	0,431	8,915	0,534	1,106
15,0	0,863	7,035	0,479	14,518	6,550	1,080	4,183	4,366	0,038	3,428	0,088	0,636	10,504	0,277	2,836
18,0	11,046	8,210	3,345	6,728	1,491	0,146	3,480	2,083	1,311	1,743	1,214	4,197	26,693	0,128	0,076
20,0	19,323	7,327	7,975	0,960	0,358	0,155	0,412	8,049	0,208	3,774	1,913	2,872	22,431	2,501	3,376
23,0	19,446	7,938	14,052	4,112	1,726	0,015	0,040	7,006	2,708	0,296	2,509	6,533	20,112	3,898	2,411
25,0	22,812	8,133	17,602	4,312	0,464	1,624	0,073	0,770	2,841	5,587	2,709	4,514	21,328	0,630	2,451
28,0	31,104	5,666	18,733	6,933	2,674	1,548	0,338	1,643	7,532	1,038	1,455	3,546	27,318	1,281	0,240
30,0	17,404	6,728	16,460	1,297	0,677	0,137	0,372	0,171	1,485	4,217	0,384	0,756	36,711	0,607	0,050
40,0	10,482	18,926	3,626	1,425	0,678	1,452	0,497	0,618	0,156	2,967	1,371	0,156	25,616	0,151	0,308
50,0	32,732	28,052	16,099	1,322	0,126	0,152	0,865	0,402	1,429	2,332	2,560	0,233	32,159	0,690	0,533

Commas indicate decimal points.

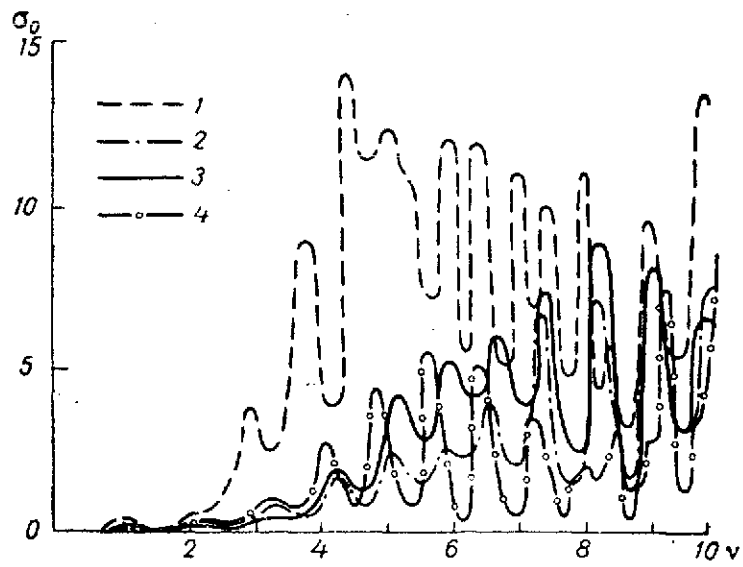

Figure 5.27. Effective Area of Radar Scatter δ_0 of Homogeneous Hailstones Having A Density of 0.916 g/cm^3 (1) and 0.600 g/cm^3 (2) and A Bilayer Hailstone Having A Layer Density of ρ_2 = 0.916 g/cm^3, ρ_1 = 0.600 g/cm^3 When $\frac{b_2}{b_1}$ = 0.5 (3) and $\frac{b_2}{b_1}$ = 0.8 (4).

TABLE 5.15. VALUES OF σ_0 OF A TWO-LAYER HAILSTONE FOR DIFFERENT COMBINATIONS OF DENSITIES OF THE CORE (ρ_2) AND SHELL (ρ_1) AT $\frac{b_2}{b_1}$ = 0.90, 0.96 AND 1.00, t = 0°C. /214

	$\rho_2=0{,}916$ g/cm^3, $\rho_1=0{,}600$ g/cm^3		$\rho_2=0{,}916$ g/cm^3, $\rho_1=0{,}380$ g/cm^3		$\rho_2=0{,}600$ g/cm^3, $\rho_1=0{,}380$ g/cm^3		$\rho_2=0{,}380$ g/cm^3, $\rho_1=0{,}600$ g/cm^3		$\rho_2=0{,}380$ g/cm^3, $\rho_1=0{,}916$ g/cm^3		$\rho_2=0{,}600$ g/cm^3, $\rho_1=0{,}916$ g/cm^3		$\rho=0{,}916$ g/cm^3	$\rho=0{,}600$ g/cm^3	$\rho=0{,}380$ g/cm^3
	$\frac{b_2}{b_1}=0{,}90$	$\frac{b_2}{b_1}=0{,}96$	$\frac{b_2}{b_1}=0{,}90$	$\frac{b_2}{b_1}=0{,}96$	$\frac{b_2}{b_1}=0{,}90$	$\frac{b_2}{b_1}=0{,}96$	$\frac{b_2}{b_1}=0{,}90$	$\frac{b_2}{b_1}=0{,}96$	$\frac{b_2}{b_1}=0{,}90$	$\frac{b_2}{b_1}=0{,}96$	$\frac{b_2}{b_1}=0{,}90$	$\frac{b_2}{b_1}=0{,}96$	$\frac{b_2}{b_1}=1{,}00$	$\frac{b_2}{b_1}=1{,}00$	$\frac{b_2}{b_1}=1{,}00$
0,1	0,000	0,000	0,000	0,000	0,000	0,000	0,000	0,000	0,000	0,000	0,000	0,000	0,000	0,000	0,000
0,3	0,004	0,005	0,004	0,005	0,002	0,002	0,001	0,001	0,002	0,002	0,003	0,003	0,005	0,002	0,001
0,5	0,028	0,031	0,025	0,030	0,013	0,015	0,009	0,007	0,012	0,009	0,024	0,017	0,033	0,016	0,007
0,8	0,186	0,204	0,163	0,194	0,080	0,089	0,050	0,043	0,069	0,050	0,121	0,106	0,217	0,096	0,038
1,0	0,442	0,482	0,389	0,459	0,183	0,203	0,109	0,094	0,149	0,109	0,269	0,238	0,511	0,218	0,084
3,0	0,408	4,592	3,708	4,352	3,111	3,300	1,199	1,723	2,659	2,008	3,789	3,564	4,896	3,412	1,555
5,0	1,492	1,531	1,780	1,444	3,583	3,746	3,849	3,582	4,654	3,880	3,535	3,959	2,188	3,916	3,374
8,0	2,779	2,568	2,538	2,569	1,690	1,581	3,501	3,624	2,804	3,410	1,982	1,801	2,834	1,792	3,506
10,0	2,040	2,382	1,891	2,263	2,434	2,737	2,319	2,351	1,591	2,314	2,799	3,189	2,397	2,868	2,523
13,0	2,359	1,974	1,994	2,169	2,164	2,113	2,093	1,932	2,231	2,166	1,847	2,003	1,977	2,280	1,704
15,0	2,660	2,510	2,207	2,618	1,956	1,989	2,476	2,556	2,684	2,744	2,448	2,335	2,575	1,999	2,425
18,0	2,106	2,039	1,972	1,971	2,571	2,607	2,442	2,619	2,025	2,556	2,241	2,469	2,314	2,458	2,668
20,0	2,524	2,262	2,365	2,336	2,178	1,931	1,919	2,319	1,809	2,009	2,132	2,053	2,322	2,047	2,363
23,0	2,231	2,478	2,112	2,197	2,435	2,302	2,026	2,185	2,532	2,049	2,358	2,543	2,348	2,419	1,854
25,0	2,197	2,224	2,435	2,040	2,388	2,368	2,390	2,290	2,341	2,430	2,001	2,084	2,057	2,251	2,153
28,0	2,331	2,274	2,381	2,424	2,079	2,035	2,292	2,490	2,065	2,260	2,373	2,283	2,234	2,204	2,483
30,0	2,052	2,073	2,347	2,048	2,407	2,385	2,023	2,128	2,088	2,084	2,120	2,292	2,161	2,356	2,229
40,0	2,273	2,330	2,122	2,190	2,082	2,063	1,991	1,102	2,202	1,986	2,336	2,202	2,173	2,058	2,196
50,0	2,135	2,085	2,208	2,176	2,182	2,218	1,932	2,106	2,325	2,022	2,065	2,033	2,101	2,170	2,187

Commas indicate decimal points.

Analysis of the σ_2 curve (Figure 5.28) shows that the dependence of the attenuation cross-section of the two-layer hailstone with the indicated layer densities on the thickness of the shell is much less pronounced than the dependence of σ_0. Thus, softening of the outer layer with $h_{sh} = 0.2\ b_1$ does not effect the magnitude of σ_2 with an accuracy of 30%.

A further increase of the less dense shell in the range $\nu \leqslant 3.5$ leads to a decrease in σ_2 to the values of a solid hailstone with $\rho = \rho_1 = 0.600$ g/cm^3, and increases by a factor of 1-2 in the range $3.5 < \nu < 6.5$ σ_2.

For $\nu > 6.5$, the σ_2 curves of hailstones with $\frac{b_2}{b_1}$, equal to 0.8 and 0.5 are oscillatory in character, asymptotically approaching one another. At $\nu > 15$, the factor for two layers may be neglected and σ_2 may be assumed to be the same as in the homogeneous hailstone.

$\rho_2 = 0.916$; $\rho_1 = 0.380$. As is evident from Table 5.14, for $1 < \nu < 15$ the σ_0 curve for the hailstone with $h_{sh} = 0.04\ b_1$ undergoes slight oscillations

about the curve for the homogeneous hailstone with $\rho = 0.916$ g/cm^3, whereas at $\nu > 15$ this shell substantially decreases the magnitude of radar scattering (for example, at $\nu = 20$ σ_0 it decreases by a factor of 22), particulary at $\nu > 30$, and σ_0 approaches the σ_0 values of the hailstone with $\rho = 0.380$ g/cm^3. As h_{sh} increases to 0.10 b_1, σ_0 at $1 < \nu < 20$ basically decreases, and at $\nu \geqslant 20$, increases and occupies an intermediate position between $h_{sh} = 0.04$ b_1 and $h_{sh} = 0.00$ b_1. An increase in the thickness of the softer shell by a factor of 2.5 (to 0.10 b_1) leads at $\nu \geqslant 20$ to a substantial increase of the radar scattering (for example, at $\nu = 20$, σ_0 increases by a factor of 8, and at $\nu = 50$, by a factor of 13). /21

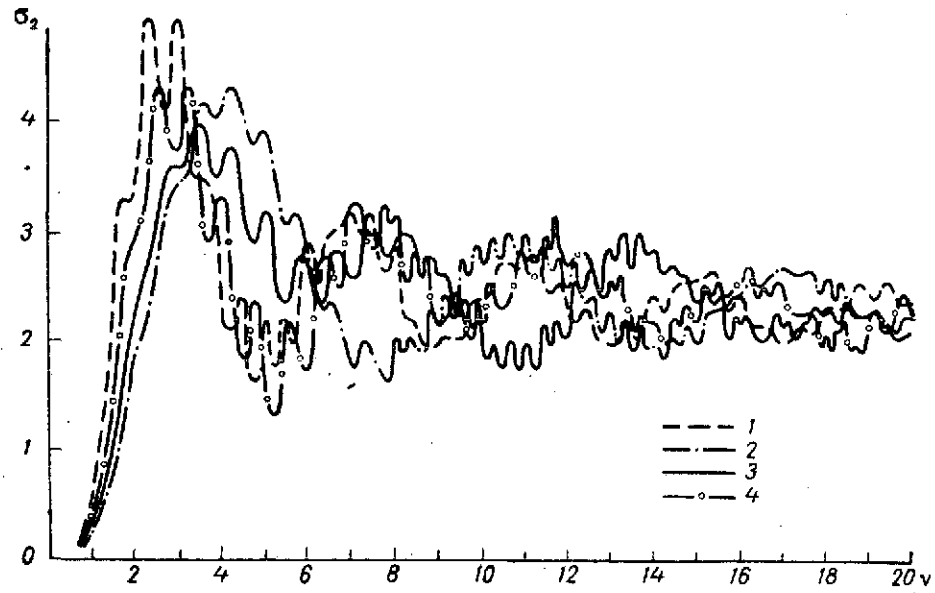

Figure 5.28. Effective Attenuation Area σ_2 of Homogeneous Hailstones With Densities of 0.916 g/cm^3 (1) and 0.600 g/cm^3 (2) and a Two-Layer Hailstone with Layer Densities $\rho_2 = 0.916$ g/cm^3, $\rho_1 = 0.600$ g/cm^3 for $\frac{b_2}{b_1} = 0.5$ (3) and $\frac{b_2}{b_1} = 0.8$ (4).

Figure 5.29 shows σ_0 curves of hailstones with a large h_{sh}: 0.2 b_1 and 0.5 b_1. It is evident that the σ_0 curve of the hailstone is $\frac{b_2}{b_1} = 0.8$ for $\nu > 1$ passes between the σ_0 curve of the homogeneous hailstone with $\rho = 0.916$

g/cm^3 and the σ_0 curve of the hailstone with $\frac{b_2}{b_1} = 0.5$, i.e., as the thickness of the shell increases from 0.2 b_1 to 0.5 b_1, σ_0 decreases, particularly at $9.5 < \nu < 15$. Moreover, the two-layer hailstone with $h_{sh} = 0.5\ b_1$ has approximately the same effect on the radar scattering as the homogeneous hailstone with $\rho = 0.380\ g/cm^3$.

The behavior of the effective attenuation area σ_2 is the same here (Figure 5.30) as in the preceding case. A characteristic feature of the layer density ratio under consideration is an increase in the oscillation amplitude of the curves and as a consequence, a somewhat greater difference in the values of σ_2 than in the preceding case (see Figure 5.28). /219

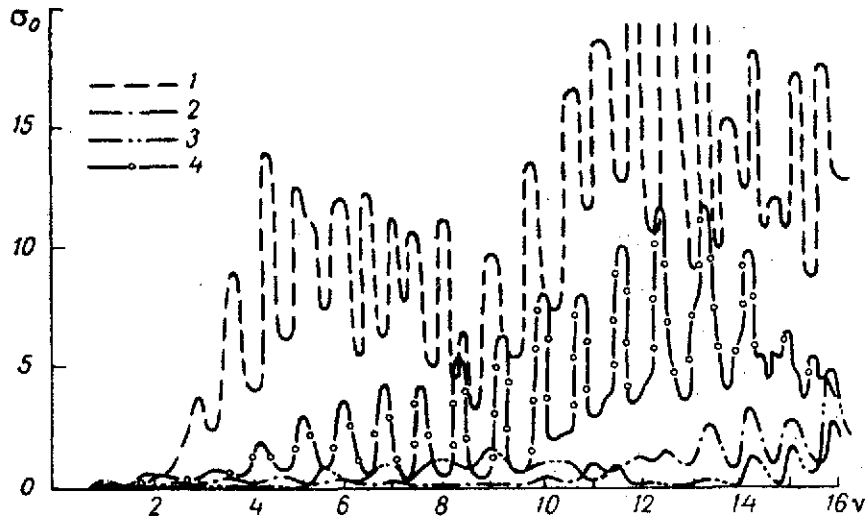

/218

Figure 5.29. Values of σ_0 of Homogeneous Hailstones with Densities of 0.916 g/cm^3 (1), 0.380 g/cm^3 (2) and a Two-Layer Hailstone with Layer Densities ρ_2 = = 0.916 g/cm^3, ρ_1 = 0.380 g/cm^3 at $\frac{b_2}{b_1} = 0.5$ (3) and $\frac{b_2}{b_1} = 0.8$ (4).

$\rho_2 = 0.600\ g/cm^3$; $\rho_1 = 0.380\ g/cm^3$. The magnitude of σ_0 at $h_{sh} = 0.04\ b_1$ and $1 < \nu < 8$ is smaller, and at $\nu > 8$ oscillates about the corresponding σ_0 values of the homogeneous hailstone with $\rho = 0.600\ g/cm^3$. As the shell

thickness increases to 0.10 b_1, σ_0 at $0 < \nu < 13$ decreases, and at $\nu > 13$ occupies an intermediate position between σ_0 for the cases $\frac{b_2}{b_1} = 0.96$ and $\frac{b_2}{b_1} = 1$.

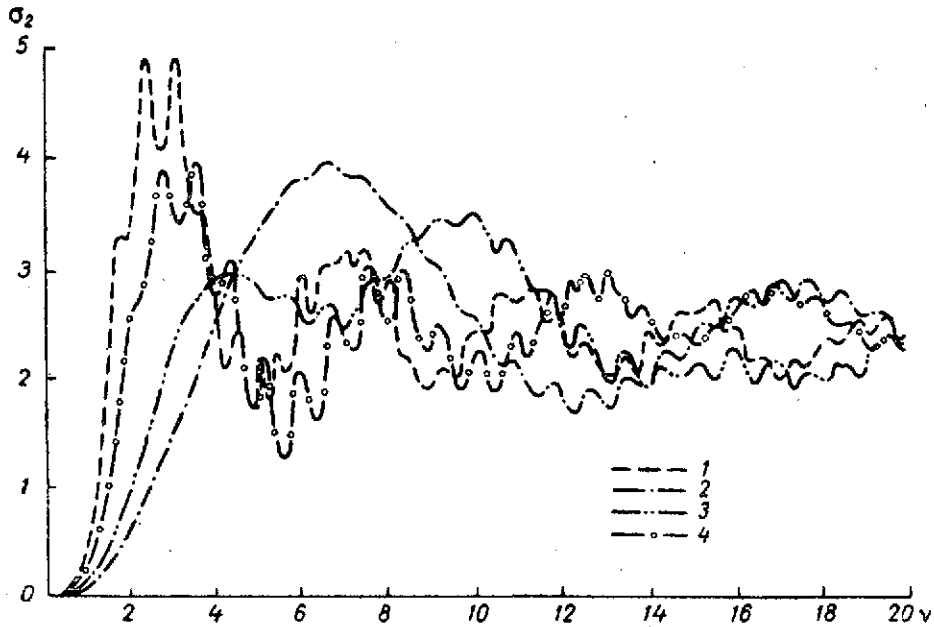

Figure 5.30. σ_2 of Homogeneous Hailstones with Densities of 0.916 g/cm^3 (1), 0.380 g/cm^3 (2), and of a Two-Layer Hailstone with Layer Densities $\rho_2 = 0.916$ g/cm^3, $\rho_1 = 0.380$ g/cm^3 of Thickness $\frac{b_2}{b_1} = 0.5$ (3) and $\frac{b_2}{b_1} = 0.8$ (4).

Figure 5.31 shows σ_0 curves for a shell thickness of 0.2 b_1 and 0.5 b_1 and $\nu < 10.5$. For $\nu > 10.5$, there is a marked oscillation of σ_0, which at $\nu > 10.5$ and $h_{sh} = 0.2\ b_1$ causes the radar reflection to be considerably exceeded in comparison with $h_{sh} = 0.0\ b_1$ for a very wide range of ν.

While it should be noted also that $h_{sh} = 0.5\ b_1$ and $\nu \leqslant 20$, in contrast to the other pairs of densities examined above, it cannot be stated that σ_0 is close to the values corresponding to a homogeneous sphere with $\rho = 0.380$ g/cm^3.

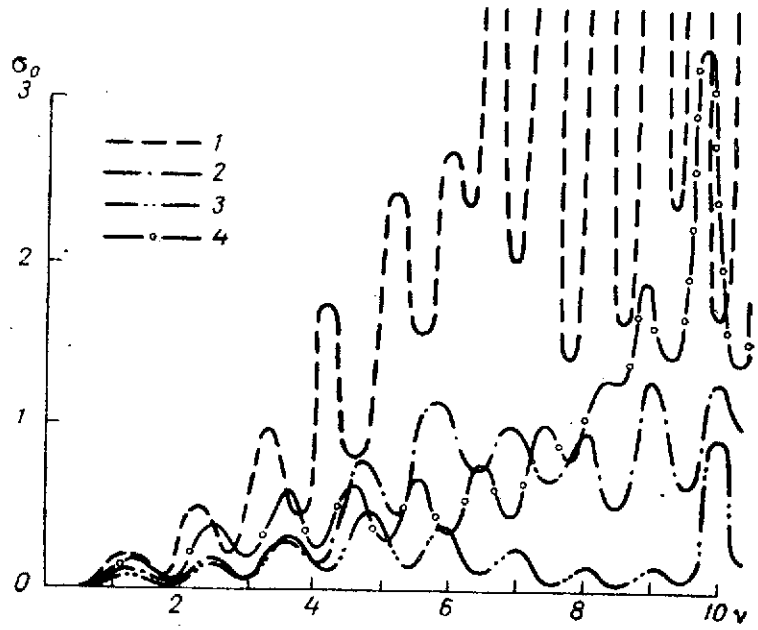

Figure 5.31. σ_0 of Homogeneous Hailstones with Densities of 0.600 g/cm^3 (1) and 0.380 g/cm^3 (2) and of a Two-Layer Hailstone with Layer Densities ρ_2 = 0.600 g/cm^3, ρ_1 = 0.380 g/cm^3 of Thickness $\frac{b_2}{b_1}$ = 0.5 (3) and $\frac{b_2}{b_1}$ = 0.8 (4).

Calculations show that the lower the layer densities, the more oscillatory /220 the variations of σ_0 with ν.

Analysis of the attenuation cross-section σ_2 (Figure 5.32), however, leads to the conclusion that the oscillation amplitudes of the corresponding curves decrease. From Figure 5.32 it is also evident that a shell less than 0.2 b_1 thick has practically no effect on the σ_2 values, whereas the magnitude of σ_2 of the hailstone with the ratio $\frac{b_2}{b_1}$ = 0.5 at $\nu \leqslant 5$ is the same as σ_2 of a homogeneous hailstone with $\rho = \rho_1$ = 0.380 g/cm^3. In contrast, in the range $9 < \nu < 15$, the hailstone with $\frac{b_2}{b_1}$ = 0.5 attenuates the radio waves in the same way as a homogeneous hailstone with $\rho = \rho_2$ = 0.600 g/cm^3. The σ_2 curves for the densities considered at all ν differ by not more than 80%. Analysis of results of the calculation of σ_2 for hailstones with shells of large thickness

(over 0.75 b_1) for all the pairs of densities considered shows that at $h_{sh} \geqslant$ $\geqslant 0.75\ b_1$, such hailstones may be considered homogeneous with densities equal to the densities of the shells.

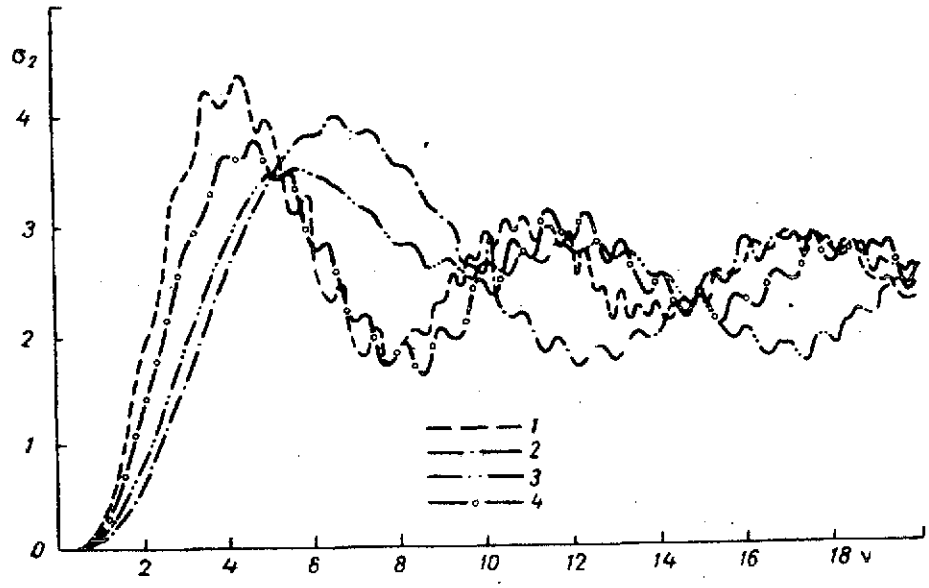

Figure 5.32. σ_2 of Homogeneous Hailstones with Densities of 0.600 g/cm^3 (1), 0.380 g/cm^3 (2) and of a Two-Layer Hailstone with Layer Densities ρ_2 = 0.600 g/cm^3, ρ_1 = 0.380 g/cm^3 of Thickness $\frac{b_2}{b_1}$ = 0.5 (3) and $\frac{b_2}{b_1}$ = 0.8 (4).

In order to establish the dependence of the radar properties of a hailstone on the shell density ρ_1 at constant core density ρ_2 = 0.916 g/cm^3, it is necessary to compare the curves for ρ_1 = 0.380 g/cm^3 and ρ_1 = 0.600 g/cm^3, corresponding to the two ratios $\frac{b_2}{b_1}$: 0.8 and 0.5. /22

It follows from the comparison that at $h_{sh} = 0.2\ b_1$ for $10 < \nu < 16$, to a smaller ρ_1 there corresponds a smaller σ_0, whereas for the remaining ν, the curves oscillate relative to one another. If however h_{sh} reaches 0.5 b_1, then at $1 < \nu \leqslant 14$, $\nu = 19$, to a larger ρ_1 there corresponds a smaller σ_0, with the exception of the range for $14 < \nu < 19$, where the curves are oscillatory in nature.

A difference in the shell densities of the hailstones with $\frac{b_2}{b_1} = 0.8$ has no effect on σ_2 and the range of 15-25% of its magnitude, whereas at $\frac{b_2}{b_1} = 0.5$ the dependence is more complex: in the ranges $\nu \leqslant 6$; $12 < \nu < 15$, a denser shell has larger σ_2 values (by 20-80%) associated with it, and at $8 < \nu < 12$, vice versa. In the remaining range of ν, the σ_2 values coincide with an accuracy not in excess of 20%.

Comparison of σ_0 and σ_2 curves at constant $\rho_1 = 0.380$ g/cm^3 and variable ρ_2 makes it possible to determine the effect of core density on the values of the radar scattering and attenuation cross-sections. Thus, at $h_{sh} = 0.2\ b_1$ for essentially all ν, a larger ρ_2 has a larger σ_0 associated with it. When the shell thickness increases to $0.5\ b_1$, this property is preserved, but starting at $\nu > 7$.

For the hailstone with $\frac{b_2}{b_1} = 0.8$ at the same densities of the core (0.916 and 0.600 g/cm^3) and shell (0.380 g/cm^3), to a larger ρ_2 there corresponds a larger effective attenuation area (20-40%) only in the range $\nu \leqslant 4$.

For $\nu > 4$, the opposite dependence is observed up to $\nu = 9$, beyond which the core density of the hailstone with $\frac{b_2}{b_1} = 0.8$ has no substantial effect on the magnitude of σ_2. As the shell thickness increases, the σ_2 values of the layered and homogeneous hailstones come closer together. For example, at $\frac{b_2}{b_1} = 0.5$ and $\nu < 5$, the core density, which substantially exceeds the shell density, plays practically no part at all, and the corresponding curves coincide with the curve of the homogeneous hailstone of the same size with $\rho = \rho_1 = 0.380$ g/cm^3.

Layered Hailstone with $\rho_1 > \rho_2$. Let us now consider the properties of a hailstone with the same densities (but taken in reverse order) and relative layer dimensions as in the case $\rho_1 < \rho_2$. Analyzing the data of Tables 5.14 and 5.15, corresponding to the condition $\rho_1 > \rho_2$, we come to the conclusion that the appearance on the hailstone of a harder layer (for example, as a result of icing over), not more than $0.1\ b_1$ thick has practically no effect on σ_0 at $\nu \leqslant 1$ and on σ_2 at any ν.

Combining this result with what was stated for the case $\rho_1 < \rho_2$, one can assert that $h_{sh} \leqslant 0.1\ b_1$, from the standpoint of radar scattering for $\nu \leqslant 1$ and attenuation for all ν, a two-layer hailstone may be considered homogeneous with $\rho = \rho_2$. /222

$\rho_2 = 0.380\ g/cm^3$, $\rho_1 = 0.600\ g/cm^3$. For $\nu > 1$, as the rule, a shell 0.04 b_1 thick causes an increase in σ_0 (in comparison with the homogeneous hailstone with $\rho = 0.380\ g/cm^3$), that is very substantial at certain ν (for example, at $\nu = 13$, σ_0 increases by a factor of 7, and at $\nu = 18$, by a factor of 30). A further increase in shell thickness to 0.1 b_1 leads to an even greater increase in the magnitude of back scattering, to approximately $\nu = 18$, after which σ_0 approaches its asymptotic values. This phenomenon is associated with a sharp decrease in the magnitude of radar scattering (for example, at $\nu = 20$, σ_0 decreases by a factor of 20, and at $\nu = 23$, by a factor of 175). Calculations show that starting at $\nu = 60$, the magnitudes of σ_0 for the indicated thicknesses differ by their limiting values.

If $\nu \leqslant 3.5$, the difference in σ_0 of the layered hailstone with $\frac{b_2}{b_1}$ equal to 0.8 and 0.5 and of a homogeneous hailstone with $\rho = 0.600\ g/cm^3$ is insignificant; if however at $3.5 < \nu < 7$, than as h_{sh} increases from 0.2 b_1 to 0.5 b_1, the value of σ_0 diminishes, approaching those of radar scattering of a homogeneous hailstone whose density is equal to that of the shell.

For $7 \leqslant \nu \leqslant 16.5$, the σ_0 curve of hailstones with $\frac{b_2}{b_1} = 0.8$ oscillates about the σ_0 values of a homogeneous hailstone with $\rho = 0.600\ g/cm^3$ and of a two-layer hailstone with $\frac{b_2}{b_1} = 0.5$, substantially exceeding them in certain regions (for example, $8 < \nu < 11$). Let us note that an increase in h_{sh} to 0.5 b_1 causes a decrease in radar scattering to σ_0 values of the homogeneous hailstone with $\rho = 0.600\ g/cm^3$. Hence it may be concluded that a layered hailstone with a shell 0.5 b_1 thick and the given densities has the same magnitude of backscattering as a hailstone with a density equal to that of the shell.

Curve σ_2 (Figure 5.33) of the shell with $\frac{b_2}{b_1} = 0.8$ occupies an intermediate position between the σ_2 curves of homogeneous hailstones with $\rho = 0.600\ g/cm^3$ and $\rho = 0.380\ g/cm^3$, and at $\nu > 6$ it has a tendency to approach the corresponding

curve for the hailstone with density 0.380 g/cm^3. A further increase in the thickness of the denser shell to 0.5 b_1 causes the two-layer hailstone with $\nu \leqslant 7$ to attenuate electromagnetic radiation to the same extent as the homogeneous hailstone with ρ = 0.600 g/cm^3. For large ν, the curves exhibit a complex oscillatory character.

ρ_2 = 0.380 g/cm^3; ρ_1 = 0.916 g/cm^3. As is evident from Table 5.14, the presence on the hailstone of the harder shell 0.04 b_1 thick for $\nu > 1$ leads to an appreciable increase in oscillations and an overall increase in σ_0, this /223
increase in certain ranges of ν being much greater than in the case of σ_0 of the hailstone with ρ_2 = 0.380 g/cm^3 and ρ_1 = 0.600 g/cm^3, this being apparently due to the higher density of its shell. As h_{sh} increases further to 0.1 b_1, the σ_0 values become much larger than σ_0 of the homogeneous hailstone of density 0.380 g/cm^3, and much lower than σ_0 of the hailstone with ρ = 0.916 g/cm^3.

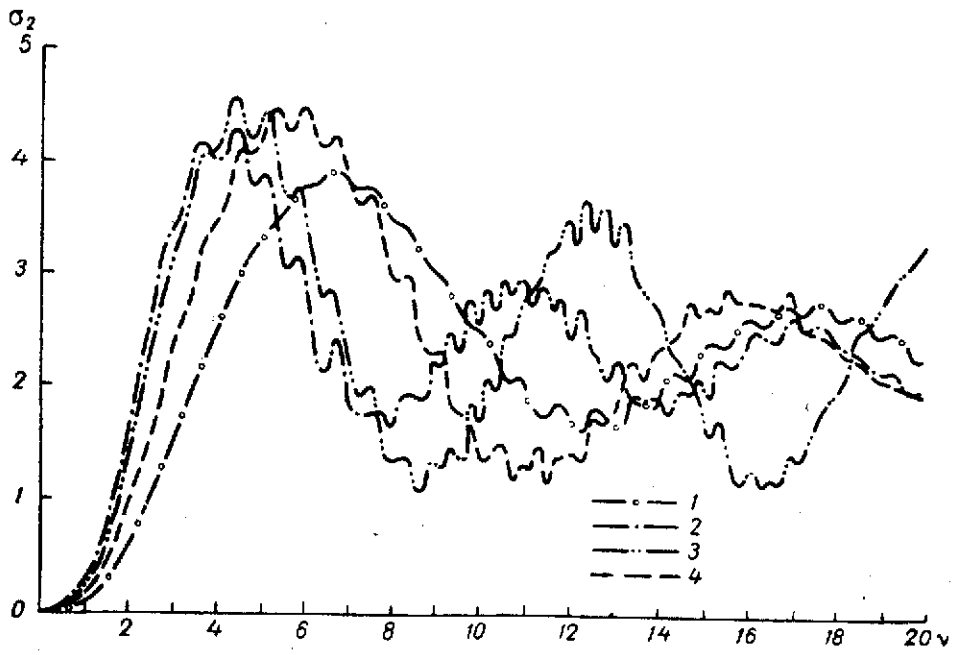

Figure 5.33. σ_2 of Homogeneous Hailstones with Densities 0.380 g/cm^3 (1), 0.600 g/cm^3 (2) and a Two-Layer Hailstone with Layer Densities ρ_2 = 0.380 g/cm^3, ρ_1 = 0.600 g/cm^3 of Thickness $\frac{b_2}{b_1}$ = 0.5 (3) and ρ_2 = 0.8 (4).

Figure 5.34 illustrates the behavior of a two-layer hailstone with $\frac{b_2}{b_1}$ equal to 0.8 and 0.5 for $\nu < 10$. It is evident that in the range $5.5 < \nu < 7.5$ the two-layer hailstone with $\frac{b_2}{b_1} = 0.8$ scatters backward much more energy than than the homogeneous hailstone with $\rho = 0.916$ g/cm^3. An increase in shell thickness from $0.2\ b_1$ to $0.5\ b_1$ results in a decrease in backscattering only at $\nu < 5$. Further, up to $\nu \sim 10$, the σ_0 values of hailstones with shells of both thicknesses are practically the same.

For $\nu > 10$, the σ_0 curve of the hailstone with $\frac{b_2}{b_1} = 0.8$ is practically the same as the σ_0 curve of the hailstone with $\rho = 0.380$ g/cm^3, while the curve for $\frac{b_2}{b_1} = 0.5$ substantially predominates over them both only in the range $10 < \nu < 13.5$.

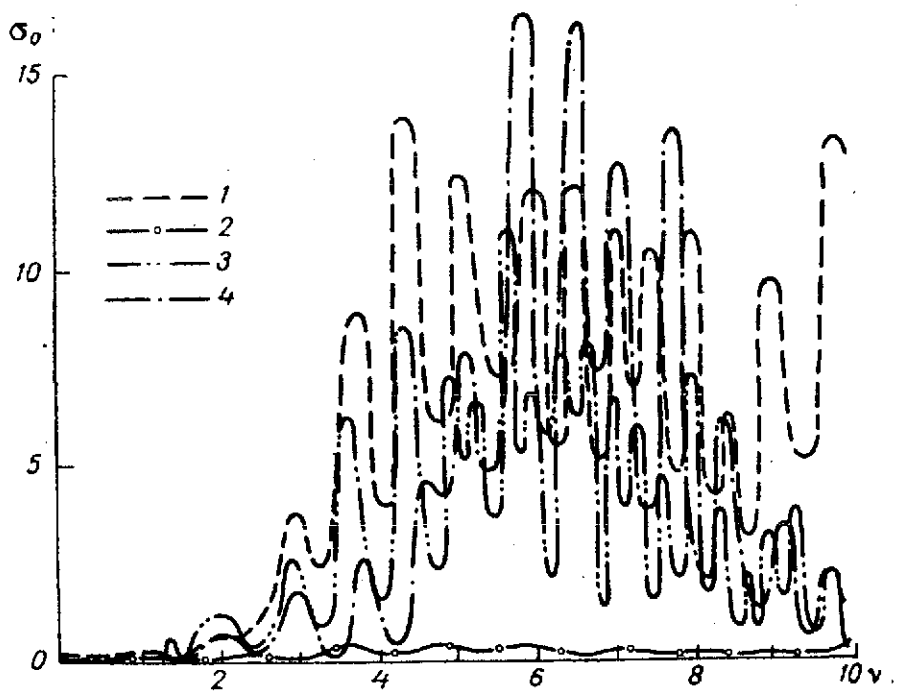

Figure 5.34. σ_2 of Homogeneous Hailstones with Densities 0.916 g/cm^3 (1), 0.380 g/cm^3 (2) and of a Two-Layer Hailstone with Layer Densities $\rho_2 = 0.380$ g/cm^3, $\rho_1 =$ $= 0.916$ g/cm^3 of Thickness $\frac{b_2}{b_1} = 0.5$ (3) and $\frac{b_2}{b_1} = 0.8$ (4).

It should be noted that for large ν, the difference between the homogeneous hailstone with $\rho = 0.916$ g/cm^3 and the two-layer with $\frac{b_2}{b_1} = 0.5$ is very substantial.

The effective attenuation area (Figure 5.35) of the hailstone with a shell $0.5\ b_1$ thick for $\nu < 3$ coincides with σ_2 of the homogeneous hailstone of density 0.916 g/cm^3. Comparing this case with the preceding one (see Figure 5.33), we see that a compaction of the shell, its thickness being the same, leads to a decrease in the limits of variation of ν within which the layered hailstone attenuates electromagnetic waves to the same extent as the homogeneous hailstone with $\rho = \rho_1$. In the range $4 \leqslant \nu \leqslant 6$, the hailstone with shell thickness $0.2\ b_1$ attenuates radio waves 3-5 times more than the hailstone with /225 $h_{sh} = 0.5\ b_1$, and at $6 \leqslant \nu \leqslant 10$, the same number of times less.

$\rho_2 = 0.600$ g/cm^3; $\rho_1 = 0.916$ g/cm^3. In this case, in contrast to those already discussed, the presence of a thin shell $\sim 0.04\ b_1$ thick and its increase have less effect on the radar scattering, this being due to a much smaller difference in the densities of the shell and the core.

Figure 5.36 shows σ_0 curves of hailstones with shells $0.2\ b_1$ and $0.5\ b_1$. For $\nu < 3$, the difference in shell thickness does not affect the radar scattering, and σ_0 is practically the same as σ_0 of a homogeneous sphere with $\rho = 0.916$ g/cm^3; at $9 < \nu < 15$, to a larger h_{sh} there corresponds a larger σ_0, and at $15 < \nu < 18$, a smaller σ_0. For $\nu > 18$, at both thicknesses, the curves approach the curve for $\rho = 0.600$ g/cm^3.

The character of the behavior of the attenuation cross-section σ_2 in this case is basically the same as in the preceding case.

Analysis of the calculations shows, as in the case $\rho_2 > \rho_1$, that for all the indicated combinations of density pairs, the layered hailstone with shells of large thickness ($h_{sh} \geqslant 0.75\ b_1$) may be regarded as a homogeneous hailstone /226 whose density is equal to that of the shell.

In order to determine the dependence of the radar properties of the hailstone on the core density, it is necessary to compare the σ_0 and σ_2 curves of the hailstones with $\rho_1 = 0.916$ g/cm^3, $\rho_2 = 0.600$ g/cm^3 and $\rho_2 = 0.380$ g/cm^3 (Figures 5.34, 5.36, 5.37). Thus, at $h_{sh} = 0.2\ b_1$ up to $\nu \sim 9$, the σ_0 curves oscillate relative to one another. For $\nu > 9$, to a denser core there

corresponds a much larger σ_0, whereas at $\nu > 20$, both curves approach their asymptotic values and differ little from each other. When the shell thickness is 0.5 b_1, the effect of core density on backscattering is less evident, this being due to the properties noted above. The establishment of oscillations about the asymptotic values for $h_{sh} = 0.5\ b_1$ also occurs somewhat earlier here, i.e., at $\nu \sim 16$.

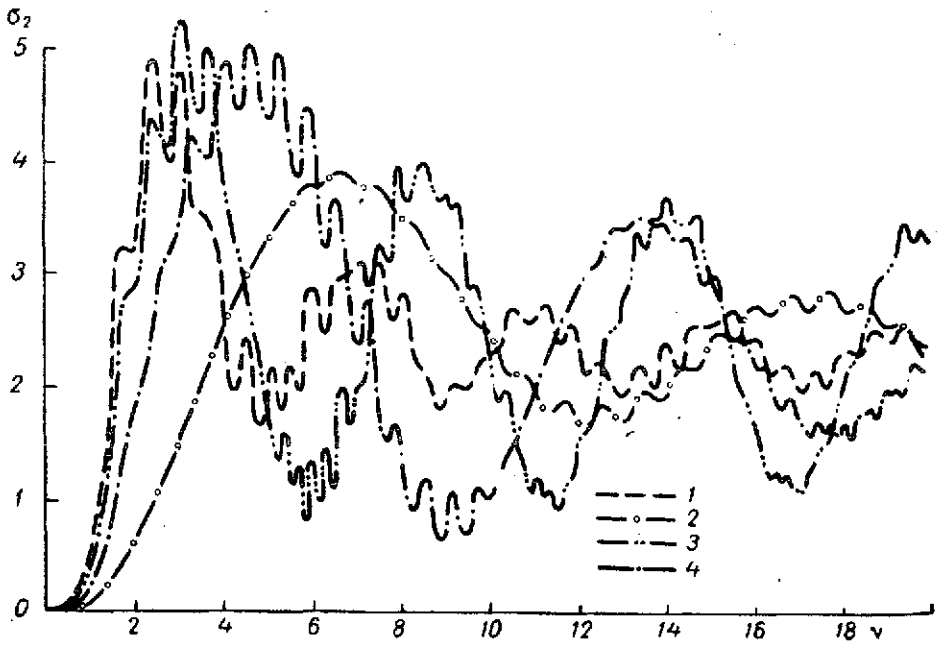

Figure 5.35. σ_2 of Homogeneous Hailstones with Densities 0.916 g/cm^3 (1) and 0.380 g/cm^3 (2) and of a Two-Layer Hailstone with Layer Densities ρ_2 = 0.380 g/cm^3, ρ_1 = = 0.916 g/cm^3 of Thickness $\frac{b_2}{b_1}$ = 0.5 (3) and $\frac{b_2}{b_1}$ = 0.8 (4).

Analysis of σ_2 curves shows that at $\frac{b_2}{b_1} = 0.8$, the core density does not play any role to within ±25% only at $\nu > 7$. However for larger ν, the σ_2 values at core densities of 0.380 and 0.600 g/cm^3 and a constant shell density ρ_1 = 0.916 g/cm^3 may differ by a factor of 2.5-3. For the case $\frac{b_2}{b_1} = 0.5$, the effect of core density decreases substantially (Figure 5.37).

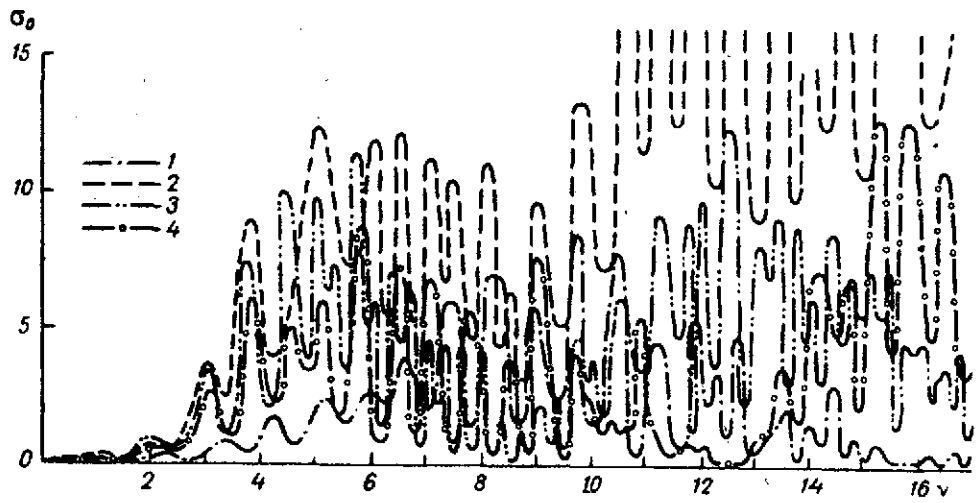

Figure 5.36. σ_0 of Homogeneous Hailstones with Densities 0.600 g/cm^3 (1), 0.916 g/cm^3 (2) and of a Two-Layer with Layer Densities ρ_2 = 0.600 g/cm^3, ρ_1 = 0.916 g/cm^3 of Thickness $\frac{b_2}{b_1}$ = 0.5 (3) and $\frac{b_2}{b_1}$ = 0.8 (4).

This one compares the dependence of σ_0 on the shell density ρ_1 at constant core density, one can note that at $h_{sh} = 0.2\ b_1$ for $1.5 < \nu < 7.5$, σ_0 of the hailstone with the shell density ρ_1 = 0.916 g/cm^3 is approximately twice as large as the radar scattering of the hailstone with a shell of lower density ρ_1 = 0.600 g/cm^3, and in the range $7.5 < \nu < 14$, almost one-half as large. At $\nu > 14$, the σ_0 values oscillate relative to one another, approaching the limiting magnitudes. /227

If however, $h_{sh} = 0.5\ b_1$, the character of radar scattering is basically preserved, with the exception of the range $7.5 < \nu < 14$, where the difference in the σ_0 values of hailstones with shells having densities of 0.916 g/cm^3 and 0.600 g/cm^3 decreases by a factor of 2-3 in comparison with the preceding case.

Comparison of σ_2 curves (Figures 5.33, 5.37) at ρ_2 = 0.380 g/cm^3 and variables ρ_1 = 0.600 g/cm^3 and ρ_1 = 0.916 g/cm^3 shows that as the shell thickness increases from 0.2 b_1 to 0.5 b_1, its effect on the magnitude of σ_2 increases sharply, chiefly at $\nu \geqslant 5$.

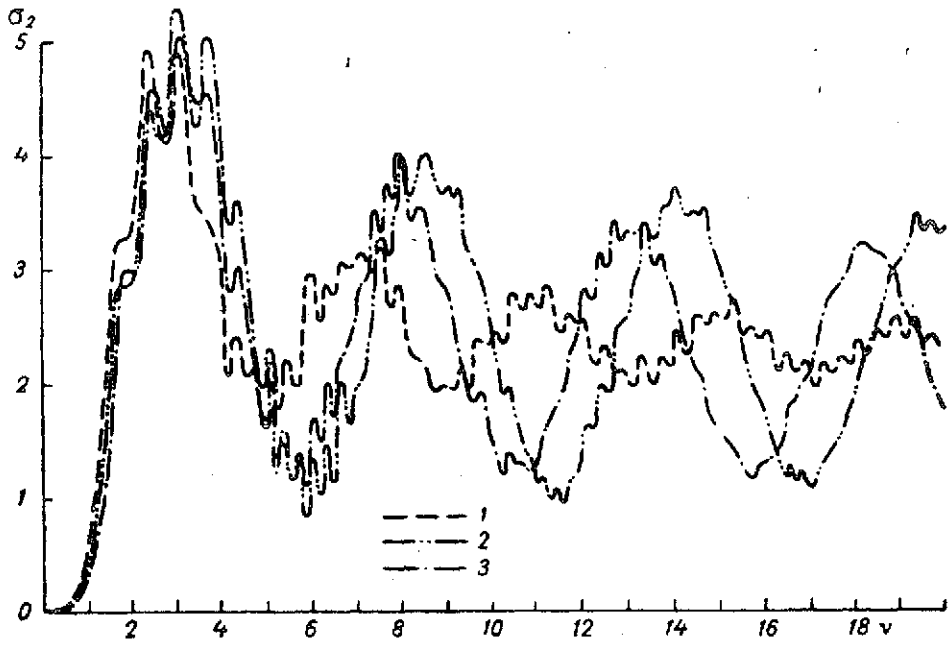

Figure 5.37. σ_2 of a Homogeneous Hailstone of Density 0.916 g/cm^3 (1) and a Two-Layer Hailstone with Shell Density ρ_1 = 0.916 g/cm^3 and Core Densities 0.380 g/cm^3 (2), 0.600 g/cm^3 (3). $\frac{b_2}{b_1} = 0.5$.

It should be noted that all of the above is essentially qualitative in character and may prove useful in a radar study of clouds and precipitation as well as in other problems.

Multilayer Hailstone. It was shown in § 5.1 that an actual hailstone is generally multilayered. In order to determine the extent to which the radar characteristics of a hailstone are effected by its layers (when there are more than two) of different densities, the effective areas of radar scattering σ_0 and attenuation σ_2 were calculated from exact diffraction formulas (1.277), (1.274), (1.248), (1.261)-(1.263) for a five-layer round hailstone with concentric layers. In the symbols of Chapter I (see Figure 1.5), the following was assumed in the calculations:[93] $b_5 = 0.65\ b_1$; $b_4 = 0.79\ b_1$; $b_3 = 0.89\ b_1$; $b_2 = 0.96\ b_1$ cm; $\rho_5 = 0.916$; $\rho_4 = 0.76$; $\rho_3 = 0.60$; $\rho_2 = 0.46$; /229

[93] b_j (j = 1, 2, 3, 4, 5) — radii of layers, $b_1 > b_2 > b_3 > b_3 > b_5$; ρ_5 — density of sphere of radius b_5, ρ_j — density of region between spheres of radii b_j and b_{j+1}, j = 4, 3, 2, 1.

$\rho_1 = 0.34$ g/cm^3; t = 0°C; $\nu = \frac{2\pi b_1}{\lambda}$; λ — wavelength of the lower portion of the centimeter range (see reference on page 212). The parameters of the layers were chosen on the basis of the experimental data cited in [228, 161-165] etc. The dielectric constants of ice of the corresponding density were chosen from Table 4.31.

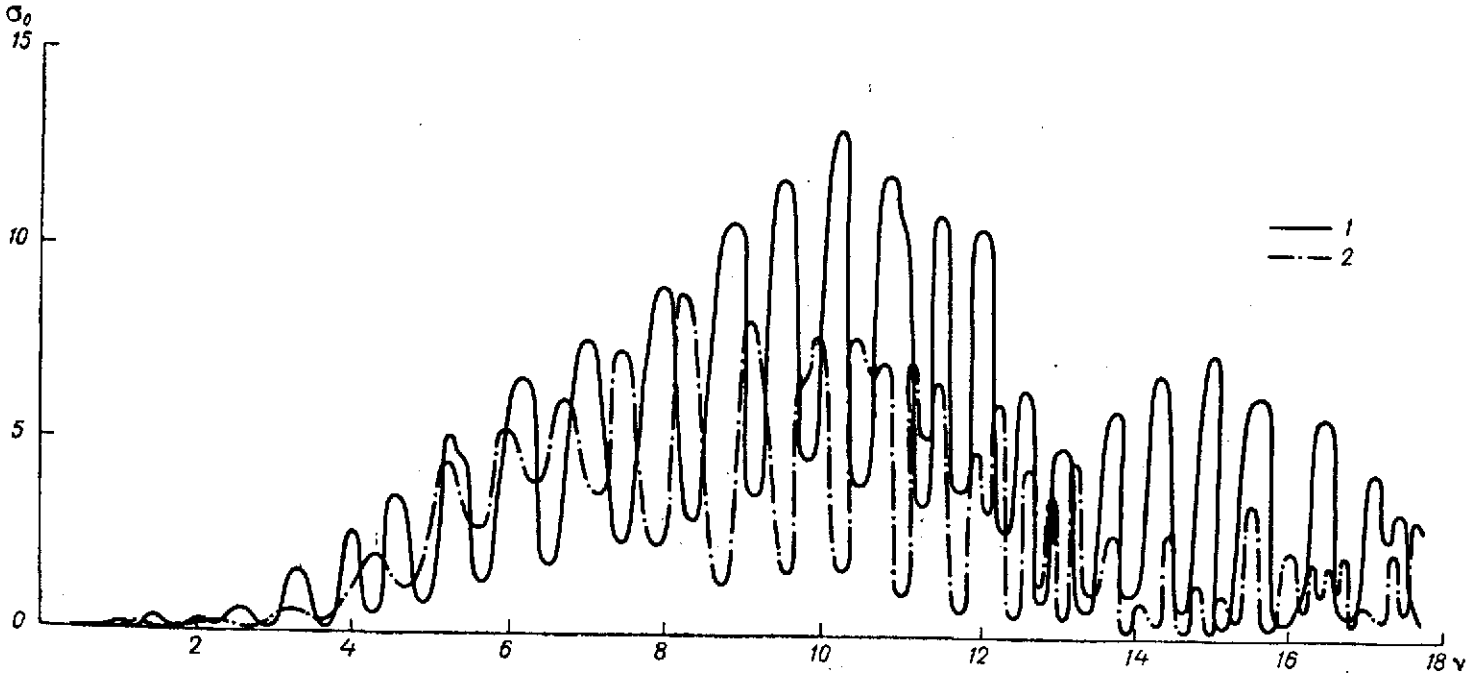

Figure 5.38. σ_0 of Five-Layer (1) and Two-Layer (2) Hailstones with $\rho_2 = 0.916$ g/cm^3, $\rho_1 = 0.600$ g/cm^3. $\frac{b_2}{b_1} = 0.5$. /228

Results of the calculation are given in Figures 5.38 and 5.39.

Illustrated for comparison are σ_0 and σ_2 curves of a two-layer hailstone with a shell density close to the mean square of the densities ρ_1, ρ_2, ρ_3, ρ_4 (0.56 g/cm^3).

It is obvious that such an approximation of the multilayer hailstone by a two-layer hailstone with averaging of the densities of all the layers beginning with the second gives a fairly good approximation from the standpoint of the radar characteristics. Thus, for all the ν considered, the magnitude of the effective attenuation area σ_2 of a multilayer hailstone differs from that of the two-layer hailstone by an average of not more than 30-50%. /230

Similar discrepancies are observed in the σ_0 values of these hailstones at $\nu < 9.5$. At greater ν, however, the oscillations and amplitudes of function σ_0 of the multilayer hailstone increase, and the discrepancies in the σ_0 values of the two-layer and multilayer hailstones increase. This is explained primarily by the fact that an increase in the number of layers of the hailstone generally has a substantial retarding effect on the tendency of the radar characteristics to reach their limiting values. It should also be noted at this point that the curves of the two-layer hailstone being compared have the $\frac{b_2}{b_1}$ parameter equal not to 0.65, but to 0.50, which also introduces the corresponding error (see Figures 5.27 and 5.28) into the final values of σ_0 and σ_2. Numerous calculations of σ_0 and σ_2 which we made for multilayer hailstones with different dimensions of the concentric layers and their densities show that the more layers the hailstone has and the smoother the transition in the values of their densities, the smaller the error of its approximation by a two-layer hailstone such as the one indicated above. The converse is also true. Thus, for some choice of the parameters of a three--layer hailstone, its σ_0 and σ_2 may differ by 400 to 600% from σ_0 and σ_2 of the two-layer hailstone corresponding to it. According to similar calculations, the discrepancies in σ_0 and σ_2 of a five to eight-layer hailstone with a core density of 1 g/cm^3 and with ρ_j = 80 to 100% ρ_{j+1} (and vice versa) from the two-layer hailstone corresponding to it are no greater than 20 to 45%.

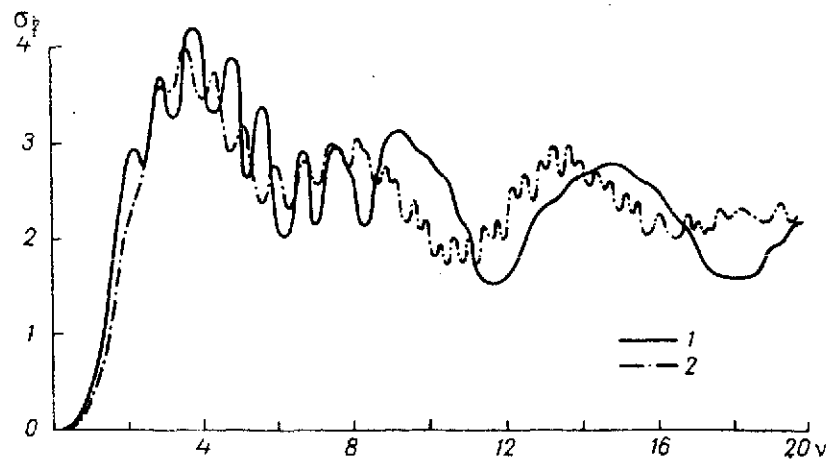

Figure 5.39. σ_2 of Five-Layer (1) and Two-Layer (2) Hailstones with ρ_2 = 0.916 g/cm^3, ρ_1 = 0.600 g/cm^3. $\frac{b_2}{b_1}$ = 0.5.

As was noted in § 5.1, actual hailstones frequently have a nonconcentric layered structure (see Figure 5.1). In order to determine the role of nonconcentricity in the arrangement of the layers, the exact diffraction formulas (1.230), (1.222), (1.240), (1.210), (1.90) were used to calculate the effective areas of radar scattering σ_0 and attenuation σ_2 for a three-layer spherical hailstone [12] with the following parameters of its layers (see Figures 1.1 and 1.4): $\frac{b_2}{b_1} = 0.8$; $\frac{b_3}{b_2} = 0.25$; $\frac{h_2}{b_2} = 0.125$; $\frac{h_3}{b_3} = 0.5$; $\chi_j = 0 = \vartheta_j$; (j = 1, 2); medium 0 — air; medium 1 — ice with density of 0.38 g/cm^3; medium 2 — ice with density of 0.60 g/cm^3; medium 3 — ice with density of 0.92 g/cm^3; λ = 3.21 cm; t = 0°C. /231

Results of the calculations are shown in Figure 5.40, 5.41.

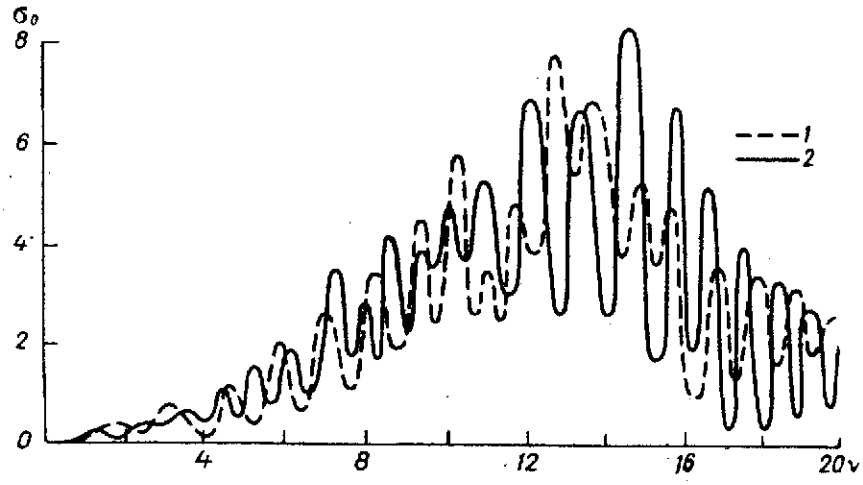

Figure 5.40. σ_0 of Three-Layer Hailstone for Concentric (1) and Nonconcentric (2) Arrangement of the Layers.

For comparison, the same figures include parts of σ_0 and σ_2 curves of a three-layer hailstone with concentric layers of the same density, formed by spheres of the same radii b_1, b_2, b_3, as in the case of a nonconcentrically layered hailstone.

It is evident from the figures that for radar scattering σ_0 at $\nu < 10$, the nonconcentricity of layers may be neglected to within 25%. In the range $\nu \geqslant 10$, the ratio of σ_0 values corresponding to the two cases of arrangement of the layers may reach 1.8-2.3.

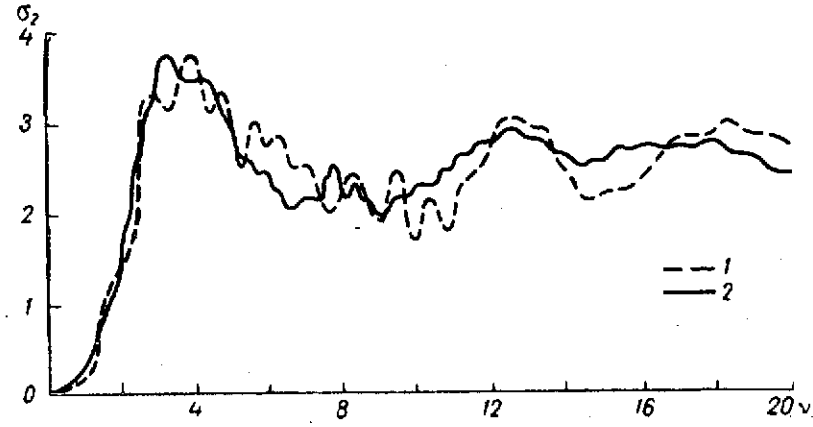

Figure 5.41. σ_2 of Three-Layer Hailstone for Concentric (1) and Nonconcentric (2) Arrangement of the Layers.

For the effective attenuation area, however, the difference in σ_2 values for all $\nu \leqslant 20$ does not exceed 20%. Such a comparatively moderate influence of nonconcentricity of the layers on a cross-section σ_0 and σ_2 should apparently be attributed only to the small values of the ratios $\frac{h_3}{b_3}$ and $\frac{h_2}{b_2}$.

Individual points of σ_0 and σ_2, calculated[94] with other, somewhat larger values of $\frac{h_3}{b_3}$ and $\frac{h_2}{b_2}$ show that they may differ by a factor of 2 to 5 from σ_0 and σ_2 of /231 a concentrically layered hailstone. Moreover, it should be noted that the dependence of σ_2 on the nonconcentricity of the layers is much less pronounced than the dependence of σ_0.

§ 5.5. Scattering and Attenuation of Microwaves By a Wet Hailstone

Wet Hailstone. In discriminating between hail and rain clouds with radar and studying the microstructure of hail clouds and other problems, of considerable interest is the investigation of the dependence of the scattering and attenuation characteristics of a wet hailstone on the thickness of the water film.

---

[94] For provided that $\chi_j = 0 = \vartheta_j$; $\lambda = 3.21$ cm, $t = 0°C$ and for the same densities and ratios $\frac{b_2}{b_1}, \frac{b_3}{b_2}$.

Some reflection aspects of these questions have been discussed in [229-232, 220, 146, 149, etc.], where it was shown that the presence of even a very thin surface film of water may appreciably affect the values of the back scattering cross-sections of the ice particles. However, these studies still do not provide a basis for a conclusion as to the manner in which the reflection and attenuation of radiowaves of various lengths take place on hailstones under natural conditions.

In order to supplement the known data by studying the cross-sections of radar and total scattering, and also the attenuation for wet ice spheres at film thicknesses occurring on hailstones during both their growth and melting, calculations were carried out [233, 234][95] to determine the dimensionless cross-sections of radar σ_0 and total σ_1 scatterings and also attenuation σ_2 over a wide range of particle sizes and wavelengths. The calculations were carried out by using the exact diffraction formulas (1.276), (1.273), (1.274), (1.281-1.283) for a two-layer (see Figure 1.6) spherical particle. The general symbols were retained here: b_2 — radius (in cm) of ice core with a density of 1 g/cm^3, b_1 — outer radius (in cm), equal to $b_1 + h_{sh}$ (h_{sh} being the thickness (in cm) of the water shell), $\nu = \frac{2\pi b_1}{\lambda}$. The temperature of the ice core and water film is assumed to be 0°C. The dielectric constants of water were chosen for the wavelengths 0.86, 3.2, 5.6, 11 and 17 cm from the appendix and those of ice from Table 4.33 after [136]. The film thickness was varied from 10^{-4} to 10^{-1} cm at each λ.

Figure 5.42 shows the dependence of σ_0 values of a wet hailstone on b_1 at different λ and h_{sh}. The curves for spheres of solid ice and water are also shown for comparison.

It is evident from Figure 5.42 that the presence on the ice sphere of a surface water film only 0.01 cm thick has an appreciable effect on σ_0, and the smaller λ, the greater the deviation from σ_0 values of equally large ice spheres; even at λ = 17.0 cm and h_{sh} = 0.01 cm, this deviation is rather substantial. /234

Hence, for the wavelengths used in meteorology, scattering by wet hailstones must not be treated as scattering by ice spheres. Because of large intervals between the individual calculated points and a marked oscillation, the curve

---

[95] Individual calculations of σ_0, σ_1, σ_2 as functions of the core radius for water film thicknesses of 0.01, 0.05 and 0.1 cm are given in [234]. In this paper, misprints in the table headings should be corrected; b should be replaced by a, σ_1 by σ_2, σ_2 by σ_1.

of the dependence of σ_0 on ν at $\lambda = 0.86$ cm has been replaced in Figure 5.42 by individual points whose location shows that even at $h_{sh} = 0.01$ cm, this curve oscillates about its asymptotic value, as in the case of σ_0 for water spheres. At $\lambda = 11.0$ and 17.0 cm, this curve moves further and further away from its asymptotes while oscillating randomly as ν increases. The σ_0 curves, however, at λ equal to 3.2 and 5.6 cm, occupy an intermediate position, and although the curve for $\lambda = 3.2$ cm is considerably closer to the curve for water spheres than for ice, the difference between the σ_0 values of wet ice spheres and σ_0 of water spheres is still fairly significant.

At h_{sh} equal to 0.05 and 0.1 cm, the curve of σ_0 versus ν for all wavelengths oscillates about a certain value σ_0^* close to the asymptotic value for spheres of continuous water, although at $h_{sh} = 0.05$ cm in the range of ν under consideration, the damping of oscillation characteristic of σ_0 of water spheres is still imperceptible (Figure 5.42, b and c).

It also follows from Figure 5.42 c that the character of scattering by wet ice spheres with a surface film 0.1 cm thick is closer to the character of scattering by water spheres. The curves for wet ice spheres have deep minima and maxima at which they differ by a factor of 10 to 100 from similar points of the curves for continuous water spheres, and even more (by a factor of 1,000 at many points) for solid ice spheres. The presence of such deep minima and maxima is confirmed by the experimental studies made by D. Atlas [149].

Thus, scattering by wet hailstones must not be regarded as scattering by water particles of equal size, let alone by particles of dry ice. It can be stated only that the total radar scattering sections of the spectrum of wet spherical hailstones at $h_{sh} = 0.1$ cm will be approximately equal to the total radar scattering cross-sections of water spheres by the same spectrum (especially at $\nu < 2$). As is shown by calculation, this conclusion applies to all the wavelengths considered. Therefore, in the part of the hail cloud where the main growth of the hailstones takes place under single crystal conditions and the water film thickness on the hailstones may reach 0.1 cm or more, the back scattering for all the λ used in meteorology may be interpreted as scattering by water particles of the same size. The same is true in the range $\lambda \leqslant 3.2$ cm of melting hail below the zero degree isotherm level, where the thickness of the surface film may reach only 0.01 cm. At $\lambda > 3.2$ cm, it is necessary to use only the values of back scattering cross-sections for two-layer particles. These conclusions are confirmed by experimental data on the size of the falling hail and on the values of the radar reflectivity of hail clouds, presented in [233]. /235

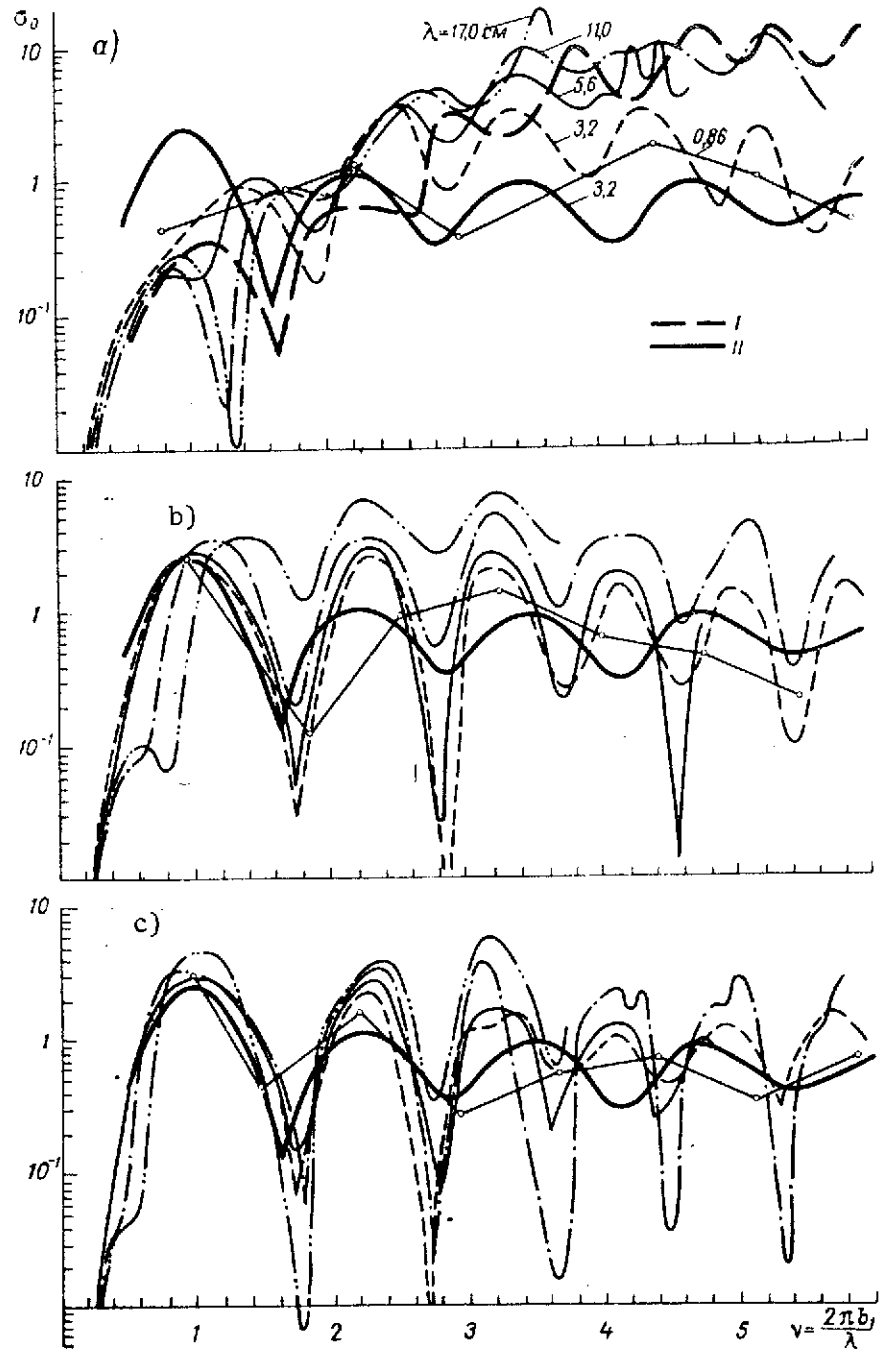

Figure 5.42. σ_0 of Spheres of Wet Ice at Different λ, and Also of Spheres of Solid Ice (Curves I) and Continuous Water (Curves II) at λ = 3.2 cm. a) h_{sh} = 0.01 cm, b) h_{sh} = 0.05 cm; c) h_{sh} = 0.1 cm.

/233

The attenuation of radar radiation in hail clouds and precipitation as well as the intensity of radar scattering depend considerably on the state of the hailstone surface (Figures 5.43, 5.44).

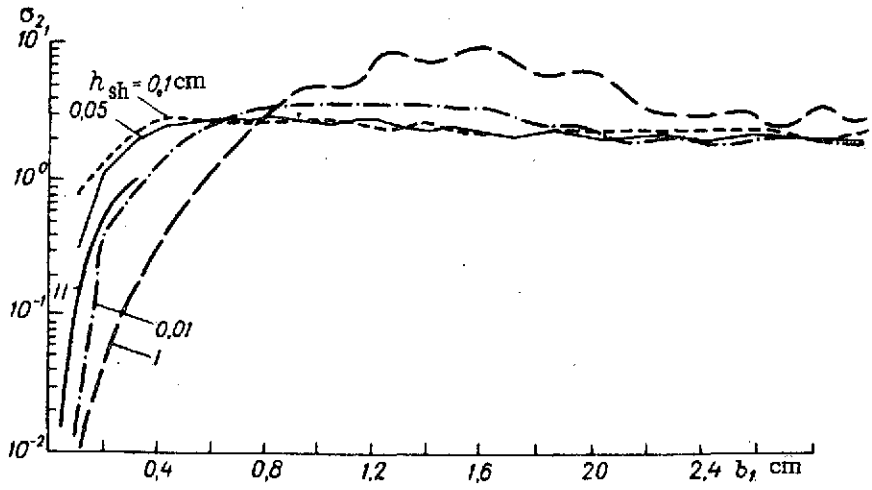

Figure 5.43. σ_2 of Wet Ice Spheres At Different h_{sh} and Spheres of Solid Ice (Curve I) and Continuous Water (Curve II) at λ = 3.2 cm.

It follows from Figure 5.43 that in the range of small particles ($b_1 < 0.7$ cm), the presence of a water film on the hailstone surface, even 0.01 cm thick, increases the values of dimensionless attenuation cross-sections σ_2 of ice spheres, and when h_{sh} becomes of the order of 0.05 cm the σ_2 values surpass the values of the cross-section corresponding to spheres of continuous water. However, in the range of large particles, the σ_2 values are almost independent of h_{sh} and even at h_{sh} = 0.01 cm are approximately equal to the attenuation cross-sections of spheres of continuous water. It should be noted that like σ_0, the σ_2 values of wet hailstones increase with increasing h_{sh} in the range of small particles, while those of large particles decrease, approaching in both cases the cross-section values characteristic of continuous water spheres; attenuation by wet spheres at h_{sh} = 0.1 cm in the range of small particles is two orders of magnitude greater, and in the range of large particles, 4 to 6 times less than attenuation by solid ice spheres.

To study the attenuation in hail clouds at different wavelengths, Figure 5.44 shows σ_2 values for h_{sh} = 0.1 cm. Analysis of the σ_2 values shows that at the hailstone concentrations possible in hail precipitation (according to

[235], an average of 10^{-3}), the attenuation of radiation with $\lambda < 11.0$ cm at $h_{sh} \approx 0.01$ cm is negligibly slight, up to $b_1 < 0.7$ cm, whereas the linear attenuation coefficient at $\lambda < 5.6$ cm may reach 5 db/km. This is satisfactorily /236 confirmed by experimental data [235]. However, at $h_{sh} = 0.1$ cm (i.e., in the zone of moist growth of hail), starting at $b_1 > 0.3$ cm, one cannot neglect the attenuation of radiation even at $\lambda = 11.0$ cm (Figure 5.44), since as h_{sh} increases from 0.01 to 0.1 cm, there is an approximately ten-fold increase in σ_1 for $\lambda = 11.0$ cm in the range of small b_1 ($b_1 < 2$).

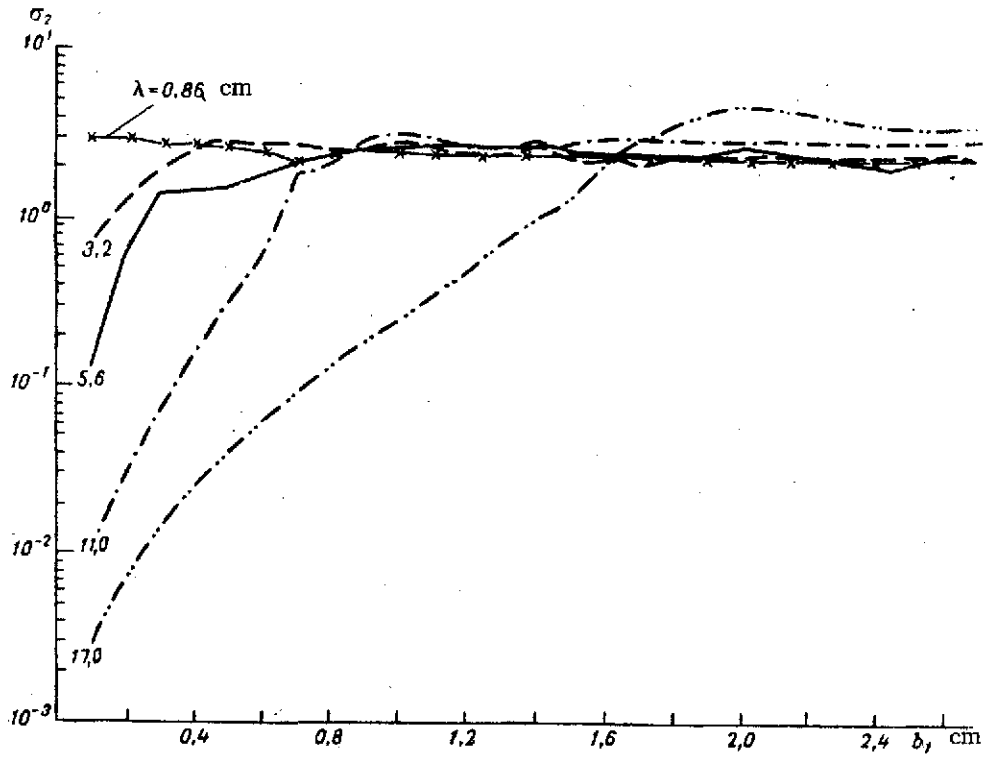

Figure 5.44. σ_2 of Wet Ice Spheres Versus Radius b_1 at Different Wavelengths. Thickness of surface water Film $h_{sh} = 0.1$ cm.

To examine the transfer of radar radiation in hail clouds, it is necessary to study the dependence of the dimensionless total scattering cross-section σ_1 of a wet hailstone on the thickness of the water film on its surface.

As follows from Figure 5.45, the dependence of σ_1 on h_{sh} is substantial only in the range of small particles, in particular, for $\lambda = 3.2$ cm at $b_1 < 0.6$

cm. In the region of large particles, however, according to Figures 5.45 and 5.46, the σ_1 values for all the h_{sh} and λ considered are approximately equal to 1.5, this value being reached at $\nu > 0.4$.

In the range $\nu < 0.4$, however, the σ_1 values for the wavelengths under consideration may differ by several orders of magnitude, decreasing with increasing λ.

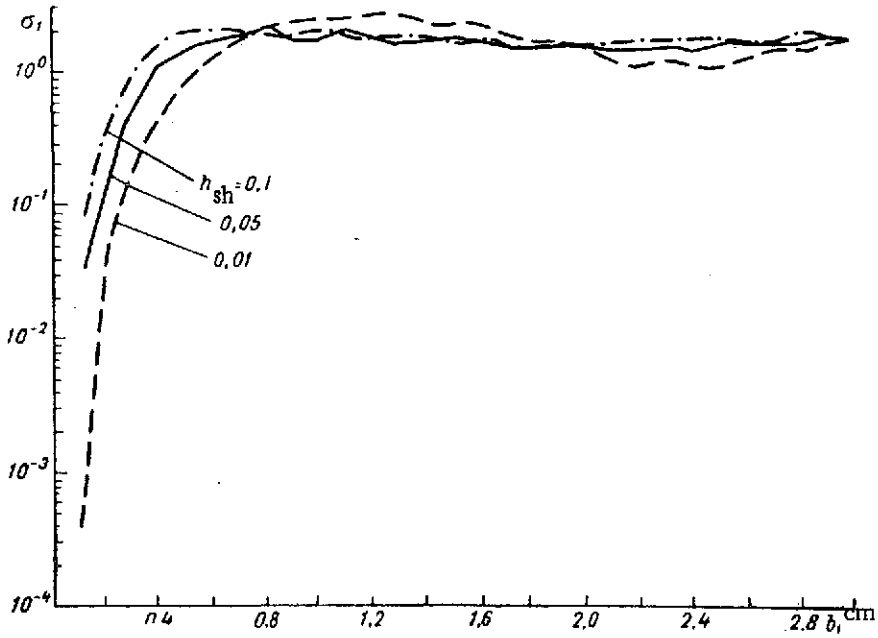

Figure 5.45. σ_1 of Wet Ice Spheres Versus b_1 for Different Thicknesses of the Water Film h_{sh}. λ = 3.2 cm. /237

Let us note in conclusion that when the relationships obtained are extended to the scattering conditions in hail clouds, it is necessary to keep in mind a number of complicating factors. First, during the fall of wet hailstones, the water film obviously will not be of uniform thickness, and according to the data of various authors, may collect in a ring in a plane perpendicular to the direction of fall of the hailstone. /238

Secondly, the radar characteristics of a hail cloud are obtained as the result of scattering not only by hailstones but also by water drops. Finally, the hailstones may be coated with a mixture of water and ice instead of a film of water.

Hailstone Coated With a Mixture of Water and Ice. There are extremely few studies dealing with such hailstones. Thus, L. Battan and B. German [146]

perform calculations of only σ_0 and only at λ = 3.21 cm, with h_{sh} equal to 0.01 and 0.1 cm; d equal to 1, 2, 3, 4, and 5 cm. J. Joss and R. List [147] used 5-cm radar to measure the radar cross-section of spheres of artificial hail consisting of a solid ice core about 2 cm in diameter and a shell 0.2 cm thick consisting of a mixture of ice and water.

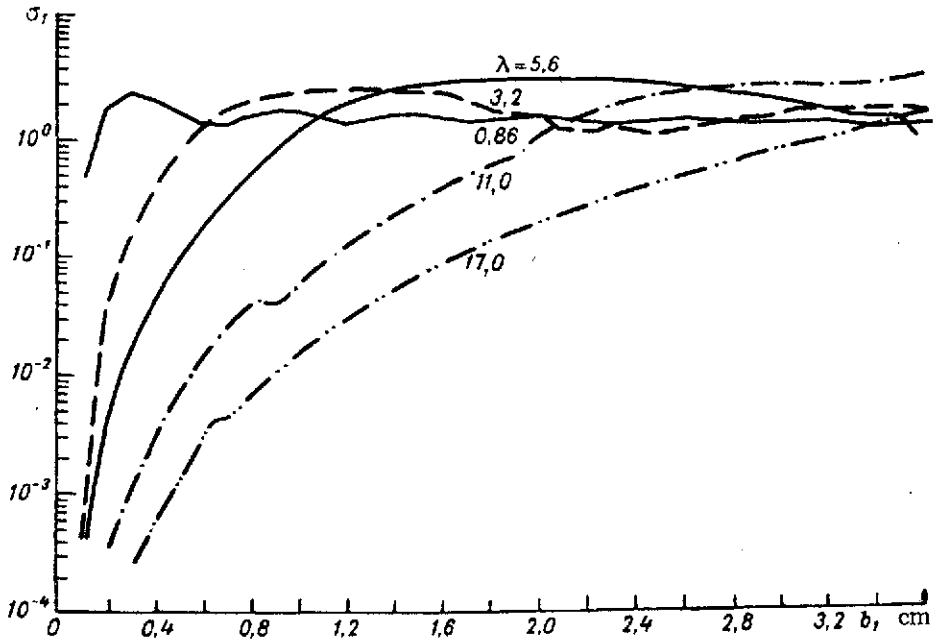

Figure 5.46. σ_1 of Wet Ice Spheres Versus Radius b_1 at Different Wavelengths. Thickness of water film h_{sh} = 0.01 cm.

The detailed analysis of these spheres can be found in [149]. Although the model representations of the dielectric constant of the shell under consideration [see formula (429)] are highly conditional, we deemed it necessary to make a more detailed qualitative study of this case as a function of a series of parameters determining it. To this end, we performed calculations of σ_0, σ_1 and σ_2 of a hailstone with a shell consisting of a homogeneous mixture of water and ice (p being the water content of the mixture in percent). The value p = 100 corresponds to the above-discussed case of a film consisting solely of water. The dielectric constants of the mixture as functions of p

and λ were chosen from Table 1.7 in [11][96]. The temperature was assumed to be 0°C.

Figure 5.47 illustrates the influence exerted by different water contents of the mixture on the effective radar scattering cross-section area σ_0 for different shell thicknesses h_{sh}. It is evident that at a shell thickness of 0.01 cm the presence of 50% of water in the mixture has practically no effect on the magnitude of σ_0. On the other hand, when p increases to 80%, as a rule, the cross-section σ_0 decreases by a factor of 2 to 3. As the shell thickness increases, the role of the water content in the mixture increases. At the same time, the σ_0 curves corresponding to p = 80% come increasingly closer to the σ_0 curves of completely wet hailstones.

A different picture is observed at wavelength λ = 11 cm (Figure 5.48). Thus, at shell thickness 0.01 cm, the water content of the mixture plays no substantial role, even when its amount in the mixture reaches 80%. In this case, the hailstone behaves as would a sphere consisting entirely of ice. As h_{sh} increases, the role of parameter p gains sharply in importance, and at h_{sh} = 0.1 cm, the hailstone with radius $b_1 > 2$ cm and p = 80% scatters backward 1.3-2.2 times as much energy as a homogeneous dry hailstone. This is explained by the fact that at these b_1, the σ_0 values of pure water spheres are much greater than those of pure ice spheres. /241

Figure 5.49 shows the effective attenuation area σ_2 versus b_1 for hailstones coated with a homogeneous mixture of water and ice. It is evident that as p increases, the σ_2 curves for all the wavelengths considered come increasingly closer to their asymptotic values. This is clearly evident from Figure 5.49 d where for $b_1 \geqslant 1$ cm, the σ_0 curves for λ = 0.86, 3.2 and 5.6 cm practically coincide. However, at p = 80% (Figure 5.49 c), the discrepancies in σ_2 values are fairly substantial. As the wavelength increases, the water content of the mixture plays an increasingly less important role, and at $\lambda \geqslant 3.2$ cm and $p \leqslant 50\%$, it can be assumed that a hailstone coated with a homogeneous mixture of water and ice has the same σ_2 values as a dry hailstone of the same radius.

---

[96] Table 1.7 in [11] was calculated from formula (4.29) with ε_w from the appendix and $\varepsilon_i = 3.17 - 4.5 \cdot 10^{-2} i$ ($n_i = 1.78$; $F_i = 12.6 \cdot 10^{-3}$), both close to the data of [132]. As was shown in § 5.2, practically the same values of scattering and attenuation cross-sections are obtained if ε_i used in the calculation is taken from Table 4.33 according to [136].

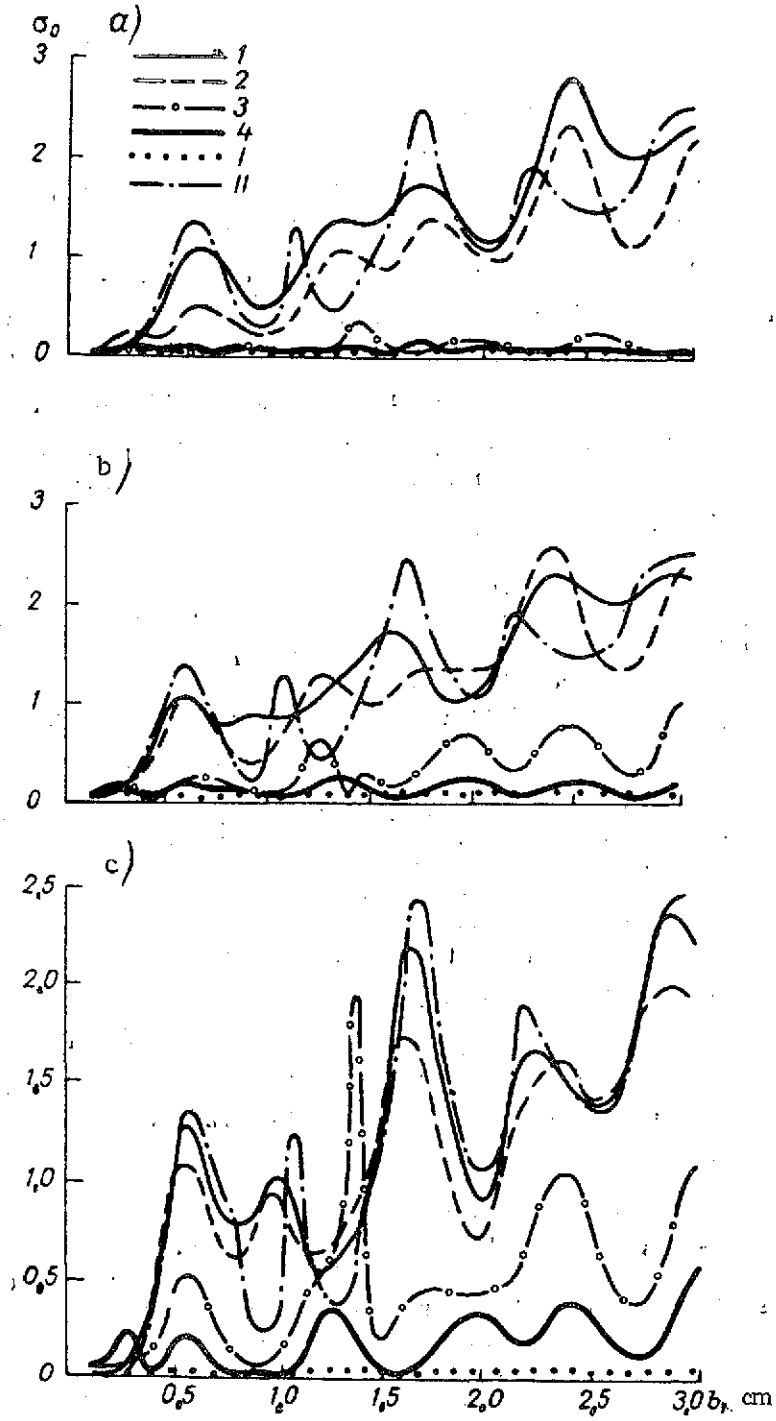

Figure 5.47. σ_0 of a Two-Layer Hailstone with the Shell Consisting of a Homogeneous Mixture of Water and Ice at Different h_{sh} and p, and Also of a Homogeneous Water Hailstone (I) and Ice Hailstone (II). λ = 0.86 cm, t = 0°C. a) h_{sh} = 0.1 cm, b) h_{sh} = 0.05 cm, 1) p = 20%, 2) p = 50%, 3) p = 80%, 4) p = 100%. /239

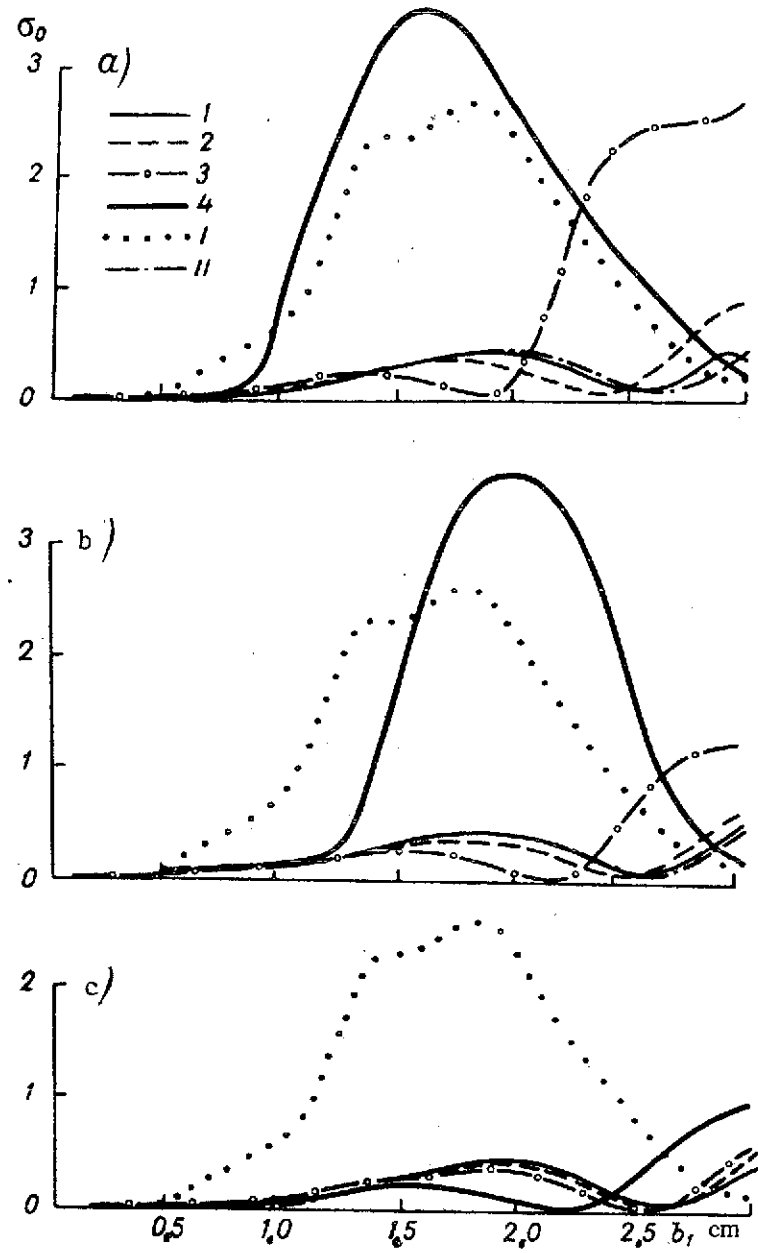

Figure 5.48. σ_0 of Two-Layer Hailstone with a Shell Consisting of a Homogeneous Mixture of Water and Ice at Various h_{sh} and p, and Also of a Homogeneous Water Hailstone and Ice Hailstone. λ = 11 cm, t = 0°C. For notations see Figure 5.47. /240

The same conclusion applies at p ~ 80% for h_{sh} = 0.01. The dependence of the effective area of total scattering on p, h_{sh} and b_1 is shown in Figure

5.50. It follows from the latter that $p \leqslant 50\%$ has no appreciable effect on σ_1 at any of the shell thicknesses considered. As h_{sh} and p increase, σ_1 of a two-layer hailstone approaches the magnitude of σ_1 of a water sphere. Thus, at $p = 80\%$ and $h_{sh} = 0.1$ cm, the total scattering cross-section of a hailstone coated with a homogeneous mixture of water and ice and the cross-section of a sphere consisting exclusively of water differ by less than 50% for $b_1 < 1.5$ cm and almost coincide at $b_1 \geqslant 1.5$ cm.

As p increases, the σ_1 curves for different λ come closer together, as do the σ_2 curves, approaching their limiting values.

Hailstone Coated With Wet Snow. Here we will examine the radar characteristics of a two-layer hailstone whose core consists of ice of different densities, and whose shell is made up of wet snow with a density of 0.38 g/cm^3. According to the arguments of § 4.2, 5.1, snow with a density of 0.34 g/cm^3 is dielectrically equivalent to small hail of the same density. Therefore, results of calculations of effective scattering and attenuation areas of such a hailstone may be interpreted in the same manner as the radar characteristics of a wet hailstone with a character (structure) of its outer shell differing from that of the hailstone already discussed above.

Calculations of σ_0 and σ_2 were made using formulas (1.276), (1.274), (1.281)-(1.283) with dielectric constants from Table 4.31, 4.32. The same symbols were used as above: b_1 — hailstone radius, b_2 — radius of its core of density ρ_2; ρ_1 — density of shell; p — water content of the shell in percent;

$$\nu = \frac{2\pi b_1}{\lambda}\ ;\ h_{sh} = b_1 - b_2.$$

Analysis of calculations of radar scattering cross-sections of a hailstone coated with wet snow of different humidities and thicknesses shows that the appearance of 0.4% of water in the snow shell of a hailstone with $\frac{b_2}{b_1} = 0.8$ decreases σ_0 by not more than 10-20%. Figure 5.51 illustrates a further 20-50% decrease in σ_0 as p rises to 1.6%. /243

The greater the shell thickness, the larger the amount by which σ_0 decreases with rising p. This fact is clearly apparent if we compare Figures 5.51 and 5.52. Thus, at a shell thickness of $0.5\ b_1$, an increase in its moisture content from 0.4 to 1.6% causes a marked decrease in σ_0, particulary in the range $14 \leqslant \nu \leqslant 20$ (by a factor of 2.5-4). /244

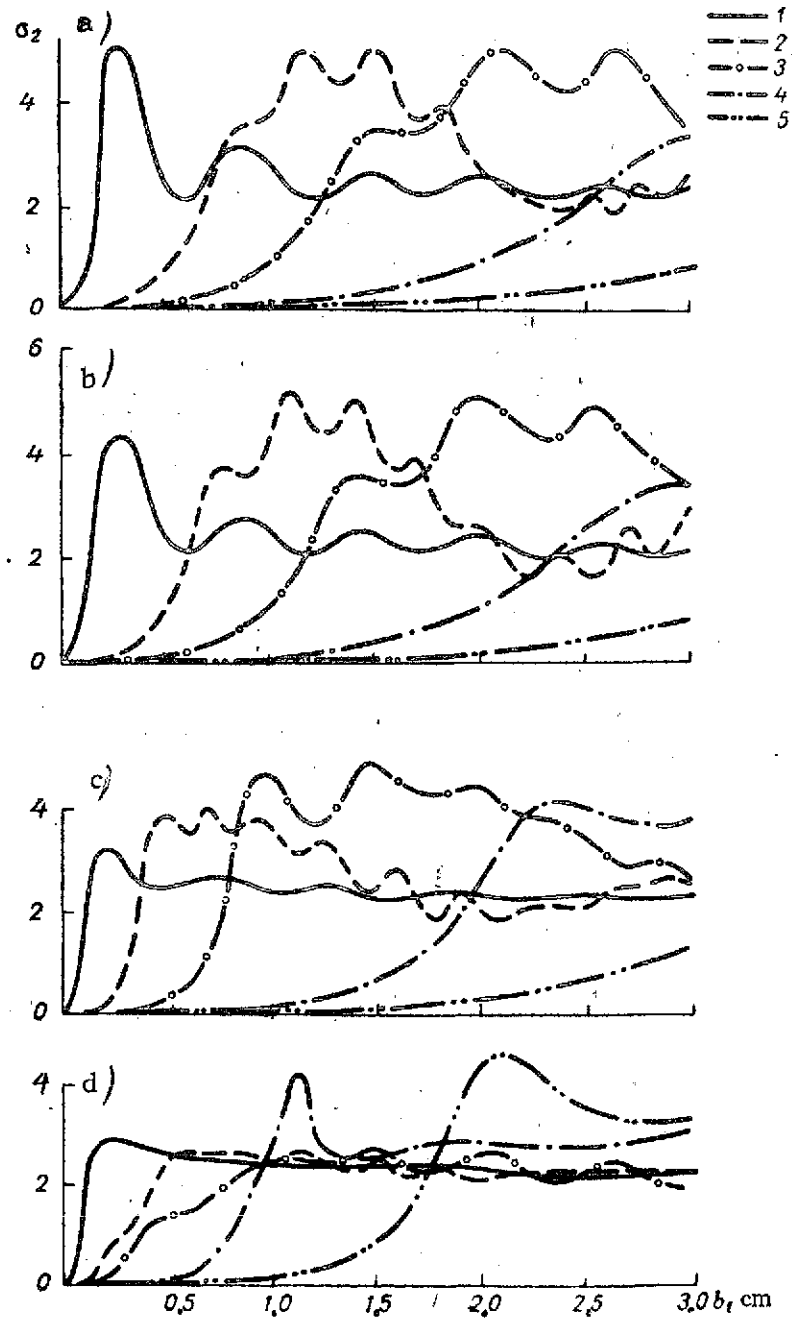

Figure 5.49. σ_2 of Two-Layer Hailstone With a Shell Consisting of a Homogeneous Mixture of Water and Ice at Different p and λ. h_{sh} = 0.1 cm, t = 0°C. a) p = 20%, b) p = 50%, c) p = 80%, d) p = 100%; 1) λ = 0.86 cm, 2) λ = 3.2 cm, 3) λ = 5.6 cm, 4) λ = 11.0 cm, 5) λ = 17.0 cm. /24

Figure 5.43 shows a fairly marked dependence of σ_0 on the shell thickness h_{sh} at a constant moisture content of the snow. Such a decrease in σ_0 (by a

factor of 3 to 15) at constant p takes place mainly as a result of an increase in the total content of the water mass in the snow shell.

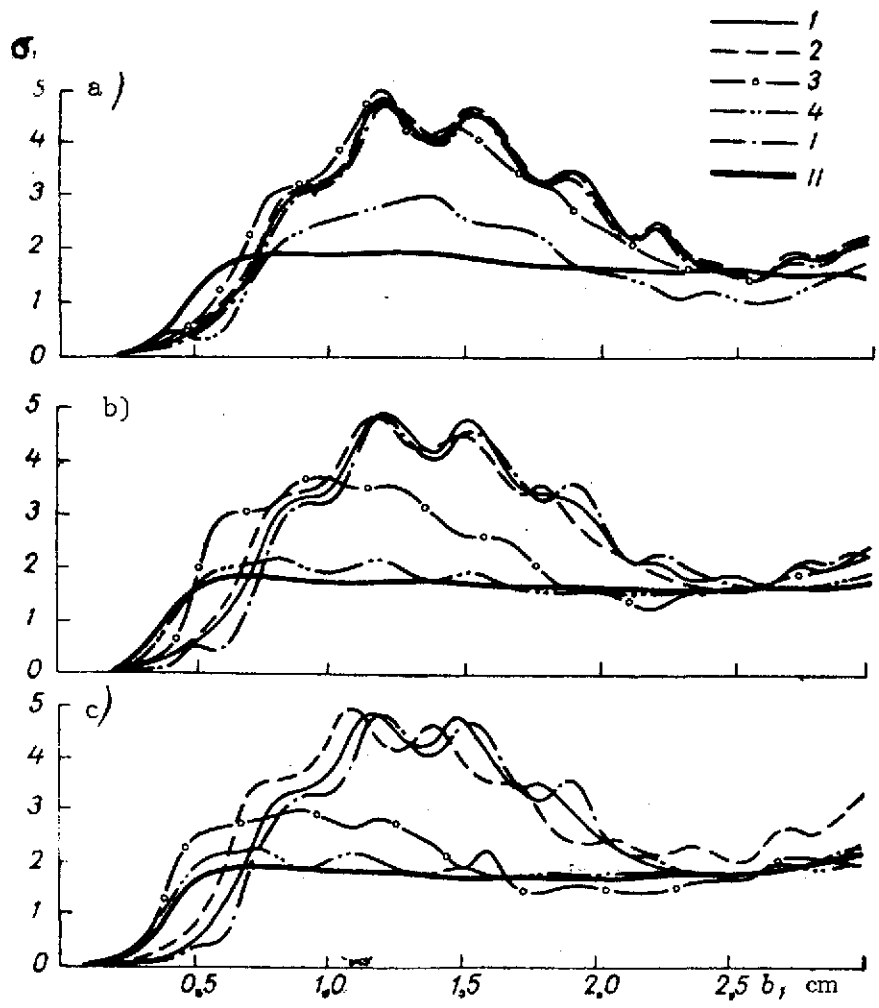

Figure 5.50. σ_0 of Two-Layer Hailstone with Shell Consisting of Homogeneous Mixture of Water and Ice at Different p and h_{sh}, and Also of a Homogeneous Water Hailstone (II) and Ice Hailstone (I). λ = 3.2 cm, t = 0°C. a) h_{sh} = 0.01 cm, b) h_{sh} = 0.05 cm, c) h_{sh} = 0.1 cm; 1) p = 20%, 2) p = 50%, 3) p = 80%, 4) p = 100%.

Figure 5.54 shows σ_0 as a function of p when the core has the same density as the shell. It is obvious that for $\nu < 11.5$, a 1.6% moisture content of the shell has practically no effect on the magnitude of σ_0. For greater ν, the influence of the moisture content of the shell is the same as

in the case discussed above of $\rho_2 = 0.916$ g/cm^3. If one compares Figure 5.54 with Figure 5.52, one can see that a decrease in core density leads to an increase in the range of ν where σ_0 is practically independent of p.

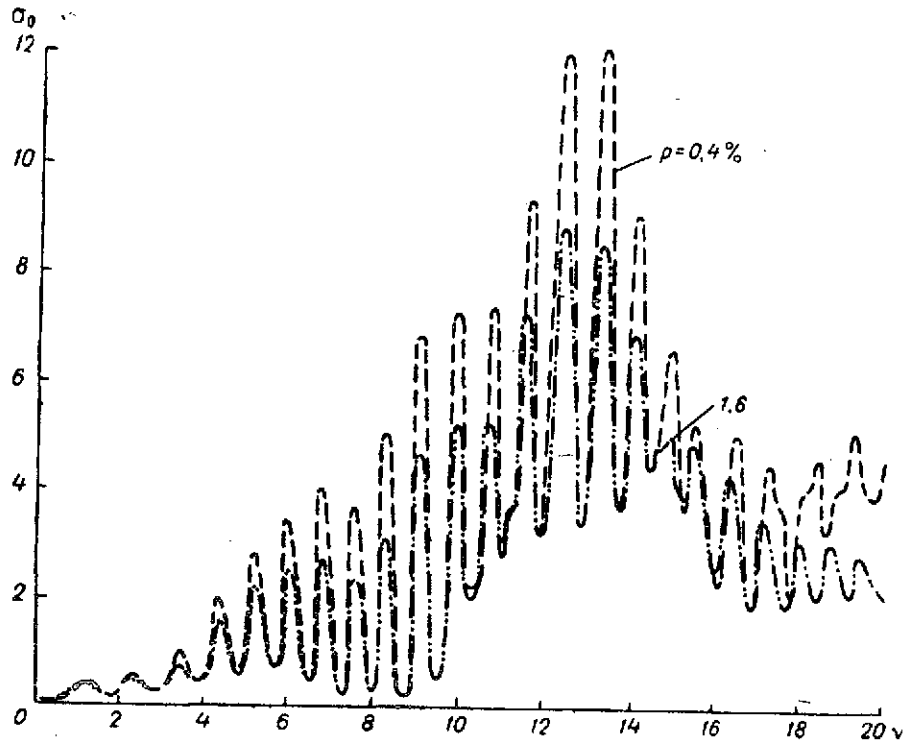

Figure 5.51. σ_0 of Two-Layer Hailstone with $\rho_2 = 0.916$ g/cm^3 and a Shell of Wet Snow with Density $\rho_1 = 0.380$ g/cm^3 at $\frac{b_2}{b_1} = 0.8$, t = 0°C and Different p.

This is also confirmed by calculations with $\rho_2 = 0.600$ g/cm^3. Finally, Figures 5.55 and 5.56 illustrate the effect of the density of a core coated with wet snow on the magnitude of σ_0. It is evident that as the shell thickness increases, the dependence of σ_0 on ρ_2 markedly decreases. Calculations for ρ_2 equal to 0.76, 0.600 and 0.46 g/cm^3 confirm this conclusion.

As for the effective attenuation area σ_2 of the hailstone coated with wet snow with $p < 1.6\%$, calculations show that it attenuates electromagnetic radiation to the same extent (to within 1-3%) as the corresponding two-layer hailstone with p = 0.

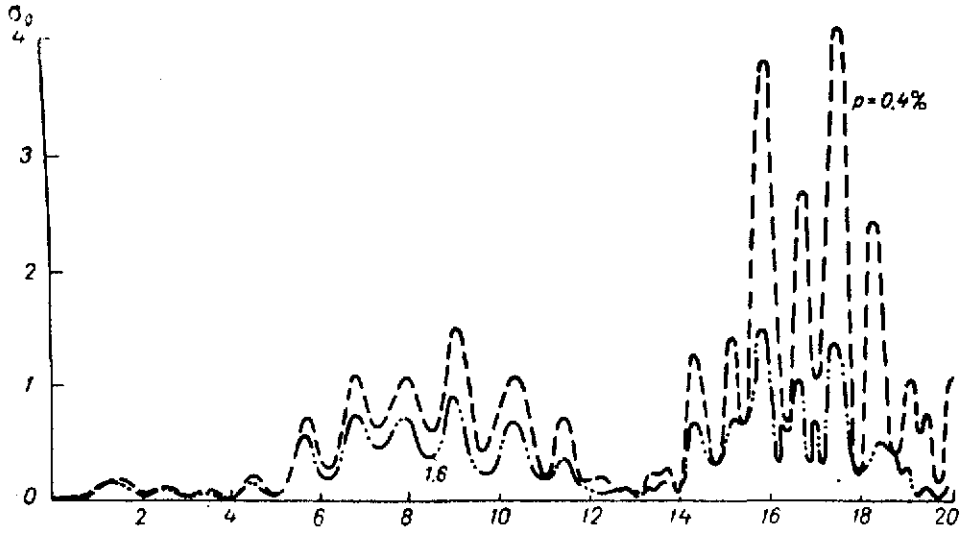

Figure 5.52. σ_0 of Two-Layer Hailstone with ρ_2 = 0.916 g/cm^3 and a Shell of Wet Snow with Density ρ_1 = 0.380 g/cm^3 at $\frac{b_2}{b_1}$ = = 0.5, t = 0°C and different p.

To conclude this section, we will consider some of the experimental studies [236-238] involving the radar characteristics of a melting hailstone.

In 1962, N. Labrum [236] first reported on variations of electromagnetic energy scattered back by an ice particle in the course of its fusion. A particle with a cross-section no greater than λ^2 was placed in a rectangular waveguide; energy variations were observed at λ = 10 cm. It was found that the energy scattered back by the ice particle increases rapidly at first, then falls off to the value corresponding to the final shape of the water droplet being formed.

In 1965, D. Nicolis [237] continued these investigations on shorter waves, from 1.20 to 1.67 cm. There different frequency groups were noted for which the laws of change in reflected energy are substantially different. /248
Thus, at frequencies of 18-19 GHz, a maximum was obtained at the instant when 40% of the mass of the sample was converted into water, this being in accord with Labrum's experiments [236]. For the intermediate frequency band (19.5-22 GHz) it was noted that as the ice sample changed into water, the reflected energy varied aperiodically with the presence of several "steps" characterizing the fusion process. Finally, at higher frequencies (23-24.8 GHz), the law of change becomes reversed, i.e., a minimum is observed where a maximum took place in the lower frequency region. As reported in [237], the experiment was repeated in the laboratory about 500 times with two identical samples which were changed at selected frequencies.

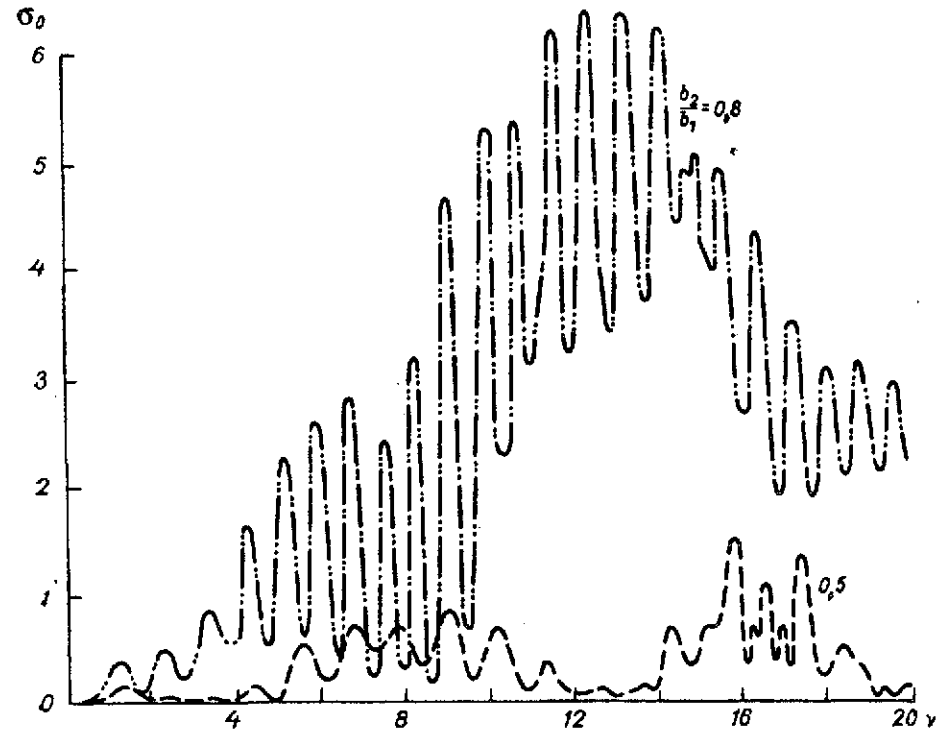

Figure 5.53. σ_0 of Two-Layer Hailstone with ρ_2 = 0.916 g/cm^3 and a Shell of Wet Snow with Density ρ_1 = 0.380 g/cm^3 at p = 1.6%, t = 0°C and Different $\frac{b_2}{b_1}$. /246

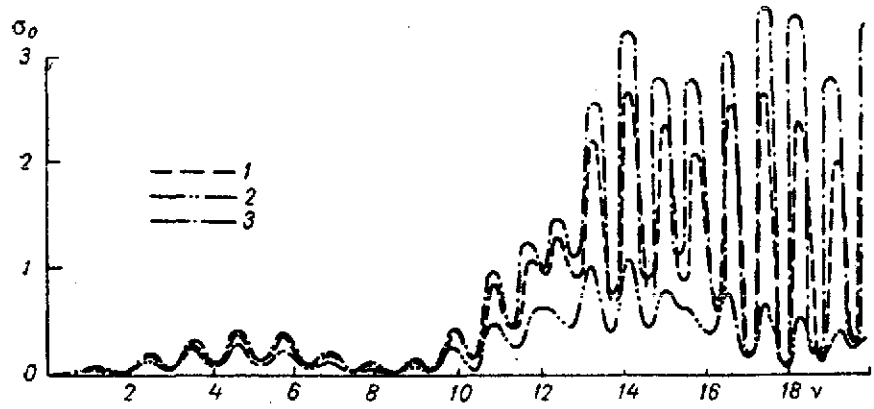

Figure 5.54. σ_0 of Two-Layer Hailstone with a Shell of Wet Snow with Density 0.380 g/cm^3 at $\frac{b_2}{b_1}$ = 0.5, t = 0°C, ρ_2 = 0.380 g/cm^3 and p = 0.4% (1) and p = 1.6% (2), and Also of a Homogeneous Hailstone (3) with Density 0.380 g/cm^3 at t = 0°C.

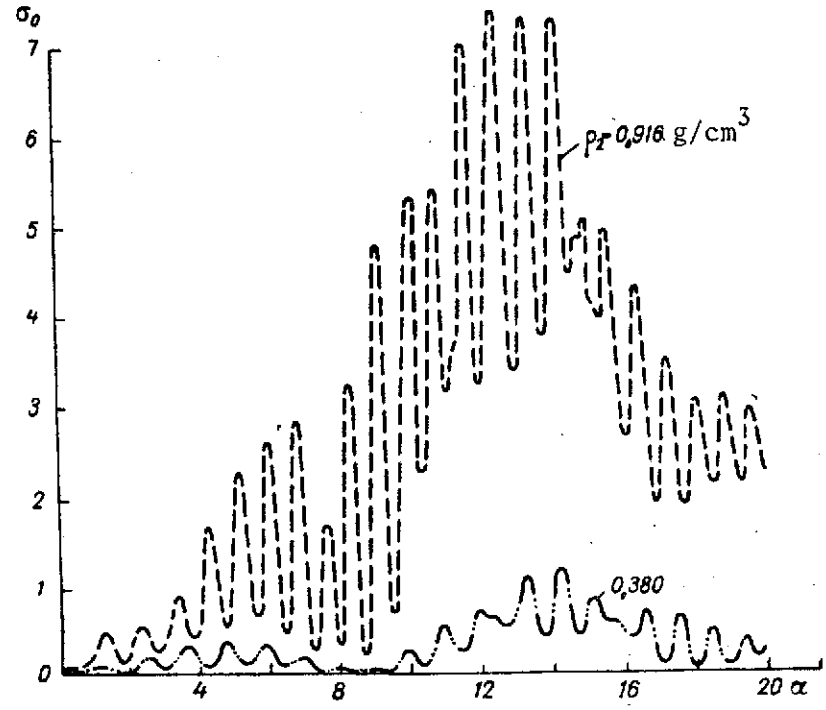

Figure 5.55. σ_0 of Two-Layer Hailstone with a Shell of Wet Snow with Density 0.380 g/cm^3 at p = 1.6%, $\frac{b_2}{b_1}$ = 0.8, t = 0°C, ρ_2 = 0.916 g/cm^3 and ρ_2 = 0.380 g/cm^3.

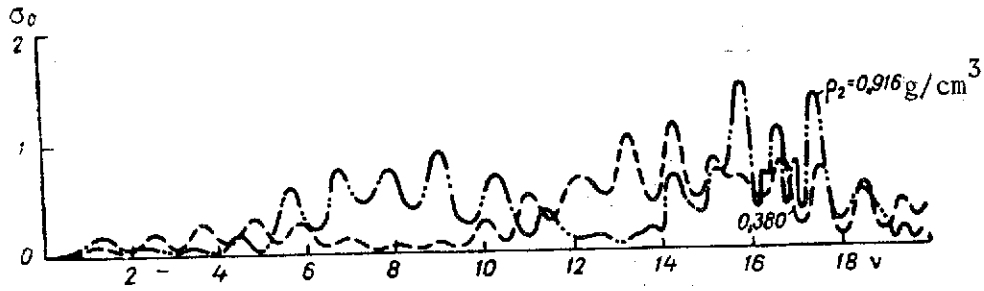

Figure 5.56. σ_0 of Two-Layer Hailstone with a Shell of Wet Snow with Density 0.380 g/cm^3 at p = 1.6%, $\frac{b_2}{b_1}$ = 0.5, t = 0°C, ρ_2 = 0.916 g/cm^3 and ρ_2 = 0.380 g/cm^3.

A year later, T. Oguchi [238] published selected results of calculations of effective scattering and attenuation areas of wet particles at 0.86 cm wavelength. It is seen that the overall character of change in σ_0 with increasing ν is very close to the experimental measurement of Nicolis [237] at frequencies of 18-25 GHz, although his model also differed substantially from the one from which the calculations were made.

§ 5.6. Scattering and Attenuation of Microwaves by a Drop Frozen on the Outside and a Hollow Hailstone

The analytical model of a two-layer particle and the computer program used above make it possible also to study the cases of other particles such as drops frozen on the outside and hollow hailstones (see § 5.1).

A drop frozen on the outside is treated as a two-layer spherical particle with inner and outer radii b_2 and b_1 respectively. The core of such a particle consists of water, and the ice shell has a density of 1 g/cm^3. Calculations of the effective area of radar σ_0 and total σ_1 scatterings and also attenuation σ_2 for the case of $t = 0°C$, $\nu = \frac{2\pi b_1}{\lambda} = 0.1$ are shown in Table 5.16. Here $h_{sh} = b_2 - b_1$; $\frac{h_{sh}}{b_1} = 0$ and $\frac{h_{sh}}{b_1} = 1$ are cases of a homogeneous water sphere and ice sphere of radius b_1 respectively.

It follows from Table 5.16 that when an ice shell 0.1 b_1 thick appears on the drop, the magnitudes of radar and total scatterings decrease by approximately 20%, and the attenuation values, by 10%.

Thus, from the standpoint of radar characteristics, a drop slightly frozen on the outside behaves as if such freezing did not occur. The dependence of the scattering cross-sections on the wavelength is very weak. As λ increases from 1 to 10 cm , the σ_2 values decrease by a factor of 7-8.

Hollow Hailstone. This example is interesting in that it permits one to track in one particular case the influence of air inclusions, so common in hailstones, on the radar properties of the latter. Calculations of σ_0 and σ_2 were made (Tables 5.17-5.19) for a two-layer particle with an air core radius b_2 and radius b_1 of an outer layer of a concentric ice shell of density 1 g/cm^3. For comparison, the tables also list σ_0 and σ_2 values of a solid ice sphere of the corresponding size ($b_1 = b_2 + h_{sh}$). /250

Analysis of Tables 5.17-5.19 leads to the following conclusions.

1. The radar scattering of a hollow hailstone may be greater than that of a solid hailstone of the same size. For instance, at $b_1 = 1$ cm, $\lambda = 3.2$ cm,

h_{sh} = 0.7 cm; b_1 = 0.5 cm, λ = 0.4 cm, h_{sh} = 1 cm; b_1 = 0.25 cm, λ = 0.2 cm and h_{sh} = 0.05 cm.

TABLE 5.16. σ_0, σ_1 AND σ_2 VALUES OF A DROP FROZEN ON THE OUTSIDE. /251

$\frac{h_{sh}}{b_1}$	$\sigma_0 \cdot 10^4$ at λ cm			$\sigma_1 \cdot 10^4$ at λ cm			$\sigma_2 \cdot 10^4$ at λ cm		
	1	3	10	1	3	10	1	3	10
0,3	1,76	1,84	1,84	1,18	1,24	1,25	2,53	1,03	0,364
0,2	2,28	2,37	2,36	1,53	1,61	1,62	3,19	1,34	0,485
0,1	2,89	2,99	2,95	1,95	2,04	2,05	3,74	1,65	0,632
0,01	3,50	3,58	3,50	2,36	2,46	2,47	4,13	1,95	0,802
0,001	3,57	3,64	3,55	2,40	2,50	2,52	4,16	1,98	0,822
0,0001	3,57	3,65	3,56	2,41	2,51	2,52	4,16	1,98	0,823
0	3,57	3,65	3,56	2,41	2,51	2,52	4,16	1,99	0,824
1	0,702	0,702	0,702	0,471	0,471	0,471	0,043	0,043	0,043

Commas indicate decimal points.

TABLE 5.17. σ_0 AND σ_2 VALUES OF A HOLLOW HAILSTONE OF RADIUS 1 CM.

λ	σ_0 at h_{sh}					σ_1 at h_{sh}				
	1	0,7	0,5	0,3	0,1	1	0,7	0,5	0,3	0,1
0,6	15,34	10,95	3,25	2,90	0,71	2,72	1,99	2,67	1,76	3,34
0,86	9,70	7,74	6,11	3,75	6,28	3,13	3,45	1,74	2,25	3,12
3,2	0,66	0,97	1,40	1,15	0,15	3,26	3,07	2,64	1,78	0,27
5,6	0,44	0,38	0,24	0,10	$1,3 \cdot 10^{-2}$	0,76	0,70	0,53	0,27	0,05
11,0	$6,8 \cdot 10^{-2}$	$6,4 \cdot 10^{-2}$	$5,1 \cdot 10^{-2}$	$2,9 \cdot 10^{-2}$	$5,4 \cdot 10^{-3}$	$5,7 \cdot 10^{-2}$	$5,4 \cdot 10^{-2}$	$4,4 \cdot 10^{-2}$	$2,7 \cdot 10^{-2}$	$5,7 \cdot 10^{-3}$
17,0	$1,3 \cdot 10^{-2}$	$1,2 \cdot 10^{-2}$	$1,0 \cdot 10^{-2}$	$6,1 \cdot 10^{-2}$	$1,2 \cdot 10^{-3}$	$1,1 \cdot 10^{-2}$	$1,0 \cdot 10^{-2}$	$8,7 \cdot 10^{-3}$	$5,7 \cdot 10^{-3}$	$1,6 \cdot 10^{-3}$

Commas indicate decimal points.

It follows from the above data that the smaller the size of the hailstone, the shorter the wavelength for which this condition is fulfilled. This is explained by such a combination of parameters b_1, h_{sh}, and λ for which, in addition to a focusing of the energy starting with certain limiting angles of incidence, there also takes place total reflection from the surface of the inner sphere as a medium that is electromagnetically less dense than ice. This also accounts for the fact that hailstones of fixed diameter with a thicker ice shell may reflect a power several times lower toward the radar

set. For instance, at b_1 = 1 cm, λ = 0.86 cm, h_{sh} = 0.3 and 0.1 cm; b_1 = 0.5 cm, λ = 0.4 cm, h_{sh} = 0.3 and 0.5 cm; b_1 = 0.25 cm, λ = 0.6 cm; h_{sh} = 0.05 and 0.02 cm.

2. For wavelengths substantially exceeding the hailstone diameter, a monotonic decrease of σ_0 with decreasing thickness of the ice shell is observed.

3. The maximum value of σ_0 of a hollow hailstone with a fixed diameter and thickness of the ice shell is reached mainly at the same wavelength as in the case of a solid hailstone. Only in the case of very thin shells is the wavelength λ_{max} at which the maximum σ_0 is reached somwhat lower. Thus, while for b_1 = 0.5 cm at h_{sh} = 0.3 cm λ_{max} = 0.6 cm, in the case of h_{sh} = 0.1 and 0.05 cm, λ_{max} = 0.4 cm, or if for b_1 = 2.5 cm at h_{sh} = 0.05 cm λ_{max} = 0.4 cm, then at h_{sh} = 0.02 cm λ_{max} = 0.2 cm.

4. For the same thickness of the ice shell, a larger σ_0 does not always correspond to a hailstone of larger diameter. For example, at h_{sh} = 0.1 cm and λ = 0.6 cm, σ_0 of a hailstone with b_1 = 0.5 cm is six times as large as σ_0 of the hailstone with b_1 = 1 cm. This shows that, as in the case of a solid hailstone, the dependence of the radar scattering on the diameter of a hollow hailstone is expressed by a sharply oscillating function.

5. The effective attenuation area σ_2 of a hollow hailstone may be greater than that of a solid hailstone of the same size. This takes place, for example, at b_1 = 1 cm, λ = 0.86 cm, h_{sh} = 0.7 cm; b_1 = 0.5 cm, λ = 0.86 cm, h_{sh} = 0.3 cm; b_1 = 0.25 cm, λ = 0.4 cm, h_{sh} = 0.1 cm.

TABLE 5.18. σ_0 AND σ_2 VALUES OF A HOLLOW HAILSTONE OF 0.5 CM RADIUS. /251

λ cm	σ_0 at h_{sh}				σ_2 at h_{sh}			
	0,5	0,3	0,1	0,05	0,5	0,3	0,1	0,05
0,4	4,36	0,84	4,53	2,96	2,61	3,43	4,53	2,98
0,6	11,95	8,36	4,22	2,29	1,91	1,54	3,83	2,28
0,86	8,92	6,81	1,07	$1,4 \cdot 10^{-2}$	3,74	4,73	2,77	1,23
3,2	0,38	0,80	$5,6 \cdot 10^{-2}$	$1,6 \cdot 10^{-2}$	0,48	0,40	$9,8 \cdot 10^{-1}$	$3,1 \cdot 10^{-2}$
5,6	$6,3 \cdot 10^{-2}$	$5,5 \cdot 10^{-2}$	$1,6 \cdot 10^{-2}$	$5,1 \cdot 10^{-3}$	$5,3 \cdot 10^{-2}$	$4,7 \cdot 10^{-2}$	$1,5 \cdot 10^{-2}$	$5,4 \cdot 10^{-3}$
11,0	$4,6 \cdot 10^{-3}$	$4,1 \cdot 10^{-3}$	$1,4 \cdot 10^{-3}$	$4,7 \cdot 10^{-4}$	$4,4 \cdot 10^{-3}$	$4,0 \cdot 10^{-3}$	$1,7 \cdot 10^{-3}$	$8,4 \cdot 10^{-4}$
17,0	$8,1 \cdot 10^{-4}$	$7,3 \cdot 10^{-4}$	$2,5 \cdot 10^{-4}$	$8,6 \cdot 10^{-5}$	$1,3 \cdot 10^{-3}$	$1,2 \cdot 10^{-3}$	$6,7 \cdot 10^{-4}$	$3,8 \cdot 10^{-4}$

Commas indicate decimal points.

TABLE 5.19. σ_0 AND σ_2 VALUES OF A HOLLOW HAILSTONE OF 0.25 CM RADIUS.

λ cm	σ_0 at h_{sh}				σ_2 at h_{sh}			
	0,25	0,1	0,05	0,02	0,25	0,1	0,05	0,02
0,2	4,36	1,68	4,53	1,58	2,61	1,19	4,53	2,55
0,4	5,87	4,11	4,54	0,11	2,93	4,75	3,28	1,00
0,6	1,52	0,46	$9,3 \cdot 10^{-3}$	$5,8 \cdot 10^{-2}$	4,31	3,40	1,91	0,38
0,86	0,58	1,11	0,40	$5,1 \cdot 10^{-2}$	3,27	2,22	0,81	0,13
3,2	$3,8 \cdot 10^{-2}$	$2,4 \cdot 10^{-2}$	$1,0 \cdot 10^{-2}$	$2,2 \cdot 10^{-3}$	$3,1 \cdot 10^{-2}$	$2,1 \cdot 10^{-2}$	$9,4 \cdot 10^{-3}$	$2,6 \cdot 10^{-3}$
5,6	$4,3 \cdot 10^{-3}$	$2,9 \cdot 10^{-3}$	$1,3 \cdot 10^{-3}$	$3,0 \cdot 10^{-4}$	$4,1 \cdot 10^{-3}$	$3,0 \cdot 10^{-3}$	$1,7 \cdot 10^{-3}$	$6,3 \cdot 10^{-4}$
11,0	$2,9 \cdot 10^{-4}$	$2,0 \cdot 10^{-4}$	$9,0 \cdot 10^{-5}$	$2,1 \cdot 10^{-5}$	$7,5 \cdot 10^{-4}$	$6,4 \cdot 10^{-4}$	$4,5 \cdot 10^{-4}$	$2,3 \cdot 10^{-4}$
17,0	$5,1 \cdot 10^{-5}$	$3,5 \cdot 10^{-5}$	$1,6 \cdot 10^{-5}$	$3,8 \cdot 10^{-5}$	$3,9 \cdot 10^{-4}$	$3,5 \cdot 10^{-4}$	$2,6 \cdot 10^{-2}$	$1,4 \cdot 10^{-4}$

Commas indicate decimal points.

A similar phenomenon is observed in the dependence of σ_2 on the thickness of the ice shell. Thus, at $b_1 = 1$ cm and $\lambda = 0.6$ cm, σ_2 at $h_{sh} = 0.1$ cm is greater than at $h_{sh} = 0.5$ cm and at $\lambda = 0.86$ cm the attenuation of a hollow hailstone of 1 cm radius with an ice shell 1 mm thick is nearly the same as that of a solid hailstone. /252

6. For wavelengths considerably exceeding the hailstone diameter, an increase in the thickness of the ice shell results in an increase of σ_2.

7. For $\lambda \geqslant 0.86$ cm at a fixed hailstone thickness ($h_{sh} = 0.1$ cm), to a larger size b_1 of the hailstone there corresponds a larger value of attenuation σ_2, but as for example at $\lambda = 0.6$ cm, σ_2 at $b_1 = 0.5$ cm is larger than at $b_1 = 1$ cm.

CHAPTER 6. /253

SCATTERING AND ATTENUATION OF MICROWAVES BY A SET OF HYDROMETEORIC PARTICLES

§ 6.1. Physical Parameters of Hydrometeors

In order to allow for the influence of hydrometeors on the operation of microwave and submillimeter radar stations, and for many other purposes, in addition to the electromagnetic parameters of hydrometeors (see Chapter 4), it is necessary to know their geometrical, temporal, probability and other physical characteristics.

According to the classification adopted in [202-204, 158, etc.][97] all the precipitation falling on the Earth's surface from clouds is subdivided into types, as shown in Figure 6.1. On the right of this figure, the international symbol is given for each type. We will give a brief description of the major ones.

Rain – precipitation in the form of water drops of different sizes, from 0.5 to 7 mm in diameter. Rain falls from cumulus rain clouds, stratified rain clouds and sometimes from altostratus clouds. The physical parameters of an individual drop are given in § 5.1.

Drizzle – precipitation consisting of a large number of fine drops less than 0.5 mm in diameter. Drizzle falls from stratified and strato-cumulus clouds. The rainfall intensity of a drizzle does not exceed 0.25 mm/hr, and the falling velocity of the drops in still air is 0.3 m/s.

Hail – precipitation in the form of spherical particles or pieces of ice (hailstones) from 5 to 50 mm in diameter, sometimes larger, falling individually or in the form of irregular aggregates. Hailstones consist only of layers of transparent ice not less than 1 mm thick, alternating with semitransparent layers. Hailstones are formed in cumulus rain clouds as the result of fusion of supercooled water drops with grains of sleet and their freezing. The largest hailstones are formed by the coalescence of finer ones. /254

The physical parameters of an individual hailstone and its layered structure were discussed in § 5.1.

Snow – precipitation falling in the form of snow and ice crystals of most diverse shapes, frequently clustered into flakes of large size. The physical parameters of ice crystals and snowflakes were indicated in § 5.1.

[97]This classification is in accordance with the definitions adopted in 1956 by the Committee of the World Meteorological Organization on the Study of Clouds and Hydrometeors, and published in the International Cloud Atlas.

The definitions of the remaining types of precipitation may be found in the works indicated above.

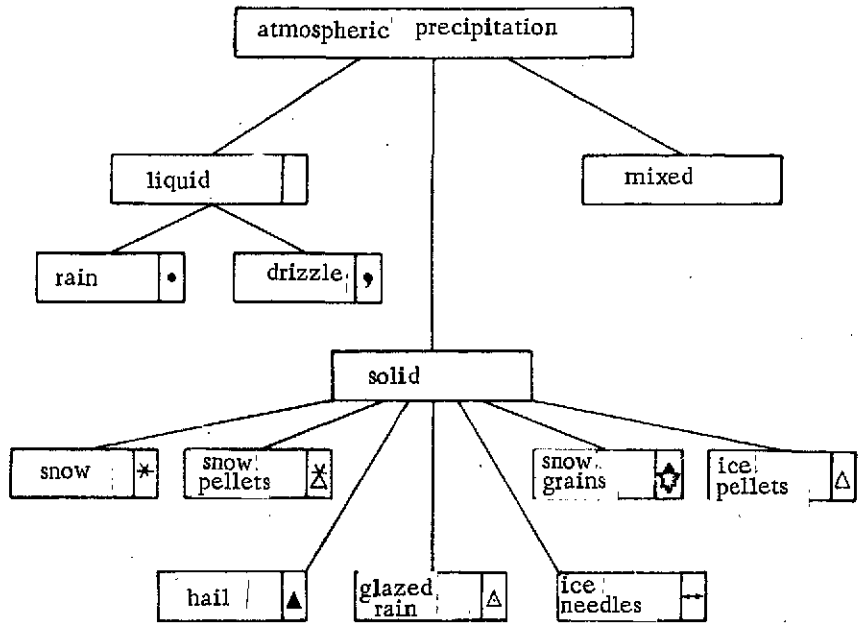

Figure 6.1. Classification of Precipitation.

In addition to liquid and solid precipitation, mixed precipitation consisting of a mixture of different types of precipitation falling simultaneously (Figure 6.1) frequently occurs, for example, rain with drizzle, snow with rain, ice pellets and rain, etc.

Depending on the physical conditions of formation, duration and intensity, precipitation is divided into 3 types [202-204, etc.].

Continuous, falling from a system of frontal, stratified rain clouds and altostratus clouds. It is of long duration and of medium intensity; it covers large areas simultaneously; it falls in the form of either medium size rain drops, or snow, or both (wet snow).

Showers, usually falling from cumulus rain clouds in the form of rain, snow, sleet or hail.

It is frequently marked by a high intensity; begins suddenly and lasts a short time, but resumes frequently; it covers a small area. Its precipitation is frequently associated with hail and squalls. /255

Drizzling precipitation falling from thick stratified and strato-cumulus clouds in the form of drizzle, finest snowflakes or ice needles. It is formed chiefly within the stable homogeneous air masses.

Individual characteristics of clouds as a function of the type of precipitation and conditions of their formation are presented in Table 6.1, after the data of G. Mann [239].

One of the most important characteristics of precipitation that permits a study of its radar properties is the distribution of the particles with size. This distribution may be represented in different ways. The most common consists of frequency diagrams of particles of different sizes. In constructing these diagrams, the diameters d_i of particles with a certain fixed increment Δd ($d_i = d_{min} + i\Delta d$, $i = 0, 1, \ldots,$ max; d_{min}, d_{max} are respectively the minimum and maximum particle diameters in the spectrum) are plotted along the abscissa axis, and the ratio of the number of particles N_i per unit volume of air with a diameter between d_i and $d_i + \Delta d$ to the quantity Δd is plotted along the ordinate axis at the point with abscissa $d_i + \frac{\Delta d}{2}$. Because of a change in the values of $n_i = \frac{N_i}{\Delta d}$ from one interval to the next, the diagram has a stepwise appearance.

Sometimes it is preferable to deal, not with an absolute, but with a relative number of particles, and for this purpose, in plotting the free particle frequency diagram, f_i is plotted along the ordinate axis instead of n_i:

$$f_i = \frac{N_i}{N\Delta d}$$

where N is the total number of particles in the selected volume:

$$N = \sum_{i=0}^{\max} N_i. \tag{6.1}$$

For a large number of particles ($N \geqslant 1000$), it is possible to obtain a smooth, continuous size spectrum, i.e., a certain curve. The equation of this curve in the form $n = n(d)$ or

$$f = f(d) = \frac{n(d)}{N} \tag{6.2}$$

is usually called the function (law) of particle distribution with diameter (size)[98].

Let us note at this point that in the case of a continuous spectrum, the expression for N in formula (6.2), in contrast to (6.1), has the form

---

[98] In probability theory, these functions are called differential distribution functions (see [241], p. 78).

$$N = \int_{d_{min}}^{d_{max}} n(d)\, dd. \tag{6.3}$$

Frequently, to simplify various theoretical investigations, it is assumed that $d_{min} = 0$ and $d_{max} = \infty$.

If we want to switch to the distribution functions and to $\tilde{n}(r)$ of a random quantity r related to the previous d by /257

$$r = \varphi(d),$$

it is necessary to transform $n = n(d)$ by using the formula [240]

$$\tilde{n}(r) = \int_{-\infty}^{+\infty} \delta[r - \varphi(d)]\, n(d)\, dd, \tag{6.4}$$

where $\delta(x)$ is the delta function.

In the special case of a linear transformation of the form $r = kd$, where k is a constant, expression (6.4) becomes:

$$\tilde{n}(r) = \frac{1}{|k|}\, n\left(\frac{r}{k}\right). \tag{6.5}$$

If variable r is treated as the particle radius, substituting $k = 1/2$ into relation (6.5), we obtain

$$\tilde{n}(r) = 2n(2r). \tag{6.6}$$

Formula (6.6) indicates the law of transformation of the particle diameter distribution function to the particle size distribution function. Similar relations will apply to the probability density function f(d). To obtain, it suffices to replace the symbol $\tilde{n}$ by $\tilde{f}$ in expressions (6.4)-(6.6). In addition to the differential functions $n = n(d)$ and $f = f(d)$, the integral particle size distribution functions $F = F(d)$ are frequently used in practice. As an example, we will give the rain water content distribution function

$$F(d) = \frac{\pi}{6} \int_{d_{min}}^{d} d^3 n(d)\, dd, \tag{6.7}$$

characterizing the part of the water mass corresponding to drops with a diameter no greater than d per unit volume of air.

From the integral representation (6.7) and the analogous rain water content distribution with radii r we have the following equality for the function $\tilde{F}(r)$:

$$\tilde{F}(r) = F(2r),$$

from which it follows that the integral distribution functions, in contrast to differential distribution functions, are formed directly by substitution of the variable.

TABLE 6.1. AVERAGED CHARACTERISTICS OF PRECIPITATION-PRODUCING CLOUDS AFTER [239]. /256

Type of precipitation	Height of cloud base, M	Cloud thickness, M	t°C at cloud base level	t°C at cloud top level	Precipitation intensity, mm/3 hr.	Number of cases
1. Precipitation near the Earth's surface						
a) Snow						
light shower	850	1750	-9.6	—	0.03	7
light steady	800	2400	-5.7	—	0.10	26
heavy shower	600	2000	-5.6	—	0.8	11
heavy study	500	2550	-2.6	—	1.3	17
b) Rain formed from snow						
light shower	1000	3250	+2.6	-15.0	0.14	5
light steady	1150	3050	1.0	-14.6	0.2	26
heavy shower	950	2850	6.4	-13.7	1.0	17
heavy steady	750	3400	4.2	-13.5	2.0	36
c) Rain near the ground (of undetermined origin)						
light shower	1600	1900	+0.8	-8.0	0.4	10
light steady	1400	1900	3.1	-7.2	0.6	27
heavy shower	1200	2050	5.4	-9.0	0.7	28
heavy steady	500	3150	3.8	-8.8	1.4	14
d) Light precipitation						
rain with drizzle	500	1400	+5.5	-0.8	—	19
drizzle	1200	2150	3.6	-8.3	—	79
individual raindrops	2600	1200	2.7	-3.3	—	9
2. Precipitation observed above, without precipitation on the ground						
trails of precipitation	3200	1150	-11.6	-14.8	—	93
snow	700	2300	-5.3	-17.1	—	61
drizzle	350	850	+1.1	-2.6	—	26
ice crystals	3300	1600	-8.1	-17.9	—	35
heavily wetting clouds containing no ice crystals	1750	1600	-2.7	-2.7	—	21

For the practice, in addition to the particle size distribution functions themselves, of definite interest are also certain characteristics of the range of determination of their argument, such as the mean arithmetic diameter $\tilde{d}_1$, mean square diameter $\tilde{d}_2$, mean cubic diameter $\tilde{d}_3$, the most probable or modal diameter $\tilde{d}_{mod}$, the diameter of the drops making the maximum contribution to the water content $\tilde{d}_W$, the median d_{med}, etc. As parameters, they may also enter into more complex characteristics of hydrometeors, such as for example the water content W, defined by the expression $W = F(d_{max})$:

$$W = \frac{2}{3}\pi N \tilde{d}_3^3.$$

We will consider specific expressions (particle frequency diagrams) for the particle size distribution functions. Considering their further use in § 6.2-6.4, we will concentrate most of our attention on precipitation.

The Laws-Parsons' distribution was given [242] in the form of the distribution of the water volume formed by raindrops of diameter d falling on the ground.[99] From this distribution, it is easy to obtain the function n(d) by transformations:

$$n(d)\,\Delta d = 0{,}529 I \frac{M(d)}{v(d)\,d^3}, \tag{6.8}$$

where v(d) is the velocity of the raindrop at the Earth's surface in m/s (Tables 5.3, 5.4); d is the diameter in cm, Δd is the interval of diameter measurements in cm; I is the precipitation intensity in mm/h; n(d) is the raindrop size distribution in m^{-3}; M(d) is the part of the total volume of the water falling on the ground formed by drops of the interval Δd (a dimensionless quantity, Table 6.2).

The Marshall-Palmer distribution [243] gives the raindrop size distribution function in the form

$$n(d) = 0{,}08 \exp[-Bd]\ \text{cm}^{-4}, \tag{6.9}$$

where $B = 41\ I^{-0.21}$, cm^{-1}, and I is the rainfall intensity in mm/h.

Comparing distribution (6.9) with (6.8), Marshall and Palmer [243] come to the conclusion that their distribution satisfactorily describes the experimental data of Laws and Parsons if one neglects the tendency toward a slight overestimation of the number of fine droplets for which $Bd < 4.5$.

---

[99] It would be more accurate to say "drops of rain with drizzle." However, strictly for the sake of brevity, the word "drizzle" may be admitted hereinafter.

Best's Distribution. Having analyzed a large number of experimental data [244, 242, 245-247], A. Best found [247] that most observations may be described with the aid of the integral function (6.7) of the water content:

$$F(d) = 1 - \exp\left[-\left(\frac{d}{a}\right)^m\right] \tag{6.10}$$

by varying the parameters a and m. Switching from the integral function to the differential function n(d), we have

$$n(d) = \frac{6}{\pi} W \frac{m d^{m-4}}{a^m} \exp\left[-\left(\frac{d}{a}\right)^m\right] \text{ cm}^{-4}, \tag{6.11}$$

where W is the rain water content per 1 cm^3 of air, $W = \delta I^f$ g/cm^3; $a = \alpha I^B$ cm, and I is the rainfall intensity in mm/h.

TABLE 6.2. M(d) FOR DIFFERENT I. /259

d cm	I mm/h							
	0,25	1,25	2,5	12,5	25	50	100	150
0,050	0,28	0,10	0,07	0,03	0,02	0,01	0,01	0,01
0,100	0,50	0,37	0,28	0,12	0,08	0,05	0,04	0,04
0,150	0,18	0,31	0,33	0,25	0,18	0,12	0,09	0,07
0,200	0,03	0,14	0,19	0,25	0,24	0,20	0,14	0,12
0,250	0,01	0,05	0,08	0,17	0,20	0,21	0,17	0,14
0,300	—	0,02	0,03	0,10	0,13	0,16	0,18	0,18
0,350	—	0,01	0,01	0,04	0,08	0,11	0,15	0,16
0,400	—	—	0,01	0,02	0,03	0,07	0,09	0,12
0,450	—	—	—	0,01	0,02	0,03	0,06	0,08
0,500	—	—	—	0,01	0,01	0,02	0,03	0,04
0,550	—	—	—	—	0,01	0,01	0,02	0,02
0,600	—	—	—	—	—	0,01	0,01	0,01
0,650	—	—	—	—	—	—	0,01	0,01

Commas indicate decimal points.
Note: The tabulated data were calculated every $\Delta d = 0.050$ cm with the exception of the first interval from 0.00 to 0.075 cm. In all the other cases, the diameter d indicated in the table corresponds to the middle of the interval.

Having treated the experimental data of different authors, Best first established the values of the parameters m, α, β, δ and f for each of them (Table 6.3), and then, after averaging them again (without considering observations made on the Hawaiian Islands) over all the observation sites, he obtained:

$$m = 2{,}25; \quad \alpha = 0{,}130 \text{ cm}; \quad \beta = 0{,}232;$$
$$\delta = 6{,}7 \times 10^{-8} \text{ g/cm}^3; \quad f = 0{,}846. \tag{6.11a}$$

The distribution of the number of drops N_i in 1 m^3 of air, belonging to the corresponding interval of change in diameter d, calculated from formulas (6.11), (6.11a) and (6.3) is shown in Table 6.4.

TABLE 6.3. MEAN VALUES OF THE PARAMETERS OF DISTRIBUTION FUNCTION (6.11) BASED ON EXPERIMENTAL DATA OF VARIOUS AUTHORS. /260

Observation site		Author	m	α cm	β	$\delta \cdot 10^8$	f
Germany (1904)		Lenard	2.59	0.142	0.272	6.1	0.840
USA		Laws et al.	2.29	0.125	0.199	7.2	0.867
Canada		Marshall et al.	1.85	0.100	0.240	7.2	0.880
Ayniles*	England	Laird	2.49	0.188	0.203	7.4	0.845
Shuberines*	England	Gemens	2.29	0.156	0.209	5.9	0.816
Ost-Khill*	England	Jones	1.99	0.138	0.269	6.5	0.829

*Translator's Note: Correct spelling of these words unknown.

Table 6.5 gives a and W as a function of I.

Litvinov's Distribution. On the basis of experimental data obtained in the upper Baksanskaya Valley on the slopes of Mount El'brus and in the Alazanskaya Valley, I. V. **Litvinov** [248-250] came to the conclusion that the size distribution function of drops in the rain is not uniquely determined by the intensity I, but substantially depends on the origin of the rain.[100]

According to their origin, rains are divided into four groups:

1) Rains formed as a result of the melting of snow grains and heavily rimed particles (rains from graupel);

2) rains formed by the melting of unrimed and slightly rimed solid particles (rains from unrimed snow);

3) rains formed by the melting of medium-rimed particles (rains from rimed snow);

4) rains formed by the melting of hail (rains from hail).

---

[100] I. V. Litvinov considered only the case of formation of rain from the solid phase.

TABLE 6.4. DISTRIBUTION OF NUMBER OF DROPS PER 1 m^3 OF AIR AFTER [247].

Interval d, mm	I, mm/h					
	0,5	1,0	2,5	5,0	10,0	25,0
0,00—0,25	1250	1585	2136	2685	3369	4538
0,25—0,50	160	208	287	364	461	625
0,50—0,75	54	74	108	140	180	248
0,75—1,00	22	33	52	71	94	132
1,00—1,25	9	16	28	40	55	80
1,25—1,50	3,55	7	15	23	34	52
1,50—1,75	1,27	3,27	8	14	22	35
1,75—2,00	0,41	1,37	4,33	8	14	25
2,00—2,25	0,11	0,53	2,20	4,87	9	17
2,25—2,50	0,03	0,19	1,07	2,76	6	12
2,50—2,75	0,01	0,06	0,49	1,52	3,60	8
2,75—3,00	—	0,02	0,21	0,81	2,21	6
3,00—3,25	—	0,004	0,09	0,41	1,32	4,03
3,25—3,50	—	—	0,03	0,20	0,77	2,74
3,50—3,75	—	—	0,01	0,10	0,43	1,83
3,75—4,00	—	—	0,004	0,04	0,24	1,20
4,00—4,25	—	—	—	0,02	0,13	0,77
4,25—4,50	—	—	—	0,01	0,06	0,49
4,50—4,75	—	—	—	0,003	0,03	0,31
4,75—5,00	—	—	—	0,001	0,015	0,19
5,00—5,25	—	—	—	—	0,007	0,11
5,25—5,50	—	—	—	—	0,003	0,06
5,50—5,75	—	—	—	—	0,001	0,04
5,75—6,00	—	—	—	—	0,001	0,02
6,00—6,25	—	—	—	—	—	0,011
6,25—6,50	—	—	—	—	—	0,006
6,50—6,75	—	—	—	—	—	0,003
6,75—7,00	—	—	—	—	—	0,001

Commas indicate decimal points.

TABLE 6.5. VALUES OF a AND W IN EXPRESSION (6.11) FOR DIFFERENT I AFTER [247]. /261

I, mm/h...	0.5	1.0	2.5	5.0	10.0	25.0
a mm.....	1.107	1.300	1.608	1.888	2.218	2.743
W mm^3/m^3..	37	67	145	261	470	1020

The spectra of raindrops of all the groups enumerated above differ from one another. Thus, rains from graupel have a much greater number of fine droplets than rains from unrimed snow. Moreover, d_{max} in rains from graupel is much smaller than in rains from unrimed snow. The parameters of the spectral distribution of drops in rains from rimed snow occupy an intermediate position. In contrast to rains of the first three groups, rains from hail are marked by a high intensity and a short duration, occur in separate showers

lasting not more than 30 min, cover a small area and are distinctly local in precipitation character. Rains from hail are characterized by large droplets. The intensity of rains formed by the melting of snow changes slowly with time, whereas the intensity of rains from hail changes very abruptly.

Analysis of measurements showed [248-250] that the functions of Marshall--Palmer (6.8) and Best (6.11) adequately describe only rains from rimed snow and are unsuitable for describing rains from graupel or unrimed snow. For rains from hail, a good approximation of the experimental data is achieved with the aid of function (6.11) with the following parameter values: $a = 0.288 I^{0.31}$ cm; $m = 2.82$;

$$W = 6.45 \cdot 10^{-8} I^{0.7} \text{ g/cm}^3.$$

Characterizing the rain spectrum as a function of rain's origin, Litvinov /262 introduced the distribution function

$$n(d) = A \exp\left(-Bd^{3/2}\right) \tag{6.12}$$

with the parameters from Tables 6.6, 6.7. It was thus found that the function

$$n(d) = Ld^2 \exp(\beta d), \tag{6.13}$$

previously proposed in [251] by Ye. A. Polyakova and K. S. Shifrin, also satisfactorily describes the distribution of drops with diameters above 1 mm in range of different origins if L and β are taken from Tables 6.6, 6.7. At values $d < 1$ mm, a deviation of the theoretical data from the experimental ones is observed.

TABLE 6.6. VALUES OF THE PARAMETERS IN DISTRIBUTIONS (6.12), (6.13) FOR RAINS FROM SNOW.

Origin of rain	A cm^{-4}	B $\text{cm}^{-\frac{3}{2}}$	L cm^{-6}	β cm^{-1}
From graupel	$0.0133I^{0.4}$	$90.43I^{-0.24}$	$64.5I^{-0.5}$	$69.5I^{-0.27}$
From rimed snow	0.009	$65.77I^{-0.31}$	$11.75I^{-0.29}$	$48.7I^{-0.2}$
From unrimed snow	$638 \cdot 10^{-5} I^{-0.4}$	$57.86I^{-0.41}$	$2.83I^{-0.18}$	$40.1I^{-0.19}$

Kelkar's Distribution. On the basis of an analysis of a large number of rains in India during August, September and October 1956, V. Kalkar [252-254]

obtained the distribution of drops with size for range with intensities from 0.2 to 34 mm/h (Table 6.8).

TABLE 6.7. VALUES OF THE PARAMETERS IN DISTRIBUTIONS (6.12), (6.13) FOR RAINS FROM HAIL.

I mm/h	A cm^{-4}	B $cm^{-\frac{3}{2}}$	L cm^{-6}	β cm^{-1}
1.76	$602 \cdot 10^{-5}$	46.48	8.7	18.4
4.28	$186 \cdot 10^{-5}$	45.53	1.0	11.8
9.33	$123 \cdot 10^{-5}$	17.14	0.55	9.4
23.0	$11 \cdot 10^{-5}$	13.84	0.372	8.0

It is evident from the table that as I increases, the spectrum shifts toward larger diameter intervals, and a marked increase in the number of drops whose diameter exceeds 1 mm is observed. For $I > 13$ mm/h, the distribution curve has two maxima: the first at $d < 1$ mm, and the second at d between 1.25 and 1.50 mm. Also observed is an anomalous increase in the number of fine droplets at I = 35 mm/h.

Having treated these data by the least squares method, Kalkar found that Best's function (6.11) will agree with them satisfactorily if one assumes that /264 in addition to a and W, m also depends on the intensity (Table 6.9).

An approximation of the numerical values of a and W leads to their dependence on I, mm/h as follows:

$$a = 0{,}11 I^{0{,}176} \text{ cm}, \qquad W = 7{,}1 \cdot 10^{-8} I^{0{,}88} \text{ g/cm}^3. \tag{6.14}$$

It is interesting to note that expressions (6.14) are rather close to the analogous expressions obtained by Marshall and Palmer, Laws and Parsons and Best [see Tables 6.3, 6.5 and expressions (6.11a)]. In addition, Kalkar obtained expressions for the different parameters of the spectrum:

a) for the mean arithmetic diameter: $d_1 = 0.63\ I^{0.25}$ mm;

b) for the modal diameter $d_{mod} = 0.63$ mm (0.50 to 0.75 mm) for all I;

c) for the mean number of drops of all sizes per 1 m^3 of air:

$$N = 282 + 220I,$$

etc.

TABLE 6.8. AVERAGE NUMBER OF DROPS IN 1 m^3 OF AIR AFTER [254].

Interval d, mm^3	I, mm/h									
	0,20	0,33	0,46	0,57	0,64	0,76	0,87	1,1	1,5	1,9
0,00—0,25	80	22	—	34	44	66	40	17	—	—
0,25—0,50	125	67	49	69	81	55	41	51	46	59
0,50—0,75	25	85	111	82	123	99	89	83	126	136
0,75—1,00	8	19	34	41	47	34	70	60	92	76
1,00—1,25	2,7	4,1	3,5	8	8,3	8	13	17	28	31
1,25—1,50	1,5	1,4	1,4	2,8	2	2,9	3,9	6,2	6,9	14
1,50—1,75	0,03	0,2	0,8	1,2	0,6	1,8	1,5	2,4	2,2	3,8
1,75—2,00	—	0,2	0,3	0,3	0,5	1,2	0,6	1,2	1,7	1,5
2,00—2,25	—	0,2	0,2	0,1	0,2	0,5	0,08	0,2	1,9	0,9
2,25—2,50						0,1	0,04	0,1	0,1	0,7
2,50—2,75						0,06	0,04	0,04	—	0,4
2,75—3,00										
3,00—3,25										
3,25—3,50										
3,50—3,75										
3,75—4,00										
Total no. of drops	242	198	200	238	307	269	259	238	305	323

Interval d, mm^3	I, mm/h									
	2,3	3,5	4,1	4,6	5,4	6,2	8,6	9,9	13,0	18,0	34,0
0,00—0,25	—	—	—	19	—	—	—	5	—	—	592
0,25—0,50	54	50	29	60	15	66	—	60	18	32	561
0,50—0,75	110	85	72	130	96	141	37	121	104	94	388
0,75—1,00	180	93	168	107	85	124	47	83	74	55	118
1,00—1,25	79	100	88	101	87	108	123	76	85	88	105
1,25—1,50	29	42	38	72	59	72	98	80	120	128	156
1,50—1,75	5,5	9,4	8,8	8,6	22	30	47	52	69	70	117
1,75—2,00	1,9	2,1	6,8	2,7	14	8	19	21	27	52	100
2,00—2,25	0,4	0,5	1,4	0,2	5,1	1,0	1,6	7	12	17	51
2,25—2,50	0,08	0,2	0,2	0,1	0,4	0,5	0,9	4,5	5,8	7,2	23
2,50—2,75	—				0,08	0,1	—	1,0	1,0	4,4	10
2,75—3,00						—	0,1	0,3	—	1,7	1,4
3,00—3,25						0,2	—	—	0,1	0,1	0,4
3,25—3,50								—	—	0,9	—
3,50—3,75								0,1	—	—	—
3,75—4,00								0,1	—	—	—
Total no. of drops	460	382	402	501	383	552	374	511	516	546	2222

Commas indicate decimal points.

TABLE 6.9. PARAMETERS n, a AND W IN DISTRIBUTION (6.11) FOR RAINS AFTER KALKAR [254].

Interval of change in I, mm/h	I, mm/h	n	a, cm	$W \cdot 10^8$ m^3/m^3
0.0-0.6	0.40	1.93	0.091	3.1
0.6-1.1	0.83	1.70	0.097	5.6
1.1-3.8	2.45	1.94	0.118	15.6
3.8-7.3	5.10	4.0	0.146	29.6
7.3-20.0	12.0	3.67	0.180	59.0
20.0-41.0	34.0	3.43	0.188	157.3

Polyakova's Distribution. On the basis of an analysis of 40 cases of rain precipitation at Voyeykovo (Leningrad province) and 19 cases in the region of subtropics, at the Chakvi agrometeorological station near Batumi in the course of 4 summer seasons of 1953-1955 and 1957, Ye. A. Polyakova [255] found that the distribution functions of raindrops with radius are:

$$n(r) = Ar^2 e^{-\beta r}, \tag{6.15}$$

$$n(r) = Le^{-\delta r}, \tag{6.16}$$

where $A = 0.0066\ \alpha\beta^5\ cm^{-6}$, $\beta = 635\left(\frac{\alpha}{I}\right)^{\frac{2}{3}}\ cm^{-1}$, $L = 0.08\ \alpha\beta^3\ cm^{-4}$, $\delta = 391\left(\frac{\alpha}{I}\right)^{\frac{2}{3}}$ cm^{-1}, α is the attenuation coefficient of visible light in the rain zone in cm^{-1} and I is the rainfall intensity in cm/s, are valid for $r > r_0 = r_0(I)$. /265 The dependence of r_0 on I is shown in Table 6.10.

TABLE 6.10. FUNCTION $r_0 = r_0(I)$.

Interval of change in I, mm/h	0.3-3	3-5	5-10	10-15	15-25	24-40	40-60
r_0, mm	0.2	0.25	0.3	0.35	0.40	0.45	0.55

As stated by its author, the method used in [255] does not permit a theoretical calculation of the distribution curve for $r < r_0$.

The paper [255] also notes that no geographical differences in the microstructure of the rains was observed.

Joss's Distribution. In a study of the size distribution of raindrops at Locarno, J. Joss et al. [256, 257] found that a function of the form

$$n(d) = Me^{-\beta d} \tag{6.17}$$

with parameters from Table 6.11 is suitable for describing rains of different types.

It is interesting to note that values of m and β for a widely distributed rain (Table 6.11) practically coincide with the corresponding quantities in the Marshall-Palmer distribution function (6.9).

TABLE 6.11. PARAMETERS M AND β OF DISTRIBUTION (6.17).

Type of rain	M cm^{-4}	β cm^{-1}
Drizzle	0.3	$57I^{-0.21}$
Steady rain	0.07	$41I^{-0.21}$
Thundershower	0.014	$30I^{-0.21}$

Donaldson's Distribution [258] is given by expression (6.17) with

$$M = 70 \text{ см}^{-4}, \quad \beta = 41I^{-0,21} \tag{6.18}$$

and is applicable to drizzle.

If this distribution is compared with the Marshall-Palmer distribution (6.9), it is easy to see that it differs from the latter in the preexponential factor (it is 875 times greater!). It should be noted that this distribution was obtained by Donaldson after only a few observations.

Distributions Proposed by Other Authors. In addition to the most common distribution functions enumerated above, the literature contains data on other n(d) functions as well, obtained on the basis of experimental studies /266 of rains in different geographical latitudes at different times of year. These functions are extremely diverse.

Thus, Best proposed in [259] a classification of rains according to 9 types: A, B, C, D, E, F, G, H, J (Table 6.12). Here A and B are ordinary rains falling over large areas; C is a rain with breaks in the cloud and solar radiance; D is a brief thundershower, E is a sudden rain from small light clouds under conditions of a windless clear atmosphere; F is a heavy rain similar to a hail shower; G, H, J is the heaviest rain with frequent brief interruptions.

TABLE 6.12. NUMBER OF DROPS PER 1 m^3 OF AIR IN DIFFERENT TYPES OF RAINS AFTER [64, 70].

d,mm	Type of rain								
	A	*B*	*C*	*D*	*E*	*F*	*G*	*H*	*J*
0,5	28,5	476	752	61,4	3,33	0,0	323	245	47,6
1,0	71,8	512	30,8	25,6	59,7	12,8	134	108	333
1,5	31,0	27	11,4	14,0	21,5	9,52	66	68,4	95,2
2,0	3,13	22	31,2	15,6	7,2	23,4	46,1	21,6	31,2
2,5	2,76	—	—	4,0	0,96	0,0	28,3	21,5	0,0
3,0	—	—	—	7,2	0,0	25,3	10,2	17,6	0,0
3,5	—	—	—	—	3,83	0,0	3,35	0,0	0,0
4,0	—	—	—	—	4,88	5,75	2,3	0,0	0,0
4,5	—	—	—	—	0,0	—	—	11,3	22,5
5,0	—	—	—	—	2,71	—	—	—	—
I,mm/h	2,46	3,6	4,0	6,0	15,2	18,7	22,6	34,3	43,1

Commas indicate decimal points.

R. Wexler and D. Atlas [260] found that the raindrop distribution function (6.9) proposed by Marshall and Palmer is unsuitable for describing fine droplets. A better suited function for fine droplets is (6.17), with the following parameters: M = 0.01 cm^{-4}, β = 20 cm^{-1} for $d \leqslant 1$ mm, I = 0.8 to 1.0 mm/h and M = 0.01 cm^{-4}, β = 15 cm^{-1} for $d \leqslant 1.5$ mm, I = 3.85 to 5.0 mm/h.

Measurements by E. Mueller and D. Jones [261] and M. Fujiaara [262] showed that the Marshall-Palmer distribution (6.9) cannot be used for showers.

Instead of an exponential decrease with size, the concentration of drops increases to a maximum, then decreases exponentially. Thus, the function n(d) may in this case be given by the expression

$$n(d) = \begin{cases} N_1 e^{\beta d}, & d \leqslant 0{,}15 \text{ cm}, \\ N_2 e^{-\delta d}, & d \geqslant 0{,}15 \text{ cm}, \end{cases} \qquad (6.19)$$

The mean value of β is 4.3 (variation range 0.6-7.1), ρ = 3.5 (range 2.6-4.6). /267

D. Atlas [149] selected a simple linear dependence of the total number of drops N in 1 m^3 on the rain intensity (in mm/h):

$$N = 100 + 7\ I.$$

From this it is easy to determine the values of coefficients n_1 and n_2 (in cm^{-4}) in expression (6.19):

$$N_1 = 3{,}05 \cdot 10^{-6} + 2{,}13 \cdot 10^{-7} I,$$
$$N_2 = 0{,}37 + 0{,}025 I.$$

J. Imai [263] found on the basis of a study of the spectra of rains falling in Japan that the quantity $d^3n(d)$ has a Gaussian distribution.

M. Sivaramakrishnan [264] studied the size distribution of drops in thundershowers in India. Using the similarity of the relationships between the reflectivity, water content, diameter of the median volume and rain intensity obtained by Marshall and Palmer, he came to the conclusion that on the average, function (6.9) adequately approximates the experimental data.

Analyzing the experimental data of [251, 242], Ye. M. Sal'man [65] obtained a size distribution function of drops in showers and steady rains starting with r = 100 μm:

$$n(r) = ar^{-2} \text{ cm}^{-4},$$

where

$$a = \frac{5120Z}{[1 - \exp(-0{,}41Z^{0{,}162})]} \text{ cm}^{-2},$$

where Z is the reflectivity factor[101] (in mm^6/m^3), related to the rainfall intensity I mm/h by the relation $Z = 220\ I^{1.54}$.

However, Ye. A. Polyakova in [255], evaluating [242] and her earlier work [251], indicates the unreliability of the method used in [251] to obtain statistical material on fine droplets and also the fact that the filter paper method employed by Laws and Parsons [242] for sampling makes it impossible to measure drops smaller than 0.3 mm in diameter.

On the basis of radar observations of rains at the Central Aerological Observatory in the summer and autumn of 1961, A. G. Gorelik and G. A. Smirnova [266] proposed the distribution function

$$n(d) = \frac{N\beta^{b+1}}{\Gamma(b+1)} d^b e^{-\beta d}, \qquad (6.20)$$

where N is the number of drops per unit volume (ranging from 100 to 1,000 per 1 m^3), b and β are parameters (b = 2 to 32; β = 50 to 640). Generalizing the extensive experimental material on rains obtained by the Central Aerological Observatory, the authors of [267, 268] propose the inverse power law /268

$$n(d) = \alpha d^{-\beta} \qquad (6.21)$$

for d changing from 0.15 mm to d_{max}, where d_{max} ranges from 0.2-0.3 to 1-1.5 mm.

[268] indicates a difference between drop spectra in continuous precipitation, which is subordinate, in most cases, to the power law (6.21), and drop spectra in shower precipitation, which is satisfactorily described by the exponential function (6.9). As noted by these authors, this difference is due to a different mechanism of enlargement of the drops.

---

[101] Concerning the determination of the reflectivity factor see, for example [149].

Analyzing the experimental data of a series of studies, the authors of [269] found that despite the diversity of these studies, it is possible to give a unique analytical description of the spectra of all rains with the aid of the generalized gamma distribution

$$n(d) = Cd^{\mu}\exp(-\beta d^{\gamma}), \tag{6.21a}$$

where $3 \leqslant \mu \leqslant 30$, $-\frac{3}{2} \leqslant \gamma \leqslant \frac{3}{2}$.

D. Deirmendjin [270] used the size distribution function of drops in this form at $N = 10^3$ m^{-3}, $\tilde{d}_{mod} = 0.1$ mm, $W = 0.495$ g/m^3 to study the scattering properties of hydrometeors.

L. M. Levin [271] showed the possibility of using the following lognormal law for describing the distribution of raindrops with diameter:

$$n(d) = \frac{N}{\sigma d\sqrt{2\pi}}\exp -\left[\frac{\ln^2 \frac{d}{\tilde{d}_0}}{2\sigma^2}\right],$$

where $\tilde{d}_0$ is the mean geometric diameter of the particles, ranging from 0.56 to 0.64 mm for range with I = 0.5 to 7.5 mm/h; σ is the dispersion, ranging from 0.41 to 0.52 for rains with I = 0.5 to 7.5 mm/h.

It was also noted [271] that the distribution function (6.9) and gamma function [272] adequately approximate a lognormal law over a fairly wide range (F. Kessler and D. Atlas [273] established that the Marshall-Palmer distribution is also applicable to the representation of the spectrum of drops of hurricane showers.

As a rule, the above distribution function of raindrops with size are the result of averaging over a large number of observations and large areas. At the same time, depending on various external factors, individual rain spectra taken simultaneously at different points of the precipitation zone separated by small distances may differ markedly from one another, as may samples (Figure 6.2) taken at different times. Moreover, the rainfall intensity I may itself change appreciably in time (Figure 6.3) and (Figure 6.4). In that case, the spectra of the rain depend on the variation of its intensity with time (Figure 6.5). It is evident that the spectra differ sharply from one another as its intensity increases and decreases. As I decreases, the spectra break off abruptly in the large drop portion, while the spectra during increasing I have a large number of large drops and a comparatively small number of fine ones. /269

Hence, the size distribution functions of raindrops discussed above can be applied only to rains of constant intensity. However, even in this case it is necessary to use them carefully, since some were obtained from the basis of samples of small volume ($\sim$ 1 m^3). As was shown by E. Mueller and A. Simms [276], for a sample volume of 1 m^3, the errors in the calculation of the

intensity and reflectivity of the precipitation on the basis of the spectrum obtained from the sample may reach 70% or more.

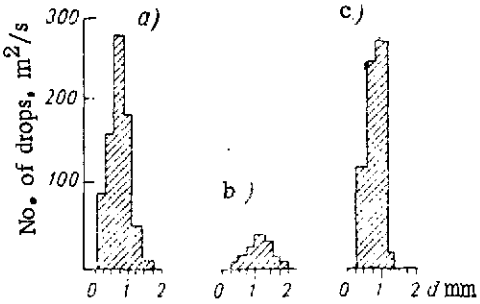

Figure 6.2. Three (a, b, c) Different Spectra of Raindrops (On the Ground) of the Same Intensity I = 0.6 mm/h After [252].

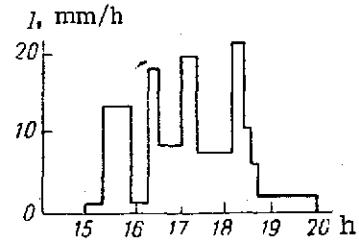

Figure 6.3. Change in Rainfall Intensity I with Time on 19 June 1951 in the Village of Voyeykovo After [204].

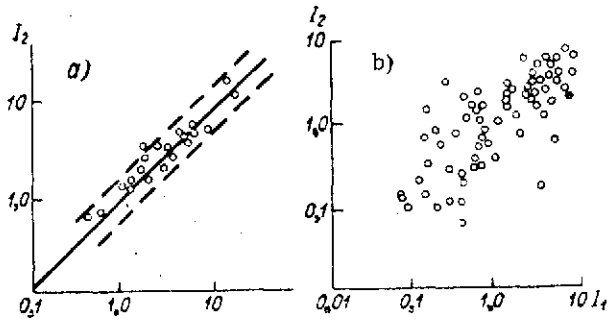

Figure 6.4. Relationship Between Rainfall Intensities (mm/h) at Points Separated by 10 m(a) and 1,200 m(b) From Each Other After [274].

Let us also note at this point that the many distribution functions given in the literature do not provide sufficiently reliable statistics on fine drops. The need for such data is very perceptible in connection with the development and perfection of submillimeter radar engineering. /270

Distribution Functions of Snow Particles. A study of the size distribution of snowflakes of uniform shape, K. Gunn and J. Marshall obtained [189]

$$n(d) = N_0 \exp(-\Lambda d), \qquad (6.22)$$

where $N_0 = 3.8 \cdot 10^{-2} I^{-0.87}$ cm^{-4}, $\Lambda = 25.5 I^{-0.48}$ cm^{-1}, I is the intensity in mm/h, and d is the diameter in cm of a drop obtained from a molten snow crystal.

I. V. Litvinov [194] came to the conclusion that the distribution curves of drops equivalent in mass to snow crystals may be represented by the gamma distribution proposed earlier by L. M. Levin [272],

$$n(d) = \frac{N d^{\alpha} e^{-\frac{d}{\beta}}}{\Gamma(\alpha+1)\beta^{\alpha+1}}, \qquad (6.23)$$

where $\Gamma(x)$ is the gamma function; α and β are parameters related by the relation $\beta = 292\alpha^{-0.67}$. Experimental analysis [194] showed that the α and N values change from one snowfall to the next over fairly wide limits. Moreover, a decrease in α with rising temperature was observed for one and the same snowfall.

On the basis of 42 spectra of snow crystals in different snowfalls, Abshayev et al. [197] obtained a distribution function of snow crystals with diameter

$$n(d) = \frac{N\beta^{\mu+1}}{\Gamma(\mu+1)} \frac{d^{\mu}}{d_3^{\mu+1}} \exp\left[-\beta \frac{d}{\widetilde{d}_3}\right], \tag{6.24}$$

analogous to function (6.23) for drops equivalent to these crystals. Here N is the number of snow crystals per unit volume; d_3 is the root-mean-cube diameter; /271

$$\beta = \sqrt[3]{(\mu+1)(\mu+2)(\mu+3)}; \tag{6.25}$$

μ is a parameter ranging from 0 to 4.

Hail Distribution Functions. Analysis [277] of 30 hail spectra collected during the spring-summer periods of 1962-1964 on the Mushtinskiy and Sasmarskiy high-mountain polygons [278, 279] and 8 spectra based on data of [280, 281] showed that of the 20 cases of hail precipitation, in 15 (28 spectra) a simultaneous unsymmetric distributions of hailstones with size was observed, and in 5 (10 spectra), both a one-peak and a two-peak distribution occurred along the hail path.

One-peak distributions are adequately described by gamma function (6.24) with μ = 0 to 10; half of them correspond to μ = 2, i.e., to the distribution obtained by the authors of [271, 283] on the basis of more limited experimental material.[102]

As was shown in [279][103] two-peak size distributions of hailstones always occur in the central portion of a hail band, and a one-peak distribution is observed along with a two-peak distribution in one and the same case of hail precipitation. Moreover, in all the cases of hail precipitation, there was not a single instance [277] of just a two-peak distribution at any of the portions along the hail path. The first maximum of the two-peak distribution was an average of 3.6 times greater than the second, and the ratio of modal dimensions of the hailstone spectrum was equal to an average of 3.1. It is noted in [277] that the second maximum for the above-mentioned 10 spectra corresponds in the majority of cases to d = 1.1 cm, the ratio of the magnitudes

[102] Data on hail concentration N may be found in [278, 279, 282]. Comparison of these data in [278] with the data of J. Ryde [139], D. Atlas, R. Donaldson, F. Ludlam and F. Macklin [282] showed the latter data to be 0.5-1 order of magnitude too low.

[103] See also [323-325].

of the maxima changes from one case to another, and a smooth transition from the one-peak to the two-peak distribution is observed.

The two-peak spectral distribution of hailstones with size is adequately represented in the form of a sum of two gamma distributions with parameters μ_1, β_1 and μ_2, β_2 [277], with μ_1 = -1 to 1; μ_2 = 4 to 8.

The paper [277] indicates the independence of the hail spectra from the climatic and geographical conditions (Northern Caucasus, Transcaucasia, England, Canada).

§ 6.2. Effect of Multiple Reemissions on the Radar Characteristics of A Set of Hydrometeoric Particles

Chapters 2 and 3 developed a rigorous theory of scattering and attenuation of electromagnetic waves by an arbitrary set of homogeneous and nonconcentrically layered spheres, and also derived expressions for its various electromagnetic and radar characteristics. /272

In this section, on the basis of the formulas and expression given in Chapters 2 and 3, and with the aid of a computer, we will make a partial study of the effect of the interaction of water drops and homogeneous and inhomogeneous hailstones on the effective areas of radar scattering and attenuation.

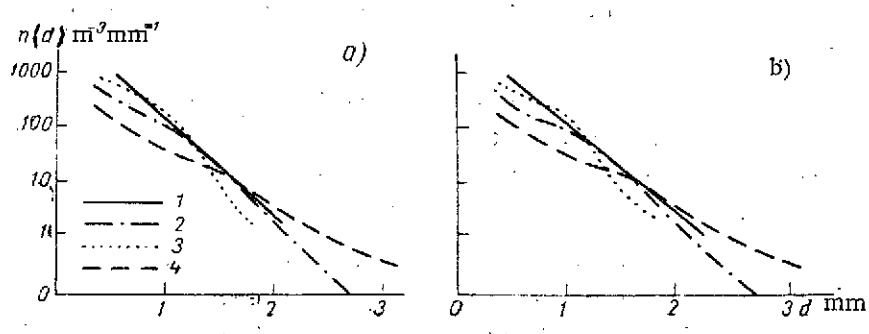

Figure 6.5. Spectral Distribution of Rain of Intensity 1 mm/h (a) and 5 mm/h (b) after [275]. 1) Calculated curve after Marshall and Palmer; 2) Average spectrum; 3) Spectrum of intensity decrease; 4) Spectrum of intensity increase.

Let the coordinate system $X_0Y_0Z_0$ (Figure 6.6)[104] contain 4 homogeneous spherical particles with diameters d_i (i = 1, 2, 3, 4); the centers of all of the particles lie in the plane $X_0Y_0Z_0$, the sphere of diameter d_1 being at the

[104] See also Figure 2.1.

origin, and the other 3 being separated from it by the same distance l. Other details of their relative positions are indicated directly in Figure 6.6.

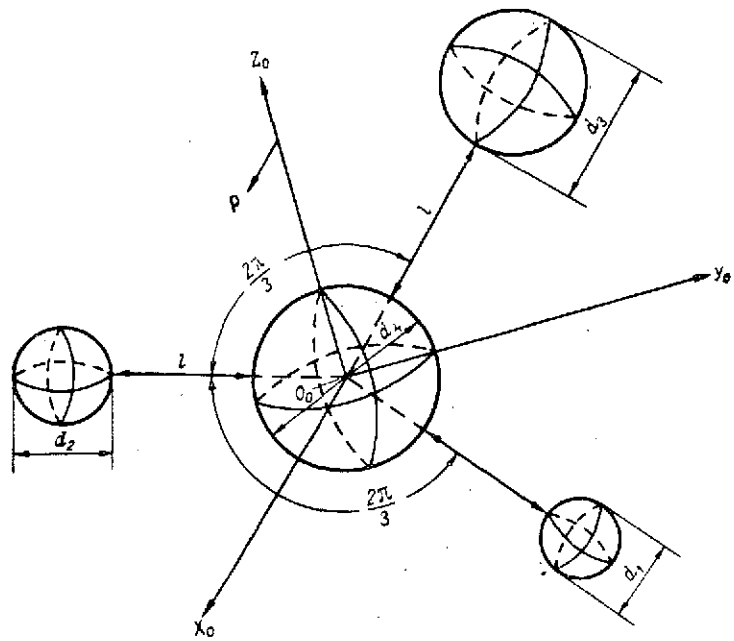

Figure 6.6. Theoretical Model of the Location of Four Spherical Particles of Different Diameters.

These assumptions were used with formulas (2.82), (2.77), (2.59) and (2.58) /27 to calculate, with an accuracy of not more than 10%, the radar scattering cross-section σ_0' and attenuation cross-section σ_2' of the particles for the following 3 cases (Figure 6.6).

1. All the particles are water drops of different diameters: d_1 = 1 mm, d_2 = 2 mm, d_3 = 3 mm, d_4 = 4 mm; wavelength[105] λ = 2.74 mm; temperature t = 16°C; the dielectric constant of water was calculated from formulas (4.13), (4.14), (4.16), (4.23), (4.24); the distance l between the particles ranged from 1.6 to 50 mm.

2. All the particles were water drops of the same diameter d_i = 4 mm (i = 1, 2, 3, 4); λ = 6 mm; t = 16°C, and the dielectric constants of water were calculated in the same way as in p. 1; l = 4.4 to 5.0 mm.

---

[105] It was assumed equal to the mean square diameter of all the spheres.

3. All the particles were homogeneous hailstones of the same diameter d_i = 6 mm (i = 1, 2, 3, 4); λ = 8 mm; t = 0°C; the dielectric constants of ice were chosen from Table 4.33 after Cumming; l = 6.0 to 50 mm.

For the sake of convenient discussion, the final quantities programmed for computation were the expressions $\Sigma_0 = \sigma'_0\left[\sum_{i=1}^{4}\sigma'_{0i}\right]^{-1}$ and $\Sigma_2 = \sigma'_2\left[\sum_{i=1}^{4}\sigma'_{2i}\right]^{-1}$, where σ'_{0i} and σ'_{2i} are respectively the cross-sections of radar scattering and attenuation by a single particle of diameter d_i (assuming that the other 3 are absent), determined from formulas (1.276), (1.274) and (1.288).

Results of calculations of Σ_0 and Σ_2 are shown in Figures 6.7 and 6.8, from which it is evident that the σ_0 and σ_2 curves for water drops and hailstones are oscillatory in character. Moreover, the quantities $\sigma^{(i)} = 1 - \Sigma_i$ (i = 0, 2), hereinafter called reemission factors of radar scattering (i - 0) and attenuation (i = 2)[106] tend to zero with increasing l. The oscillatory character of the $\Sigma^{(i)}$ curves is responsible for the fact that for two distances l' and l'' between particles, with $l' \gg l''$, the reemission factors may be considerably greater at $l = l'$ than at $l = l''$. /274

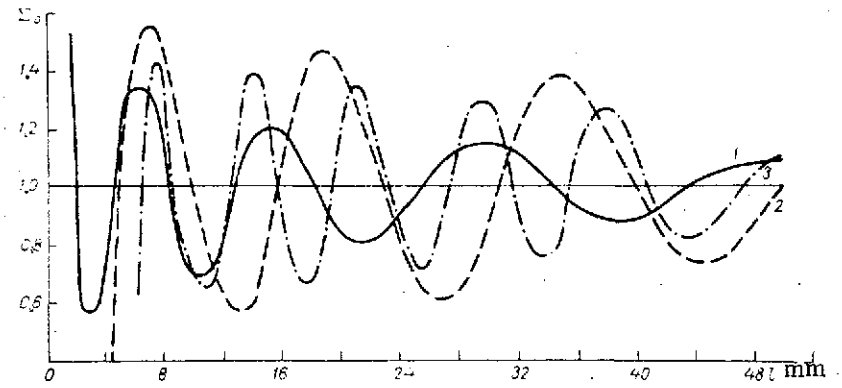

Figure 6.7. Dependence of Σ_0 of Four Particles on the Distance Between Them. 1) Case 1; 2) case 2; 3) case 3.

[106] In terms of reemission factors, the effective areas of radar scattering σ'_0 and attenuation σ'_2 of a set of four meteorological particles may be represented in the form

$$\sigma'_i = \sum_{j=1}^{4}\sigma'_{ij} + \Sigma^{(i)}\left(\sum_{j=1}^{4}\sigma'_{ij}\right), \quad i = 0, 2.$$

In the calculated range of l, the largest contribution of multiple reemission between particles[107] to the σ_0' and σ_2' values amounts to, respectively: for case 1, 55 and 38%; for case 2, 59 and 48%; for case 3, 37 and 40% of $\sum_{j=0}^{4}\sigma'_{0j}$ and $\sum_{j=0}^{4}\sigma'_{2j}$. It should be assumed, that as l decreases, the maximum of $\Sigma^{(i)}$ increases.

Comparing cases 1 and 2, one can easily note that the reemission factors for both radar scattering and attenuation for hailstones are an average of 20% lower than for water drops.

At $\frac{l}{\lambda} > l^{(0)}$ for σ_0' and $\frac{l}{\lambda} > l^{(2)}$ for σ_2' with an error no greater than δ%, the scattering multiplicity may be neglected, i.e., the scattering may be considered incoherent (Table 6.13).

The curves of Figures 6.7 and 6.8 also show that the reemission factors of radar scattering in the integral average are greater than $\Sigma^{(2)}$ for each of the cases discussed.

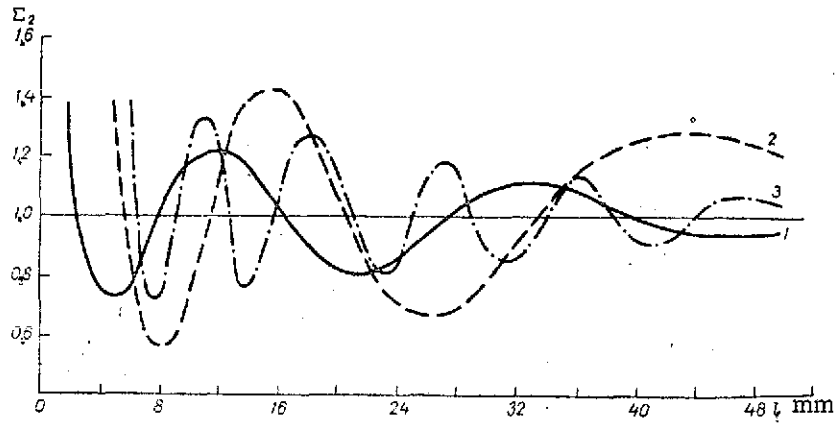

Figure 6.8. Dependence of Σ_0 of Four Particles on the Distance Between Them. 1) Case 1; 2) case 2; 3) case 3.

Let us know consider the effect of interaction of two nonconcentrically layered hailstones. We will take two completely identical three-layered hailstones (Figure 6.9) with the following parameters: d_1 = 2 cm; d_2 = 1.6 cm; d_3 = 0.4 cm; h_2 = 0.1 cm = h_3; medium (1) is ice of density 0.38 g/cm^3, medium /27

[107] More accurately, the largest value of $\Sigma^{(i)}$.

(2) is ice of density 0.60 g/cm^3, medium (3) is ice of density 0.92 g/cm^3; λ = 3.2 cm; t = 0°C. We will place them at a distance l cm from one another as shown in Figure 6.9. The radar characteristics of each such hailstone have already been determined in § 5.4 (see Figures 5.40 and 5.41). We will concentrate our attention here on the reemission factors of radar scattering $\Sigma^{(0)}$ and attenuation $\Sigma^{(2)}$ of a set of such hailstones.

TABLE 6.13. VALUES OF PARAMETERS $l^{(0)}$ (IN THE NUMERATOR) AND $l^{(2)}$ (IN THE DENOMINATOR)

Case	δ %			
	30	20	15	10
1	2,7 / 0,72	5,8 / 4,8	8,4 / 8,8	14,6 / 13,1
2	6,1 / 4,7	—	—	—
3	2,7 / 0,77	4,7 / 2,3	5,6 / 3,5	5,8 / 4,6

Commas indicate decimal points.
Note: Dashes in case 2 signify that in the calculation range $\frac{l}{\lambda}\left(\frac{l}{\lambda} \leqslant 6.25\right)$, there are no values of $l^{(i)}$ (i = 0, 2), such that the inequality $\Sigma^{(i)} < 20$ is fulfilled uniformly for all $\frac{l}{\lambda} > l^{(i)}$, (i = 0,2).

/276

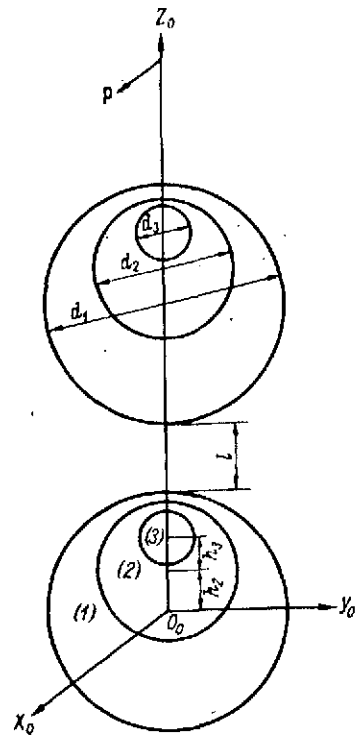

Figure 6.9. Theoretical Model of the Location of Two Nonconcentrically Layered Hailstones.

Results of their calculation from exact diffraction formulas (3.26), (3.26a), (2.104), (2.108), etc. (expressed in percent accurately to ±15%) as a function of the ratio $\frac{l}{\lambda}$ are shown in the form of curves in Figure 6.10. It is evident that the $\Sigma^{(i)}$ curves (i = 0, 2) are oscillatory in character, with an amplitude tending to zero as the distance between the hailstones increases. The largest value of $\Sigma^{(0)}$ is 120%, $\Sigma^{(2)}$ is 78%, reached at $\frac{l}{\lambda}$ = 1.2. At distances greater than 6.0, for σ_2' and 7.6 for σ_0', the multiple reemission of the hailstones under consideration may be neglected with an accuracy of not more than 25%.

/278

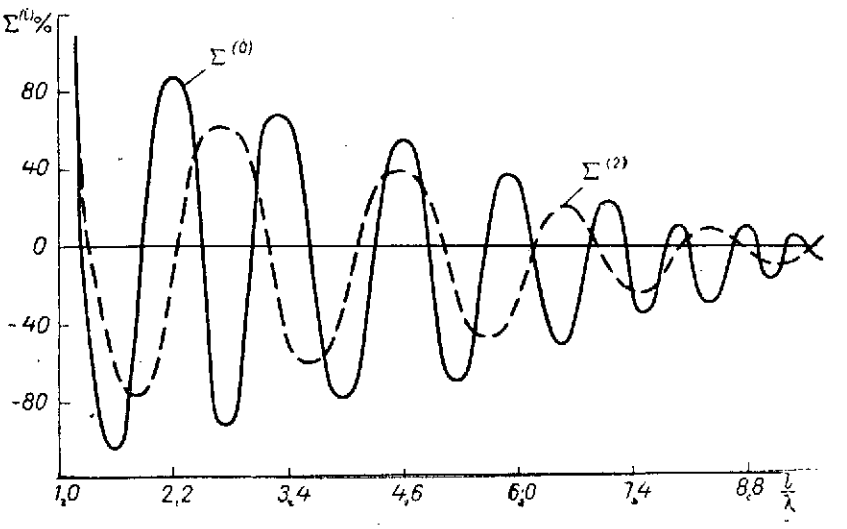

Figure 6.10. Dependence of $\Sigma^{(0)}$ and $\Sigma^{(2)}$ of Two Nonconcentrically Layered Hailstones on $\frac{l}{\lambda}$.

Thus, it follows from the above examples that for certain relative magnitudes of the particle diameters, distances between the particles, length of the emitted wave and other factors[108], the additional total field due to multiple reemissions may prove to be of the same order as the field of single reflection, and consequently the radar characteristics of a set of such particles in the incoherent approximation become substantially inaccurate even in the case of relatively large distances between them.

Average parameters of the most typical hydrometeors are listed in Table 6.14, compiled on the basis of the data of [81, 278]. It is evident that $\frac{l}{d} > 20$ for all of them. The value of $\frac{l}{\lambda}$ in the millimeter and submillimeter range of radiowaves is close to unity only for clouds and fogs. For precipitation, it ranges from 7.0 to 5,770. This makes it possible to assume, with sufficient accuracy for radio meteorology and radar that the scattering of microwaves of this range by rains, hail and pellets is incoherent.

In the case of centimeter waves, however, the ratio $\frac{l}{\lambda}$ may be correspondingly much lower (clouds, fogs, rains), of the same order of magnitude, and much greater than unity. Therefore, in this range of λ, multiple reemission of particles may prove to have an appreciable effect on the radar characteristics of hydrometeors.

---

[108] For example, the arrangement of the layers in a nonconcentrically layered hailstone.

TABLE 6.14. MEAN VALUES OF PARTICLE DIAMETERS d, DISTANCES l BETWEEN THEM AND OTHER PARAMETERS OF VARIOUS HYDROMETEORS

Types of Hydrometeors	d mm	l mm	$\frac{l}{d}$	0.1 mm $\leqslant \lambda \leqslant$ 1 mm	
				$\frac{d}{\lambda}$	$\frac{l}{\lambda}$
Clouds (of all types).....	0,008	1,3	162	0,08—0,008	13,0—1,3
Fog:					
Thin.....	0,01	4,3	430	0,1—0,01	43—4,3
Medium.....	0,1	21,0	210	1,0—0,1	210—21
Rain:					
Light (1 mm/h).....	0,45	70,0	155	4,5—0,45	700—7,0
Moderate (4 mm/h).....	1,0	123,0	123	10—1,0	1230—123
Heavy (15 mm/h).....	1,5	130,0	86,6	15—1,5	1300—130
Very Heavy (40 mm/h).....	2,1	138,0	65,6	21—2,1	1380—138
Shower (100 mm/h).....	4,0	137,0	34,3	40—4,0	1370—137
Hail.....	7,9	353	44,7	79—7,9	3530—353
	14,2	57,7	40,6	142—14,2	5770—577
Ice Pellets.....	3,0	123	41,0	30—3,0	1230—123
	5,1	227	40,6	51—5,1	2270—227
	6,3	128	20,3	63—6,3	1280—128

Types of Hydrometeors	1 mm $\leqslant \lambda \leqslant$ 10 mm		1 cm $\leqslant \lambda \leqslant$ 10 cm		10 cm $\leqslant \lambda \leqslant$ 20 cm	
	$\frac{d}{\lambda}$	$\frac{l}{\lambda}$	$\frac{d}{\lambda}$	$\frac{l}{\lambda}$	$\frac{d}{\lambda}$	$\frac{l}{\lambda}$
Clouds (of all types).....	0,008—$8,10^{-4}$	1,3—0,13	$8,10^{-4}$—$8,10^{-5}$	0,13—0,013	$8,10^{-5}$—$4,10^{-5}$	0,013—0,007
Fog:						
Thin.....	0,01—10^{-3}	4,3—0,43	10^{-3}—10^{-4}	0,43—0,043	10^{-4}—$5,10^{-5}$	0,043—0,021
Medium.....	0,1—0,01	21—2,1	0,01—0,001	2,1—0,21	0,001—$5\cdot10^{-4}$	0,21—0,1
Rain:						
Light (1 mm/h)...	0,45—0,045	70—7,0	0,045—$4,5\cdot10^{-3}$	7,0—0,7	$4,5\cdot10^{-3}$—$2,3\cdot10^{-3}$	0,7—0,4
Moderate (4 mm/h)	1,0—0,1	123—12,3	0,1—0,01	12,3—1,2	0,01—0,005	0,12—0,06
Heavy (15 mm/h)..	1,5—0,15	130—13,0	0,15—0,02	13,0—1,3	0,02—0,01	1,3—0,6
Very heavy (40 mm/h)	2,1—0,21	138—13,8	0,21—0,02	13,8—1,4	0,02—0,01	1,4—0,7
Shower (100 mm/h)	4,0—0,4	137—13,7	0,4—0,04	13,7—1,4	0,04—0,02	1,4—0,7
Hail.....	7,9—0,79	353—35,3	0,79—0,08	35,3—3,5	0,08—0,04	3,5—1,8
	14,2—1,4	577—57,7	1,4—0,14	57,7—5,8	0,14—0,07	5,8—2,9
Ice pellets.....	3,0—0,3	123—12,3	0,3—0,03	12,3—1,2	0,03—0,015	1,2—0,2
	5,1—0,5	227—22,7	0,5—0,05	22,7—2,3	0,05—0,03	2,3—1,1
	6,3—0,6	128—12,8	0,6—0,06	12,8—1,3	0,06—0,03	1,3—0,7

Commas indicate decimal points.

Remarks: 1. For hail and ice pellets, the root-mean-cube diameter is given in the column d, mm. 2. l are the closest distances between the particles.

Let us note also that at $\frac{l}{\lambda} \ll 1$, a set of scattering particles (for example, clouds[109] at $\lambda \geqslant 10$ cm may be regarded as a continuous medium. In this case, the principal role in the determination of the signal power may be played by the interference of waves scattered by individual particles.

§ 6.3. Radar Characteristics of Rain Precipitation

Various types of hydrometeors may have a substantial influence on the propagation of microwaves in the Earth's atmosphere. The associated effects are used both for studying the atmosphere itself, and for planning and operating various types of radar equipment.

As is evident from the general radar equation [149, 326], a key role in the study of all these questions is played by the radar characteristics of the unit volume of a hydrometeor: the specific effective area of radar scattering η and attenuation coefficient γ given in the incoherent approximation by the formulas: /27

$$\eta = \int_{d_{\min}}^{d_{\max}} n(d)\, \sigma_0'(d)\, dd \ \text{cm}^{-1} \tag{6.26}$$

$$\gamma = 4{,}343 \cdot 10^5 \int_{d_{\min}}^{d_{\max}} n(d)\, \sigma_2'(d)\, dd \ \text{db/km}, \tag{6.27}$$

where
- $n(d)$ is the particle distribution function with diameter (see § 6.1),
- $\sigma_i(d)$ are the normalized effective areas of radar scattering ($i = 0$) and attenuation ($i = 2$) of an individual particle[110] of diameter d,
- $d_{\min}$ and $d_{\max}$ are the minimum and maximum particle diameters in the selected volume.

Chapter 5 analyzed in detail the radar characteristics σ_0 and σ_2 of an individual particle as a function of its temperature, dielectric properties, size, wave length, and other factors, and in § 6.1, various laws of size distribution of precipitation particles were discussed.

On the basis of this material, a computer was also used to study the dependence of η and γ of rain on its intensity, wave length of the emitted wave in the centimeter, millimeter and submillimeter ranges, on the type of

---

[109] See Table 6.14.

[110] Determined via expressions (1.276), (1.274), (1.288) as follows: $\sigma_i'(d) = \pi d^2 \sigma_i(d)$.

distribution function, dielectric and temperature properties of the particles, minimum and maximum diameters in the particle spectrum, and other factors. Certain aspects of these problems are dealt with in many publications, a survey of which may be found, for example, in [46, 149, 64, 189, 204, 284-289, etc.].

The material presented below is based chiefly on studies made by the author [289-295].

Effect of Temperature. To determine the effect of temperature t of the drops on the radar characteristics of rain, calculations were made for η and γ at temperatures from 0 to 40°C, and also for the temperature coefficients $\varphi(t)$ and $\psi(t)$, which are defined by the expressions

$$\varphi(t) = \frac{\gamma_{t^\circ C}}{\gamma_{18^\circ C}}, \qquad \psi(t) = \frac{\gamma_{t^\circ C}}{\gamma_{18^\circ C}}.$$

The computations were carried out by using formulas (6.26), (6.27), (1.276), (1.274), and (1.288) at d_{min} = 0.05 cm, d_{max} = 0.55 cm, using different laws n(d) of drop size distribution (6.9)-(6.14). Since the character of the effect of temperature obtained was the same ±10% for all the n(d) considered, we will cite (Table 6.15) only the temperature coefficients obtained by using function (6.9). /280

TABLE 6.15. COEFFICIENTS $\varphi(t)$ AND $\psi(t)$ (MARSHALL-PALMER RAINDROP DISTRIBUTION)

I, mm/h	λ cm	$\varphi(t)$ at t°C				$\psi(t)$ at t°C			
		0	10	30	40	0	10	30	40
0,1	0,1	1,10	1,00	1,11	1,12	1,04	1,02	0,99	0,98
	0,4	0,78	0,91	1,10	1,16	0,97	0,99	1,01	1,02
	0,8	0,93	0,99	1,08	1,11	1,02	1,00	1,03	1,07
	3,0	1,03	1,02	0,99	0,98	1,48	1,19	0,79	0,65
1,0	0,1	1,01	0,97	1,13	1,16	1,01	1,00	1,00	1,00
	0,4	0,78	0,92	1,09	1,15	0,99	1,00	0,99	0,98
	0,8	0,87	0,95	1,05	1,09	1,00	1,00	1,02	1,04
	3,0	1,05	1,02	0,97	0,95	1,23	1,10	0,84	0,71
10,0	0,1	0,93	0,95	1,28	1,20	1,00	1,02	1,00	1,00
	0,4	0,80	0,93	1,08	1,13	1,02	1,01	0,98	0,98
	0,8	0,88	0,96	1,04	1,06	1,03	1,01	0,98	0,98
	3,0	0,97	0,99	1,01	1,02	0,87	0,95	1,03	1,04
30,0	0,1	0,86	0,93	1,12	1,22	1,00	1,00	1,00	1,00
	0,4	0,81	0,93	1,08	1,12	1,02	1,01	0,99	0,98
	0,8	0,90	0,96	1,03	1,04	1,04	1,01	0,98	0,97
	3,0	0,87	0,94	1,09	1,16	0,85	0,94	1,07	1,12
100,0	0,1	0,86	0,93	1,13	1,23	1,00	1,00	1,00	1,00
	0,4	0,81	0,93	1,08	1,13	1,02	1,01	0,99	0,98
	0,8	0,91	0,97	1,03	1,04	1,04	1,02	0,98	0,97
	3,0	0,85	0,94	1,09	1,18	0,85	0,94	1,08	1,13

Commas indicate decimal points.

It is evident from the table that in the millimeter range of radiowaves, a temperature change from 0 to 40°C causes variations in η and γ ($\Delta\eta$ and $\Delta\gamma$) of not more than 25 and 7% respectively.

Analysis of the behavior of $\Delta\eta$ and $\Delta\gamma$ at other n(d) shows that the quantities $|1-\varphi(t)|$ and $|1-\psi(t)|$ in the range λ = 1 to 10 mm do not exceed 0.25.

In the centimeter region of λ variation, as is particularly evident from Table 6.16, taken from [45], these variations may increase appreciably, reaching 100% or more in some cases.

The diverse character of the behavior of the radar characteristics of rain in the millimeter and centimeter ranges of λ is mainly due to the difference in the dependences on t for $\lambda > 1$ cm and $\lambda < 1$ cm of the dielectric constants of water (see Figures 4.11, 4.12) and also to the difference in the effective areas of radar scattering and attenuation of individual drops (see § 5.3).

The effect of temperature on the magnitudes of η and γ in the submillimeter range of λ variation is much smaller than in the millimeter range. This follows from the temperature dependences of ε of the type of (4.26b) and Figure 4.13. /28.

TABLE 6.16. COEFFICIENT $\psi(t)$ (LAWS-PARSONS RAINDROP DISTRIBUTION).

I, mm/h	λ cm	$t°$ C			
		0	10	30	40
0,25	0,5	0,85	0,95	1,02	0,99
	1,25	0,95	1,00	0,90	0,81
	3,2	1,21	1,10	0,79	0,55
	10,0	2,01	1,40	0,70	0,59
2,5	0,5	0,87	0,95	1,03	1,01
	1,25	0,85	0,99	0,92	0,80
	3,2	0,82	1,01	0,82	0,64
	10,0	2,02	1,40	0,70	0,59
12,5	0,5	0,90	0,96	1,02	1,00
	1,25	0,83	0,96	0,93	0,81
	3,2	0,64	0,88	0,90	0,70
	10,0	2,03	1,40	0,70	0,59
50,0	0,5	0,94	0,98	1,00	1,00
	1,25	0,84	0,95	0,95	0,83
	3,2	0,62	0,87	0,99	0,81
	10,0	2,01	1,40	0,70	0,58
150,0	0,5	0,96	0,98	1,00	1,00
	1,25	0,86	0,96	0,97	0,87
	3,2	0,66	0,88	1,03	0,89
	10,0	2,00	1,40	0,70	0,58

Commas indicate decimal points.

Effect of Particle Shape. There is a very limited number of papers devoted to the effect of nonsphericity of drop shape on the radar characteristics of rain.[111]

Thus, T. Oguchi [296] found that the error in γ due to nonsphericity of the drops at wave length λ = 8.6 mm does not exceed 16%; after measuring the effective radar scattering area of water drops at wave length λ = 5.33 mm, U. Lammers [297] came to the conclusion that the effect of particle shape in actual range is smoothed out statistically; I. Kh. Vakser, Yu. I. Malyshenko, and L. Ye. Kopilovich [298] established that in a rainshower with I = 50 mm/h for λ = 8.6 mm, the error in calculations of radar characteristics of rain as a result of the hypothesis of sphericity of the drops is 14%, for /282
λ = 2 mm it decreases to 7%, and in the submillimeter range, to 5%. In a moderate rain with I $\leqslant$ 10 mm/h, these errors decrease further by a factor of 3.

Effect of the Law of Size Distribution of Drops. Studying the role of various laws of size distribution of drops, we will strictly adhere to the classification of rain precipitation given in § 6.1 (see Figure 6.1).

Calculations of η and γ of rain precipitation with different n(d) were /283
made on a computer using formulas (6.26), (6.27) at d_{max} = 0.51 cm and d_{min} = = 0.05 cm for rain; d_{max} = 0.05 cm and d_{min} = 0.01 cm for drizzle; d_{max} = 0.51 cm and d_{min} = 0.01 cm for rain with drizzle.

Figures 6.11 and 6.12 show η and γ curves of rains of different intensities with a drop distribution after Marshall-Palmer (6.9), Best (6.11), (6.11a) and Kalkar (6.11), (6.14) in the submillimeter, millimeter and centimeter ranges of radiowaves. An analysis of these curves shows that to each rainfall intensity there corresponds a λ_0 such that for all $\lambda > \lambda_0$, the η and γ values calculated according to Marshall-Palmer, Best and Kalkar agree to within 25%. As I increases, λ_0 shifts into the long wave length part of the microwave /284
region. Thus, at an intensity equal to 0.1, 1.0, 10.0 and 100 mm/h, the corresponding λ_0 values are 0.35, 0.46, 0.72, and 1.74 cm. If however $\lambda < \lambda_0$, the ratio η_M/η_B has a tendency to increase with increasing I and may reach a maximum value equal to 1.8-2.0.[112]

---

[111] Pertinent surveys of these papers and their results may be found in [117, 149, 11, 327, etc.]

[112] η_M, γ_M denoted η, γ of rain with a drop distribution according to Marshall and Palmer, and η_B, γ_B denote those of rain with a distribution according to Best.

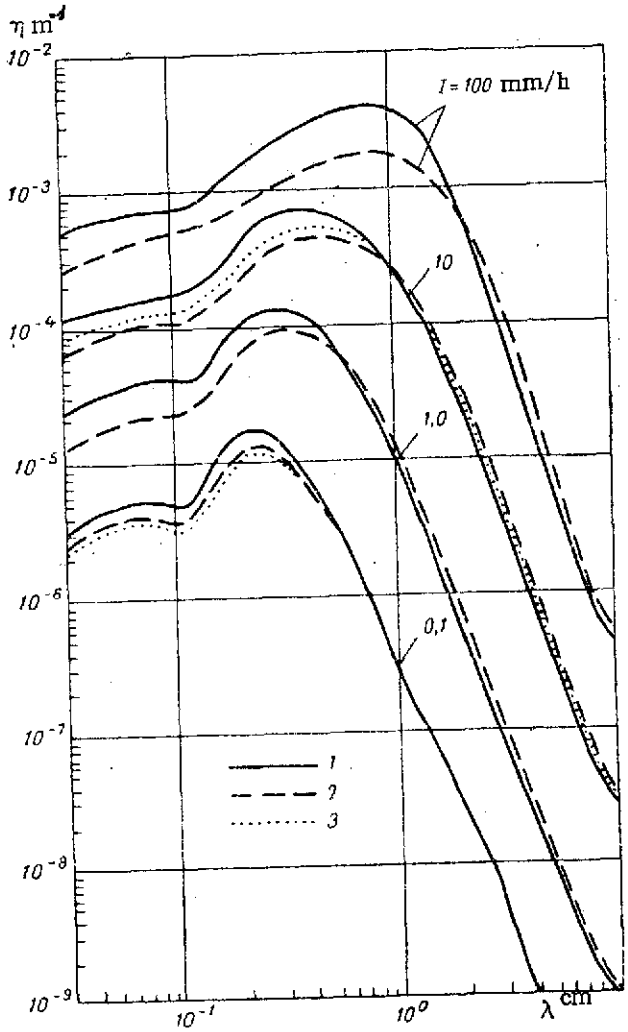

Figure 6.11. Specific Effective Radar Scattering Area η of Rains With Different Spectra of Drops at t = 18°C. 1) After Marshall and Palmer; 2) after Best; 3) after Kalkar.

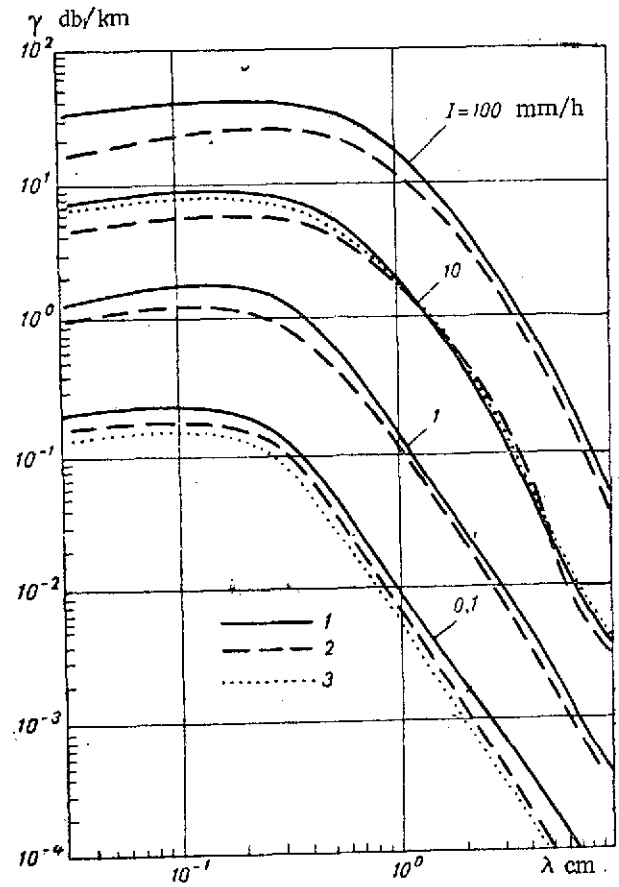

Figure 6.12. Attenuation Coefficient γ of Rains With Different Drop Spectra at t = 18°C. 1) After Marshall and Plamer; 2) after Best; 3) after Kalkar.

For γ, the magnitude of γ_M/γ_B at $I > 2.5$ mm/h increases with increasing λ and I. The maximum value of this ratio is 1.5-1.7. At $I < 2.5$ mm/h, discrepancies of γ_B and γ_M do not exceed 25%. Since the parameters of the Laws-Parsons n(d) distribution (see Table 6.3) are close to the parameters of the Best distribution, all of the above applies equally to this type of the drop spectrum. It is also easy to see that the η_K and the γ_K of rains with n(d) after Kalkar and an intensity of less than 6 mm/h for all the λ under

consideration are located somewhat lower[113] than the η_B and γ_B curves, and the /286
η_K and γ_K curves of rains with intensities above 6 mm/h occupy an intermediate position between curves η_M, η_B and γ_M, γ_B respectively.

It was pointed out in § 6.1 that in an analysis of rains as a function of their origin, I. V. Litvinov proposed for their description the functional relations (6.12), (6.13) with parameters from Tables 6.6, 6.7.

Figures 6-13-6.15 show results of calculation of η and γ of rains of different origins, using formulas (6.26), (6.27), (6.12). For comparison, the same figures show the η_M and γ_M curves. It is obvious that the longer the /287
wave length λ, the greater the intensity range in which a practical agreement of η of rains from rimed and unrimed snow and of η_M is observed. Thus, at λ = 337 μm, agreement takes place for $I < 1$ mm/h, at λ = 0.5 cm, for $I \leqslant 3$ mm/h, and at λ = 3 to 10 cm, practically for all I considered.

In the centimeter range of λ, rain formed from pellets differs from rains of other origin of any I by a 1.5-3 times smaller value of η, and in the millimeter and submillimeter ranges this conclusion applies only to rains with $I < 2$ to 1 mm/h. For γ, the corresponding dependences are somewhat less pronounced. Thus, in the centimeter region of λ variation, rains from rimed and unrimed snow and according to Marshall-Palmer for all I have γ values differing from each other by not more than 10-20%; in the millimeter region of λ, this applies at $I < 5$ mm/h, and in the submillimeter region, at still lower values of I.

Let us note that in [248], n(d) were determined from rains of different origins on the basis of processing of experimental data at $I < 15$ mm/h. For this reason, all the radar characteristics not pertaining to these I should be regarded as an analytical continuation of η and γ into a wider region of I.

In the study of the effect of the type of approximation there were calculations made for η and γ of rains of different origins with distribution n(d) described by expression (6.13). The η and γ curves of rain from pellets, calculated for n(d) from (6.12) and (6.13) for individual wave lengths of the submillimeter, millimeter and centimeter ranges are plotted in Figures 6.16 and 6.17. It is evident from the latter that a fairly good agreement for η is observed only in the range I = 1 to 10 mm/h at all λ simultaneously. The greatest discrepancies (factor of 2-4) are noted for rains of low intensity (< 0.5 mm/h) and high intensity (> 20 mm/h), these differences being much smaller at $\lambda < 2$ mm. η of rains with I = 0.3 to 20 mm/h and at $\lambda \geqslant 2$ mm agree to within 25%. At $\lambda < 2$ mm, discrepancies even in the range I = 1 to 10 mm/h may reach 40-60%.

[113] Not more than 20%.

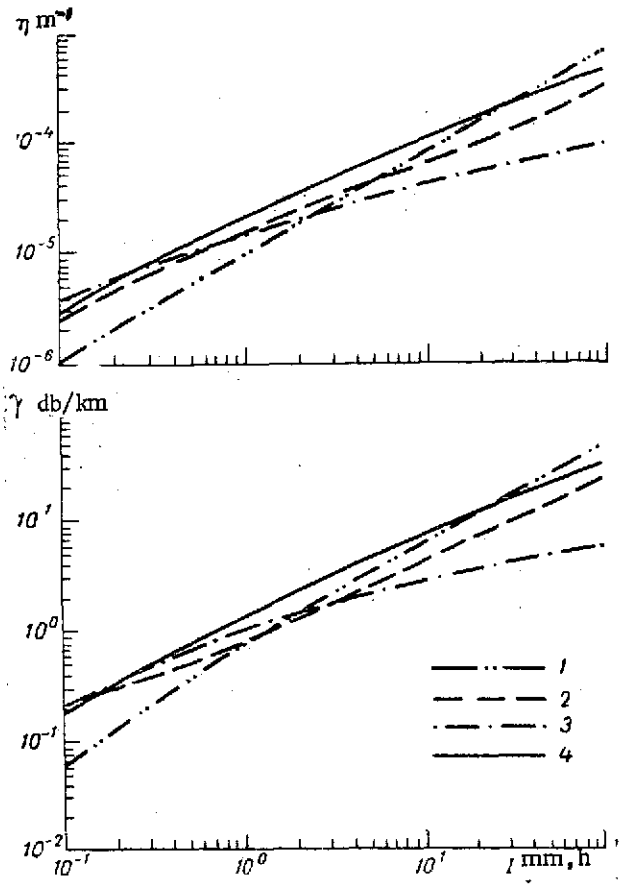

Figure 6.13. Dependence of η and γ of Rains of Different Origins on I at λ = 337 μm. t = 20°C. 1) Rain from pellets; 2) rain from rimed snow; 3) rain from unrimed snow; 4) rain with n(d) after Marshall and Palmer.

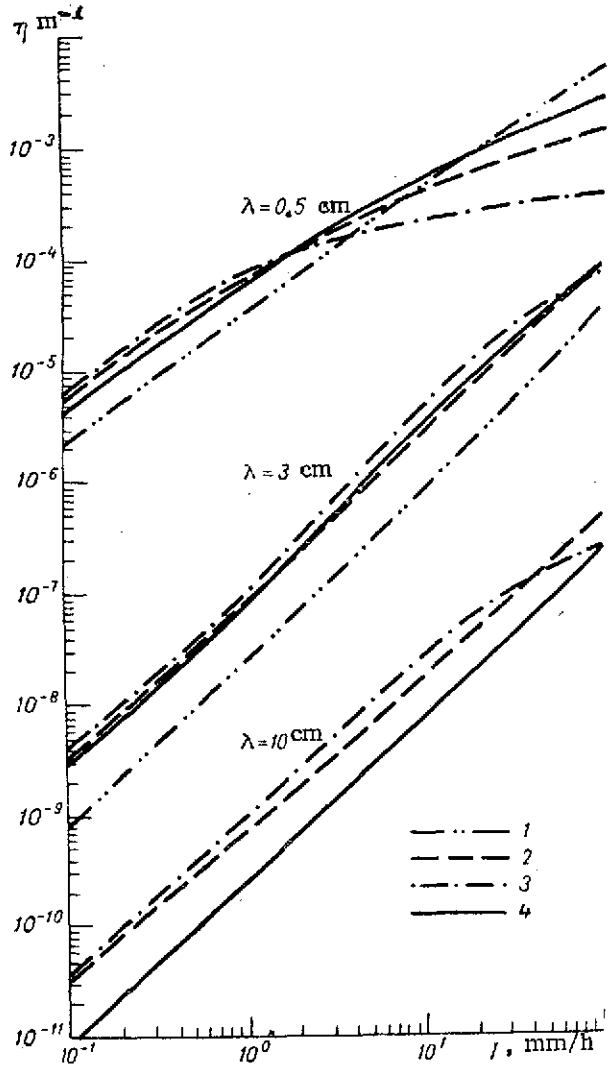

Figure 6.14. Dependence of η of Rains of Different Origins on I at Different λ. t = 18°C. 1) Rain from pellets; 2) rain from rimed snow; 3) rain from unrimed snow; 4) rain with n(d) after Marshall and Palmer.

Analysis of cases of rains from rimed and unrimed snow for both approximations (6.12), (6.13), eventually leads to the same relationships as those already disscussed, and is therefore omitted.

Let us know consider another type of precipitation — drizzle. The η and γ values were calculated from formulas (6.26), (6.27) at d_{min} = 0.01 cm and d_{max} = 0.05 cm.

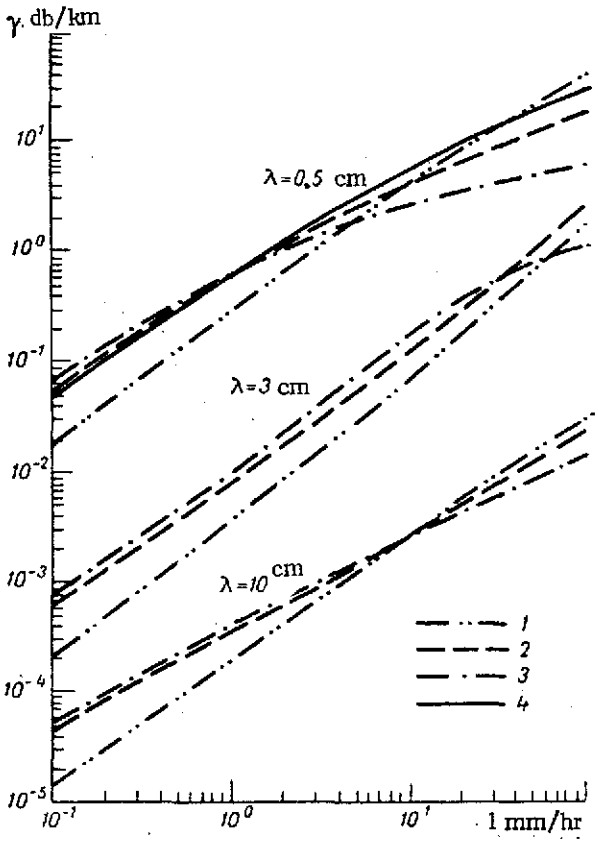

Figure 6.15. Dependence of γ of Rains of Different Origins on I at Different λ. t = 18°C. 1) Rain from pellets; 2) rain from rimed snow; 3) rain from unrimed snow; 4) rain with n(d) after Marshall and Palmer.

Figure 6.18 shows the dependence of η and γ of drizzle on the wave length λ in the submillimeter, millimeter and centimeter ranges for drop distributions according to Marshall--Palmer (6.9), Best (6.11), (6.11a), Kalkar (6.11), (6.14) and Joss (6.17). It is evident from the figure that the highest value of η is in the upper portion of the submillimeter range and lower portion of the millimeter range. The η and γ values of drizzle with I = = 0.1 mm/h but different n(d) differ by a factor of 1.2-3.5. At the same time, if one compares the η and γ values of drizzle calculated for n(d) according to Donaldson (6.18), with η and γ presented in Figure 6.18, it is easy to see that the latter will be 800--3,000 times smaller. Although Donaldson obtained distribution (6.18) from only a few observations, it is evident that the radar characteristics of hydrometeors may in some cases substantially surpass the average values. /289

This is also clearly confirmed by Figure 6.19, which shows the radar characteristics of drizzle in rain with drizzle for a distribution of drops based on different authors. It is evident that the η and γ values corresponding to different n(d) at a fixed intensity may differ by hundreds of times.

The above discussed pronounced scatter in the values of η and γ for rains and drizzle also leads to a corresponding difference in the radar characteristics of precipitation consisting of rain with drizzle. Their η and γ are obtained additively from η and γ of drizzle and η and γ of rain. This is equivalent to calculating η and γ of rain with drizzle directly from formula (6.26), (6.27) at d_{min} = = 0.01 cm, d_{max} = 0.51.

Results of calculations of the specific effective area of radar scattering and of the attenuation coefficient for nine laws of particle distribution (of submillimeter and millimeter ranges) are shown in Tables 6.17 and 6.18. /293

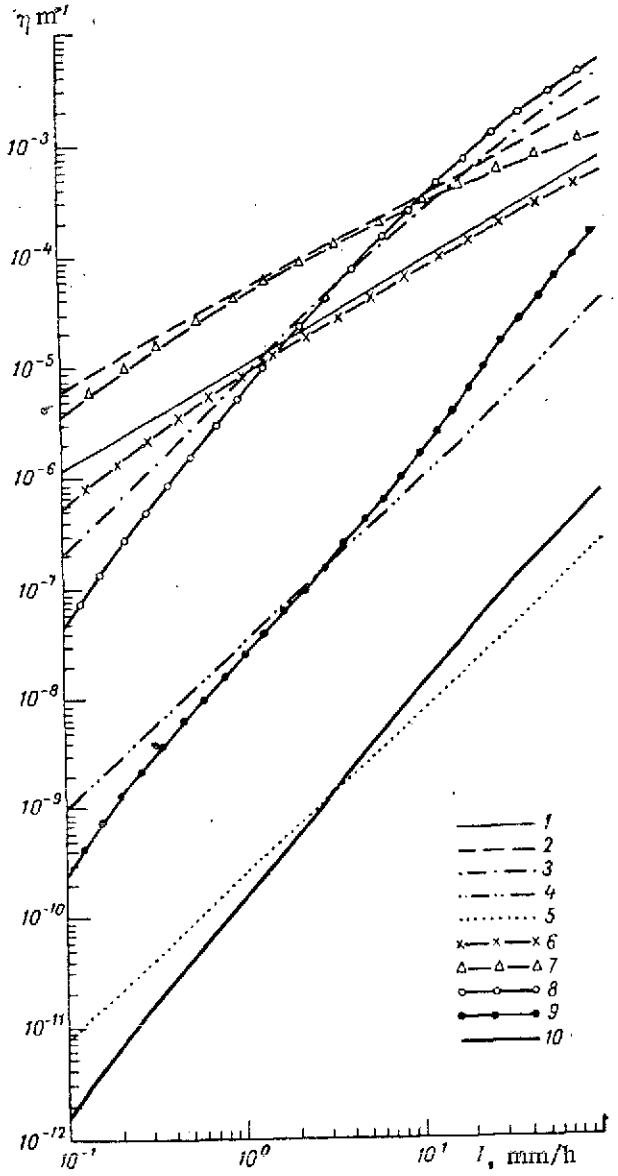

Figure 6.16. Dependence of η of Rains from Pellets for n(d) Determined According to Expression (6.12) (Curves 1-5) and (6.13) (Curves 6-10). t = 18 to 20°C. 1, 6) λ = 337 μm; 2, 7) λ = 2 mm; 3, 8) λ = 8 mm; 4, 9) λ = 3 cm; 5, 10) λ = 10 cm.

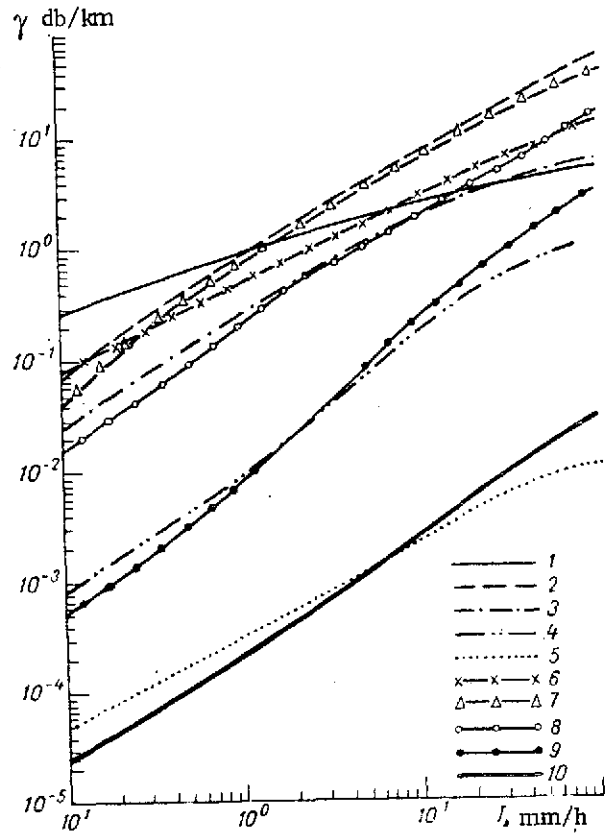

Figure 6.17. Dependence of γ of Rains from Pellets for n(d) According to Expression (6.12) (Curves 1-5) and (6.13) (Curves 6-10) t = 18 to 20°C. For notation see Figure 6.16.

Here I is the law of drop distribution after Marshall-Palmer (6.9); II — after Best (6.11), (6.11a); III — after Kalkar (6.11), (6.14); IV, V, VI — respectively rain from pellets, rain from rimed snow, and rain from unrimed snow after Litvinov (6.12); VII, VIII, IX — respectively, rain from pellets, rain from rimed snow, and rain from unrimed snow after Polyakova-Shifrin (6.13). /288

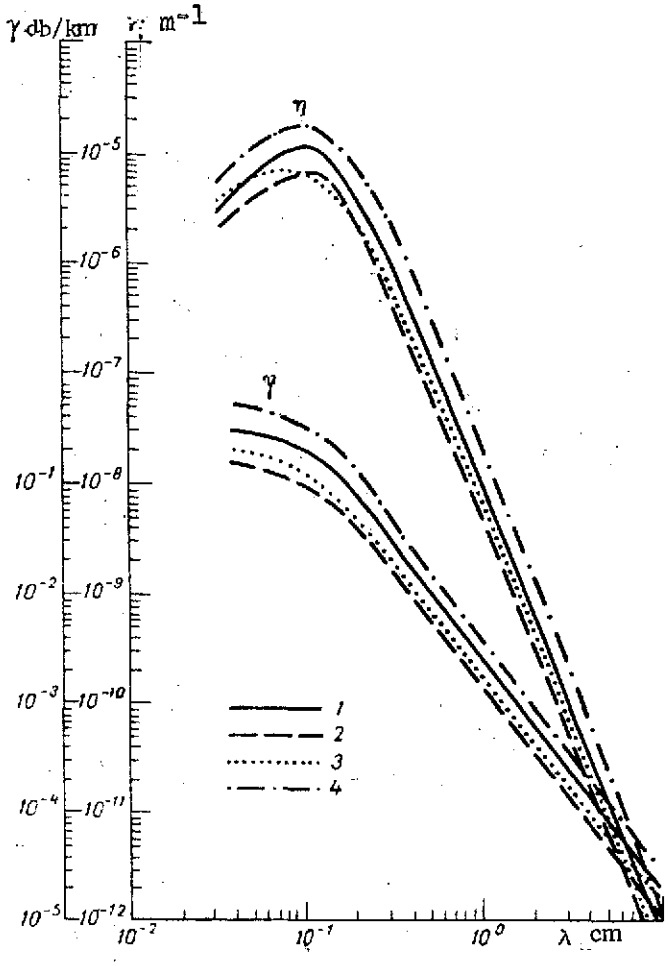

Figure 6.18. η and γ of Drizzle with Drop Distribution After Marshall--Palmer (1), Best (2), Kalkar (3), and Joss (4). t = 18 to 20°C, I = = 0.1 mm/h.

It follows from Tables 6.17 and 6.18 that the η and γ values for rain with drizzle also vary over fairly wide limits. It is easy to see that the η and γ values of rain with drizzle for n(d) after Laws-Parsons (in the centimeter region – Table 6.19, in the millimeter – Figure 6.20), after Best for rains with drizzle of nine types[114] (Table 6.20), after Polyakova (Table 6.21), after Polyakova (6.15) for drizzle and after Best for rain (Figure 6.21) and others lie within the same limits.

However, if the various distributions of drops of drizzle are varied with different distributions of drops of rain as was done, for example, in [298], then on the basis of the above it is evident that the η and γ values of rain with drizzle thus obtained may differ by several orders of magnitude from one another.

Let us note in conclusion that the qualitative relationships established here, particularly for drizzle, are tentative in view of the imperfection of the technique used for measuring fine droplets. Thus, for example in [255] it is noted that the filter paper method used by Laws and Parsons in [242] does not permit one to measure a drop smaller than 0.3 mm in diameter; the data of Polyakova and Shifrin [251] yield unreliable statistics for fine droplets; one cannot theoretically calculate the distribution curve after Polyakova [255] with $d < 0.4$ to 0.5 mm. It is noted in [248] that Best's measurement method [247] introduces significant distortions into the fine droplet portion of the spectrum at $d < 0.5$ mm.

Effect of d_{min} and d_{max}. The limits of drop size distribution in rain precipitation are not constant. Thus, d_{max} according to observational data is equal to 6 mm [203], 7.0-7.3 mm [247], 5.0-6.4 mm [204], etc. The case of d_{min} is similar. If in addition one considers that these parameters change

[114] See Table 6.12.

as a function of various external conditions and that a reliable experimental determination of d_{min} and d_{max} is difficult, it becomes evident that in order to study the radar properties of precipitation in the form of rain it is necessary to know the extent to which it is influenced by η and γ of the initial and final portions of the distribution functions.

TABLE 6.17. VALUES OF $\eta \cdot 10^m$ m^{-1} (IN THE NUMERATOR) AND $\gamma \cdot 10^n$ db/km (IN THE DENOMINATOR) OF RAIN WITH DRIZZLE AT λ = 337 μm AND DIFFERENT n(d). t = 20°C. /292

I_* mm/h	$\frac{m}{n}$	n(d) I	II	III	IV	V	VI	VII	VIII	IX
0,1	6 / 1	6,01 / 5,01	4,80 / 3,31	5,90 / 3,61	1,52 / 1,31	3,66 / 3,00	5,22 / 4,39	1,19 / 1,28	2,24 / 1,78	1,30 / 0,96
0,3	5 / 1	1,21 / 9,84	0,94 / 6,45	1,26 / 7,89	0,42 / 3,35	0,76 / 5,96	0,88 / 6,71	0,35 / 3,14	5,14 / 3,78	0,31 / 2,18
0,6	5 / 0	1,90 / 1,49	1,43 / 0,98	2,09 / 1,29	0,79 / 0,61	1,19 / 0,87	1,21 / 0,89	0,68 / 0,55	0,86 / 0,68	0,54 / 0,37
1,0	5 / 0	2,66 / 2,04	1,95 / 1,33	2,90 / 1,85	1,25 / 0,95	1,65 / 1,19	1,52 / 1,07	1,09 / 0,84	1,24 / 0,82	0,80 / 0,54
3,0	5 / 0	5,44 / 3,98	3,82 / 2,57	6,24 / 4,01	3,38 / 2,43	3,31 / 2,27	2,44 / 1,64	2,91 / 2,05	2,75 / 1,84	1,87 / 1,22
6,0	5 / 0	8,53 / 6,05	5,84 / 3,90	10,13 / 6,52	6,27 / 4,43	5,12 / 3,45	3,29 / 2,17	5,34 / 3,62	4,50 / 2,97	3,19 / 2,05
10,0	4 / 0	1,19 / 8,25	0,80 / 5,28	1,44 / 9,33	0,99 / 6,88	0,71 / 4,68	0,41 / 2,64	0,82 / 5,50	6,48 / 4,21	0,47 / 3,02
30,0	4 / −1	2,39 / 1,61	1,55 / 1,01	3,12 / 2,00	2,62 / 1,78	1,40 / 0,91	0,63 / 3,98	2,19 / 1,50	1,41 / 8,90	1,08 / 6,83
60,0	4 / −1	3,70 / 2,45	2,33 / 1,50	— / —	4,86 / 3,23	2,14 / 1,56	0,79 / 3,94	3,79 / 2,51	2,28 / 1,44	1,80 / 1,13
100,0	4 / −1	5,09 / 3,32	3,11 / 1,99	— / —	7,62 / 5,02	2,91 / 2,06	0,90 / 5,68	5,76 / 3,71	3,23 / 2,02	2,59 / 1,63

Commas indicate decimal points.

Since it is rather difficult to obtain an estimate of this influence in general form from expressions (6.26), (6.27), an attempt was made in [295] to set up numerical experiments on a computer for varied n(d) and λ at d_{min} = 0.01 cm, d_{max} = 0.05 cm (initial portion of the spectrum), on the one hand, and d_{min} = 0.05 cm, d_{max} = 0.51 cm on the other. These data have already been discussed in a study of the radar characteristics of drizzle. We will discuss them here /296

from the standpoint of the relationships of η, γ of drizzle and η, γ of rain respectively.

TABLE 6.18. VALUES OF $\eta \cdot 10^m$ m^{-1} (IN THE NUMERATOR) AND $\gamma \cdot 10^n$ db/km (IN THE DENOMINATOR) OF RAIN WITH DRIZZLE AT λ = 3 mm AND DIFFERENT n(d). t = 18°C.

I, mm/h	m/n	n(d) I	II	III	IV	V	VI	VII	VIII	IX
0,1	5	1,58	1,40	1,23	0,56	1,59	2,26	0,23	1,13	0,78
	1	1,82	1,48	1,36	0,60	1,65	2,12	3,14	1,10	0,82
0,3	5	4,72	3,63	3,38	2,01	4,15	4,87	1,32	3,08	1,91
	1	5,10	3,95	3,78	2,05	4,31	5,05	3,12	3,24	2,19
0,6	5	8,64	6,02	6,11	4,20	6,91	7,11	3,36	5,30	3,17
	0	0,94	0,70	0,70	0,43	0,75	0,79	0,34	0,59	0,40
1,0	4	1,30	0,85	0,93	0,70	0,97	0,88	0,62	0,76	0,45
	0	1,45	1,03	1,09	0,73	1,11	1,06	0,63	0,90	0,63
3,0	4	2,87	1,66	2,17	1,97	1,83	1,25	1,80	1,52	0,98
	0	3,46	2,31	2,73	2,23	2,43	1,87	2,05	2,11	1,48
6,0	4	4,50	2,48	3,64	3,65	2,64	1,51	3,11	2,28	1,42
	0	5,80	3,74	4,80	4,38	3,90	2,57	4,03	3,56	2,54
10,0	4	6,15	3,31	5,28	5,62	3,42	1,72	4,47	3,06	1,96
	0	8,38	5,27	7,18	7,13	5,72	3,20	6,46	5,17	3,76
30,0	3	1,14	0,64	1,16	1,38	0,59	0,23	0,92	0,57	0,39
	1	1,79	1,07	1,70	1,98	1,09	0,49	1,69	1,12	0,86
60,0	3	1,67	0,87	—	2,40	0,84	0,26	1,45	0,84	0,61
	1	2,81	1,79	—	3,74	1,67	0,61	3,01	1,81	1,42
100,0	3	2,18	1,12	—	3,60	1,08	0,29	2,04	1,13	0,84
	1	3,91	2,20	—	5,93	2,27	0,69	4,54	2,55	2,01

Commas indicate decimal points.

Analysis of the results of the calculations shows that the initial portion of the spectrum in comparison with the entire remaining portion has the greatest influence on η and γ at different n(d) and $\lambda \leqslant 2$ mm for rain precipitation of low intensity. In these regions of λ and I, the η and γ values for the various laws of distribution of drops with size at $0.01 < d < 0.05$ cm may significantly exceed η and γ at 0.05 cm $< d <$ 0.51 cm.

The literature [301-306, etc.] contains a considerable amount of data of experimental character showing that the Marshall-Palmer distribution (6.9) slightly exaggerates the number of fine droplets in rain with drizzle (see for example Figure 6.22).

TABLE 6.19. VALUES OF γ OF RAIN WITH DRIZZLE WITH n(d) AFTER LAWS-PARSONS AT t = 18°C AFTER [189]. /294

λ mm	I, mm/h								
	0,25	1,25	2,5	5,0	12,5	25,0	50,0	100,0	150,0
0,3	0,25	1,29	2,19	3,68	7,08	11,7	19,6	33,7	46,8
0,5	0,159	0,764	1,43	2,63	5,46	9,86	17,0	29,4	40,9
1,0	$0,349\cdot10^{-1}$	0,210	0,447	0,933	2,43	4,87	9,59	18,4	26,8
1,5	$0,136\cdot10^{-1}$	$0,878\cdot10^{-1}$	0,196	0,427	1,18	2,49	5,15	10,4	15,7
2,0	$0,572\cdot10^{-2}$	$0,423\cdot10^{-1}$	0,100	0,233	0,709	1,53	3,28	6,77	10,2
3,0	$0,172\cdot10^{-2}$	$0,116\cdot10^{-1}$	$0,284\cdot10^{-1}$	$0,718\cdot10^{-1}$	0,240	0,602	1,45	3,43	5,49
4,0	$0,757\cdot10^{-2}$	$0,434\cdot10^{-2}$	$0,101\cdot10^{-1}$	$0,252\cdot10^{-1}$	$0,848\cdot10^{-1}$	0,223	0,590	1,55	2,71
5,0	$0,442\cdot10^{-2}$	$0,218\cdot10^{-2}$	$0,465\cdot10^{-2}$	$0,107\cdot10^{-1}$	$0,336\cdot10^{-1}$	$0,882\cdot10^{-1}$	0,235	0,639	1,13
5,5	$0,309\cdot10^{-2}$	$0,160\cdot10^{-2}$	$0,339\cdot10^{-2}$	$0,749\cdot10^{-2}$	$0,226\cdot10^{-1}$	$0,580\cdot10^{-1}$	0,152	0,416	0,739
6,0	$0,242\cdot10^{-3}$	$0,123\cdot10^{-2}$	$0,257\cdot10^{-2}$	$0,554\cdot10^{-2}$	$0,159\cdot10^{-1}$	$0,383\cdot10^{-1}$	$0,971\cdot10^{-1}$	0,260	0,472
6,5	$0,196\cdot10^{-3}$	$0,986\cdot10^{-3}$	$0,203\cdot10^{-2}$	$0,430\cdot10^{-2}$	$0,120\cdot10^{-1}$	$0,279\cdot10^{-1}$	$0,678\cdot10^{-1}$	0,174	0,313
7,0	$0,162\cdot10^{-3}$	$0,809\cdot10^{-3}$	$0,165\cdot10^{-2}$	$0,346\cdot10^{-2}$	$0,941\cdot10^{-2}$	$0,213\cdot10^{-1}$	$0,499\cdot10^{-1}$	0,123	0,214
8,0	$0,119\cdot10^{-3}$	$0,572\cdot10^{-3}$	$0,112\cdot10^{-2}$	$0,234\cdot10^{-2}$	$0,586\cdot10^{-2}$	$0,127\cdot10^{-1}$	$0,283\cdot10^{-1}$	$0,659\cdot10^{-1}$	0,110
9,0	$0,939\cdot10^{-4}$	$0,434\cdot10^{-3}$	$0,851\cdot10^{-3}$	$0,170\cdot10^{-2}$	$0,429\cdot10^{-2}$	$0,900\cdot10^{-2}$	$0,194\cdot10^{-1}$	$0,432\cdot10^{-1}$	$0,700\cdot10^{-1}$
10,0	$0,780\cdot10^{-4}$	$0,350\cdot10^{-3}$	$0,678\cdot10^{-3}$	$0,133\cdot10^{-2}$	$0,330\cdot10^{-2}$	$0,678\cdot10^{-2}$	$0,142\cdot10^{-1}$	$0,309\cdot10^{-1}$	$0,492\cdot10^{-1}$
15,0	$0,396\cdot10^{-4}$	$0,159\cdot10^{-3}$	$0,294\cdot10^{-3}$	$0,550\cdot10^{-3}$	$0,128\cdot10^{-2}$	$0,247\cdot10^{-2}$	$0,489\cdot10^{-2}$	$0,989\cdot10^{-2}$	$0,151\cdot10^{-1}$

Commas indicate decimal points.

TABLE 6.20. VALUES OF γ OF RAIN WITH DRIZZLE OF VARIOUS TYPES OF RAIN AT t = 18°C AFTER [64, 70].

Type of precipitation	λ cm											
	0,1	0,3	0,5	0,75	1,0	1,25	3,0	5,0	8,0	10,0	15,0	20,0
A	1,64	1,82	1,43	8,11	$4,80\cdot10^{-1}$	$1,93\cdot10^{-1}$	$4,92\cdot10^{-2}$	$4,24\cdot10^{-3}$	$1,23\cdot10^{-3}$	$7,34\cdot10^{-4}$	$2,80\cdot10^{-4}$	$1,52\cdot10^{-4}$
B	7,44	7,63	4,44	2,24	1,14	—	—	—	—	—	—	—
C	3,61	2,45	1,90	1,37	7,75	$3,18\cdot10^{-1}$	$8,63\cdot10^{-2}$	$7,11\cdot10^{-3}$	$2,04\cdot10^{-3}$	$1,19\cdot10^{-3}$	$4,69\cdot10^{-4}$	$2,53\cdot10^{-4}$
D	1,99	2,13	2,01	1,69	1,26	$6,15\cdot10^{-1}$	$1,92\cdot10^{-1}$	$1,25\cdot10^{-2}$	$3,02\cdot10^{-3}$	$1,67\cdot10^{-3}$	$5,84\cdot10^{-4}$	$3,02\cdot10^{-4}$
E	2,76	3,17	2,93	2,46	2,19	2,12	$6,13\cdot10^{-1}$	$5,91\cdot10^{-2}$	$1,17\cdot10^{-2}$	$5,68\cdot10^{-3}$	$1,69\cdot10^{-3}$	$7,85\cdot10^{-4}$
F	3,75	4,25	4,35	4,11	3,64	2,37	$8,01\cdot10^{-1}$	$5,13\cdot10^{-2}$	$1,10\cdot10^{-2}$	$6,46\cdot10^{-3}$	$1,85\cdot10^{-3}$	$9,09\cdot10^{-4}$
G	7,93	8,35	7,61	6,20	4,56	2,40	$7,28\cdot10^{-1}$	$5,29\cdot10^{-2}$	$1,21\cdot10^{-2}$	$6,96\cdot10^{-3}$	$2,27\cdot10^{-3}$	$1,17\cdot10^{-3}$
H	8,03	8,61	8,14	6,98	5,73	4,51	1,28	$1,12\cdot10^{-1}$	$2,32\cdot10^{-2}$	$1,17\cdot10^{-2}$	$3,64\cdot10^{-3}$	$1,75\cdot10^{-3}$
J	9,82	1,12	9,60	7,30	5,88	6,17	1,64	$1,65\cdot10^{-1}$	$3,33\cdot10^{-2}$	$1,62\cdot10^{-2}$	$4,96\cdot10^{-3}$	$2,29\cdot10^{-3}$

Commas indicate decimal points.

Hence, the calculations (Figure 6.23) of η and γ for n(d) according to expression (6.9) make it possible to obtain the upper estimate of the specific effective radar scattering area and of the attenuation coefficient of microwaves in rains and also in rains with drizzle.

Let us note that the lower limit that we took for the size of drizzle drops is slightly low. For example, according to [159], the minimum drop diameter can be no smaller than 0.02 cm. As a result, the estimate obtained for the upper limit of η and γ is too high.

TABLE 6.21. VALUES OF γ OF RAIN WITH DRIZZLE WITH n(d) AFTER BEST (B) AND POLYAKOVA (P) AT t = 20°C ACCORDING TO THE CALCULATIONS OF SOKOLOV AND SUKHONIN IN [300]*. /295

I, mm/h	λ mm									
	2,0		1,0		0,8		0,5		0,1	
	Б	П	Б	П	Б	П	Б	П	Б	П
0,5	0,7	0,8	0,9	0,8	0,9	0,8	0,9	0,8	0,8	0,6
1,0	1,5	1,3	1,7	1,3	1,6	1,2	1,6	1,1	1,5	1,0
2,5	2,3	2,6	2,4	2,5	2,4	2,4	2,3	2,2	2,1	2,0
5,0	3,6	4,1	3,7	3,9	3,6	3,8	3,5	3,4	3,2	3,1
10,0	5,6	7,7	5,7	7,2	5,6	7,0	5,4	6,3	4,9	5,8
25,0	9,3	13,8	9,9	12,8	9,6	12,5	9,3	11,3	8,3	10,4
50,0	16,0	22,1	15,6	20,5	15,3	20,0	14,7	18,1	12,7	16,6
100,0	23,0	34,0	22,7	31,5	22,1	30,0	21,3	28,4	18,0	26,5

Commas indicate decimal points.
*See also [328].

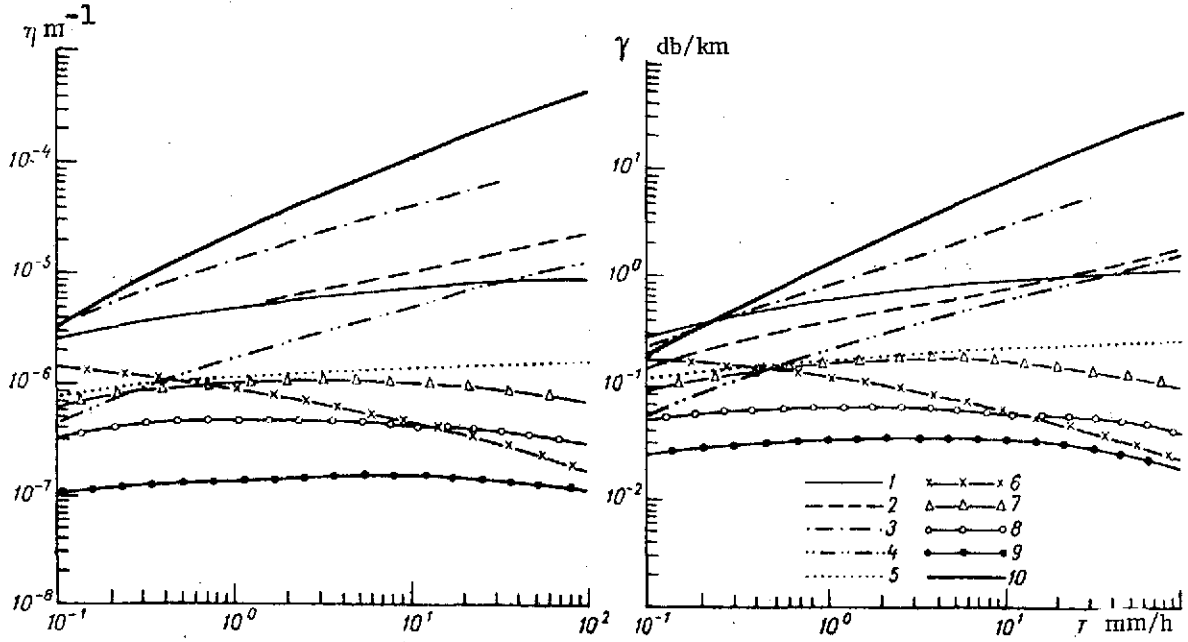

Figure 6.19. η and γ of Drizzle in Rain Precipitation of Different Intensities of λ = 337 μm and t = 20°C with Drop Distribution After Marshall-Palmer (6.9) (1); Best (6.11), (6.11a) (2); Kalkar (6.11), (6.14) (3); After Litvinov (6.12): Rain from Pellets (4), Rain From Rimed Snow (5), Rain from Unrimed Snow (6); After Polyakova-Shifrin (6.13): Rain from Pellets (7), Rain from Rimed Snow (8), Rain from Unrimed Snow (9). η and γ of Rain After Marshall-Palmer (10). /291

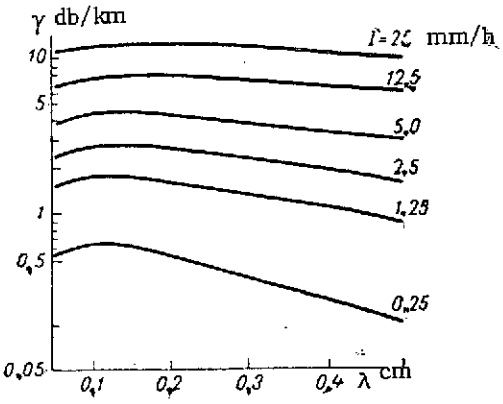

Figure 6.20. γ of Rain with Drizzle for n(d) After Laws--Parsons in the Millimeter and Submillimeter Region. t = 20°C [299].

It is evident from Figure 6.23 that the η values at $0.01 \leqslant d \leqslant 0.05$ cm may surpass η at $0.05 \text{ cm} \leqslant d \leqslant 0.51$ cm by a factor of 1-3, and for γ by a factor no greater than 1-1.8. The effect of the initial portion of function n(d) decreases with increasing λ at I = const or with increasing I at λ = const and is practically insignificant in the upper portion of the millimeter range and in the centimeter range. /297

To estimate the effect of the end portion of the n(d) spectrum on the radar characteristics of rain, η and γ were calculated from formulas (6.26), (6.27) with d_{min} = 0.05 cm and d_{max} = f(I), where f(I) is given in the form of Table 6.22, compiled from the data of [247, 45]. Results of calculation for different n(d) showed that in the millimeter and submillimeter regions of change in λ, the variations in η and γ values of rain due to variations in d_{max} according to Table 6.22 at $0.1 \leqslant I \leqslant 100$mm/h do not exceed 20%, and in the centimeter range at I < 30 mm/h amount to no more than 25%.

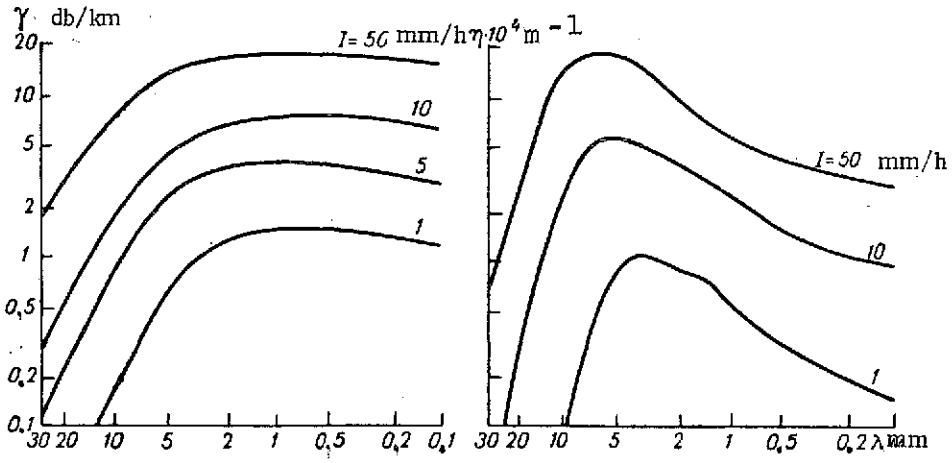

Figure 6.21. η and γ of Rain (n(d) After Best) with Drizzle (n(d) After Polyakova) in the Millimeter and Submillimeter Regions. t = 20°C [298].

The greatest contribution to the end portion of the n(d) spectrum into the radar characteristics of rain is observed in the centimeter region of change in λ at $\pi \geqslant 30$ mm/h. For nine types of distribution (the same as in Table 6.17), Table 6.23 gives the values of δ_η and δ_γ, defined by the formulas: /299

$$\delta_\eta = \frac{|\eta^{(0)} - \eta^{(1)}|}{\eta^{(0)}}, \qquad \delta_\gamma = \frac{|\gamma^{(0)} - \gamma^{(1)}|}{\gamma^{(0)}},$$

where $\eta^{(0)}$, $\gamma^{(0)}$ are the η, γ of rain at $0.05 \leqslant d \leqslant 0.51$ cm, $\eta^{(1)}$, $\gamma^{(1)}$ are the η, γ of rain at $0.5 \leqslant d \leqslant f(I)$ cm, and $f(I)$ is determined from Table 6.22.

TABLE 6.22. DEPENDENCE OF d_{max} ON RAINFALL INTENSITY I.

I mm/h	0.1	0.3	0.6	1.0	3.0	6.0	10.0	30.0	60.0	100.0
d_{max} cm	0.20	0.25	0.35	0.40	0.45	0.50	0.55	0.60	0.65	0.70

TABLE 6.23. VALUES OF ε_η % (IN THE NUMERATOR) AND δ_γ % (IN THE DENOMINATOR) FOR RAINS (I-IX) WITH DIFFERENT n(d).

	$\lambda = 3$ cm							
I, mm/h	I	II	IV	V	VI	VII	VIII	IX
10	2,1 / 0,5	3,5 / 0,0	0,0 / 0,0	0,6 / 0,0	4,3 / 0,9	0,5 / 0,0	1,9 / 0,0	5,5 / 0,8
30	1,01 / 1,8	15,6 / 3,1	0,0 / 0,0	6,6 / 1,2	27,7 / 7,6	6,1 / 0,9	11,0 / 2,1	20,2 / 4,7
60	22,5 / 4,3	36,5 / 11,7	0,5 / 0,0	15,5 / 4,0	66,2 / 19,8	18,2 / 3,5	24,0 / 5,5	40,7 / 10,9
100	37,7 / 7,8	72,7 / 20,6	1,6 / 0,0	32,5 / 7,9	117,5 / 39,7	35,6 / 8,4	39,8 / 9,8	66,2 / 18,4

	$\lambda = 10$ cm							
I, mm/h	I	II	IV	V	VI	VII	VIII	IX
10	0,8 / 0,3	0,9 / 0,3	0,0 / 0,0	0,5 / 0,0	2,6 / 1,1	0,0 / 0,0	1,5 / 0,3	3,4 / 1,6
30	6,6 / 1,7	12,0 / 5,9	0,0 / 0,0	4,0 / 0,5	24,1 / 14,0	4,0 / 0,8	7,2 / 2,9	16,3 / 8,9
60	16,0 / 7,3	35,6 / 20,1	0,7 / 0,0	13,1 / 6,3	60,9 / 42,9	11,1 / 6,5	18,7 / 10,1	35,3 / 22,4
100	28,7 / 14,1	65,0 / 43,2	1,0 / 0,3	26,1 / 15,4	114,3 / 88,5	29,1 / 17,5	33,9 / 20,8	58,6 / 41,2

Commas indicate decimal points.

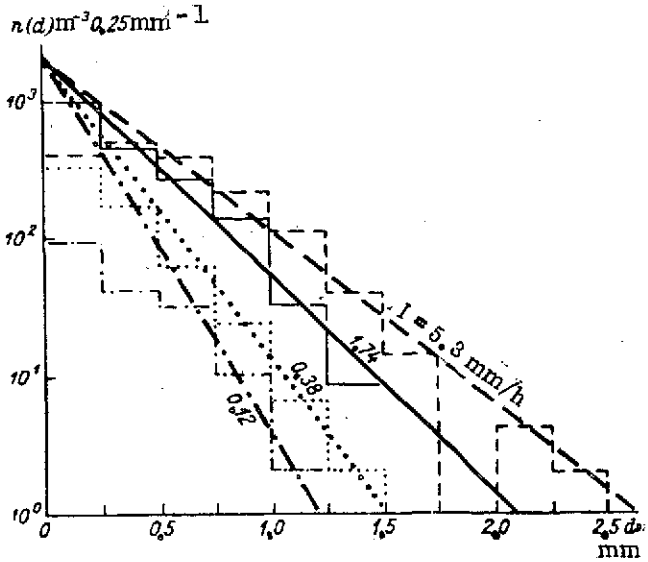

Figure 6.22. Distribution Functions n(d) [306] of Rain With Drizzle, Obtained from Experimental Data (Step Function) and Calculated Data After Marshall-Palmer (Straight Line).

Although distributions IV-IX at large I are used as noted earlier, with the aid of far extrapolation of the experimental data obtained at $I \leqslant 15$ mm/h, nevertheless there is no doubt that the values of $\eta^{(1)}$, $\gamma^{(1)}$ for the corresponding parameters λ, I and n(d) may exceed $\eta^{(0)}$, $\gamma^{(0)}$ by a factor of 2 or more.

Effective dielectric constants. /301

It is well known that the Debye relation (4.16) is unsuitable for determining the dielectric constants (ε) of water in the submillimeter range. At the same time, the data on ε available in the literature (see § 4.1) have a certain spread. In § 5.2 we already discussed the question of effect of errors in the determination of ε of water on the radar characteristics of a single drop. Here we will extend these results to polydisperse particles.

Calculations of η and γ of rain with drizzle for λ from 5 mm to 500 μm were made in [299]. In this entire region of change in λ, the authors of [299] used dielectric constants of water calculated from the Debye relation. Of interest is the magnitude of error introduced into η and γ.

Calculations (Table 6.24) of η and γ of rain (d_{min} = 0.05 cm, d_{max} = 0.51 cm) were carried out by using formulas (6.26), (6.27); ε of water was determined from expressions (4.16), (4.14), (4.23), (4.24), on the one hand, and experimental data (Tables 4.24, 4.29) on the other hand, with n(d) after Marshall-Palmer (6.9) for wave lengths of 300 and 500 μm and t = 20 to 25°C. It is obvious that the smaller error introduced into η and γ by the Debye values of ε does not exceed 25% for η and 10% for γ. Calculations for other types of distributions with ε found from formulas (4.26a), (4.26b) and taken from Table 4.30 and also from the Debye expression show that in determining the dielectric constant of water in the submillimeter range up to λ = 200 μm with an accuracy up to 20-30% for η and 10-25% for γ, use may be made of the Debye expressions.

Experimental Data. There are a number of papers [46, 11, 149, 189, 267, 287, 288, 298, etc.] which give surveys and contain results of experimental studies on the scattering and attenuation of microwaves in rain precipitation.[115]

[115] See also [328-330].

It was found that the theoretical calculations are frequently in only qualitative agreement with the experimental data. The disagreement may be due in part to inaccuracies in the measurement of the intensity of the rain precipitation and their nonuniformity along the route (see §6.1), usually neglected in the calculations.

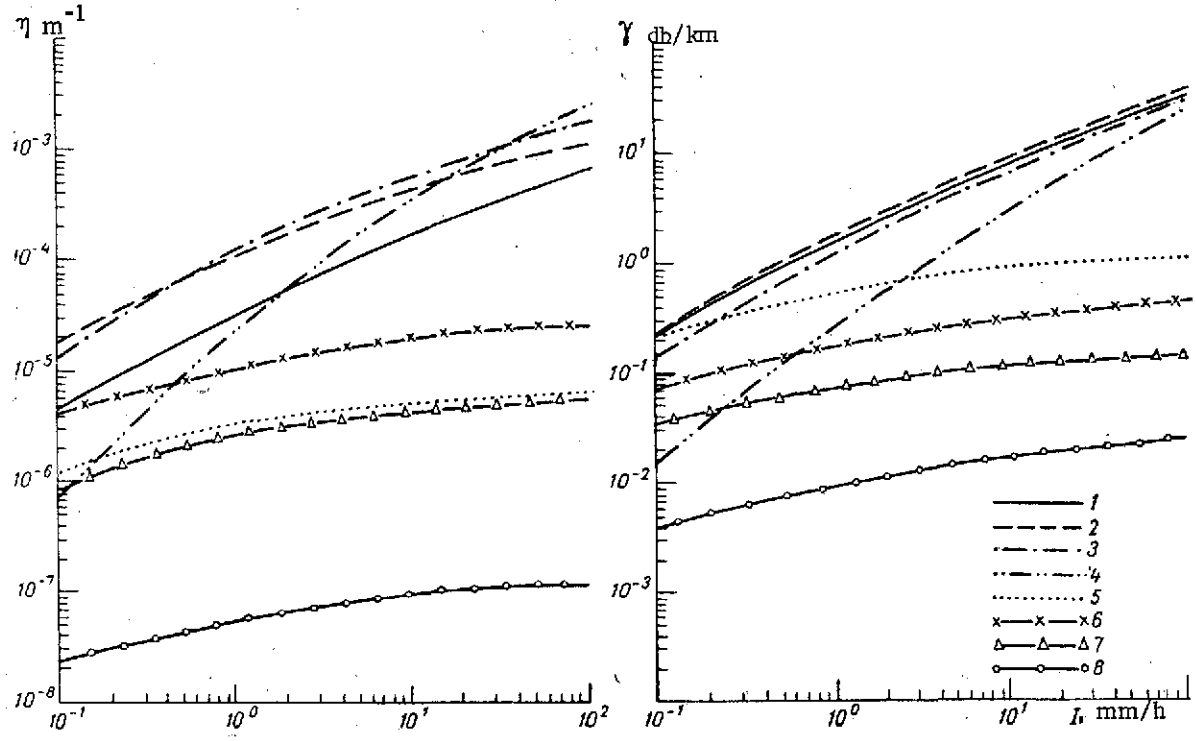

Figure 6.23. η and γ of Rain with Drizzle, n(d) After Marshall-Palmer. At 0.05 cm ⩽ d ⩽ 0.51 cm; 1) λ = 0.1 cm, 2) λ = 0.2 cm, 3) λ = 0.3 cm, 4) λ = 0.8 cm; at 0.01 cm ⩽ d ⩽ 0.05 cm: 5) λ = 0.1 cm, 6) λ = 0.2 cm, 7) λ = = 0.3 cm, 8) λ = 0.8 cm. /298

However, in addition to the measurement errors, the quantitative disagreement between existing theory and experiment is also due to other factors. One of them, according to R. G. Medhurst [201] is the use of a more simplified model of actual rain precipitation in the form of a set of individual randomly situated circle drops separated by gaps whose average size is much greater than their own. Thus, the experimental data of [307] indicate that rain precipitation consists rather of a collection of groups, each of which is made up of two or more closely situated drops. Such a grouping of drops must introduce substantial changes into the radar characteristics of liquid precipitation, which should be examined on the basis of the theory developed in /301 Chapter 2.

In addition, the calculations of radar characteristics of rains took no account of the fact that, as we were shown by V. G. Khorguani [205], the

falling velocity of a collection of closely situated particles may be several times as high as that of a single particle.[116]

TABLE 6.24. VALUES OF η AND γ OF RAIN, CALCULATED ON THE BASIS OF DIELECTRIC CONSTANTS AFTER DEBYE (IN THE NUMERATOR) AND EXPERIMENTAL DATA [118-112] (IN THE DENOMINATOR).

i mm/h	$\eta \cdot 10^5$ м$^{-3}$ at λ μm		γ db/km at λ μm	
	300	500	300	500
0,1	0,238 / 0,307	0,407 / 0,420	0,195 / 0,200	0,210 / 0,211
0,3	0,698 / 0,817	1,05 / 1,12	0,526 / 0,539	0,563 / 0,565
0,6	1,29 / 1,44	1,81 / 1,96	0,929 / 0,948	0,994 / 0,996
1,0	1,98 / 2,14	2,67 / 2,91	1,38 / 1,41	1,48 / 1,48
3,0	4,69 / 4,80	5,86 / 6,50	3,11 / 3,16	3,30 / 3,31
6,0	7,81 / 7,81	9,42 / 10,55	5,04 / 5,12	5,34 / 5,36
10,0	11,2 / 11,1	13,2 / 14,9	7,12 / 7,23	7,53 / 7,56
30,0	23,8 / 23,0	27,1 / 30,9	14,6 / 14,9	15,4 / 15,5
60,0	37,5 / 36,1	42,1 / 48,4	22,7 / 23,2	23,8 / 24,1
100,0	51,8 / 49,9	57,6 / 66,7	31,0 / 31,8	32,5 / 33,1

Commas indicate decimal points. Note: the column λ = 300 μm for η and γ give values calculated and λ = 337 μm, t = 18°C in the denominator; in the numerator, all the values correspond to t = 20°C.

Another factor causing disagreement between theory and measurements is the use in the calculations of distributions of drops with size different from those which actually take place in rain. Corresponding examples may be found in § 3.6 [149]. /302

§ 6.4. Radar Characteristics of Hail.

A theoretical study of the scattering and attenuation of electromagnetic radiation by polydispersed hail [149, 308-310][117] poses certain difficulties, since η and γ depend[118] not only on the wave length, size distribution functions of the particles and its parameters, but also on the shape, state of the surface and density of the hailstones. As already indicated in Chapter 5, the surface of hailstones under natural conditions may be dry (in the course of buildup of the dull layer) and moist (in the course of monocrystalline growth and melting). Moreover, depending on the thickness of the water film, scattering by hailstones may be equivalent to scattering by equal-sized particles of solid ice or continuous water and may differ from these limiting cases.

In this paragraph, on the basis of the concepts given in Chapter 5 and [308-310], we will examine the specific effective radar scattering area η and attenuation coefficient γ of polydispersed hail clouds and precipitation with different ratios of dry to wet hailstones, obeying

[116] For more details see page 188.
[117] References to other studies can also be found there.
[118] As in the case of rain precipitation, for example.

the γ distribution, as a function of their density and temperature and also of the parameters of the spectrum.

Calculations of η and γ of homogeneous water and ice spheres were carried out by using formulas (6.26), (6.27) with n(d):

$$n(d) = N \frac{\beta^{\mu+1}}{\Gamma(\mu+1)\, d_3^{\mu+1}} d^{\mu} \exp\left(-\beta \frac{d}{d_3}\right), \tag{6.28}$$

where N is the total concentration of hailstones per unit volume; $\Gamma(\mu + 1)$ is the gamma function; d_3 is the root-mean-cube diameter of the hail spectrum; β is a parameter defined by expression (6.25).

The calulations were performed by assuming that t = 0°C; λ = 0.86, 3.2, 10, 11, 17 cm; μ = 0, 2, 4, 6, 8, 10; d_3 = 0.1, 0.2, 0.3,..., 5.0 cm; N = 1 m^{-3}; d_{min} = 0. In view of the fact that the experimental hail spectra [277] break off at such d_{max}, when the hailstone concentration amounts to about 0.02-0.01 of the concentration of hailstones of modal diameter d_{mod}, we assumed in the calculations that

$$d_{max} = cd_3, \tag{6.29}$$

where c values were found for different μ from the condition $N_{d_{max}} = 0.01\, N_{d_{mod}}$ (Table 6.25).

TABLE 6.25. VALUE OF PARAMETER c IN RELATION (6.29). /303

μ	0	2	4	6	8	10
c	2.14	2.11	2.06	2.00	1.94	1.88

Figures 6.24 and 6.25 give the dependences of normalized values of specific effective radar scattering areas

$$\eta^{(n)} = \frac{4\eta}{N\pi d_3^2}$$

and attenuation coefficients

$$\gamma^{(n)} = \frac{4\gamma}{4{,}343 \cdot 10^5 N\pi d_3^2}.$$

of water and ice spheres at μ = 0 to 10 for λ = 0.86 cm. It is obvious from these figures that $\eta^{(n)}$ and $\gamma^{(n)}$ change little as functions of parameter μ. Similar graphs for λ equal 3.2, 11 and 17 cm indicate a tendency toward an even greater attenuation of the dependence on μ with increasing wave length. Thus, when λ = 17 cm, the curves for all μ almost merge.

Nevertheless, in the region of small particles $\left(\alpha^{(n)} = \frac{\pi d_3}{\lambda} < 0.4\right)$, the $\eta^{(n)}$ and $\gamma^{(n)}$ values decrease with increasing μ, and in the region of large particles ($\alpha^{(n)} > 0.4$), they increase. At large μ values, this dependence is less pronounced than at small ones.

Thus, in calculations of the radar reflectivity and attenuation in the centimeter wave length range in the case of hail clouds, one can use the two-parameter distribution function of hailstones with size at μ = const with an error not exceeding the error of measurement of these characteristics. Since according to [277], over one half of the spectra of hail obey (see § 6.1) the distribution (6.28) with $\mu = 2$, and, as is evident from Figures 6.24, 6.25, the dependence of $\eta^{(n)}$ and $\gamma^{(n)}$ on $\alpha^{(n)}$ at $\mu = 2$ is approximately average; hereinafter, neglecting the dependence of the radar characteristics on μ, we will consider only the case of $\mu = 2$.

The $\eta^{(n)}$ and $\gamma^{(n)}$ curves for water spheres have a maximum at $\alpha^{(n)} = 0.8$, and as $\alpha^{(n)}$ increases further, tend toward asymptotic values, approaching them at $\alpha^{(n)} = 4$.

For ice spheres, the maximum of $\gamma^{(n)}$ is reached at $\alpha^{(n)} = 2.8$, beyond which the curve slowly approaches the asymptote. The function $\eta^{(n)}$, which increases slowly with increasing $\alpha^{(n)}$, does not reach a maximum.

It is also evident from Figures 6.24, 6.25 that the $\gamma^{(n)}$ values for water and ice spheres differ appreciably in the region of small particles ($\alpha^{(n)} < 4$) and are the same in the region of large particles ($\alpha^{(n)} > 4$), whereas the $\eta^{(n)}$ values for water and ice spheres differ significantly at any $\alpha^{(n)}$. It should /306 be noted that the dependences of $\eta^{(n)}$ and $\gamma^{(n)}$ on $\alpha^{(n)}$ for the spectrum of ice spheres are analogous to the corresponding dependence for individual ice particles.

Figures 6.26, 6.27 show the η and γ curves of water and ice spheres at different λ. A characteristic feature is a rapid growth of η and γ with increasing $\alpha^{(n)}$ to a definite value equal to 0.8 for water spheres and 2.8 for ice spheres. For the growth of η and γ for $\alpha^{(n)}$ greater than the indicated values is insignificant. Hence, the sharp increase in radar reflectivity and attenuation in clouds with coarse hail ($\alpha^{(n)} > 1$), sometimes detected in radar observations is evidently explained not so much by an increase in the size of the hail falling from these clouds as an increase in its concentration.

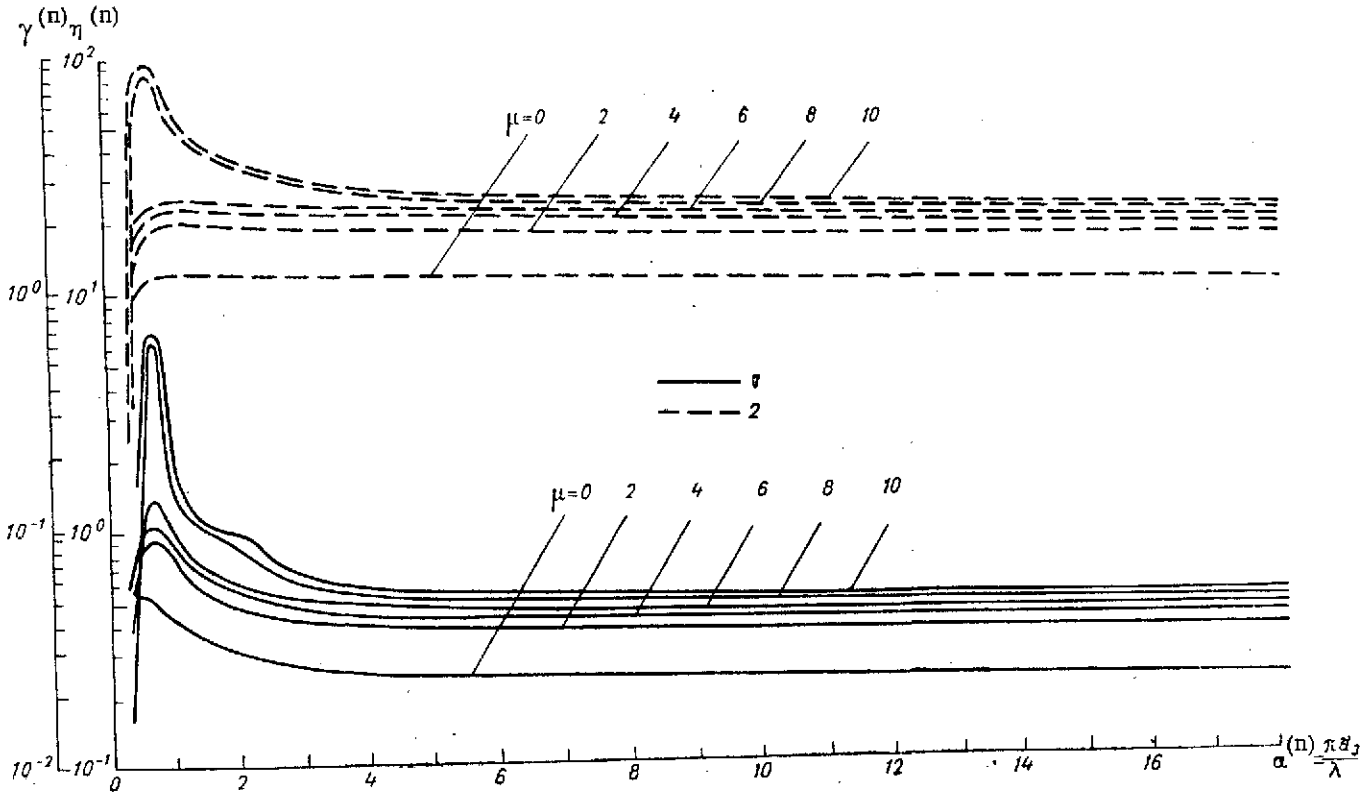

Figure 6.24. Dependence of $\eta^{(n)}$ (1) and $\gamma^{(n)}$ (2) of Water Spheres on $\alpha^{(n)}$ at λ = 0.86 cm and for Gamma Distribution. /304

The change in the η and γ values for different λ as a function of d_3 is not proportional (particularly in the case of water spheres), so that ratios of the type $\eta_{\lambda_i}/\eta_{\lambda_j}$ or $\gamma_{\lambda_i}/\gamma_{\lambda_j}$, which are independent of the particle concentration, /307 may prove useful in determining[119] d_3.

It also follows from Figures 6.26, 6.27 that in coarse hail, the attenuation of electromagnetic radiation may be significant even at λ = 11.0 and 17.0 cm.

Figure 6.28 illustrates the comparative dependence of η and γ values on /308 d_3 for water and ice spheres at a fixed wave length. It is evident that the

[119] See [149, 311, etc.]. In addition to other factors, the calculations require a correct consideration of the phase state of the hailstone surface [312, 310].

η values for water and ice spheres differ substantially from one another. From the region of small particles, η of water spheres exceed the η values of ice spheres by approximately one order of magnitude, and in the region of coarse particles, ice spheres scatter back better than water spheres. The behavior of the attenuation coefficient γ is similar.

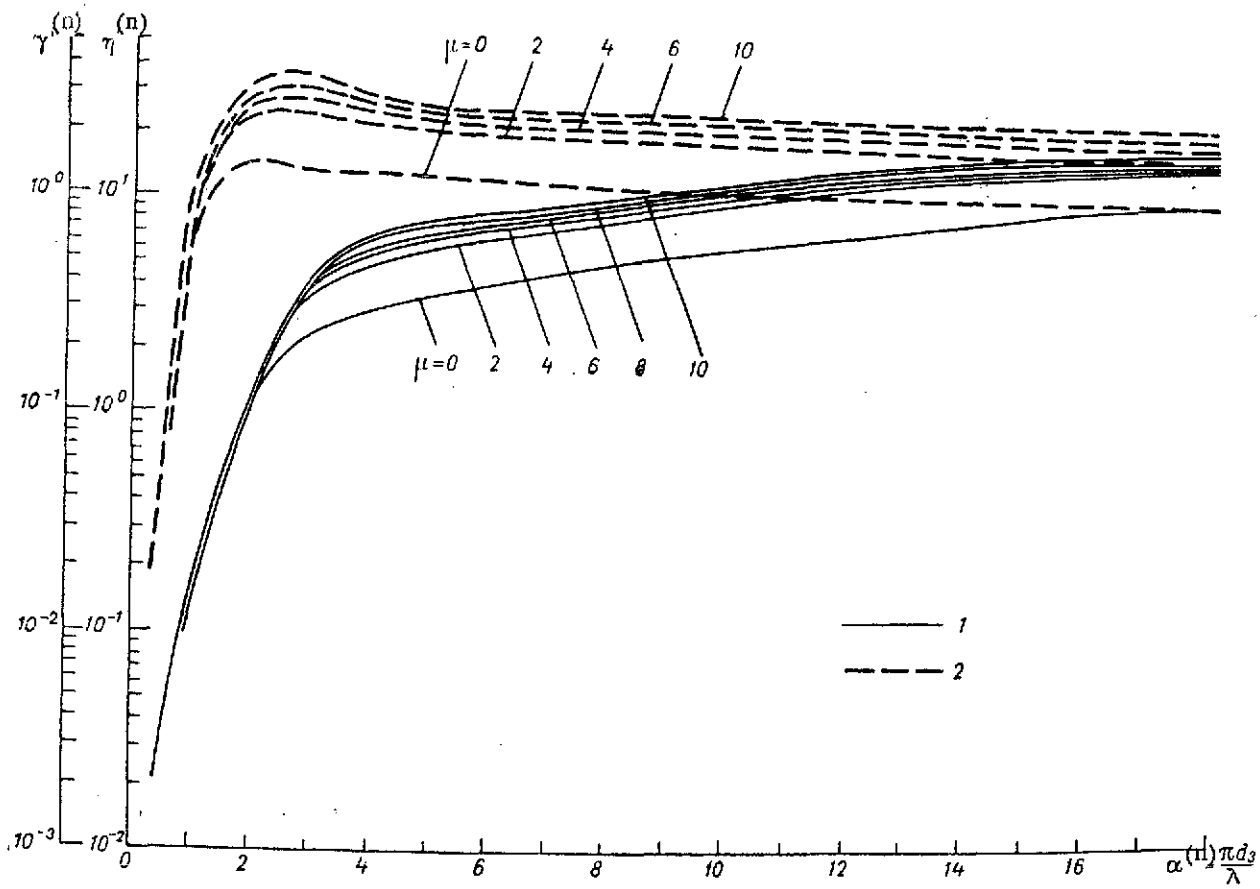

Figure 6.25. Dependence of $\eta^{(n)}$ (1) and $\gamma^{(n)}$ (2) of Ice Spheres on $\alpha^{(n)}$ at λ = 0.86 cm and for Gamma Distribution. /305

Above, the radar characteristics of hail were studied under the assumption that all the hailstones in the spectrum are homogeneous in structure and have a density of 1 g/cm^3. We will remove these limitations [310] and consider the scattering and attenuation of electromagnetic radiation in polydispersed hail clouds by taking into account the crystallization processes determining the phase state of the surface (ice-water), the thickness of the water film and the density of the growing hailstones. /309

As was indicated in § 5.1, according to modern views, the growth of hail nuclei formed as a result of the freezing of a small number of large cloud drops is due to their coalescence with supercooled drops. Moreover, depending

on the thermodynamic parameters of the cloud and size of the hailstone, one of two markedly different crystallization regimes of the water reaching the hailstone is established: the supercritical or the subcritical regime. The criterion of separation of the two regimes is the quantity h_s defined by formula (5.1).

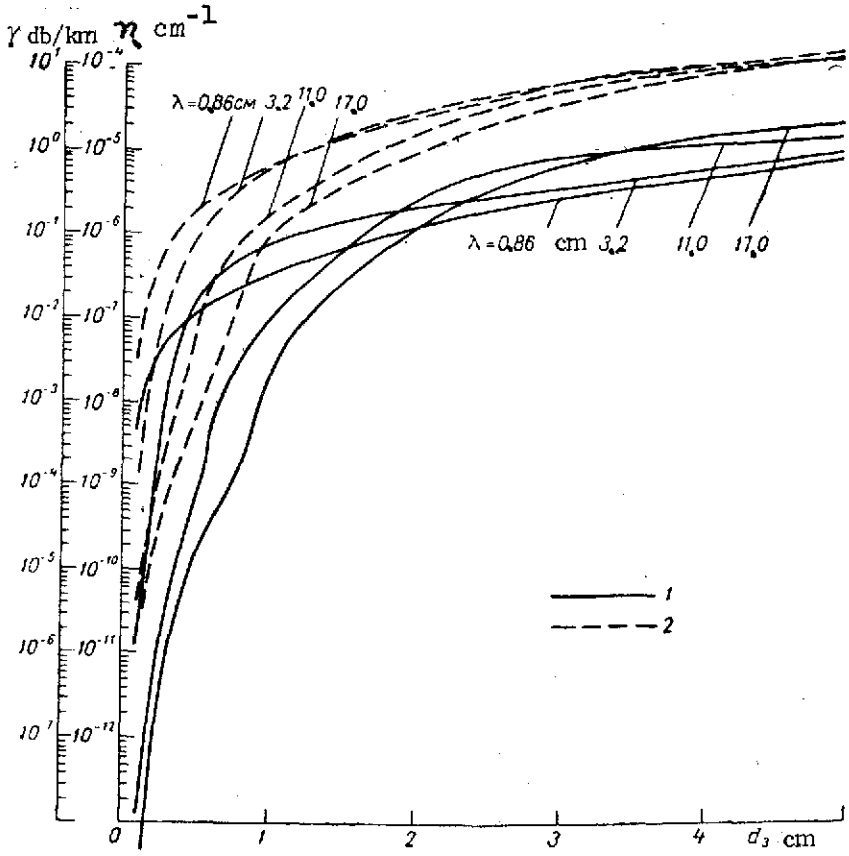

Figure 6.26. Dependence of η (1) and γ (2) of Water Spheres on d_3 for Gamma Distribution of μ = 2 and Different λ.

We introduce into consideration the critical hailstone diameter d_c, which is the value of d at which h_s reaches the critical value, equal to 0.1 cm. Taking into account the dependence [158] of the falling velocity of the hailstones on their integral density and size, and also on the air density, from expression (5.1)[120] we can easily obtain:[121]

---

120 Normalized for the case of a rotating hailstone [310].

121 The meaning of the symbols used here is the same as in § 5.1, d_c in cm, ρ_i in g/cm^3, $q\bar{E}$ in g/m^3.

$$d_к = \frac{0{,}20}{\rho_i} \exp\left[-0{,}017\,(t_0 - t)\right] \left(\frac{t_0 - t}{q\bar{E}}\right)^2. \qquad (6.30)$$

The air density (ρ_a) as a function of temperature t was approximated by the relation

$$\rho_a = 0{,}863 \exp\left[-0{,}017\,(t_0 - t)\right],$$

obtained by processing data of temperature sounding of the atmosphere on days with hail.

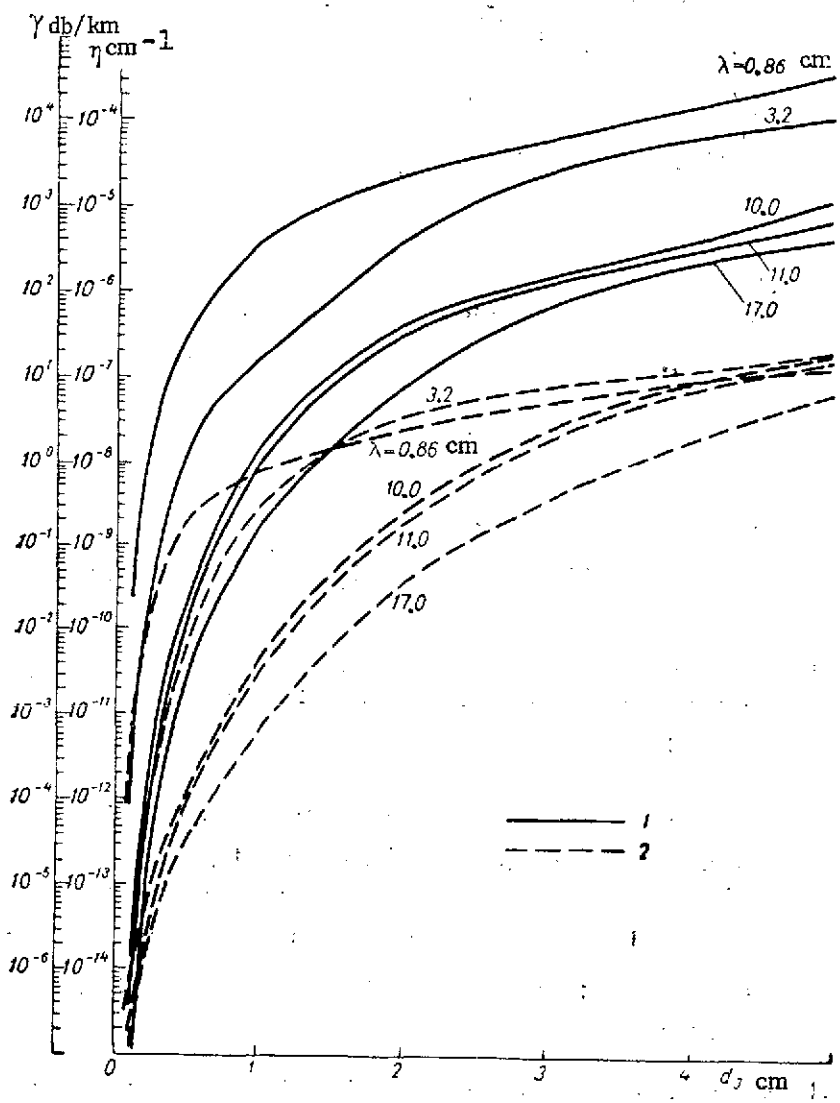

Figure 6.27. Dependence of η (1) and γ (2) of Ice Spheres on d_3 for Gamma Distribution with μ = 2.

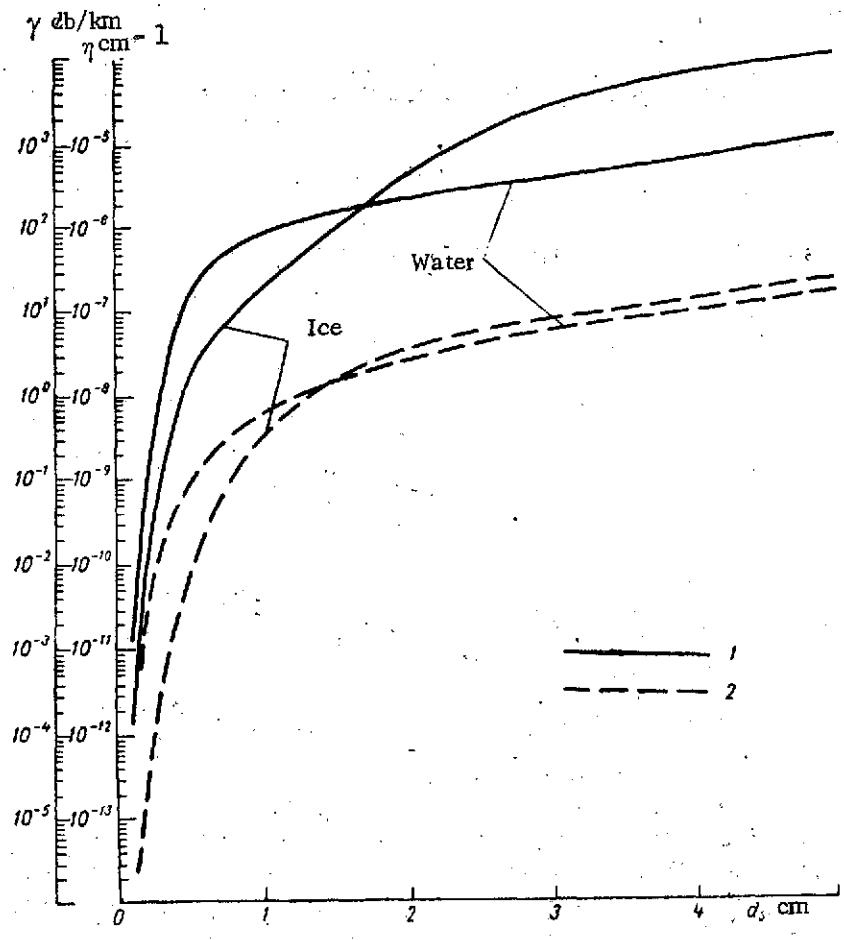

Figure 6.28. Dependence of η (1) and γ (2) of Water and Ice Spheres on d_3 for Gamma Distribution with $\mu = 2$. $\lambda = 3.2$ cm.

Formula (6.30) is convenient in the sense that d_c for the given values of temperature t and effective water content $q\bar{E}$ divides the hail spectrum in the cloud into two parts (Figure 6.29): wet hailstones (region B at $d > d_c$) and dry hailstones (region A at $d < d_c$). Specific results of the calculation of /310 the critical diameters of hailstones under different conditions of their growth in the cloud are shown in Figure 6.30.

It is evident from Figures 6.29, 6.30 that the relative number of wet hailstones in the spectrum increases either when the supercooling of the cloud decreases or when the effective water content increases, or finally when the values of the root-mean-cube diameter of the hailstones increases. The thickness of the water film h_{sh} on the surface of wet hailstones may be

calculated from formula (5.2) by considering the approximate equality

$$\left(\frac{q\bar{E}}{t_0 - t}\right)^{1/4} \approx 1.$$

Results of calculations of h_{sh} made under this assumption are presented in Figure 6.31, from which it is evident that the thickness of the water film on the surface of hailstones growing in the subcritical regime amounts to fractions of a millimeter and decreases with increasing size of the hailstones.

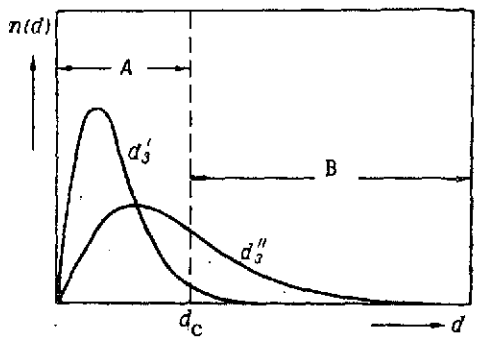

Figure 6.29. Relationships of "Dry" and Wet Hailstones in Two Spectra Differing by the Root-Mean-Cube Diameter d_3 ($d_3'' > d_3'$).

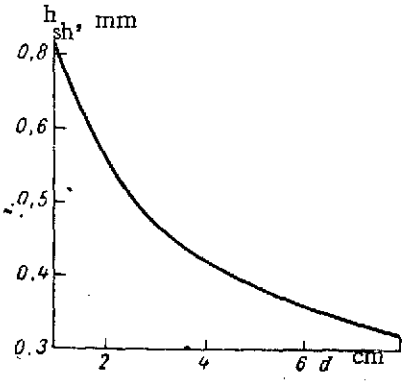

Figure 6.31. Dependence of Thickness of Water Film h_{sh} on the Hailstone on Its Size d and on the Temperature in the Cloud t. ρ_i = 0.800 g/cm^3.

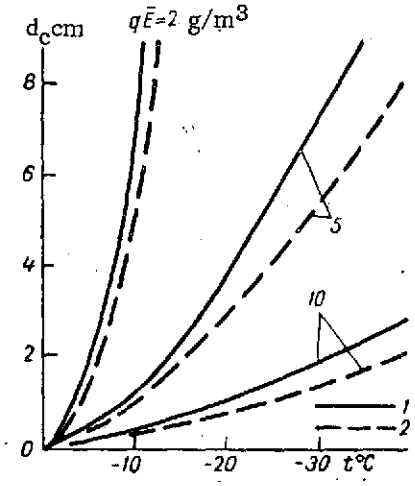

Figure 6.30. Dependence of d_c on Temperature t and All the Effective Water Content $q\bar{E}$ in the Cloud. 1) ρ_i = 0.600 g/cm^3; 2) ρ_i = 0.800 g/cm^3.

Considering the characteristics of formation of structurally inhomogeneous hail, calculations were made to determine its specific effective radar scattering area

$$\eta_i = \int_{d_{min}}^{d_c} n(d)\,\sigma_0(d)\,dd + \int_{d_c}^{d_{max}} n(d)\,\sigma_0(d,\ h_{sh})\,dd \text{ cm}^{-1}$$

and attenuation coefficient /311

$$\gamma = \int_{d_{min}}^{d_c} n(d)\,\sigma_2(d)\,dd + \int_{d_c}^{d_{max}} n(d)\,\sigma_2(d,\ h_{sh})\,dd \text{ db/km},$$

where $\sigma_0(d)$ and $\sigma_2(d)$ are respectively the effective radar scattering and

attenuation areas of dry hailstones [see formulas (1.270), (1.274), (1.288)]; $\sigma_0(d, h_{sh})$ and $\sigma_2(d, h_{sh})$ are respectively the effective radar scattering and attenuation areas of wet hailstones with diameter d and thickness of water film h_{sh} [see formulas (1.276), (1.274), (1.281)-(1.283), (5.2)]; n(d) is the size distribution function of the particles (6.28) for $N = 1\ m^{-3}$, $\mu = 2$, $\lambda = 3.2$ cm, $d_{min} = 0.3$ cm, $d_{max} = 2.11\ d_3$, $d_3 = 0.3\ (0.1)\ 3.0$, $t = -10°C$, $q\bar{E}$ equal to 2.5, 5.0, 10.0 g/m^3, $\rho_i = 0.916\ g/cm^3$, d_c was determined from formula (6.30) and the dielectric constants of supercooled water were taken from the appendix. /312

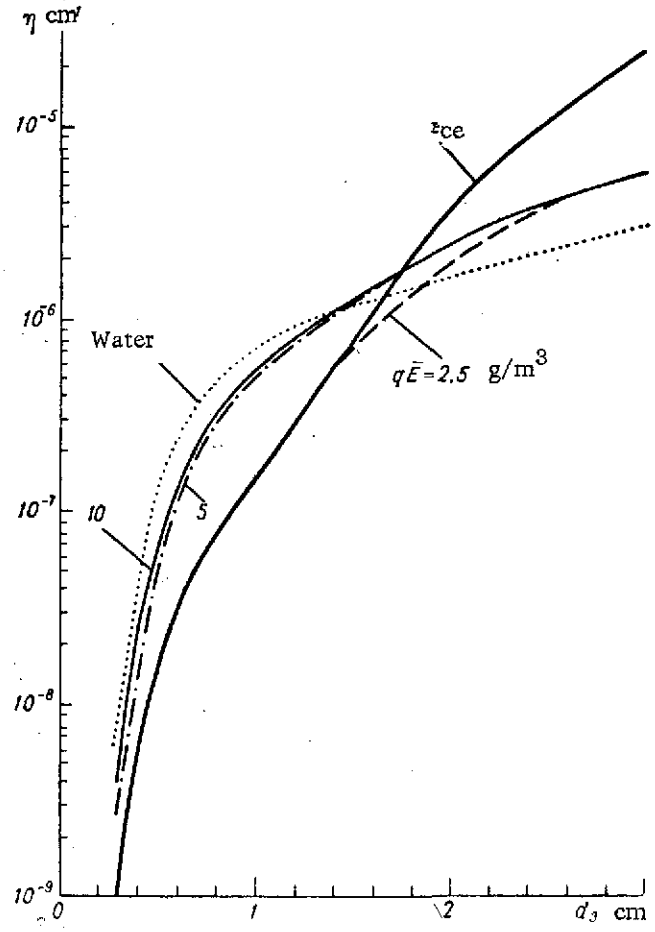

Figure 6.32. Dependence of η of Hail with an Inhomogeneous Spectrum on d_3 for Different Water Contents of the Cloud $q\bar{E}$. $t = -10°C$, $\lambda = 3.2$ cm, $\rho_i = 0.916\ g/cm^3$.

Results of the calculations are presented in Figures 6.32, 6.33 in the form of curves. It is evident from the figures that the scattering and attenuation of radar radiation with 3.2 cm wave length by hail growing in a cloud has a fairly complex character and differs substantially in many cases from the scattering and attenuation of electromagnetic waves by pure water or pure ice spheres.[122] This is explained by a change in the relative amounts of dry and wet hailstones in the spectrum, and also in the thickness of the water film as a function of the parameters of the cloud (t, $q\bar{E}$) and hailstones ($d_з$).

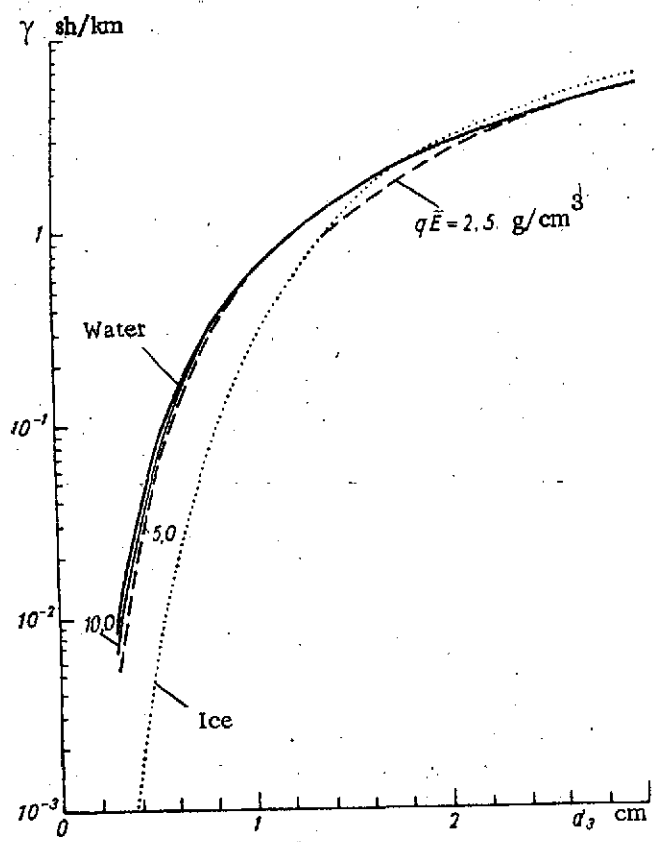

Figure 6.33. Dependence of γ of Spectrally Inhomogeneous Hail on $d_з$ for Different Water Contents of the Cloud $q\bar{E}$. t = –10°C, λ = 3.2 cm, ρ_i = 0.916 g/cm^3.

[122] In Figures 6.32, 6.33, they are denoted by a heavy solid line and points. We will note tentatively that comparison of η and γ of pure ice spheres for gamma distribution at t = –10°C (Figures 6.32, 6.33) and t = 0°C (Figure 6.28) shows that they are practically independent of temperature (with an error of not more than 20-25%). See also § 5.3.

Dry and wet hailstones in turn, like wet hailstones of the same size but with a different thickness of the water film, are not equivalent to one another "radarwise," which in the final analysis determines the complex character of the relationships discussed.

Analysis of Figures 6.32, 6.33 shows that only the spectra of hail with $d_3 \leqslant 1.4$ may be considered at $q\bar{E} = 2.5$ g/m^3 to be "radar dry". At higher /314
values of d_3 in the larger-drop portion of hail growing at the same water content, wet hailstones begin to appear whose relative number and contribution to the total scattering and attenuation of electromagnetic radiation increases with increasing d_3.

As $q\bar{E}$ rises, the fraction of wet hailstones in the spectrum increases (Figure 6.30), so that at $t = -10°C$ and $q\bar{E} = 10$ g/m^3, all the hailstone with $d \geqslant 0.2$ cm are coated with a water film. It is easy to note (Figure 6.32) that the η curve of such a completely wet hail occupies some intermediate position between the η curves for pure water and pure ice spheres, but a position closer to the η curve for water spheres.

At the same time, γ of wet hail at $q\bar{E} = 10$ g/m^3 practically coincides with γ for water spheres (Figure 6.33). This is explained by the characteristics of scattering and attenuation of microwaves by individual wet hailstones. The thickness of the water film on them is such that wet hailstones are equivalent to water drops in attenuation of electromagnetic radiation.

In the case of radar scattering, the water film on the hailstones proves insufficiently "thick" to produce a similar electromagnetic effect.

The same conclusions can be reached by examining the η and γ curves at a water content $q\bar{E} = 5$ g/m^3. Let us note at this point that the calculations given in Figures 6.32, 6.33, were made for different values of the water content $q\bar{E}$, but at a constant temperature in the cloud equal to $-10°C$. It is clear that under other thermodynamic conditions in the cloud, the functions of scattering η and attenuation γ may differ substantially from those shown in Figures 6.32, 6.33.

In addition to the effects discussed above, a substantial influence on the character of scattering and attenuation of microwaves in hail clouds is that of the density of ice in hailstones, which usually changes (see § 5.1) over fairly wide limits: from 0.3 to 0.9 g/cm^3. As was shown by calculations (Figure 6.34) made by using formula (6.26)-(6.29), hail of low density ($\rho_i = 0.600$ g/cm^3) scatters and attenuates radar radiation ($\lambda = 3.2$ cm) much worse than hail with density $\rho_i = 0.92$ g/cm^3.

Thus, scattering and attenuation of radar radiation by hail occurring under natural conditions largely depends on the cloud parameters (t, $q\bar{E}$), density and characteristics of the hailstone spectrum (d_3), which determine

the relative amounts of dry and wet hailstones, and also on the thickness of the water film on their surface.

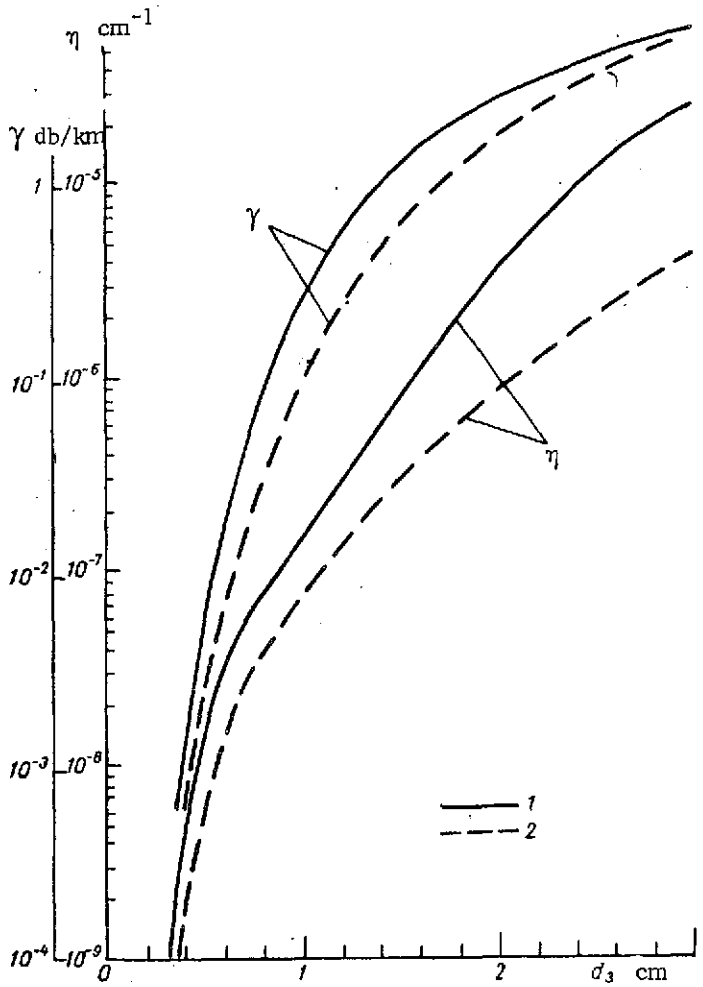

Figure 6.34. Dependence of η and γ of Ice Spheres of Different Densities on d_3 for Gamma Distribution with $\mu = 2$. $t = -10°C$, $\lambda = 3.2$ cm. 1) $\rho_i = 0.916$ g/cm^3, 2) $\rho_i = 0.600$ g/cm^3.

APPENDIX

VALUES OF DIELECTRIC CONSTANTS OF WATER

The tables list values of ε', ε'', n and κ of water for various combinations of wave lengths λ from 0.08 to 20 cm and temperatures t from 0 to 40°C, and also of supercooled water at λ = 0.08 to 17 cm and t = –2, –40°C.

All the values were determined from formulas (4.3), (4.13), (4.16), (4.14), (4.23) and (4.24) for ε_0 = 5.5.

λ cm	ε'	ε''	n	κ	ε'	ε''	n	κ	ε'	ε''	n	κ
	$t = 0°$ C				$t = 2°$ C				$t = 4°$ C			
0,08	5,55	1,98	2,39	0,41	5,55	2,10	2,40	0,44	5,56	2,23	2,40	0,46
0,09	5,56	2,23	2,40	0,46	5,57	2,37	2,41	0,49	5,58	2,51	2,42	0,52
0,10	5,58	2,47	2,42	0,52	5,58	2,63	2,42	0,54	5,60	2,79	2,43	0,57
0,20	5,80	4,94	2,59	0,95	5,84	5,24	2,62	1,00	5,88	5,56	2,64	1,05
0,30	6,16	7,37	2,81	1,31	6,25	7,82	2,85	1,37	6,36	8,29	2,90	1,43
0,40	6,67	9,77	3,04	1,61	6,83	10,36	3,10	1,67	7,01	10,96	3,16	1,73
0,50	7,31	12,11	3,28	1,85	7,56	12,83	3,35	1,91	7,83	13,56	3,43	1,98
0,60	8,09	14,39	3,51	2,05	8,44	15,23	3,59	2,12	8,82	16,07	3,68	2,18
0,62	8,26	14,84	3,55	2,09	8,63	15,70	3,64	2,15	9,03	16,55	3,73	2,21
0,70	8,98	16,61	3,73	2,22	9,45	17,54	3,83	2,29	9,95	18,47	3,93	2,35
0,80	9,99	18,74	3,95	2,37	10,58	19,75	4,06	2,43	11,22	20,76	4,17	2,49
	$t = 0°$ C				$t = 2°$ C				$t = 4°$ C			
0,86	10,64	19,97	4,08	2,45	11,31	21,03	4,19	2,51	12,04	22,07	4,31	2,56
0,90	11,10	20,78	4,16	2,50	11,82	21,86	4,28	2,55	12,60	22,93	4,40	2,60
1,00	12,31	22,73	4,37	2,60	13,17	23,85	4,50	2,65	14,02	24,96	4,62	2,70
1,24	15,52	26,99	4,83	2,79	16,73	28,16	4,97	2,83	18,00	29,28	5,12	2,86
1,50	19,38	30,91	5,29	2,92	20,95	32,04	5,44	2,94	22,57	33,06	5,59	2,95
2,00	27,33	36,46	6,04	3,02	29,45	37,25	6,20	3,00	31,58	37,88	6,36	2,98
2,50	35,20	39,68	6,64	2,99	37,63	39,99	6,80	2,94	40,01	40,09	6,95	2,88
3,00	42,43	41,12	7,12	2,89	44,96	40,92	7,27	2,81	47,36	40,52	7,41	2,74
3,20	45,08	41,31	7,29	2,83	47,60	40,93	7,43	2,75	49,96	40,35	7,56	2,67
3,50	48,79	41,31	7,51	2,75	51,25	40,66	7,64	2,66	53,52	39,85	7,75	2,57
4,00	54,23	40,69	7,81	2,60	56,53	39,69	7,92	2,50	58,59	38,55	8,02	2,40
4,50	58,83	39,58	8,05	2,46	60,91	38,31	8,15	2,35	62,74	36,94	8,23	2,24
5,00	62,69	38,20	8,25	2,32	64,54	36,73	8,33	2,20	66,13	35,22	8,40	2,10
5,50	65,93	36,69	8,41	2,18	67,54	35,09	8,48	2,07	68,90	33,48	8,53	1,96
5,60	66,50	36,38	8,44	2,16	68,07	34,76	8,50	2,04	69,39	33,14	8,55	1,94

Commas indicate decimal points.

λ cm	ε'	ε''	n	x	ε'	ε''	n	x	ε'	ε''	n	x
6,00	68,64	35,15	8,54	2,05	70,04	33,46	8,59	1,95	71,19	31,80	8,64	1,84
6,50	70,93	33,62	8,64	1,94	72,13	31,89	8,69	1,84	73,09	30,20	8,72	1,73
7,00	72,87	32,14	8,73	1,84	73,88	30,39	8,77	1,73	74,68	28,70	8,79	1,63
7,50	74,52	30,73	8,81	1,74	75,37	28,98	8,84	1,64	76,01	27,30	8,85	1,54
8,00	75,93	29,40	8,87	1,66	76,63	27,66	8,89	1,56	77,14	26,01	8,90	1,46
8,50	77,15	28,15	8,92	1,58	77,72	26,43	8,94	1,48	78,11	24,81	8,95	1,39
		$t = 0°$ C				$t = 2°$ C				$t = 4°$ C		
9,00	78,20	26,98	8,97	1,50	78,65	25,29	8,98	1,41	78,94	23,70	8,98	1,32
9,50	79,11	25,88	9,01	1,44	79,46	24,22	9,01	1,34	79,65	22,67	9,01	1,26
10,00	79,91	24,85	9,04	1,37	80,17	23,23	9,05	1,28	80,28	21,72	9,04	1,20
11,00	81,22	22,99	9,10	1,26	81,32	22,44	9,09	1,18	81,29	20,01	9,08	1,10
12,00	82,26	21,36	9,14	1,17	82,23	19,89	9,13	1,09	82,10	18,54	9,12	1,02
14,00	83,75	18,67	9,21	1,01	83,54	17,34	9,19	0,94	83,24	16,13	9,17	0,88
16,00	84,75	16,54	9,25	0,89	84,41	15,34	9,22	0,83	84,00	14,25	9,20	0,77
17,00	85,13	15,64	9,26	0,84	84,73	14,50	9,24	0,78	84,28	13,46	9,21	0,73
18,00	85,45	14,83	9,28	0,80	85,01	13,74	9,25	0,74	84,53	12,75	9,22	0,69
20,00	85,96	13,44	9,30	0,72	85,46	12,44	9,27	0,67	84,91	11,53	9,24	0,62
		$t = 6°$ C				$t = 8°$ C				$t = 10°$ C		
0,08	5,57	2,36	2,41	0,49	5,58	2,49	2,42	0,52	5,59	2,63	2,43	0,54
0,09	5,59	2,66	2,43	0,55	5,60	2,81	2,44	0,58	5,61	2,96	2,44	0,60
0,10	5,61	2,95	2,44	0,60	5,62	3,12	2,45	0,63	5,64	3,28	2,47	0,67
0,20	5,93	5,88	2,67	1,10	5,99	6,20	2,70	1,15	6,05	6,53	2,73	1,20
0,30	6,47	8,76	2,95	1,49	6,59	9,24	2,99	1,54	6,72	6,72	3,04	1,60
0,40	7,20	11,57	3,23	1,79	7,41	12,18	3,29	1,85	7,64	12,80	3,36	1,91
0,50	8,13	14,29	3,51	2,04	8,45	15,03	3,58	2,10	8,79	15,76	3,66	2,15
0,60	9,23	16,91	3,77	2,24	9,68	17,74	3,87	2,29	10,16	18,57	3,96	2,35
0,62	9,47	17,41	3,83	2,27	9,95	18,27	3,92	2,33	10,45	19,11	4,01	2,38
0,70	10,50	19,40	4,03	2,40	11,08	20,31	4,14	2,46	11,71	21,21	4,24	2,50
0,80	11,91	21,75	4,28	2,54	12,64	22,73	4,40	2,59	13,42	23,67	4,51	2,63
0,86	12,81	23,10	4,43	2,61	13,64	24,09	4,55	2,65	14,51	25,05	4,66	2,69
0,90	13,44	23,96	4,52	2,65	14,32	24,97	4,64	2,69	15,26	25,94	4,76	2,72
1,00	15,08	26,02	4,75	2,74	16,12	27,04	4,88	2,77	17,21	28,01	5,00	2,80
1,24	19,39	30,32	5,26	2,88	20,73	31,28	5,40	2,90	22,17	32,15	5,53	2,91
1,50	24,25	33,97	5,74	2,96	25,97	34,76	5,89	2,95	27,71	35,42	6,03	2,94
2,00	33,71	38,33	6,51	2,94	35,82	38,61	6,65	2,90	37,88	38,73	6,78	2,85
2,50	42,31	40,00	7,09	2,82	44,51	39,74	7,22	2,75	46,59	39,31	7,33	2,68
3,00	49,61	39,94	7,53	2,65	51,70	39,22	7,63	2,57	53,61	38,36	7,73	2,48
		$t = 6°$ C				$t = 8°$ C				$t = 10°$ C		
3,20	52,15	39,61	7,67	2,58	54,16	38,73	7,77	2,49	55,99	37,74	7,86	2,40
3,50	55,60	38,89	7,86	2,47	57,47	37,82	7,95	2,38	59,14	36,66	8,02	2,28
4,00	60,44	37,31	8,11	2,30	62,06	36,01	8,18	2,20	63,47	34,67	8,24	2,10
4,50	64,34	35,52	8,30	2,14	65,70	34,07	8,36	2,04	66,86	32,62	8,40	1,94
5,00	67,48	33,68	8,45	1,99	68,61	32,15	8,50	1,89	69,54	30,64	8,53	1,80
5,50	70,03	31,88	8,57	1,86	70,95	30,31	8,61	1,76	71,68	28,78	8,63	1,67
5,60	70,48	31,53	8,59	1,83	71,36	29,95	8,62	1,74	72,05	28,43	8,65	1,64
6,00	72,12	30,17	8,67	1,74	72,85	28,59	8,69	1,64	73,41	27,07	8,71	1,55
6,50	73,84	28,57	8,75	1,63	74,41	27,00	8,76	1,54	74,81	25,51	8,77	1,45
7,00	75,27	27,08	8,81	1,54	75,70	25,54	8,82	1,45	75,97	24,08	8,82	1,36
7,50	76,47	25,71	8,86	1,45	76,77	24,20	8,87	1,36	76,93	27,78	8,86	1,28
8,00	77,48	24,45	8,91	1,37	77,67	22,98	8,91	1,29	77,74	21,60	8,90	1,21
8,50	78,34	23,28	8,95	1,30	78,44	21,85	8,94	1,22	78,42	20,52	8,93	1,15
9,00	79,08	22,21	8,98	1,24	79,09	20,83	8,97	1,16	79,01	19,54	8,96	1,09
9,50	79,71	21,22	9,01	1,18	79,66	19,88	8,99	1,11	79,51	18,63	8,98	1,04

Commas indicate decimal points.

λ cm	ε′	ε″	n	x	ε′	ε″	n	x	ε′	ε″	n	x
10,00	80,26	20,31	9,03	1,12	80,15	19,01	9,01	1,05	79,94	17,81	9,00	0,99
11,00	81,16	18,69	9,07	1,03	80,94	17,47	9,05	0,97	80,64	16,34	9,03	0,91
12,00	81,87	17,29	9,10	0,95	81,56	16,14	9,07	0,89	81,19	15,09	9,05	0,83
14,00	82,87	15,01	9,14	0,82	82,44	14,00	9,11	0,77	81,97	13,06	9,08	0,72
16,00	83,53	13,25	9,17	0,72	83,02	12,34	9,14	0,68	82,48	11,51	9,10	0,63
17,00	83,78	12,51	9,18	0,68	83,24	11,65	9,15	0,64	82,66	10,86	9,11	0,60
18,00	83,99	11,85	9,19	0,64	83,43	11,03	9,15	0,60	82,83	10,28	9,12	0,56
20,00	84,33	10,71	9,20	0,58	83,72	9,96	9,17	0,54	83,09	9,28	9,13	0,51
		$t = 12°$ C				$t = 14°$ C				$t = 16°$ C		
0,08	5,60	2,77	2,43	0,57	5,61	2,90	2,44	0,59	5,62	3,04	2,45	0,62
0,09	5,62	3,11	2,45	0,63	5,64	3,27	2,47	0,66	5,65	3,42	2,48	0,69
0,10	5,65	3,45	2,48	0,70	5,67	3,62	2,49	0,73	5,69	3,80	2,50	0,76
0,20	6,11	6,87	2,77	1,24	6,18	7,21	2,80	1,29	6,25	7,55	2,83	1,33
0,30	6,86	10,20	3,09	1,65	7,01	10,69	3,15	1,70	7,17	11,19	3,20	1,75
		$t = 12°$ C				$t = 14°$ C				$t = 16°$ C		
0,40	7,89	13,42	3,42	1,96	8,15	14,04	3,49	2,01	8,43	14,66	3,56	2,06
0,50	9,16	16,49	3,74	2,20	9,56	17,22	3,82	2,25	9,98	17,94	3,91	2,30
0,60	10,67	19,39	4,05	2,39	11,21	20,20	4,14	2,44	11,79	20,99	4,23	2,48
0,62	11,00	19,95	4,11	2,43	11,57	20,77	4,20	2,47	12,18	21,57	4,30	2,51
0,70	12,37	22,10	4,34	2,54	13,07	22,95	4,44	2,58	13,81	23,78	4,54	2,62
0,80	14,24	24,59	4,62	2,66	15,10	25,47	4,73	2,69	16,00	26,30	4,84	2,72
0,86	15,43	25,98	4,78	2,72	16,39	26,85	4,89	2,75	17,38	27,68	5,00	2,77
0,90	16,24	26,86	4,88	2,75	17,26	27,73	5,00	2,78	18,32	28,55	5,11	2,79
1,00	18,35	28,91	5,13	2,82	19,52	29,75	5,25	2,83	20,73	30,52	5,37	2,84
1,24	23,64	32,93	5,66	2,91	25,14	33,60	5,79	2,90	26,65	34,18	5,92	2,89
1,50	29,46	35,96	6,16	2,92	31,21	36,36	6,29	2,89	32,93	36,64	6,41	2,86
2,00	39,88	38,69	6,91	2,80	41,80	38,50	7,02	2,74	48,62	38,19	7,13	2,68
2,50	48,53	38,74	7,44	2,60	50,34	38,06	7,53	2,53	52,01	37,27	7,62	2,45
3,00	55,35	37,40	7,82	2,39	56,92	36,37	7,89	2,30	58,32	35,27	7,95	2,22
3,20	57,62	36,66	7,93	2,31	59,08	35,52	8,00	2,22	60,36	34,35	8,06	2,13
3,50	60,62	35,45	8,09	2,19	61,91	34,20	8,14	2,10	63,02	32,93	8,19	2,01
4,00	64,68	33,30	8,29	2,01	65,70	31,93	8,33	1,92	66,56	30,58	8,36	1,83
4,50	67,82	31,17	8,44	1,85	68,61	29,76	8,47	1,76	69,24	28,38	8,49	1,67
5,00	70,29	29,16	8,56	1,70	70,87	27,74	8,57	1,62	71,31	26,37	8,58	1,54
5,50	72,24	27,31	8,64	1,58	72,65	25,90	8,65	1,50	72,93	24,56	8,66	1,42
5,60	72,58	26,96	8,66	1,56	72,95	25,55	8,67	1,47	73,20	24,22	8,67	1,40
6,00	73,80	25,62	8,72	1,47	74,07	24,25	8,72	1,39	74,21	22,94	8,71	1,32
6,50	75,07	24,09	8,77	1,37	75,21	22,76	8,77	1,30	75,25	21,50	8,76	1,23
7,00	76,12	22,71	8,82	1,29	76,15	21,41	8,81	1,22	76,09	20,20	8,80	1,15
7,50	76,98	21,45	8,86	1,21	76,93	20,21	8,84	1,14	76,79	19,04	8,83	1,08
8,00	77,70	20,31	8,89	1,14	77,57	19,11	8,87	1,08	77,37	18,00	8,85	1,02
8,50	78,31	19,28	8,92	1,08	78,12	18,13	8,90	1,02	77,85	17,05	8,88	0,96
9,00	78,83	18,34	8,94	1,03	78,58	17,23	8,92	0,97	78,27	16,20	8,89	0,91
9,50	79,28	17,48	8,96	0,98	78,98	16,41	8,93	0,92	78,62	15,42	8,91	0,87
10,00	79,66	16,69	8,97	0,93	79,32	15,66	8,95	0,88	78,93	14,71	8,92	0,82
11,00	80,28	15,30	9,00	0,85	79,87	14,34	8,97	0,80	79,41	13,46	8,94	0,75
12,00	80,77	14,12	9,02	0,78	80,30	13,23	8,99	0,74	79,80	12,40	8,96	0,69
		$t = 12°$ C				$t = 14°$ C				$t = 16°$ C		
14,00	81,45	12,21	9,05	0,67	80,91	11,43	9,02	0,63	80,34	10,71	8,98	0,60
16,00	81,90	10,75	9,07	0,59	81,31	10,05	9,03	0,56	80,69	9,42	9,00	0,52
17,00	82,07	10,14	9,08	0,56	81,45	9,48	9,04	0,52	80,82	8,88	9,00	0,49
18,00	82,22	9,59	9,08	0,53	81,58	8,97	9,05	0,50	80,94	8,40	9,01	0,47
20,00	82,44	8,66	9,09	0,48	81,78	8,09	9,05	0,45	81,11	7,57	9,02	0,42

Commas indicate decimal points.

λ cm	ε′	ε″	n	x	ε′	ε″	n	x	ε′	ε″	n	x
	$t = 18°$ C				$t = 20°$ C				$t = 22°$ C			
0,08	5,63	3,19	2,46	0,65	5,65	3,33	2,47	0,67	5,66	3,47	2,48	0,70
0,09	5,67	3,58	2,49	0,72	5,69	3,74	2,50	0,75	5,71	3,91	2,51	0,78
0,10	5,71	3,98	2,52	0,79	5,73	4,16	2,53	0,82	5,75	4,34	2,55	0,85
0,20	6,33	7,89	2,87	1,38	6,42	8,24	2,90	1,42	6,51	8,59	2,94	1,46
0,30	7,35	11,68	3,25	1,80	7,53	12,17	3,31	1,84	7,73	12,66	3,36	1,88
0,40	8,73	15,28	3,63	2,11	9,04	15,89	3,70	2,15	9,38	16,50	3,77	2,19
0,50	10,42	18,65	3,99	2,34	10,89	19,35	4,07	2,38	11,38	20,03	4,15	2,41
0,60	12,39	21,76	4,33	2,51	13,02	22,51	4,42	2,55	13,69	23,23	4,51	2,58
0,62	12,81	22,35	4,39	2,54	13,48	23,10	4,48	2,58	14,18	23,83	4,58	2,60
0,70	14,58	24,58	4,65	2,65	15,38	25,34	4,74	2,67	16,22	26,06	4,84	2,69
0,80	16,94	27,09	4,94	2,74	17,91	27,83	5,05	2,76	18,90	28,02	5,15	2,77
0,86	18,42	28,45	5,11	2,78	19,48	29,17	5,22	2,79	20,57	29,82	5,33	2,80
0,90	19,42	29,30	5,22	2,80	20,54	29,99	5,33	2,81	21,68	30,62	5,44	2,81
1,00	21,97	31,21	5,48	2,85	23,23	31,83	5,60	2,84	24,51	32,36	5,71	2,84
1,24	28,17	34,64	6,03	2,87	29,69	35,00	6,15	2,85	31,19	35,26	6,26	2,82
1,50	34,63	36,80	6,53	2,82	36,28	36,83	6,63	2,78	37,88	36,76	6,73	2,73
2,00	45,35	37,75	7,22	2,61	46,96	37,21	7,31	2,54	48,47	36,58	7,39	2,48
2,50	53,52	36,40	7,69	2,37	54,89	35,46	7,75	2,29	56,12	34,48	7,81	2,21
3,00	59,55	34,14	8,01	2,13	60,62	32,98	8,05	2,05	61,55	31,81	8,09	1,97
3,20	61,48	33,14	8,10	2,05	62,44	31,93	8,14	1,96	63,26	30,72	8,17	1,88
3,50	63,97	31,66	8,23	1,92	64,77	30,39	8,26	1,84	65,42	29,15	8,28	1,76
4,00	67,25	29,25	8,38	1,74	67,81	27,96	8,40	1,66	68,24	26,70	8,41	1,59
4,50	69,72	27,04	8,50	1,59	70,08	25,76	8,51	1,51	70,32	24,53	8,51	1,44
	$t = 18°$ C				$t = 20°$ C				$t = 22°$ C			
5,00	71,61	25,05	8,59	1,46	71,81	23,80	8,59	1,39	71,90	22,61	8,58	1,32
5,50	73,09	23,28	8,65	1,35	73,15	22,08	8,65	1,28	73,12	20,93	8,64	1,21
5,60	73,34	22,95	8,67	1,32	73,38	21,75	8,66	1,26	73,33	20,62	8,65	1,19
6,00	74,25	21,71	8,71	1,25	74,21	20,55	8,69	1,18	74,08	19,46	8,68	1,12
6,50	75,19	20,31	8,75	1,16	75,05	19,20	8,73	1,10	74,85	18,16	8,71	1,04
7,00	75,95	19,07	8,78	1,09	75,74	18,01	8,76	1,03	75,46	17,02	8,74	0,97
7,50	76,57	17,96	8,81	1,02	76,30	16,94	8,79	0,96	75,97	16,00	8,76	0,91
8,00	77,09	16,96	8,83	0,96	76,77	15,99	8,81	0,91	76,39	15,09	8,78	0,86
8,50	77,53	16,06	8,85	0,91	77,16	15,13	8,83	0,86	76,75	14,27	8,80	0,81
9,00	77,90	15,24	8,87	0,86	77,49	14,36	8,84	0,81	77,04	13,53	8,81	0,77
9,50	78,22	14,50	8,88	0,82	77,77	13,65	8,85	0,77	77,30	12,87	8,82	0,73
10,00	78,49	13,83	8,89	0,78	78,02	13,02	8,86	0,73	77,52	12,26	8,83	0,69
11,00	78,92	12,65	8,91	0,71	78,41	11,89	8,88	0,67	77,86	11,20	8,85	0,63
12,00	79,27	11,65	8,93	0,65	78,72	10,95	8,89	0,62	78,14	10,31	8,86	0,58
14,00	79,75	10,05	8,95	0,56	79,14	9,44	8,91	0,53	78,52	8,88	8,88	0,50
16,00	80,06	8,83	8,96	0,49	79,42	8,29	8,92	0,46	78,77	7,80	8,89	0,44
17,00	80,18	8,32	8,97	0,46	79,52	7,81	8,93	0,44	78,86	7,35	8,89	0,41
18,00	80,28	7,87	8,97	0,44	79,62	7,39	8,93	0,41	78,95	6,95	8,89	0,39
20,00	80,44	7,10	8,98	0,40	79,76	6,66	8,94	0,37	79,07	6,26	8,90	0,35
	$t = 24°$ C				$t = 26°$ C				$t = 28°$ C			
0,08	5,68	3,62	2,49	0,73	5,70	3,77	2,50	0,75	5,71	3,91	2,51	0,78
0,09	5,73	4,07	2,53	0,81	5,75	4,23	2,54	0,83	5,77	4,40	2,55	0,86
0,10	5,78	4,52	2,56	0,88	5,81	4,70	2,58	0,91	5,83	4,89	2,59	0,94
0,20	6,60	8,94	2,98	1,50	6,71	9,29	3,01	1,54	6,82	9,64	3,05	1,58
0,30	7,94	13,16	3,41	1,93	8,16	13,64	3,47	1,97	8,39	14,13	3,52	2,01
0,40	9,73	17,10	3,83	2,23	10,10	17,69	3,90	2,27	10,49	18,27	3,97	2,30
0,50	11,90	20,70	4,23	2,45	12,44	21,35	4,31	2,48	13,00	21,98	4,39	2,50
0,60	14,38	23,92	4,60	2,60	15,09	24,59	4,69	2,62	15,83	25,22	4,78	2,64
0,62	14,90	24,52	4,67	2,63	15,65	25,18	4,76	2,65	16,43	25,81	4,85	2,66
0,70	17,07	26,74	4,94	2,71	17,96	27,38	5,04	2,72	18,87	27,97	5,13	2,73

Commas indicate decimal points.

λ см	ε′	ε″	n	x	ε′	ε″	n	x	ε′	ε″	n	x
	$t = 24°$ C				$t = 26°$ C				$t = 28°$ C			
0,80	19,92	29,15	5,26	2,77	20,96	29,73	5,35	2,78	22,02	30,24	5,45	2,77
0,86	21,68	30,41	5,43	2,80	22,80	30,94	5,53	2,80	23,94	31,39	5,63	2,79
0,90	22,85	31,17	5,54	2,81	24,02	31,65	5,65	2,80	25,20	32,07	5,74	2,79
1,00	25,79	32,81	5,81	2,82	27,07	33,19	5,91	2,81	28,35	33,48	6,01	2,79
1,24	32,67	35,42	6,36	2,79	34,11	35,48	6,45	2,75	35,52	35,45	6,55	2,71
1,50	39,42	36,58	6,83	2,68	40,90	36,30	6,91	2,63	42,30	35,94	6,99	2,57
2,00	49,86	35,87	7,46	2,40	51,13	35,10	7,52	2,33	52,29	34,27	7,58	2,26
2,50	57,22	33,46	7,86	2,13	53,18	32,41	7,90	2,05	59,02	31,36	7,93	1,98
3,00	62,34	30,64	8,12	1,89	63,01	29,49	8,14	1,81	63,55	28,35	8,16	1,74
3,20	63,94	29,53	8,20	1,80	64,49	28,35	8,21	1,73	64,94	27,20	8,23	1,65
3,50	65,95	27,93	8,29	1,68	66,37	26,75	8,30	1,61	66,68	25,60	8,31	1,54
4,00	68,55	25,49	8,42	1,51	68,77	24,33	8,42	1,45	68,89	23,21	8,41	1,38
4,50	70,47	23,35	8,51	1,37	70,53	22,23	8,50	1,31	70,51	21,16	8,49	1,25
5,00	71,91	21,48	8,57	1,25	71,84	20,41	8,56	1,19	71,71	19,40	8,54	1,14
5,50	73,02	19,85	8,62	1,15	72,86	18,84	8,61	1,09	72,63	17,88	8,59	1,04
5,60	73,21	19,54	8,63	1,13	73,03	18,54	8,61	1,08	72,79	17,59	8,59	1,02
6,00	73,89	18,43	8,66	1,06	73,64	17,47	8,64	1,01	73,35	16,56	8,62	0,96
6,50	74,58	17,19	8,69	0,99	74,27	16,28	8,67	0,94	73,92	15,42	8,64	0,89
7,00	75,14	16,09	8,72	0,92	74,78	15,22	8,69	0,88	74,38	14,41	8,66	0,83
7,50	75,60	15,12	8,74	0,86	75,19	14,29	8,71	0,82	74,75	13,53	8,68	0,78
8,00	75,98	14,25	8,75	0,81	75,53	13,47	8,73	0,77	75,06	12,74	8,69	0,73
8,50	76,30	13,47	8,77	0,77	75,82	12,73	8,74	0,73	75,32	12,03	8,71	0,69
9,00	76,57	12,77	8,78	0,73	76,06	12,06	8,75	0,69	75,54	11,40	8,72	0,65
9,50	76,79	12,14	8,79	0,69	76,27	11,46	8,76	0,65	75,72	10,83	8,72	0,62
10,00	76,99	11,56	8,80	0,66	76,45	10,91	8,77	0,62	75,88	10,31	8,73	0,59
11,00	77,30	10,55	8,81	0,60	76,73	9,96	8,78	0,57	76,14	9,40	8,74	0,54
12,00	77,55	9,71	8,82	0,55	76,95	9,16	8,79	0,52	76,34	8,65	8,75	0,49
14,00	77,89	8,36	8,84	0,47	77,26	7,88	8,80	0,45	76,62	7,44	8,76	0,42
16,00	78,12	7,34	8,85	0,41	77,46	6,92	8,81	0,39	76,80	6,53	8,78	0,37
17,00	78,20	6,91	8,85	0,39	77,53	6,52	8,81	0,37	76,86	6,15	8,77	0,35
18,00	78,27	6,54	8,85	0,37	77,60	6,16	8,82	0,35	76,92	5,81	8,78	0,33
20,00	78,38	5,89	8,86	0,33	77,70	5,55	8,82	0,31	77,01	5,24	8,78	0,30
	$t = 30°$ C				$t = 32°$ C				$t = 34°$ C			
0,08	5,73	4,06	2,53	0,80	5,75	4,21	2,54	0,83	5,77	4,36	2,55	0,86
0,09	5,79	4,57	2,57	0,89	5,82	4,74	2,58	0,92	5,85	4,91	2,60	0,94
0,10	5,86	5,07	2,61	0,97	5,89	5,26	2,63	1,00	5,93	5,44	2,64	1,03
0,20	6,93	9,99	3,09	1,62	7,05	10,34	3,13	1,65	7,18	10,69	3,17	1,69
0,30	8,84	14,61	3,58	2,04	8,90	15,09	3,63	2,08	9,17	15,57	3,69	2,11
0,40	10,90	18,84	4,04	2,33	11,32	19,40	4,11	2,36	11,76	19,94	4,18	2,39
0,50	13,59	22,59	4,47	2,53	14,19	23,17	4,55	2,55	14,82	23,73	4,63	2,56
0,60	16,59	25,81	4,86	2,65	17,37	26,37	4,95	2,67	18,17	26,89	5,03	2,67
0,62	17,23	26,40	4,94	2,67	18,04	26,95	5,02	2,68	18,88	27,46	5,11	2,69
0,70	19,79	28,51	5,22	2,73	20,73	29,00	5,31	2,73	21,69	29,44	5,40	2,73
0,80	23,08	30,70	5,54	2,77	24,16	31,09	5,64	2,76	25,24	31,42	5,72	2,74
0,86	25,08	31,78	5,73	2,78	26,22	32,10	5,82	2,76	27,37	32,35	5,91	2,74
0,90	26,39	32,41	5,84	2,78	27,56	32,68	5,93	2,76	28,74	32,87	6,02	2,73
1,00	29,62	33,69	6,10	2,76	30,88	33,82	6,19	2,73	32,11	33,88	6,28	2,70
1,24	36,88	35,33	6,63	2,66	38,20	35,13	6,71	2,62	39,47	34,86	6,79	2,57
1,50	43,62	35,49	7,07	2,51	44,87	34,98	7,13	2,45	46,03	34,41	7,19	2,39
2,00	53,34	33,41	7,63	2,19	54,29	32,50	7,67	2,12	55,13	31,60	7,70	2,05
2,50	59,74	30,30	7,96	1,90	60,36	29,25	7,98	1,83	60,88	28,20	8,00	1,76
3,00	63,99	27,23	8,17	1,67	64,34	26,14	8,18	1,60	64,60	25,08	8,18	1,53

Commas indicate decimal points.

λ cm	ε'	ε''	n	x	ε'	ε''	n	x	ε'	ε''	n	x
3,20	65,29	26,08	8,23	1,58	65,54	24,99	8,24	1,52	65,71	23,94	8,24	1,45
3,50	66,90	24,50	8,31	1,47	67,03	23,43	8,31	1,41	67,09	22,41	8,30	1,35
4,00	68,94	22,15	8,41	1,32	68,91	21,13	8,40	1,26	68,83	20,16	8,38	1,20
4,50	70,42	20,15	8,48	1,19	70,27	19,18	8,46	1,13	70,07	18,27	8,44	1,08
5,00	71,52	18,44	8,53	1,08	71,28	17,53	8,51	1,03	70,99	16,68	8,48	0,98
5,50	72,36	16,98	8,56	0,99	72,05	16,03	8,54	0,94	71,69	15,32	8,51	0,90
5,60	72,50	16,70	8,57	0,97	72,17	15,86	8,55	0,93	71,81	15,07	8,52	0,88
6,00	73,01	15,71	8,59	0,91	72,64	14,91	8,57	0,87	72,24	14,16	8,54	0,83
6,50	73,53	14,62	8,62	0,85	73,11	13,86	8,59	0,81	72,66	13,16	8,56	0,77
7,00	73,95	13,65	8,64	0,79	73,49	12,94	8,61	0,75	73,01	12,28	8,57	0,72
7,50	74,29	12,81	8,65	0,74	73,80	12,14	8,62	0,70	73,29	11,51	8,59	0,67
8,00	74,57	12,06	8,66	0,70	74,05	11,42	8,63	0,66	73,52	10,83	8,60	0,63
8,50	74,80	11,39	8,67	0,66	74,26	10,78	8,64	0,62	73,71	10,22	8,61	0,59
		$t = 30°$ C				$t = 32°$ C				$t = 34°$ C		
9,00	75,00	10,78	8,68	0,62	74,44	10,21	8,65	0,59	73,87	9,67	8,61	0,56
9,50	75,16	10,24	8,69	0,59	74,59	9,69	8,65	0,56	74,01	9,18	8,62	0,53
10,00	75,31	9,75	8,70	0,56	74,72	9,23	8,66	0,53	74,13	8,74	8,62	0,51
11,00	75,54	8,89	8,71	0,51	74,93	8,41	8,67	0,48	74,31	7,96	8,63	0,46
12,00	75,72	8,17	8,71	0,47	75,09	7,73	8,68	0,45	74,47	7,32	8,64	0,42
14,00	75,97	7,03	8,73	0,40	75,32	6,65	8,69	0,38	74,67	6,29	8,65	0,36
16,00	76,13	6,16	8,73	0,35	75,47	5,83	8,69	0,34	74,80	5,52	8,65	0,32
17,00	76,19	5,80	8,73	0,33	75,52	5,49	8,70	0,32	74,85	5,19	8,66	0,30
18,00	76,24	5,49	8,74	0,31	75,57	5,19	8,70	0,30	74,89	4,91	8,66	0,28
20,00	76,32	4,95	8,74	0,28	75,64	4,67	8,70	0,27	74,96	4,42	8,66	0,26
		$t = 36°$ C				$t = 38°$ C				$t = 40°$ C		
0,08	5,80	4,52	2,56	0,88	5,82	4,67	2,58	0,91	5,85	4,82	2,59	0,93
0,09	5,88	5,08	2,61	0,97	5,91	5,25	2,63	1,00	5,94	5,42	2,64	1,02
0,10	5,96	5,63	2,66	1,06	6,00	5,82	2,68	1,09	6,04	6,01	2,70	1,11
0,20	7,31	11,04	3,21	1,72	7,46	11,39	3,25	1,75	7,60	11,74	3,29	1,79
0,30	9,45	16,04	3,75	2,14	9,75	16,50	3,80	2,17	10,06	16,95	3,86	2,20
0,40	12,22	20,47	4,25	2,41	12,70	20,98	4,31	2,43	13,20	21,48	4,38	2,45
0,50	15,46	24,26	4,70	2,58	16,12	24,76	4,78	2,59	16,80	25,23	4,85	2,60
0,60	18,99	27,37	5,11	2,68	19,82	27,81	5,19	2,68	20,66	28,21	5,27	2,67
0,62	19,73	27,93	5,19	2,69	20,59	28,35	5,27	2,69	21,47	28,72	5,35	2,68
0,70	22,65	29,83	5,48	2,72	23,62	30,16	5,56	2,71	24,59	30,45	5,64	2,70
0,80	26,32	31,68	5,81	2,73	27,39	31,89	5,89	2,71	28,45	32,03	5,97	2,68
0,86	28,50	32,54	5,99	2,72	29,62	32,66	6,07	2,69	30,72	32,71	6,15	2,66
0,90	29,89	33,00	6,10	2,70	31,03	33,06	6,18	2,67	32,14	33,05	6,26	2,64
1,00	33,31	33,86	6,36	2,66	34,48	33,77	6,43	2,63	35,61	33,62	6,50	2,58
1,24	40,67	34,51	6,86	2,52	41,81	34,10	6,92	2,46	42,89	33,63	6,98	2,41
1,50	47,12	33,78	7,25	2,33	48,11	33,11	7,30	2,27	49,03	32,40	7,34	2,21
2,00	55,87	30,66	7,73	1,98	56,52	29,73	7,76	1,92	57,08	28,79	7,78	1,85
2,50	61,30	27,18	8,01	1,70	61,64	26,17	8,02	1,63	61,90	25,19	8,02	1,57
3,00	64,77	24,06	8,18	1,47	64,88	23,07	8,18	1,41	64,92	22,11	8,17	1,35
		$t = 36°$ C				$t = 38°$ C				$t = 40°$ C		
3,20	65,81	22,93	8,23	1,39	65,84	21,96	8,22	1,34	65,81	21,02	8,21	1,28
3,50	67,08	21,42	8,29	1,29	67,02	20,48	8,28	1,24	66,90	19,59	8,26	1,18
4,00	68,68	19,23	8,37	1,15	68,49	18,35	8,35	1,10	68,26	17,52	8,33	1,05
4,50	69,83	17,41	8,42	1,03	69,54	16,59	8,40	0,99	69,23	15,81	8,37	0,94
5,00	70,67	15,87	8,46	0,94	70,32	15,11	8,43	0,90	69,94	14,39	8,41	0,86
5,50	71,31	14,57	8,49	0,86	70,90	13,86	8,46	0,82	70,47	13,19	8,43	0,78
5,60	71,42	14,32	8,49	0,84	71,00	13,62	8,46	0,80	70,56	12,96	8,44	0,77
6,00	71,81	13,46	8,51	0,79	71,36	12,79	8,48	0,75	70,88	12,17	8,45	0,72
6,50	72,20	12,49	8,53	0,73	71,71	11,87	8,50	0,70	71,21	11,29	8,46	0,67

Commas indicate decimal points.

λcm	ε′	ε″	n	x	ε′	ε″	n	x	ε′	ε″	n	x
7,00	72,51	11,66	8,54	0,68	72,00	11,07	8,51	0,65	71,47	10,52	8,48	0,62
7,50	72,76	10,92	8,55	0,64	72,23	10,37	8,52	0,61	71,68	9,85	8,49	0,58
8,00	72,97	10,27	8,56	0,60	72,42	9,75	8,53	0,57	71,86	9,26	8,49	0,55
8,50	73,15	9,69	8,57	0,57	72,58	9,20	8,54	0,54	72,00	8,74	8,50	0,51
9,00	73,30	9,17	8,58	0,53	72,71	8,70	8,54	0,51	72,12	8,26	8,51	0,49
9,50	73,42	8,71	8,58	0,51	72,83	8,26	8,55	0,48	72,23	7,84	8,51	0,46
10,00	73,53	8,28	8,59	0,48	72,92	7,86	8,55	0,46	72,32	7,46	8,52	0,44
11,00	73,70	7,54	8,60	0,44	73,08	7,15	8,56	0,42	72,45	6,79	8,52	0,40
12,00	73,83	6,93	8,60	0,40	73,20	6,58	8,56	0,38	72,57	6,24	8,53	0,37
14,00	74,02	5,96	8,61	0,35	73,37	5,65	8,57	0,33	72,72	5,36	8,53	0,31
16,00	74,14	5,22	8,62	0,30	73,48	4,95	8,58	0,29	72,82	4,70	8,54	0,28
17,00	74,18	4,92	8,62	0,29	73,51	4,66	8,58	0,27	72,85	4,42	8,54	0,26
18,00	74,22	4,65	8,62	0,27	73,55	4,41	8,58	0,26	72,89	4,18	8,54	0,24
20,00	74,28	4,19	8,62	0,24	73,61	3,97	8,58	0,23	72,94	3,76	8,54	0,22
		$t = -2°$ C				$t = -4°$ C				$t = -6°$ C		
0,08	5,54	1,86	2,39	0,39	5,54	1,74	2,38	0,37	5,53	1,63	2,38	0,34
0,10	5,56	2,32	2,41	0,48	5,56	2,18	2,40	0,45	5,55	2,03	2,39	0,42
0,20	5,76	4,63	2,56	0,90	5,72	4,34	2,54	0,85	5,69	4,06	2,52	0,81
0,30	6,08	6,93	2,77	1,25	6,00	6,49	2,72	1,19	5,94	6,07	2,69	1,13
0,40	6,52	9,18	2,98	1,54	6,39	8,62	2,92	1,47	6,27	8,06	2,87	1,40
		$t = -2°$ C				$t = -4°$ C				$t = -6°$ C		
0,50	7,09	11,40	3,20	1,78	6,88	10,71	3,13	1,71	6,70	10,02	3,06	1,64
0,60	7,76	13,57	3,42	1,98	7,48	12,76	3,34	1,91	7,21	11,96	3,25	1,84
0,62	7,91	14,00	3,46	2,02	7,61	13,16	3,38	1,95	7,33	12,34	3,29	1,87
0,70	8,55	15,68	3,64	2,16	8,17	14,76	3,54	2,09	7,82	13,85	3,44	2,01
0,80	9,44	17,72	3,84	2,31	8,95	16,70	3,73	2,24	8,50	15,70	3,63	2,16
0,86	10,03	18,91	3,96	2,38	9,46	17,84	3,85	2,32	8,95	16,79	3,74	2,24
0,90	10,43	19,69	4,04	2,43	9,82	18,59	3,93	2,37	9,26	17,50	3,81	2,30
1,00	11,50	21,57	4,24	2,54	10,78	20,41	4,11	2,48	10,10	19,25	3,99	2,41
1,24	14,39	25,76	4,68	2,75	13,34	24,49	4,54	2,70	12,37	23,19	4,40	2,64
2,0	25,26	35,49	5,87	3,03	23,25	34,38	5,69	3,02	21,32	33,13	5,51	3,01
3,0	39,81	41,09	6,96	2,95	37,18	40,83	6,79	3,01	34,40	40,33	6,61	3,05
3,2	42,44	41,48	7,13	2,91	39,71	41,41	6,97	2,97	36,91	41,10	6,79	3,03
5,6	64,66	37,96	8,36	2,27	62,54	39,47	8,26	2,39	60,13	40,85	8,15	2,51
10,0	79,47	26,58	9,04	1,47	78,84	28,41	9,02	1,58	77,98	30,35	8,99	1,69
11,0	80,97	24,65	9,10	1,35	80,54	26,42	9,09	1,45	79,90	28,32	9,07	1,56
17,0	85,45	16,90	9,29	0,91	85,68	18,27	9,31	0,98	85,81	19,78	9,32	1,06
		$t = -8°$ C				$t = -10°$ C				$t = -12°$ C		
0,08	5,53	1,52	2,37	0,32	5,52	1,41	2,57	0,30	5,52	1,31	2,37	0,28
0,10	5,54	1,90	2,39	0,40	5,54	1,76	2,38	0,37	5,53	1,64	2,38	0,34
0,20	5,67	3,79	2,50	0,76	5,64	3,52	2,48	0,71	5,62	3,27	2,46	0,66
0,30	5,87	5,67	2,65	1,07	5,82	5,27	2,61	1,01	5,77	4,90	2,58	0,95
0,40	6,16	7,53	2,82	1,34	6,07	7,01	2,77	1,27	5,99	6,51	2,72	1,20
0,50	6,53	9,37	3,00	1,56	6,39	8,73	2,93	1,49	6,27	8,12	2,87	1,41
0,60	6,98	11,18	3,18	1,76	6,77	10,43	3,10	1,68	6,59	9,70	3,03	1,60
0,62	7,08	11,54	3,21	1,80	6,86	10,77	3,13	1,72	6,66	10,02	3,06	1,64
0,70	7,50	12,97	3,35	1,93	7,22	12,10	3,26	1,85	6,97	11,27	3,18	1,77
0,80	8,10	14,72	3,53	2,09	7,73	13,75	3,43	2,01	7,41	12,81	3,33	1,92
0,86	8,49	15,75	3,63	2,17	8,07	14,72	3,53	2,09	7,70	13,73	3,42	2,00
0,90	8,76	16,42	3,70	2,22	8,31	15,36	3,59	2,14	7,91	14,33	3,48	2,06

Commas indicate decimal points.

λ cm	ε′	ε″	n	x	ε′	ε″	n	x	ε′	ε″	n	x
	$t = -8°$ C				$t = -10°$ C				$t = -12°$ C			
1,00	9,49	18,09	3,87	2,34	8,94	16,94	3,75	2,26	8,45	15,82	3,63	2,18
1,24	11,48	21,88	4,25	2,57	10,68	20,57	4,11	2,50	9,96	19,27	3,98	2,42
2,0	19,50	31,76	5,33	2,98	17,80	30,29	5,14	2,94	16,23	28,74	4,96	2,90
3,0	31,68	39,58	6,42	3,08	29,01	38,60	6,22	3,10	26,44	37,39	6,01	3,11
3,2	34,09	40,52	6,60	3,07	31,29	39,69	6,40	3,10	28,56	38,62	6,19	3,12
5,6	57,45	42,07	8,02	2,62	54,49	43,08	7,87	2,74	51,30	43,82	7,71	2,84
10,0	76,85	32,36	8,95	1,81	75,42	34,43	8,90	1,94	73,65	36,52	8,83	2,07
11,0	79,02	30,31	9,05	1,68	77,87	32,39	9,01	1,80	76,40	34,54	8,95	1,93
17,0	81,81	21,42	9,33	1,15	85,64	23,21	9,34	1,24	85,30	25,15	9,33	1,35
	$t = -14°$ C				$t = -16°$ C				$t = -18°$ C			
0,08	5,52	1,21	2,36	0,26	5,51	1,12	2,36	0,24	5,51	1,03	2,36	0,22
0,10	5,53	1,52	2,37	0,32	5,52	1,40	2,37	0,30	5,52	1,29	2,36	0,27
0,20	5,60	3,03	2,45	0,62	5,59	2,80	2,43	0,57	5,57	2,58	2,42	0,53
0,30	5,73	4,54	2,55	0,89	5,70	4,19	2,58	0,83	5,67	3,86	2,50	0,77
0,40	5,91	6,03	2,68	1,13	5,85	5,58	2,64	1,06	5,79	5,15	2,60	0,99
0,50	6,14	7,52	2,82	1,34	6,04	6,96	2,76	1,26	5,96	6,42	2,71	1,18
0,60	6,42	9,00	2,96	1,52	6,28	8,33	2,89	1,44	6,16	7,69	2,83	1,36
0,62	6,49	9,29	2,98	1,56	6,33	8,60	2,92	1,47	6,20	7,94	2,85	1,39
0,70	6,75	10,46	3,09	1,69	6,56	9,68	3,02	1,60	6,39	8,94	2,95	1,52
0,80	7,13	11,90	3,24	1,84	6,88	11,03	3,15	1,75	6,66	10,19	3,07	1,66
0,86	7,38	12,76	3,33	1,92	7,09	11,83	3,23	1,83	6,84	10,93	3,14	1,74
0,90	7,55	13,33	3,38	1,97	7,24	12,36	3,28	1,88	6,97	11,43	3,19	1,79
1,00	8,02	14,73	3,52	2,09	7,64	13,67	3,41	2,00	7,31	12,64	3,31	1,91
1,24	9,32	17,99	3,85	2,34	8,75	16,73	3,72	2,25	8,25	15,52	3,59	2,16
2,0	14,78	27,14	4,78	2,84	13,48	25,50	4,61	2,77	12,32	23,86	4,43	2,70
3,0	23,97	35,99	5,80	3,10	21,66	34,42	5,58	3,08	19,52	32,71	5,37	3,05
3,2	25,93	37,32	5,97	3,12	23,44	35,82	5,75	3,11	21,12	34,16	5,54	3,09
5,0	47,90	44,25	7,52	2,94	44,36	44,34	7,32	3,03	40,75	44,06	7,10	3,10
10,0	71,53	38,59	8,74	2,21	69,02	40,58	8,63	2,35	66,13	42,43	8,51	2,49
11,0	74,58	36,70	8,88	2,07	72,39	38,85	8,79	2,21	69,79	40,91	8,68	2,36
17,0	84,72	27,23	9,32	1,46	83,88	29,45	9,29	1,58	82,73	31,80	9,26	1,72
	$t = -20°$ C				$t = -22°$ C				$t = -24°$ C			
0,08	5,51	0,95	2,35	0,20	5,51	0,87	2,35	0,19	5,51	0,80	2,36	0,17
0,10	5,52	1,19	2,36	0,25	5,51	1,09	2,36	0,23	5,51	1,00	2,37	0,22
0,20	5,56	2,37	2,41	0,49	5,55	2,18	2,40	0,45	5,54	1,99	2,39	0,42
0,30	5,64	3,56	2,48	0,72	5,62	3,26	2,46	0,66	5,60	2,99	2,44	0,61
0,40	5,72	4,73	2,57	0,92	5,71	4,35	2,54	0,86	5,67	3,98	2,51	0,79
0,50	5,88	5,91	2,67	1,12	5,82	5,43	2,62	1,03	5,77	4,97	2,59	0,96
0,60	6,05	7,08	2,77	1,28	5,96	6,50	2,72	1,20	5,88	5,96	2,67	1,12
0,62	6,09	7,31	2,79	1,31	5,99	6,72	2,74	1,23	5,91	6,16	2,69	1,15
0,70	6,25	8,24	2,88	1,43	6,13	7,57	2,83	1,34	6,02	6,94	2,76	1,26
0,80	6,48	9,39	2,99	1,57	6,32	8,64	2,92	1,48	6,18	7,92	2,85	1,39
0,86	6,63	10,08	3,06	1,65	6,44	9,27	2,98	1,56	6,28	8,51	2,90	1,46
0,90	6,73	10,54	3,10	1,70	6,53	9,69	3,02	1,61	6,36	8,89	2,94	1,51
1,00	7,02	11,67	3,21	1,82	6,77	10,74	3,12	1,72	6,56	9,86	3,03	1,63
1,24	7,81	14,34	3,47	2,06	7,44	13,22	3,36	1,97	7,12	12,15	3,26	1,87
2,0	11,29	22,23	4,26	2,61	10,38	20,63	4,09	2,52	9,56	19,07	3,93	2,42
3,0	17,56	30,90	5,15	3,00	15,80	29,02	4,94	2,94	14,23	27,12	4,74	2,86
3,2	18,98	32,37	5,31	3,04	17,04	30,49	5,10	2,99	15,30	28,55	4,88	2,92
5,6	37,13	43,41	6,87	3,16	33,58	42,39	6,62	3,20	30,16	41,04	6,37	3,22
10,0	62,84	44,06	8,35	2,64	59,20	45,40	8,18	2,78	55,25	46,37	7,98	2,91
11,0	66,79	42,82	8,55	2,50	63,39	44,49	8,39	2,65	59,62	45,86	8,21	2,79
17,0	81,23	34,23	9,20	1,86	79,33	36,72	9,13	2,01	76,99	39,20	9,04	2,17

Commas indicate decimal points.

λ cm	ε′	ε″	n	x	ε′	ε″	n	x	ε′	ε″	n	x
	$t = -26°$ C				$t = -28°$ C				$t = -30°$ C			
0,08	5,51	0,73	2,35	0,16	5,50	0,67	2,35	0,14	5,50	0,61	2,35	0,13
0,10	5,51	0,91	2,36	0,19	5,51	0,83	2,35	0,18	5,51	0,76	2,35	0,16
0,20	5,54	1,82	2,38	0,38	5,53	1,66	2,38	0,35	5,52	1,51	2,37	0,32
0,30	5,58	2,73	2,43	0,56	5,57	2,49	2,41	0,52	5,55	2,27	2,40	0,47
0,40	5,64	3,64	2,49	0,73	5,62	3,32	2,46	0,67	5,60	3,03	2,45	0,62
0,50	5,72	4,55	2,55	0,89	5,68	4,15	2,52	0,82	5,65	3,78	2,49	0,76
0,60	5,82	5,45	2,62	1,04	5,76	4,98	2,59	0,96	5,72	4,53	2,55	0,89
0,62	5,84	5,63	2,64	1,07	5,78	5,14	2,60	0,99	5,73	4,68	2,56	0,91
	$t = -26°$ C				$t = -28°$ C				$t = -30°$ C			
0,70	5,93	6,35	2,70	1,17	5,86	5,80	2,66	1,09	5,79	5,28	2,61	1,01
0,80	6,06	7,25	2,79	1,30	5,96	6,62	2,73	1,21	5,88	6,03	2,67	1,13
0,86	6,15	7,79	2,83	1,37	6,04	7,11	2,77	1,28	5,94	6,48	2,71	1,19
0,90	6,21	8,14	2,86	1,42	6,09	7,44	2,80	1,33	5,98	6,78	2,74	1,24
1,00	6,38	9,03	2,95	1,53	6,22	8,25	2,88	1,43	6,10	7,52	2,81	1,34
1,24	6,84	11,14	3,16	1,77	6,61	10,19	3,00	1,66	6,41	9,30	2,98	1,56
2,0	8,91	17,57	3,78	2,32	8,33	16,14	3,64	2,22	7,84	14,77	3,50	2,11
3,0	12,84	25,21	4,54	2,78	11,64	23,33	4,34	2,69	10,60	21,51	4,16	2,59
3,2	13,77	26,60	4,68	2,84	12,43	24,67	4,47	2,75	11,27	22,77	4,28	2,66
5,6	26,93	39,40	6,11	3,22	23,93	37,51	5,85	3,21	21,21	34,45	5,59	3,17
10,0	51,06	46,92	7,76	3,02	46,73	46,99	7,52	3,13	42,35	46,56	7,26	3,21
11,0	55,53	46,84	8,01	2,93	51,21	47,36	7,78	3,04	46,75	47,39	7,53	3,15
17,0	74,18	41,60	8,92	2,33	70,89	43,84	8,78	2,50	67,14	45,82	8,61	2,66
	$t = -32°$ C				$t = -34°$ C				$t = -36°$ C			
0,08	5,50	0,55	2,35	0,12	5,50	0,50	2,35	0,11	5,50	0,45	2,35	0,10
0,10	5,50	0,69	2,35	0,15	5,50	0,62	2,35	0,13	5,50	0,57	2,35	0,12
0,20	5,52	1,38	2,37	0,29	5,52	1,25	2,36	0,26	5,51	1,13	2,36	0,24
0,30	5,54	2,06	2,39	0,43	5,54	1,87	2,39	0,39	5,53	1,70	2,38	0,36
0,40	5,58	2,75	2,43	0,57	5,56	2,50	2,41	0,52	5,55	2,26	2,40	0,47
0,50	5,62	3,44	2,47	0,70	5,60	3,12	2,45	0,64	5,58	2,83	2,43	0,58
0,60	5,68	4,12	2,53	0,82	5,64	3,74	2,49	0,75	5,62	3,39	2,47	0,69
0,62	5,69	4,26	2,53	0,84	5,65	3,87	2,50	0,77	5,62	3,50	2,48	0,71
0,70	5,74	4,81	2,57	0,93	5,70	4,36	2,54	0,86	5,66	3,95	2,50	0,79
0,80	5,81	5,49	2,63	1,04	5,76	4,98	2,59	0,96	5,71	4,52	2,55	0,89
0,86	5,86	5,89	2,66	1,11	5,79	5,36	2,62	1,02	5,74	4,85	2,57	0,94
0,90	5,90	6,17	2,69	1,15	5,82	5,60	2,64	1,06	5,76	5,08	2,59	0,18
1,00	5,99	6,85	2,75	1,25	5,90	6,22	2,69	1,16	5,82	5,64	2,64	1,07
1,24	6,25	8,47	2,90	1,46	6,11	7,70	2,82	1,36	6,00	6,98	2,76	1,27
2,0	7,42	13,49	3,38	2,00	7,07	12,29	3,26	1,85	6,78	11,17	3,15	1,77
	$t = -32°$ C				$t = -34°$ C				$t = -36°$ C			
3,0	9,72	19,75	3,98	2,48	8,97	18,07	3,81	2,37	8,34	16,49	3,66	2,25
3,2	10,27	20,94	4,10	2,55	9,43	19,18	3,92	2,44	8,72	17,52	3,76	2,33
5,6	18,77	33,25	5,34	3,12	16,61	30,99	5,09	3,05	14,74	28,71	4,85	2,96
10,0	38,02	45,65	6,98	3,27	33,86	44,29	6,69	3,31	29,95	42,54	6,40	3,32
11,0	42,45	46,91	7,26	3,23	37,85	45,92	6,98	3,29	33,61	44,47	6,68	3,33
17,0	62,95	47,43	8,42	2,82	58,40	48,59	8,20	2,96	53,59	49,22	7,95	3,10

Commas indicate decimal points.

λ cm	ε'	ε''	n	x	ε'	ε''	n	x	ε'	ε''	n	x
	$t = -38°$ C				$t = -40°$ C							
0,08	5,50	0,41	2,35	0,09	5,50	0,37	2,35	0,08				
0,10	5,50	0,51	2,35	0,11	5,50	0,46	2,35	0,10				
0,20	5,51	1,02	2,36	0,22	5,51	0,92	2,36	0,20				
0,30	5,52	1,54	2,37	0,32	5,52	1,39	2,37	0,29				
0,40	5,54	2,05	2,39	0,43	5,53	1,85	2,38	0,39				
0,50	5,57	2,55	2,42	0,53	5,55	2,31	2,41	0,48				
0,60	5,59	3,07	2,45	0,62	5,58	2,77	2,43	0,57				
0,62	5,60	3,17	2,45	0,65	5,58	2,86	2,43	0,59				
0,70	5,63	3,58	2,48	0,72	5,60	3,23	2,46	0,66				
0,80	5,67	4,09	2,52	0,81	5,64	3,69	2,49	0,74				
0,86	5,69	4,39	2,54	0,87	5,66	3,97	2,51	0,79				
0,90	5,71	4,60	2,55	0,90	5,67	4,15	2,52	0,82				
1,00	5,76	5,11	2,59	0,98	5,71	4,61	2,56	0,90				
1,24	5,90	6,32	2,70	1,17	5,83	5,72	2,64	1,08				
2,0	6,54	10,13	3,05	1,66	6,34	9,17	2,96	1,55				
3,0	7,81	15,00	3,52	2,13	7,38	13,61	3,38	2,01				
3,2	8,13	15,95	3,61	2,21	7,64	14,48	3,46	2,09				
5,6	13,13	26,47	4,62	2,86	11,77	24,28	4,40	2,76				
10,0	26,34	40,46	6,11	3,31	23,08	38,14	5,82	3,28				
11,0	29,63	42,63	6,39	3,34	26,02	40,47	6,09	3,32				
17,0	48,63	49,27	7,67	3,21	43,67	48,72	7,39	3,30				

Commas indicate decimal points.

REFERENCES

1. Logan, N. A., "Review of Certain Early Works on the Theory of Scattering of Plane Waves on a Sphere," *Tr. Instituta inzhenerov po elektrotekhnike i radioelektronike*, USA (Translated from English), No. 8, p. 895, 1965.
2. Shifrin, K. S., "Scattering of Light on Two-Layer Particles," *Izv. AN SSSR*, Geophysics Series, No. 2, p. 15, 1952.
3. Aden, A. L. and M. Kerker, "Scattering of Electromagnetic Waves from Two Concentric Spheres," *J. Appl. Phys.*, Vol. 22, No. 10, p. 1242, 1951.
4. Kul'ko, V. F. and V. N. Mikhaylovskiy, *Elektromagnitnoye pole v sloistykh sredakh* [Electromagnetic Field in Stratified Media], Kiev, "Naukova dumka" Press, 1967.
5. Miculski, J. J. and E. L. Murphy, "The Computation of Electromagnetic Scattering from Concentric Spherical Structures," *IEEE Trans. Anten. Propag.*, Vol. AP-11, No. 2, p. 169, 1963.
6. D'yakonov, B. P., "Diffraction of Electromagnetic Waves on Sphere in Half-Space," *Izv. AN SSSR*, Geophysics Series, No. 11, p. 1579, 1959.
7. Negi, J. G., Discussion on "Diffraction of Electromagnetic Waves by an Inhomogeneous Sphere," *Geophysics*, Vol. 28, No. 4, p. 665, 1963.
8. Ivanov, Ye. A., "Sphere of Arbitrary Conductivity with Nonconcentric Spherical Inclusion in the Field of Vertical Electric Dipole," *Izv. VUZov SSSR, Radiofizika*, Vol. 6, No. 5, p. 992, 1963.
9. Ivanov, Ye. A., *Difraktsiya elektromagnitnykh voln na dvukh telakh.* [Diffraction of Electromagnetic Waves on Two Bodies], Minsk, "Nauka i tekhnika" Press, 1968.
10. Rozenberg, V. I., "Diffraction and Scattering of Electromagnetic Waves on Inhomogeneous Sphere," *Izv. VUZov SSSR*, Radiophysics, Vol. 13, No. 3, p. 431, 1970.
11. Krasyuk, N. P. and V. I. Rozenberg, *Korabel'naya Radiolokatsiya Meteorologiya* [Marine Radar and Meteorology], Leningrad, "Sudostroyeniye" Press, 1970
12. Rozenberg, V. I., "Diffraction of Electromagnetic Waves on Spheres, Arbitrarily Placed One Inside Another," *Izv. VUZov, SSSR*, Radiophysics, Vol. 13, No. 10, p. 1541, 1970.
13. Trinks, W., "Multiple Scattering on Small Spheres," *Annalen der Physik*, Vol. 22, No. 6, p. 561, 1935.
14. Mevel, J, "Contribution to the Study of Electromagnetic Wave Diffraction by the Spheres," *Ann. de Phys.*, Vol. 5, Nos. 3-4, p. 265, 1960.
15. Germogenova, O. A., "Scattering of Electromagnetic Wave on Two Spheres," *Izv. AN SSSR*, Geophysics Series, No. 4, p. 648, 1963.
16. Sato Yasuo, "Addition Theorems," *Bull. Earthquake Res. Institute*, Tokyo, No. 28, p. 1, 1950.
17. Friedman, B, and J. Russek, "Addition Theorems for Spherical Waves," *Quart. Appl. Math.*, Vol. 12, No. 1, p. 13, 1954.
18. Ben-Menahem, A., "An Operational Representation of the Addition Theorems for Spherical Waves," *J. Math. and Phys.*, Vol. 41, No. 3, p. 201, 1962.

19. Stein, S., "Addition Theorems for Spherical Wave Functions," *Quart. Appl. Math.*, Vol. 19, No. 1, p. 15, 1961.
20. Crusan, O. R., "Translational Addition Theorems for Spherical Vector Wave Functions," *Quart. App. Math.*, Vol. 20, No. 1, p. 33, 1962.
21. Ivanov, Ye. A., "Addition Theorem for Elementary Functions of Spheroidal Waves," *DAN BSSR*, Vol. 4, No. 1, p. 3, 1960. /334
22. Ivanov, Ye. A., "Scattering of Plain Electromagnetic Waves on Several Spheres," *Differentsialynye Uravneniya*, Vol. 2, No. 6, p. 828, 1966.
23. Edmonds, A. R., *Angular Momentum Quantum Mechanics*, Princeton, N. Y., Princeton Univ. Press, Chapter 4, 1957.
24. Li Tszun-Dao, *Matematicheskiye Metody v Fizike* [Mathematical Methods in Physics], Moscow, "Mir" Press, 1965.
25. Gel'fand, I. M., R. Ya. Minlos and Z. Ya. Shapiro, *Predstavleniye Gruppy Vrashcheniy i Gruppy Lorentsa* [Representation of Revolutions Group and Lorentz Group], Moscow, "Fizmatgiz," 1958.
26. Vilenkin, N. Ya., *Spetsial'nye Funktsii i Teoriya Predstavleniya Grupp.* [Special Functions and Group Representation Theory], Moscow, "Nauka" Press, 1965.
27. McIntosh, H., A. Kleppner and D. F. Minner, "Tables of the Herglots Polynomials of Orders 3/2, 8/2 Transformation Coefficients for Spherical Harmonics," *B. R. L. Mem. Rept.*, No. 1097, Ballistic Res. Lab. Aberdeen Prov. Ground, Md., 1957.
28. Gradshteyn, I. S. and I. M. Ryzhik, *Tablitsy Integralov, Summ, Ryadov i Proizvedeniy* [Tables of Integrals, Sums, Series and Products], Moscow, GIFML Press, 1963.
29. Morse, F. M. and G. Feshbah, *Metody Teoreticheskoy Fiziki* [Methods of Theoretical Physics], Vol. 2, Moscow, Foreign Literature Press, 1960.
30. Jones, A. L., "An Extension of an Inequality Involving Modified Bessel Functions," *J. Math. and Phys.*, Vol. 47, No. 2, p. 220, 1968.
31. Cochran, J. A., "The Monotonicity of Modified Bessel Functions with Respect to Their Order," *J. Math. and Phys.*, Vol. 46, No. 2, p. 220, 1967.
32. Flammer, Carson, *Spheroidal Wave Functions*, Stanford University Press, 1957.
33. Rozenberg, V. I., "Addition Theorems for Modified Bessel and Hankel Functions," *Izv. VUZov SSSR*, Mathematics, No. 11, p. 72, 1969.
34. Beytmen, G. and A. Erdeyn, *Vysshiye Transtsendentnyye Funktsii* [Higher Transcendental Functions], Vol. 2, Moscow, "Nauka" Press, 1966.
35. Natanson, I. P., *Teoriya Funktsiy Veshchestvennoy Peremennoy* [Theory of Real Variable Functions], Moscow, GITTL, 1957.
36. Nikol'skiy, S. M., "Linear Equations in Linear Standard Spaces," *Izv. AN SSSR*, Mathematics Series, Vol. 7, No. 3, p. 147, 1943.
37. Vulikh, B. Ye., *Vvedeniye v Funktsional'nyy Analiz* [Introduction to Functional Analysis], Moscow, "Nauka" Press, 1967.
38. Faddeyev, D. K. and V. N. Faddeyeva, *Vychislitel'nyye Metody Lineynoy Algebry* [Computation Methods of Linear Algebra], Moscow-Leningrad, "Fizmatgiz," 1963.
39. Kupradze, V. D., *Granichnyye Zadachi Teorii Kolebaniy i Integral'nyye Uravneniya* [Boundary Problems of Vibrations Theory and Integral Equations], Moscow-Leningrad, Gostekhizdat, 1962.

40. Kantorovich, L. V., "Functional Analysis and Applied Mathematics," *Uspekhi Matematicheskikh Nauk*, Vol. 3, No. 6 (28), p. 89, 1948.
41. Kantorovich, L. V. and G. P. Akilov, *Funktsional'nyy Analiz v Normirovannykh Prostranstvakh* [Functional Analysis Spaces with Norms], Moscow, Fizmatgiz, 1958.
42. Vatson, G. N., *Teoriya Besselevykh Funktsii* [Theory of Bessel Functions], Foreign Literature Press, 1949.
43. Khynl, Kh., A. Mauye and K. Vestpfal', *Teoriya Diffraktsii* [Diffraction Theory], Moscow, "Mir" Press, 1964.
44. Khyulet, G., *Rasseyaniye Sveta Malymi Chastitsami* [Scattering of Light by Small Particles], Moscow, Foreign Literature Press, 1961.
45. *Rasprostraneniye Ul'trakorotkikh Voln.* [Propagation of Ultrashort Waves], translated from the English, edited by B. A. Shillerova, Moscow, "Sovetskoye Radio" Press, 1954.
46. Blacksmith, P., E. Hiatt and R. B. Mack, "Introduction to Radar Cross-Section Measurements," *Proc. IEEE*, Vol. 53, No. 8, p. 901, 1965.
47. Stretton, D., *Teoriya Elektromagnetizma* [Theory of Electromagnetism], Moscow, Gostekhizdat, 1948.
48. Born, M. and E. Bol'f, *Osnovy Optiki* [Fundamentals of Optics], Moscow, "Nauka" Press, 1970.
49. Krasnosel'skiy, M. A. et al., *Priblizhennoye Resheniye Operatornykh Uravneniy* [Approximate Solution of Operator Equations], Moscow, "Nauka" Press, 1969.
50. Forsight, D. and K. Moler, *Chislennoye Resheniye Sistem Lineynykh Algebraicheskikh Uravneniy* [Numerical Solution of Linear Algebraic Equation Systems], Moscow, "Mir" Press, 1969.
51. Shebeko, G. A., "Diffraction of Electromagnetic Field of Elementary Electric Dipole on Two Spheres," *Izv. An BSSR*, Physical-Technical Series, No. 2, p. 72, 1967.
52. Ivanov, Ye. A., "Diffraction of Field of Dipole Emitter on Two Spheres," *Zh. Vychislitel'noy Matem. i Matem. Fiziki*, Vol. 7, No. 6, p. 1285, 1967.
53. Liang, C. and V. T. Lo., "Scattering by Two Spheres," *Radio Sci.*, Vol. 2, No. 12, p. 1481, 1967.
54. Levine, S. and G. O. Olaofe, "Scattering of Electromagnetic Waves by Two Equal Spherical Particles," *J. Colloid. and Interface Sci.*, Vol. 27, No. 3, p. 442, 1968. /335
55. Shebeko, G. A. "Diffraction of Electromagnetic Field on Several Spheres," in the book: *Trudy II Respublikanskoy Konferentsii Matematikov Belorussii* [Proceedings of the Second Republic Conference of Belorussian Mathematicians], Vol. 1, Minsk, Belorussian State Univ., p. 293, 1969.
56. Rozenberg, V. I., "Diffraction of Electromagnetic Waves on Arbitrary Set of Spheres," *Radiotekhnika i Elektronika (AN SSSR)*, Vol. 16, No. 2, p. 245, 1971.
57. Shebeko, G. A., "Solution of Some Boundary Problems of Theory of Wave Diffraction on the Spheres in Space and Half-Space," Candidate dissertation, Minsk, Belorussian State Univ., 1970.

58. Rozenberg, V. I. "Diffraction of Waves on Arbitrary Set of Nonconcentrically Stratified Spheres," *Doklady na v Vsesoyuznom Simpoziume po Difraktsii i Rasprostraneniyu Radiovoli* [Report to Fifth All-Union Symposium on Radio Wave Diffraction and Propagation],, Leningrad, 1970; *Zh. Vychislitel'noy Matem. i Matem. Fiziki*, Vol. 12, No. 1, p. 266, 1972.
59. Debay, P., *Polyarnyye Molekuly*. [Polar Molecules], translated from the English by K. Shchedro, GONTI, 1931.
60. Debay, P. and G. Zakk, *Teoriya Elektricheskikh Svoystv Molekul* [Theory of Electrical Properties of Molecules], GONTI, 1963.
61. Cole, R. H., "Dielectric Absorption in Polar Media and the Local Field," *J. Chem. Phys.*, Vol. 6, No. 7, p. 385, 1938.
62. Onsager, L., "Electric Moments of Molecules in Liquids," *J. Am. Chem. Soc.*, Vol. 58, No. 7, p. 1486, 1936.
63. Van Vleck, "The Role of Dipole Coupling in Dielectric Media," *J. Chem. Rhys.*, Vol. 5, No. 4, p. 566, 1937.
64. Radio Wave Propagation," *Consolid. Summary Technical Report Comit. Propag. Nation. Defense Research Comit.*, Editor S. S. Atwood, Acad. Press, Inc. N. Y., 1949.
65. Hippel, R., "Progress Report on Ultra High Frequency Dielectrics," *OEM sr-191, NDRC Division 14, Report 121, Laboratory Insulation Res.*, MIT, Jan. 1943.
66. Dorsey, N. E., *Properties of Ordinary Water Substance*, Reinhold Pub. Co., N. Y., 1940.
67. Saxton, J. A. and J. A. Lane, "The Anomalous Dispersion of Water at Very High Radio Frequencies, Part 1: Experimental Determination of the Dielectric Properties of Water in the Temperature Range 0°C to 40°C for Wavelength of 1.24 and 1.58 cm. Meteorological Factors in Radiowave Propagation," London, *Phys. Soc. and Roy. Meteorl. Soc.*, p. 278, 1946.
68. Saxton, J. A., "The Anomalous Dispersion of Water at Very High Radio Frequencies. Part 2: Relation of Experimental Observations to Theory. Meteorological Factors in Radiowave Propagation," *Phys. Soc. and Roy. Meteorl. Soc.*, London, p. 292, 1946.
69. Saxton, J. A., "The Anomalous Dispersion of Water at Very High Radio Frequencies. Part 3: The Dipole Relaxation Time and Its Relation to the Viscosity. Meteorological Factors in Radiowave Propagation," *Phys. Soc. and Roy. Meteorol. Soc.*, London, p. 306, 1946.
70. Chu Ch.-M, "Scattering and Absorption of Water Droplets at Millimeter Wavelength," a dissertation for the degree of Doctor of Philosophy, Univ. Michigan, 1952.
71. Lindeman, K. L., "Anomalous Electrical Dispersion in Water in the 0.014--10.4 cm Wavelength Region," *Acta Acad. Aboensis, Math. et Phys.*, Vol. 15, No. 9, p. 1, 1947.
72. Collie, C. H., J. B. Hasted and D. M. Ritson, "The Dielectric Properties of Water and Heavy Water," *Proc. Phys. Soc.*, Vol. 60, Part 2, No. 338, p. 145, 1948.

73. Buchanan, M. A., "Balance Methods for the Measurement of Permeability in the Microwave Region," *Proc. Inst. Electr. Eng.*, Vol. 99, Part III, No. 57, p. 61, 1952.
74. Magat, M. M., "On the Dielectric Dispersion of Liquid Water," *J. Chimie Physique, Physico-Chimie Biologique*, Vol. 45, No. 4, 5, p. 93, 1948.
75. Rubens, H., "Of Normal and Anomalous Scatter in Long Wave Range and of Molecular Dipoles Theory by Herrn Debye," *Deutschen Physik Gesellshaft J.*, Vol. 17, No. 16, p. 315, 1915. /336
76. Cartwright, C. H. and J. Errera, "Extreme Infrared Dispersion of Polar and Non-Polar Liquids," *Proc. Roy. Soc.*, London, Ser. A, Vol. 154, No. 88, p. 138, 1936.
77. Cartwright, C. H., "Extreme Infrared Investigation of Hindered Rotation in Water," *Nature*, Vol. 135, No. 3421, p. 872, 1935.
78. Cartwright, C. H., "Extreme Infrared Absorption of D_2O, ice, and D_2O in Dioxane," *Nature*, Vol. 136, No. 3431, p. 181, 1935.
79. Saxton, J. A., "Electrical Properties of Water. Wireless Engineer," *J. Radio Res. Progress*, Vol. 26, No. 312, p. 288, 1949.
80. Kiely, D. G., "Measurement of the Reflection Coefficient of Water at a Wavelength of 8.7 mm," *Proc. Phys. Soc.*, Sect. B, Vol. 63, Part 1, No. 361, p. 46, 1950.
81. Shifrin, K. S., *Rasseyniye Sveta v Mutnoy Srede* [Scattering of Light in Turbid Medium], Moscow-Leningrad, GITTL Press, 1951.
82. Lane, J. A. and J. A. Saxton, "Dielectric Dispersion in Pure Polar Liquids at Very High Radio Frequencies," *I. Proc. Roy. Soc.*, Ser. A, Vol. 213, No. 1114, p. 400, 1952.
83. Goe, J. R. and T. B. Godfrey, "Viscosity of Water," *J. Appl. Phys.*, Vol. 15, No. 8, p. 625, 1944.
84. Saxton, J. A., "Dielectric Dispersion in Pure Polar Liquids at Very High Radio Frequencies," *II. Proc. Roy. Soc.*, Ser. A, Vol. 213, No. 1115, p. 473, 1952.
85. Saxton, J. A., "Electrical Properties of Sea Water. Wireless Engineer," Vol. 29, No. 349, p. 269, 1952.
86. Frelikh, G., *Teoriya Dielektrikov. Dielektricheskaya Pronitsayemost' i Dielektricheskiye Poteri.* [Theory of Dielectrics. Permittivity and Dielectric Losses], Moscow, Foreign Literature Press, 1960.
87. Maryott, A. and F. Buckley, "Tables of Dielectric Dispersion Data for Pure Liquids and Dilute Solutions," Washington, U. S., 1958.
88. Hertel, P. J., A. W. Straiton and C. W. Tolbert, "Dielectric Constant. Measurements at 8.6 mm Wavelength," *J. Appl. Phys.*, Vol. 24, No. 7, p. 956, 1953.
89. Little, V. J., "A Standing Wave Method for Measuring Electromagnetic Absorption in Polar Liquids at Frequencies of the Order $3 \cdot 10^9$ c/s," *Proc. Phys. Soc.*, Ser. B, Vol. 66, London, Part 3, No. 399, p. 175, 1953.
90. Poley, J. P., "Microwave Dispersion of Some Polar Liquids," *Appl. Sci. Res.*, Ser. B, Vol. 4, No. 5, p. 337, 1955.
91. Strivastava, G. P. and Y. P. Varshni, "Variation of Dielectric Constant with Temperature," *Physica*, Vol. 22, No. 7, p. 584, 1956.

92. Varshni, V. P. and G. P. Strivastava, "Temperature Dependence of Dielectric Constant," *J. Phys. Chem.*, Vol. 210, Leipzig, No. 3, 4, p. 144, 1959.
93. Drake, F. H., G. W. Pierce and M. T. Dow, "Measurement of the Dielectric Constant and Index of Refraction of Water and Aqueous Solutions of KCl at High Frequencies," *Phys. Review*, Ser. 2, No. 35, No. 6, p. 613, 1930.
94. Zinchenko, N. S., "Measurement of Coefficients of Reflection and Permittivity of Water in Millimeter Wavelength Range," *Uchenyye Zapiski*, Vol. 102, 1959; *Tr. Radiofizicheskogo F-ta*, Vol. 3, p. 81, Kharkhov State Univ., 1959.
95. Usikov, O. Ya., V. L. German and I. Kh. Vakser, "Consequences of Absorption and Scattering of Millimeter Waves in Precipitation," *Ukrainskiy Fizicheskiy Zhurnal*, Vol. 6, No. 5, p. 618, 1961.
96. Rampolla, R. W., R. C. Miller and C. P. Smyth, "Microwave Absorption and Molecular Structure in Liquids. XXV Measurements of Dielectric Constant and Loss at 3.1 mm Wavelength by an Interferometric Method," *J. Chem. Phys.*, Vol. 30, No. 2, p. 566, 1959.
97. Kislovskiy, L. D., "Optical Characteristics of Water and Ice in the Infrared and Radiowave Regions of the Spectrum," *Optika i Spektroskopiya*, Vol. 7, No. 3, p. 311, 1959.
98. Stanevich, A. Ye. and N. G. Yaroslavskiy, "Absorption of Water in Long-wave Region of Spectrum (42-2,000 μ)," *Optika i Spektroskopiya*, Vol. 10, No. 4, p. 53, 1961. /337
99. Lane, J. A., "Far-Infrared Spectrum of Liquid Water," *J. Opt. Soc. Am.*, Vol. 56, No. 10, p. 1398, 1966.
100. Draegert, D. A. et al., "Far-Infrared Spectrum of Liquid Water," *J. Opt. Soc. Am.*, Vol. 56, No. 1, p. 64, 1966.
101. Goronina, K. A., R. K. Belov and E. P. Sorokina, "Determination of Permittivity by Change of Polarization of Wave on Reflection," *Izv. VUZov SSSR*, Radiophysics Series, Vol. 9, No. 5, p. 975, 1966.
102. Rozenberg, V. I., "Permittivity of Water at Wavelength 1.2-1.6 mm," *Izv. VUZov SSSR*, Radiophysics Series, Vol. 11, No. 2, p. 322, 1968.
103. Khvostova, A. I., "Change of Permittivity of Water at λ = 0.85 mm," ↑ζ× *Izv. VUZov SSSR*, Radiophysics Series, Vol. 10, No. 2, p. 292, 1967.
104. Hoffman, N. J., "A Decimeter Wave Measurement Method, Independent of Detector Characteristics, For Determination of the Complex Dielectric Constants of Water and Aqueous Solutions Up to a Loss Factor of tan δ = 0.87," *J. Phys. Chem. (Leipzig)*, Vol. 225, No. 5-6, p. 372, 1964.
105. Cole, K and R. Cole, "Dispersion and Absorption in Dielectrics," *J. Chem. Phys.*, Vol. 9, No. 4, p. 341, 1941.
106. Fuoss, R. and J. G. Kirkwood, "Electrical Properties of Solids," *J. Am. Chem. Soc.*, Vol. 63, No. 1, p. 385, 1941.
107. Grant, E., T. Buchanan and H. F. Cook, "Dielectric Behavior of Water at Microwave Frequencies," *J. Chem. Phys.*, Vol. 26, No. 1, p. 156, 1957.
108. Hasted, J. B. and G. W. Roderick, "Dielectric Properties of Aqueous and Alcoholic Electrolytic Solutions," *J. Chem. Phys.*, Vol. 29, No. 1, p. 17, 1958.

109. Nora, E. H., "Interpretation of the Dielectric Properties of Water," *Trans. Faraday Soc.*, Vol. 59, No. 482, Part 2, p. 344, 1963.
110. Hasted, J. B., "Dielectric Properties of Water," *Progress in Dielectrics*, Vol. 3, p. 100, 1961.
111. Hasted, J. B. and S. H. M. Saben, "The Dielectric Properties of Water in Solutions," *Trans. Faraday Soc.*, Vol. 49, Part 9, p. 1003, 1953.
112. Chamberlain, J. E. et al., "Submillimeter Absorption and Dispersion of Liquid Water," *Nature*, Vol. 210, No. 5038, p. 790, 1966.
113. Ryde, J. W. and D. Ryde, "Attenuation of Centimeter and Millimeter Waves by Rain, Hail, Fogs and Clouds," *Rept. 8670, General Electric Co.*, Wembley, England, 1945.
114. Ozawa, Y. and D. Kuroiwa, "Dielectric Properties of Ice, Snow and Supercooled Water," *Monograph. Ser. Res. Inst. Appl. Electricity*, Hokkaido Univ., No. 6, p. 31, 1958.
115. Basharinov, A. Ye. and B. G. Kutuza, "Investigations of Radioemission and Absorption of Cloud Atmosphere in Millimeter and Centimeter Wavelength Ranges," *Tr. Tret'yego Vsesoyuznogo Soveshchaniya po Radiolokatsionnoy Meteorologii*, Moscow, Gidrometeoizdat, p. 96, 1968.
116. Collie, C. H., "Preliminary Report on the Dielectric Properties of Water in the K-band," *CL Misc. 25, CVD Report*, May 1944.
117. Stepanenko, V. D., *Radiolokatsiya v Meteorologii* [Radar in Meteorology], Leningrad, Gidrometeoizdat, 1966.
118. Zolotarev, V. M. et al., "Dispersion and Absorption of Liquid Water in Infrared and Radio Ranges of Spectrum," *Optika i Spektroskopiya*, Vol. 27, No. 5, p. 790, 1969.
119. Pontier, L, and C. Dechambenoy, "Determination of Optical Constants of Liquid Water between 1 and 40. Application to the Calculation of its Reflectivity and Emissivity," *Ann. de Geophys.*, Vol. 22, No. 4, p. 633, 1966.
120. Kondrat'ev, K. Ya. et al., "Infrared Absorption Spectrum of Liquid Water," from the book: *Problemy Fiziki Atmosfery* [Problems of Atmospheric Physics], Vol. 2, Leningrad State Univ. Press, p. 87, 1963.
121. Sonchik, V. K., "Experimental Determination of Components of Complex Refraction Index of Water in Visible and Infrared Regions of Spectrum," *Izv. AN SSSR*, Physics of Atmosphere and Ocean, Vol. 5, No. 7, p. 745, 1969.
122. Zolotarev, V. M. "Absolute Absorption Intensities and Optical Constants of Light (H_2O) and Heavy (D_2O) Water in Region 4,000-1,000 cm^{-1} of Spectrum," *Optika i Spektroskopiya*, Vol. 23, No. 5, p. 817, 1967. /338
123. Plyler, E. K. and N. Griff, "Absolute Absorption Coefficients of Liquid Water at 2.95, 4.7 and 6.1 μ," *Appl. Optics*, Vol. 4, No. 12, p. 1663, 1965.
124. Zuyev, V. Ye., *Rasprostraneniye Vidimykh i Infrakrasnykh Voln v Atmosfere* [Propagation of Visible and Infrared Waves in Atmosphere], Moscow, "Sovetskoye Radio" Press, 1970.
125. Apletalin, V. N., V. V. Meriakri and Ye. Ye. Chigryay, "Measurement of Absorption and Reflection Properties of Water at Wavelengths of 2 to 0.8 mm, *Radiotekhnika i Elektronika*, Vol. 15, No. 7, p. 1502, 1970.

126. Malyshenko, Yu. I. and I. Kh. Vakser, "Calculation of Permittivity of Water in Submillimeter Wavelength Range," *Ukrainskiy Fizicheskiy Zhurnal*, Vol. 15, No. 9, p. 1496, 1970.
127. Kozlov, A. I. and V. L. Mendel'son, "On Electric Parameters of Water and Ice," *Tr. Rizhskogo Instituta Grazhdanskoy Aviatsii*, No. 127, p. 5, 1969.
128. Evans, S., "Dielectric Properties of Ice and Snow," a review, *J. Glaciology*, Vol. 4, No. 42, p. 773, 1965.
129. Bogorodskiy, V. V. and V. N. Rudakov, "Electromagnetic Paramters of Snow, Ice, Fresh and Sea Water," in the book: *Primeneniye Radiofizicheskikh Metodov v Okeanograficheskikh i Ledovykh Issledovaniyakh*, [Application of Radiophysical Methods in Oceanologic and Ice Studies], Leningrad, Arctic and Antarctic Institute Press, p. 21, 1965.
130. Yonker, E. L., "Dielectric Properties of Water and Ice at K-Band," *OEM sr, 262, Service Project AN-25, Division 14*, Report 644, RL, Dec. 4, 1944.
131. Dunsmuir, R., and J. Lamb, "The Dielectric Properties of Ice at Wavelengths of 3 and 9 cm," *Report No. 61*, Manchester Univ. Press, 1945.
132. Lamb, J., "Measurements of the Dielectric Properties of Ice," *Trans. Faraday Soc.*, Vol. 42A, No. 1-2, p. 238, 1946.
133. Rudakov, V. N. and V. V. Bogorodskiy, "On the Problem of Measurement of the Thickness of Glaciers by Electromagnetic Methods," *Zh. Tekhnichekoy Fiziki*, Vol. 30, No. 1, p. 82, 1960.
134. Auty, R. P. and R. H. Cole, "Dielectric Properties of Ice and Solid D_2O," *J. Chem. Phys.*, Vol. 20, No. 8, p. 1309, 1952.
135. Lamb, J. and Turney, "The Dielectric Properties of Ice at 1.25 cm Wavelength," *Proc. Phys. Soc.*, Ser. B., Vol. 62, London, Part 4, No. 352, p. 272, 1949.
136. Cumming, W. A., "The Dielectric Properties of Ice and Snow at 3.2 cm," *J. Appl. Phys.*, Vol. 23, No. 7, p. 768, 1952.
137. Marshall, J. S. and K. L. S. Gunn, "Measurement of Snow Parameters by Radar," *J. Meteorol.*, Vol. 9, No. 5, p. 322, 1952.
138. Humbel, F., F. Jona and P. Schekker, "Anisotropy of Dielectric Constant of Ice," *Helv. Phys. Acta*, Vol. 26, No. 1, p. 17, 1953.
139. Ryde, J. W., "The Attenuation and Radar Echoes Produced at Centimeter Wavelengths by Various Meteorological Phenomena," *Meteorological Factors in Radio Wave Propagation, London Phys. Soc.*, p. 169, 1946.
140. Wiener, O., "Theory of Refraction Constants," *Berichte ueber die Verhandlungen der Koeniglichen Saechsischen Gesellschaft der Wissenschaften zu Leipzig, Math.-Phys. Klasse*, Vol. 62, No. 5, p. 256, 1910.
141. Wagner, K. W., "Explanation of the Electrical After-Effect Processes on the Basis of Maxwellian Considerations," *Archiv fuer Elektrotechnik*, Vol. 2, No. 1, p. 371, 1913.
142. Pearce, C. A. R., "The Permittivity of Two Phase Mixtures," *Brit. J. Appl. Phys.*, Vol. 6, No. 10, p. 358, 1955.
143. Reynolds, J. A. and J. M. Hough, "Formulae for Dielectric Constant of Mixture," *Proc. Phys. Soc.*, Ser. B, Vol. 70, London, Part 8, No. 452, p. 769, 1957.

144. Dichburn, R. W., *Light*, New York, Interscience Publ., p. 458, 1958.
145. Gunn, K. L. S. and T. W. R. East, "The Microwave Properties of Precipitation Particles," *Quart. J. Meteorol. Soc.*, Vol. 80, No. 346, p. 522, 1954.
146. Battan, L. J. and B. M. Herman, "The Radar Cross-Sections of 'Spongy' Ice Spheres," *J. Geophys. Res.*, Vol. 67, No. 13, p. 5139, 1962.
147. Joss, J. and R. List, "Radar Back-Scattering of Ice-Water Mixtures," *Z. Angew. Math. Phys.*, Vol. 14, No. 4, p. 376, 1963.
148. Joss, J. "Determination of the Back-Scattering Cross Section of Ice--Water Mixtures at a Wavelength of 5.05 cm," *Z. Angew. Math. Phys.*, Vol. 15, No. 5, p. 509. 1964. /339
149. Atlas, D., *Uspekhi Radarnoy Meteorologii* [Successes in Radar Meteorology], Leningrad, Gidrometeoizdat, 1967.
150. Rozenberg, V. I., "Permittivity of Homogeneous Mixture of Water and Ice," *Tr. Severo-Zapadnogo Politekhnicheskogo Instituta*, Radioelectronics Series, No. 5, p. 34, 1969.
151. Bogoroditskiy, N. P. et al., *Teoriya Dielektrikov* [Dielectric Theory], Moscow, "Energiya" Press, 1965.
152. Parnas, Ya. M. and K. I. Lebedeva, "Dielectric Properties of Inhomogeneous Dielectrics at Superhigh Frequencies," in the book: *Fizika Dielektrikov* [Dielectric Physics], Moscow, Academy of Sciences of the USSR Press, p. 65, 1960.
153. Landau, L. D. and Ye. M. Lifshits, *Elektrodinamika Sploshnykh Sred.* [Electrodynamics of Continua], Moscow-Leningrad, GIFML, 1958.
154. Howorka, F., "Dielectric Measurement of the Free Water Content of the Snow Cover," Dissertation, Innsbruck, 1964.
155. Ambach, W., W. Bitterlich and F. Howorka, "A Device for Determining the Free Water Content in the Snow Cover by Dieletric Measurement," *Acta Phys. Austriaca*, Vol. 20, No. 1-4, p. 247, 1965.
156. Kuroiva, D., "The Dielectric Property of Snow," *Union Geodesique et Geophysique Internationale, Association Internationale d'Hydrologie Scientifique, Assemblee General de Rome*, Vol. 4, p. 52, 1954.
157. Khippel', A. R., *Dielektriki i ikh Primeneniye* [Dielectrics and Their Application], Moscow, Gosenergoizdat, 1959.
158. Genev, R., *Grad* [Hail], translated from the French, Leningrad, Gidrometeoizdat, 1966.
159. Meyson, B. Dzh., *Fizika Oblakov* [Cloud Physics], translated from the English, Leningrad, Gidrometeoizdat, 1961.
160. Clark, V., "Icing Nomenclature," *Harvard-Mount Washington Icing. Res., 1946-47. U.S.A.F. Tech. Rep.*, No. 5676, p. 415, 1948.
161. Browning, K. A., "The Lobe Structure of Giant Hailstones," *Quart. J. Roy. Meteorol. Soc.*, Vol. 92, No. 391, p. 1, 1966.
162. Browning, K. A., F. H. Ludlam and W. C. Macklin, "The Density and Structure of Hailstones," *Quart. J. Roy. Meteorol. Soc.*, Vol. 89, No. 379, p. 75, 1963.

163. Browning, K. A., "The Growth Environment of Hailstones," *Met. Magazine*, Vol. 96, No. 1140, p. 202, 1967.
164. Bartishvili, G. S., *Mekhanizm Obrazovaniya Osobo Krupnykh Gradin (str. 66).* [Mechanism of Formation of a Specially Large Hailstones (p. 66)], *Raznovidnosti Ledyanykh Nasloyeniy Gradin i Usloviya ikh Obrazovaniya (str. 74)* [Varieties and Conditions of Ice Deposition on Hailstones of Formation (p. 74)]. *Nepravil'nyye Formy Gradin (str. 89)* [Irregular Hailstone Shapes (p. 89)] *Konicheskiye Gradiny i ikh Obrazovaniye (str. 95)* [Conical Hailstones and Their Formation (p. 95)]. from the collection: *Tr. Zakavkazskogo Nauchno-Issled. Gidromet. in-ta*, No. 25 (31), 1969.
165. Shumann, T. E. W., "The Theory of Hailstone Formation," *Quart. J. Roy. Meteorol. Soc.*, Vol. 64, No. 273, p. 1, 1938.
166. Ludlam, F. H., "The Composition of Coagulation Elements in Cumulonimbus," *Quart. J. Roy. Meteorol. Soc.*, Vol. 76, No. 327, p. 52, 1950.
167. Ludlam, F. H., "The Hail Problem," *Nubila*, Vol. 1, No. 1, p. 13, 1958.
168. List, R., "Growth and Structure of Graupel and Hailstones. Physics of Precipitation," *Geophys. Mon., Am. Geophys. Un.*, Washington, No. 5, p. 317, 1960.
169. List, R., "Thermodynamics of Partially Liquid Hailstones," *Zeit. Angew. Math. Phys.*, Vol. 273, No. 4, p. 11, 1960.
170. Macklin, W. C., "The Density and Structure of Ice Formed by Accretion," *Quart. J. Roy. Meteorol. Soc.*, Vol. 88, No. 375, p. 30, 1962.
171. Kachupin, L. G., "On the Theory of Aircraft Icing," *Izv. AN SSSR*, Geofiz. Series, No. 6, p. 823, 1962.
172. Kachurin, L. G., L. I. Gashin and Yu. G. Osipov, "Equation of Structural Crystals Growing in Supercooled Aerosol Flow," *DAN SSSR*, Vol. 147, No. 4, p. 833, 1962.
173. Kachurin, L. G. and L. I. Gashin, "On Density and Structure of Ice Growing in Supercooled Aerosol Flow," *AN SSSR*, Atmospheric and Oceanic Physics Ser., Vol. 4, No. 1, p. 93, 1968.
174. Mazin, I. P., *Fizicheskiye Osnovy Obledeneniya Samoletov* [Physical Principles of Aircraft Icing], Moscow, Gidrometeoizdat, 1957.
175. Kachurin, L. G. and V. G. Morachevskiy, *Kinetika Fazovykh Perekhodov Vody v Atmosfere* [Kinetics of Phase Transitions of Water in the Atmosphere], Leningrad State Univ. Press, 1965.
176. Byers, H. R. and R. R. Braham, "The Thunderstorm Report of the Thunder-Storm Project," Washington, U. S. Govt. Print. Office, 1949. /340
177. Shmeter, S. M., "Structure of Fields of Meteorological Elements in Cumulus Cloud Zone," *Tr. Tsentral'noy Aerolog. Observatorii*, No. 88, 1969.
178. Kachurin, L. G., V. I. Bekryayev and B. M. Vorob'yev, "Application of Turbulent Flow Method for Calculation of Convective Motions in the Atmosphere," *Tr. VIII Vsesoyuznoy Konferentsii po Fizike Oblakov i Aktivnym Vozdeystviyam* [Proceedings of the VIII All-Union Conference on Cloud Physics and Active Control], Leningrad, Gidrometeoizdat p. 213, 1970.
179. Sulakvelidze, G. K., *Livnevyye Osadki i Grad* [Shower Precipitation and Hail], Leningrad, Gidrometeoizdat, 1967.

180. Vorob'yev, B. M., *Chislennoye Modelirovaniye Protsessov, Protekayushchikh v Razvitykh Kuchevykh Oblakakh, Primenitel'no k Probleme Grada* [Numerical Simulation of Processes Occurring in Well-Developed Cumulus Clouds in Application to the Problem of Hail], Candidate's dissertation, Leningrad, Hydrometeorology Institute, 1971.
181. Brooks, C. F., "Hail Shells," *Bull. Amer. Met. Soc.*, Vol. 24, No. 2, p. 53, 1943.
182. Gvelesiani, A. I., *Nekotoryye Voprosy Evolyutsii Gradovykh Chastits* [Some Aspects of Hail Particle Evolution], Candidate's dissertation, Institute of Geophysics, Academy of Sciences GSSR, Tbilisi, 1970.
183. Gokhale, N. R. and K. M. Rao, "Theory of Hail Growth," *J. Rech. Atmosph.*, Vol. 4, 1st edition, p. 153, Oct. 1969.
184. Zamorskiy, A. D. *Atmosfernyy Led.* [Atmospheric Ice], Moscow-Leningrad, AN SSSR Press, 1955.
185. Bentley, W. A. and W. J. Humphreys, *Snow Crystals*, McGraw-Hill Press, London, New York, 1931.
186. Magono, C. and C. Lee, "Meteorological Classification of Natural Snow Crystals," *J. Facul. Sci., Hokkaido Univers.*, Ser. VII, Vol. II, Japan, No. 4, p. 325, 1966.
187. Gold, L. W. and B. W. Power, "Dependence of the Forms of Natural Snow Crystals on Meteorological Conditions," *J. Met.*, Vol. 11, No. 1, p. 35, 1954.
188. Imai, J. et al., "Radar Reflectivity of Falling Snow," *Papers in Meterorol. Geoph.*, Vol. 6, Tokyo, No. 2, p. 130, 1955.
189. Gunn, K. L. S. and J. S. Marshall, "The Distribution with Size Aggregate Snowflakes," *J. Meteorol.*, Vol. 15, No. 5, p. 452, 1958.
190. Magono, C., "Distribution of the Large Precipitation Elements," *J. Meteorol. Soc.*, Second edition, Japan, Ser. 31, No. 8, p. 12, 1953.
191. Kumai, M. and K. Higudi, "Measurement of the Mass and Number of Falling Snow Crystals in the Atmosphere," *J. Meteorol. Japan*, Second edition, Ser. 32, No. 3, p. 23, 1954.
192. Nakaya, U. and T. Terada, "Simultaneous Observations of the Mass, Rate of Fall and Shape of Individual Snow Crystals," *Mitt. des. Dent. Akad. Luft-fahrtforschung*, Vol. 2, No. 1, 1943.
193. Litvinov, I. V., "Determination of Steady State Fall Velocity of Snowflakes," *Izv. AN SSSR*, Geophysics Series, No. 7, p. 853, 1956.
194. Litvinov, I. V., "Experience of Investigation of Snowflake Distribution by Size," *Izv. AN SSSR*, Geophysics Series, No. 10, p. 1473, 1959.
195. Atlas, D., H. Kerker and W. Hitschfeld, "Scattering and Attenuation by Non-Spherical Atmospheric Particles," *J. Atmosph. Terrest. Phys.*, Vol. 3, No. 2, p. 108, 1953.
196. Magono, C. and T. Nakamura, "Aerodynamic Studies of Falling Snowflakes," *J. Meteorol. Soc. Japan*, Vol. 43, No. 3, p. 139, 1965.
197. Abshayev, M. T., Yu. A. Dadali and V. I. Rozenberg, "Radar Determination of Microstructural and Integral Characteristics of Snow," *Tr. Vysokogornogo Geofiz. in-ta*, [Proceedings of Alpine Geophysical Institute], No. 17, p. 260, 1970.
198. Magono, "On the Falling Velocity of Solid Precipitation Elements," *Sci. Rep. Yokahama Nat. Univ.*, Sec. 1, No. 3, 1954.

199. Battan, L. D., *Radiolokator Nablyudayet za Pogodoy* [Radar Watches the Weather], translated from the English, Gidrometeoizdat, 1964.
200. Gunn, R. and G. D. Kinzer, "The Terminal Velocity of Fall for Water Droplets in Air," *J. Meteorol.*, Vol. 6, No. 4, p. 243, 1949.
201. Medhurst, R. G., "Railfall Attenuation of Centimeter Waves: Comparison of Theory and Measurement," *IEEE Trans. Anten. and Propag.*, Vol. AP-13, No. 4, p. 550, 1965.
202. Tverskoy, P. N., *Kurs Meteorologii* [Course in Meteorology], Leningrad, Gidrometeoizdat, 1962. /341
203. Khrgian, A. Kh., *Fizika Atmosfery* [Atmospheric Physics], Leningrad, Gidrometeoizdat, 1969.
204. Matveyev, L. T., *Osnovy Obshchey Meteorologii, Fizika Atmosfery* [Fundamentals of General Meteorology. Atmospheric Physics], Leningrad, Gidrometeoizdat, 1965.
205. Khorguani, V. G., "Features of the Character and Velocity of Particle Systems," *Tr. Vysokogornogo Geofiz. in-ta*, No. 3 (5), p. 39, 1966.
206. Atlas, D. et al., "Back-Scatter by Dielectric Spheres (Reflective Index 1.6)," *IEEE Trans. Anten. and Propag.*, Vol. AP-11, No. 1, p. 68, 1963.
207. Deutsch, K., E. A. W. Hoff and W. Redish, "Relation Between the Structure of Polymers and Their Dynamic, Mechanical and Electrical Properties," *J. Polymer Sci.*, Vol. 13, No. 72, p. 565, 1954.
208. Dave, J. V., "Scattering of Electromagnetic Radiation by a Large Absorbing Sphere," *IBM J. Res. and Developm.*, Vol. 13, No. 3, p. 302, 1969.
209. Kattawar, W. and G. N. Plass, "Electromagnetic Scattering From Absorbing Spheres," *Appl. Optics*, Vol. 6, No. 8, p. 1377, 1967.
210. Herman, B. M. and L. J. Battan, "Calculation of Mie Back-Scattering of Microwaves from Ice Spheres," *Quart. J. Roy. Met. Soc.*, Vol. 87, No. 372, p. 223, 1961.
211. Denman, H. H., W. Heller and W. J. Pangonis, *Angular Scattering Functions for Spheres*, Detroit, Wayne State Univ. Press, 1966.
212. Corbato, F. J. and J. L. Uretsky, "Generation of Spherical Bessel Functions in Digital Computers," *J. Assoc. Comput. Machinery*, Vol. 6, No. 3, p. 366, 1959.
213. Shifrin, K. S. and I. L. Zel'manovich, *Tablitsy po Svetorasseyaniyu, T. III. Koeffitsiyenty Oslableniya, Rasseyaniya i Luchevogo Davleniya* [Tables on Light Scattering, Vol. III.] [Coefficients of Attenuation, Scattering and Radiant Pressure], Leningrad, Gidrometeoizdat, 1968.
214. Rozenberg, V. I., "Radar Characteristics of Hail with Various Dielectric Properties and Temperatures," *Tr. Vysokogornogo Geofiz. in-ta*, No. 13, p. 206, 1969.
215. Atlas, D. and K. M. Glover, "Back-Scatter by Dielectric Spheres with and Without Metal Caps," *Proc. Interdisciplinary Conf. on Electromagnetic Scattering*, New York, Pergamon Press, p. 213, 1963.
216. Krasyuk, N. P. and V. I. Rozenberg, "Effect of Variations of Complex Refraction Coefficients on Radar Characteristics of Ice Sphere," *Tr. Vysokogornogo Geofiz. in-ta*, No. 13, p. 215, 1969.
217. Donaldson, R. J., "Analysis of Severe Convective Storms Observed by Radar," *J. Meteorol.*, Vol. 15, No. 1, p. 44, 1958.

218. Herman, B. M. and L. J. Battan, "Calculation of the Total Attenuation and Angular Scatter of Ice Spheres," *Proc. 9th Weather Radar Conf. Am. Meteorol. Soc.*, Boston, p. 259, 1961.
219. Gerhardt, J. R. et al., "Experimental Determinations of the Back--Scattering Cross-Sections of Water Drops and of Wet and Dry Ice Spheres at 3.2 cm," *J. Meteorol.*, Vol. 18, No. 3, p. 340, 1961.
220. Gerhardt, J. R., C. W. Tolbert and S. A. Brunstein, "Further Studies of the Back-Scattering Cross-Sections of Water Drops and Wet and Dry Ice Spheres," *J. Meteorol.*, Vol. 18, No. 5, p. 688, 1961.
221. Glover, K. M. and D. Atlas, "On the Backscatter Cross-Sections of Ice Spheres," *Proc. 10th Weather Radar Conf. Am. Met. Soc.*, Boston, p. 157, 1963.
222. Stephens, J. J., "Radar Cross-Sections for Water and Ice Spheres," *J. Meteorol.*, Vol. 18, No. 3, p. 348, 1961.
223. Von, M. H. et al., "An Investigation of Mie and Rayleigh Backscattering at 3.2 and 10.3 Centimeter Wavelengths," *J. Geophys. Res.*, Vol. 69, No. 14, p. 2873, 1964.
224. Shifrin, K. S. and M. M. Chernyak, "Absorption and Scattering of Micro-Radiowaves in Precipitation," *Tr. Glavnoy Geofiz. Observatorii*, No. 222, p. 74, 1968.
225. Shifrin, K. S. and M. M. Chernyak, "Attenuation and Scattering of Centimeter Radiation by Raindrops," *Tr. Glavnoy Geofiz. Observatorii*, No. 203, p. 109, 1967.
226. Shupyatskiy, A. B., "Radar Measurement of Average Drop Size and Moisture Content in Heavy Rain," *Tr. Tsentral'noy Aerolog. Observatorii*, No. 20, p. 58, 1958.
227. Rozenberg, V. I., "Scattering of Microradio Waves by Lamellar Hail," /342 *Izv. AN SSSR*, Atmospheric and Oceanic Physics Ser., Vol. 6, No. 2, p. 168, 1970.
228. Rosinski, J., "Solid Water-Insoluble Particles in Hailstones and Their Geophysical Significance," *J. Appl. Meteorol.*, Vol. 5, No. 4, p. 481, 1966.
229. Atlas, D. et al., "Radar Scatter by Large Hail," *Quart. J. Roy. Meterol. Soc.*, Vol. 86, No. 370, p. 468, 1960.
230. Herman, B. M. and L. J. Battan, "Calculations of Mie Back-Scattering From Melting Ice Spheres," *J. Meteorol.*, Vol. 18, No. 4, p. 468, 1961.
231. Harper, W. G., "Radar Back-Scattering from Oblate Spheriods," *Nubila*, Vol. 5, No. 1, p. 60, 1962.
232. Willis, J. T., K. A. Browning and D. Atlas, "Radar Observations of Ice Spheres in Free Fall," *J. Atmosph. Sci.*, Vol. 21, No. 1, p. 103, 1964.
233. Abshayev, M. T. and V. I. Rozenberg, "Scattering and Attenuation of Radar Emission by Hailstones," *Izv. AN SSSR*, Atmospheric and Oceanic Physics Ser., Vol. 5, No. 9, p. 973, 1969.
234. Abshayev, M. T. and V. I. Rozenberg, "Calculations of Scattering and Attenuation Characteristics of Radar by Hailstones with Surface Layer of Water," *Tr. Vysokogornogo Geofiz. in-ta*, No. 13, p. 183, 1969.
235. Abshayev, M. T. and Yu. A. Dadali, "Capability of Microstructural Investigations of Clouds and Precipitation by Radar," *Tr. VGI*, No. 5, p. 71, 1966.

236. Labrum, N., "Some Experiments on Centimeter Wavelength Scattering by Small Obstacles," *J. Appl. Phys.*, Vol. 23, No. 12, p. 1320, 1962.
237. Nikolis, D., "Frequency Dependence of Back-Scattered Energy from Small Ice Particles During Falling Process,(in 18-25 GHz Band)," *Tr. Instituta Inzhenerov po Elektrotekhnike i Radioelektronike SShA*, Vol. 53, No. 5, p. 639, 1965.
238. Oguchi, T., "Scattering and Absorption of Millimeter Waves by Spherical Ice Particles During Falling Process," *Tr. Instituta Inzhenerov po Elektrotekhnike i Radioelektronike SShA*, Vol. 54, No. 6, p. 78, 1966.
239. Mann, G., "Studies of the Aerological Conditions for Precipitation in the Atmosphere in the Light of Data from the Weather Station at Koenigsberg," *Beitr. Phys. Frei. Atmos.*, Vol. 26, No. 3, p. 121, 1940.
240. Pugachev, V. S., *Teoriya Sluchaynykh Funktsii* [Random Functions Theory], Moscow, GIFML Press, 1962.
241. Venttsel', G. S., *Teoriya Veroyatnostey* [Probability Theory], Moscow, GIFML Press, 1962.
242. Laws, J. O, and D. A. Parsons, "The Relation of Raindrop Size to Rain Intensity," *Trans. Am. Geophys. Union*, Vol. 24, Part II, p. 452, 1943.
243. Marshall, J. S. and W. M. Palmer, "The Distribution of Raindrops with Size," *J. Meteorol.*, Vol. 5, No. 4, p. 165, 1948.
244. Lenard, P. "On Rain," *Met. Z.*, Vol. 21, p. 248, 1904.
245. Marshall, J. S., R. C. Langille and W. H. Palmer, "Measurement of Rainfall by Radar," *J. Meteorol.*, Vol. 4, No. 6, p. 186, 1947.
246. Anderson, L., "Drop-Size Distribution Measurements in Orographic Rains," *Bull. Am. Meteorol. Soc.*, Vol. 29, No. 7, p. 362, 1948.
247. Best, A. C., "The Size Distribution of Raindrops," *Quart. J. Roy. Meteorol. Soc.*, Vol. 76, No. 327, p. 16, 1950.
248. Litvinov, I. V. "Liquid Precipitation Particles Distribution Functions," *Izv. AN SSSR*, Geophysics Ser., No. 12, p. 1474, 1956.
249. Litvinov, I. V., "On Liquid Precipitation Particle Distribution Functions," *Izv. AN SSSR*, No. 6, p. 838, 1957.
250. Litvinov, I. V., "Spectral Distribution of Raindrops Formed by Melting of Hail," *Izv. AN SSSR*, Geophysics Ser., No. 7, p. 903, 1958.
251. Polyakova, Ye. A. and K. S. Shifrin, "Microstructure and Transparency of Rain," *Tr. Glavnoy Geofiz. Observatorii*, No. 42 (104), p. 84, 1953.
252. Kelkar, V. N., "Size Distribution of Raindrops, I," *Indian J. Meteorol. Geophys.*, Vol. 10, No. 2, p. 125, 1959.
253. Kelkar, V. N., "Size Distribution of Raindrops, II," *Indian J. Meteorol. Geophys.*, Vol. 11, No. 4, p. 323, 1960.
254. Kelkar, V. N., "Size Distribution of Raindrops, III," *Indian J. Meteorol. Geophys.*, Vol. 12, No. 4, p. 553, 1961.
255. Barteneva, O. D., Ye. K. Dovgyallo and Ye. A. Polyakova, "Experimental Investigations of Optical Properties of Near-Earth Atmosphere Layer," *Tr. Glavnoy Geofiz. Observatorii*, No. 220, p. 2, 1967. /343
256. Joss, J. J., C. Thams and A. Waldvogel, "The Variation of Raindrop Size Distributions at Locarno," *Proc. Intern. Conf. Cloud Phys.*, Toronto, p. 369, 1968.

257. Joss, J. and A. Waldvogel, "Raindrop Size Distribution and Sampling Size Errors," *J. Atmosph. Sci.*, Vol. 26, No. 3, p. 566, 1969.
258. Donaldson, R. J., "Drop-Size Distribution, Liquid Water Content, Optical Transmission and Radar Reflectivity in Fog and Drizzle," *Proc. 5th Weather Radar Conf.*, Asbury Park, New Jersey, p. 275, 1955.
259. Best, A. C., "Water in Atmosphere," *Interim Report of the U. S. W. Panel Working Commit.*, Part I, JEIA 7607, Report AC-7375, MO-USW, Aug. 14, 1944.
260. Wexler, R. and D. Atlas, "Radar Reflectivity and Attenuation of Rain," *J. Appl. Meteorol.*, Vol. 2, No. 2, p. 276, 1963.
261. Mueller, E. A. and D. M. Jones, "Drop Size Distribution in Florida," *Proc. 8th Weather Radar Conf. Am. Meteorol. Soc.*, Boston, p. 299, 1960.
262. Fujiwara, M., "An Analytical Investigation of the Variability of Size Distribution of Raindrops in Convective Storms," *Proc. 8th Weather Radar Conf. Am. Meteorol. Soc.*, Boston, p. 159, 1960.
263. Imai, J. "A Fitting Equation for Raindrop Size Distributions in Various Weather Situations," *Proc. 11th Weather Radar Conf. Am. Meteorol. Soc.*, p. 74, 1962.
264. Sivaramakrishnan, M. V., "Studies of Raindrop Size Characteristics in Different Types of Tropical Rain Using a Simple Raindrop Recorder," *Indian J. Meteorol. Geophys.*, Vol. 12, No. 2, p. 189, 1961.
265. Sal'man, Ye. M., "Radar Investigation of the Structure of Showers and Thunderstorms," *Tr. Glavnoy Geofiz. Observatorii*, No. 72, p. 46, 1957.
266. Gorelik, A. G. and G. A. Smirnova, "On Relation Between Water Content and Intensity of Clouds with Radar Reflectivity for Various Drop Size Distribution Parameters," *Tr. Tsentral'noy Aerolog. Observatorii*, No. 48, p. 98, 1963.
267. Borovikov, A. N. et al., *Radiolokatsionnyye Izmereniya Osadkov.* [Radar Measurement of Precipitation], Leningrad, Gidrometeoizdat, 1967.
268. Mazin, I. P. and A. N. Nevzorov, "Distribution of Raindrops by Size," *Meteorol. i Gidrol.*, No. 4, p. 99, 1968.
269. Dadali, Yu. A. and N. M. Mal'bakhova, "On the Character of Scattering and Attenuation of Micro-radiowaves in Precipitation," *Tr. Vysokogornogo Geofiz. in-ta*, No. 13, p. 153, 1969.
270. Deirmendjian, D., "Complete Scattering Parameters of Polydispersed Hydrometeors in the 0.1 to 10 cm Range," *Radio Sci. J. Res. Nat. Bur. Stand.*, Vol. 69D, No. 6, p. 893, 1965.
271. Levin, L. M., "On the Distribution Function of Cloud and Raindrops by Size," *DAN SSSR*, Vol. 94, No. 6, p. 1045, 1954.
272. Levin, L. M., "On Distribution Functions of Raindrops by Size," "Optical Density of Clouds," *Izv. AN SSSR*, Geophys. Ser., No. 10, p. 1211, 1958.
273. Kessler, F. and D. Atlas, "Radar-Synoptic Analysis of Hurricane 'EDNA'," *Geophys. Res. Paper, No. 50, Air Force Cambridge Res. Cent.*, Cambridge, Massachusetts, 1956.

274. Litvinov, I. V., "Procedural Aspects of Investigation of the Spectral Distribution of Precipitation Particles," *Tr. El'brusskoy Vysokogornoy Ekspeditsii* [Proceedings of El'brus Alpine Expedition], Vol. 2, No. 5, *Izd. AN SSSR*, p. 87, 1961.
275. Litvinov, I. V., "On the Rain Spectrum," *Izv. AN SSSR*, Geophys. Ser., No. 1, p. 114, 1956.
276. Mueller, E. A. and A. H. Sims, "The Influence of Sampling Volume on Raindrop Size Spectra," *12th Conf. Radar Met.*, Normal, Okla., p. 79, 1966.
277. Abshayev, M. T. and O. I. Chepovskaya, "On Hail Distribution Function," *Meteorol. i Gidrol.*, No. 6, p. 36, 1967.
278. Abshayev, M. T., "On Hailstone and Hail Nucleus Concentration in Cumulus Clouds," *Tr. Vysokogornogo Geofiz. in-ta*, No. 3 (5), p. 191, 1966.
279. Chepovskaya, O. I., "Preliminary Study Results of Hail Distribution on the Earth's Surface," *Tr. Vysokogornogo Geofiz. in-ta*, No. 3 (5), p. 117, 1966. /344
280. Douglas, R. H. and W. Hitschfeld, "Studies of Alberta Hailstorms," *Sci. Rept. MW-27*, McGill Univ., 1958.
281. Atlas, D. and F. Ludlam, "Multi-Wavelength Radar Reflectivity of Hailstorms," *Quart. J. Roy. Met. Soc.*, Vol. 87, No. 374, p. 523, 1961.
282. Ludlam, F. H. and W. K. Macklin, "Some Aspects of Severe Storm in SE England," *Nubilia*, Vol. 3, p. 38, 1959.
283. Abshayev, M. T. and N. Sh. Bibilashvili, "Radar Method of Determining Spectrum and Concentration of Hailstones in Convective Clouds," *Tr. Vysokogornogo Geofiz. in-ta*, No. 3(5), p. 117, 1966.
284. Hunter, I. B., "Attenuation of Microwaves in the Troposphere," *Marconi Review*, Vol. 27, No. 154, p. 122, 1964.
285. Bean, B. R., "Attenuation of Radio Waves in the Troposphere," *Advances in Radio Research*, Vol. 1, Academic Press, London, N. Y., p. 121, 1964.
286. Rider, G. C., "Propagation Measurements of Q-Band Rainfall Attenuation," *Marconi Review*, Vol. 29, No. 160, p. 24, 1966.
287. Kolosov, M. A. and A. V. Sokolov, "Some Aspects of Propagation of Millimeter and Submillimeter Radio Waves," *Radiotekhnika i Elektronika (AN SSSR)*, Vol. 15, No. 4, p. 667, 1970.
288. Basharinov, A. Ye. et al., "Investigation of Field of Radiothermal Radiation of the Earth," *Izv. AN SSSR*, Atmospheric and Oceanic Physics Ser., Vol. 6, No. 4, p. 366, 1970.
289. Krasyuk, N. P., V. I. Rozenberg and D. A. Chistyakov, "Radar Characteristics of Precipitation of Various Nature, Spectra, Intensities and Temperatures in Centimeter and Millimeter Wavelength Ranges," *Tr. Vysokogornogo Geofiz. in-ta*, No. 11, p. 147, 1968.
290. Rozenberg, V. I., "Radar Characteristics of Rain in Submillimeter Range," *Radiotekhnika i Elektronika (AN SSSR)*, Vol. 15, No. 12, p. 2443, 1970.
291. Krasyuk, N. P., V. I. Rozenberg and D. A. Chistyakov, "Consideration of Effect of Rain with Different Drop Spectra on Radar Operations," *Radiotekhnika i Elektronika (AN SSSR)*, Vol. 13, No. 5, p. 780, 1968.

292. Krasyuk, N. P., V. I. Rozenberg and D. A. Chistyakov, "Attenuation and Scattering of Radar Signals by Rain with Droplet Size Distribution According to Shifrin and Marshall-Palmer," *Radiotekhnika i Elektronika, (AN SSSR)*, Vol. 13, No. 10, p. 1872, 1968.
293. Krasyuk, N. P., V. I. Rozenberg and D. A. Chistyakov, "Attenuation and Scattering of Radio Waves by Rain of Different Origin," *Izv. AN SSSR*, Atmospheric and Oceanic Physics Series, Vol. 4, No. 11, p. 1209, 1968.
294. Krasyuk, N. P., V. I. Rozenberg and D. A. Chistyakov, "Attenuation and Scattering of Electromagnetic Waves by Rain of Different Nature," *Izv. VUZov SSSR*, Radiophysics Ser., Vol. 12, No. 1, p. 54, 1969.
295. Rozenberg, V. I., "Effect of Initial and Final Segments of Droplet Spectrum on Radar Characteristics of Rain," *Izv. AN SSSR*, Atmospheric and Oceanic Physics Series, Vol. 6, No. 8, p. 854, 1970.
296. Oguchi, T., "Attenuation of Electromagnetic Waves Due to Rain with Distorted Raindrops," *J. Radio Res. Labs (Tokyo)*, Vol. 7, No. 9, p. 467, 1960.
297. Lammers, U., "Back-Scattering Measurements on Water Droplets and the Influence of Their Shape in the Millimeter-Wave Region," *Nachrichten Tech. Zeitschrift*, Vol. 19, No. 10, p. 591, 1966.
298. Vakser, I. Kh., Yu. I. Malyshenko and L. Ye. Kopilovich, "On the Effect of Rain on The Distribution of Millimeter and Submillimeter Radio Waves," *Izv. AN SSSR*, Atmospheric and Oceanic Physics Ser., Vol. 6, No. 9, p. 956, 1970.
299. Naumov, A. P. and V. S. Stankevich, "On Attenuation of Millimeter and Submillimeter Radio Waves in Rain," *Izv. VUZov SSSR*, Radiophysics Series, Vol. 12, No. 2, p. 181, 1969.
300. Valitov, R. A. et al., *Tekhnika Submillimetrovykh Voln.* [Submillimeter Wave Technology], Moscow, "Sovetskoye Radio" Press, 1969.
301. Atlas, D. and A. C. Chmela, "Physical-Synoptic Variations of Drop-Size Parameters," *Proc. 6th Weather Radar Conf., Am. Meteorol. Soc.*, Boston, Vol. 4, p. 21, 1957. /345
302. Hardy, K. R. and A. N. Dingle, "Raindrop Size Distributions in a Cold Frontal Shower," *Proc. 8th Weather Radar Conf. Am. Meteorol. Soc.*, Boston, p. 179, 1960.
303. Imai, I., "Raindrop Size Distributions and Z-R Relationships," *Proc. 8th Weather Radar Conf. Am. Meteorol. Soc.*, Boston, p. 211, 1960.
304. Hardy, K. R., "The Development of Raindrop Size Distributions and Implications Related to the Physics of Precipitation," *J. Atmosph. Sci.*, Vol. 20, No. 4, p. 299, 1963.
305. Boyenval, E. H., "Echoes from Precipitation Using Pulsed Doppler Radar," *Proc. 8th Weather Radar Conf. Am. Meteorol. Soc.*, Boston, p. 57, 1960.
306. Mason, B. J. and J. B. Andrews, "Drop-Size Distributions from Various Types of Rain," *Quart. J. Roy. Met. Soc.*, Vol. 86, No. 369, p. 346, 1960.
307. Dingle, A. N., "The Micro-Structure of Rain in a Summer Shower," *Proc. 8th Weather Radar Conf.*, p. 99, 1960.
308. Abshayev, M. T. and V. I. Rozenberg, "Scattering and Attenuation of Radio Emission of Centimeter Wavelength Range by Hail," *Izv. AN SSSR*, Atmospheric and Oceanic Physics Series, Vol. 5, No. 8, p. 803, 1969.

309. Abshayev, M. T. et al., "Radar Investigations of Cumulus Clouds," *Tr. VIII Vsesoyuznoy Konferentsii po Fizike Oblakov i Aktivnym Vozdeystviyam* [Proceedings of VIII All-Union Conference on Cloud Physics and Active Control], Leningrad, Gidrometeoizdat, p. 325, 1970.

310. Rozenberg, V. I. and B. M. Vorob'yev, "Scattering Attenuation of Electromagnetic Waves of Length 3.2 cm by Inhomogeneous Hail," *Izv. AN SSSR*, Atmospheric and Oceanic Physics Series, Vol. 7, No. 6, p. 632, 1971.

311. Abshayev, M. T., "Radar Methods of Measuring Microstructural Characteristics of Clouds," in the book: *Tr. III Vsesoyuznogo Soveshchaniya po Radiolokatsionnoy Meteorologii* [Proceedings of the Third All-Union Conference on Radar Meteorology], Moscow, Gidrometeoizdat, p. 72, 1968.

312. Kachurin, L. G. and B. M. Vorob'yev, "Features of Vertical Structure of Radio Echo of Hail Clouds, Attributed to Crystallization Processes," *Izv. AN SSSR*, Atmospheric and Oceanic Physics Series, Vol. 4, No. 5, p. 525, 1968.

313. Voronov, G. S., "Observations of Hail in Samsar Expedition," *Tr. Tsentral'noy Aerolog. Observatorii*, No. 51, p. 42, 1963.

314. Voronov, G. S., "Some Data from Investigation of Hail in Alazanskaya Valley," *Tr. Tsentral'noy Aerolog. Observatorii*, No. 65, p. 93, 1965.

315. Akhvlediani, Ya. R., O. V. Lomats and L. S. Sarkisova, "Hail Phenomena in Alazanskaya Valley According to Meteorological Data," *Tr. in-ta Geofiziki AN GSSR*, Cloud Physics Series, Vol. 25, No. 1, p. 65, 1963.

316. Voronov, G. S. et al., "Hail Phenomena in Alazanskaya Valley According to Expedition Observation Data," *Tr. in-ta Geofiziki AN GSSR*, Cloud Physics Series, Vol. 25, No., p. 75, 1963.

317. Kartsivadze, A. I. and P. I. Makharashvili, "Some Data on Physical Characteristics of Hail," *Tr. in-ta Geofiziki AN SSSR*, Cloud Physics Series, Vol 25, No. 1, p. 84, 1963.

318. Knight, C. A. and N. C. Knight, "Hailstone Embryos," *J. Atmosph. Sci.*, Vol. 27, No. 4, p. 659, 1970.

319. Knight, C. A. and N. C. Knight, "Lobe Structures of Hailstones," *J. Atmosph. Sci.*, Vol. 27, No. 4, p. 667, 1970.

320. Knight, C. A. and N. C. Knight, "The Falling Behavior of Hailstones," *J. Atmosph. Sci.*, Vol. 27, No. 4, p. 672, 1970.

321. List, R., J. G. Cantin and M. G. Ferland, "Structural Properties of Two Hailstone Samples," *J. Atmosph. Sci.*, Vo.. 27, No. 7, p. 1080, 1970.

322. Babkin, Yu. S. et al., "On the Problem of Attenuation of Radiation at Wavelength 0.96 mm in Snow," *Radiotekhnika i Elektronika (AN SSSR)*, Vol. 15, No. 12, p. 2459, 1970.

323. Voronov, G. S. and I. I. Gayvoronskiy, "Results of Active Actions on Hail Processes," *Tr. Tsentral'noy Aerolog. Observatorii*, No. 100, p. 11, 1970.

324. Sulakvelidze, G. K., N. Sh. Bibilashvili and V. F. Laicheva, *Obrazovaniye Osadkov i Vozdeystviye na Gradovyye Protsessy* [Formation of Precipitation and Action on Hail Processes], Leningrad, Gidrometeoizdat, 1965. /346

325. Voronov, G. S. and I. I. Gayvoronskiy, "Radar Investigations of Hail Processes in Moldavia," *Meteorol. i Gidrol.*, No. 4, p. 48, 1969.
326. Beryulev, G. P. et al., "Equation of Radar Observation of Precipitation and Calibration of Radar System for Measuring Reflectivity of Multiple Target," *Tr. III Vsesoyuznogo Soveshchaniya po Radiolokatsionnoy Meteorologii* [Proceedings of Third All-Union Conference on Radar Meteorology], Moscow, p. 22, 1968.
327. Shupyatskiy, A. B., "Scattering of Radio Waves by Aspherical Atmospheric Particles," *Tr. Tsentral'noy Aerolog. Observatorii*, No. 30, p. 39, 1959.
328. Sokolov, A. V. and Ye. V. Sukhonin, "On Attenuation of Submillimeter Radio Waves in Rain," *Radiotekhnika i Elektronika (AN SSSR)*, Vol. 15, No. 12, p. 2454, 1970.
329. Babkin, Yu. S. et al., "Measurement of Attenuation in Rain on 1 km Path and Wavelength of 0.96 mm," *Radiotekhnika i Elektronika (AN SSSR)*, Vol. 15, No. 12, p. 2451, 1970.
330. Malyshenko, Yu. I. and I. Kh. Vakser, "Measurement of Radio Wave Attenuation Coefficient on 1.3 and 0.86 mm in Rain," *Izv. VUZov SSSR*, Radiophysics Series, Vol. 14, No. 5, p. 958, 1971.

Translated for the National Aeronautics and Space Administration Under Contract No. NASw-2485 by Techtran Corporation, P. O. Box 645, Silver Spring, Maryland 20901, translator: Adam Peiperl.

*U.S. GOVERNMENT PRINTING OFFICE: 1974-739-157/95